The Design and Synthesis of αvβ6 Antagonists and PI3K Inhibitors as Small Molecule Therapies for Respiratory Diseases

Thesis submitted to the University of Strathclyde as part of the assessment towards a degree of Doctor of Philosophy

Christopher J Tame

2014

University of Strathclyde
Glasgow

gsk
do more
feel better
live longer

Lex I: Corpus omne perseverare in statu suo quiescendi vel movendi uniformiter in directum, nisi quatenus a viribus impressis cogitur statum illum mutare.

Lex II: Mutationem motus proportionalem esse vi motrici impressae, et fieri secundum lineam rectam qua vis illa imprimitur.

Christopher J Tame

Abstract

The respiratory system controls gas exchange in the process of respiration, a function essential for human life. Consequently, disorders in respiratory function significantly impact the quality of life and are often fatal. These disorders usually occur in the lungs, the major respiratory organ.

Current treatments for respiratory diseases often possess undesired side-effects due to off-target biological activity,[1] whilst others are only suitable for specific patient populations.[2] Consequently, respiratory diseases are responsible for millions of hospitalisations and deaths every year. In the USA alone, the cost of asthma to the economy is estimated at $55 billion per year, and is increasing at a rate of over $3000 per person, per year.[3] Taken together with the substantial reduction in the quality of life associated with these disorders, it is clear that research towards improved treatments for respiratory diseases have the potential to significantly impact both patients and economies.

This thesis presents scientific research towards the identification of small molecule therapies for two respiratory diseases, Idiopathic Pulmonary Fibrosis (IPF) and Asthma. Chapter 1 presents the design and synthesis of the first series of orally bioavailable $\alpha v \beta 6$ selective antagonists for the treatment of IPF, whilst Chapter 2 concerns the design and synthesis of two orthogonal series of small molecule PI3K inhibitors for the treatment of asthma.

The research aims were to identify safe and efficacious treatments that are also convenient for the patient to administer. Investigations have, therefore, focussed on selectively modulating a specific biological target and designing a suitable pharmacokinetic profile for oral delivery, where possible. The results presented in this document demonstrate significant advancements towards this goal, and offer encouragement that an improved standard of care for respiratory disorders is possible. The human biological samples were sourced ethically and their research use was in accord with the terms of the informed consents.

Christopher J Tame

Acknowledgements

Firstly, I would like to thank my academic supervisor, Dr. Craig Jamieson. Thanks for including me as an integral member of your research group and making the distance between Strathclyde and Stevenage feel very short indeed. Your energy, effort and rigour have made a significant impact on my scientific and personal development and I would not have been able to complete my studies without you. A special thank you also for meticulously reviewing all of my report submissions and for developing my report writing technique.

I would also like to thank my industrial supervisor, Dr. Simon Peace. I feel incredibly fortunate to have been able to work under your guidance in the PI3Kδ team and to have your valuable insight whilst working on the PI3Kγ and αvβ6 programs. Thank you for providing guidance in the synthetic route design for the PI3Kδ inhibitors and teaching me the subtleties (and limitations) of analysis of PK and PD data. Thanks especially for giving me the time and space to investigate the development of the cyclotrimerisation methodology, and for teaching me the value of careful thought and consideration of synthetic and medicinal chemistry strategies. A final thank you is for teaching me the importance of rigorous scientific research.

Thanks very much to my internal examiner Professor William Kerr, for your rigorous scientific examination of my periodical report submissions and enlightening me to the philosophical value of Isaac Newton's first two laws of motion.

A very special thank you to Professor Harry Kelly, for conceiving and successfully managing the GSK postgraduate certificate scheme and the industrial Ph.D. scheme. None of this would have been possible without your tireless effort and energy towards my professional development. Remember Harry, every day...

Thank you to Dave Allen, Dr. Patrick Vallance and Sir Andrew Witty for their financial and moral support of my postgraduate development through the GSK certificate scheme and the Ph.D. programme.

Christopher J Tame

Christopher J Tame

Contents

Christopher J Tame

5

Christopher J Tame

Christopher J Tame

Abbreviations

acac:	Acetylacetonate
Ac:	Acetyl
ACD:	Advanced Chemistry Development Labs Inc.
AGP:	Alpha glycoprotein
Akt:	Also known as Protein Kinase B (PKB)
AMU:	Atomic mass unit.
Aq:	Aqueous
Arg:	Arginine
Asn:	Asparagine
Asp:	Aspartate
ATP:	Adenosine triphosphate
ATS:	American Thoracic Society
αLβ2:	Alpha lymphocyte beta two integrin
AUC:	Area under curve
αvβ3:	Alpha vitronectin beta three integrin
αvβ5:	Alpha vitronectin beta five integrin
αvβ6:	Alpha vitronectin beta six integrin
αvβ8:	Alpha vitronectin beta eight integrin
BAL:	Bronchioalveolar lavage
BCR-ABL:	Breakpoint cluster region – Abelson
	Also known as the Philadelphia chromosome.
BINAP	2,2'-*Bis*(diphenylphosphino)-1,1'-binaphthyl
BM:	Basement membrane
BMP:	Bone morphogenetic protein
BMS:	Bristol Myers Squibb
Bn:	Benzyl
Boc:	*tert*-Butyloxycarbonate
br:	Broad
°C:	Degrees Celsius
CAD:	Cationic ambiphilic drug

Christopher J Tame

c-Bu:	Cyclobutyl
Cbz:	Carboxybenzyl
CD4$^+$:	Cluster of differentiation four
Chrom Log D:	Chromatographic log D – measured lipophilicity at pH 7.4
Cl:	Clearance
cLog P:	Daylight calculated lipophilicity
CLND:	Chemi-luminescent nitrogen detection
cod:	Cyclcooctadiene
CPME:	Cyclopentyl methyl ether
c-Pr:	Cyclopropyl
CTGF:	Connective tissue growth factor
Cy:	Cyclohexane
dba:	Dibenzylideneacetone
DCE:	Dichloroethane
DCM:	Dichloromethane
DIPEA:	Diisopropylethylamine
DMF:	*N,N*-Dimethylformamide
DMSO:	Dimethylsulfoxide
DNA PK:	DNA-dependant protein kinase
dppb:	1,4-*Bis*(diphenylphosphino)butane
dppf:	1,1'-*Bis*(diphenylphosphino)ferrocene
dppp:	1,3-*Bis*(diphenylphosphino)propane
dtbpy:	4,4'-Di-*tert*-butyl-2,2' -bipyridine
ECM:	Extra-cellular matrix
Et:	Ethyl
EMT:	Epithelial-mesenchymal transition
ERS:	European Respiratory Society
EWG:	Electron-withdrawing group
F:	Bioavailability
Fabs:	Fraction absorbed
FaSSIF:	Fasted-state simulated intestinal fluid
FDA:	Food and drug administration

9

Christopher J Tame

FGFR:	Fibroblast growth factor receptor
FiZZ1:	Resisten-like molecule alpha 1
FP:	Fluticasone propionate
FRAP:	FK506 binding protein 12-rapamycin associated protein.
FVC:	Forced vital capacity
Gln:	Glutamine
Glu:	Glutamic acid
GSK:	GlaxoSmithKline
h:	Hour
HATU:	O-(7-Azabenzotriazol-1-yl)-N,N,N',N'-tetramethyluronium hexafluorophosphate
His:	Histidine
HPLC:	High performance liquid chromatography
HPV:	Hepatic portal vein
HRMS:	High-resolution mass spectrometry
HSA:	Human serum albumin
IHC:	Inhaled corticosteroid
IFNγ:	Interferon gamma
IgG2a:	Immunoglobulin G2a
IL:	Interleukin
Ile:	Isoleucine
IPF:	Idiopathic Pulmonary Fibrosis
i-pr:	Isopropyl
i.v.	Intra veneous
IVC:	in-$vitro$ clearance
JRS:	Japanese Respiratory Society
L*:	Ligand
LABA:	Long-acting beta agonist
LAD:	Leukocyte adhesion deficiency
LAP:	Latency associated peptide
LCMS:	Liquid chromatography mass spectrometry
Let-7d:	Lethal seven d micro ribonucleic acid

Christopher J Tame

Leu:	Leucine
LOXL2:	Lysyl oxidase-like two
LPA:	Lysophosphatidic acid
Lys:	Lysine
Lysosome:	Cellular organelles which contain acid hydrolase enzymes
M6PR:	Mannose-six phosphate receptor
mAb:	Monoclonal antibody
MDAP:	Mass directed auto preparative chromatography
Mesitylene:	1,3,5-Trimethylbenzene
MDCK:	Madine-Derby canine kidney
MDI:	Metered-dose inhaler
Me:	Methyl
Met:	Methionine
MHz:	Megahertz
Min:	Minutes
mTOR:	Mechanistic target of rapamycin
MW:	Molecular weight
nbd:	Norbornadiene
NHBE:	Normal human bronchial epithelium
NICE:	National Institute of Clinical Excellence
NMP:	*N*-Methylpyrrolidine
NMR:	Nuclear magnetic resonance
PAI-1:	Plasminogen activator inhibitor-one
PBMC:	Peripheral blood mono-nuclear cells
PBS:	Phosphate buffered saline
PD:	Pharmacodynamic
Perm:	Permeability
Ph:	Phenyl
Phe:	Phenylalanine
PI3K:	Phosphoinositide-3-kinase
PIK3C2B:	Phosphatidylinositol-4-phosphate 3-kinase C2 domain-containing beta polypeptide

Christopher J Tame

pIC_{50}:	The log of the concentration of compound required to reduce the activity of the biological target in question by 50%
PIP_2:	Phosphatidylinositol 4,5-bisphosphate
PIP_3:	Phosphatidylinositol 3,4,5-triphosphate
pin:	Pinacol
PK:	Pharmacokinetic
PKB:	Protein kinase B
PDGFR:	Platelet derived growth factor
p.o.	*Per os*
PPB:	Plasma protein binding
ppm:	Parts per million
Pr:	Propyl
Pro:	Proline
PTEN:	Phosphatase and tensin homologue
quin:	Quintet
RCT:	Randomised placebo-controlled trial
RGD:	Arginine-glycine-aspartic acid
RNA:	Ribonucleic acid
ROS:	Reactive oxygen species
r.t.:	Room temperature
Ruphos:	2-Dicyclohexylphosphino-2'-6'-diisopropoxybiphenyl
SAR:	Structure activity relationship
s.c.:	Subcutaneous
SCX:	Strong cation exchange
Ser:	Serine
SHH:	Sonic hedgehog signalling protein
SHIP:	SH-2 domain-containing inositol phosphotase
S_NAr:	Nucleophilic aromatic substitution
SOA:	Short oral absorption
Suc:	Succinimide
SVM:	Support vector machine
SYS	Systemic

Christopher J Tame

T ½:	Half life
TBAHS:	*tert*-Butylammoniumhydrogen sulfate
TBME:	*tert*-Butylmethyl ether
t-Bu	*tert*-Butyl
TGFβ	Transforming growth factor beta
TGM2:	Transglutaminase two
THF:	Tetrahydrofuran
THN:	Tetrahydronaphthyridine
Thr:	Threonine
TLR4:	Toll-like receptor 4
TMEDA:	Tetramethylethylenediamine
TMS:	Trimethylsilyl
TPSA:	Topological polar surface area
Tr/ Trityl	Triphenylmethyl
Trp:	Tryptophan
TSP1:	Thrombospondin one
Tyr:	Tyrosine
UPLC:	Ultra-performance liquid chromatography
Val:	Valine
Vdss:	Volume of distribution
VEGFR:	Vascular endothelial growth factor receptor
Wnt:	Wingless-related integration site
Xantphos:	4,5-*Bis*(diphenylphosphino)-9,9-dimethylxanthene
X-Phos:	2-Dicyclohexylphosphino-2′,4′,6′-triisopropylbiphenyl
μ-wave:	Microwave

Christopher J Tame

CHAPTER 1

The development of orally bioavailable alpha vitronectin beta six (αvβ6) antagonists for the treatment of Idiopathic Pulmonary Fibrosis (IPF)

1   Introduction

1.1   Fibrosis

The general term for fibrosis is the natural proliferation of connective tissue to replace damaged or lost tissue, usually caused by injury or infection.[4]   Fibrotic diseases, however, are characterised by the deposition of connective tissue over healthy tissue, which results in impaired organ function.[5]   Most organs in the body can become fibrotic, although the lungs,[6,7] heart,[8,9,10] peritoneum,[11] and kidney[12] are most common.[5]

The causes of many fibrotic diseases are not well understood, although they are usually the result of sustained and chronic injury to the organ. These idiopathic fibrotic diseases have all shown to be associated with increased levels of the pro-inflammatory cytokine, transforming growth factor β_1 (TGF-β_1), which seems to play a central role in disease progression.[10,12,13]

1.2   Idiopathic Pulmonary Fibrosis (IPF)

Idiopathic pulmonary fibrosis (IPF) is a progressive lung disease concerning the tissue and space around the alveoli (interstitium). IPF has unknown aetiology, although most patients are current or past smokers and have a median age of 60 years.[14] A 2006 study showed that there were 50,000 new cases of IPF and 40,000 deaths from IPF in the USA, per year.[15]

Christopher J Tame

Current studies suggest that IPF is a result of an abnormal epithelial wound healing process, which can progress to a fibroproliterative state in genetically susceptible individuals. This results in the overall loss of lung architecture, thus preventing gas exchange.[16,17] This degradation of lung structure can be seen in lung cross sections taken from IPF autopsies and is known as 'honeycombing' (**Figure 1**).

Cross-section of an IPF lung

Figure 1: An idiopathic pulmonary fibrotic lung.[18]

Sufferers of IPF usually experience shortness of breath (dyspnea) and a dry, unproductive cough, whilst 25-50% of patients also develop clubbing of the hands and feet.[6,19] The classical clinical finding in IPF is considered to be the sound of Velcro-like crackles at the bottom of both sides of the lung when examined with a stethoscope.[16] These symptoms, however, are not unique to IPF patients, therefore making it difficult to distinguish from other fibrotic or respiratory disorders.[16] IPF can, however, be distinguished from other lung diseases using histological lesions, whereby IPF is classified as a 'usual interstitial pneumonia'.[20]

The median survival rate of IPF sufferers ranges from just 2 to 3 years after diagnosis, but can vary in clinical course.[21] The main method of determining disease progression is through lung function, expressed as forced vital capacity (FVC): the maximum amount of air one can dispel from the lungs after a maximal inhalation.[6] It was originally considered that lung function would slowly decline over time, leading to death after 3-5 years.[22] Recently, however, it has been shown that there are multiple types of disease progression, including rapid, slow and stable (**Figure**

Christopher J Tame

2).[21,23] Some patients may also demonstrate unpredictable acute disease progression, shown here as a lightning bolt. The reasons for this are not fully understood, but have previously coincided with the onset of other complications, such as emphysema.[24]
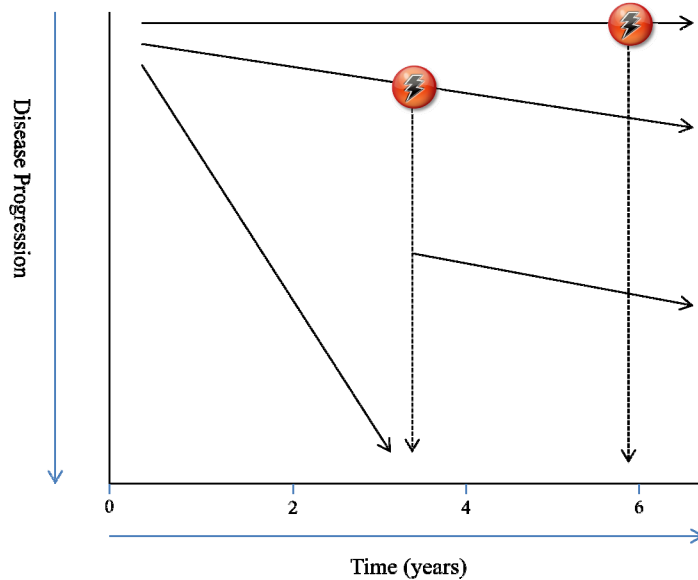
Figure 2: The varying types of disease progression in IPF patients.

The different IPF progression profiles demonstrate the importance of cohort selection for clinical research, as a mixture of patients may distort findings. It has been shown that patients with a rapid clinical course have a different gene expression to those with stable profiles. This is despite both profiles displaying similar lung function, chest imaging and histology at the time of diagnosis.[25] In addition, lung molecular signatures at the time of diagnosis can also discriminate between the two disease progression profiles.[26] Utilising these techniques during patient recruitment may help produce more reliable results, although predicting 'lightning-bolt' episodes remains challenging.

1.3   Current treatments for IPF

Perfinidone (**1**) is the only drug which has been approved for the treatment of IPF, which is now for sale in 35 countries, including China, Japan, India, Canada, Germany and the UK.[27]

Christopher J Tame

Pirfenidone is a small molecule drug dosed three times a day, at a total daily intake of 2 g (**Figure 3**).[28] The cost for treatment is similar in most countries and is equivalent to around £26,000 per patient, per year.[28] The large dose, frequent dosing regimen, and high cost are all areas that can be reduced by developing improved medicines.

1
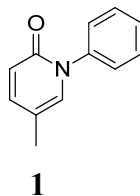
Figure 3: The molecular structure of Pirfenidone.

There are a number of side effects that have been identified during clinical trials with Pirfenidone, the most severe include photosensitivity, which prevents the patient from being exposed to sunlight, fatigue, dizziness, weight loss, gastroesophageal reflux disease, and hepatic dysfunction.[29]

The mechanism of action of Pirfenidone is unknown, but it has shown reduced TGFβ-mediated collagen production in human[30] and rat[31] fibroblasts *in vitro*, and has also reduced fibrosis in a number of animal models *in vivo*.[32] Pirfenidone is likely to work *via* multiple mechanisms, due to its antioxidant, anti-transforming growth factor, and antiplatelet properties.[33]

A joint statement from the American Thoracic Society (ATS), the European Respiratory Society (ERS), the Japanese Respiratory Society (JRS), and Latin American Thoracic Society (ALAT) (referred to herein as the 'joint committee') was published in 2011, which advises physicians on the course of treatment for IPF patients.[6] Interestingly, their recommendation was *not* to prescribe Pirfenidone. This was due to significant limitations in a randomised placebo-controlled trial (RCT) undertaken in Japan,[34] as well as inconsistencies with other international RCTs in satisfying their primary endpoints.[35] In addition, the significant side-effects were considered to out-weigh the marginal therapeutic benefit displayed in the

Christopher J Tame

clinical trials.[6] It is expected that further clinical trials will help to clarify the efficacy of Pirfenidone in IPF patients.

In 2013, the National Institute for Clinical Excellence in England and Wales (NICE) approved Pirfenidone for use by the National Health Service (NHS). This is provided certain criteria are met,[28] which is predicted to only apply to 10-15% of IPF sufferers.[36] Considering its marginal therapeutic benefit (if any), its expensive cost, and undesirable side-effects, the global approval of Pirfenidone highlights the urgent requirement for new treatments of IPF, and the importance of further research in this area.

The main recommendation, proposed by the joint committee for treatment of IPF, was that appropriate patients should undergo lung transplantation. This was due to findings which suggested improved long-term survival[37] and reduced risk of death over 5 years by employing such an approach.[38] Other recommendations focused on symptomatic treatments, rather than the fibrosis itself. This included the use of corticosteroids for patients suffering from acute exacerbations, and long-term oxygen therapy for those with IPF and resting hypoxemia (low blood-oxygen partial pressure).[6] The recommendation of corticosteroid use is based on "anecdotal reports of benefits..." and "...very low-quality evidence", in combination with the high mortality of patients with acute exacerbations.[6]

Around half of IPF patients also suffer from abnormal gastroesophageal reflux (GER), which may contribute to inflammation and fibrosis of the airways.[39] It has been shown that surgical removal of GER can stabilise lung function,[40] and has therefore been recommended for use by the committee.

These findings show that there is significant, unmet need for a safe and efficacious pharmacological treatment of idiopathic pulmonary fibrosis (IPF). Research in this area is likely to improve the understanding of this fatal disease, and has the ultimate aim of delivering new medicines for the treatment of IPF.

Christopher J Tame

1.4 Other clinical trials for IPF indications

There are a number of potential therapeutic agents for the treatment of IPF that are being evaluated with clinical studies, a selection of which are displayed in **Table 1**. The most advanced compound is the receptor tyrosine kinase inhibitor BIBF 1120 (**2**), which is currently in phase III clinical trials[41] and has an expected market launch date of 2015 (**Figure 4**).[42] BIBF 1120 inhibits the ATP-binding site of a number of growth factor receptors, including vascular endothelial growth factor receptor (VEGFR), fibroblast growth factor receptor (FGFR) and platelet derived growth factor receptor (PDGFR).[43] Numerous growth factors are involved in the injury-repair process in the alveolar-capillary barrier,[44] making BIBF 1120 a potential fibrotic treatment. BIBF 1120 has also shown to inhibit tumour angiogenesis (blood vessel formation),[43] and is, therefore, involved in clinical trials for a range of cancers.[45]

2
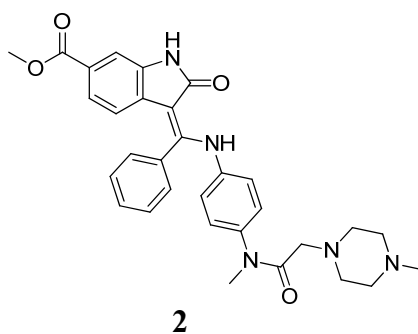
Figure 4: The molecular structure of BIBF 1120, currently undergoing phase III trials for IPF.

The majority of clinical trials ongoing for IPF indications are with biologicals, specifically monoclonal antibodies (**Table 1**). These engineered antibodies specifically bind to a single target cell or protein,[46] removing the risk of side-effects from off-target activity. Whilst they have the advantage of exhibiting high selectivity for the desired biological target, they are also expensive to produce[47] and rely on intravenous (i.v.) or sub-cutaneous (s.c.) administration.[48]

Name	Company	Clinical Trial	Type	Mechanism of Action	Route of Administration
BIBF-1120.[41]	Varatef, B.I.	Phase III	Small molecule	Tyrosine kinase inhibitor	Oral (p.o.)
BMS-986202.[49]	BMS	Phase II	Small molecule	LPA1 antagonist	Oral (p.o.)
PXS-64.[50]	Pharmaxis	Phase I	Small molecule	M6PR inhibitor	Intravenous (i.v.)
GSK 2126458[51]	GSK	Phase I	Small molecule	PI3K inhibitor	Oral (p.o.)
GC-1008.[52]	Genzyme/ Sanofi	Phase II	Humanised monoclonal antibody (mAb)	TGFβ antagonist	Intravenous (i.v.)
STX-100.[53]	Stromedix	Phase II	Humanised monoclonal antibody (mAb)	αvβ6 antagonist	Sub-cutaneous (s.c.)
GS-6624.[54]	Gilead	Phase II	Humanised monoclonal antibody (mAb)	LOXL2 inhibitor	Intravenous (i.v.) / sub-cutaneous (s.c.)
FG-3019.[55]	FibroGen	Phase II	Fully-humanised monoclonal antibody (mAb)	CTGF antagonist	Intravenous (i.v.)

Table 1: Potential therapeutic agents for the treatment of IPF, continues overleaf.

Christopher J Tame

Name	Company	Clinical Trial	Type	Mechanism of Action	Route of Administration
CAT-354.[56]	AZ/ MedImmune	Phase II	Fully-humanised monoclonal antibody (mAb)	IL-13 antagonist	Intravenous (i.v.)
SAR-156597.[57]	Sanofi	Phase II	Bi-specific antibody	IL4/ IL 13 antagonist	Sub-cutaneous (s.c.)
PRM-151.[58]	Promedior	Phase I	Recombinant human serum amyloid P	Unknown	Intravenous (i.v.)

Table 1 continued: Potential therapeutic agents for the treatment of IPF.

1.5   Biological rationale for (IPF)

Originally, it was thought that IPF developed as a result of chronic inflammation in the lung.[59,44] However, patients did not respond to anti-inflammatory drugs and clinical research found little correlation between inflammation and disease severity.[17] Current consensus now considers IPF to result from an impaired wound-healing response to injured lung epithelial tissue.[13,44,60]

To distinguish between a normal and abnormal response to lung injury, it is first necessary to describe the structure of the alveoli-capillary barrier (**Figure 5**).[61] This is the surface of the lungs and facilitates gas exchange; damage to this tissue would result in loss of organ function.

Christopher J Tame
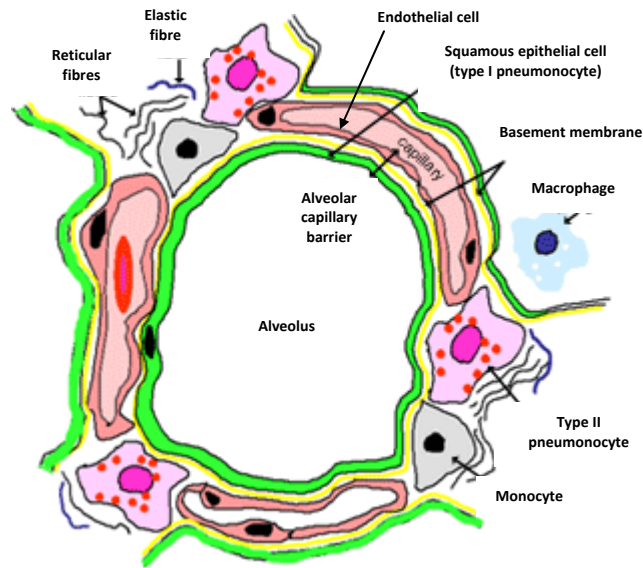
Figure 5: A diagram of the alveolar-epithelial barrier.[61]

The alveolus is an air sac located at the bottom of the airways, and is surrounded by very thin epithelial cells, also known as type I pneumonocytes (~0.3 μm thick).[62] Type II pneumonocytes secrete surfactants to help gas exchange by decreasing the surface tension between the thin cells, and helps prevent cell collapse during exhalation.[61] A basement membrane (BM) separates the edges of the cells with the extra-cellular matrix (ECM), shown in yellow in **Figure 5**. The ECM provides structural support to the cells and regulates nutrient transfer, and is composed of fibrous proteins like collagen and fibronectin, as well as glycosaminoglycans.[61] Whilst epithelial cells line the alveoli, endothelial cells line the capillaries. Macrophages are present to engulf bacteria and particulates, and originate from monocytes, a type of white blood cell.[61]

A 2009 review, published by Strieter and Mehrad, presents a useful overview of the factors that affect fibrosis.[44] A schematic presented in this publication helps to demonstrate the differences between a normal response to lung injury and the formation of fibrosis, and is reproduced in **Figure 6**.
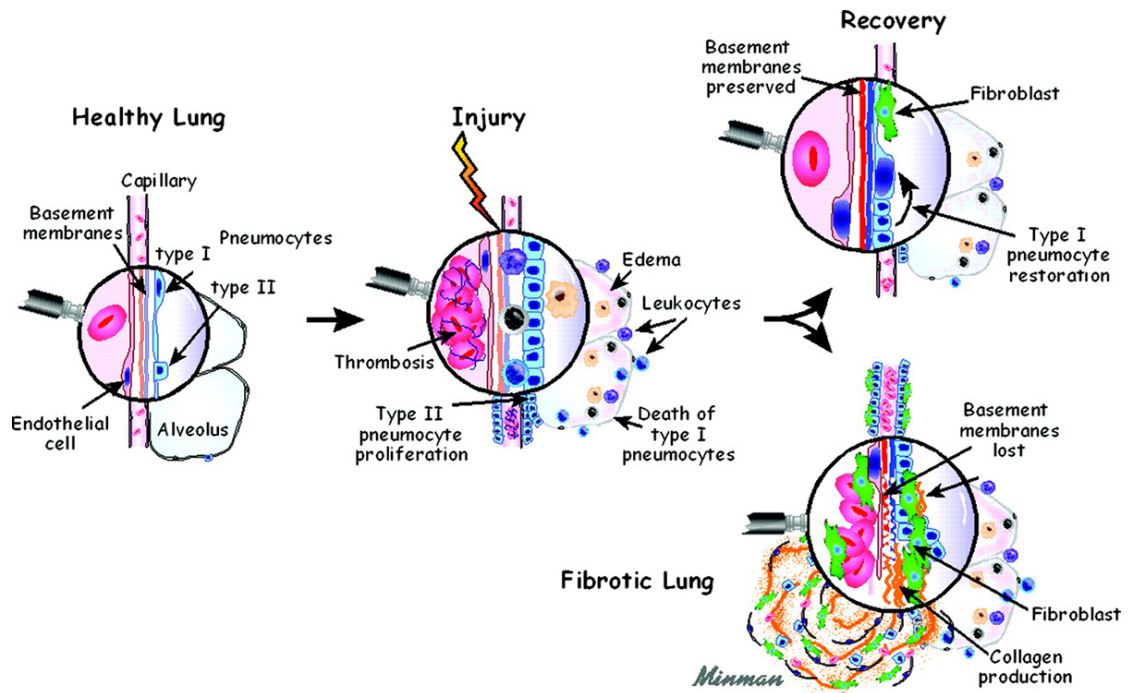
Figure 6: The normal and abnormal healing process in response to epithelial cell injury in the lung.[44]

An injury to the lung more specifically involves damage to the epithelial and endothelial cells, which causes leakage of plasma from the capillary into the lung tissue. This provokes degranulation (bursting) of white blood cells located nearby, which exposes the tissue to lipid mediators and cytokines. These cell messengers activate the formation of fibroblast/myofibroblasts, epithelial and endothelial cells, and other white blood cells. Fibroblasts and myofibroblasts help remodel the extra-cellular matrix (ECM), which in turn provides stabilisation for repair of the endothelium and epithelium with new cells. This process can only happen if the basement membrane (BM) is intact.[44,63]

If the basement membrane is lost, the production of ECM is uncontrolled and can spill-out into the alveoli air space, which causes the loss of the alveolar-capillary barrier. Epithelial cells will attempt to re-form at the leading edge of the ECM, which causes incorrect re-modelling of the alveoli. This causes increased proliferation of fibroblasts and myofibroblasts, which in turn accelerate the

Christopher J Tame

deposition of collagen-rich ECM. This self-activating fibrotic feedback loop is uncontrolled and ultimately destroys the ability for gas exchange and, therefore, lung function.[44]

Myofibroblasts are formed from fibroblasts during lung injury and stain for α-smooth muscle actin, used for wound-closing in the alveolar-capillary barrier.[64,65] They are concentrated in fibrotic foci, formed in IPF patients.[13] Interestingly, myofibroblasts are not found in healthy lung tissue and their numbers increase during IPF disease progression.[13] Preventing the formation of myofibroblasts is, therefore, expected to prevent the formation of IPF.

The origin of myofibroblasts is still debatable, but could form from a variety of sources. These include circulating progenitor cells such as fibrocytes, mesenchymal cells *via* epithelial to mesenchymal transition (EMT), or local mesenchymal cells such as fibroblasts (**Figure 7**).[13,44] Mesenchymal cells are a type of stem cell which usually develops into lymphatic, circulatory or connective tissue.[66] EMT is the process whereby epithelial cells detach from the epithelium, lose their usual cell properties and become mesenchymal cells (**Figure 8**).[67]
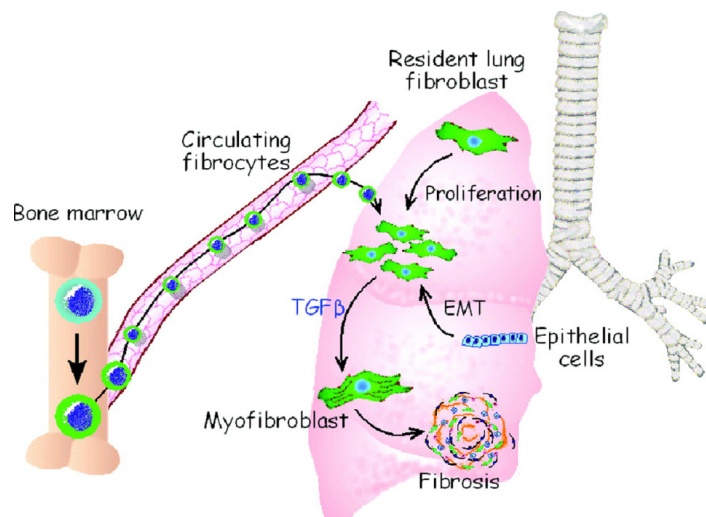
Figure 7: The possible sources of myofibroblasts.[44]

Christopher J Tame
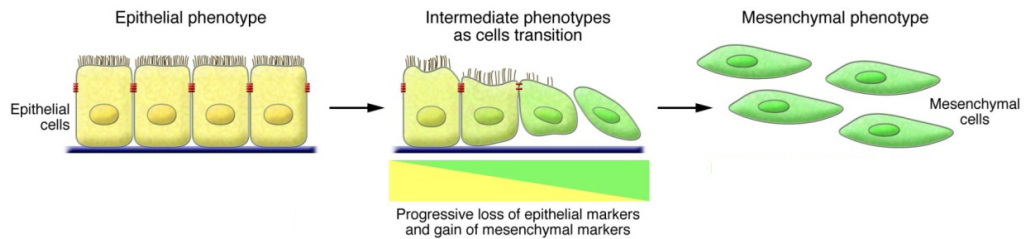
Figure 8: Epithelial to mesenchymal transition.[67]

The pro-inflammatory cytokine, transforming growth factor β (TGFβ), is considered central to the development and sustainability of the fibrotic process in IPF. TGFβ has been shown to influence the major routes of myofibroblast formation, such as epithelial to mesenchymal transition (EMT)[68,69] and fibrocyte differentiation.[70] In addition, severe and prolonged fibrosis occurred when active TGFβ$_1$ was over-expressed in rat lungs.[71]   Another study developed transgenic mice that over-expressed TGFβ in the airways. After fibrosis had developed, the TGFβ transgene was deactivated. This resulted in the receding of fibrosis and the restoration of normal lung architecture.[72] These studies suggest that blocking the action of TGFβ may provide a therapeutic treatment for IPF patients.

Conversely, TGFβ has been shown to regulate a range of *natural* processes, such as inflammation, immune tolerance and cancer biology.[73] Studies conducted with TGFβ-deficient transgenic mice actually induced a range of cancers (termed carcinogenesis).[74] This suggests that IPF treatments which modulate TGFβ levels would need to be localised to the lung and not cause complete TGFβ removal.

In addition to TGFβ, there are a variety of other cell-signalling mediators, collagen cross-linking enzymes, development pathways and micro RNA sequences, which have been implicated in idiopathic pulmonary fibrosis (**Table 2**).

Christopher J Tame

Cell-signalling mediators	Collagen cross-linking enzymes	Development Pathways	Micro RNA
LPA1[75]	LOXL2[76]	SHH[77]	Let-7d[78]
TLR4[79]	TGM2[80]	Wnt,[81]	
		FiZZ1/Notch1[82]	
		BMP[83]	

Table 2: A selection of biological targets associated with IPF.

1.6   Integrins and αvβ6

Integrins are signalling and adhesion proteins that transverse the cell membrane and connect the internal components of the cell with the surrounding environment. More specifically, integrins bind the structural architecture of the cell (cytoskeleton) with components in the extracellular environment, such as receptors on other cell surfaces or on proteins in the extracellular matrix. This allows the cell to respond to changes in its environment, which it does by initiating signalling cascades that control cell proliferation, survival and behaviour.

The extracellular component of an integrin is composed of a α and a β subunit, which form a heterodimer when bound to another ligand (**Figure 9**). Integrins can exist as either two separated subunits or as a heterodimer, which is only formed when the subunits are in their activated conformations. The heterodimer-ligand complex is the activated form of the integrin and triggers subsequent signalling.

Integrins can be activated in two ways: externally by ligand receptors, which result in intracellular signalling; or internally by cytoskeletal proteins such as Talins and Kindlins, which result in ECM changes.[84]

Christopher J Tame
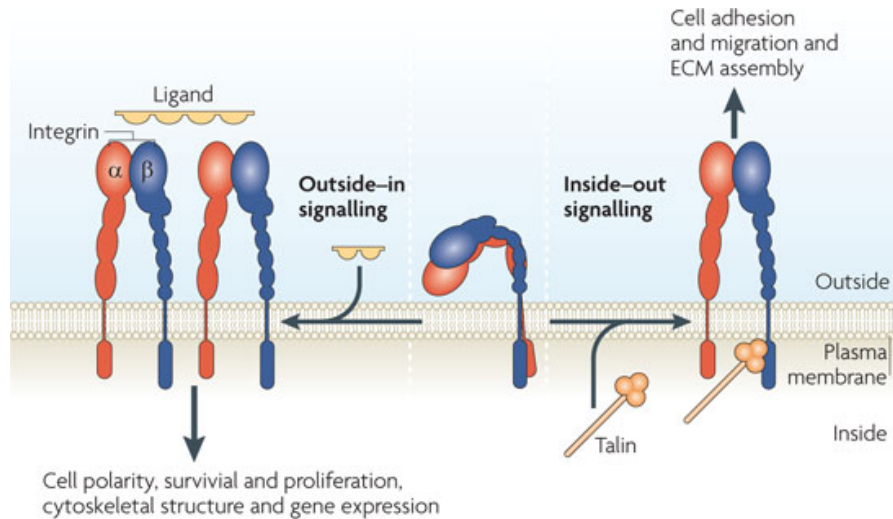
Figure 9: A schematic of the structure and function of integrins.[84]

To date, 24 distinct heterodimeric integrin complexes have been identified, which are made up of 18 α and 8 β subunits. The separate subunits and the complexes they form are displayed in **Figure 10** and are grouped according to the nature of extracellular binding ligand.[85] The α4 and α9 have limited expression and are coloured green accordingly. These subunits are exclusive to the biological taxonomic group phylum chordate, which is composed of some 75,000 animal species and includes all vertebrates.[85]
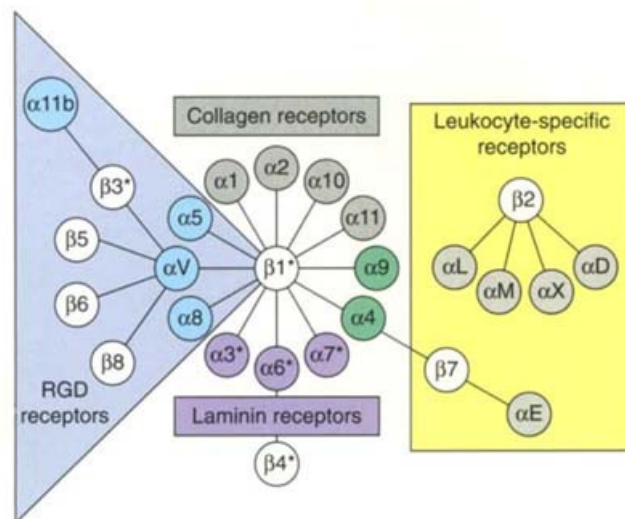
Figure 10: The different integrin subunits and heterodimeric complexes.[85]

Christopher J Tame

Laminin is a glycoprotein located in the basement membrane of cell tissue[86] and is involved in cell adhesion and migration.[87] Many laminin-binding intergins do not have exclusive complementarity to any one laminin target and pharmacological responses often require multiple laminin integrin activation.[88] An example is α6β4 and α3β1, which both bind to laminin 10 and are involved in colon cancer.[89]

A leukocyte is a general term for any marrow-derived cell which is involved in an immune response, and integrins that are exclusively expressed on their cell surface are grouped accordingly. Leukocyte integrins are involved in cell behaviour which is critical during an immune response, such as cell adhesion and migration.[90] An example of a leukocyte integrin is αLβ2, which is found on T-helper cells[91] and is implicated in leukocyte adhesion deficiency syndrome (LAD-1).[92,93]

Collagen is a fibrous structural protein which is formed by fibroblasts and is present in many tissues throughout the body, including the extracellular matrix (ECM).[94] Many different cells bind to collagen, and therefore collagen-binding integrins are widely expressed. For example, the collagen integrin α1β1 is found in fibroblasts, liver cells (hepatocytes) and smooth muscle cells. Accordingly, α1β1 is a potential therapeutic target for arthritis.[95]

The RGD-binding integrins are not grouped according to the cell-type of their complementary extacellular ligands. Instead, they are grouped according to the amino-acids they bind to: the arginine (R) - glycine (G) - aspartic acid (D) sequence (**Figure 11**). An example of an RGD-binding integrin is αvβ3, which binds to vitronectin and is involved in blood vessel formation (angiogenesis) in tumours.[96,97]
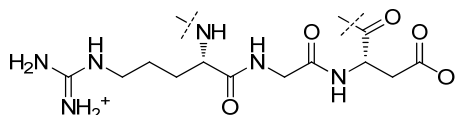
Figure 11: The arginine-glycine-aspartic acid (RGD) sequence.

Christopher J Tame

A number of studies have been conducted to identify the biological roles of different intergrins. A common method of experimentation is to genetically engineer rodents without the relevant integrin. This is done by removing the complementary gene that codes for the specific integrin and is termed a 'knock-out'. These studies have been very successful in identifying the pharmacological roles of integrins, and some have subsequently been investigated as potential therapeutic targets for disease modification. **Table 3** shows how knock-out mice and monoclonal antibodies have been used to help elucidate the function and therapeutic indication of the integrins previously discussed.

Christopher J Tame

Integrin [ref.]	Family	Experimental method	Expressing Cells	Extracellular Ligand	Phenotypes	Therapeutic Indication
α1β1 [95]	Collagen	α1 knockout	Fibroblasts, liver cells (hepatocytes), smooth muscle cells.	Type IV collagen	Decreased formation of immune cells (leukocytes) and excess tissue fluid (oedema).	Arthritis
αvβ3 [96,97]	RGD	αvβ3 monoclonal antibody (mAb)	Blood vessel cells (endothelial cells), tumour cells.	Vitronectin	Blood vessel formation (angiogenesis) in tumours	Cancers, arthritis, Osteoporosis.
αLβ2 [90,91,92]	Leukocyte	β2 knockout	T-helper (CD4+) immune system cells.	Intracellular adhesion molecule-2 (ICAM-2) (P1)	Impaired production of cell messengers (cytokines: IL-2, IFN-γ, and IgG2a).	Leukocyte adhesion deficiency (LAD I) syndrome
α6β4 / α3β1 [89]	Laminin	α3β1, or α6, or β4 monoclonal antibody (mAb)	Colon cancer cells.	Laminin-10	Inhibited cell migration during an immune response.	Colon cancer

Table 3: The roles of different integrins and some associated therapeutic indications.

Christopher J Tame

1.7   The role of αvβ6 in IPF

The RGD-binding integrin αvβ6 has been critically implicated in the fibrosis of a range of organs, including kidney,[98] liver[99] and lung.[100]   In particular, multiple studies have highlighted the importance of αvβ6 in idiopathic pulmonary fibrosis (IPF).[101,102] Histological studies on healthy and diseased human lung tissue identified fibrosis-mediated up-regulation of αvβ6 (**Figure 12**).[103]   The almost exclusive presence of αvβ6 in fibrotic tissue highlights the potential for selective pharmacological manipulation of diseased tissue through this integrin.
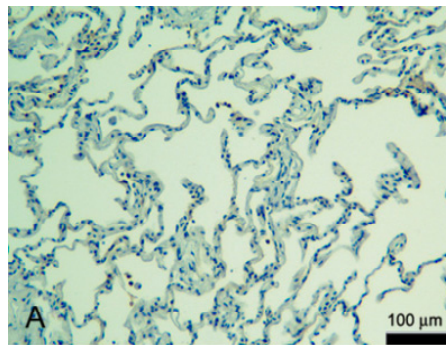
A: Healthy lung tissue
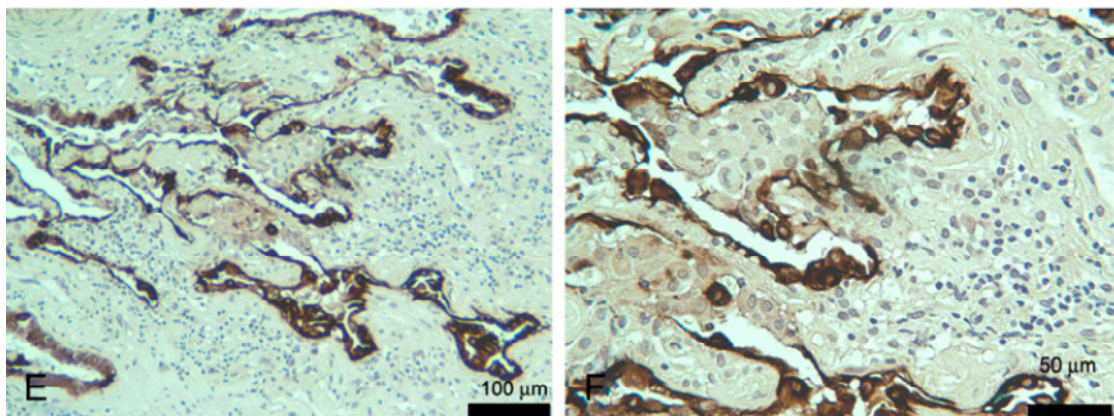
E and F: Lung tissue from IPF patients

Figure 12: Immunohistological staining of αvβ6 in the pulmonary epithelial tissue of different fibrotic diseases.[103] The tissue was stained brown for αvβ6 and the nuclei stained blue.

Christopher J Tame

The role of αvβ6 in fibrosis is believed to be mediated through its activation of transforming growth factor β$_1$ (TGFβ$_1$).[101] The role of this cytokine in IPF is well documented and has been discussed previously.[32-36] TGFβ is produced as part of a larger complex, where it is non-covalently bound to latency-associated peptide (LAP). When complexed in this fashion, TGFβ is inactive, and requires changes to the structural conformation of LAP for activation.[104]

All RGD-binding integrins can bind to LAP, and therefore influence the production of TGFβ by inducing conformational change.[105] With the exception of αvβ6, all other RGD-binding integrins are ubiquitously expressed. This indicates that a selective αvβ6 antagonist is required to avoid undesired side-effects related to TGFβ reduction in healthy tissues. Even though all of these integrins possess an RGD binding site, selectivity can be achieved, as demonstrated with a range of αvβ6 human monoclonal antibodies (mAbs).[106] Replicating the selectivity of an antibody with a small molecule, however, may be challenging.

It has been shown that αvβ6 binds to an RGD amino-acid sequence on the LAP-TGFβ$_1$ complex, which facilitates intracellular binding of β6 to the cytoskeleton. This is then thought to induce a structural change on LAP, which allows the presentation of TGFβ$_1$ to its receptor and subsequent activation the TGFβ$_1$–mediated signalling pathway (**Figure 13**).[101]
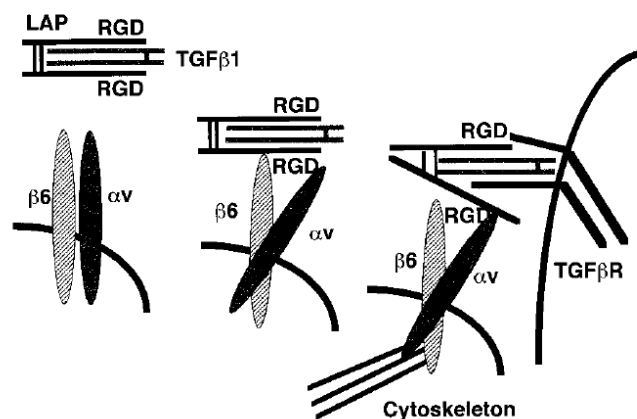
Figure 13: An illustration of αvβ6-mediated activation of TGFβ$_1$.[101]

Christopher J Tame

The exact mechanisms that are involved in TGFβ activation are not fully understood, however, a range of mediators other than αvβ6 have also been identified. These include the angiogenic mediator Thrombospondin 1 (TSP1),[107] the blood-plasma degrading protein Plasmin,[108,109] and reactive oxygen species (ROS).[110] Transgenic removal of these mediators results in the same inflammatory phenotype as with TGFβ knockout mice, although with much less severity.[109,111] For example, αvβ6 knock-out mice have a normal life span and only develop mild lung inflammation and late-onset emphysema,[112] whereas TGFβ knockout mice suffer from severe multi-organ inflammation and die after just 2-3 weeks.[113] This suggests that multiple LAP binders are required to enact the full pharmacological effect of TGFβ, and provides an opportunity to achieve an ideal balance of TGFβ expression for sufficient disease modification whilst maintaining its essential homeostatic roles.

A study which treated bleomycin-induced IPF in mice with an αvβ6 monoclonal antibody (3G9 mAb) at various doses demonstrated that a balance of significant antifibrotic activity without increased inflammation can be achieved.[102] Transgenic mice were engineered to produce lung luciferase in a collagen Iα2-dependent manner, which therefore served as a quantitative determinant of collagen production. Bleomycin was then dosed intra-tracheally, followed by the weekly intravenous administration of 3G9 mAb. The mice were culled after 14 days and lung luciferase levels were quantified. The positive control for the experiment was the TGFβ antibody rs-TGFβRII-Fc, which was delivered in phosphate-buffered saline (PBS) and has shown efficacy in range of TGFβ-dependent disease models. The results show clear dose-dependent inhibition, with an unexplained rebound effect at 10 mg/Kg and 3 x 4 mg/Kg dose levels (**Figure 14**).[102]

Christopher J Tame
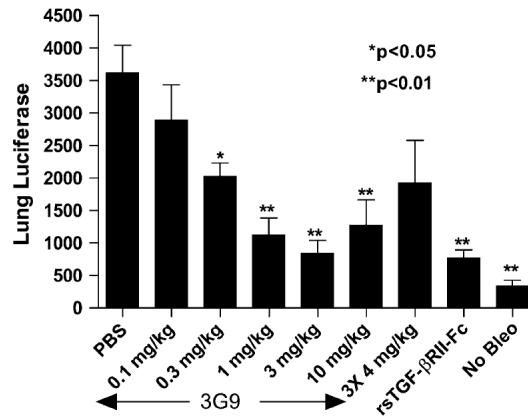
Figure 14: A dose-response study with an αvβ6 monoclonal antibody in a bleomycin IPF rat model. The significance is described as $p<0.05$ or $p<0.01$.[102]

This study was also used to identify the effect of αvβ6-inhibition on respiratory inflammation.[102] Mice were culled on days two, five, eight, and 11 of the study and a bronchial alveolar lavage (BAL) was performed. The washings were analysed for the presence of white blood cells which are up regulated during an inflammatory response. The results showed that doses up to 3 mg/Kg did not result in significant respiratory inflammation (**Figure 15**).[102] Although data are not presented for doses at 10 mg/Kg and 3 x 4 mg/kg, potential inflammation at these doses could explain why a rebound effect in lung luciferase production is observed, as shown in **Figure 14**.
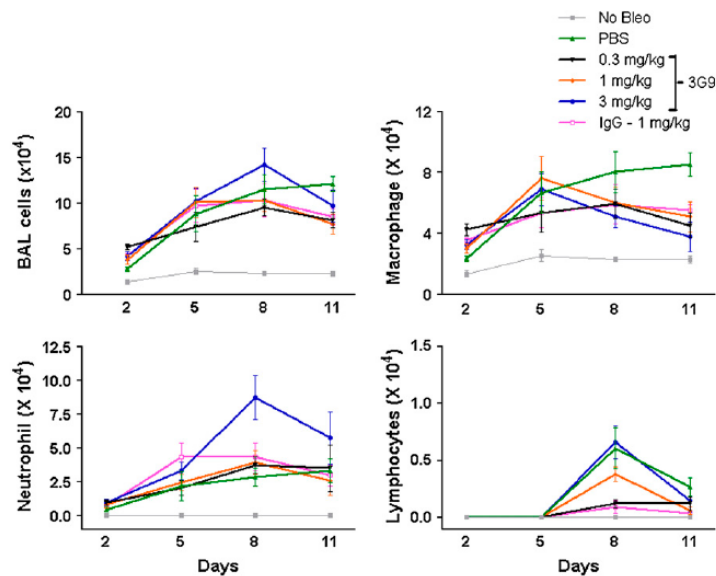
Figure 15: Measurement of white blood cells from BAL after αvβ6 inhibition with 3G9 mAb in a bleomycin IPF mouse model.[102]

Christopher J Tame

The localisation of αvβ6 to diseased pulmonary tissue is a significant factor in preventing systemic inflammation or other undesired side effects which may occur with less specific treatments. These results highlight the importance of αvβ6 in the development of IPF and the therapeutic potential of balanced αvβ6 inhibition. The positive results achieved with the αvβ6 mAb have resulted in subsequent clinical trials to further investigate the effects seen in murine systems.[53] While the αvβ6 mAb provides an exciting prospect for the treatment of IPF, its intravenous or sub-cutaneous mode of administration is a significant drawback. The development of an inhaled or orally-administered selective αvβ6 inhibitor is, therefore, expected to provide enhanced patient benefit.

1.8   Small molecule inhibitors of RGD integrins

Of the RGD binding integrins, αvβ3 has received the most attention as a therapeutic target. This is partly due to its role in new blood vessel formation (angiogenesis) in a wide range of cancers and tumours, such as ovarian,[114] breast,[115] and colon cancer[116] as well as glioblastoma brain tumours.[117] It is also the first integrin to have its three-dimensional structure determined by X-ray crystallography.[118,119,120] This provides a greater understanding of the location of residues with which to interact for improved ligand efficiency and selectivity. The structures of disclosed αvβ3 antagonists are similar in that they resemble the RGD sequence: possessing a hydrogen bond acceptor moiety at one end and a hydrogen bond donor-acceptor moiety at the other (**Table 4**).[121,122]

Christopher J Tame

The RGD amino acid sequence

3

4

5

6
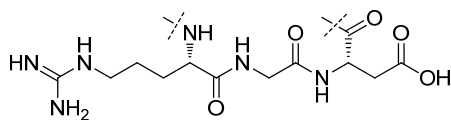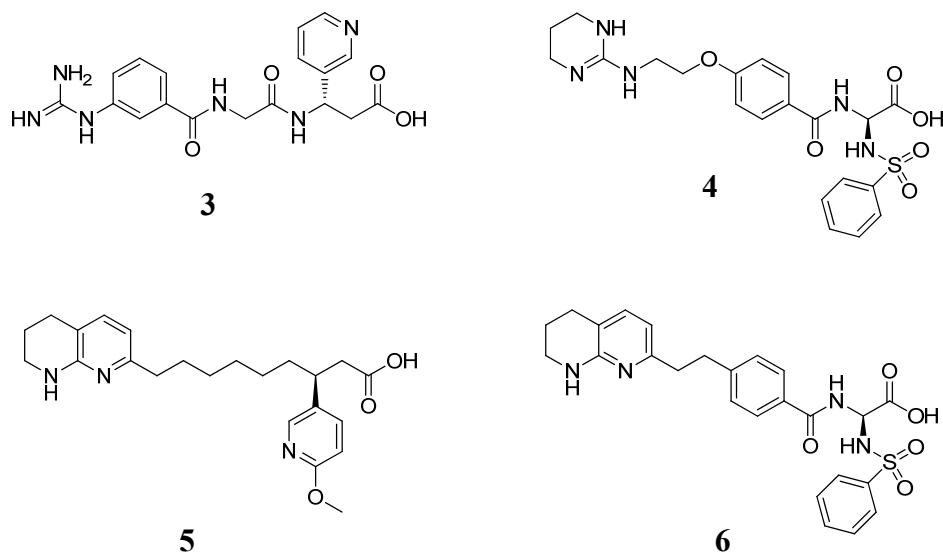
Compound no.	$\alpha v\beta 3$ cell adhesion pIC_{50}
3	9.3
4	9.1
5	9.2
6	10.0

Table 4: The structures and cell adhesion activities for a range of $\alpha v\beta 3$ antagonists.[121,122] The pIC_{50} values were generated from different assays, therefore care must be taken in directly comparing potency data.

A solved crystal structure of an RGD-containing cyclic peptide bound to $\alpha v\beta 3$ can help rationalise the structural similarities in disclosed $\alpha v\beta 3$ antagonists (**Figure 16**).[118] The crystal structure and associated interaction map identify a key bidentate interaction between the arginine residue of the ligand with an aspartic acid of the αv subunit. The structure also highlights an interaction between the aspartic acid residue of the ligand and a manganese cation in the $\beta 3$ subunit, along with multiple hydrogen bonding interactions with nearby polar residues.   The residues in the αv and $\beta 3$

Christopher J Tame

subunits which interact with the cyclic peptide are conserved across the RGD integrins, and interaction with both subunits are required for the formation of the heterodimeric complex.[118,120] Based on this, antagonising RGD integrins will require similar structural motifs at both ends of the molecule.
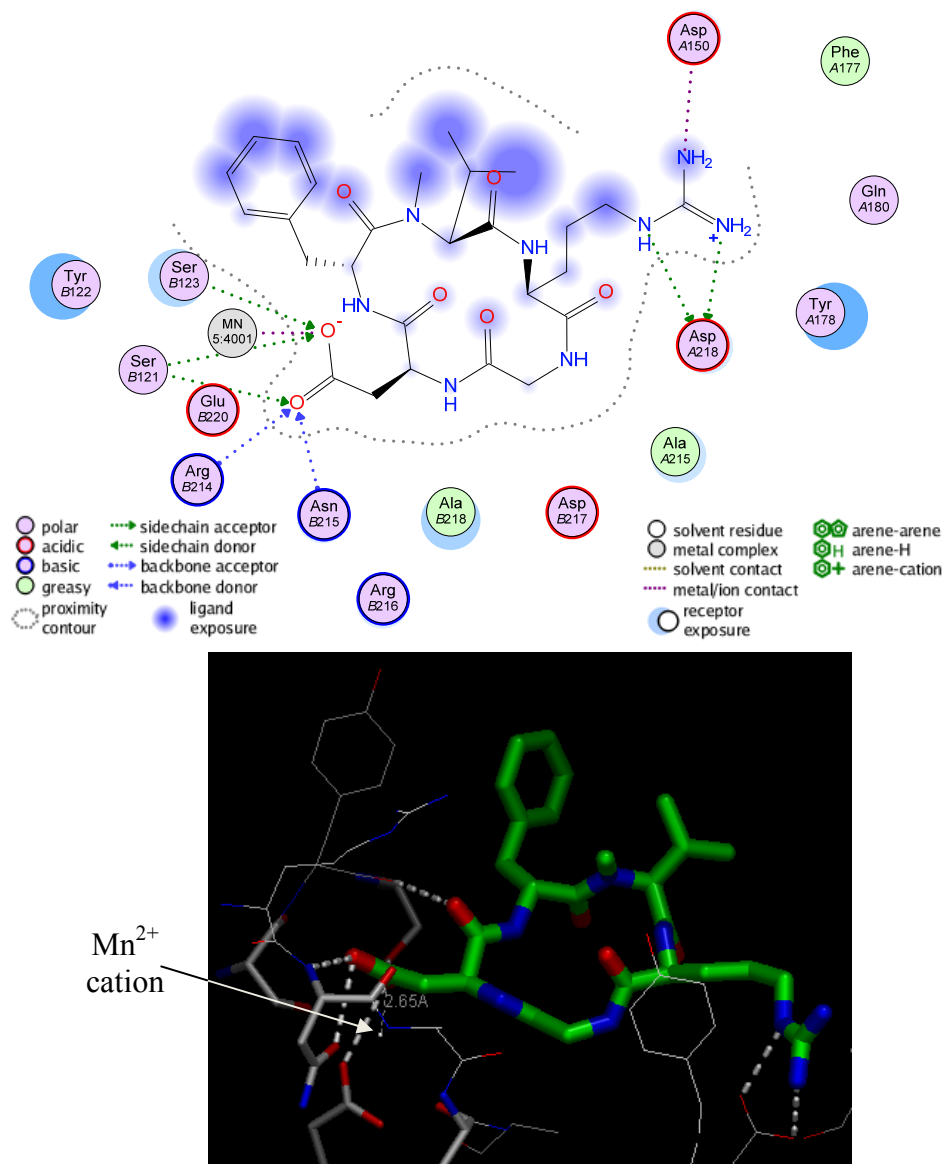
Figure 16: A solved crystal structure of an RGD-containing cyclic peptide in αvβ3.[118]

In 2002, researchers at Merck KGaA published a range of small molecules which selectively antagonised αvβ6 or αvβ3.[123] The structures and RGD integrin selectivity

Christopher J Tame

profiles are displayed in **Table 5**. Data for the related integrin αIIbβ3 is not included due to the lack of activity of these compounds to the receptor. The different selectivity profiles were achieved through substituent modifications on the phenyl ring and changes to the central peptide linker. These initial data provides confidence that selectivity for αvβ6 can be achieved against the other RGD integrins.

The RGD amino acid sequence

7

8

9

10

11
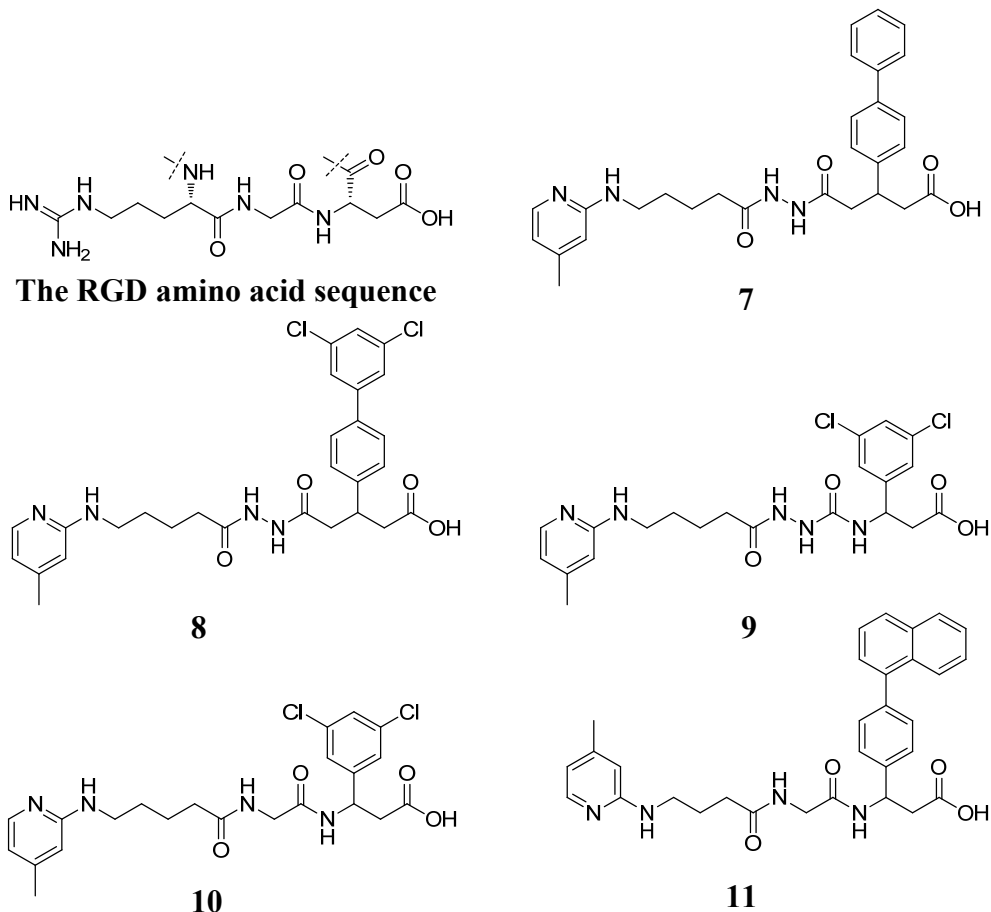
Compound no.	Cell adhesion (pIC$_{50}$)		
	αvβ6	αvβ3	αvβ5
7	5.4	6.0	4.6
8	5.8	4.7	4.7
9	6.5	4.9	5.3
10	6.5	4.8	5.7
11	6.7	5.5	4.7

Table 5: The structures and cell adhesion affinities for a range of RGD integrin antagonists.[123] The absolute stereochemistry of each analogue was not disclosed.

Christopher J Tame

Compound **11** was selected for further profiling in our laboratories in order to more fully benchmark the series.[124] The results are displayed in **Table 6**, which show a somewhat different selectivity profile to that disclosed in the literature.

Compound 11	Cell adhesion (pIC$_{50}$)		
	αvβ6	αvβ3	αvβ5
Literature assay	6.7	5.5	4.7
In-house assay	6.6	7.1	6.4

Table 6: The RGD integrin potencies for compound **12** in the literature[14] and in-house assays.[124]

Cell adhesion assays are developed by artificially expressing the integrin under study on the surface of a particular cell. Variations exist between the nature of cells and the extent of integrin expression, which help account for the differences observed in **Table 6**. These assays, therefore, do not provide results that are physiologically relevant, but serve to relate different compounds profiled in the same assay.

As a result, work undertaken in our laboratories aimed to identify compounds which displayed at least 10-fold selectivity for αvβ6 in our hands. Subsequent studies in disease-relevant animal models are expected to identify any unwanted side-effects relating to off-target integrin activity. This will help elucidate the required potency and selectivity profile in the *in vitro* assays for future lead optimisation efforts.

1.9   Previous unpublished research from our laboratories

Unfortunately, the peptidic nature of the molecules disclosed in the literature renders them unsuitable for oral administration, due to their anticipated poor oral absorption and high clearance.[125] This was confirmed with a pharmacokinetic (PK) study of compound **11** carried out in our laboratories, which was dosed intravenously (i.v.) and orally (p.o.) to rats (**Table 7**).[126] The data shows poor bioavailability and moderate clearance, short half life and a low volume of distribution. The resulting

Christopher J Tame

PK profile taken from combining these parameters was considered inadequate for an oral medicine.

11

Bioavailability (F) (%)	Clearance (Cl) (ml/min/kg)	Half Life (T ½) (h)	Volume of distribution (Vdss) (L/kg)
7	51.5	0.64	0.81

Table 7: The pharmacokinetic profile of compound **11**.[126]

Initial investigations in our laboratories, therefore, focused on developing non-peptidic, αvβ6-selective molecules with enhanced oral bioavailability, for the treatment of IPF. This resulted in the identification of two novel series of αvβ6 antagonists (**Table 8**).[127] Compound **12** was identified from a high throughput screen against αvβ6. Optimisation of the RGD integrin selectivity profile of this initial hit furnished compound **13**, which possesses a novel core composed of a piperidine ring.

12   **13**

Compound no.	Cell adhesion pIC$_{50}$				Mouse AUC ng/h/mL (1.0 mg/kg p.o. dose)
	αvβ6	αvβ3	αvβ5	αvβ8	
12	6.9	8.0	8.2	7.1	3770.0
13*	7.6	6.8	6.9	7.5	75.5

Table 8: The RGD integrin affinity and rat oral bioavailability of two novel series of RGD integrin antagonists.[124,127] * denotes single enantiomer of unknown absolute stereochemistry.

Christopher J Tame

The molecules **12** and **13** are structurally similar to the other RGD antagonists discussed previously, but differ in the nature of the core. Compound **12** possesses a 2-amino-5-oxopyridine moiety in place of an amide linker which was used in preceding integrin antagonists. Pharmacokinetic studies in mice with Pyridine **12** displayed very high levels of oral absorption; high exposure was measured in the blood after a 1 mg/Kg oral dose in mice, and excellent bioavailability (98%) was observed after administrating a 1 mg/Kg dose to rats by oral and intravenous routes.[126] Unfortunately, however, this series does not display any selectivity for αvβ6 in our assays.[124]

Subsequent modification of the core involved replacing the aromatic ring with a saturated analogue. Piperidine **13** was an example of this, which was linked through the nitrogen for synthetic expediency. In contrast to pyridine **12**, piperidine **13** imparted reasonable selectivity but displayed low exposure in the blood after oral administration (**Table 8**). Having stated this, piperidine **13** is the first example of a non-peptidic integrin antagonist to display some degree of selectivity for αvβ6 in our assays.

Both of these molecules exploited the use of a cyclopropyl substituent at the 3-position of the phenyl ring, which was identified as the most atom-efficient moiety to impart αvβ6 selectivity based on the SAR developed in this series (**Table 9**). The data refer to racemic compounds with the exception of those denoted (*) which refer to a single unknown enantiomer.

Christopher J Tame
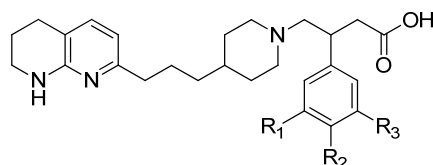
N	R$_1$	R$_2$	R$_3$	MW	Cell adhesion pIC$_{50}$			
					αvβ6	αvβ3	αvβ5	αvβ8
A	Cl	H	H	456	7.0	6.6	6.5	6.8
B	Pr	H	H	464	7.4	6.5	6.6	7.3
C	c-Pr	H	H	462	7.4	6.5	6.8	7.5
D	c-Pr*	H	H	462	7.6	6.8	6.9	7.5
E	c-Pr	H	c-Pr	502	7.4	5.9	5.8	7.4
F	c-Pr	c-Pr	H	502	7.2	6.5	6.2	7.7
G	c-Bu	H	H	475	7.3	6.4	7.0	7.4
H	H	OMe	H	452	7.2	7.2	6.8	6.4
I	c-Pr	OMe	H	492	7.9	6.7	6.4	7.7
J	N-Morpholine	H	H	507	7.4	6.2	6.5	7.4
K	N-Pyrazole	H	H	488	7.6	6.2	7.2	7.3

Table 9: Modifications to the phenyl ring substituent of piperidine **13** can manipulate the RGD integrin selectivity profile.[124,127] * denotes single enantiomer.

Despite the poor bioavailability of compound **13**, it is potentially suitable for topical administration, as it localises the concentration of the dose to the administered tissue. This helps reduce the risk of off target effects which cause systemic toxicity. Accordingly, antagonists similar to piperidine **13** are undergoing further investigation elsewhere in our laboratories for delivery *via* the inhaled route.

1.10   Route of administration

Although the inhaled route is attractive, there could be a number of complications with this delivery mode resulting from the reduced lung function and severe obstruction of the airways of IPF patients. This could prevent the drug from accessing the source of fibrosis at the alveolar-capillary barrier, and therefore from

delivering efficacy. Consequently, the development of an orally bioavailable, αvβ6-selective antagonist represents the best chance of providing an efficacious treatment for IPF.

Two approaches can be considered to identify an orally bioavailable, αvβ6-selective antagonist:

1: To develop αvβ6-selectivity in a compound with existing good oral bioavailability (for example, pyridine **12**).

2: To develop oral bioavailability in a compound with existing good αvβ6-selectivity (for example, piperidine **13**).

It has been previously demonstrated that manipulation of phenyl ring substituents can influence the RGD integrin selectivity profile (**Table 9**). Current efforts in our laboratories are attempting to transfer this SAR onto a series of antagonists with good oral bioavailability, such as pyridine **12**.

The aim of this research, however, is to develop oral bioavailability in compounds which possess αvβ6 selectivity, such as piperidine **13**. In order to identify methods of improving oral bioavailability, it is first necessary to understand the pharmacokinetic (PK) factors which determine it.

1.11 Understanding the cause of poor bioavailability

Typical PK studies dose the compound in question *via* oral (p.o.) and intravenous (i.v.) routes and compare the relative levels of drug found in the blood at different time points throughout the study (**Figure 17**). The drug levels found after i.v. administration then represent the behaviour of 100% of the dose in the systemic circulation. Relating the difference between these levels and the levels found after oral administration defines the percentage of dose which is orally absorbed, which is quoted as bioavailability (F%).

Christopher J Tame
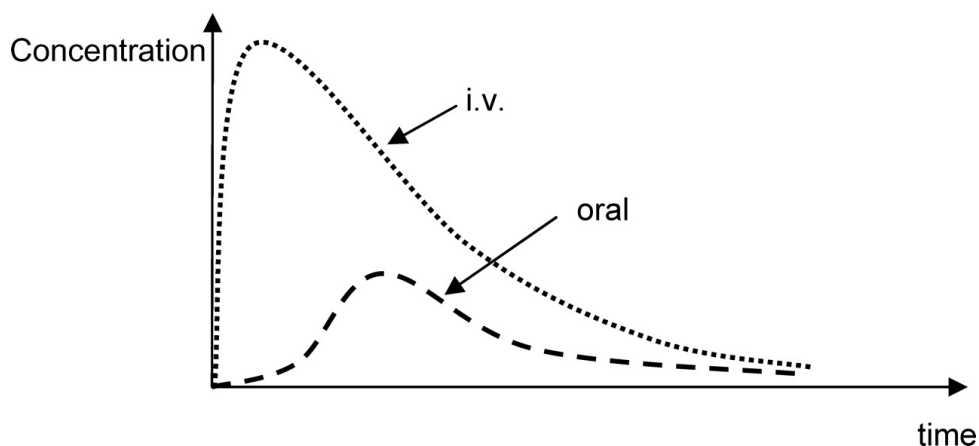
Figure 17: A diagram of drug levels in the blood after i.v. and p.o. dosing.[128]

However, factors such as rapid first-pass hepatic metabolism could also affect oral bioavailability.[129] Drug which is absorbed from the gut will first be transported to the liver *via* the hepatic portal vein (**Figure 18**). The liver is the metabolic engine of the body, containing a high density of metabolic enzymes and cells which readily drain unwanted material into the bile for excretion. Compounds which are rapidly removed (cleared) from the blood in the liver are unlikely to reach the systemic circulation beyond the liver, which is where blood samples are taken. Therefore, low levels of orally-administered drug may be due to factors other than poor oral absorption.
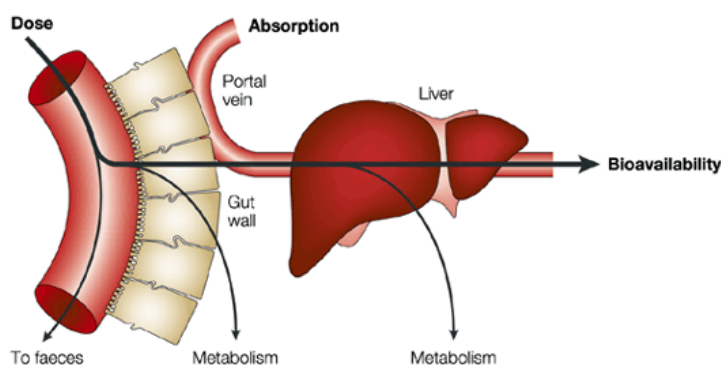
Figure 18: The passage of drug from digestive system to systemic circulation.[129]

In order to better understand oral absorption, compounds can be studied in a mouse short oral absorption model. This study takes blood samples in the hepatic portal vein and the systemic circulation after oral administration, which helps determine liver-

Christopher J Tame

related clearance mechanisms and the amount of drug present in the hepatic portal vein before it is exposed to first-pass clearance mechanisms.[126]
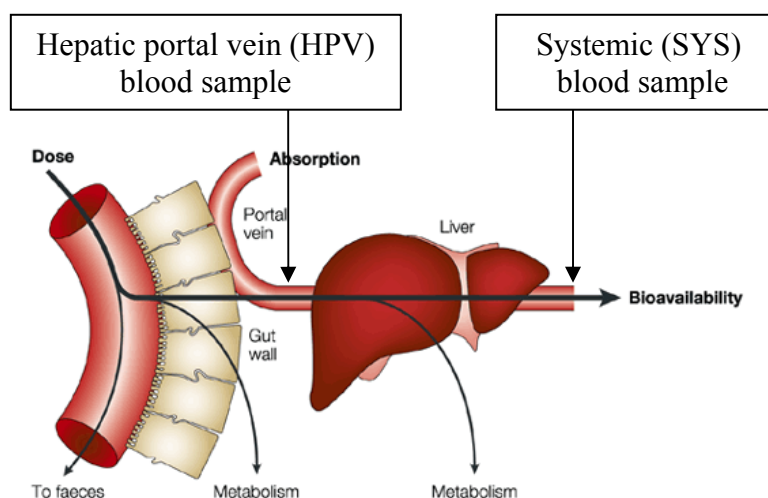
Figure 19: A diagram representing the short oral absorption pharmacokinetic model.[126]

To understand the cause of low oral bioavailability, two αvβ6-selective antagonists with a piperidine core were tested in a mouse short oral absorption (SOA) model with a 3.0 mg/kg p.o. dose (**Table 10**). The results also show low oral absorption determined by the total amount of drug detected in the hepatic portal vein (HPV) during the study, which is expressed as area under curve (AUC). This is especially apparent when comparing the data to pyridine **12**, which has a systemic AUC of 3770 ng/h/mL after a 1 mg/kg oral dose in rats, which could scale to 11310 ng/h/mL in order to match the 3 mg/kg dose.[126]

The results also show moderate hepatic clearance, which is calculated by dividing the systemic AUC by the hepatic AUC and multiplying this factor by mouse liver blood flow (90 mL/min/kg). These results suggest that the main contributing factor towards the observed low oral bioavailability of piperidine **13** and **14** is poor oral absorption.

Christopher J Tame

13   **14**
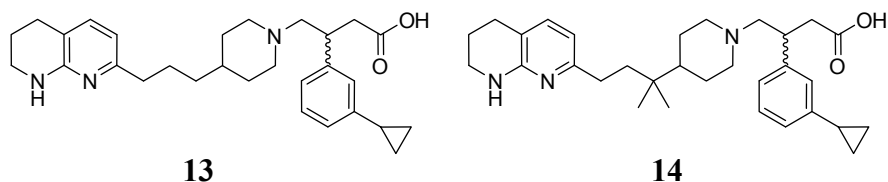
Compound no.	Hepatic Clearance (mL/min/Kg) [% mouse liver blood flow]	HPV AUC, (ng/h/mL)
13	51 [57%]	382
14	36 [40%]	234

Table 10: Results from a mouse short oral absorption (SOA) model with piperidine-containing compounds **13** and **14**. Both compounds were administered with doses of 3 mg/kg.[126]

1.12   Physicochemical property guidelines for an orally-administered medicine

In order to improve the oral absorption, it is first necessary to understand the factors that influence it and how these can be modified on a chemical level.   The requirement for an oral drug to be absorbed from the digestive system into the blood circulation distinguishes this mode of administration from other delivery methods. The degree of oral absorption is dependent on the aqueous solubility and permeability of the drug.[130]   The solubility determines how much of the formulated dose can be dissolved in the intestinal fluids (which is around 500 mL), whilst the permeability controls the rate and extent of absorption through the gut wall.[131]   Both of these factors control a third parameter, the dose, which cannot exceed an amount which saturates the intestinal fluids.[131] It follows, therefore, that all three factors are inter-related. For example, if the solubility and permeability are low then the dose would also need to be very low in order to achieve complete oral absorption. This would require a drug molecule to be very potent to achieve efficacy.

A study by Amidon and co-workers attempted to predict the *in vivo* bioavailability of orally administered drugs with *in vitro* solubility and permeability parameters.[130]   A biopharmaceutical classification system using this data was accordingly generated, which has been widely used for the optimisation of oral dose formulation.

Christopher J Tame

A more recent study by other members of our laboratories revised these parameters and identified a more reliable developability classification system (DCS),[131] which helps identify the dose and particle size required to achieve sufficient *in vivo* absorption in humans. In this case, fewer liabilities are encountered for drugs with high permeability and solubility. It follows that drug discovery programmes seeking to develop medicines with oral bioavailability should strive to identify drug candidates with good permeability and aqueous solubility.

In order to utilise DCS for oral bioavailability predictions, data on human jejunal permeability, fasted state simulated intestinal fluid (FaSSIF) solubility, and predicted dose are required. These factors require expensive and low throughput experiments and are normally only available for advanced compounds with extensive potency and selectivity data. Such requirements render this method unsuitable for early stage drug discovery. Consequently, other methods of predicting oral absorption were required.

High throughput *in vitro* assays for permeability and solubility are regularly used in our laboratories to help predict the human jejunal permeability and FaSSIF solubility, respectively. The Madine Derby Canine Kidney (MDCK) permeability assay has a sigmoidal relationship with human jejunal permeability.[132] Compounds with an MDCK value above 100 nm/sec are more likely to achieve 80% human jejunal permeability, although this only accounts for passive permeability by diffusion and may discount other active uptake and efflux mechanisms.[132]

As previously discussed, the aqueous solubility required for good oral absorption is dependent both on permeability and particle size, although a minimum value operated by chemists at Pfizer is 50 μg/mL if permeability is high.[133] The *in vitro* solubility assay run in our laboratories utilises a stock DMSO solution of the compound in question, which is subjected to chemi-luminescent nitrogen detection (CLND) to confirm the concentration. This solution is then added a microlitre at a time to an aqueous solution buffered to pH 7 until precipitation is observed, which identifies the maximum aqueous solubility of the compound.

Christopher J Tame

The limitations of the MDCK permeability and CLND solubility assays are that they are not accurate representations of the true biological environment present in the human intestine, and cannot, therefore, accurately predict human oral absorption for all compounds. In addition, these methods still require molecules to be synthesised and are not suitable for medicinal chemistry drug design. A relationship between oral absorption and the physical properties of a molecule, however, would allow medicinal chemists to design and optimise molecules which have an increased likelihood of oral absorption in humans.

In 1997, Lipinski and co-workers at Pfizer Central Research identified the correlation of physicochemical properties with permeability and solubility.[133] In this seminal work he identified that the molecular weight, lipophilicity and hydrogen bond donor/acceptor capability of a molecule determined its likelihood to achieve oral efficacy. His findings were summarised as the 'rule of five', which represented the first attempt of limiting drug design to within specific physicochemical parameters (**Table 11**). It was shown that approximately 90% of orally efficacious molecules do not violate more than one of the four rules.

Physicochemical property	Value
Molecular Weight (Da)	<500
Lipophilicity (cLogP)	<5
Number of H-bond donors	<5
Number of H-bond acceptors	<10

Table 11: Lipinski's rule of five.[133]

The key to the success of the 'rule of 5' was that the physicochemical properties of molecules required could be readily measured or calculated *a priori* using routine analytical methods. Subsequent studies followed, and as evidence supporting the use of physicochemical properties as descriptors of oral absorption increased, so did the development of increasingly sophisticated electronic models to accurately calculate

Christopher J Tame

these parameters. A review of some of the key studies which contributed towards the use of physicochemical parameters in drug discovery today is presented below.

In 2003 AstraZeneca published findings of a study comparing the physicochemical properties of marketed compounds with those throughout the various stages of development.[134]   The findings correlated well with Lipinski's original results, showing the mean molecular weight and lipophilicity of compounds to gradually decrease as they progressed through the development pipeline towards market. This indicated that compounds of generally lower molecular weight and lipophilicity had a greater probability of clinical success.

In 2002 at GlaxoSmithKline, Veber, *et. al.* showed that the oral bioavailability of compounds in rats decreased proportionally to increased rotatable bond count, with the upper limit being set at 7-10.[135] This was augmented by Gleeson, *et. al.* in 2008, who showed that ideal ADMET values reduced with increasing size and lipophilicity, based on ionisation state.[136]

In a related fashion, Pfizer published an insight into toxicity relationships with physicochemical properties, which showed that their clinical candidates were 2.5 times more likely to exhibit toxicity if they possessed a topological polar surface area (TPSA) under 75 and a cLogP over 3.[137] More recently, Ritchie and Macdonald showed that low topological polar surface area (TPSA) and high aromatic ring count increased the chances of developing negative developability parameters such as poor solubility and permeability.[138]

1.13:   Lipophilicity: Measurements and calculations

The majority of early work that studied the relationship between physiochemical properties and oral absorption used LogP as a measure of lipophilicity. LogP is the partition coefficient of a compound between octanol and water.[139]   The standard experimental procedure for calculating LogP is the so-called 'shake flask' experiment.   This involves shaking the compound in octanol and water, then

Christopher J Tame

analysing the fractions using quantitative LCMS analysis.[139] The more rapid, and therefore widely-used method of generating LogP values, utilises chromatographic methods. The injected compound is submitted to a reverse-phase eluent graduated between water and octanol. The retention time of the compound is a measure of its lipophilicity, and is used to generate a LogP value, known more specifically as Chrom LogP.[140]

A calculated LogP value is readily obtained by matching a test compound with a range of related fragments with measured LogP values. The additive sum of the LogP values for these fragments give the overall cLogP value.[141] There are now a range of commercially available programs which will rapidly compute cLogP values, such as Daylight and Advanced Chemistry Development (ACD/LogP DB).[139] These programs are based on statistical analysis of thousands of molecular fragments and their associated Log P values.[139]

A much earlier study, carried out by Scherrer and Howard in 1977, observed that LogP values are not an accurate physiological representation of the lipophilicity of compounds with ionisable groups.[142] The degree of ionisation is dependent on the pH of the solution to which it is dissolved in. They reasoned that a more accurate representation would, therefore, involve undertaking the partition experiment in a solvent buffered to physiological pH (pH 7.4). They termed this the distribution coefficient, expressed as LogD.

At the time of Lipinski's initial publication, the standard method of determining lipophilicity was cLogP, due to the availability of a number of methods for the expedient calculation of LogP values. In 2007, Bhal and co-workers utilised recent chromatographic methods of rapidly generating LogD values to revisit Lipinski's original data set.[143] They calculated LogD values for marketed drugs at pH 5.5, in an attempt to represent the pH of the small intestine, where the majority of drug absorption occurs. This revealed a better correlation between marketed compounds and a $LogD_{5.5} \leq 5$, than with a $LogP \leq 5$. [144]

Christopher J Tame

The lipophilicity of a compound has been shown to influence a range of factors that determine ADMET parameters. This includes: the volume of distribution,[145] protein binding,[146] and hERG activity – a cardiac ion channel associated with toxicity.[147] All of these factors are dependent on the behaviour of the compound in the blood. For this reason, LogD values are typically measured and calculated at the pH of the blood, known as physiological pH (7.4).

The generation of lipophilicity values in our laboratories use a chromatographic hydrophobicity index (CHI).[148] This reverse phase HPLC method utilises a water-acetonitrile gradient, which was developed to overcome the poor solubility observed with many compounds in octanol. The retention time is used in combination with the hydrogen bond donor count (HBC) to calculate the relative lipophilicity value in octanol (LogP) using **Equation 1** in **Figure 20**, below.[149] Undertaking the experiment at a specific pH will afford the relative LogD value using equation **2**.[150] Routine experiments are run at three pH levels in our laboratories; 2.0, 7.4 and 10.5.

$$LogP = 0.05CHI + 0.41HBC - 1.41 \qquad \textbf{(Equation 1)}$$

$$LogD_{pH} = CHI_{pH} -1.46 \qquad \textbf{(Equation 2)}$$

Figure 20: The equations used for calculating LogP and LogD values from CHI chromatographic retention times.[149]

Based on data generated elsewhere in our laboratories, it was observed that CHI LogD lipophilicity does not correlate well to LogD measurements generated from shake-flask experiments. A mathematical expression was subsequently derived to convert CHI LogD values into Chrom LogD values, which more closely correlate to shake-flask LogD results (**Equation 1**, **Figure 19**).[151]

$$Chrom\ LogD_{pH} = 0.08CHI_{pH} - 2 \qquad \textbf{(Equation 1)}$$

Figure 21: The equation used for calculating Chrom LogD values, which more accurately represent LogD values derived from shake-flask experiments.[151]

Christopher J Tame

When collated together, these findings show that larger, poorly soluble, low polarity and highly lipophilic molecules are less likely to make orally-efficacious drugs. The current trend in the literature is to formulate rules based on the findings; however, the precise boundaries proposed are often disputable, making this approach less useful.

As a result of this research, the *in vitro* permeability, solubility and physicochemical properties were, next investigated for compound **13** and **14**, to help identify possible causes of poor oral absorption (**Table 12**). Compound **12** was also included in this analysis to provide a representative comparison for good oral bioavailability. With the exception of calculated pKa values, the analysis shows no clear relationship between oral absorption and physicochemical properties, permeability or solubility.

Unfortunately, the absence of measured pKa values for compounds **12** and **13** resulted in the use of pKa measurements for closely related analogues. In the case of compound **12**, the representative compound had replaced the cyclopropyl group with a chlorine atom. Alternatively, the pKa value used to represent compound **13** was taken from an analogue which reduced the length of the propyl chain linking the piperidine and tetrahydronaphthyridine by one methylene unit, resulting in an ethyl chain. The use of representative pKa values for **12** and **13** meant that the data could only be used as a rough estimate to predict the actual pKa values. However, the identical pKa measurements obtained for compounds **14** and **13**, and their similarity to the calculated values, provided confidence that the representative pKa values used for compound **12** and **13** were good predictors in the absence of true pKa measurements.

Christopher J Tame
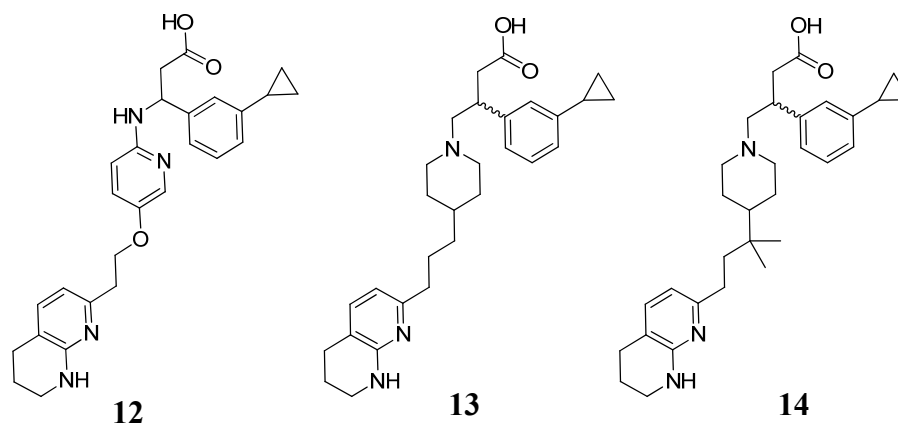
Compound no.	12	13	14
Mouse AUC (ng/h/mL)	3770 (SYS)	382 (HPV)	234 (HPV)
p.o. dose (mg/kg)	1.0	3.0	3.0
MW	459	461	489
Chrom LogD pH 2.0, 7.4, 10.5	0.6, 2.7, 2.5	0.2, 3.7, 3.9	0.5, 4.4, 4.6
Aromatic ring count	3	2	2
Rotatable bond count	9	9	9
Calculated pKa (Chemaxon)	7.2, 5.9, 4.0	9.9, 7.5, 4.0	9.7, 8.9, 3.9
Measured pKa (Potentiometric)	7.6, 5.5, NT[†]	9.7, 8.1, 3.9[†]	9.7, 8.1, 3.9
MDCK Permeability (nm/sec)	68	43	106
CLND Solubility (µg/mL)	153	218	208

Table 12: The comparison of *in vitro* permeability, *in vitro* solubility, and physicochemical properties of compounds **12**, **13** and **14**.[152] [†]pKa values were obtained on closely related analogues of **12** and **13**.

Focusing on absorption, the surface of cells is composed of a phospholipid bilayer, which creates a lipophilic barrier which molecules must pass through in order to passively enter the cell.[153] The hydrophobic nature of the bilayer renders it intolerable to water or charged species. It follows, therefore, that molecules must be desolvated and uncharged in order to passively permeate a cell membrane. Charged species, however, can still be transported into the cell *via* specific proteins or ion channels (**Figure 22**).[154]

Christopher J Tame
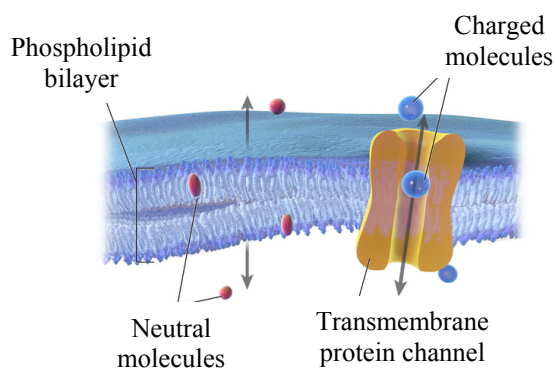
Figure 22: The methods of cellular permeability for neutral and charged molecules.[154]

The zwitterionic nature of these molecules indicates the predominance of a charged form across a range of pHs, suggesting that their absorption is likely to be driven by active transporters. As stated above, these are transmembrane proteins that can facilitate the transport of molecules across a biological membrane. Considering this, it is reasonable to suggest that the presence of an extra basic centre may reduce the recognition of the compound in the active transporter, thus reducing oral absorption.

It is difficult to reliably identify the reasons behind the poor oral absorption of compounds with a piperidine core, which is largely due to the lack of precedence of zwitterionic drug molecules with an extra basic centre. The data clearly suggested, however, that incorporation of a basic nitrogen in the core of the molecule reduced oral bioavailability and improved selectivity for αvβ6 (cf. **12** and **13**).

1.14   Research aims

Considering that the basic amine of piperidine **13** may be responsible for both poor bioavailability and good selectivity, it is reasonable to suggest that reducing the pKa to a value between that of pyridine **12** and piperidine **13** could achieve a balance of suitable oral bioavailability and RGD-integrin selectivity.

Christopher J Tame

To investigate this hypothesis, research in our laboratories has focused on reducing the pKa of the core nitrogen using three methods: addition of fluorine; addition of oxygen; and addition of a fused aromatic ring.

Research is ongoing elsewhere in our laboratories concerning the addition of fluorine and oxygen, which are expected to reduce the pKa through inductive effects.[155] It has been shown by measured pKa values that the conjugate acids of benzylic amines are more acidic than alkylamines. For example, the pKa of benzylamine (10.2) is lower than *n*-butylamine (11.1) when measured in DMSO.[156] This could be explained by a reduction in stability of the quaternary ammonium species resulting from depleted hyperconjugation from the benzylic methylene unit. This decrease in hyperconjugation could be a result of the slightly electron-withdrawing nature of the aromatic ring.

In addition to the reduction of pKa, the incorporation of a fused aromatic ring also reduces the number of rotatable bonds, which has been shown to improve oral bioavailability.[135]

The aim of this research is to develop an orally bioavailable, αvβ6-selective antagonist for the treatment of idiopathic pulmonary fibrosis (IPF). This will be attempted by reducing of pKa of the RGD integrin-selective αvβ6 antagonist **13** by fusing an aromatic ring to the central core of the molecule (**Figure 23**).

15
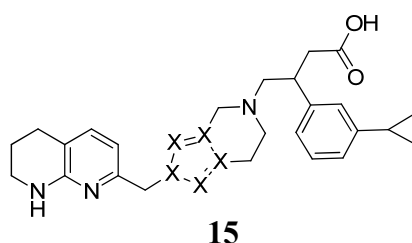
Figure 23: An aromatic ring fused onto the piperidine-containing αvβ6-selective antagonist **13**.

1.15   Compound analysis

As stated above, this work focussed on the identification of an oral αvβ6 antagonist which is considered suitable for extensive safety assessment in preparation for testing in human studies. In order to achieve this, a compound must be able to satisfy the following key criteria:

- Demonstration of significant reduction of fibrotic biomarkers after dosing in a diseased animal model,

- Calculated daily dose < 100 mg.

- > 10 fold selectivity against αvβ3 in cell adhesion assay,

- > 100 fold selectivity against other biological targets tested in a range of non-RGD integrin assays available in our laboratories.

- Inactive (<4.5) in hERG assays

- Drug classification system class 1 (DCS class 1).

In an attempt to reduce the number of animals used in the drug discovery process, *in vitro* assays, such as microsomal IVC, will be used to help select optimal compounds for testing in animal models.

As discussed previously, cell adhesion affinity assays are generated by culturing cells with artificially expressed levels of integrins.[124] As the levels of integrin expression are artificial, the results cannot be used as a method of determining physiologically relevant potency and selectivity. Instead, the data can be used to help rank different compounds on their *relative* potency and selectivity profiles.

An *in vitro* assay has been developed in our laboratory which provides a more pharmacologically-relevant measure of αvβ6 potency in a fibrotic environment by using normal human bronchial epithelial (NHBE) cells.[157] This assay works by applying NHBE cells to wells coated with collagen. In a physiological environment, the NHBE cells will bind to collagen through αvβ6, which will initiate the release of a range of cell signalling mediators. The supernatant media is removed after 24

Christopher J Tame

hours and replaced with a solution containing the antagonist of interest or a solvent control. The wells are left for 48 hours, then the supernatant is analysed for levels of PAI-1, a cytokine which has shown to be expressed as a result of αvβ6 activation.[158] Comparing the levels of PAI-1 versus the solvent control provides a potency measurement. This is undertaken at a range of concentrations to achieve a pIC50 measurement.

Unfortunately, the NHBE assay is very low throughput and is not routinely run. Therefore, testing in this assay is reserved for compounds selected for *in vivo* pharmacodynamic (PD) studies. Activity in this assay is indicative of a functional inhibition of αvβ6 and will be required for progression to an *in vivo* PD study.

Previously, molecules from other chemical series developed in our laboratories only gave measurable potency in the NHBE assay when the αvβ6 cell adhesion potency was greater than a pIC50 of 7.[127] Accordingly, only compounds which exceed an αvβ6 cell adhesion pIC50 of 7 will be progressed for further study.

The highly charged nature of integrin antagonists suggests that oral absorption may be controlled by transmembrane proteins, which makes prediction of human jejunal absorption difficult. A sigmoidal relationship has been shown between MDCK permeability and human jejunal permeability (the top of the small intestine) with compounds possessing MDCK values between one and 50 nm/sec, which represents high variability in the assay (**Figure 24**).[159] Therefore, whilst compounds with MDCK values of over 50 nm/sec are desired, compounds with lower values will not be discounted based on permeability alone.

Christopher J Tame
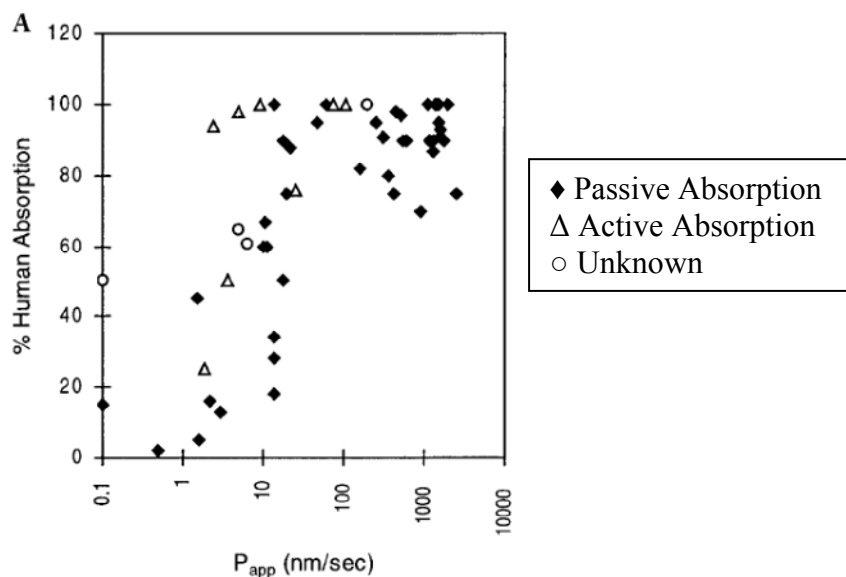
Figure 24: Relationship between MDCK permeability and human absorption (%).[159]

The zwitterionic nature of αvβ6 antagonists also results in high aqueous solubility, with the majority of compounds synthesised in our laboratories possessing solubility higher than Pfizer's minimum requirement of 50 μg/mL for highly permeable compounds.[127,133,152] Therefore, it is expected that oral absorption will not be limited by solubility provided the dose is not high.[152]

Before progressing suitable compounds to an animal diseased model, pharmacokinetic (PK) studies are conducted in a relevant animal species to determine the exposure of the drug in the body over time. Compounds will be prioritised for study based on their *in vitro* clearance in mouse, rat and human liver microsomes, which will help predict their relative *in vivo* clearance. Selected compounds will be screened initially in a short oral absorption model to determine oral absorption. Promising compounds will have an HPV AUC higher than 1000 ng/h/mL and hepatic clearance less than 50% liver blood flow (LBF) after a 3 mg/Kg dose to give the best chance of delivering improved oral absorption when compared to piperidine **13**.

Christopher J Tame

Suitable compounds will then be studied in a mouse PK study with intravenous (i.v.) and oral (p.o.) arms. Compounds with a bioavailability > 30% and clearance < 60% liver blood flow (LBF) are considered to have sufficient exposure to deliver a therapeutic response in a diseased animal model. This has been supported with previous compounds tested in our laboratories.[126]

In summary, the compounds tested will follow a defined screening cascade, which is designed to optimise the use of *in vitro* assays to select compounds for further studies in an *in vivo* environment (**Figure 25**).
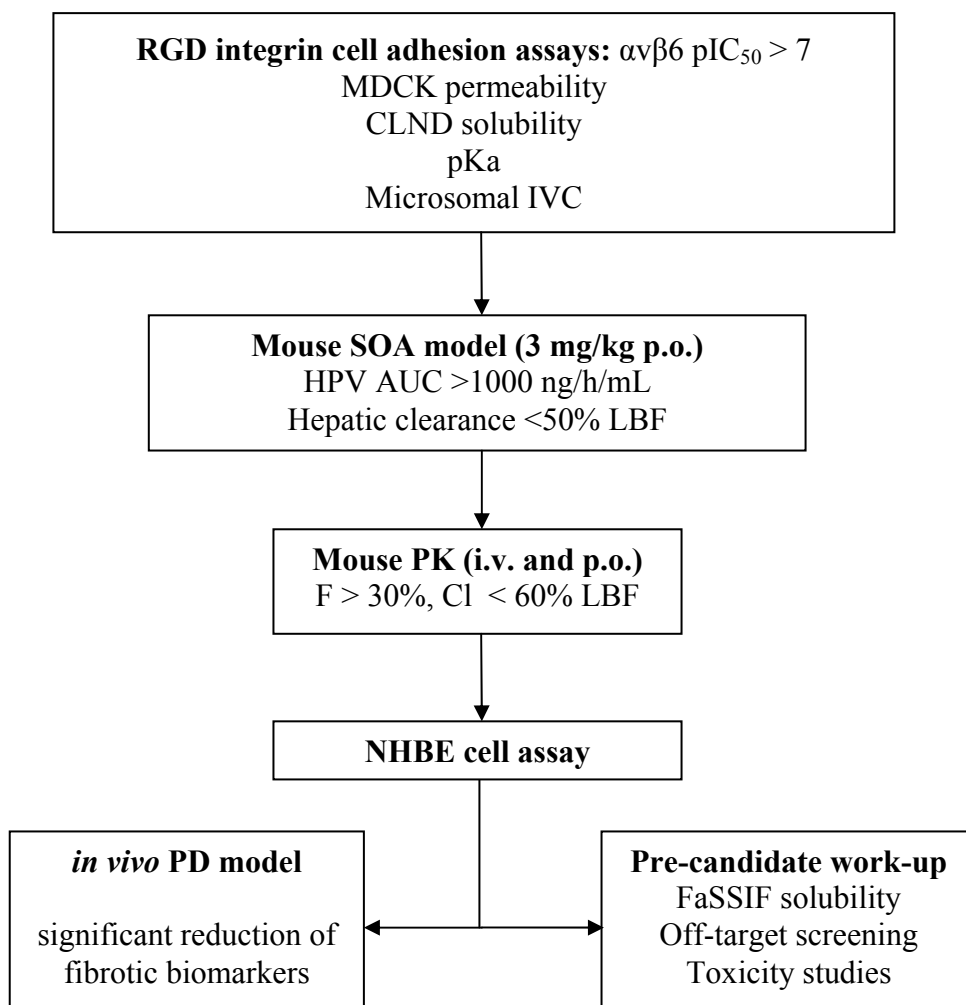
Figure 25: A progression cascade for the identification of an RGD integrin-selective αvβ6 inhibitor with oral bioavailability and *in vivo* efficacy, for the treatment of IPF.

Christopher J Tame

1.16   αvβ6 antagonists containing a pyrazolopiperidine core

Previous work in our laboratories identified the RGD integrin antagonist **16**, which contains a pyrazolopiperidine bicyclic system in the core of the molecule.[160]   The pKa values of the two basic centres have been reduced when compared to an analogue of piperidine **13** (**Table 13**), suggesting that it could have improved oral absorption. However, the reduction in pKa was also hypothesised to be responsible for the loss of αvβ6-selectivity. Previous work with another series of integrin antagonists developed in our laboratories demonstrated that replacing the chlorine with a cyclopropyl substituent gave a measurable increase in selectivity (**Table 9**).[124,160] Accordingly. this strategy was selected for the optimisation of pyrazolopiperidine **16**.

16
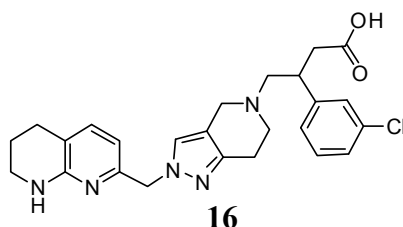
	Cell adhesion pIC$_{50}$				Calculated pKa	Potentiometric pKa
	αvβ6	αvβ3	αvβ5	αvβ8		
16	6.5	6.5	6.2	6.2	8.0, 6.6, 3.8	7.7, 6.2, 4.1
12*	6.9	8.0	8.2	7.1	7.2, 5.9, 4.0	7.6, 5.5, NT[†]
13*	7.6	6.8	6.9	7.5	9.9, 7.5, 4.3	9.7, 8.1, 3.9[†]

Table 13: The cell adhesion affinity and calculated pKa of compound **16**, compared with **12** and **13**.[124,160] * denotes single enantiomer. [†]pKa values of analogues as described in **Table 11.**

A mouse short oral absorption model was subsequently planned to investigate the effect of reduced pKa on oral absorption. Compound **17** was selected for synthesis, as it had the potential of providing both oral bioavailability and αvβ6 selectivity (**Figure 26)**.

Christopher J Tame
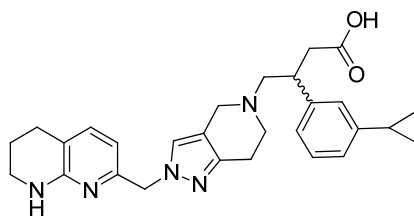
17

Figure 26: Target compound for investigation in the short oral absorption model.

The existing synthetic route used to access compound **16** is displayed in **Schemes 1** and **2**, which utilises commercially available starting materials.[127]   The yields are moderate to good, although a low yield was obtained during preparative HPLC separation of the two *N*-regioisomers. This poor recovery was considered to be due to the low solubility of the product in the reverse-phase eluents used.

Christopher J Tame
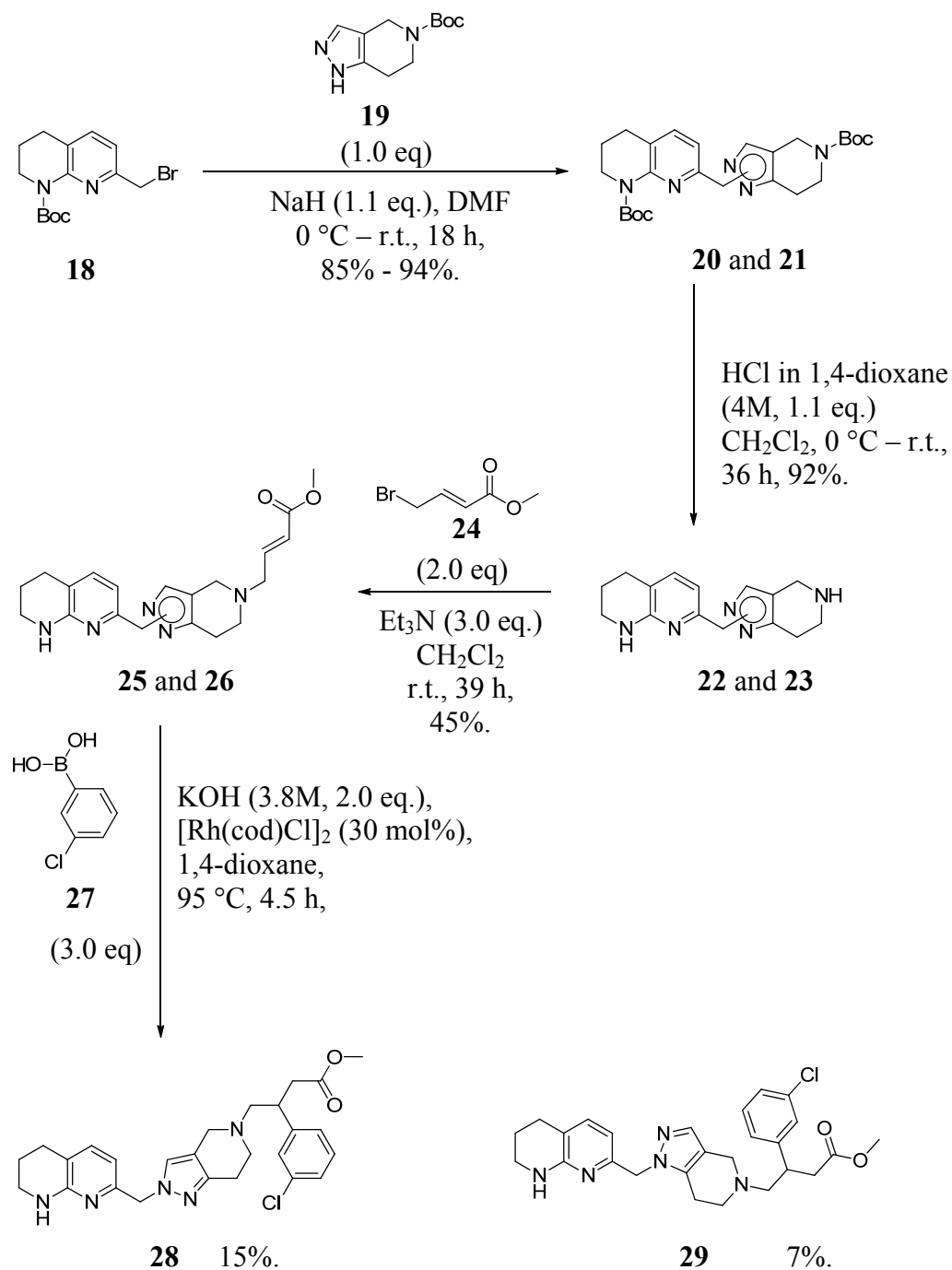
Scheme 1: The previous synthetic approach towards a pyrazolopiperidine-containing αvβ6 antagonist.[127]

Christopher J Tame
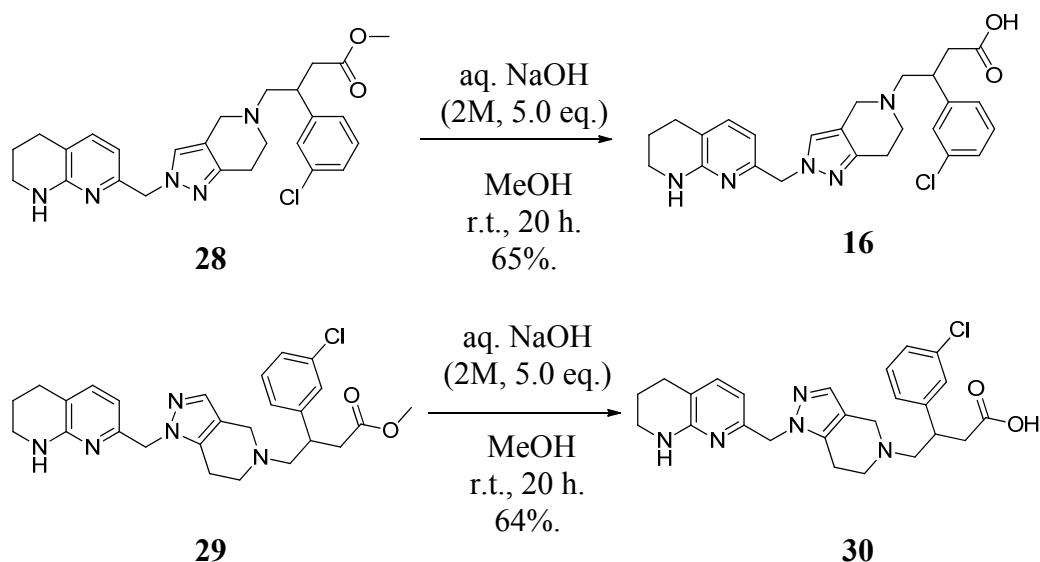
Scheme 2: Base-mediated ester hydrolysis to afford the final racemic products as single regioisomers.[127]

The key step in the synthetic route is the rhodium-catalysed 1,4-addition of 3-chlorophenylboronic acid **27** to α,β-unsaturated ester **24**. The synthetic route has been designed to enable the efficient introduction of a range of substituted phenyl rings from a late-stage intermediate (**25** and **26** as a mixture of regioisomers). Consequently, the structure activity relationships (SAR) identified in previous series can be expediently investigated on this new template, and is ideal for the synthesis of cyclopropyl analogue **17**. Given that metal-catalysed conjugate addition is a key step in accessing target compounds within this series of interest, it is pertinent to briefly review the associated literature.

1.17 Metal-catalysed conjugate additions of organometallic reagents to α,β-unsaturated substrates

The first metal-catalysed 1,4-conjugate addition of a carbon nucleophile to a carbon electrophile was demonstrated in 1941, when Kharasch and Tawney reacted methylmagnesium bromide and isophorone in the presence of copper (I) chloride (**Scheme 3**).[161]

Christopher J Tame
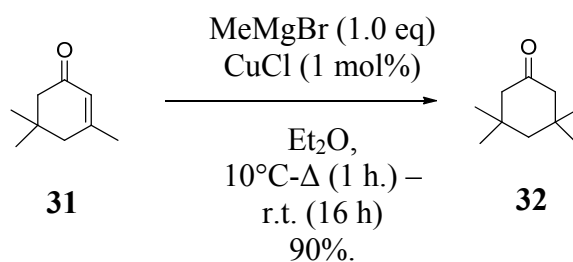
Scheme 3: The copper-catalysed 1,4-addition of methylmagensium bromide to isophorone.[161]

The use of copper salts in this manner has since been extensively investigated and developed, with asymmetric conditions being identified in recent years.[162,163] The drawback with this approach, however, is the instability of many of the organometallic reagents to air and water.

The identification of arylboronic acids as organometallic reagents with improved air and moisture stability has revolutionised carbon-carbon bond forming reactions. The use of arylboronic acids to effect palladium-catalysed sp^2-sp^2 carbon-carbon bond forming reactions under mild conditions was pioneered by Suzuki and Miyaura, for which Suzuki received the Nobel prize in 2011 (**Scheme 4**).[164]
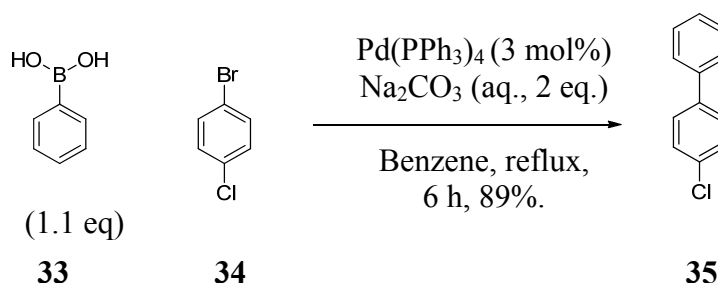
Scheme 4: The first application of phenylboronic acid to metal-catalysed biaryl cross-couplings.[164]

The first application of arylboronic acids in metal-catalysed 1,4-addition reactions was also developed by Miyaura and co-workers.[165] These reactions utilised catalytic amounts of rhodium and actually *required* the use of water (**Scheme 5**). Subsequent collaboration between the Miyaura and Hayashi laboratories in 1998 identified the

Christopher J Tame

first asymmetric conditions for 1,4-addition reactions using arylboronic acids (**Scheme 6**).[166]
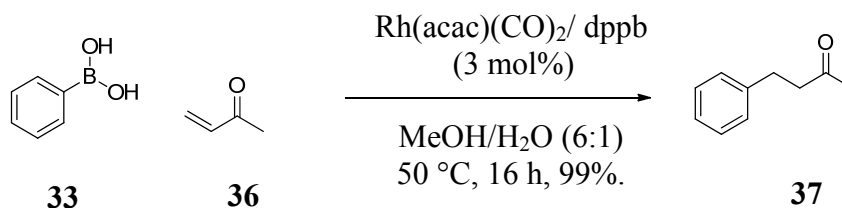
Scheme 5: Rhodium-catalysed 1,4-addition of phenylboronic acid to methyl vinyl ketone (MVK).[165]
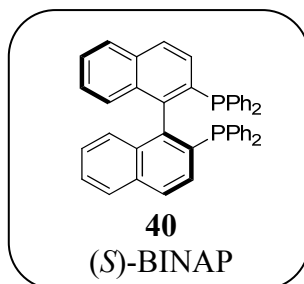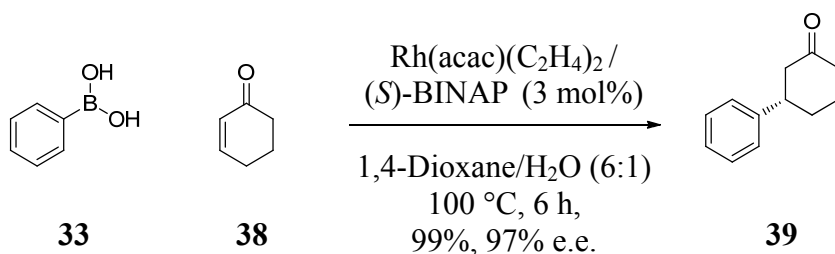
Scheme 6: The asymmetric 1,4-addition of *p*-tolylboronic acid to cyclohexenone.[166]

A variety of advancements in this area have since been demonstrated, including the use of palladium[167] and a range of α,β-unsaturated substrates, such as aldehydes[168] and carboxylic acids[169] which are displayed in **Schemes 7** and **8**, respectively. A comprehensive review of rhodium-catalysed conjugate addition of arylboronates can be obtained from recent articles by Frost[170] and Lin[171]

Christopher J Tame

43
(*R,R*)-Bn-bod*
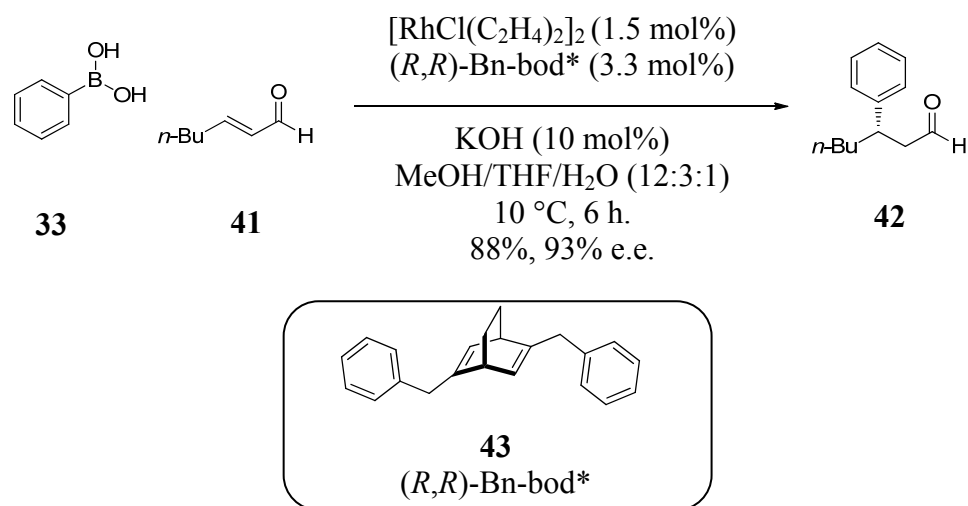
Scheme 7: Rhodium-catalysed 1,4-addition of phenylboronic acid **33** to α,β-unsaturated aldehyde **41**.[168]
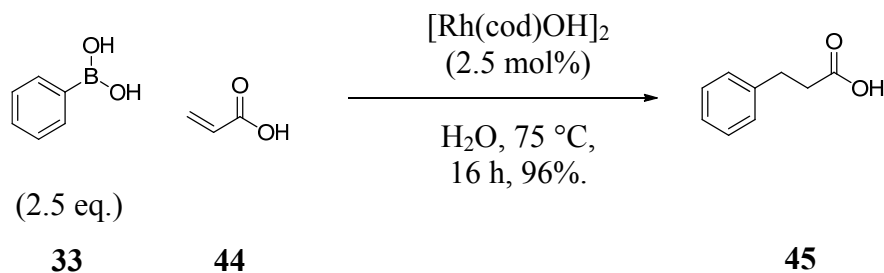
Scheme 8: Rhodium-catalysed 1,4-addition of phenylboronic acid **33** to α,β-unsaturated carboxylic acid **44**.[169]

A recent publication from our own laboratories demonstrated the 1,4-addition of arylboronic acids to α,β-unsaturated esters containing a basic γ-amino group (**Scheme 9**).[172] The addition of 20 mol% (*R*)-BINAP was also investigated, which gave products with good to excellent enantiomeric excesses. The yields were considerably lower when 3-(cyclopropylphenyl)boronic acid was employed, although subsequent work in our laboratories have shown that this can be improved by increasing the catalyst loading to 30 mol% (60 mol% Rh).

Christopher J Tame
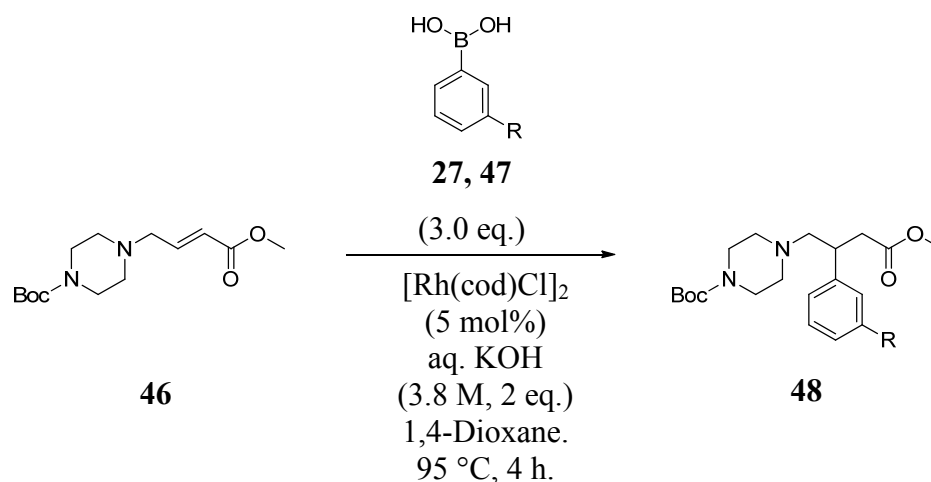
Scheme 9: Rhodium-catalysed addition of arylboronic acids to acyclic unsaturated esters containing a basic γ-amino group.[172]

The generally accepted mechanism for this transformation is presented in **Scheme 10**.[173] Proposed by Hayashi in 2002, the mechanism requires the formation of a hydroxyl-rhodium species (**49**), which undergoes transmetallation with the arylboronic acid (**33**) to form intermediate **50**. The next step involves co-ordination of the rhodium with an α,β-unsaturated system (**38**), which is in competition with hydrolysis of the organometallic species to form **54** (**Pathway II**). In order to minimise the effects of hydrolysis, excess arylboronic acid (**33**) is typically employed. Once co-ordinated to the alkene, the aryl group is inserted in a 1,4-addition fashion and rhodium forms an oxa-π-allyl species (**52**). The final step is hydrolysis of intermediate (**52**) to release the desired product (**53**) and regenerate the catalyst (**49**).
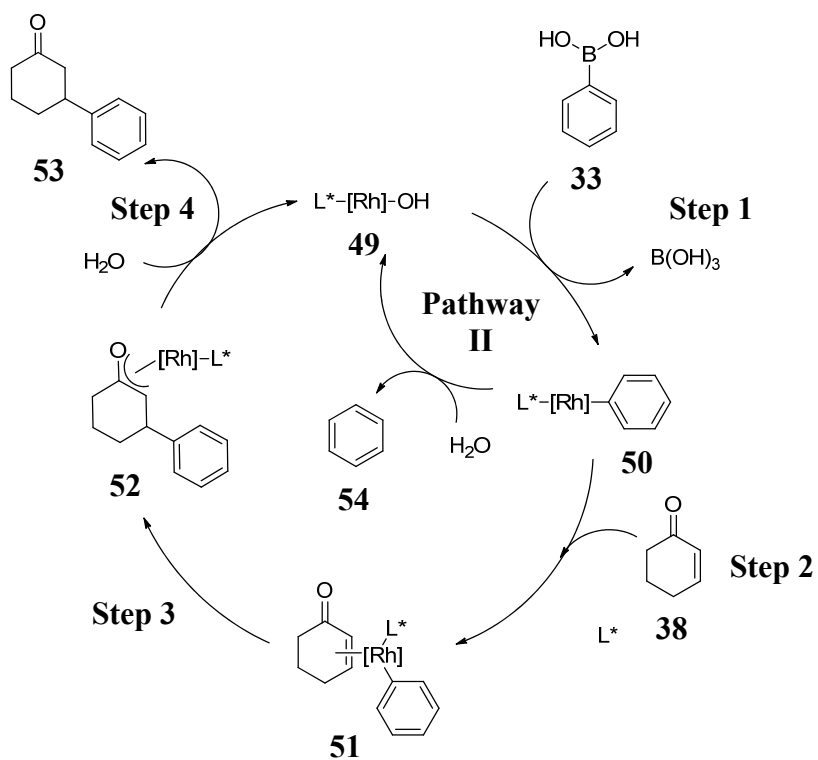
Christopher J Tame

Scheme 10: Proposed mechanism for rhodium-catalysed 1,4-addition of arylboronic acid to cyclic or acyclic α,β-unsaturated systems.[173]

2   Results and Discussion

2.1   Synthetic approach towards pyrazolopiperidine 17

The previously-disclosed synthesis of 3-chlorophenyl **16** provided an expedient route for accessing related compounds.   The unselective pyrazole alkylation gave a mixture of *N*-regioisomers, which required separation using preparative HPLC at a later stage. Optimisation efforts would, therefore, benefit from developing a selective alkylation protocol.   As a rapid synthesis of pyrazolopiperidine **17** was required, however, optimisation was not initially considered.   Future optimisation would be attempted if a large scale synthesis was required to support subsequent biological studies.

Accordingly, the existing synthetic route was used to access pyrazolopiperidine **17**, which was achieved in comparable yields to those obtained for the synthesis of chlorophenyl **16** (**Scheme 11**). Characterisation of the *N*-regioisomers was achieved using NOESY ^{1}H NMR, which were separated using preparative HPLC. Regular reaction monitoring allowed the reaction times to be reduced in many of the synthetic steps, and the use of environmentally-hazardous dichloromethane[174] was successfully replaced with MeOH for the acid-mediated Boc-deprotection step.

Christopher J Tame
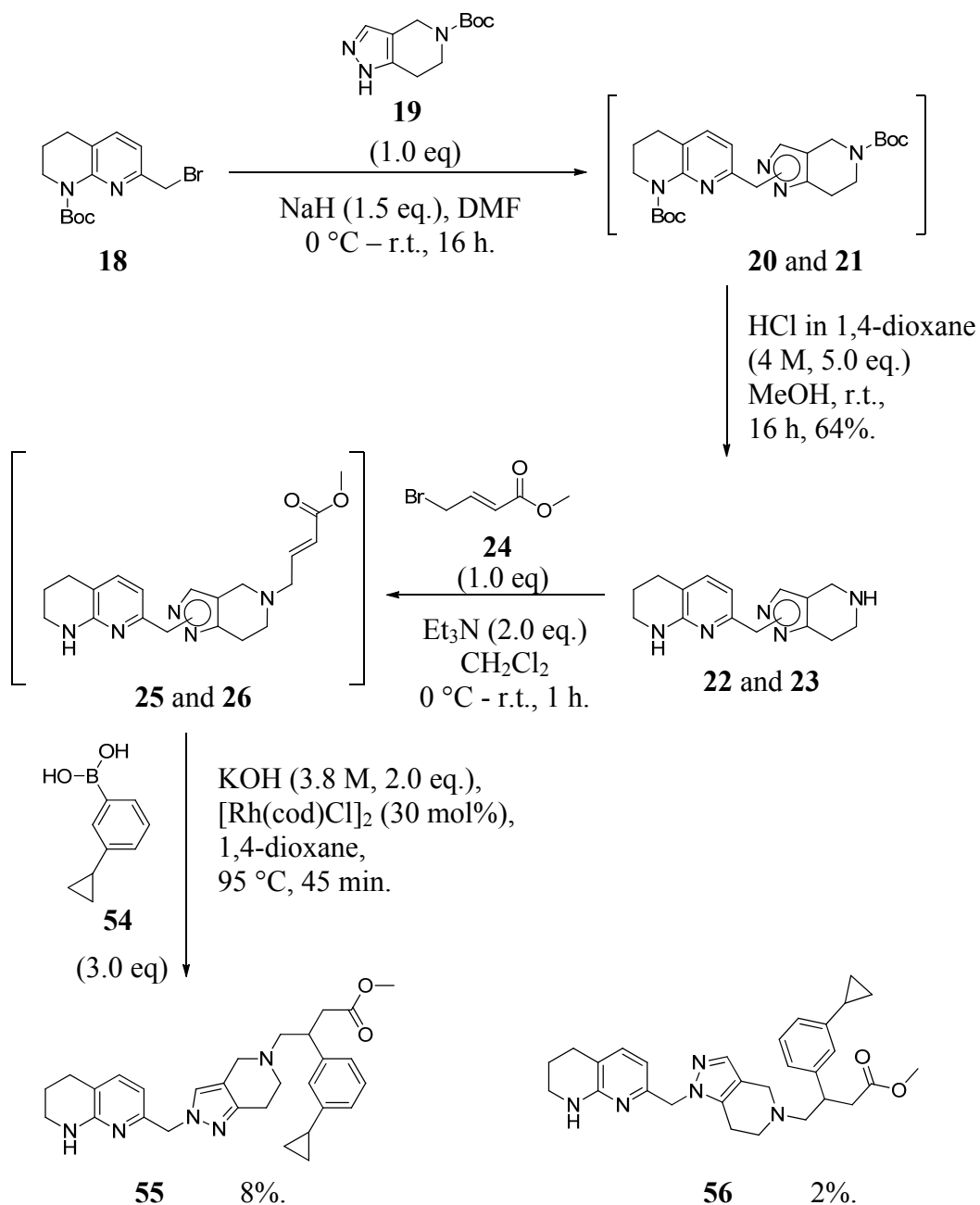
Scheme 11: The synthesis of compounds **55** and **56** from commercially available starting materials.

The racemic mixture of desired regioisomer **55** was resolved using chiral HPLC.[175] This was undertaken on the methyl ester due to perceived difficulties in the separation of the final zwitterionic compound, which had been observed in other related series. This afforded the single enantiomers **57a** and **57b** in >99% enantiomeric excess (**Scheme 12**).

Christopher J Tame
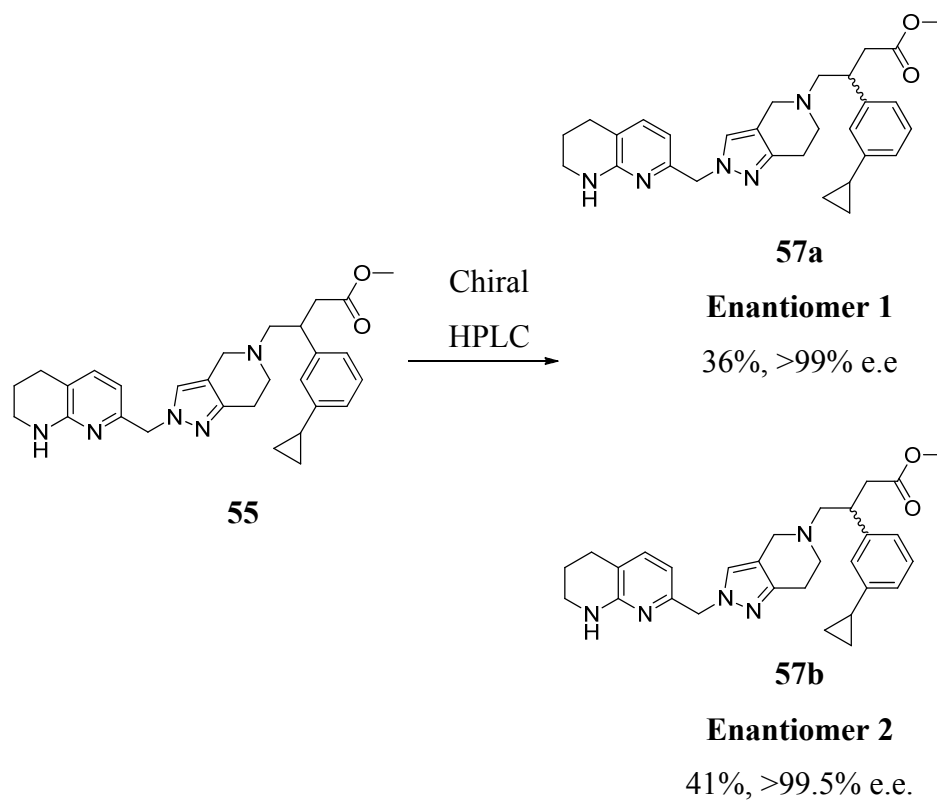
Scheme 12: Chiral HPLC to afford the isolated single enantiomers.[175]

Base-mediated ester hydrolysis was then undertaken on the methyl esters **56**, **57a** and **57b** to afford target compounds **58**, **17a** and **17b** in moderate yields (**Scheme 13**). The solvent was changed from MeOH to MeCN in an attempt to improve the solubility of the starting material.   Mass-directed purification (MDAP) was used to isolate the final products in sufficient quantities for further profiling, although this technique is likely to be the cause of the varying yields observed.
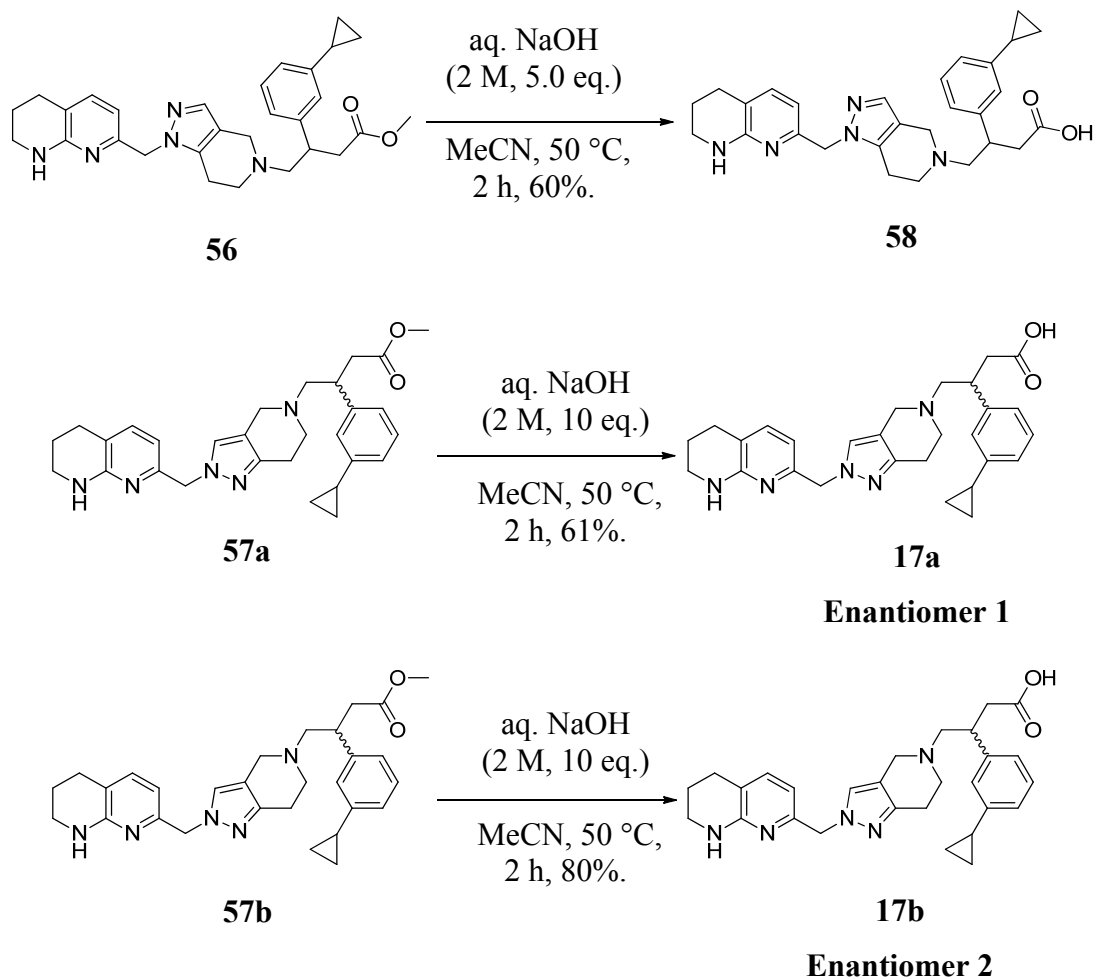
Scheme 13: Base-mediated ester hydrolysis afforded racemic **58** and single enantiomers **17a** and **17b**.

2.2 Biological data and evaluation of pyrazolopiperidine 17

Compounds **58**, **17a** and **17b** were screened in the cell adhesion assays for relevant RGD integrins and the results were compared with exemplars from the pyridine core (**12**), the piperidine core (**13**), and pyrazolopiperidine core (**16**), (**Table 14** and **Figure 27**). As anticipated, replacement of the 3-chloro substituted phenyl ring with a 3-cyclopropyl analogue improved the αvβ6 potency and RGD integrin selectivity, and the regioisomeric compound **58** exhibited lower potency.

Christopher J Tame

Compound	Cell adhesion pIC$_{50}$			
	αvβ6	αvβ3	αvβ5	αvβ8
12*	6.9	8.0	8.2	7.1
13*	7.6	6.8	6.9	7.5
16	6.5	6.5	6.2	6.2
17a*	5.8	5.2	5.6	5.9
17b*	7.3	6.5	6.4	6.4
58	6.0	5.8	5.3	5.0

Table 14: Cell adhesion pIC$_{50}$ values for a range of αvβ6 antagonists.[124] * denotes single enantiomer.
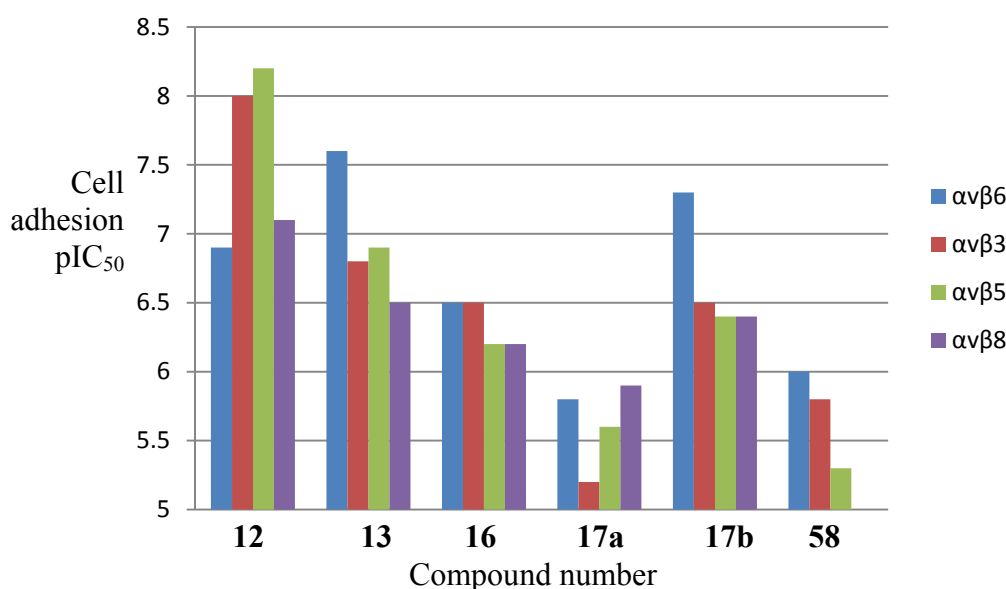
Figure 27: Cell adhesion pIC$_{50}$ values for a range of αvβ6 antagonists.[124]

The pKa values of the various ionisable centres of compound **17b** were subsequently measured and compared with the representative compounds from each series (**Table 15**). Interestingly, the pKa of the second basic centre has a difference of 0.7 log units between cyclopropylphenyl **17b** and chlorophenyl **16**. It is unclear how structural changes to substituents of the phenyl ring could invoke the observed differences in pKa. It is possible that this result could be due to experimental error, although additional tests were not undertaken to investigate this further.

Christopher J Tame

Compound number	Potentiometric pKa
12	7.6, 5.5, NT[†]
13	9.7, 8.1, 3.9[†]
16	7.7, 6.2, 4.1
17b	7.8, 5.5, 4.0

Table 15: Measured pKa values for a range of integrin antagonists.[152] [†]pKa values obtained on closely related analogues as described in **Table 12**.

In addition to improving selectivity, a reduction in the most basic pKa was expected to improve oral absorption. Compound **17b** satisfied this requirement, and was therefore profiled in the mouse short oral absorption model (**Table 16**). The results show a reduction in the hepatic clearance, although the oral absorption, measured as HPV AUC values, was not considerably improved.

Compound no.	Hepatic Clearance (mL/min/Kg) [% mouse liver blood flow]	HPV AUC (ng/h/mL)
13	51 [57%]	382
17b	23 [27%]	417

Table 16: The results of a mouse short oral absorption model after a 3 mg/kg dose of compound **13** and **17b**.[126]

The hepatic clearance displayed by compound **17b** is the lowest observed from any compound tested, which may be due to the reduced flexibility in the core of the molecule.[135] Compound **17b** possesses 7 rotatable bonds, 2 less than compounds previously profiled in this assay, such as piperidine **13**. Veber and co-workers have shown that oral bioavailability is improved when the number of rotatable bonds is limited to ≤7, supporting this hypothesis.[135]

The reduced basicity of compound **17b** unfortunately did not improve the oral absorption to the desired HPV AUC level of 1000 ng/h/mL as hypothesised. The improved hepatic clearance, however, warrants further optimisation of the oral

Christopher J Tame

absorption of αvβ6 antagonists with similar bicyclic cores. Subsequently, the physicochemical properties of compound **17b** were reviewed in an attempt to elucidate other possible causes of low oral absorption. These were compared with exemplar compounds **12** and **13**, and are displayed in **Table 17**.

Compound no.	12	13	17b
Species	Rat	Rat	Mouse
p.o. dose (mg/kg)	1.0	3.0	3.0
HPV AUC (ng/h/mL)	3770	382	417
MW	459	461	472
Chrom LogD pH 2.0, 7.4, 10.5	0.6, 2.7, 2.5	0.2, 3.7, 3.9	-0.3, 3.1, 2.0
Aromatic ring count	3	2	3
Rotatable bond count	9	9	7
pKa (potentiometric	7.6, 5.5, NT[†]	9.7, 8.1, 3.9[†]	7.8, 5.5, 4.0
Permeability (MDCK nm/sec)	68	43	23
Solubility (CLND μg/mL)	153	218	173

Table 17: The physicochemical properties of compounds **12**, **13** and **17b**.[152] [†]pKa values obtained on closely related analogues as described in **Table 12**.

The measured Chrom LogD data shows that pyrazole **17b** has a lower lipophilicity than piperidine **13**. Considering this, it is plausible that the reduction in pKa observed in pyrazole **17b** was insufficient to improve permeability due to the concomitant reduction in lipophilicity. It is possible, therefore, that increasing the lipophilicity of pyrazole **17b** to a similar level as piperidine **13** would more accurately test the hypothesis that a reduction in pKa may improve oral absorption.

2.3   Optimisation of lipophilicity for improved oral absorption

Accordingly, methods to tune the lipophilicity of **17b** were investigated further. Some of the structural modifications which could be made to compound **17b** to improve the lipophilicity are shown in **Figure 28**.

Christopher J Tame
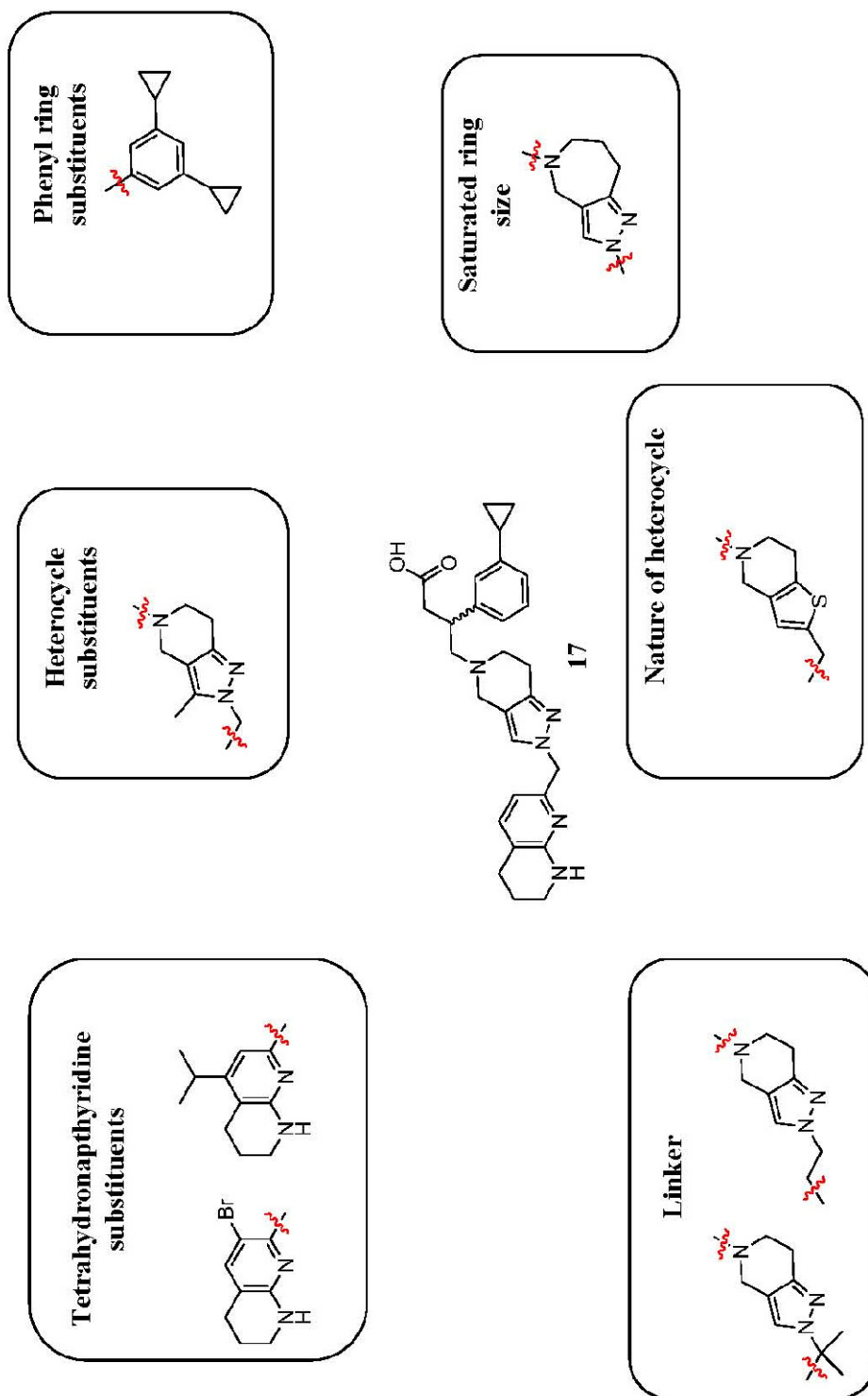
Figure 28: Potential modifications to pyrazolopiperidine **17b** for increased lipophilicity.

Christopher J Tame

Substitution at the phenyl ring had been investigated in the literature[116] as well as in our laboratories[127] and was likely to be tolerated in this series, whereas substitution on the tetrahydronaphthyridine, linker and core had less precedence. The modification of the heterocycle in the core of the molecule presented an atom-economic method of increasing the lipophilicity without making significant changes to the size and shape of the molecule, and was subsequently selected for further investigation.

Due to the wide range of heterocycles available for consideration, a thorough analysis was undertaken to ensure the most appropriate heterocycles were selected for synthesis. This did not include an analysis of 6-membered aromatic rings due to earlier molecular modelling work in our laboratories, which suggested poor activity at αvβ6.[176]

The possible bicyclic systems composed of a 5-membered heterocycle fused to a piperidine ring were identified and a methyl group was included at the appropriate place to represent the substitution pattern when incorporated into an αvβ6 antagonist molecule. The lipophilicity of these isolated cores was then calculated and compared to the core of compound **17b** (**67**, **Table 18**). A 0.5 log unit cut off was used to ensure that the compounds selected would significantly affect the lipophilicity. Accordingly, cores **70**, **71** and **74 - 77** were discounted from further investigation.

The calculated lipophilicity value used for this analysis was LogP, as this provides a value independent on ionisation state. This was considered important because the behaviour of a zwitterion with an extra basic centre may be poorly predicted by pKa models used in Chrom LogD calculations. Indeed, research elsewhere in our laboratories have concluded that pKa values are poorly predicted for basic amines,[152] which may be compounded in this case by potential for intramolecular interactions on these flexible molecules.

Christopher J Tame

Compound no.	Structure	cLogP	Increase lipophilicity?
59		3.9	Yes
60		3.9	Yes
61		4.6	Yes
62		4.9	Yes
63		5.7	Yes
64		5.7	Yes
65		5.0	Yes
66		5.0	Yes
67		**3.2**	-
68		3.2	No
69		3.5	No
70		2.9	No
71		3.3	No
72		4.4	Yes
73		4.4	Yes

Table 18: Calculated lipophilicities for a range of fused heterocycles (cores only). Continues overleaf.

Christopher J Tame

Compound no.	Structure	cLogP	Increase lipophilicity?
74		3.2	No
75		3.2	No
76		2.5	No
77		2.4	No

Table 18 (continued): Calculated lipophilicities for a range of fused heterocycles (cores only).

In an attempt to reduce attrition, our laboratories have compiled a database containing known toxicities of drug compounds and molecules in development.[177] This enables correlation of a given sub-structure with an undesirable off target effect, allowing further prioritisation of the systems proposed for synthesis. These results must be analysed carefully, however, as there could be other moieties on the molecule which are responsible for the toxicity. It follows that if a particular substructure is present in a number of toxic compounds then it could be contributing to that toxicity. Removing these toxic liabilities at the design stage of medicinal chemistry has the aim of reducing toxicity-based attrition later on in the development process.

In the same vein, identifying a particular structural motif in a marketed drug will provide confidence that it has successfully passed all stages of safety assessment, and is thus less likely to be toxic. Accordingly, substructures of the remaining cores were screened in the toxicity database and compared with the top 100 marketed drugs in 2011 (by US sales),[178] the results of which are displayed in **Table 19**.

Christopher J Tame

Structure	Toxicity flag? (Exemplar structure)	Marketed drug? (Exemplar structure)
59/60	Acute toxicity[179]	Negative search result
61	Acute toxicity[180] 78	Negative search result
62	Acute toxicity[181,182] 79	Negative search result
63 64	Cytotoxicity[183] 80	Zyprexa (Olanazpine) 81 Also: Plavix and Spiriva (inhaled)
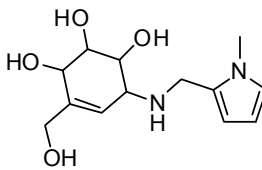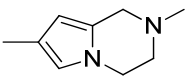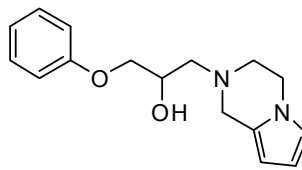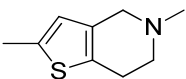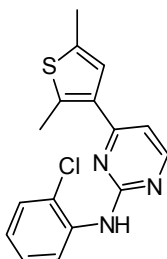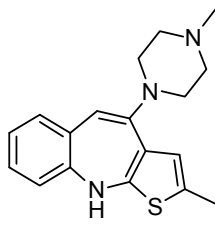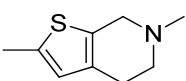
Table 19: The presence of relevant substructures in the top 100 marketed drugs, or with known toxicity. Continues overleaf.

Christopher J Tame
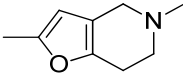
Structure	Toxicity flag? (Exemplar structure)	Marketed drug? (Exemplar structure)
65 **66**	Acute toxicity, Cytotoxicity.[184] **82**	Veramyst (inhaled) **83**
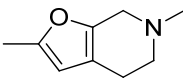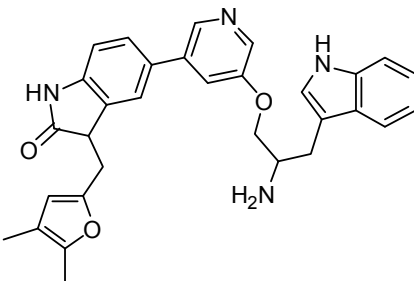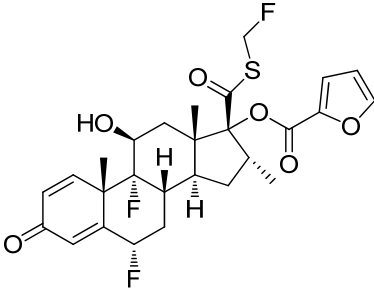
Table 19, continued: The presence of relevant substructures in the top 100 marketed drugs, or with known toxicity.

Based on the analysis presented above, cores **59-62** were not investigated further. Some furan-containing compounds also demonstrated some associated toxicity, such as **82**, although the presence of a marketed drug containing a furan restored confidence in the safety profile of this moiety. Consequently, the remaining compounds were considered for synthesis and are presented along with their calculated physicochemical properties in **Table 20**.

The most lipophilic compounds were calculated to be the thiophene-containing compounds **84** and **85**. These were subsequently prioritised for synthesis because they presented the best chance of balancing low pKa and a greater degree of lipophilicity, which was expected to result in improved oral absorption.

Christopher J Tame
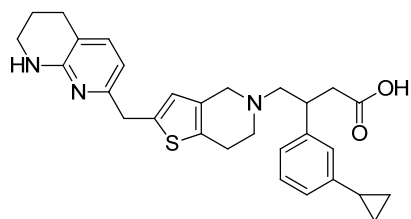
84
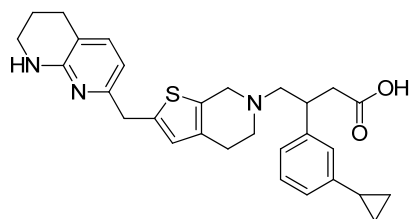
85
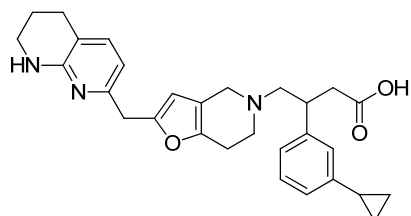
86
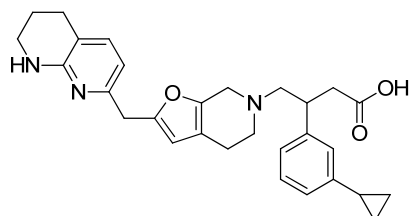
87
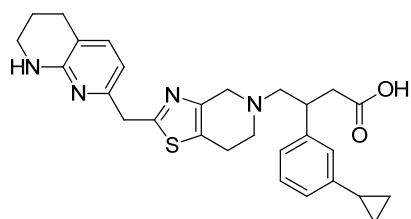
88
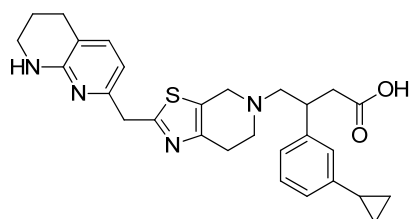
89

Compound no.	MW	cLogP	No. of aromatic rings	No. of rotatable bonds	Calculated pKa	
					Basic	Acidic
84	487.7	5.3	3	7	9.4, 6.4	4.6
85	487.7	5.3	3	7	9.7, 6.4	4.6
86	471.6	4.8	3	7	9.0, 6.2	4.4
87	471.6	4.8	3	7	9.1, 6.2	4.3
88	488.6	4.3	3	7	8.0, 6.0	4.2
89	488.6	4.3	3	7	8.9, 6.0, 0.5	4.3

Table 20: Calculated physicochemical properties of proposed compounds for synthesis.

Christopher J Tame

2.3.1 Synthetic route design for thiophenes 84 and 85

The retrosynthetic analysis of thiophene **84** is shown in **Scheme 14**, which utilises the commercial availability of the core fragments to facilitate a reproducible procedure which can be applied to both regioisomers.
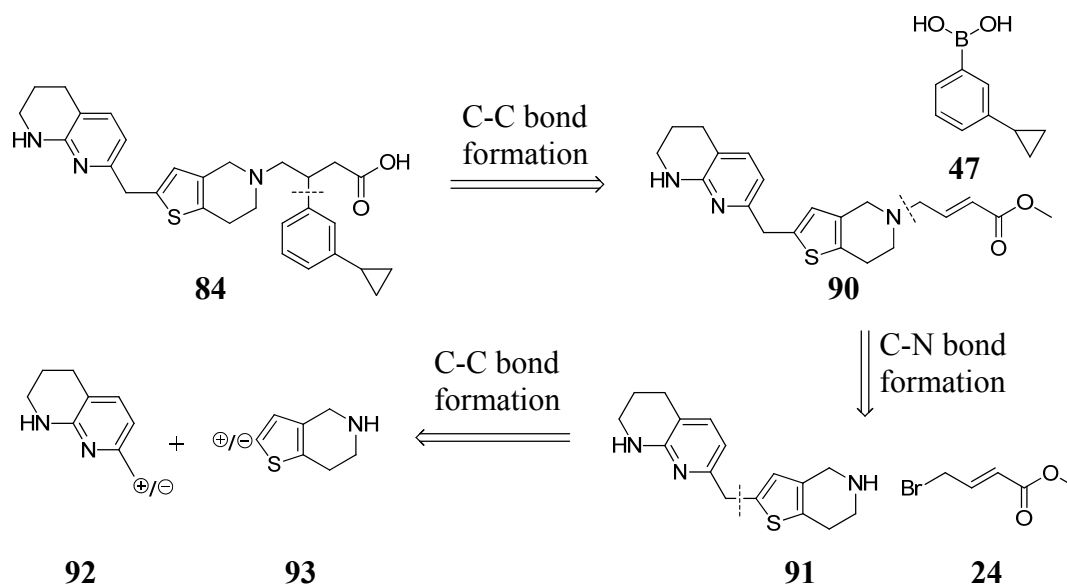
Scheme 14: The retrosynthesis of thiophene **84**.

The first and second disconnections follow the synthetic route used to access pyrazolopiperidine **17b** *via* alkylation of the piperidine nitrogen with bromocrotonate **24**, followed by rhodium-catalysed 1,4-addition of an appropriately substituted phenylboronic acid (**Scheme 11**).

The last disconnection breaks the carbon-carbon bond joining the core and the tetrahydronaphthyridine. This was chosen due to the expedient access to the respective monomers, which are shown in **Figure 29**.
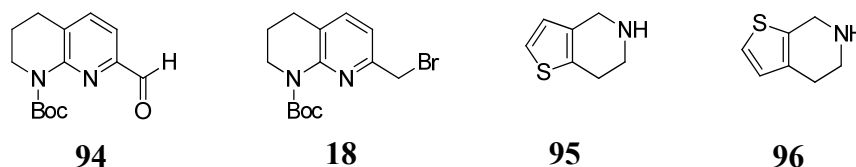
Figure 29: Commercially available tetrahydronaphthyridine-containing compounds and thiophene-containing bicyclic systems.

Christopher J Tame

A survey of the literature highlighted the reliable application of C-H lithiation followed by reaction with benzyl bromide to form the required bond (**Scheme 15**).[185] These conditions require the use of a strong base in order to selectively lithiate the C-H bond α- to the sulfur atom.
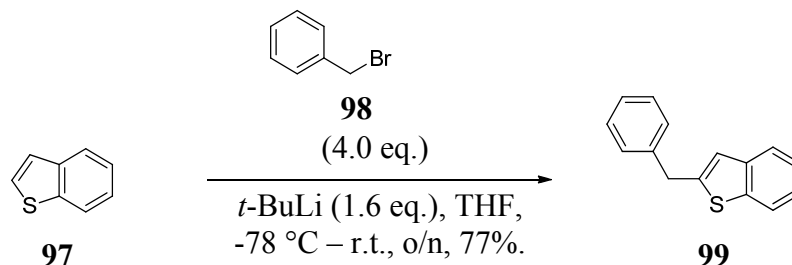
Scheme 15: *t*-BuLi mediated C-H lithiation followed by reaction with benzyl bromide.[185]

It is also possible to direct lithiation with the incorporation of a halogen atom at the desired lithiation site.[186] The increased rate of halogen-lithium exchange when compared to C-H lithiation greatly facilitates this transformation. Electrophilic aromatic substitution can efficiently introduce the halogen at the desired position.[187]

The use of strong bases, however, is expected to be incompatible with thiophenylpiperidine **95**, which contains other potential sites for lithiation on the piperidine ring. The use of metal-catalysed cross-coupling conditions with benzylic organometallic species such as Grignards[188] and organozincates[189] provides a milder approach for this bond forming reaction, thus avoiding undesired reactivity

The formation of these organometallic species, however, has no precedence on benzylic heterocycles such as tetrahydronaphthyridine **18**, which is expected to be due to instability issues. Consequently, this approach was not considered further.

Recent advancements from Fairlamb[190] and Buchwald[191] have identified palladium catalysts which enable efficient cross coupling of heterarylboronic acids and benzylhalides (**Schemes 16** and **17**). Such an approach could be relevant to the current target systems.

Christopher J Tame
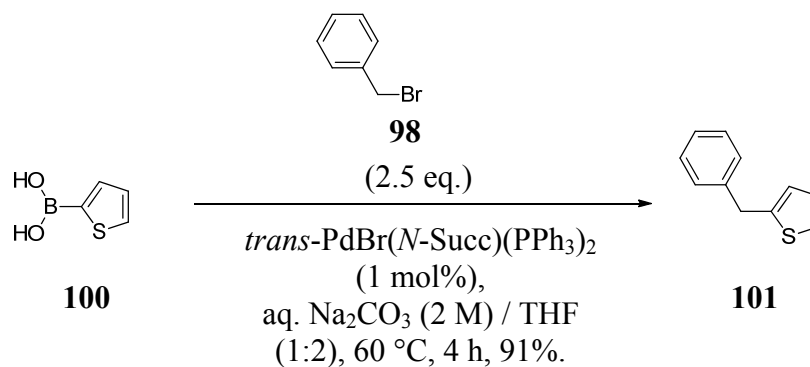
Scheme 16: Palladium-catalysed cross-coupling of heteroarylboronic acid **100** with benzyl bromide **98**.[190]
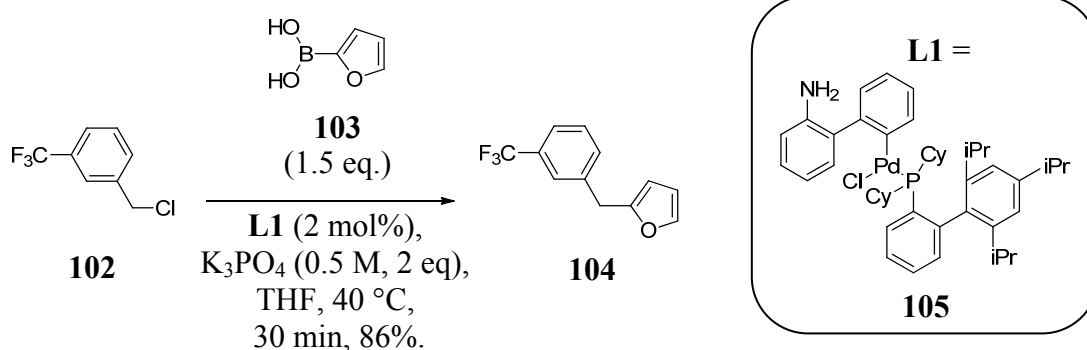
Scheme 17: Palladium-catalysed cross-coupling of heteroarylboronic acid **103** with benzyl chloride **102**.[191]

An organometallic centre on thiophene **95** was considered to be more stable and, therefore, more straightforward to access than the other organometallic components required in the previously discussed techniques. As a result, this approach was selected to access desired intermediate **91**.

Although the palladium catalyst prepared by Buchwald had not been applied to the cross-coupling of a thiophene with an arylbromide, a thiophene had been used in an analogous sp^2-sp^2 cross coupling.[191] In addition, these conditions had been successfully reproduced in our laboratories,[192] providing confidence that they could be applied to the reaction of thiophene **95** with bromomethyl **18**. Consequently, these conditions were chosen in preference to those disclosed by Fairlamb and co-workers. Consideration was then given to accessing the required boronic acid.

Christopher J Tame

The formation of arylboronic acids usually requires a strong base and is potentially unsuitable for use in the presence of other exchangeable centres as is the case with thiophene **95**.[193] Boronic esters provide a more attractive synthetic handle because they can be formed under more mild conditions and are readily hydrolysed to the corresponding boronic acid under reaction conditions. The formation of 2-heteroarylboronic esters can be achieved *via* a number of methods, including: base-mediated lithiation, followed by reaction with trialkoxyborane[194] palladium-catalysed cross-coupling of 2-bromoheteroaromatics with bispinacolatodiboron[195] and iridium-catalysed C-H borylation with pinacolborane or bispinacolatodiboron (**Scheme 26**).[196]

The regioselective C-H borylation of thiophene **97** presents an attractive opportunity for direct functionalisation under mild conditions. This is in contrast to other methods which require the pre-formation of the 2-bromothiophene analogue. Subsequent palladium-catalysed cross coupling of pinacolboronate **108** with tetrahydronaphthyridine **18** is then expected to form the desired product **109** (**Scheme 18).** The relatively mild conditions used in this scheme are expected to help suppress undesired side-reactions, thus ensuring regioselectivity.

The use of a carboxybenzyl (Cbz) protecting group was selected because it significantly increases the molecular weight of thiophene **106**, which would reduce volatility and facilitate work-up procedures. In addition, the Cbz group could be either selectively or simultaneously removed, relative to the Boc-protected tetrahydronaphthyridine on intermediate **109**. This could be achieved using either hydrogenation[197] or acidic conditions,[198] respectively. The conditions required for the protection of secondary amines with Cbz groups typically involve the use of a carboxybenzyl chloride and a weak organic base.[199]

The complete proposed synthetic route to access the desired thiophene-containing αvβ6 antagonist **84** is displayed in **Scheme 18**. The route exploits three transition metal-catalysed cross coupling procedures to efficiently access the desired product in seven linear steps.

Christopher J Tame
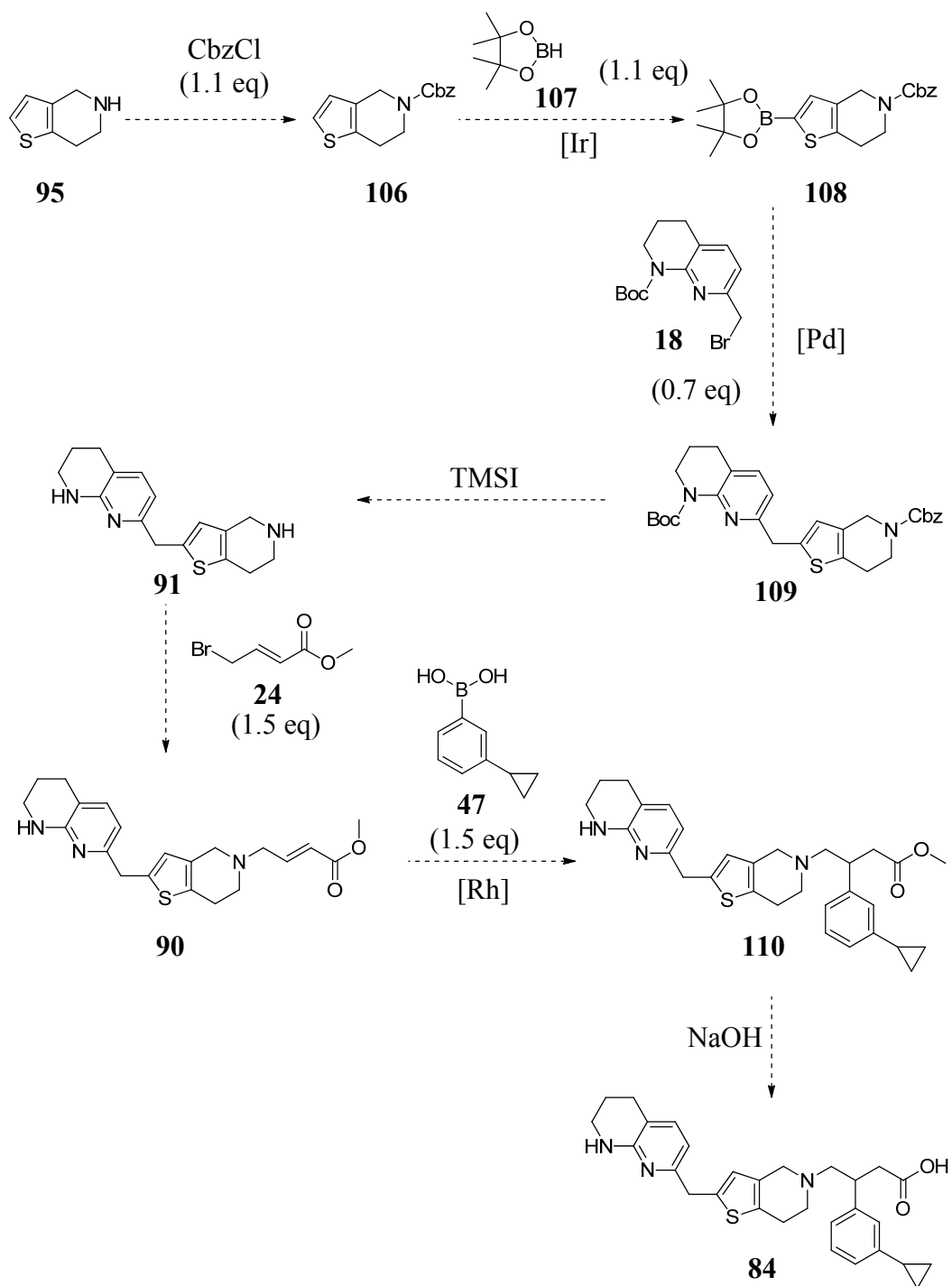
Scheme 18: Proposed synthetic route to access desired αvβ6 antagonist **84**.

2.3.2   Synthesis of thiophenes 84a and 84b

The synthesis of the αvβ6 antagonist target **84** commenced with the protection of thiophene **95** using carboxybenzyl chloride and proceeded well using literature conditions to afford the desired product (**106**) in quantitative yield (**Scheme 19**).
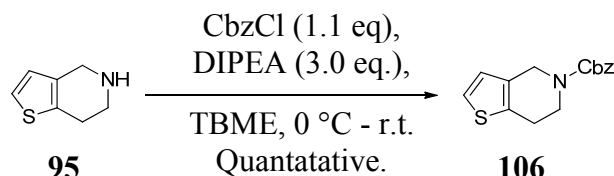
Scheme 19: Cbz protection of the piperidine nitrogen of thiophene **95**.

Iridium-catalysed C-H borylation of thiophene **106** with pinacolborane was subsequently attempted to access the appropriately functionalised thiophene **108** (**Scheme 20**). LCMS and ^{1}H NMR analysis of the reaction mixture after an aqueous work-up identified borylated thiophene **108**. Unfortunately, however, this decomposed to starting material **106** when exposed to air.
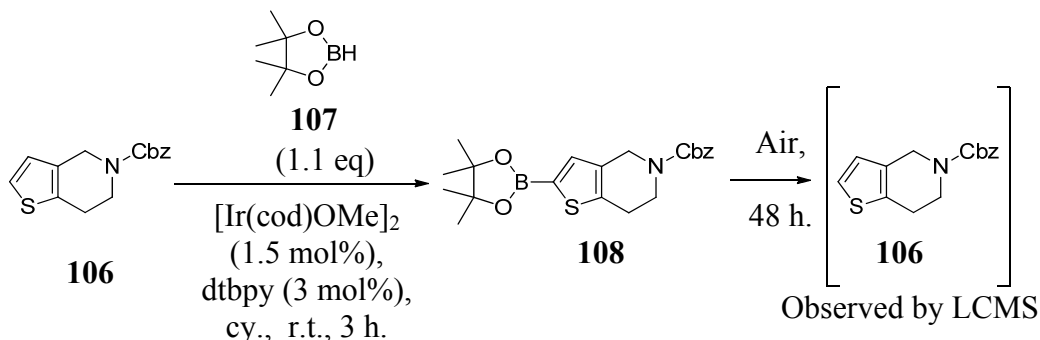
Scheme 20: Iridium-catalysed C-H borylation of thiophene **126**, followed by protodeborylation in air.

In an attempt to avoid protodeborylation of borylated thiophene **108**, it was reasoned that a one-pot protocol which included the palladium-catalysed sp^2-sp^3 cross coupling conditions could access the more stable intermediate **109** (**Scheme 21**). This procedure would avoid prolonged exposure of borylated thiophene **108** to air and moisture, which was believed to be the cause of rapid protodeborylation which was observed previously.

Christopher J Tame
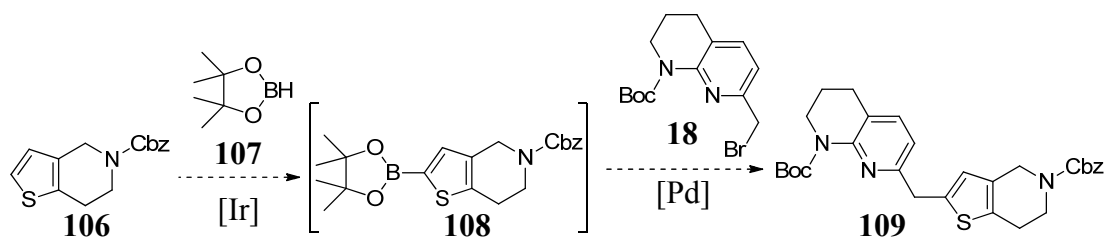
Scheme 21: A proposed one pot C-H borylation/ sp^2-sp^3 cross coupling protocol to afford methylene-linked **128**.

Hartwig and Miyaura described a similar one-pot procedure, which involved iridium-catalysed C-H borylation followed by palladium-catalysed sp^2-sp^2 cross-coupling (**Scheme 22**).[196] This supported the proposed approach by demonstrating the tolerance of the palladium-catalysed cross-coupling conditions to an iridium catalyst, the di(*tert*-butyl)bipyridine (dtbpy) ligand, and a non-polar solvent.
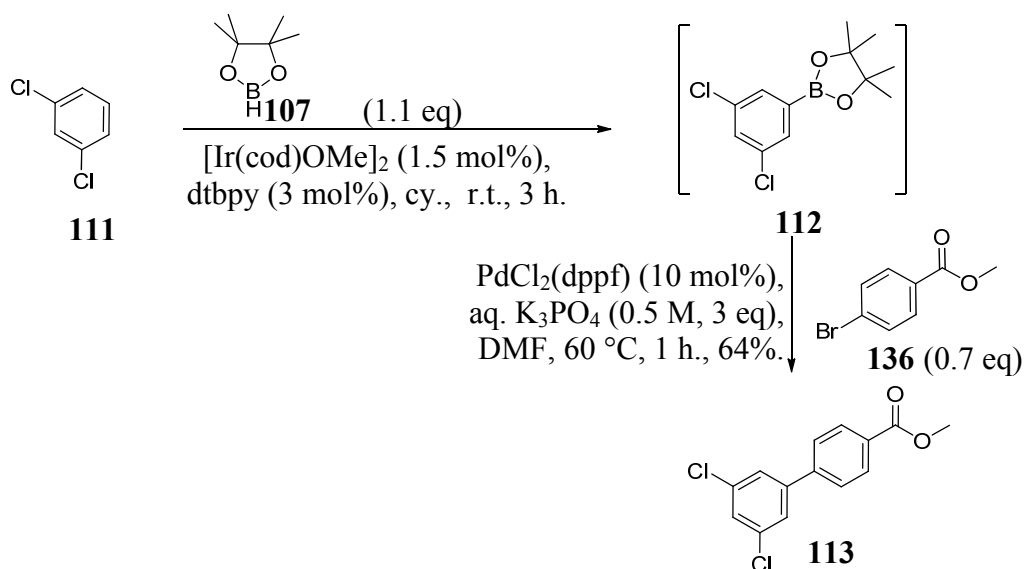
Scheme 22: A one pot protocol for iridium-catalysed C-H borylation followed by palladium-catalysed sp^2-sp^2 cross coupling.[196]

Accordingly, the one pot procedure was undertaken on thiophene **106** to successfully access the desired methylene-linked **109** in 60% overall yield. The palladium loading was increased from 2 mol% to 10 mol% in an attempt to increase the rate of reaction and ensure optimal conversion of pinacolboronate **127** to methylene-linked **128**.

Christopher J Tame

The sub-stoichiometric amount of alkyl bromide **18** limited the yield to a maximum of 70%. Considering this, the yield can be recalculated as 92% with respect to the limiting reagent (**Scheme 23**). LCMS analysis of the crude reaction mixture after 16 hours indicated complete consumption of pinacolboronate **106** and a small amount of alkyl bromide **18**, suggesting some protodeborylation. Therefore, increasing the number of equivalents of alkyl bromide **18** was not expected to lead to an improvement of the yield. The yield obtained in this reaction demonstrates the successful application of this methodology to more structurally complex molecules without compromising on yield, which highlights its robustness and applicability.
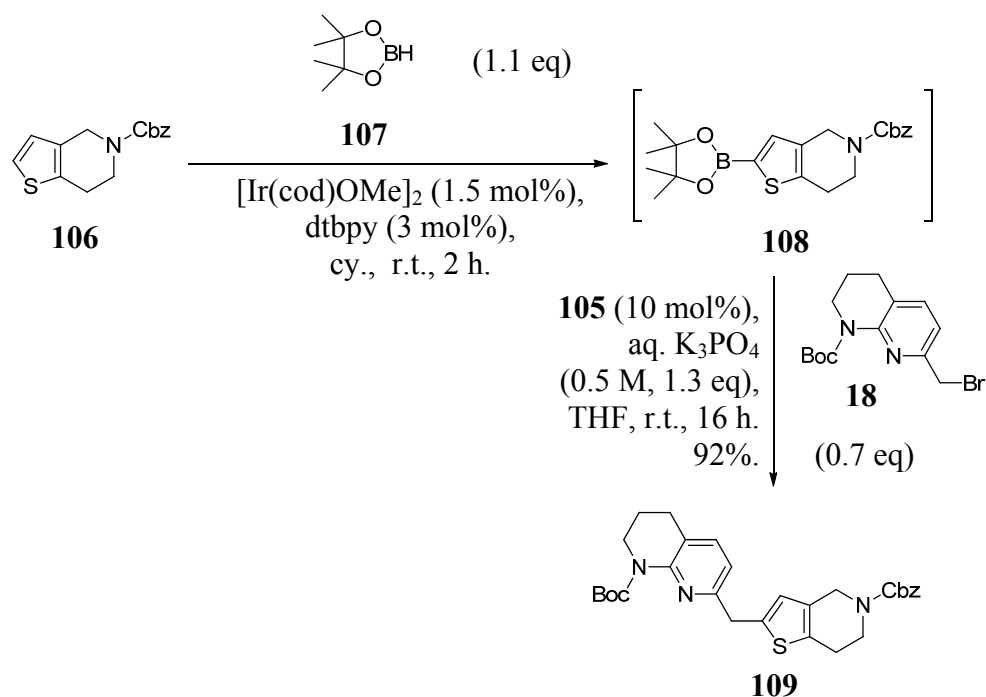
Scheme 23: Iridium-catalysed C-H borylation of thiophene **106**, followed by palladium-catalysed sp^2-sp^3 cross coupling with alkyl bromide **18** to afford methylene-linked **109**.

The next step involved TMSI-mediated global deprotection of methylene-linked **109** to access amine **91** in 86% yield (**Scheme 24**). Selective deprotection of the Cbz group was not attempted because the tetrahydronaphthyridine was expected to have insufficient nucleophilicity to alkylate under the reaction conditions in the subsequent step. This, however, could be considered if problems were encountered.

Christopher J Tame
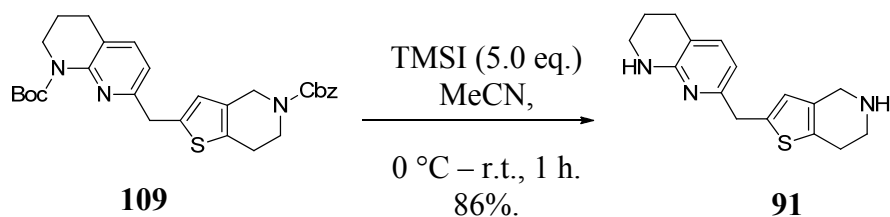
Scheme 24: TMSI-mediated global deprotection of methylene-linked **109**.

The previously developed conditions for the alkylation of amine **91** with bromocrotonate **24**, followed by rhodium-catalysed 1,4-addition of aryl boronic acid **47**, were subsequently undertaken to access methyl ester **110** in 59% overall yield over the two steps (**Scheme 25**). Separation of the enantiomers by chiral HPLC afforded **110a** and **110b** as single enantiomers in moderate yields. [175].
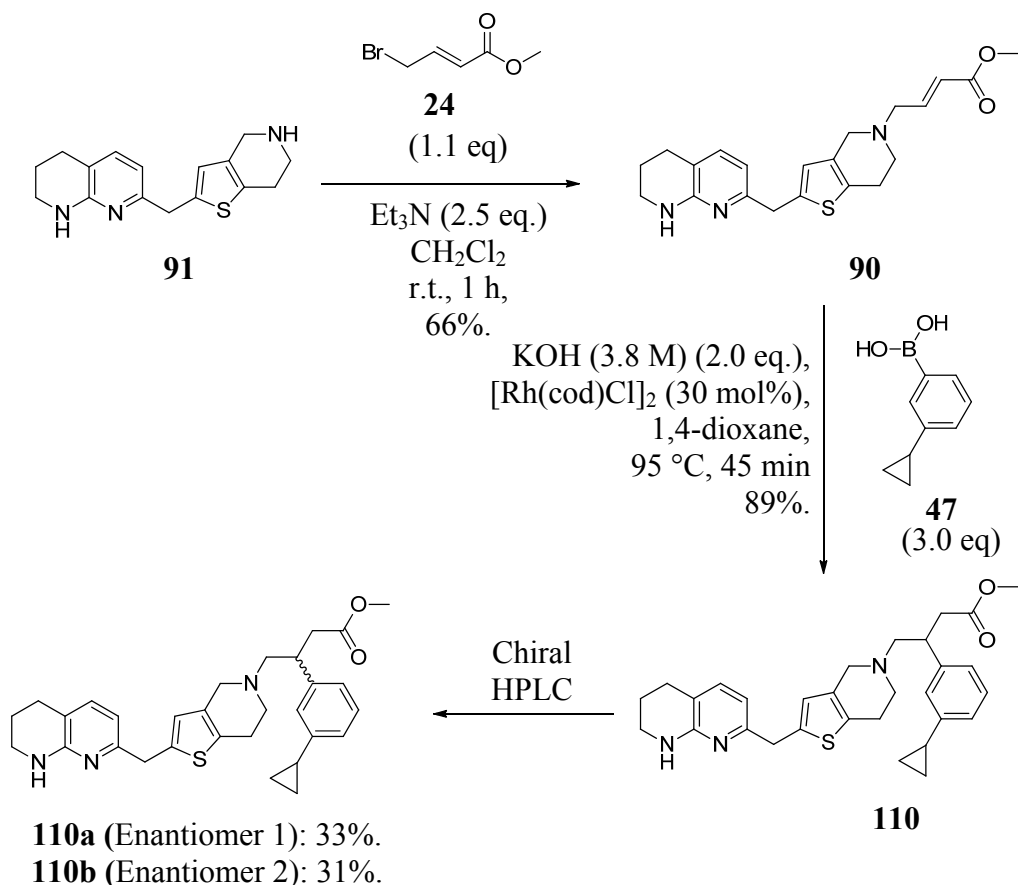
Scheme 25: The alkylation of amine **91** with bromocrotonate **24**, followed by rhodium-catalysed 1,4-addition of arylboronic acid **47** and chiral chromatography.[175]

Christopher J Tame

The hydrolysis of methyl esters **110a** and **110b** gave carboxylic acids **84a** and **84b** in 82% and 83% yield, respectively (**Scheme 26**).
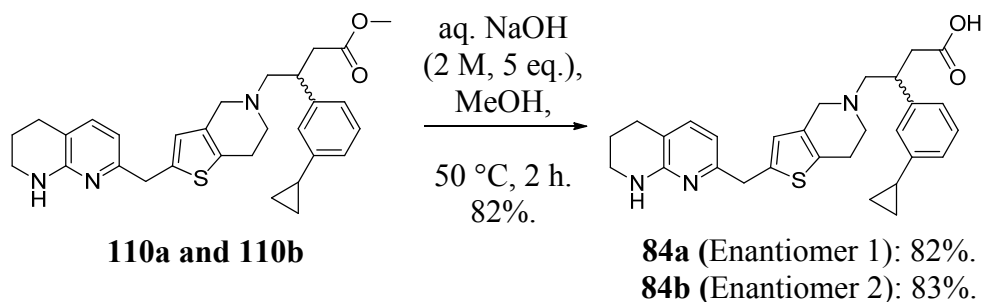
Scheme 26: The sodium hydroxide mediated hydrolysis of methyl esters **133a** and **133b** to afford the corresponding carboxylic acids.

The chiral HPLC purification was responsible for the lowest yield in the synthetic route used to access **84a** and **84b**, which was also the case for the synthesis of pyrazolopiperidine-containing **17a** and **17b**. Consequently, investigations focused on a method to circumvent this issue. Recent work in our laboratories has focused on the optimisation of the catalytic system used for the 1,4-conjugate addition reactions on similar templates. Unfortunately, this work could only afford moderate levels of enantioselectivity, which would require further purification by chiral HPLC.[200] In an attempt to identify alternative approaches, the retrosynthetic analysis of thiophene **84** was revisited to provide further inspiration.

It was recognised that the synthesis of thiophene **84** contains a two step route to access synthon **114** (**Scheme 27**). Therefore, an alternative strategy could be the convergent synthesis of a synthetic equivalent of synthon **114**. If an asymmetric route could be developed, it would also avoid the low-yielding chiral HPLC purification. The use of commercially available materials to access this compound would also be essential, in order to compete with the existing route.

Christopher J Tame
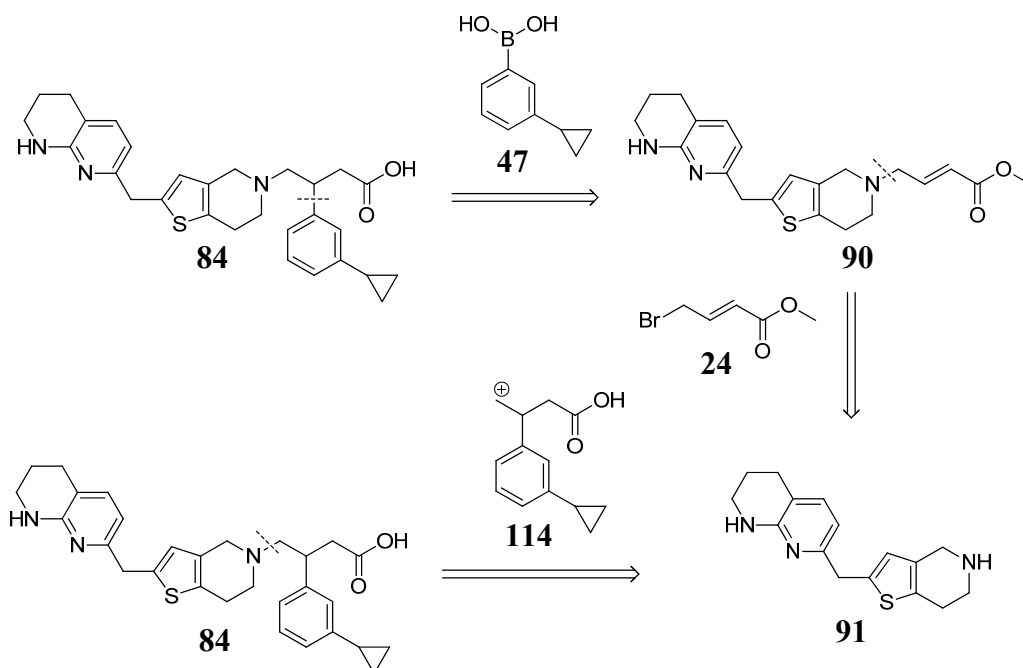
Scheme 27: The retrosynthetic analysis of thiophene **84**.

A survey of the literature revealed the successful use of rhodium-catalysed 1,4-addition of arylboronic acids to γ-crotonolactone (**Scheme 28**).[201] It has also been shown that treatment of these systems with HBr gas can facilitate ring-opening to form the electrophile **118** (**Scheme 29**),[202] although other examples generate HBr *in situ* using the more convenient protocol with acetyl bromide in ethanol.[203] This two step process presented a potentially efficient method of accessing desired alkylating agent **121**, which is displayed in **Scheme 30**.
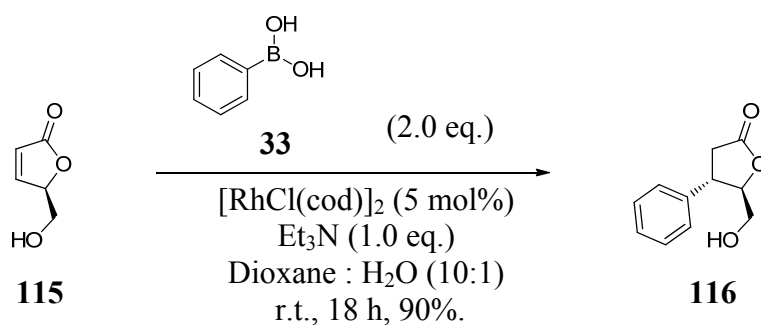
Scheme 28: Rhodium-catalysed 1,4-addition of phenylboronic acid **33** to γ-crotonolactone **115**.[201]

117 → **118** ≡ **118**
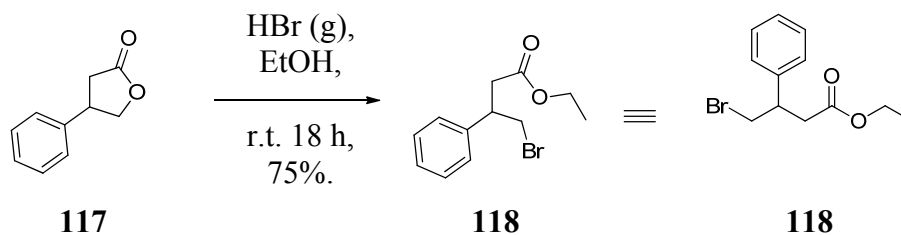
Scheme 29: HBr-mediated ring opening of lactone **117** to afford ethyl ester **118**.[202]

119 → **120** → **118**
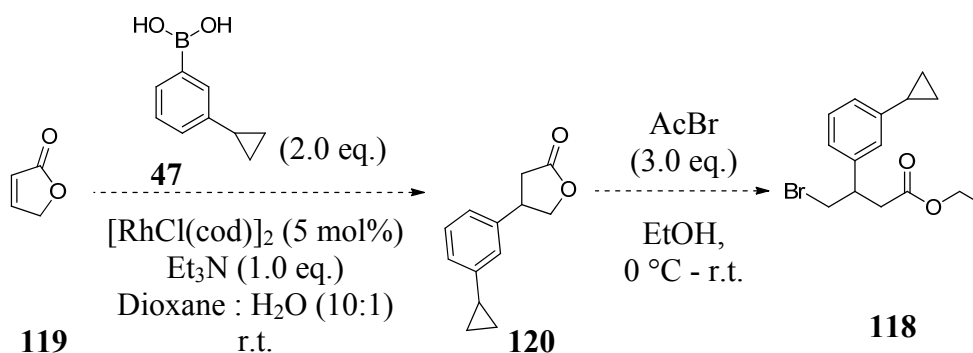
Scheme 30: Proposed route to access electrophile **121**.[201,203]

The rhodium-catalysed 1,4-addition of boronic acid **47** to γ-crotonolactone **119** was initially attempted using literature conditions, which afforded the desired product in low yield (**Scheme 31**).

119 → **120**
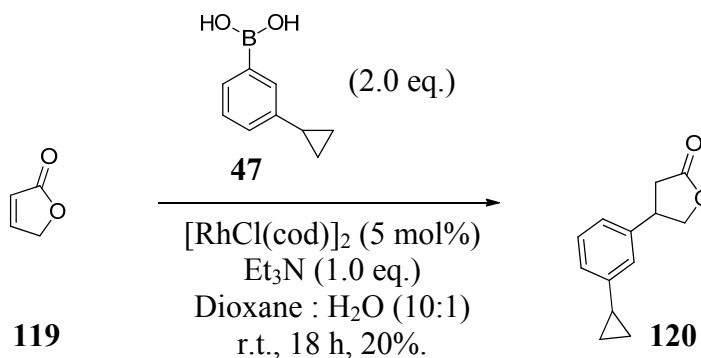
Scheme 31: The rhodium-catalysed 1,4-addition of boronic acid **47** to γ-crotonolactone **119** using literature conditions.

Examination of the catalytic cycle highlighted the competing hydrolysis of intermediate **50 (Pathway II)**, which provided an explanation for the low isolated yield (**Scheme 10**). Consequently, an excess of boronic acid has been typically

Christopher J Tame

employed in the literature to account for this competing pathway. It is reasonable to suggest, therefore, that increasing the equivalents of boronic acid **33** would improve the reaction efficiency.
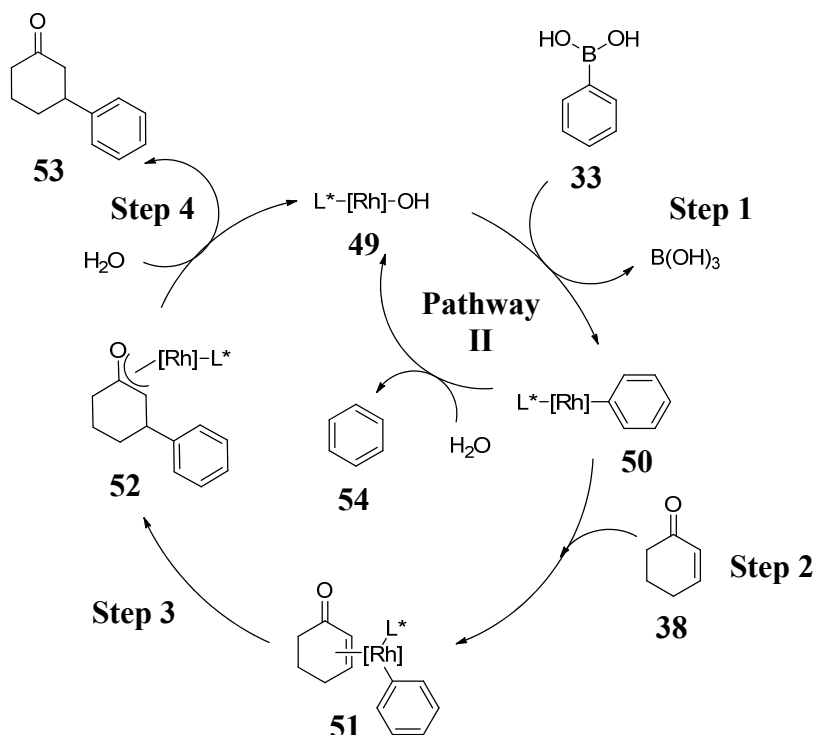
Scheme 10: Proposed mechanism for rhodium-catalysed 1,4-addition of arylboronic acid to cyclic or acyclic α,β-unsaturated systems.[173]

An excess of the α,β-unsaturated component **38**, however, would also be expected to increase the rate of **Step 2**, providing an alternative strategy for suppressing **Pathway II**. It is envisaged that this has not been considered in the literature because the α,β-unsaturated system is usually the most valuable component. In contrast to the literature examples, however, the boronic acid required for the synthesis of desired product **120** is the most valuable component of the reaction. Consequently, in an attempt to improve the efficiency of the reaction with respect to the boronic acid, the reaction was repeated with an excess of γ-crotonolactone **119**.

A wide range of bases have been utilised in rhodium-catalysed 1,4-additions, and optimisation efforts on other templates in our laboratories have identified that 3 equivalents of KOH (3.8 M) and 10 mol% catalyst loading considerably enhances the

Christopher J Tame

rate of reaction.[204]   It was considered that these conditions would help reduce **Pathway II**, and were subsequently selected for use.

Based on all of the above, two equivalents of γ-crotonolactone **119** were reacted with 3-(cyclopropylphenyl)boronic acid **47** using 10 mol% rhodium catalyst and 3 equivalents of KOH (**Scheme 32**). LCMS analysis indicated complete consumption of boronic acid **47** after 30 minutes, which gave the desired product in 36% yield. This is in contrast to 10% yield from the literature conditions, relative to the boronic acid component.

Scheme 32: The rhodium-catalysed 1,4-addition of boronic acid **47** to 2 equivalents of γ-crotonolactone **143**.[172]

In an attempt to improve the efficiency of the reaction further, five equivalents of γ-crotonolactone **119** were employed (**Scheme 33**). The reaction was found to reach completion in just ten minutes and the yield was increased from 36% to 57%.

Scheme 33: The rhodium-catalysed 1,4-addition of boronic acid **47** to 5 equivalents of γ-crotonolactone **119**.

Christopher J Tame

Following on from this result, asymmetric conditions were investigated. A recent publication from our laboratories investigated the asymmetric conjugate addition of aryl boronic acids to γ-amino α,β-unsaturated esters.[172] This work demonstrated that the addition of the chiral bisphosphine ligand (*R*)-BINAP imparted excellent levels of enantioselectivity. (*R*)-BINAP and hydroxide readily displace the cyclooctadiene and chloride ligands to form the active chiral catalytic species [Rh((*R*)-BINAP)OH] *in situ*.[166]

These conditions were applied to the conjugate addition of boronic acid **47** and α,β-unsaturated ester **119** (**Scheme 34**), although this failed to provide any asymmetry. This could be a result of background reactions with small amounts of cyclooctadiene-bound rhodium, which would catalyse the reaction under achiral conditions. The use of preparative HPLC methods of purification facilitated expedient access to the product for further analysis of enantioinduction. The low yields associated with this process were not considered to be detrimental at this stage, as it was considered that silica gel column chromatography could be applied once optimal asymmetric conditions were identified.
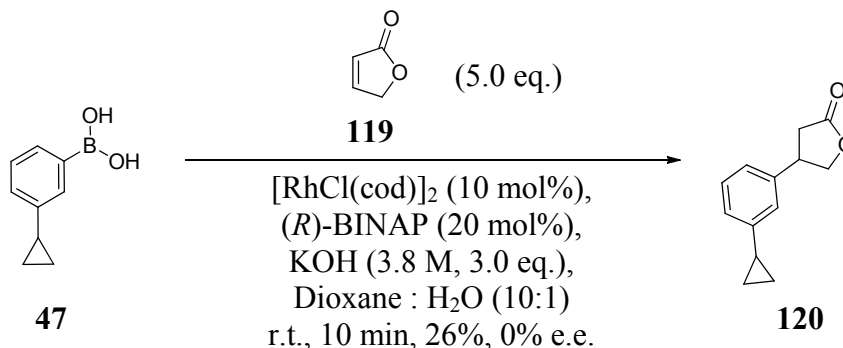
Scheme 34: The attempted asymmetric synthesis of lactone **120** using [RhCl(cod)]$_2$ and (*R*)-BINAP.

Examination of the literature revealed two alternative applications of commercially available catalysts and ligands for the enantioselective 1,4-addition of arylboronic acids to α,β-unsaturated systems. The first was developed by Hayashi and co-workers for the asymmetric addition of arylboronic acids to enones using Rh(acac)(C$_2$H$_4$)$_2$ as catalyst and an excess of boronic acid.[166] These conditions,

Christopher J Tame

however, did not show any conversion when applied to the desired substrates (**Scheme 35**).
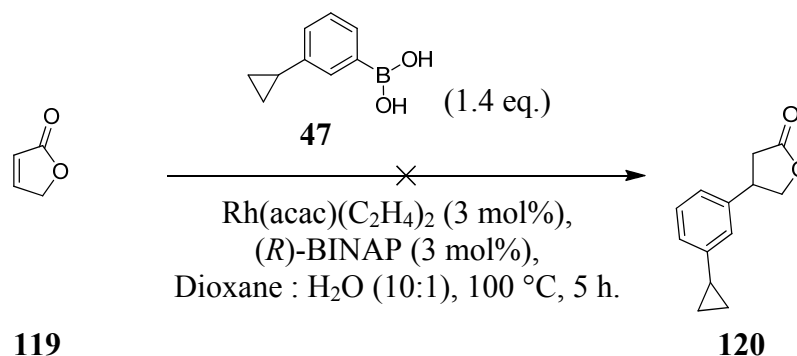
Scheme 35: The attempted synthesis of lactone **120** using $Rh(acac)(C_2H_4)_2$.[166]

The reactivity of esters such as lactone **119** is expected to be lower than the enones used to validate these conditions. In addition, the absence of base in this reaction could also affect the rate of formation of the active hydroxyrhodium species, which could result in protodeboronation of boronic acid **47**. Taken together, both of these reasons were used to explain the lack of reactivity observed.

Work by process chemists at Abbott pharmaceuticals investigated the same catalytic conditions as those used in the achiral formation of desired product **120**.[205] Arriving at the same hypothesis that background reactions from cyclooctadiene-bound rhodium negated any asymmetric induction, they demonstrated that *in situ* removal of cyclooctadiene by vacuum gave enantiomeric excesses of around 90%, although this was difficult to reproduce. Consequently, they hypothesised that the introduction of a commercially available pre-catalyst which had no catalytic activity would avoid any achiral background reactions. To this end, they selected ([Rh(nbd)$_2$]BF$_4$), which uses the sterically constrained norbornadiene ligand. This was successfully applied to the 1,4-addition of a range of arylboronic acids and enones, which gave enantiomeric excesses between 91.6-98.7%.[205]

Accordingly, these conditions were subsequently applied to the reaction of 3-(cyclopropylphenyl)boronic acid **47** with γ-crotonolactone **119** (**Scheme 36**). This pleasingly afforded the desired chiral product **120a** in 96% e.e., albeit in low yield.

Christopher J Tame
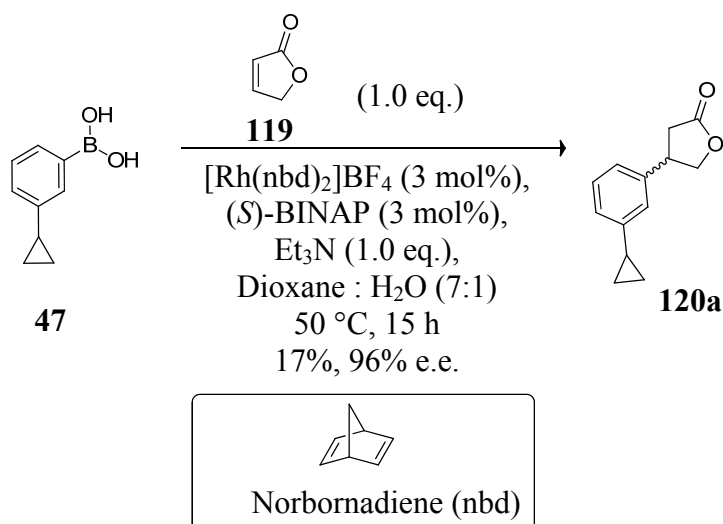
Scheme 36: The asymmetric rhodium-catalysed 1,4-addition of cyclopropylphenyl boronic acid **47** to γ-crotonolactone **120a** with [Rh(nbd)$_2$]BF$_4$.[205]

Although no further optimisation efforts were attempted, it is expected that the yield could be improved in the same areas as previously demonstrated, which include: increased equivalents of γ-crotonolactone **119**; increased catalyst and ligand loading and replacement of Et$_3$N with KOH.

With the appropriately functionalised achiral lactone **120** in hand, subsequent HBr-mediated ring-opening was next investigated. The optimal conditions developed on this substrate were then expected to be transferred to the chirally-enriched analogue, which was less readily available.

The *in situ* formation of HBr by treatment of EtOH with acetyl bromide circumvents the use of inconvenient HBr gas cylinders, which would also deliver an uncontrollable excess of HBr into the reaction mixture. The treatment of lactones with HBr generated *in situ* has been demonstrated in the literature to affect ring opening in moderate yield.[203] Accordingly, these conditions were applied to lactone **120**, which after 2 hours at room temperature suggested incomplete conversion to alkyl bromide **121**, as determined by LCMS analysis (**Scheme 37**).

Christopher J Tame
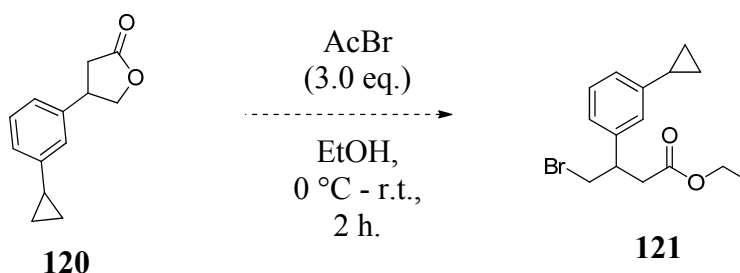
Scheme 37: Attempted synthesis of alkyl bromide **121** *via* HBr mediated ring opening of lactone **120**.

In an attempt to drive the reaction to completion, it was repeated with nine equivalents of acetyl bromide (**Scheme 38**). The reaction was monitored by LCMS analysis, which indicated around 50% conversion of the starting material after 1 hour. After this period, an impurity observed by LCMS analysis increased significantly, which was isolated and characterised as the dialkylbromide **122**.
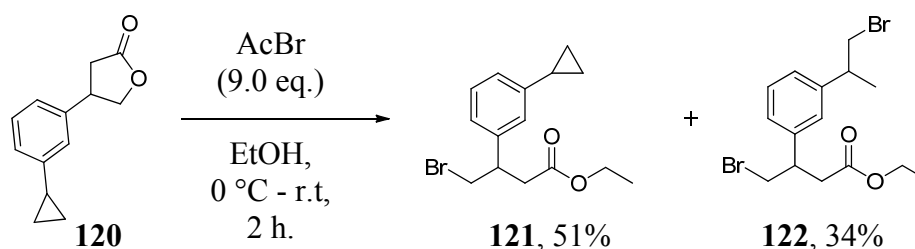
Scheme 38: HBr mediated ring opening of lactone **120** to afford alkyl bromide **121** and bisalkylbromide **122**.

Consequently, the reaction was repeated using six equivalents of acetyl bromide and was stopped after 1 hour, which gave a comparable yield to that obtained after 2 hours and nine equivalents of acetyl bromide (**Scheme 39**).
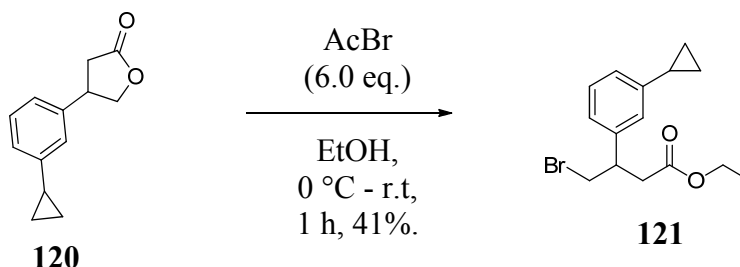
Scheme 39: HBr mediated ring opening of lactone **120** to afford alkyl bromide **121**

Christopher J Tame

With the appropriate alkyl bromide (**121**) in-hand, investigations focused on alkylation with amine **91**. An analysis of the literature revealed that the alkylation of weakly nucleophilic secondary amines with alkyl bromides required heating to 120 °C (**Scheme 40**).[206]
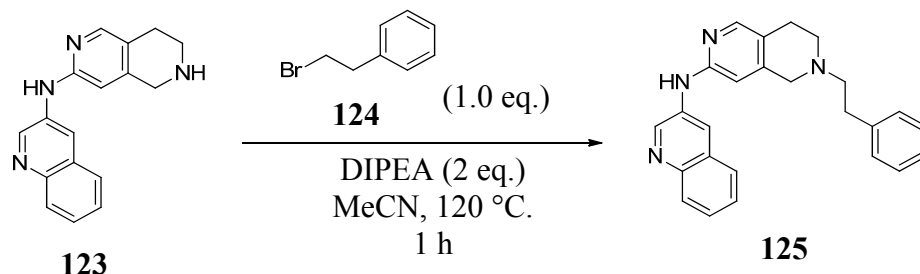
Scheme 40: The alkylation of amine **123** with alkyl bromide **124** at 120 °C.[206]

Based on this, it was expected that alkylation of relatively hindered electrophiles such as alkyl bromide **121** would require even higher temperatures. Consequently, an alkylation was attempted at 150 °C, which was undertaken using a Biotage microwave reactor for convenience (**Scheme 41**). The poor solubility of the starting materials in acetonitrile at room temperature prompted replacement with isopropanol.
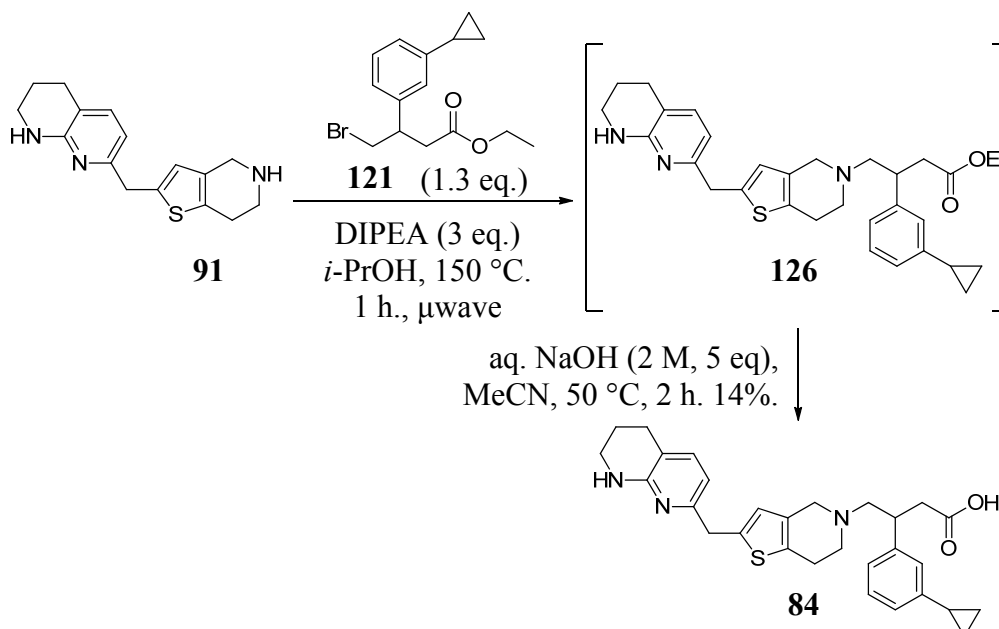
Scheme 41: Conditions attempted for the alkylation of alkyl bromide **121** with amine **91**.

Christopher J Tame

The formation of carboxylic acid **84** was achieved in poor yield, which was considered to be a result of using a number of low yielding purification techniques. Future efforts could focus on optimising this yield by purifying the ethyl ester **150** prior to hydrolysis. Alternatively, reverse phase column chromatography or MDAP purification with acidic eluent modifier could be investigated for purification of the carboxylic acid **84**.

In conclusion, a novel route has been developed to access alkyl bromide **121**, which requires just two steps and uses commercially available reagents. The conjugate addition of aryl boronic acid **47** to crotonolactone **119** was optimised to limit the use of expensive boronic acid, as well as demonstrating high enantiomeric control. However, significant optimisation of the asymmetric conjugate addition step and purification methods is required before this route could be considered more efficient and applicable than the original conditions. Before further optimisation of this route was considered, however, work undertaken in parallel identified a superior asymmetric route (section **2.3.3**). This precluded any further investigation from being carried out on the route described above.

2.3.3   Synthesis of thiophene 85b

The synthesis of thiophene analogue **85** was required for comparison of structure activity relationships with thiophene **84**, which represents the isomeric compound. The successful regioselective C-H borylation of thiophene intermediate **126** prompted the retrosynthetic analysis to be revisited, in an attempt to optimise the synthetic route further.

A shorter route was identified which removed the need of a protecting group on the thiophene core (**Scheme 42**). This sequence required a challenging regioselective C-H borylation and subsequent sp^2-sp^3 cross coupling of a highly polar and functionalised intermediate (**127**). The route could be further optimised with the incorporation of alkyl bromide **121**, although this was not fully validated on thiophene **84** at the time of synthesis, and for that reason was not considered.

Christopher J Tame
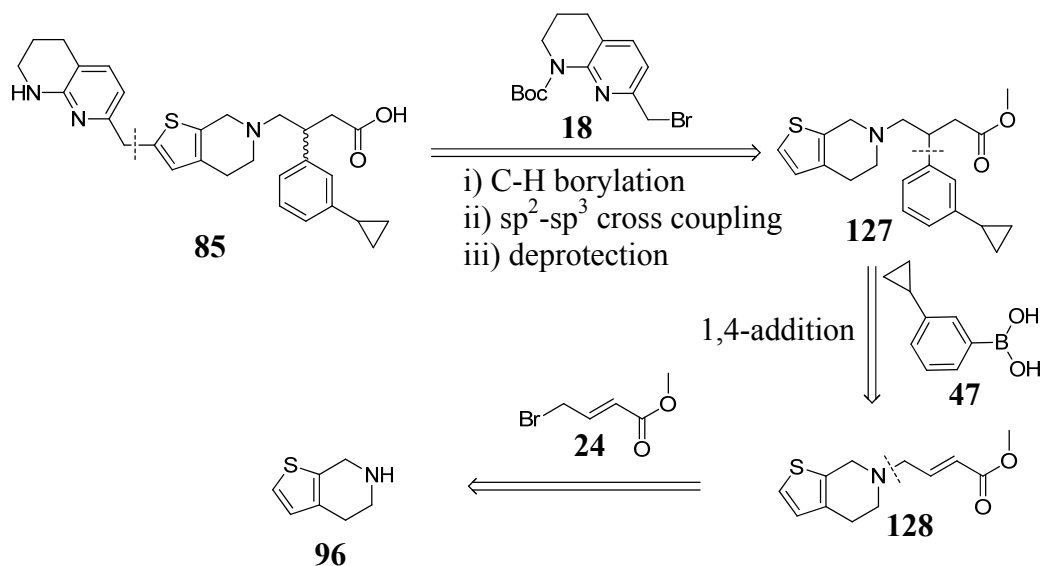
Scheme 42: The retrosynthesis of thiophene **85**.

The synthetic route was subsequently initiated, which started with alkylation of thiophene **96** with bromocrotonate **24**, followed by rhodium-catalysed 1,4-addition with arylboronic acid **47** (**Scheme 43**). The one-pot borylation/cross coupling conditions were then applied to intermediate **127**, which pleasingly afforded desired thiophene **128** in 22% yield. The final steps involved removal of the protecting groups, which was undertaken using the standard conditions to afford desired target **85** in 23% yield.

Christopher J Tame
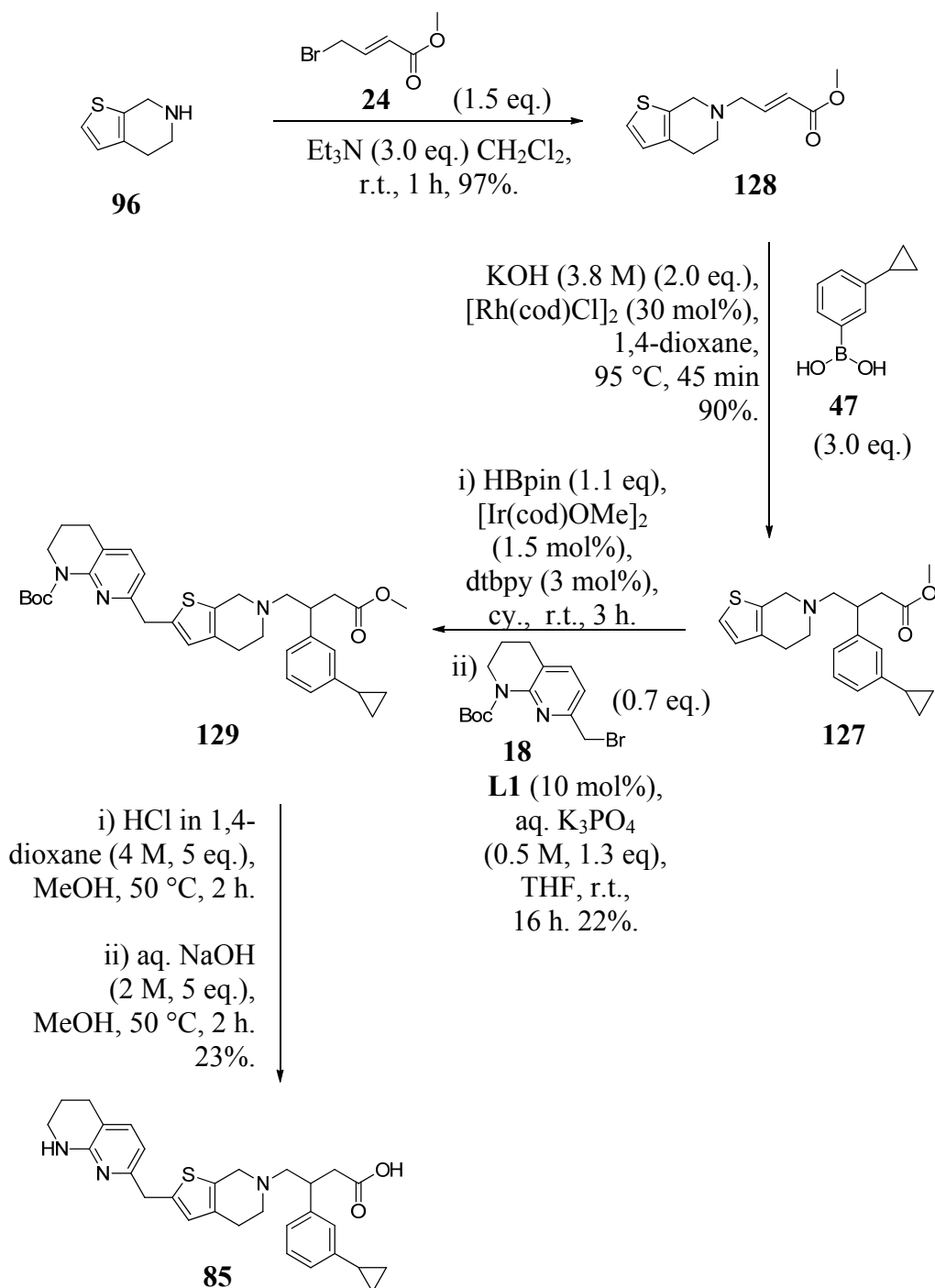
Scheme 43: The synthetic route to access thiophene **85**.

The yield obtained for the one pot borylation/cross coupling transformation (**127** to **129**) was significantly lower than with Cbz-protected thiophene analogue (**106**), although it reduced the number of synthetic steps, providing a more concise route to access thiophene **85**. However, this low yield did not provide a sufficient amount of

Christopher J Tame

thiophene **128** for chiral HPLC purification. Therefore, the synthetic route was repeated on a larger scale. In an attempt to improve the yield, the rhodium-catalysed conjugate addition step was undertaken using (*R*)-BINAP. This was expected to form a chirally-enriched mixture of the more active enantiomer, with the aim of improving the yield after chiral HPLC purification.

Whilst the exact stereochemical configuration of the more active enantiomer at αvβ6 was unknown, previous investigations in our laboratories have shown that the predominant enantiomer formed from (*R*)-BINAP-controlled conjugate addition reactions is the most active when subjected to the appropriate bioassay.[127] Consequently, the rhodium-catalysed conjugate addition reaction was undertaken with (*R*)-BINAP, which could potentially afford the desired enantiomer in an increased overall yield.

The use of CH_2Cl_2 for the alkylation of amine **96** with bromocrotonate **24** was targeted for replacement with a more environmentally sustainable alternative. Consequently, the reaction was attempted in TBME,[207] although poor solubility resulted in the requirement of 20% CH_2Cl_2 to achieve solubility (**Scheme 44**). This afforded alkylated thiophene **128** in 72% yield, which is 25% lower than previously obtained when exclusively using CH_2Cl_2. Therefore, the use of CH_2Cl_2 is recommended for future alkylation attempts.
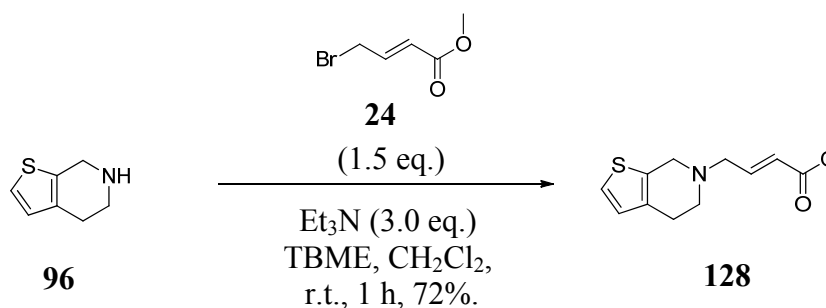
Scheme 44: The alkylation of thiophene **96** with bromocrotonate **24** in a 5:1 mixture of TBME and CH_2Cl_2.

Christopher J Tame

The asymmetric conditions selected for the rhodium-catalysed 1,4-addition of arylboronic acid **47** to crotonate **128** were identified from two trial reactions (**Schemes 45** and **46**). The conditions in **Scheme 45** were selected because of their precedence to afford good asymmetric control on α,β-unsaturated esters with γ-amino groups.[172]   In contrast, the conditions in **Scheme 46** were optimised previously to impart excellent asymmetric control in the conjugate addition of arylboronic acid **47** to crotonolactone **119** (**Scheme 36**).[205]
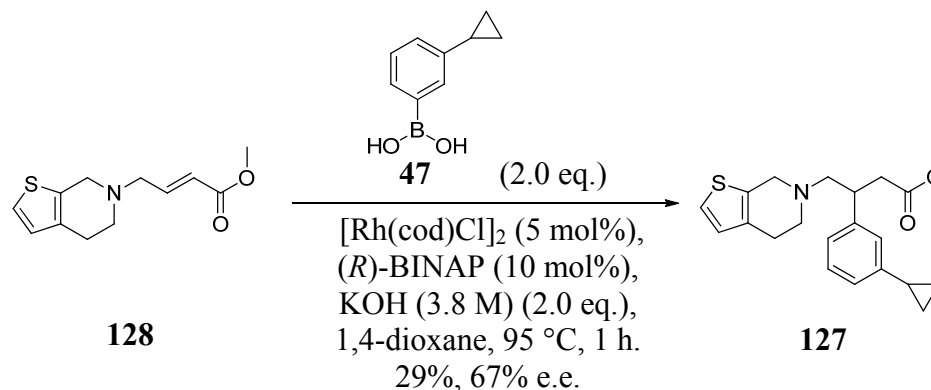
Scheme 45: Rhodium-catalysed 1,4-addition of arylboronic acid **47** to crotonate **128**.
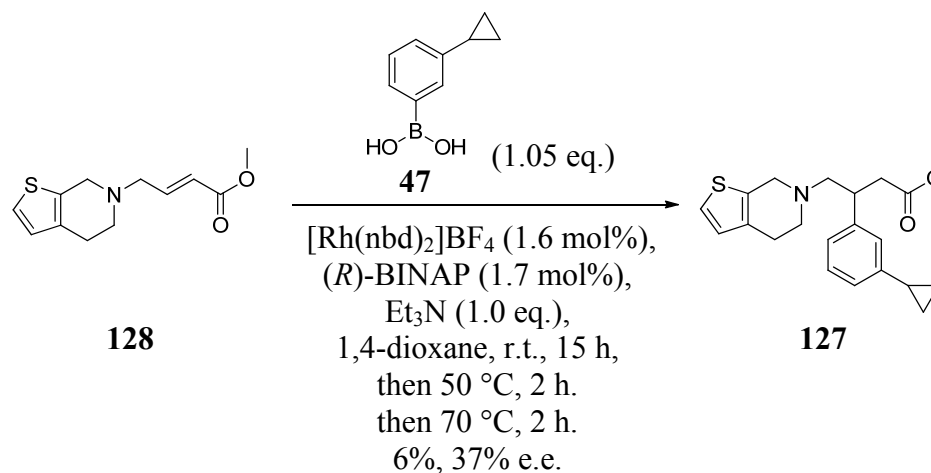
Scheme 46: Rhodium-catalysed 1,4-addition of arylboronic acid **47** to crotonate **128**.

The reactions were purified by MDAP chromatography to conveniently access a pure sample suitable for enantiomeric excess determination, which provides some explanation for the low isolated yields. The reaction in **Scheme 46** did not proceed at room temperature and required heating to 70 °C to show some conversion. Chiral

Christopher J Tame

HPLC analysis identified a low enantiomeric excess of 37%, which was clearly inferior to the conditions described in **Scheme 45**, which gave a 67% enantiomeric excess.

Consequently, the conditions in **Scheme 45** were reproduced on 8.9 g of crotonate **128**, which pleasingly produced desired thiophene **127** in 72% enantiomeric excess and 75% yield after column chromatography (**Scheme 47**). Resolution of the chirally-enriched mixture was achieved using chiral HPLC, to afford the desired single enantiomers in excellent yields (**Scheme 48**). The recovery of 88% is an improvement of 21% when compared to the earlier chiral resolution of thiophene **110**, which could be explained by purification problems with the tetrahydronaphthyridine moiety.
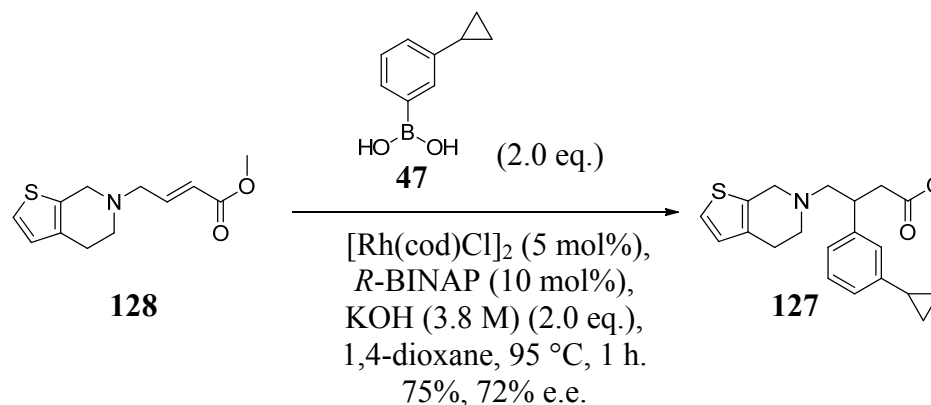
Scheme 47: Rhodium-catalysed 1,4-addition of arylboronic acid **47** to crotonate **128**.

127a (Enantiomer 1): 10%.
127b (Enantiomer 2): 78%.
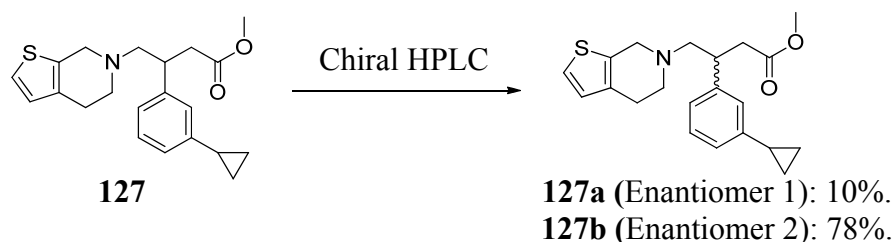
Scheme 61: Resolution of a chirally enriched mixture of thiophenes **127a** and **127b** using chiral HPLC.

The major enantiomer (thiophene **127b**) was subsequently carried through the remaining steps of the synthetic route to access final compound **85b** (**Schemes 49**

Christopher J Tame

and **50**). The one-pot C-H borylation/sp^2-sp^3 cross coupling protocol was repeated using a stoichiometric amount of alkyl bromide **18**, rather than the 0.7 equivalents used previously (**Scheme 43**). This had the aim of improving the low yield previously obtained and pleasingly, doubled the yield to 40%. However, because a comparative reaction was not undertaken at this scale under the original conditions, it is difficult to assign the improvement in the yield to the increased equivalents of alkyl bromide **18**. Nevertheless, this result highlights the robustness and applicability of this transformation.
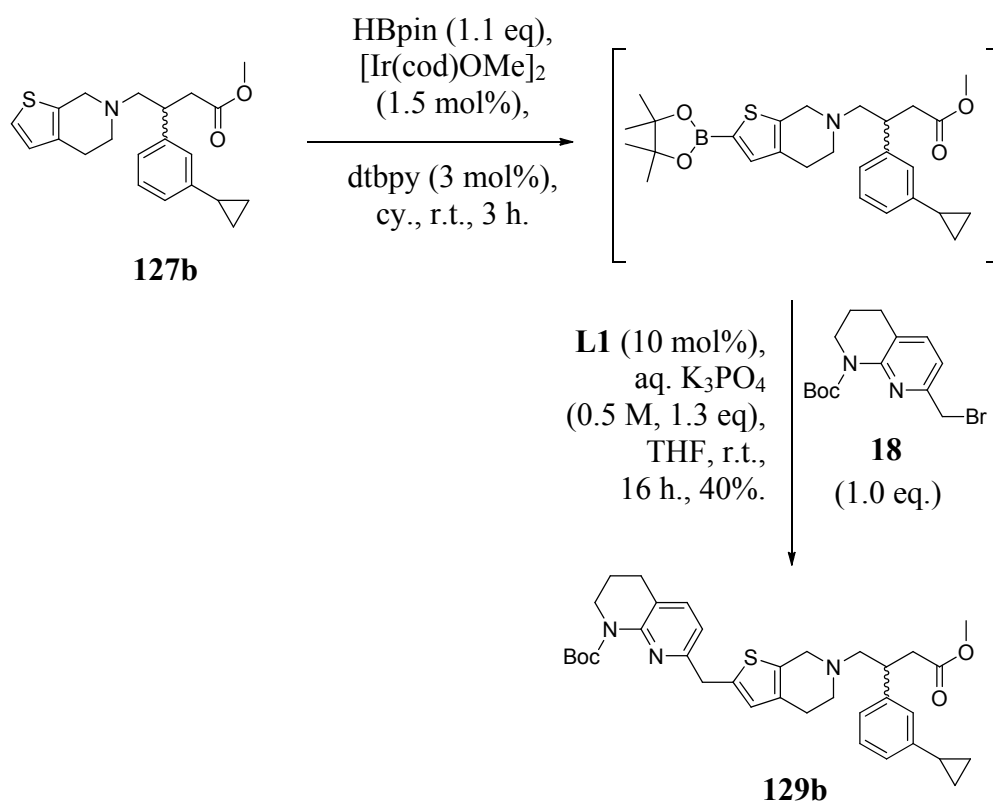
Scheme 62: Iridium-catalysed C-H borylation of thiophene **127b**, followed by palladium-catalysed sp^2-sp^3 cross coupling with alkyl bromide **18** to afford methylene-linked **129b**.

Finally, global deprotection was undertaken to afford 750 mg of desired target **85b** (**Scheme 50**). Difficulties were encountered in the isolation of **85b**, which resulted in the use of multiple purification techniques and a low isolated yield. Whilst sufficient material was obtained to facilitate the required biological testing, future

Christopher J Tame

optimisation of this step could investigate the use of reverse phase column chromatography.
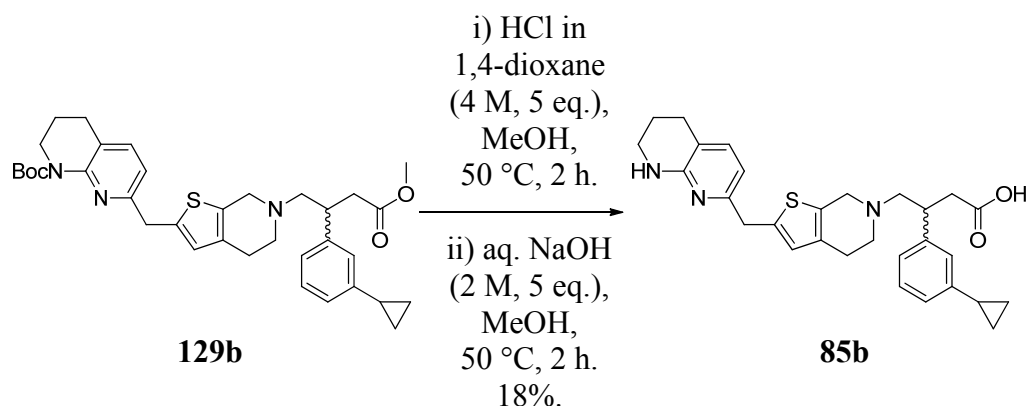
Scheme 50: The global deprotection of thiophene **129b** to afford final compound **85b**.

2.3.4 Biological data and evaluation

The RGD integrin cell adhesion affinities for thiophenes **84a**, **84b** and **85b** were compared against pyrazole **17b**, piperidine **12** and pyridine **13** (**Table 21**).[124] Thiophenes **84b** and **85b** were shown to be the most active enantiomers of the thiophene cores, which displayed a similar potency and RGD-integrin selectivity profile to pyrazole **17b**. The increased potency of thiophene **84b** verses **84a** confirms that the use of (*R*)-BINAP in the rhodium-catalysed conjugate addition step preferentially forms the more active enantiomer.

Christopher J Tame
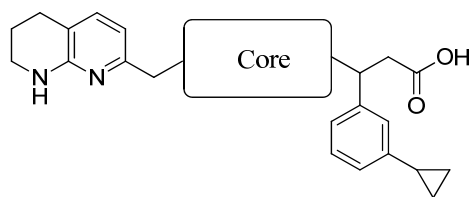
Compound	Core structure	Cell adhesion pIC$_{50}$			
		αvβ6	αvβ3	αvβ5	αvβ8
13		6.9	8.0	8.2	7.1
12		7.6	6.8	6.9	7.5
17b		7.3	6.5	6.4	6.4
84a		5.3	6.1	6.0	5.8
84b		7.1	6.6	6.3	6.9
85b		7.4	6.2	6.4	6.9

Table 21: The cell adhesion pIC$_{50}$ data of thiophene-containing integrin antagonists, compared against representative examples from different chemical series. The data are taken as an average of at least 4 tests (n ≥ 4).[124]

Whilst thiophene compounds **84b** and **85b** display different selectivities for αvβ6 against αvβ3, the relatively similar pIC$_{50}$ values fall within assay variability, and would need to be tested multiple times before reliable conclusions could be drawn. Taking this into account, it is reasonable to conclude that both thiophene compounds display at least five-fold selectivity for αvβ6 against αvβ3, which will require further optimisation to achieve the desired 10-fold selectivity profile, which was set out in the research aims. Even when considering this, the identification of an orally-bioavailable compound which has some selectivity for αvβ6 would still be a significant achievement within this research programme. Consequently, these compounds were progressed for further evaluation in the appropriate pharmacokinetic assays.

Christopher J Tame

Thiophenes **84b** and **85b** were then studied in a range of *in vitro* assays in order to predict their *in vivo* pharmacokinetic profile (**Table 22**).[126] Both compounds exhibited higher levels of lipophilicity, 1.5 log units higher than pyrazolopiperidine **17b** when Chrom LogD was measured at pH 7.4. This was the desired outcome of replacing the pyrazole ring with a thiophene, which had the aim of improving oral absorption through increased lipophilicity.

The pKa data was obtained on the less active enantiomer (**84a**).[152] It was considered that the pKa of both enantiomers would be identical, and using the inactive enantiomer in this way helped conserve supplies of the active enantiomer **84b** for other studies. The pKa data from thiophene **84a** suggested an increase versus pyrazole **17b**, although it was still considerably lower than piperidine **12** (*cf*. pKa: 9.9, 7.5, 4.0) and, therefore, not considered problematic. The measured pKa data for **84a** (8.2) was also much lower than the calculated value of 9.4 (**Table 19**), which confirmed the assumption that pKa values of these amines would be poorly predicted.

The MDCK permeability and CLND solubility of both thiophene-containing compounds was measured to be significantly higher than pyrazolopyrrolidine **17b**, which increases the likelihood of good oral absorption *in vivo*.[126] To help prioritise the compounds for further investigation, the *in vitro* clearance was accordingly measured in mouse liver microsomes.

The *in vitro* clearance value of 0.5 mL/min/Kg displayed by pyrazolopiperidine **17b** is the lowest measurable value in the assay, and predicts very low clearance in mouse *in vivo* PK studies. Unlike pyrazolopiperidine **17b**, however, the *in vitro* clearance displayed by thiophenes **84b** and **85b** was measured at the higher values of 1.4 and 2.8 mL/min/Kg, respectively (**Table 22**). Previous studies on other molecular series in our laboratories have shown that compounds with *in vitro* clearance values in this region (1.0 – 3.0 mL/min/Kg) are more likely to exhibit moderate clearance in mouse *in vivo* PK studies.[126] Although moderate clearance is predicted, *in vitro* clearance values in this range are still acceptable for further investigation in an *in vivo* study.

Christopher J Tame
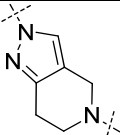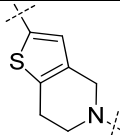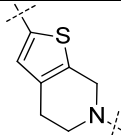
Compound no.	17b	84b	85b
Molecular weight	472	488	488
Chrom LogD pH 2.0, 7.4, 10.5	-0.3, 3.0, 2.0	0.1, 4.5, 3.3	0.3, 4.6, 3.1
pKa (potentiometric)	7.8, 5.5, 4.0	8.2, 6.8, 4.1*	NT
Permeability (MDCK, nm/sec)	23	427	349
Solubility (CLND, µg/mL)	173	162	128
IVC (mouse microsomes, mL/min/g)	0.5	1.4	2.8

* pKa data obtained on enantiomer **84a**.

Table 22: The comparison of physicochemical properties and *in vitro* pharmacokinetic data between pyrazole **17b**, thiophene **84b** and thiophene **85b**.[152] NT = not tested.

To summarise, the lipophilicity, pKa and mouse microsomal clearance of thiophene **84b** satisfied the requirements which were anticipated to impart good oral absorption in the mouse. Accordingly, thiophene **84b** was progressed to the mouse short oral absorption study (**Table 23**).[126]

After being dosed orally at 3 mg/kg, thiophene **84b** demonstrated a moderate hepatic clearance of 47 mL/min/kg, which equates to 52% liver blood flow and was on the upper limit of acceptability.[126] Pleasingly, the total drug level in the hepatic portal vein was considerably higher than pyrazole **17b**, with an AUC value of 2502 ng/h/mL. This significant increase in oral absorption represented the first αvβ6-selective antagonist to display high levels of absorption in the SOA model, which warranted further investigation.

Christopher J Tame

Compound number	Structure	Hepatic clearance (mL/min/Kg) [% mouse liver blood flow]	HPV AUC (ng/h/mL)
17b		23 [27%]	417
84b		47 [52%]	2502
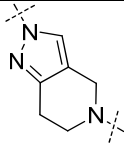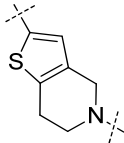
Table 23: Thiophene **84b** and pyrazole **17b** in the short oral absorption *in vivo* mouse model.[126]

To provide a more accurate representation of the pharmacokinetic profile of thiophene **84b**, a conventional mouse PK study was run using intravenous (i.v.) and oral (p.o.) administration techniques (**Table 24**).[126]

Pharmacokinetic studies in our laboratories usually administer a test compound intravenously using a bolus dose. This is a single injection of the full dose, which is used to help minimise discomfort to the animal and to improve ease of administration. However, this technique is unlikely to provide an accurate representation of complete oral absorption, which is what the i.v. leg is intended for. In reality, the dose is more likely to be absorbed more slowly. The i.v. infusion administration technique more accurately represents this by slowly dosing the compound over a longer time course. To compare these two methods, both were investigated with thiophene **86b**.

113

Christopher J Tame
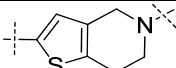
84b in C57BL6/J Jax female mice	p.o.	i.v. bolus	i.v. infusion
Dose (mg/kg)	3.2	1.1	1.2
AUC$_{(0-\infty)}$ (ng/h/mL)	1075	642	441
Bioavailability (F%)	-	58	93
Clearance (Cl$_b$) (mL/min/Kg), (% liver blood flow)	-	29 (32%)	45 (50%)
Half life (T ½) (h)	2.2	1.7	2.0
Volume of distribution (V$_d$) (L/Kg)	-	1.7	4.1

Table 24: Mouse *in vivo* PK study using i.v. and p.o. administration of **84b**.[126]

Pleasingly, both administration methods showed good oral bioavailability and moderate clearance, which supported the findings in the SOA model. The lower clearance observed after bolus administration could be a result of the highly concentrated dose saturating clearance mechanisms. This would result in lower levels of recorded clearance and a higher overall drug level (AUC). This higher AUC level also explains why the bioavailability is lower after bolus administration than *via* infusion, as when comparing to p.o. the i.v. dose is considered 100% absorption.

The lower volume of distribution observed after the bolus dose could also be explained by the saturation of tissue after the highly concentrated dose. This explains why the half lives of the two administration techniques are similar, even though the clearances are different. A half life of 2 hours could potentially be too short to support a twice daily dosing regimen, which would be required to improve upon the three daily doses required for IPF treatments with Pirfenidone. Based on this, further optimisation of the half life may be required.

Thiophene **84b** represents the first compound to display good oral bioavailability and selectivity for αvβ6 over the other RGD integrins in our assays. This breakthrough demonstrates that zwitterionic integrin inhibitors with a second basic centre can be

Christopher J Tame

readily absorbed in mice, and display suitable clearance levels for oral administration. These findings prompted further investigation into the *in vivo* activity of thiophene **84b**.

The relationship between *in vivo* activity and the fraction of free drug available to interact with the biological target is a contentious issue. The accepted theory suggests that a drug molecule cannot interact with its biological target when it is bound to other proteins in the blood.[208] It follows, therefore, that a drug is also shielded from clearance mechanisms whilst protein bound, which helps improve the pharmacokinetic profile.[208] *In vitro* assays are routinely used to assess the extent of plasma protein binding, although the ability of these assays to predict the *in vivo* efficacy of a drug is disputed.[209,210]

The plasma protein binding has been assessed for thiophenes **84b** and **85b** using a number of *in vitro* assays (**Table 25**).[152] Human serum albumin (HSA) and α-glycoprotein (AGP) are the two most abundant forms of plasma proteins and are used in high throughput assays which measure binding of lead compounds to both of these proteins. These assays use columns with the protein as a stationary phase and record the time taken for the compound to elute. The more sophisticated blood binding assay analyses the concentration of the compound between two chambers separated by a permeable membrane. An initial measurement is taken when both chambers contain a saline solution. Blood is then added to one of the chambers and the compound concentration is reanalysed. The difference between the two measurements indicates the amount of compound bound to the blood.[126]

	HSA (%)	AGP (%)	Blood (%)		
			Mouse	Rat	Human
Thiophene **84b**	97.3	94.4	-	-	-
Thiophene **85b**	97.4	93.2	99.5	> 99.9	> 99.9

Table 25: *In vitro* protein binding assays for Thiophenes **84b** and **85b**.[126,152]

Christopher J Tame

When assessed in the various assay formats, both compounds demonstrated very high levels of protein binding and thiophene **85b** displayed very high levels of blood binding. These high levels, however, do not necessarily indicate low *in vivo* efficacy. Some marketed drugs such as the orally administered asthma treatment Montelukast,[211,212] have similar levels of protein and blood binding when profiled in our assays.[126] The use of a mouse *in vivo* study would, therefore, help understand whether this high protein binding negatively affects efficacy. However, reliable *in vivo* disease models of fibrosis are rare and expensive to run when compared to the cost of molecular optimisation. Consequently, further modification of the core was attempted to reduce protein binding whilst maintaining good oral absorption.

It was observed that the HSA and AGP binding of these compounds increased with lipophilicity (**Table 26**), which is in accord with literature findings.[213] A compound which possessed an intermediate level of lipophilicity between pyrazole **17b** and thiophene **84b** could potentially reduce protein binding compared to thiophene **84b**, but still impart sufficient oral absorption for *in vivo* efficacy.

	HSA (%)	AGP (%)	Chrom LogD pH 2.0, 7.4, 10.5
Pyrazole **17b**	93.5	81.9	-0.3, 3.1, 2.0
Thiophene **84b**	97.3	94.4	0.1, 4.5, 3.3

Table 26: The protein binding and lipophilicity values for Pyrazole **17b** and Thiophene **84b**.[152]

2.4   Optimisation of lipophilicity for improved free fraction

The thiophene-containing αvβ6 antagonists show some promise, certainly in terms of oral absorption and bioavailability in the mouse. However, the high plasma protein binding associated with these compounds may preclude any *in vivo* efficacy. This was thought to be driven by lipophilicity, which prompted investigation into replacing the thiophene with less lipophilic analogues.

Christopher J Tame

Accordingly, the analysis of fused bicyclic cores was revisited to identify compounds which possessed lipophilicity greater than pyrazole **17b** but less than thiophene **84b**. This identified furan (**86**/**87**) and thiazole (**88**/**89**) containing cores as potential replacements to test this hypothesis (**Table 28**).

These cores were initially to be synthesised as one regioisomer of the core, which was selected based on synthetic tractability and availability of the appropriate starting materials. In addition, these compounds would be submitted to biological screening as racemic mixtures, which would avoid the time-consuming and low yielding chiral HPLC step. Compounds which displayed promising potency and physicochemical properties would then be synthesised as single enantiomers of both regioisomers for more complete pharmacological evaluation.

It is possible that different enantiomers of a compound bind differently to plasma proteins, as a result of their chiral nature. Consequently, it follows that the racemate may not provide an accurate representation of the plasma protein binding for either enantiomer. To investigate this further, analysis of the plasma protein binding of thiophene and pyrazole-containing compounds was undertaken (**Table 27**). This revealed very little variation in HSA and AGP binding and supported the use of racemic mixtures to investigate the effect of lipophilicity on protein binding.

Compound	HSA (%)	AGP (%)
Pyrazole **17a**	92.2	78.7
Pyrazole **17b**	93.5	81.9
Thiophene **84a**	97.0	94.4
Thiophene **84b**	97.3	94.4

Table 27: The comparison of plasma protein binding between enantiomers of pyrazole and thiophene containing $\alpha v\beta 6$ antagonists.

Christopher J Tame
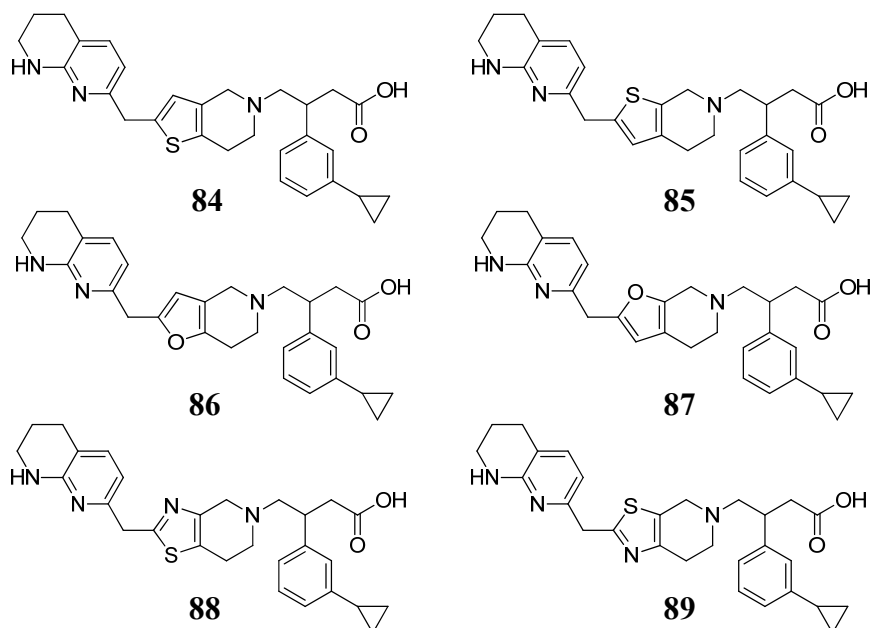
n.	MW	cLogP	Aromatic ring no.	Rotatable bond no.	Calculated pKa Basic	Acidic
84	487.7	5.3	3	7	9.4, 6.4	4.6
85	487.7	5.3	3	7	9.7, 6.4	4.6
86	471.6	4.8	3	7	9.0, 6.2	4.4
87	471.6	4.8	3	7	9.1, 6.2	4.3
88	488.6	4.3	3	7	8.0, 6.0	4.2
89	488.6	4.3	3	7	8.9, 6.0, 0.5	4.3

Table 28: The physicochemical properties of a range of potential integrin inhibitors with fused heterocyclic cores.

2.4.1 Synthesis of furan 86

The synthesis of furan and thiazole-containing αvβ6 antagonists was undertaken in parallel and the synthesis of furan **86** is presented first to provide continuity with the previous synthetic methodology used to access thiophenes **84** and **85**.

The commercial availability of furanylpiperidine **130** prompted the application of the same synthetic route used to access thiophene **85b**, which successfully delivered the desired target **86** in just four steps and in similar yields (**Scheme 51**). The rhodium-

Christopher J Tame

catalysed 1,4-addition was undertaken with 10 mol% catalyst loading, rather than the 30 mol% used previously in the synthesis of thiophene **127**. This required a longer reaction time and resulted in a lower yield when compared to the formation of thiophene **127** *cf*. 90% (**Scheme 43**). A complex reaction profile was observed by LCMS analysis of the crude reaction mixture, which could be a result of increased side-reactions at longer reaction times. Repeating the reaction using 30 mol% catalyst loading is, therefore, expected to reduce reaction time and improve the yield to comparable levels observed with thiophene **127**. The overall success of this synthetic route also demonstrates the applicability of the one-pot C-H borylation / cross-coupling protocol to different heterocycles.
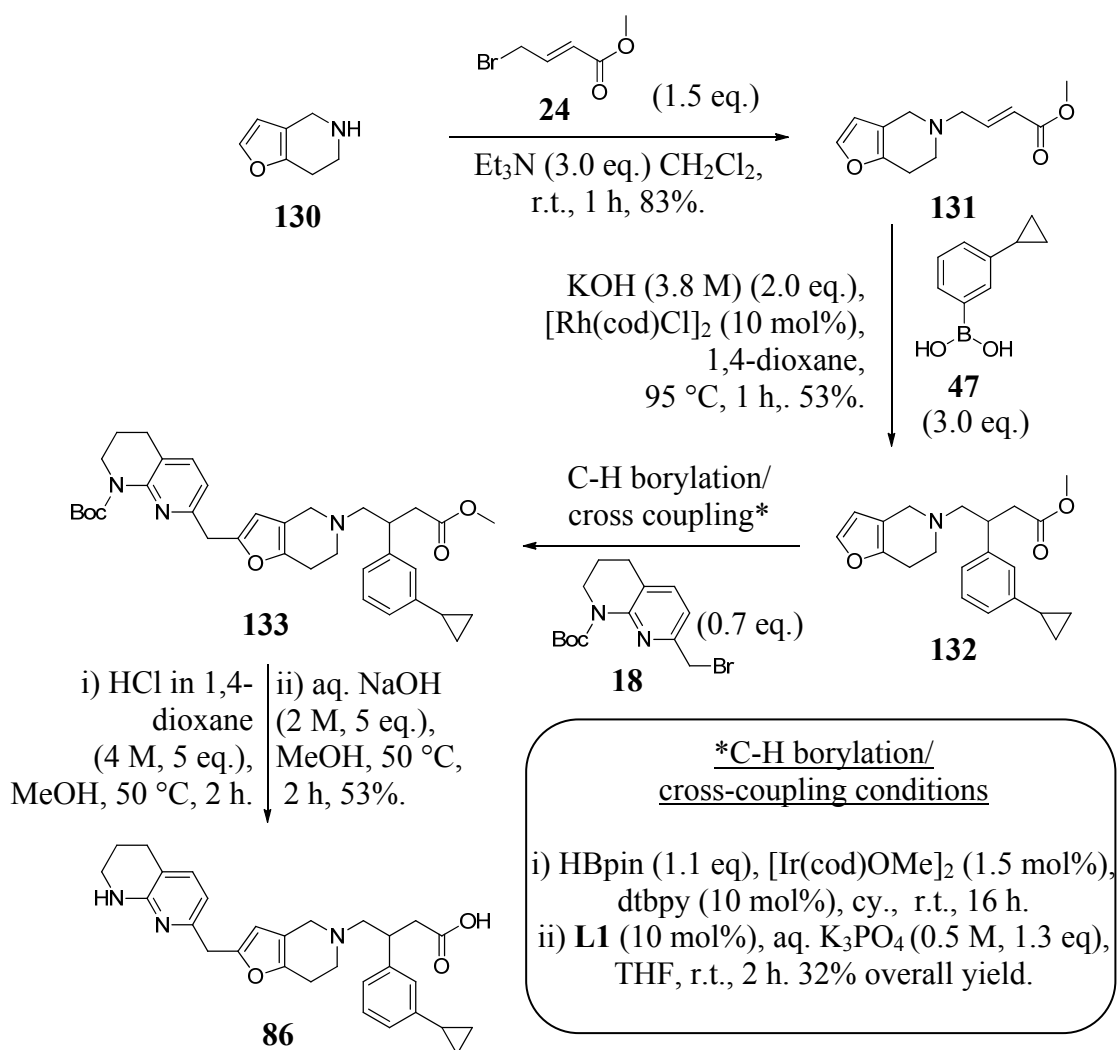
Scheme 51: The synthetic route to access furan **86**.

Christopher J Tame

2.4.2 Synthesis of thiazole 89

Initial synthetic efforts towards thiazole **89** attempted to reproduce the route used to access thiophene **85b** and furan **86** (**Scheme 54**). This was based on the commercial availability of thiazolopiperidine **134** and the synthetic efficiency of the already validated route, which only required four steps. A search of the literature, however, did not reveal any precedence for the isolation or characterisation of 2-thiazoleboronate species. Having stated this, previous success with thiophene **85b** and furan **86** provided confidence to attempt this approach.

In contrast to the synthesis of thiophene **85b**, purification of α,β-unsaturated intermediate **135** was attempted (**Scheme 52**), which aimed to improve the yield of the following conjugate addition step. However, poor recovery from column chromatography resulted in a disappointing yield. It is unclear why a low yield was obtained, although analysis of the impurities isolated after chromatography could have helped this. Even though a low yield was obtained, a sufficient quantity of material was recovered to enable the next synthetic transformation. Further investigation into the low recovery of intermediate **135** was, therefore, not undertaken.
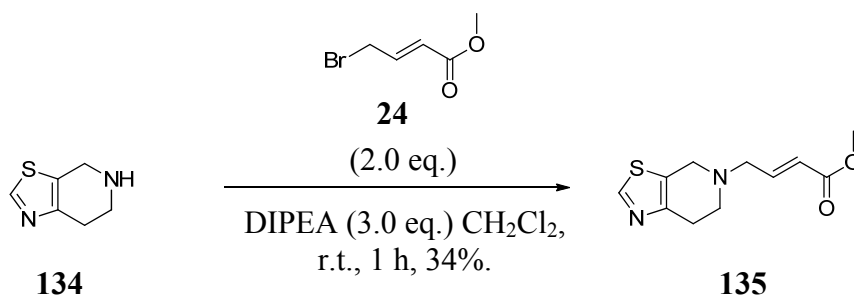
Scheme 65: The alkylation of thiazole **134** with bromocrotonate **24**.

The rhodium-catalysed 1,4-addition of arylboronic acid **47** with α,β-unsaturated **135** proceeded well to afford thiazole **136** in good yield (**Scheme 53**). The higher catalyst loadings were used to ensure optimal conversion, and were not considered an issue on this relatively low scale (1.4 mmol).

Christopher J Tame
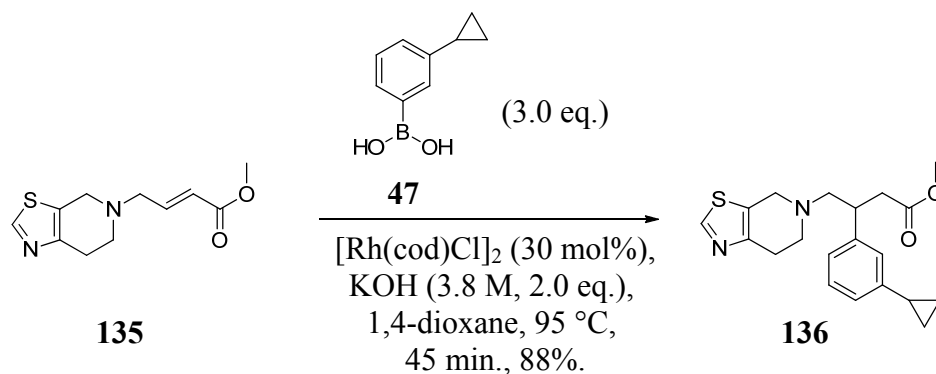
Scheme 53: Rhodium-catalysed 1,4-addition of arylboronic acid **54** to crotonate **135**.

With the appropriately decorated intermediate (**135**) in-hand, the one-pot C-H borylation/cross coupling conditions were attempted (**Scheme 54**). Thiazole **136** was submitted to iridium-catalysed borylation conditions, but after three hours at room temperature, LCMS analysis of the crude reaction mixture did not indicate any reaction to have occurred. It was reasoned that borylated intermediate **137** was unstable under the analytical conditions and rapidly decomposed to give thiazole **136**. Although the next step was subsequently undertaken, LCMS analysis of the crude reaction mixture could not identify any material consistent with the product.
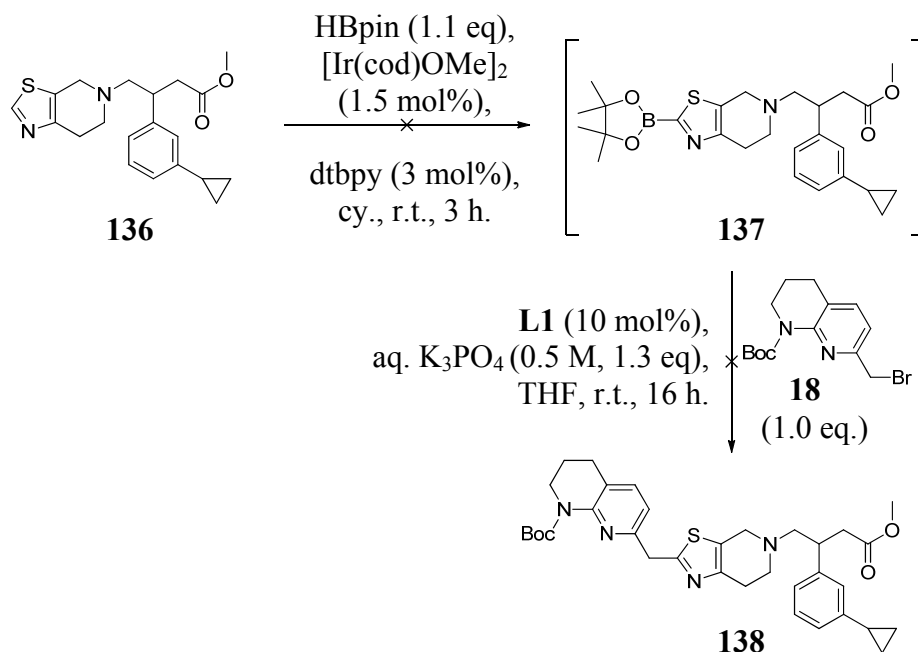
Scheme 67: Attempted synthesis of thiazole **138** using the developed one-pot C-H borylation/cross coupling protocol.

Christopher J Tame

A survey of the literature revealed a direct sp^2-sp^3 cross coupling reaction between benzothiazole **139** and benzyl carbonate **140** had been reported (**Scheme 55**).[214] This reaction proceeded without the need of an organometallic intermediate such as pinacolborane **141**, which avoided the problems with formation and reactivity of these species.
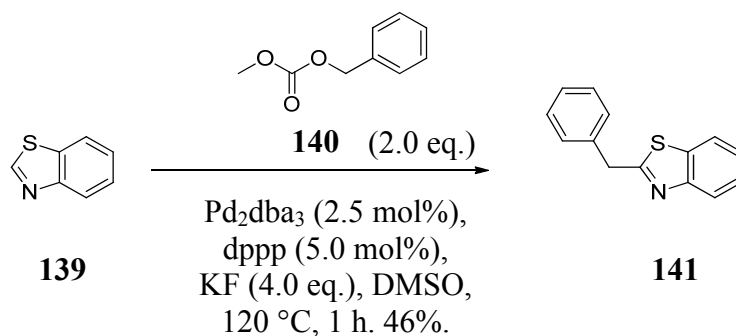
Scheme 55: Palladium-catalysed direct benzylation of benzothiazole **165** with benzyl carbonate **139**.[214]

Accordingly, these conditions were applied to the reaction of thiazole **136** with benzyl carbonate **144** (**Scheme 57**), which was formed in two steps from commercially available aldehyde **96** (**Scheme 56**).
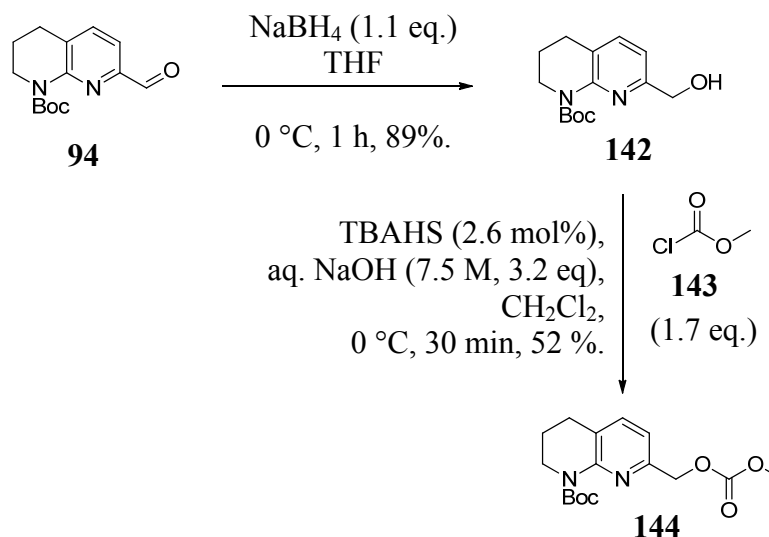
Scheme 56: The formation of methyl carbonate **144** from commercially available aldehyde **96**.

Christopher J Tame

Benzyl carbonate **144** was subsequently submitted to the palladium-catalysed cross coupling protocol with thiazole **136** (**Scheme 70**). Unfortunately, LCMS analysis of the crude reaction mixture indicated only unchanged starting materials. Consequently, further investigation in to this reaction was abandoned and other methods of accessing the desired thiazole **89** were subsequently investigated.
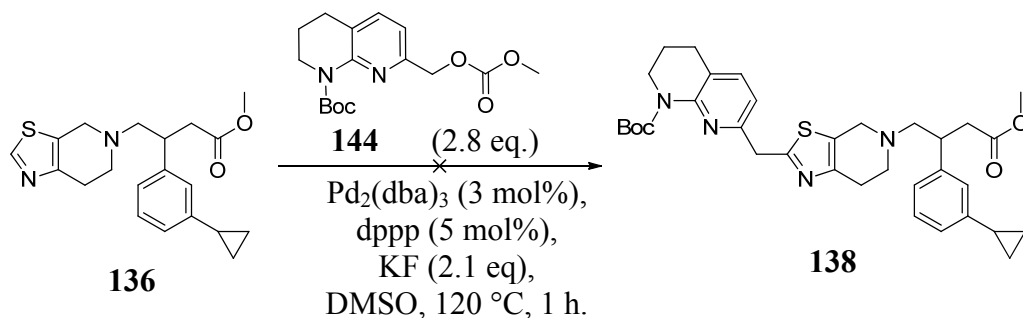
Scheme 57: Attempted synthesis of thiazole **89**.

The reaction between thioamides and α-bromo ketones provides an alternative method to access fully-substituted thiazoles.[215,216,217] This ring-forming reaction has been utilised in the synthesis of a closely related thiazolopiperidine ring system (**147**, **Scheme 58**),[218] which provides confidence of its successful application in the synthesis of thiazole **89**.
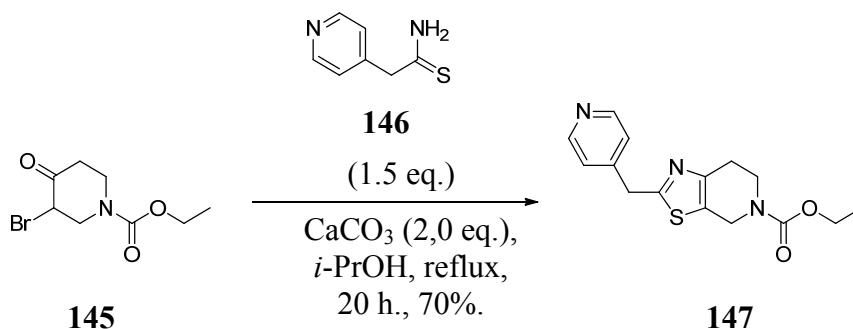
Scheme 58: The condensation of thioamide **146** and α-bromopiperidine **145** to form thiazole **147**.

An alternative proposed route used to access thiazole **89** is therefore presented in **Scheme 59**, which incorporates this key ring forming step. Thioamide **150** is expected to be formed in two steps from commercially available methyl ester **148** using methanolic ammonia solution to form primary carboxamide **149**,[219] followed by treatment with Lawesson's reagent.[220]

Christopher J Tame
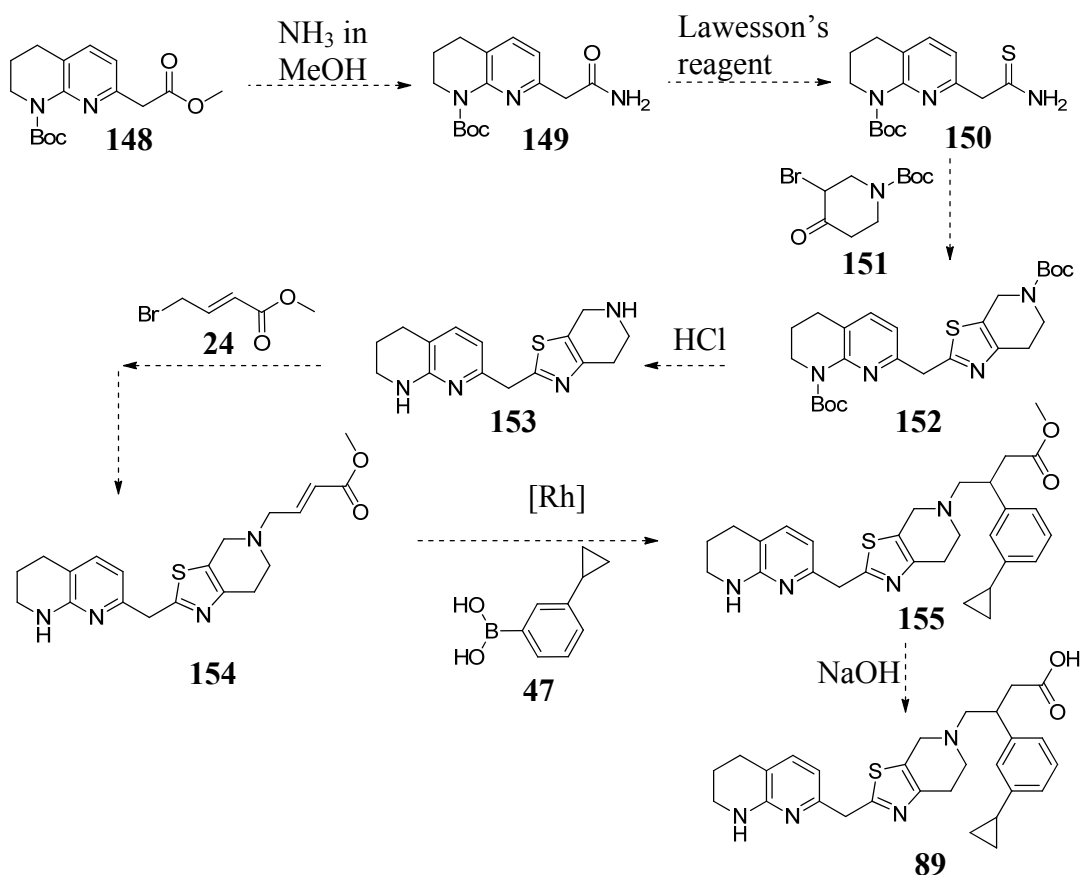
Scheme 72: Proposed route to access thiazole **89**.

It was considered that an unprotected tetrahydronaphthyridine could participate in unwanted alkylation reactions during the ring forming step of thiazole **152**. As a result, the conditions used to access thioamide **152** were modified to ensure Boc-protection of the tetrahydronaphthyridine was maintained. Accordingly, the formation of primary carboxamide **149** was attempted using a more concentrated methanolic ammonia solution at room temperature, rather than the elevated temperatures utilised in the literature. Pleasingly, this accessed primary carboxamide **149** in quantitative yield. (**Scheme 60**).
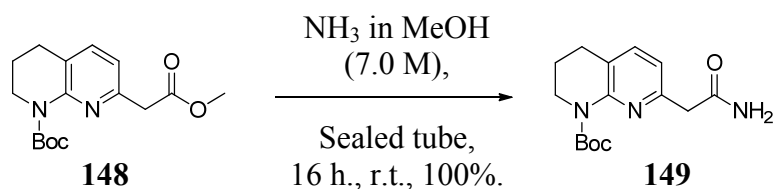
Scheme 60: The transformation of methyl ester **148** to primary carboxamide **149** under mild conditions.

Christopher J Tame

The formation of thioamide **150** was attempted using literature conditions, although LCMS analysis of the crude reaction mixture indicated mainly the Boc-deprotected analogue (**156**), along with a range of unidentifiable impurities (**Scheme 61**).
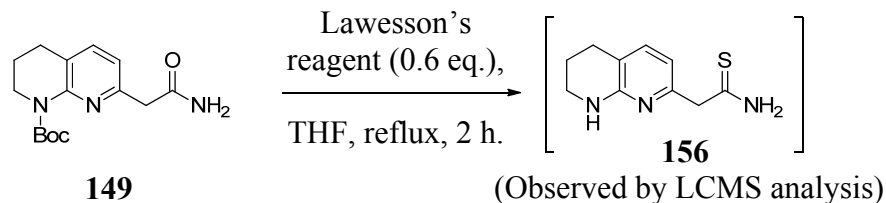
Scheme 61: The formation of thioamide **156** with Boc deprotection of the tetrahydronaphthyridine.

It was reasoned that Boc deprotection could be suppressed by reducing the reaction temperature. It was also observed that primary carboxamide **149** was poorly soluble in THF, which may be preventing the reaction to proceed at a lower temperature. A brief solvent screen with alternative ethereal solvents TBME, CPME and 1,4-dioxane revealed that 1,4-dioxane gave complete dissolution at room temperature. The reaction was subsequently repeated in 1,4-dioxane at room temperature, which accessed the desired Boc-protected thioamide **150** in moderate yield (**Scheme 62**). Good conversion to the desired product was observed from analysis of the crude reaction mixture by LCMS, suggesting that the disappointing yield could be due to inefficient work-up and purification techniques.
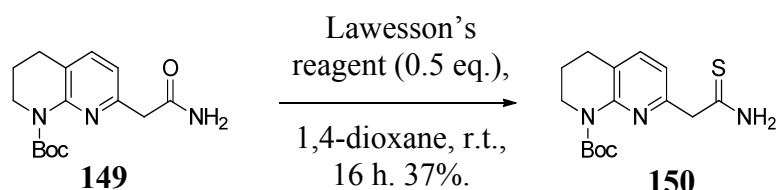
Scheme 62: The formation of thioamide **150** with Boc protection of the tetrahydronaphthyridine retained.

With thioamide **150** in-hand, subsequent thiazole ring formation with commercially available α-bromopiperidone **151** was undertaken using the literature conditions, which gave thiazole **157** in good yield (**Scheme 63**). The solvent was changed from

Christopher J Tame

isopropanol to 1,4-dioxane as a result of its superior solvation properties. Boc-deprotection of the tetrahydronaphthyridine was observed after ring formation, although this was planned for removal in the next step, and was therefore not considered an issue.
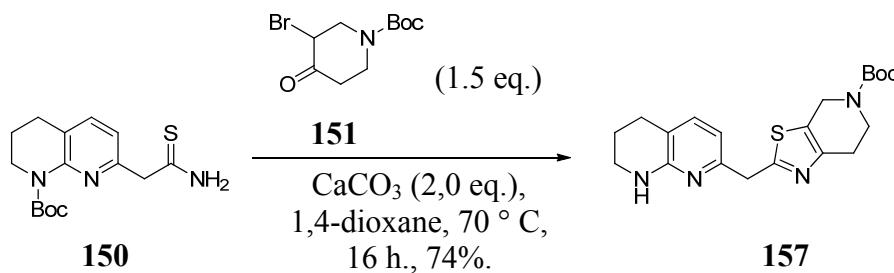
Scheme 63: Thiazole ring formation from thioamide **150** and α-bromopiperidone **151**.

The transformation of thiazole **157** to final product **89** was achieved using the previously established conditions validated in the synthesis of pyrazole **17b** and thiophene **84b** (**Scheme 64**). The alkylation of amine **153** with bromocrotonate **24** used increased equivalents of alkylating agent and base to form the α,β-unsaturated ester **154** in excellent yield (96%). The rhodium-catalysed 1,4-addition of arylboronic acid **47** to α,β-unsaturated ester **154** reached completion in just 5 minutes, which was accomplished using a pre-heated oil bath. SCX-silica chromatography of methyl ester **155** gave sufficient purity by LCMS to attempt the next step directly. Subsequent sodium hydroxide-mediated hydrolysis of methyl ester **155** gave desired product **89** in 63% overall yield, which was isolated using MDAP purification.

Christopher J Tame
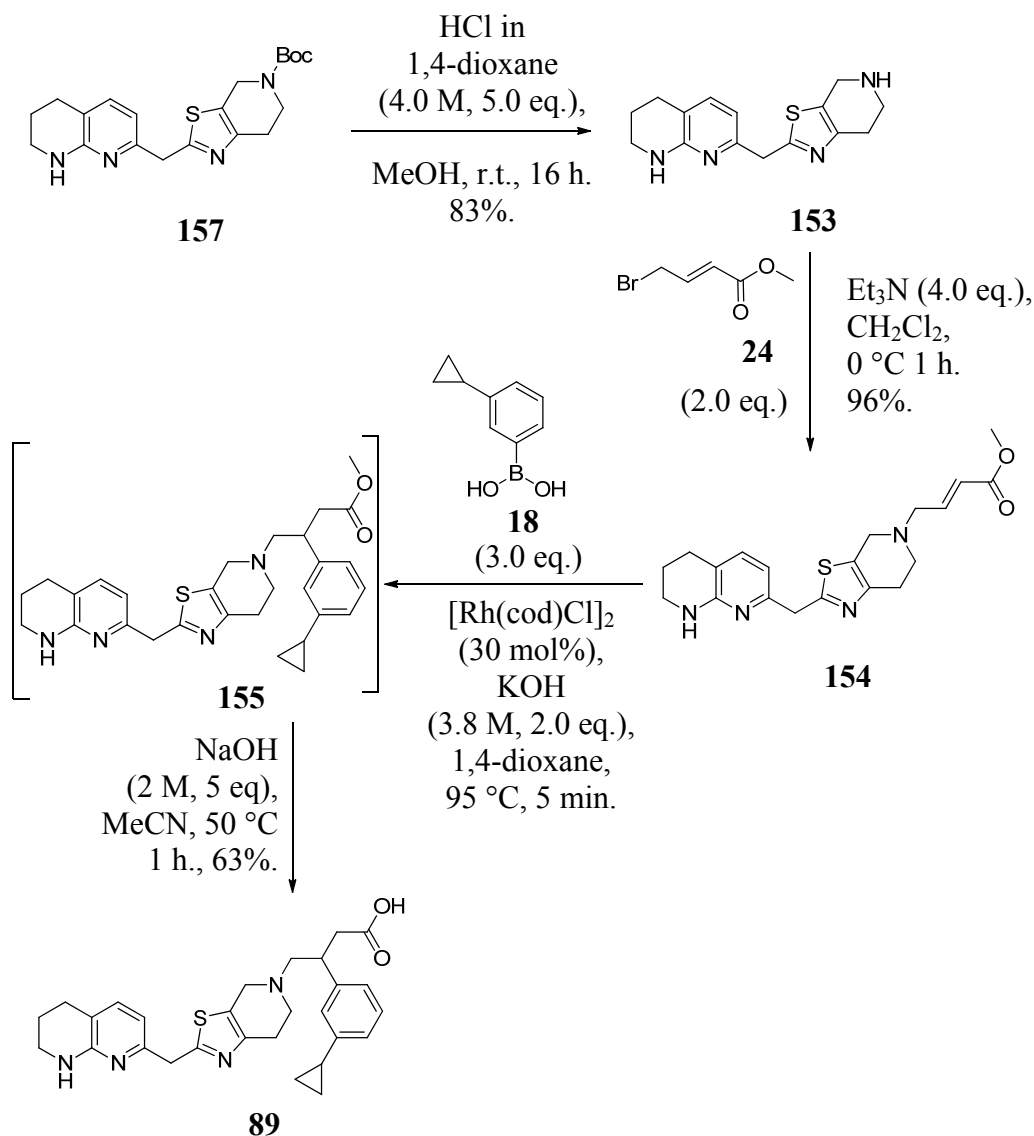
Scheme 64: The transformation of thiazole **157** to final target **89**.

2.4.3   Biological data and evaluation

With furan **86** and thiazole **89** successfully synthesised, the RGD integrin affinities, physicochemical properties, and protein binding data were subsequently obtained (**Table 29**). The results show that both compounds impart good potency for αvβ6, however they exhibit marginal selectivity over the other RGD integrins. Both compounds also have good solubility, which was expected to be driven mainly by the zwitterionic nature of the molecules. The lipophilicity of furan **86** and thiazole **89**

Christopher J Tame

neatly occupy the middle ground between pyrazole **17b** and thiophene **84b**, which is likely to be the main contributing factor to the permeability values observed, which also reside between pyrazole **17b** and thiophene **84b**. Unfortunately, whilst the lipophilicity was reduced in both cases, no significant reduction in protein binding was observed.

Compound no.	17b*	89	86	84b*
$\alpha v \beta 6$ (pIC$_{50}$)	7.3	7.1	7.3	7.1
$\alpha v \beta 3 / \alpha v \beta 5 / \alpha v \beta 8$ (pIC$_{50}$)	6.5/6.4/6.4	6.5/6.7/6.7	6.4/6.7/6.6	6.6/6.3/6.9
Molecular weight	472	489	472	488
Chrom LogD pH 2.0/7.4/10.5	**-0.3/3.1/2.0**	**-0.1/3.7/2.4**	**0.0/4.2/3.0**	**0.1/4.5/3.3**
pKa (potentiometric)	7.8, 5.5, 4.0	NT	8.4, 7.2, 4.5	8.2, 6.8, 4.1*
Plasma protein binding (HSA%/ AGP%)	**93.5/ 81.9**	**97.0/ 87.4**	**96.6/ 89.0**	**97.3/ 93.4**
Perm. (MDCK nm/sec)	23	217	196	320
Solubility (CLND µg/mL)	173	182	147	162

Table 29. The RGD binding affinities and physicochemical properties of **17b**, **89**, **86** and **84b**. * denotes single enantiomer.[124,126,152]

2.4.4 Summary of optimisation efforts towards enhancing the lipophilicity of pyrazolopiperidine 17b

In summary, increasing the lipophilicity of a pyrazolopiperidine integrin antagonist (**17b**) has identified a number of compounds which possess improved permeability. The most lipophilic example, thiophene **84b**, displayed good oral absorption and excellent bioavailability in mouse *in vivo* PK studies. A moderate clearance and half

life were also determined, which potentially would require further optimisation before candidate selection could be made.

Despite the improvements, all compounds with increased lipophilicity possess high levels of plasma protein and blood binding, which could negatively impact *in vivo* efficacy. Before an *in vivo* study can be initiated, further investigation towards the identification of selective αvβ6 antagonists with good oral bioavailability and reduced protein binding was warranted.

The original hypothesis (a reduction in pKa improved oral absorption) could not be accurately investigated from comparisons between pyrazolopiperidine **17b** and other, more basic, antagonists. This was a result of the low lipophilicity of **17b**, which resulted in relatively low oral absorption. The greater lipophilicity of thiophene **84b**, however, enabled comparisons between compounds possessing similar physicochemical properties. The similar lipophilicities of thiophene **84b** and piperidine **14** more reliably suggest that the improved oral absorption could also be a function of the reduced pKa of thiophene **84b**, rather than increased lipophilicity (**Table 30**).
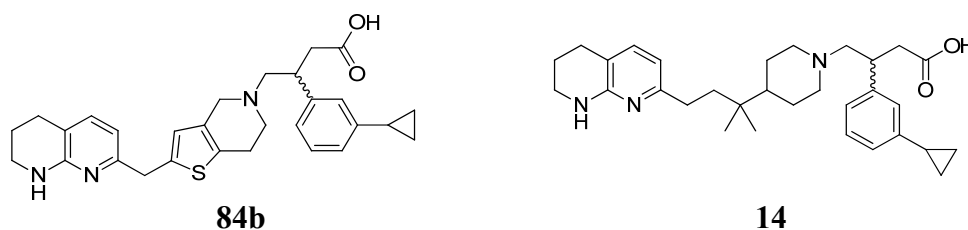
Compound no.	Chrom LogD	pKa (potentiometric)	MDCK (nm/sec)	HPV AUC (ng/h/mL)
Thiophene **84b**	4.5	8.2, 6.8, 4.1	320	2502
Piperidine **14**	4.6	9.7, 8.9, 3.9	106	234

Table 30: The comparison of lipophilicity, pKa and oral absorption after a 3mg/Kg p.o. dose of thiophene **87b** with piperidine **14**.[152]

Christopher J Tame

2.5 Efforts towards balancing oral absorption and free fraction

From comparing piperidine **14** with thiophene **84b**, an alternative approach to improving the oral absorption of pyrazole **17b** could involve reducing the pKa further, rather than increasing the lipophilicity. If this was achieved whilst maintaining a similar lipophilicity to **17b**, then it is feasible that the plasma protein binding would also stay at a lower level. Based on this, the previous analysis of fused-heterocyclic cores was subsequently revisited in order to identify compounds to test this hypothesis.

In contrast to the previous analysis, the LogP and pKa values were calculated for the entire molecule rather than the isolated cores. This was to ensure that all pKa values could be analysed, particularly the tetrahydronaphthyridine, which could vary depending on the nature of the heterocyclic atom connecting it. Reducing the pKa of this centre is expected to reduce key interactions with the aspartic acid residue in the αv subunit, which could result in loss of activity. A minimum reduction of pKa was set at 0.5 log units to allow for inaccuracies in the calculation. The results are displayed in **Table 31**, and suitable compounds were progressed to *in silico* toxicity profiling as described previously.
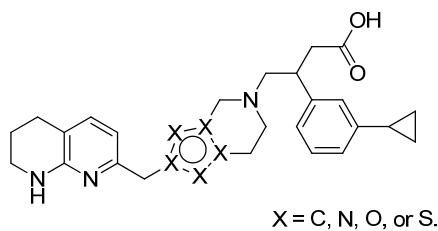
Christopher J Tame

X = C, N, O, or S.

Compound no.	Core structure	cLogP	ChemAxon pKa	Decrease pKa and maintain/reduce cLogP vs 17?
158		3.8	8.2, 6.6, 4.3	No
159		3.8	8.0, 6.6, 4.3	No
160		4.2	8.3, 7.0, 4.3	No
161		3.4	7.7, 6.7, 4.3	Yes
84		5.3	9.4, 6.4, 4.6	No
85		5.3	9.7, 6.4, 4.6	No
86		4.8	9.0, 6.2, 4.6	No
87		4.8	9.1, 6.2, 4.6	No
17		**3.5**	**8.2, 6.6, 4.0**	-
162		3.5	7.8, 6.5, 4.0	No

Table 31: Calculated lipophilicities and pKas for a range of fused heterocycles. Continues overleaf

Christopher J Tame

Compound no.	Core structure	cLogP	ChemAxon pKa	Decrease pKa and maintain/reduce cLogP vs 17?
163		3.6	7.5, 6.3, 4.0	No
164		2.8	7.8, 6.4, 4.0	No
165		3.4	7.2, 6.2, 3.8	Yes
88		4.3	8.0, 6.0, 4.2	No
89		4.3	8.9, 6.0, 4.3	No
166		3.4	8.6, 5.8, 4.2	No
167		3.4	7.8, 5.8, 4.2	No
168		3.1	7.6, 6.2, 3.8	Yes
169		2.9	7.0, 5.9, 3.8	Yes
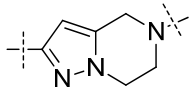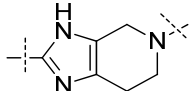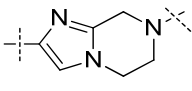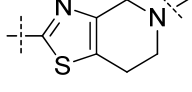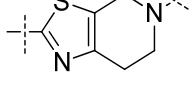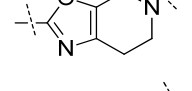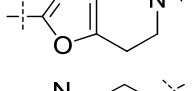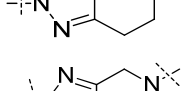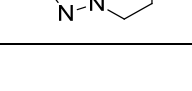
Table 31 continued: Calculated lipophilicities and pKas for a range of fused heterocycles.

Other methods of reducing the pKa of pyrazole **17b** was also considered (**Figure 30**). This identified manipulation of the saturated ring as a potentially subtle method of reducing the pKa, without relying on the addition of new functionalities which add molecular weight and may not be tolerated. Accordingly, pyrazole **170** was selected for further investigation (**Table 32**).

Christopher J Tame

170
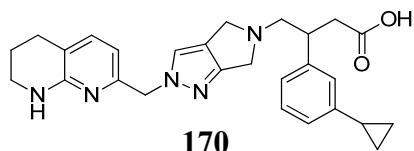
Compound no.	cLogP	ChemAxon pKa	Decrease pKa and maintain/reduce cLogP vs 17?
170	3.2	7.2, 6.3, 3.8	Yes

Table 32: Calculated lipophilicities and pKas for pyrazolopyrrolidine **170**.

The relevant compounds of interest were then screened against an in-house toxicity database. As previously discussed, this is compiled from published toxicity studies from drug discovery projects, and can help identify structural motifs that may be toxic liabilities. The results generated from thus study suggest that no cores possess any significant toxic liabilities (**Table 33**).

Christopher J Tame
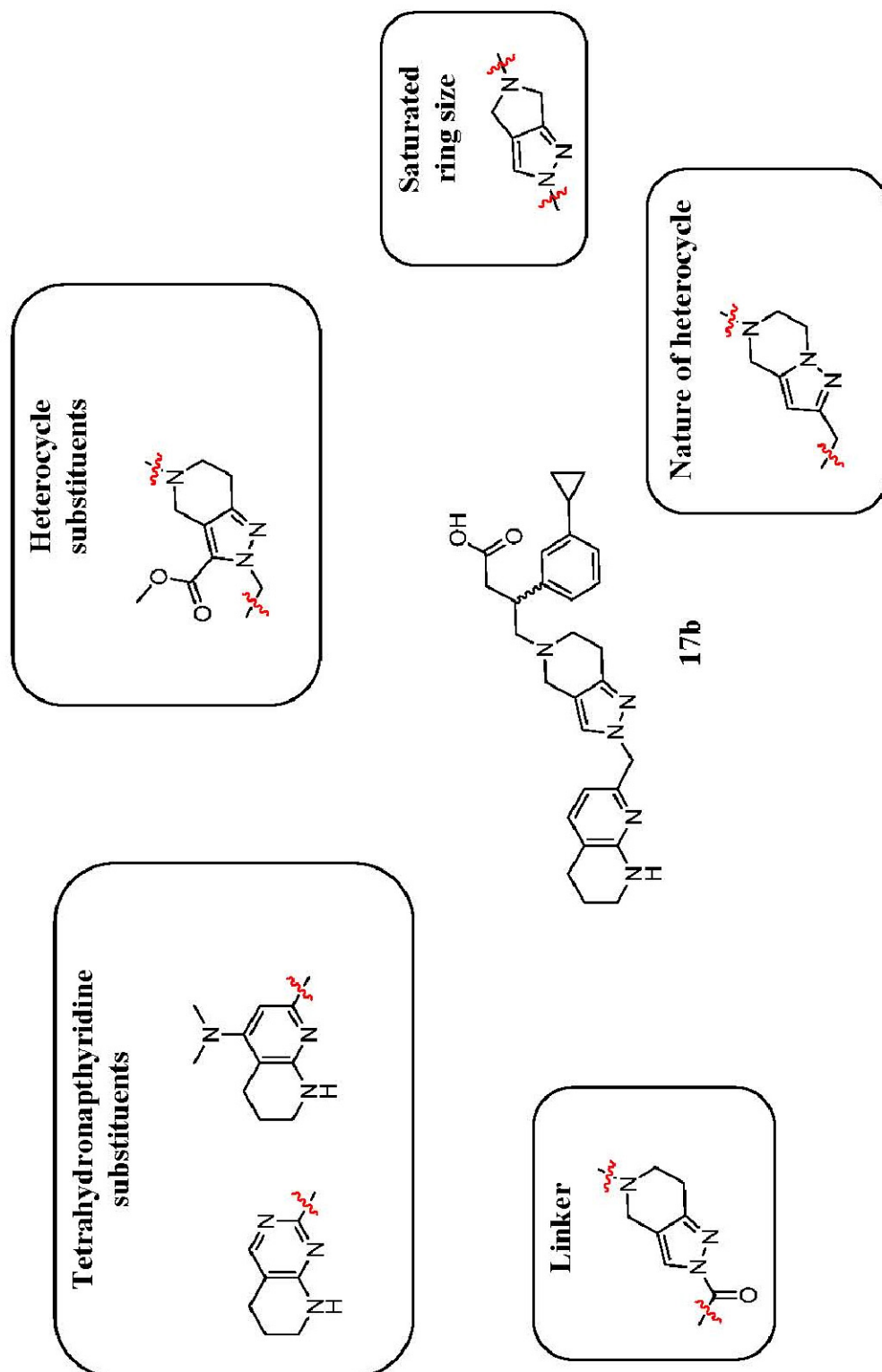
Figure 30: Potential modifications to pyrazolopiperidine **17b** for reduced pKa.

Christopher J Tame

Structure	Toxicity flag?	Marketed drug?
71 **(cf. 165)**	No	No
76 **(cf. 168)**	No. Other data: SLV317 , NK-1 antagonist (1,2,3-triazole) Phase I, positive outcome.[221]	No.
77 **(cf. 169)**	Cytotoxic.[222] However, other toxic pharmacophores are present.	1,2,4-triazoles present in: Januvia, Maxalt, Femara, and Forasartan.
171 **(cf. 170)**	No.	No.
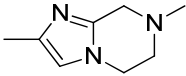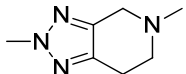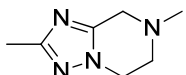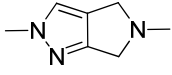
Table 33: The potential toxic liabilities and presence in marketed drugs for a selection of fused heterocyclic motifs.

The lipophilicity and pKa data for the cores identified for synthesis are compared with pyrazole **17b** in **Table 34** and **Figure 31**. Imidazole **165** was removed from further evaluation or synthesis because of its similar calculated pKa but increased cLogP when compared to pyrazolopyrrolidine **170**, which was expected to be efficiently synthesised using the already validated synthetic route for pyrazolopiperidine **17b**. This resulted in three new molecules being prioritised for synthesis (**Figure 32**).

Christopher J Tame

Compound no.	Structure of Core	cLogP	ChemAxon pKa
17b		3.5	8.2, 6.6, 4.0
165		3.4	7.2, 6.2, 3.8
168		3.1	7.6, 6.2, 3.8
169		2.9	7.0, 5.9, 3.8
170		3.2	7.2, 6.3, 3.8
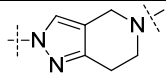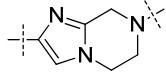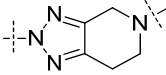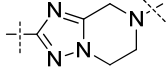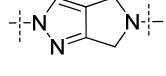
Table 34: Lipophilicity and pKa values for pyrazolopiperidine **17b** and a selection of compounds shortlisted for synthesis.
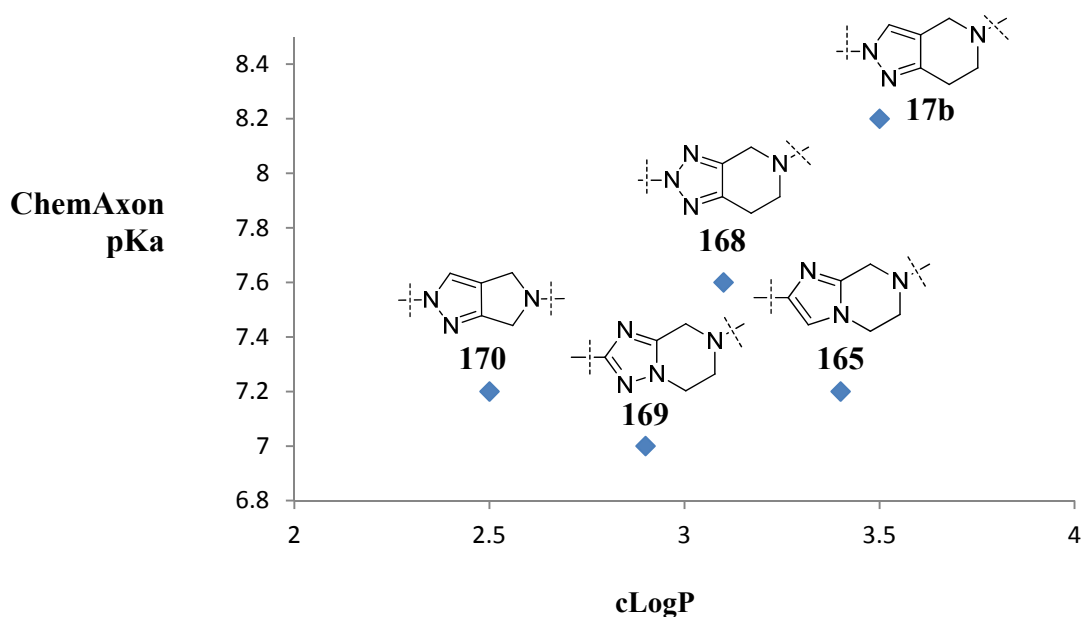
Figure 31: Lipophilicity and pKa values for pyrazolopiperidine **17b** and a selection of compounds shortlisted for synthesis.

Christopher J Tame
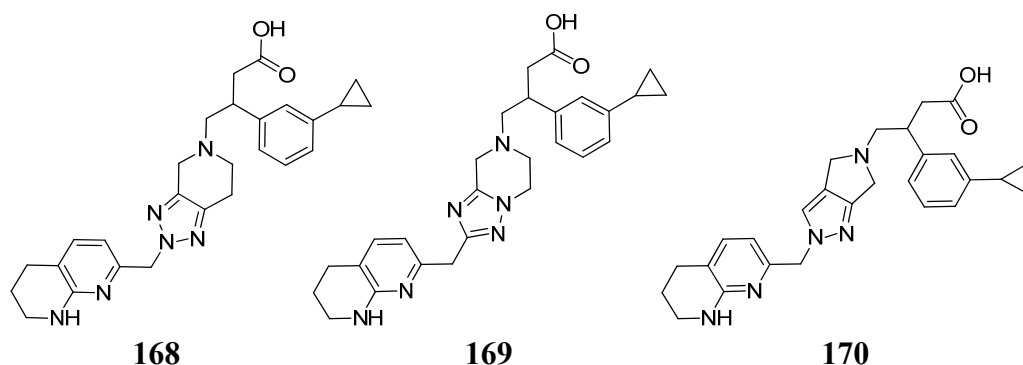
Figure 32: The molecules selected for synthesis with the aim of balancing good oral absorption and low protein binding.

2.5.1 Synthesis of 1,2,4-triazole 168

The synthesis of 1,2,4-triazole **168** was initially attempted using the one pot C-H borylation/cross coupling methodology, which was previously successful in accessing thiophene and furan analogues such as **84b** and **86**, respectively. Commercially available triazolopyridine **172** was hydrogenated and then Cbz protected to afford intermediate **174** (**Scheme 65**).[223]
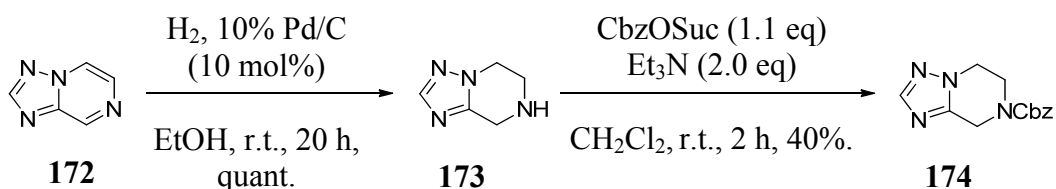
Scheme 65: Hydrogenation followed by Cbz protection of **172**.[223]

The suitably-protected triazolopiperidine (**174**) was then submitted to iridium-catalysed C-H borylation conditions. It was reasoned that the triazole ring could co-ordinate with iridium, which would detract from its catalytic activity. To account for this, the catalyst and ligand loadings were increased from 1.5 mol% and 3 mol% to 5 mol% and 10 mol%, respectively. The poor solubility of triazolopiperidine **174** in cyclohexane resulted in it being applied to the reaction mixture in chloroform.

Christopher J Tame

After 1 h at room temperature, no reaction could be identified by LCMS analysis of the crude reaction mixture. In the case of thiophene **84b** C-H borylation went to completion between 1-2 hours. It was considered that rapid protodeborylation of the desired pinacolboronate intermediate during LCMS analysis could complicate reaction monitoring efforts. Consequently, the reaction was progressed to the cross-coupling step, although no desired reaction occurred (**Scheme 66**).
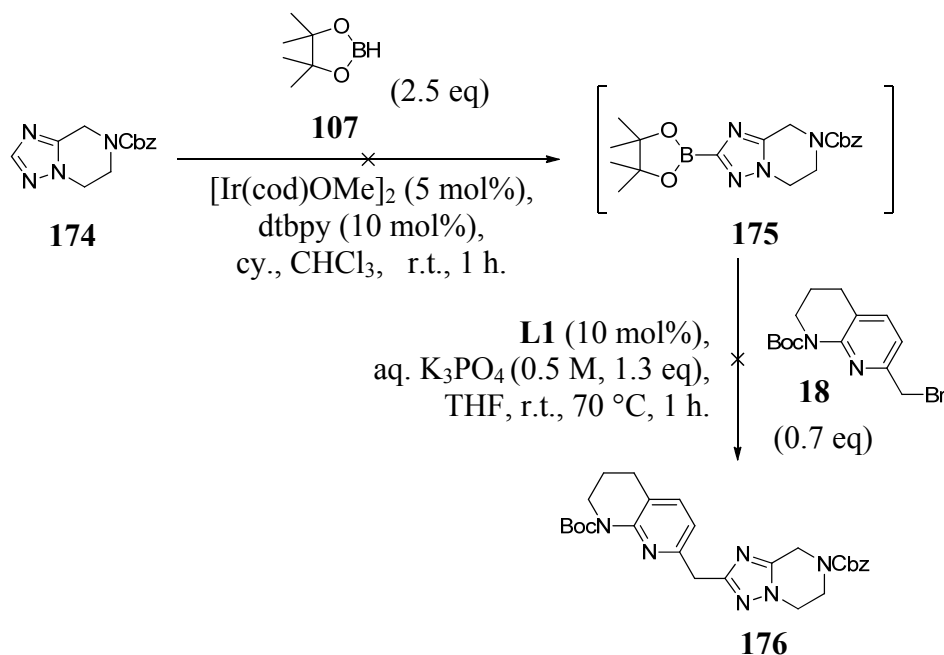
Scheme 66: Attempted iridium-catalysed C-H borylation of triazolopiperidine **174**, followed by palladium-catalysed sp^2-sp^3 cross coupling with alkyl bromide **18**.

The reaction was repeated to investigate the potential for C-H borylation at elevated temperatures (**Scheme 67**). After heating at 50 °C for 1 h., LCMS analysis of the crude reaction mixture did not identify any of the desired pinacolboronate **175**. However, heating to 70 °C for just 15 min did show a new peak with a mass ion corresponding to pinacolboronate **175**. Partial borylation and diborylation of the dtbpy ligand was also observed, although isolation and full characterisation was not attempted.

Further LCMS analysis after 1 hour indicated complete conversion to the new peak which ionised to the desired intermediate **175**. The reaction mixture was then submitted to the cross-coupling conditions at 70 °C, which resulted in rapid

Christopher J Tame

degradation of the intermediate back to starting material. It was rationalised that a lower temperature for the cross-coupling may slow down protodeborylation and, therefore, promote the desired reaction. Accordingly, the reaction was repeated twice and the mixture was cooled to 0 °C or 50 °C before the cross coupling reagents were added. Whilst LCMS analysis confirmed that lower temperatures inhibited the degradation of the proposed boronate intermediate, no cross-coupling was observed.
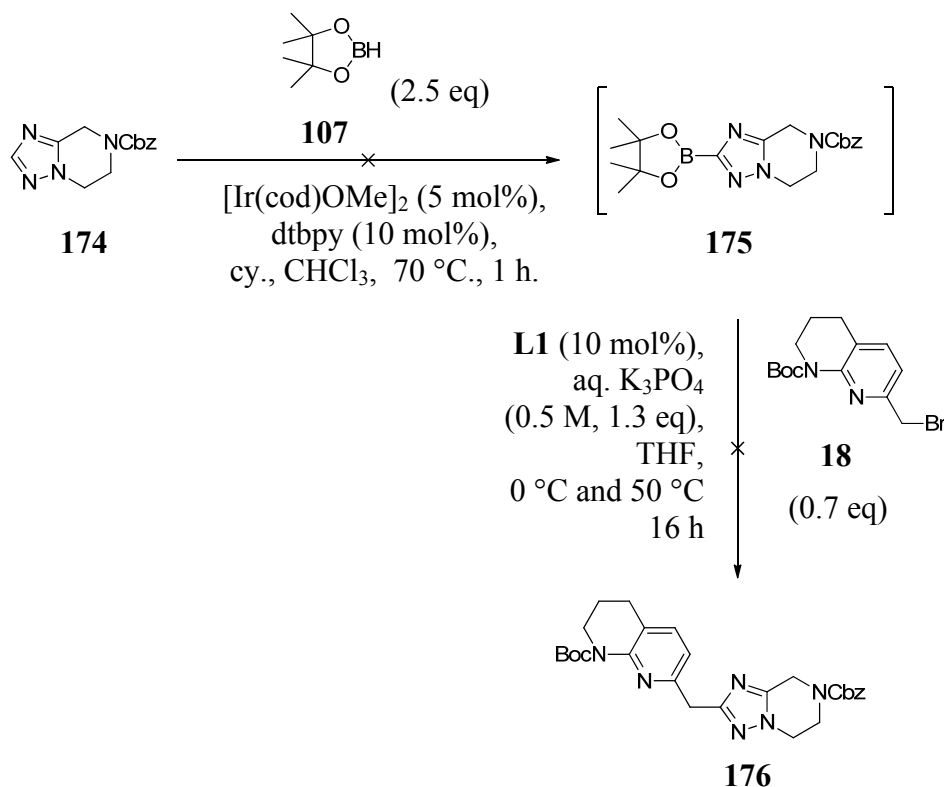
Scheme 67: Attempted iridium-catalysed C-H borylation of triazolopiperidine **174**, followed by palladium-catalysed sp^2-sp^3 cross coupling with alkyl bromide **18**.

The unsuccessful attempt to access the triazole-containing target **176** using C-H activation prompted investigation in to other approaches. The commercially-available bromotriazole **177** (**Figure 31**) was accordingly used to design a number of C-X activation approaches to access the desired target **169**.
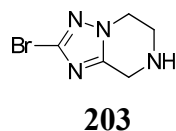
Figure 33: Commercially available bromotriazolopiperidine **177**.

Christopher J Tame

It was previously speculated that C-X activation approaches to access thiophene-containing targets were unlikely to be successful. This was due to the predicted instability of sp³-centred organometallic species for metal-catalysed cross-coupling reactions, as well as the presence of a number of reactive methylene units under base-mediated deprotonation reactions (**Scheme 81**). Therefore, these reactions were discounted from further investigation and alternatives were explored.
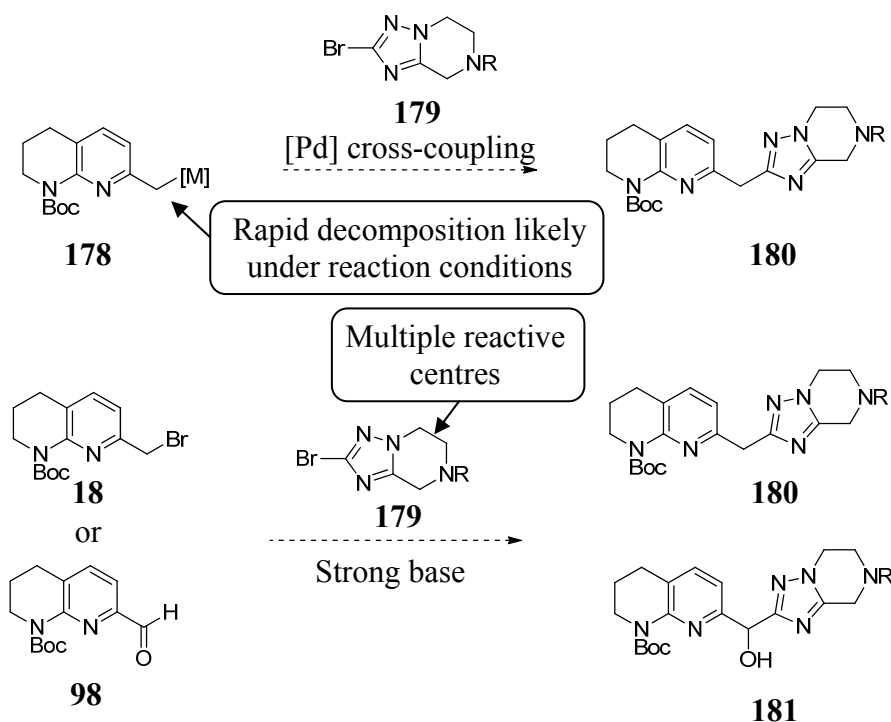
Scheme 68: Potential drawbacks of a C-X activation approach to accessing triazole **180**. 'R' is a suitable protecting group

Decarboxylative coupling provides a method of undertaking a cross-coupling reaction with two stable intermediates (**Scheme 69**). These reactions are typically promoted by palladium,[224] copper[225] or silver,[226] either singularly or in combinations.
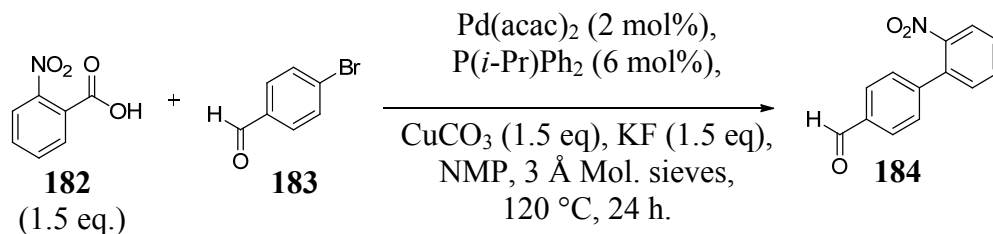
Scheme 69: Palladium-catalysed and copper mediated decarboxylative biaryl coupling.[227]

Christopher J Tame

A recent study by Liu and co-workers demonstrated the cross-coupling of 2-pyridyl acetates with bromo-aryl and heteroaryl systems (**Scheme 70**).[228] The structural similarity of these systems with the tetrahydronaphthyridine moiety encouraged application for the synthesis of triazole **180** (**Scheme 71**).
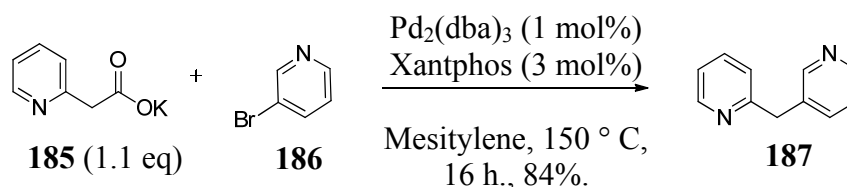
Scheme 70: Palladium-catalysed decarboxylative coupling of a 2-pyridyl acetate with 3-bromopyridine.[228]
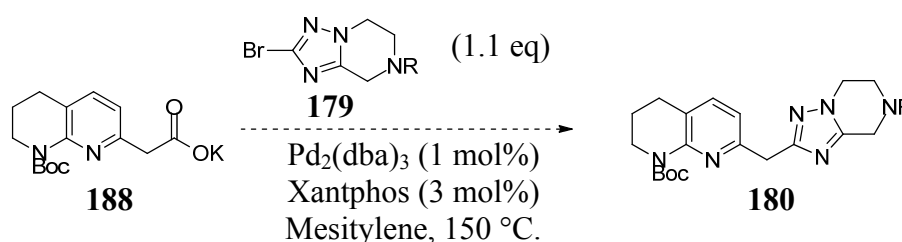
Scheme 71: Proposed route to access triazole **180** *via* a palladium-catalysed decarboxylative cross-coupling protocol. 'R' is a suitable protecting group.

Mechanistic studies have suggested that decarboxylation is the rate-limiting step in these reactions. Therefore, it is reasonable to suggest that rapid oxidative addition of arylbromides could hamper the reaction profile. In an attempt to circumvent this, bromotriazole **177** was trityl protected, which was not considered to increase the electron-withdrawing effect of the nitrogen, which is the case with carbamate protecting groups (**Scheme 72**).
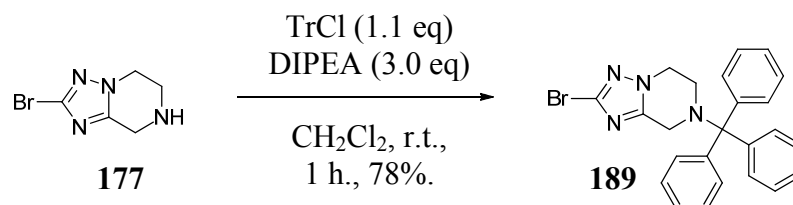
Scheme 72: Trityl protection of bromotriazole **177**.[229]

Christopher J Tame

Subsequently, commercially available methyl ester **148** was hydrolysed to form acetic acid **190**, which was then submitted to decarboxylative cross-coupling conditions with bromotriazole **189** (**Scheme 73**). A structure for the isolated product (**191**) has been tentatively assigned using ^{1}H NMR, which is likely to have occurred *via* Boc-deprotection of the tetrahydronaphthyridine **188**, followed by palladium-catalysed amination with bromotriazole **189**. LCMS analysis indicated deprotection of the trityl-protected analogue of this product during work-up.
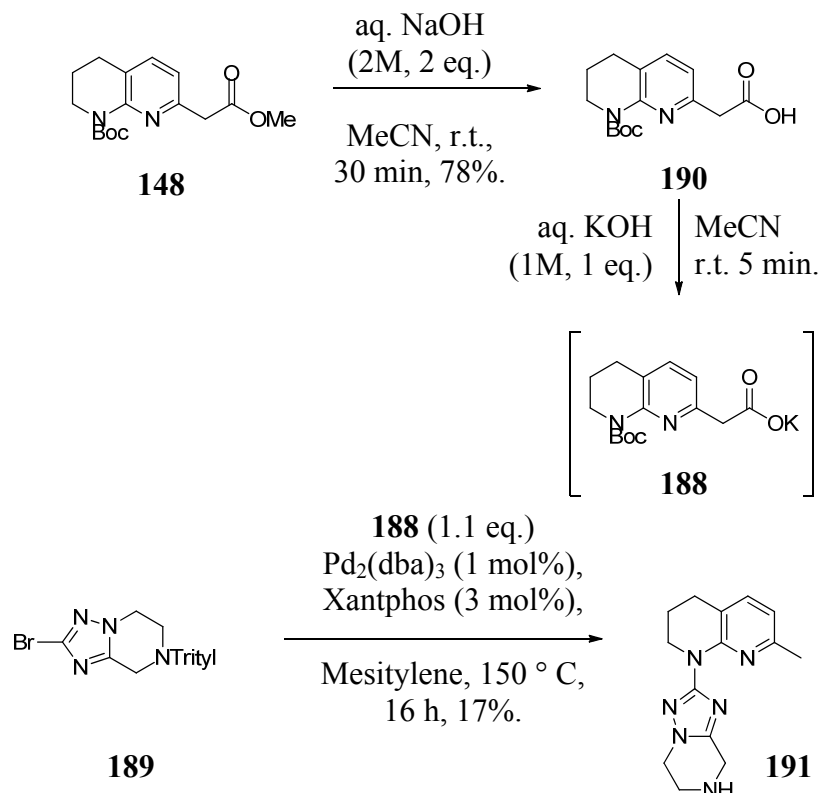
Scheme 73: Palladium-catalysed decarboxylative coupling of bromotriazole **189** with tetrahydronaphthyridine **188**.

LCMS analysis could not identify any carboxylate-related products in the reaction mixture, suggesting that decarboxylation occurred but was not favoured for cross-coupling. It is unclear whether the rate of Boc-deprotection was faster than decarboxylation, although this could be readily identified from regular reaction monitoring using LCMS.

Christopher J Tame

2.5.1.1   Future work

Unfortunately, time constraints prevented further investigation into the synthesis of triazolopiperidine target **195**.   Future work could attempt to repeat the decarboxylative coupling conditions using naphthyridine **194**, which could be readily accessed from methylnaphthyridine **192**[228] and potentially circumvents any palladium-catalysed amination side-reactions (**Scheme 74**).   Replacing the trityl protecting group of triazolopiperidine **189** with a benzyl moiety is likely to increase the stability of the reagents.   In addition, hydrogenation of the naphthyridine ring is also expected to facilitate benzyl deprotection to afford the desired intermediate **197** in one step.
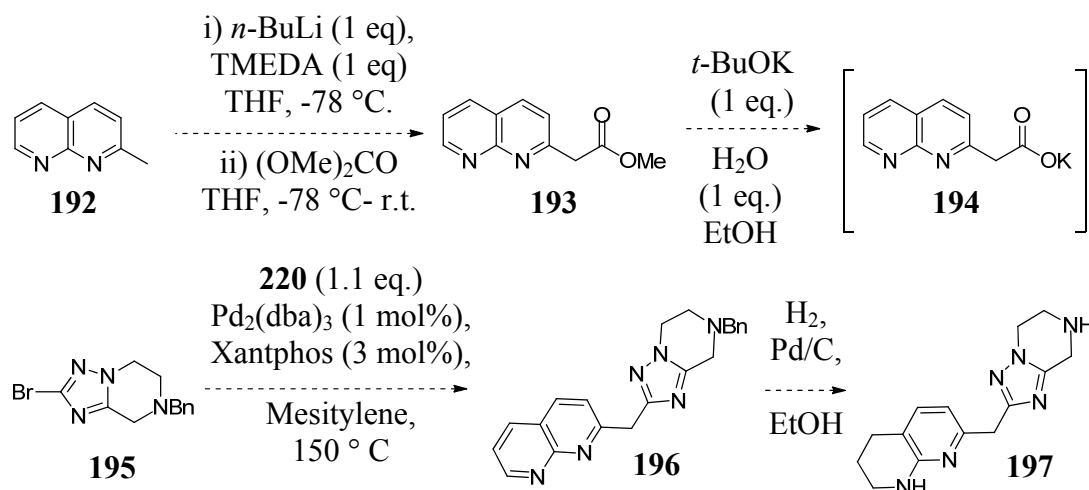
Scheme 74: Proposed modifications to the palladium-catalysed decarboxylative cross-coupling approach to access triazolopiperidine **197**.

An alternative method could involve the application of Fagnou's protocol for the C-H cross coupling of 2-methylheteroaryl *N*-oxides with aryl bromides (**Scheme 75**).[230,231]   As with decarboxylative couplings, these conditions do not require the use of unstable organometallic species, and are therefore suitable for application in the synthesis of triazolopiperidine **197**.

Christopher J Tame
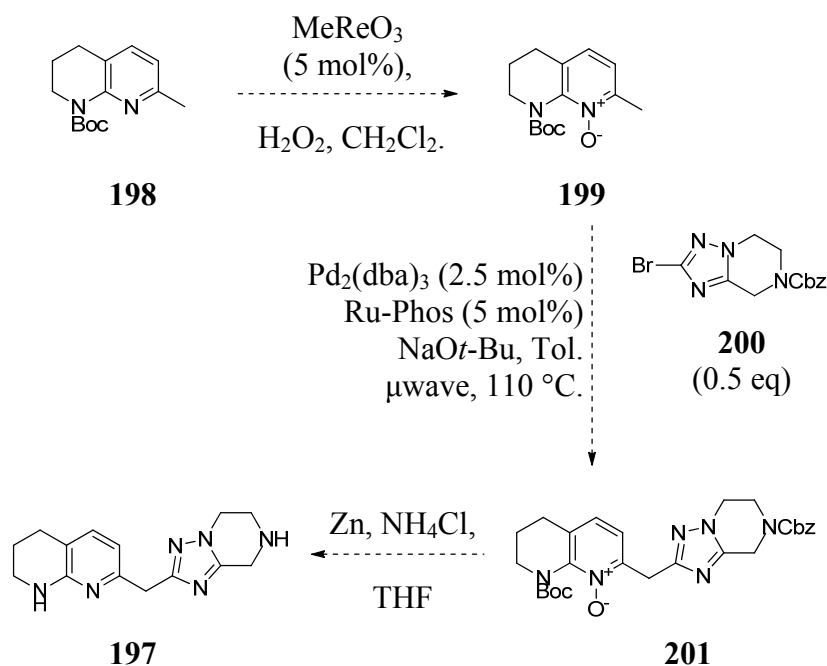
Scheme 75: Proposed synthesis of triazolopiperidine **197** *via* palladium-catalysed C-H activation of pyridine *N*-oxide **199**.[230, 231]

Some potential drawbacks of this approach are that lower yields are observed with electron-poor aryl bromides, and that a relatively strong base is required. The former drawback is postulated to be a result of multiple reactive centres which are susceptible to C-H activation and co-ordination to the metal, which is expected to inhibit reaction progression.[231] Consequently, it is expected that this reaction would not be successful.

2.5.2   Synthesis of pyrazolopyrrolidine 170

2.5.2.1 Application of the synthetic route used to access pyrazolopiperidine 17b

The existing synthetic route used to access pyrazolopiperidine **17b** was applied to pyrazolopyrrolidine **196**, which delivered the desired targets in very low yields, although this was comparable to previous attempts (**Schemes 76**, **77** and **78**). ^{1}H NMR analysis of the mixture of *N*-alkylated regioisomers (**205** and **206**) revealed a 2:1 ratio, an improvement from 1.3:1 shown with pyrazolopiperidine **17**.   The

Christopher J Tame

mixture was resolved at a later stage using preparative HPLC (**Scheme 76**) and ^{1}H NMR NOESY experiments determined the desired regioisomer (**209**) to be the major component. Once resolved, the desired regioisomer **209** was then submitted to chiral HPLC purification, followed by base-mediated hydrolysis, to afford the desired products **170a** and **170b** as single enantiomers (**Schemes 77 and 78**).

The preparative HPLC techniques were, once again, the lowest yielding steps in the synthetic route. It has been shown previously that the use of (*R*)-BINAP can impart enantioselectivity for the desired enantiomer in the rhodium-catalysed conjugate addition step which, accordingly, also improved the yield (*cf.* **Scheme 47**). Therefore, application of these conditions to this template was expected to improve the yield of this step.

Resolution of the regioisomers **209** and **210** by preparative HPLC required 43 x 100 μL injections to achieve resolution, which makes this step both the lowest yielding and the most time-consuming.[175] The reliance on reverse phase preparative HPLC was a result of the inability to resolve the mixture of *N*-alkylated regioisomers by column chromatography (**Scheme 76**).

To compound matters, this synthetic route afforded insufficient amounts of final compound to support the necessary biological testing. Re-synthesis was required, which prompted investigation into optimisation of the synthetic route. This focused on avoiding the necessity for a low-yielding and time-consuming achiral HPLC purification.

Christopher J Tame
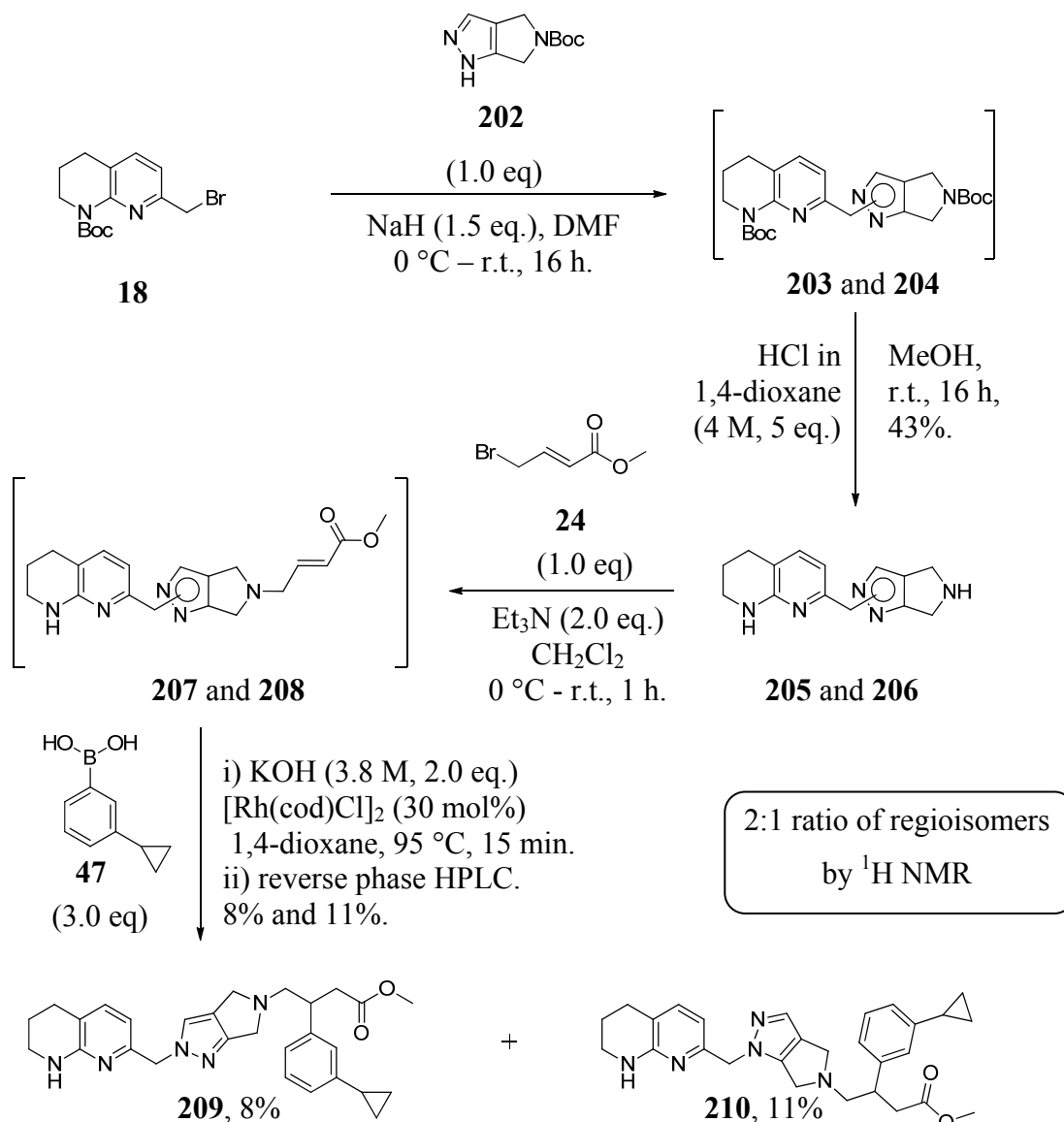
Scheme 76: Sequential alkylation and Boc-deprotection steps of commercially available **202** afforded a mixture of **209** and **210**.

209a (**Enantiomer 1**): 20%, >96% e.e
209b (**Enantiomer 2**): 21%, >99% e.e
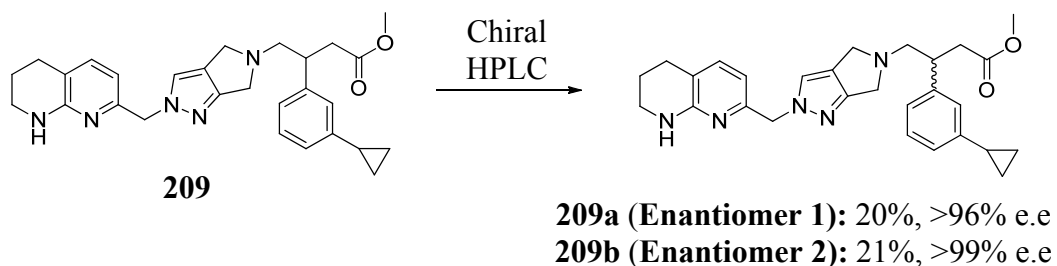
Scheme 77: Chiral HPLC to afford the isolated single enantiomers in greater than 96% and 99% enantiomeric excess, respectively.[175]

Christopher J Tame
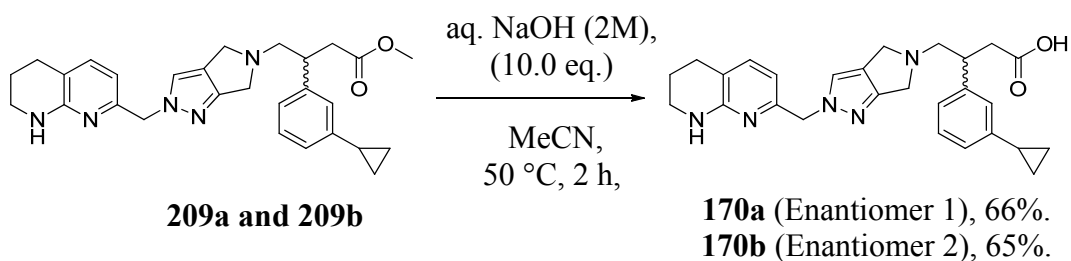
Scheme 78: Base-mediated ester hydrolysis to afford the final products **170a** and **170b** as single enantiomers.

2.5.2.2   Synthetic route optimisation

The requirement for preparative HPLC in the previous synthesis of pyrazolopyrrolidine **170b** was considered unsuitable for large scale resynthesis, as this purification approach would limit capacity. It was hypothesised that subtle changes in polarity associated with protecting group modification could be sufficient to enable separation using column chromatography. This modification would require commercially available protecting groups and well established synthetic chemistry techniques for protection and deprotection of the relevant amines.

The synthesis of thiophene **84** used a carboxybenxyl (Cbz) protecting group, which was readily synthesised and removed in good yields in previous syntheses (**Schemes 19** and **24**). The Cbz protecting group can also be removed under either Lewis acid or hydrogenation conditions, which provided an orthogonal deprotection strategy. Accordingly, a synthetic route was designed to incorporate Cbz protection for the resolution of *N*-regioisomers by column chromatography (**Scheme 79**).

The reagent used for Cbz protection of pyrazolopyrrolidine **211** was Cbz-OSuc,[232] which possesses fewer hazards than the more commonly used CbzCl and is therefore more suitable for use on larger scale.[233] The *N*-hydroxysuccinimide leaving group is water soluble and can be readily removed upon aqueous work-up.

The rhodium-catalysed arylation of α,β-unsaturated ester **215** was designed with the addition of (*R*)-BINAP, which was expected to produce a chirally-enriched mixture

Christopher J Tame

of the desired enantiomer. This was previously shown from the synthesis of thiophene **85**, providing confidence in this approach. A trial reaction with (*R*)-BINAP and Boc-deprotected α,β-unsaturated ester **207**, however, gave a relatively low 62% e.e. (c.f. thiophene **85** 72% e.e.).[234] It was considered that an unprotected tetrahydronaphthyridine could compete with (*R*)-BINAP to act as a ligand to rhodium, which could reduce the enantioselectivity or catalytic efficiency of the reaction. The orthogonal deprotection strategy was, therefore, implemented to maintain Boc deprotection for the alkylation and arylation stages. The potential for partial Boc deprotection during chiral HPLC purification resulted in its planned deprotection directly after the rhodium-catalysed conjugate addition of boronic acid **47** to enone **240**.
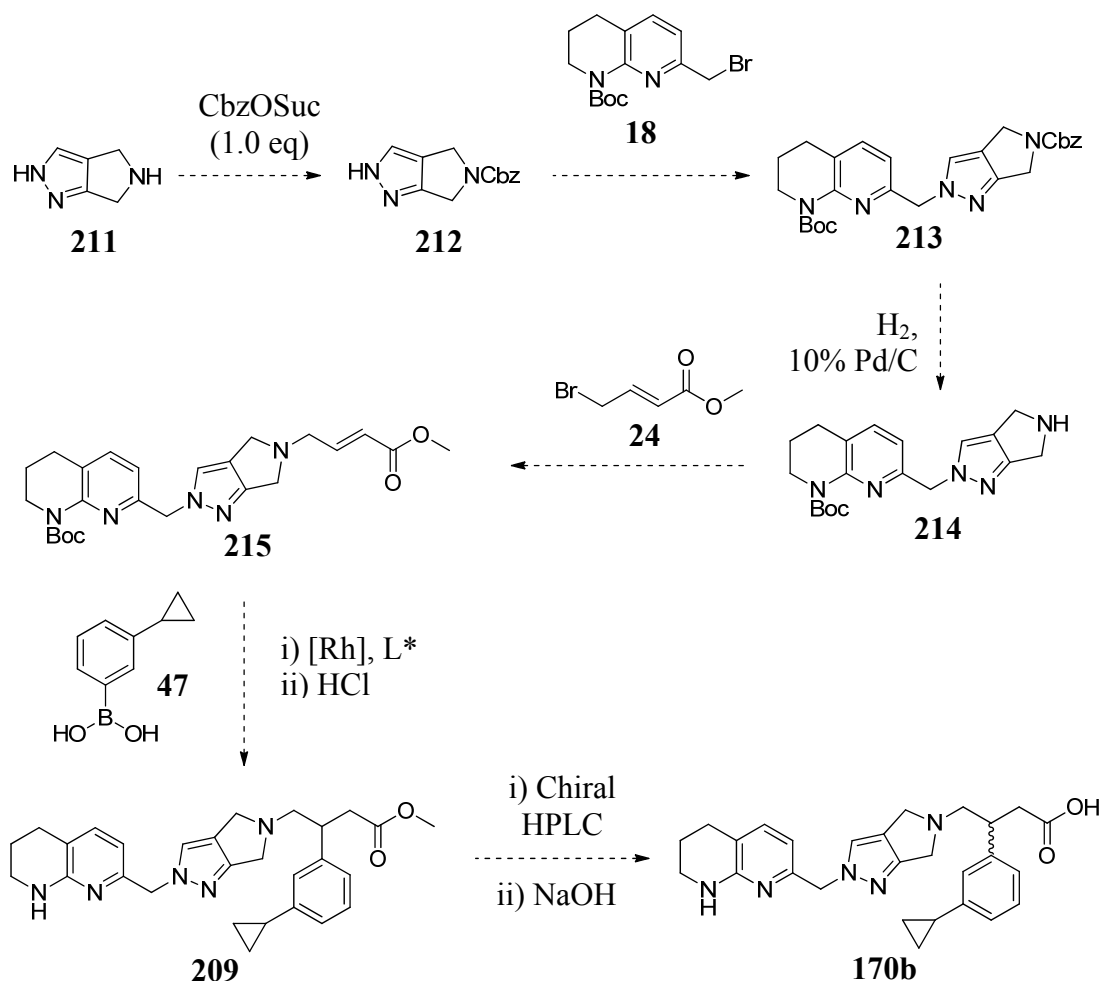
Scheme 79: Proposed route to access pyrazolopyrrolidine **170b** without preparative achiral HPLC.

In commencing the synthesis, alkylation of the pyrazolopyrrolidine core **211** was attempted with Cbz-OSuc, which gave an undesired a mixture of mono- and di-substituted products that were recovered in 35% and 15% yields, respectively (**Scheme 80**).
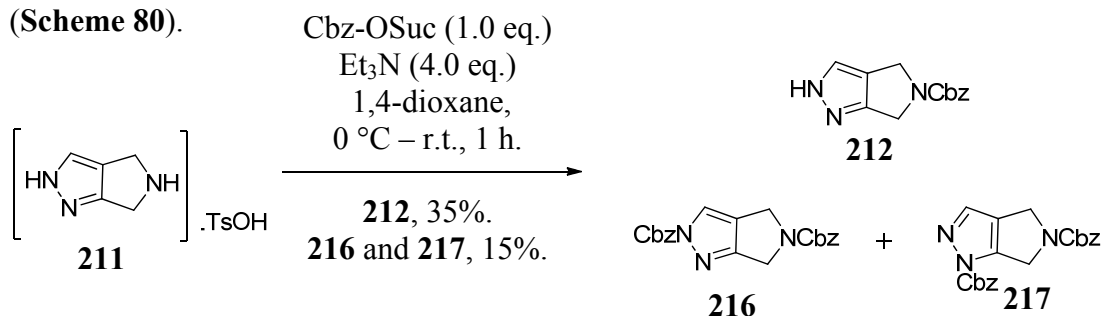
Scheme 80: Unselective alkylation of **211** with one equivalent of Cbz-OSuc.

It was reasoned that carbamates formed on pyrazoles would be labile to weak nucleophiles and could be selectively removed using a secondary amine. A literature search revealed that a Cbz-protected imidazole nitrogen had been successfully deprotected using diisopropylamine, which provided some support to the theory.[235] This would allow an over-alkylated pyrazolopyrrolidine core to be transformed to the mono protected core using mild and benign conditions.

Treatment of dialkylated **216** and **217** with isopropylamine pleasingly facilitated rapid and selective Cbz deprotection of the pyrazole-linked Cbz group, which afforded the desired mono protected **212** (**Scheme 81**), as observed by crude LCMS analysis. The reaction was subsequently repeated with an excess of Cbz-OSuc, in order to ensure complete protection of the pyrrolidine nitrogen. The mixture was then treated directly with isopropylamine, which afforded the desired product in 66% yield after column chromatography (**Scheme 82**). This provided a convenient and efficient one-pot synthesis of mono-Cbz protected pyrazolopyrrolidine **212**.
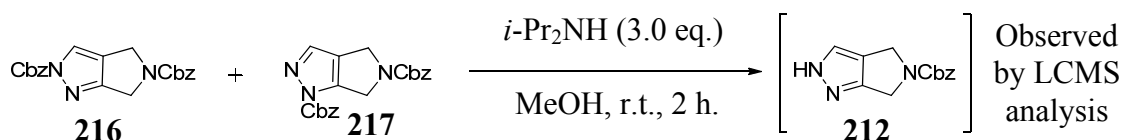
Scheme 81: Treatment of a mixture of **216** and **217** with isopropylamine gave the desired mono protected product **212**.

Christopher J Tame
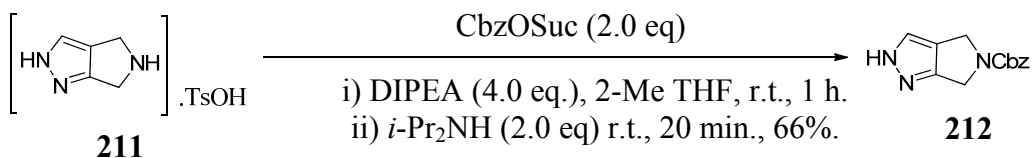
Scheme 82: Formation of the desired Cbz-protected product **212** by alkylation with an excess of Cbz-OSuc, followed by treatment with isopropylamine.

The alkylation of Cbz-protected pyrazolopyrrolidine **212** with bromo compound **18** gave a mixture of *N*-regioisomers by crude LCMS analysis. Pleasingly, column chromatography successfully resolved the isomeric mixture and **212** was isolated as a single regioisomer, although in moderate yield (**Scheme 83**). The analogous reaction with Boc-protected pyrazolopyrrolidine core **202** and bromo compound **18** (**Scheme 76**) afforded an inseparable mixture of regioisomers in 59% yield, which translates to a relative yield of 43% for regioisomer **203**. When purified later in the synthetic route, the individual regioisomers were only isolated in around 10% yield. Considering this, the isolated yield of 29% for Cbz-protected **213** is a significant improvement in the efficiency of this step, both in terms of mass recovery and time.
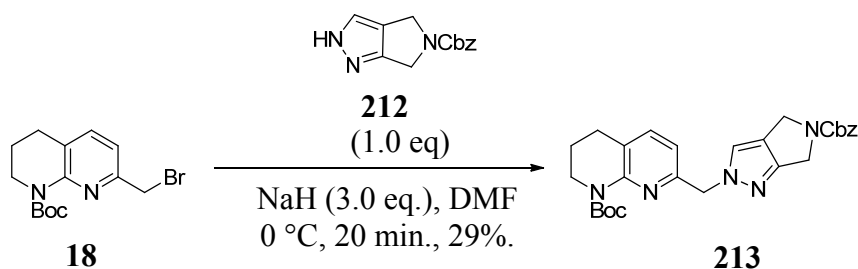
Scheme 83: Alkylation of Cbz-protected pyrazolopyrrolidine **212** with bromo **18**.

Selective deprotection of the Cbz group was initially attempted using classical hydrogenation conditions which employed a palladium on carbon catalyst and ethanol as solvent (**Scheme 84**).[236] LCMS analysis of the crude reaction mixture suggested the presence of only small quantities of the desired product, along with a range of unidentifiable impurities. This was considered to be a result of excess reactivity, and was subsequently repeated with different solvents in an attempt to slow the reaction. Ethyl acetate and chloroform were chosen due to their different solvation properties with Pd/C, as determined by a shake-flask screening method and

Christopher J Tame

qualitative analysis by eye. LCMS analysis of these crude reaction mixtures gave similar profiles, with ethyl acetate providing a slight improvement for the formation of the desired product **214**.
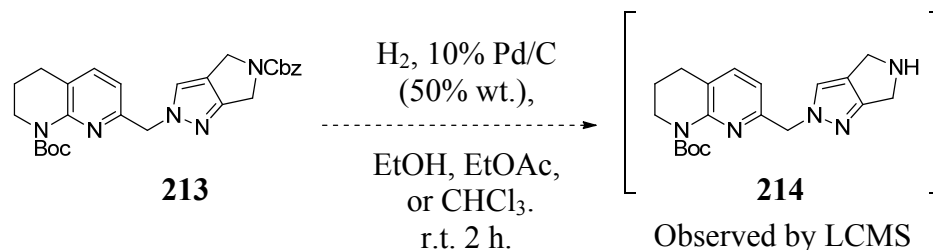
Scheme 84: Selective removal of a Cbz protecting group under hydrogenation conditions using different solvents.

It was thought that the unprotected pyrrolidine nitrogen was in some way unstable to the reaction conditions and facilitating decomposition. Subsequent consultation with other members of our laboratory suggested the incorporation of acetic acid in the reaction mixture to help stabilise the secondary amine through protonation.[237] The reaction was consequently repeated with these modified conditions which pleasingly gave clean conversion to the desired product *via* crude LCMS analysis (**Scheme 85**). Unfortunately the product persisted in aqueous phase during work-up procedures. Extraction with 2-butanol was partially successful, although subsequent preparative HPLC failed to isolate the desired product.
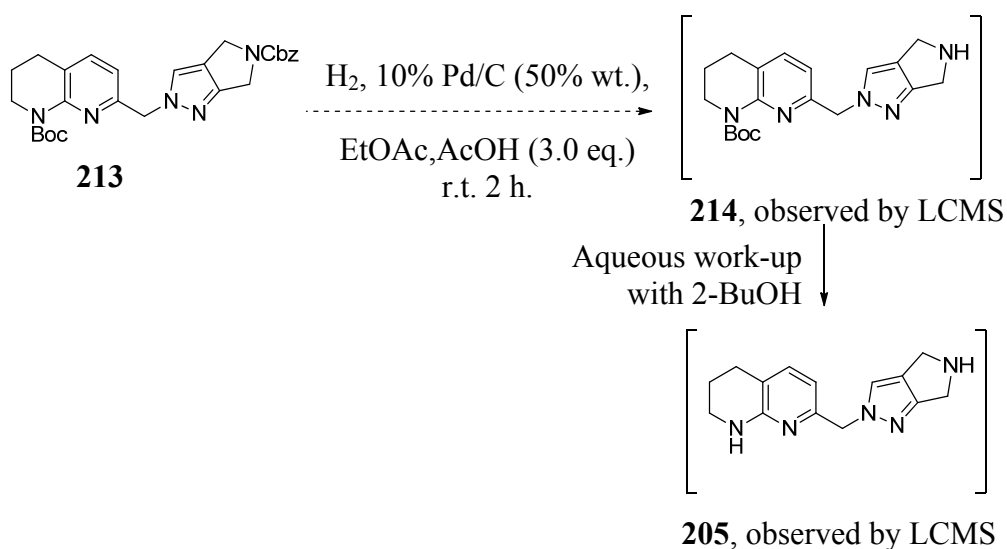
Scheme 85: Attempted removal of a Cbz protecting group under hydrogenation conditions.

Christopher J Tame

The reaction was repeated and isolation was achieved using an amino-propyl pre-packed silica cartridge and sequential elution with ethyl acetate and ethanol to afford the desired product as a free base in 73% yield (**Scheme 86**).
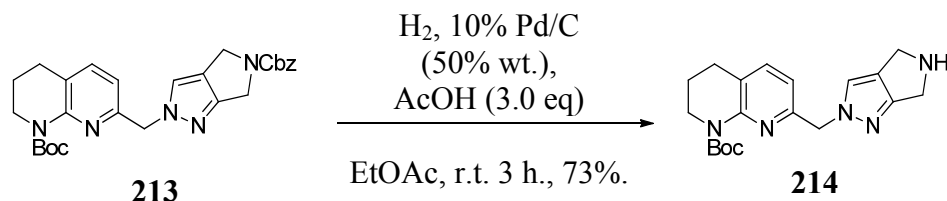
Scheme 86: Selective removal of Cbz protecting group under hydrogenation conditions.

Alkylation of secondary amine **214** with bromo crotonate **24** gave the desired product **215** in 49% yield (**Scheme 87**). LCMS analysis of the crude reaction mixture suggested a clean reaction profile and good conversion to the desired product. It is proposed that the product **215** is slightly unstable to silica column chromatography used for purification, potentially accounting for the lower yield observed.
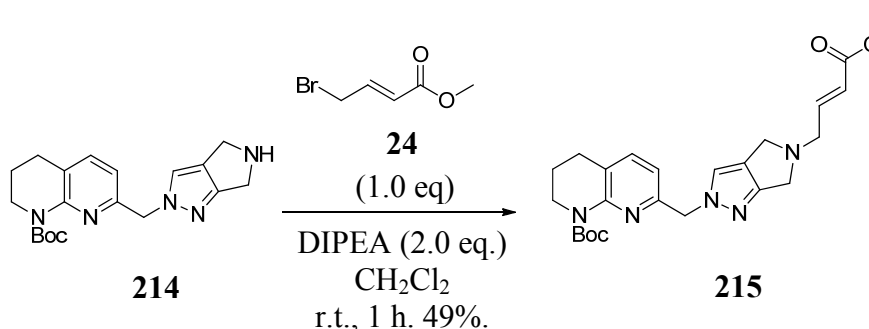
Scheme 87: Alkylation of pyrazolopyrrolidine **214** with bromo crotonate **24**.

The enoate **215** was then submitted to asymmetric rhodium-catalysed 1,4-addition conditions with arylboronic acid **47**. Acid-mediated Boc-deprotection was directly undertaken on the crude mixture to furnish chirally-enriched **209** in 36% yield and 75% enantiomeric excess (**Scheme 88**). These improved conditions were then applied to a large scale re-synthesis of **170b**, which was carried out elsewhere in our laboratories.[238] This was successfully reproduced on a 45 g scale based on the pyrazolopyrrolidine starting material **211**. Purification of the final product was

Christopher J Tame

achieved using reverse phase column chromatography, followed by strong cation exchange chromatography with a propylsulfonic acid-modified silica column.
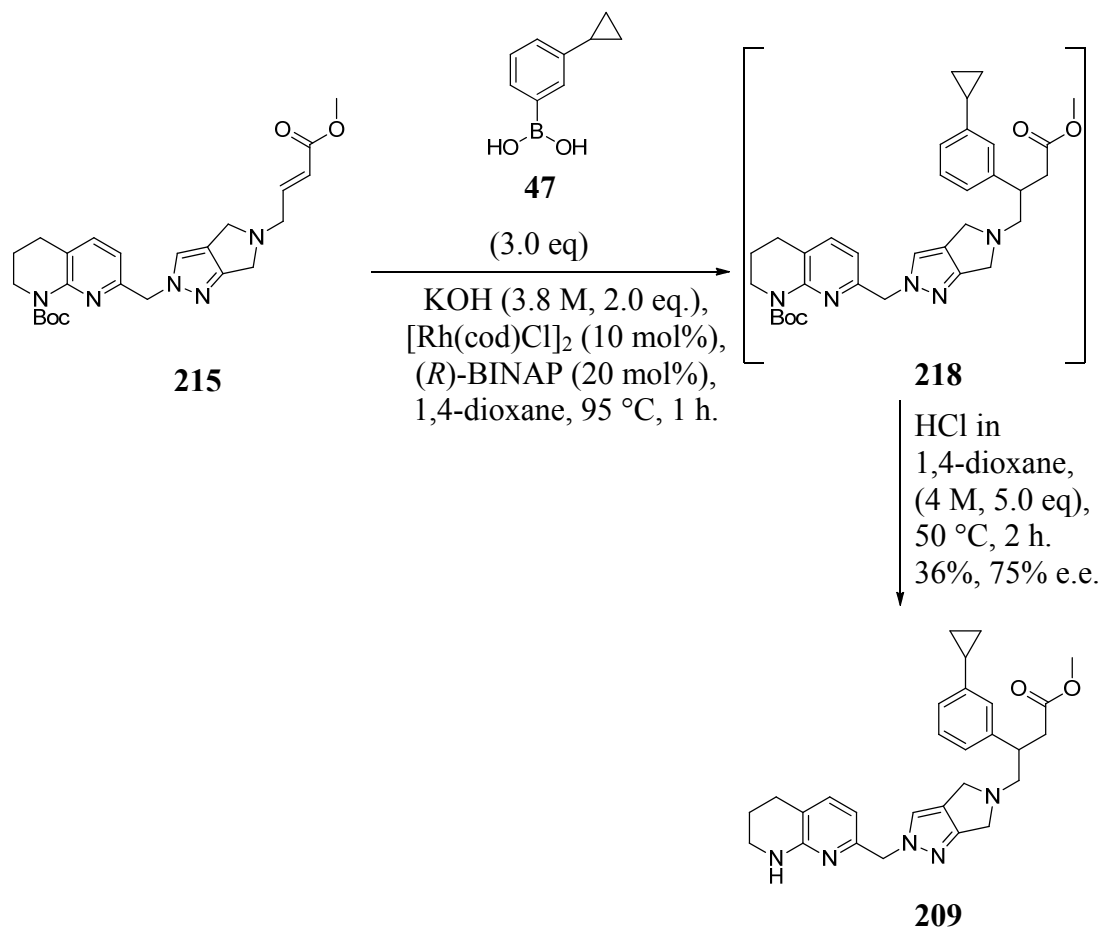
Scheme 88: Rhodium-catalysed 1,4-addition of arylboronic acid **47** to α,β-unsaturated ester **218**, followed by acid-mediated BOC deprotection.

In summary, a *t*-butoxycarbonyl (Boc) protecting group on the pyrazolopyrrolidine core was replaced with a carboxybenzyl (Cbz) moiety. This facilitated *N*-regioisomer separation using silica-gel column chromatography, which removed a low-yielding and time-consuming achiral preparative HPLC step. In addition, hydrogenation conditions were developed to enable selective deprotection of the Cbz group in presence of the Boc group. This allowed the Boc group to be maintained

for the asymmetric rhodium-catalysed 1,4-addition of boronic acid **47** to α,β-unsaturated ester **215**, which improved the enantiomeric excess from 62% to 75%.

2.5.2.3   Future synthetic work

Whilst incorporation of the Cbz group has enabled a large scale re-synthesis of desired enantiomer **170b**, the unselective alkylation of pyrazolopyrrolidine **212** with bromo compound **18** and the associated purification difficulties have not been fully-avoided and remain largely responsible for the low overall yield provided by this route. Further optimisation efforts should therefore focus on regioselective synthesis of the *N2*-alkylated pyrazolopyrrolidine ring system **213**, which would circumvent these issues.

In 2011 Takahashi and co-workers investigated the selective formation of *N2*-functionalised pyrazoles.[239] Initial attempts involved pyrazole alkylation or condensation of a 1,3-dicarbonyl with alkylated hydrazines, both of which resulted in a mixture of *N1* and *N2* regioisomers (**Scheme 90**).
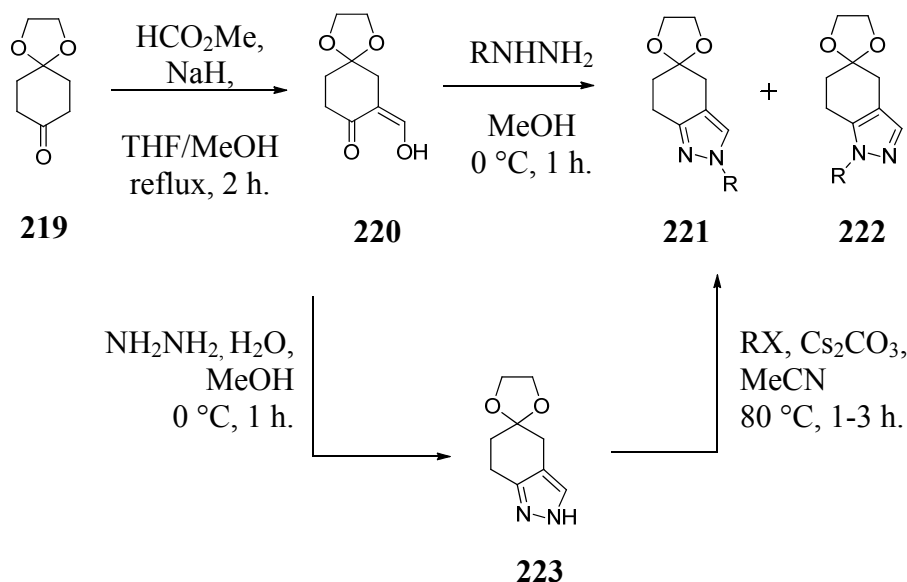
Scheme 90: The general conditions used by Takahashi and co-workers to access a mixture of *N*-alkylated pyrazoles.[239]

Christopher J Tame

It was considered that the unselective addition of alkylated hydrazines to the 1,3-dicarbonyl was a result of similar electrophilicity at the ketone and aldehyde carbon centres. The 1,3-dicarbonyl **220** was subsequently converted to the enol acetate **224**, which regioselectively reacted with Boc protected alkylhydrazines to form desired intermediates **225**, which cyclised upon TFA-mediated Boc deprotection to afford the *N*2-functionalised pyrazoles **221** (**Scheme 91**).[239]
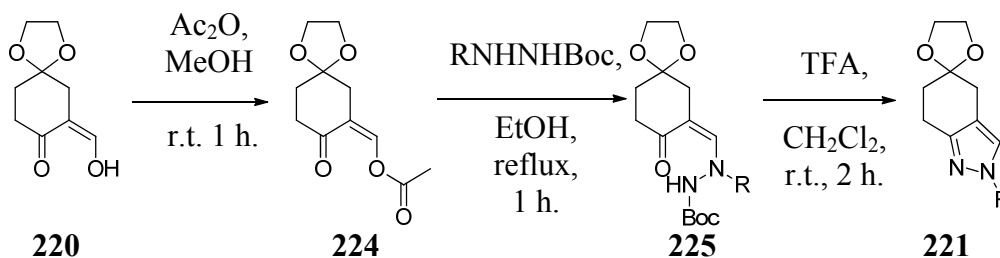
Scheme 91: General conditions for the regioselective formation of *N*2 functionalised pyrazoles.[239]

^{1}H NMR analysis could detect up to 10% of the undesired regioisomer **222** in final product **221**, which is not expected to be problematic in the synthesis of pyrazolopyrrolidine **170b** due to the use of chiral preparative HPLC later in the synthetic sequence.

Based on the above, a proposed synthetic sequence for the selective formation of the *N*2-regioisomer is displayed in **Scheme 92**. The selection of the carboxybenzyl (Cbz) protecting group on pyrrolidinone **227** was due to its predicted stability under TFA-mediated cyclisation conditions. The formation of hydrazine intermediate **226** was expected to be formed by reductive amination of aldehyde **94**.[240,241]

Christopher J Tame
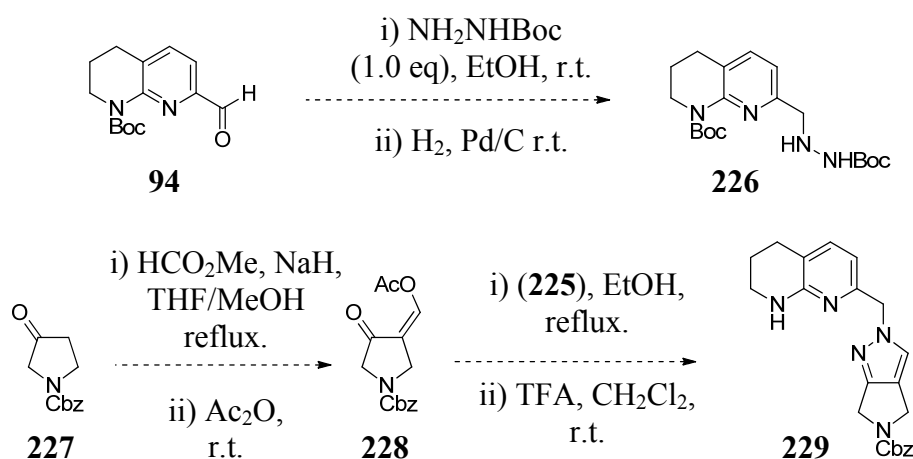
Scheme 92: Proposed route for regioselective formation of pyrazolopyrrolidine **229**.[239,240,241]

Deprotection of the tetrahydronaphthyridine is likely to occur under cyclisation conditions, but was not expected to prove problematic in the subsequent steps. Selective formation of intermediate **228** is supported by literature evidence with the reaction of Boc-protected analogue **230** with DMF-DMA (**Scheme 93**),[242] which is expected to have similar reactivity to Cbz-protected pyrrolidinone **227**.
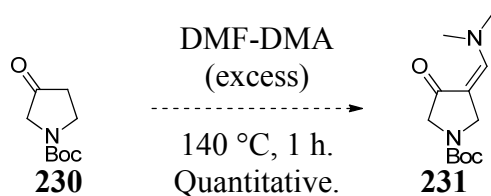
Scheme 93: Literature precedence for the regioselective formation of bis-electrophile **231**.[242]

Christopher J Tame

2.5.3 Synthesis of 1,2,3-triazole 168

To expedite the investigation of reduced pKa for improved permeability, the synthesis of 1,2,3-triazole **168** was undertaken elsewhere within our laboratory.[243] The optimised synthetic route used to access pyrazolopyrrolidine **170b** was successfully replicated, with mostly comparable yields (**Scheme 94**) to furnish the compound as a racemic mixture.

The yield observed for the alkylation of triazole **233** with bromo compound **18** was around twice as much to that observed with the pyrazole analogues. Under these reaction conditions, the desired 2-position of the triazole was the favoured alkylation site, with crude LCMS analysis suggesting a 1:10:1 alkylation ratio. This vastly differs from the 2:1 alkylation ratio observed with pyrazolopyrrolidine **202** (**Scheme 76**), which explains the different isolated yields.

The rhodium-catalysed arylation of enoate **236** also differed from previous examples, with twice as many equivalents of boronic acid required to reach reaction completion. The rapid protodeborylation observed could be a result of poor co-ordination of the enoate to rhodium, as a result of the increased electron-withdrawing nature of the triazolopiperidine core. This poor co-ordination would slow the rate of reaction versus the rate of hydrolysis of the rhodium-aryl intermediate, thus increasing the incidence of protodeborylation.

Christopher J Tame
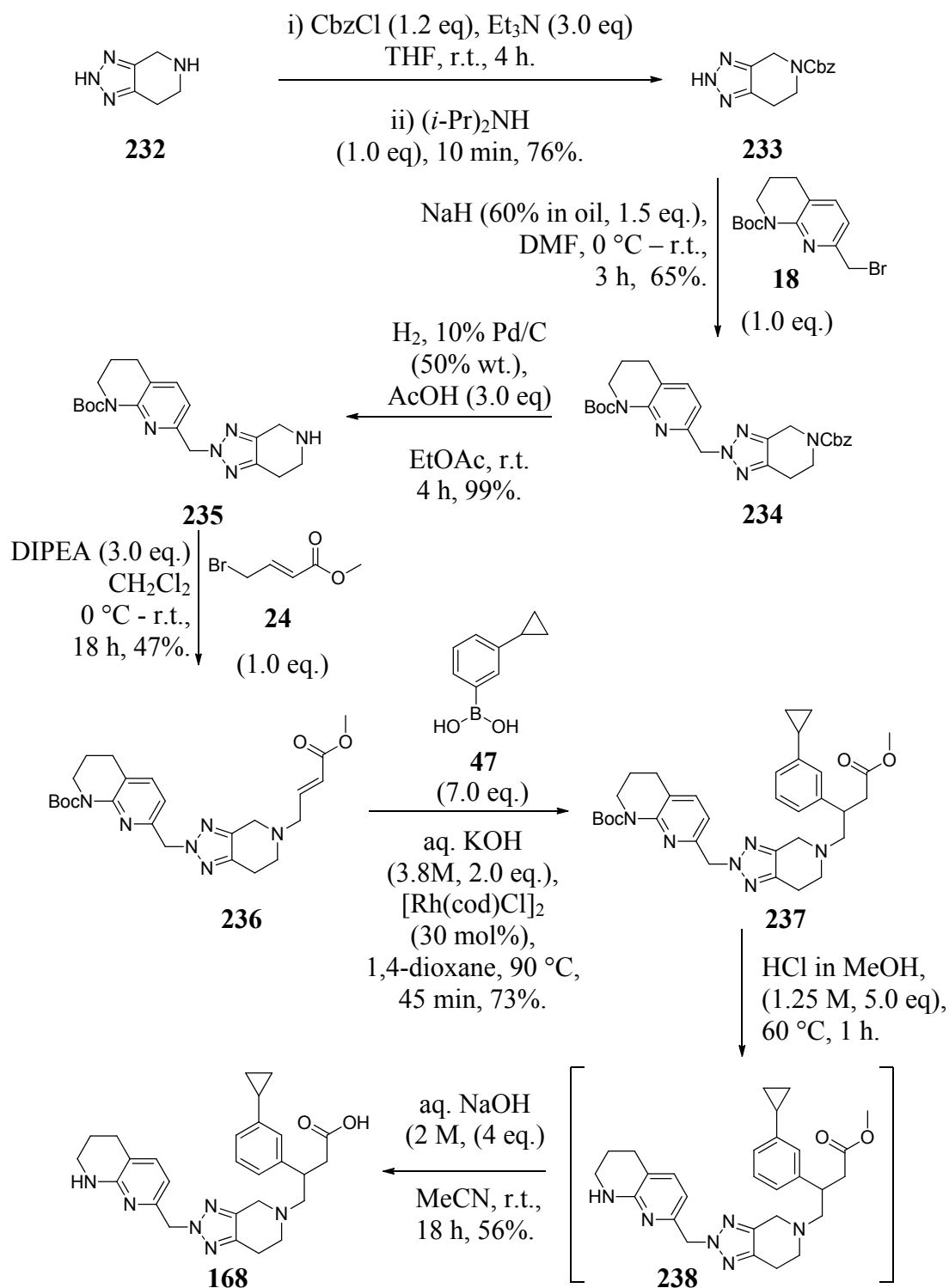
Scheme 94: The synthetic route used to access 1,2,3-triazole **168**.[243]

Christopher J Tame

2.5.4 Biological data and evaluation

The RGD integrin binding affinities and physicochemical properties of triazole **168** and pyrazoles **170a** and **170b** are compared with pyrazolopiperidine **17b** in **Table 34**.
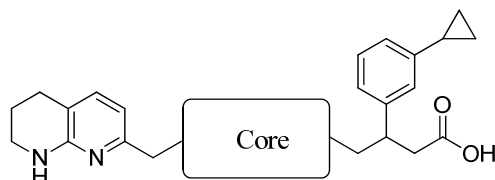
Compound no.	17b*	168	170a*	170b*
Core Structure				
αvβ6 (pIC$_{50}$)	7.3	5.6	5.8	7.9
αvβ3/αvβ5/αvβ8 (pIC$_{50}$)	6.5/6.4/6.4	6.1/5.9/5.7	5.2/5.4/5.8	6.5/6.7/7.5
Molecular weight	472	473	457	457
Chrom LogD pH 2.0, 7.4, 10.5	-0.3, 3.0, 2.0	0.0, 3.4, 2.2	-0.4, 3.0, 2.0	-0.5, 3.0, 1.9
pKa (potentiometric)	7.8, 5.5, 4.0	6.6, 5.7, 4.0	NT	7.4, 5.7, 4.1
Plasma protein binding (HSA % /AGP %)	93.5/ 81.9	96.7/ 84.5	93.0/ 75.2	91.9/ 83.1
Permeability (AMP/ MDCK nm/sec)	23/ 23	81/ NT	22/ 22	22/ 32
Solubility (CLND µg/mL)	173	136	264	216

Table 35. The RGD binding affinities and physicochemical properties of **17b**, **168**, **170a** and **170b**.[124,126,152] * denotes single enantiomer. NT =not tested.

Triazole **168** displayed the lowest activity of any racemic compound made in this series to date. The most basic centre on **168** has a measured pKa of 6.6, which is one log unit lower than **17b** and could potentially explain the poor potency against αvβ6. Having stated this, compounds such as pyridine **12** have shown good affinity for

159

Christopher J Tame

αvβ6 (cf. 6.9 pIC$_{50}$), whilst possessing no basic centre in the core of the molecule. In addition, the second pKa measurement for **168** is 5.7, which is similar to 5.5 obtained for pyrazole **17b**.

The lipophilicity of triazole **168** has increased by 0.4 log units when compared to pyrazole **17b**, which is also related to an increase in permeability and plasma protein binding. The relationship between lipophilicity and plasma protein binding correlates with previous examples such as thiophene **84b** and furan **86**, supporting the requirement for low Chrom LogD for suitable free fraction.

The only structural difference between **17b** and **168** is the replacement of a carbon atom for a nitrogen atom in the core of the molecule. Unlike the observations here, the addition of nitrogen is usually related to an *increase* in hydrogen-bonding interactions, and therefore a reduction in lipophilicity. In this case, however, the reduction in basic pKa (caused by the addition of nitrogen) is likely to have caused the increased lipophilicity by reducing the percentage of hydrogen bonding interactions with water. These findings suggest that reducing the pKa of **17b** by the addition of nitrogen in the core of the molecule actually increases lipophilicity and, therefore, plasma protein binding.

Unlike triazole **168**, pyrazolopyrrolidine **170** was designed to reduce the pKa of **17b** by removing a carbon from the saturated ring in the core of the molecule. This pleasingly resulted in an improvement in the αvβ6 potency and RGD integrin selectivity profile (**Table 34**). In fact, when compared with the other molecules made in this series, pyrazole **170b** was shown to be the most potent and RGD integrin-selective compound made to date (**Figures 34 and 35**).

Christopher J Tame
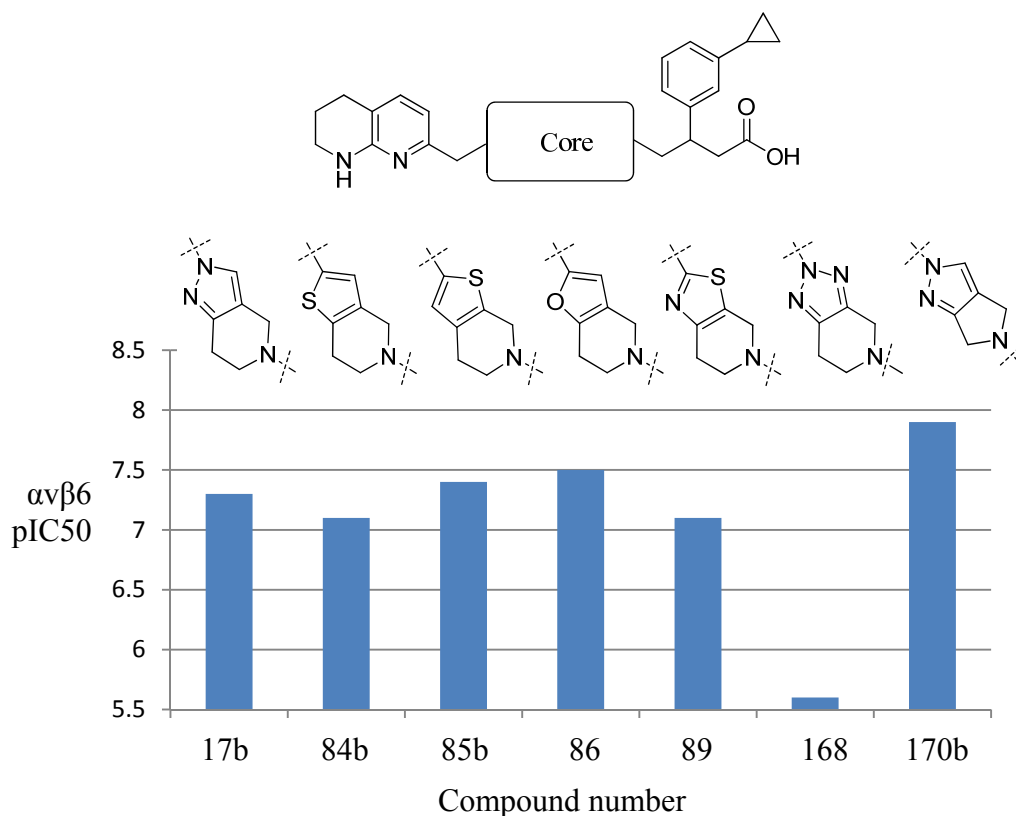
Figure 34: αvβ6 pIC50 values for a selection of molecules with a fused aromatic ring in the core of the molecule.[124]
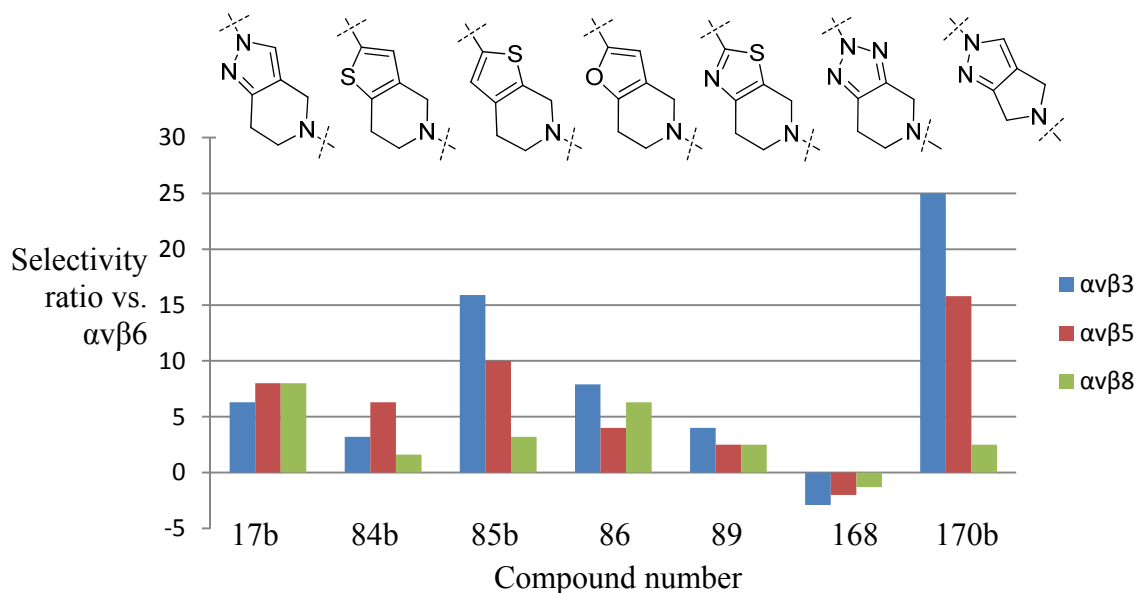
Figure 35: The selectivity ratios for αvβ6 verses the RGD binding integrins αvβ3, 5 and 8, which shows **170b** to be the most selective.[124]

Christopher J Tame

Analysis of the physicochemical properties of **170b** revealed a slight reduction in pKa when compared to **17b**, whilst maintaining a similar protein binding value (**Table 35**). This balance between pKa and protein binding fulfils the desired physicochemical parameters set out at the start of this work, which were expected to balance oral absorption and free fraction for suitable *in vivo* efficacy.

Whilst accepting the caveat that the reduction in pKa could be within error of the assay, it was rationalised that if real, the drop of 0.4 log units could improve oral absorption. Consequently, **170b** was selected for further investigation in a mouse PK study.[126]

To help predict the metabolic clearance of **170b**, it was first studied in mouse, rat and human microsomes *in vitro* (**Table 36**).[126] The results displayed good stability in all species tested, which supported the use of an *in vivo* study to fully assess the pharmacokinetic profile of **170b**.
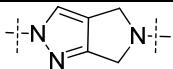
Species	170b Microsomal IVC (mL/min/g)
Mouse	< 0.5
Rat	< 0.5
Human	< 0.5

Table 36: The microsomal *in vitro* clearance (IVC) for pyrazolopyrrolidine **170b**.[126]

The results of the mouse pharmacokinetic study of **170b** are displayed in **Table 37**, which pleasingly show low-moderate clearance and moderate bioavailability. The total amount of drug observed after oral administration, however, is similar to that observed with thiophene **84b** (cf. 1075 ng/h/mL). The lower bioavailability relative to **84b** (cf. 91%) is a reflection of the greater stability of **170b** in blood, which

Christopher J Tame

increased the drug levels recorded when dosed intravenously. This is supported with the lower clearance observed with **170b** when compared with **84b**.
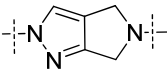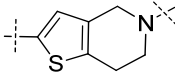
	170b		84b	
	p.o.	i.v. infusion	p.o.	i.v. infusion
Dose (mg/kg)	3.1	1.1	3.2	1.2
AUC$_{(0-\infty)}$ (ng/h/mL)	1010	1015	1075	441
Bioavailability (F%)	34	-	91	-
Clearance (Cl$_b$) (mL/min/Kg)	-	18	-	45
Half life (T ½) (h)	-	1.9	-	2.0
Volume of distribution (V$_d$) (L/Kg)	-	1.4	-	4.0

Table 37: The female C57BL6/J mouse PK profile of pyrazolopyrrolidine **170b** and thiophene **84b**.[126]

The volume of distribution is relatively low when compared to thiophene **84b** (*cf*. 3.5 L/Kg), which is potentially a reflection of the reduced lipophilicity of **170b**. The half life is moderate, which may need to be improved if a once-daily oral dose were to be administered.

When considering the low HPV AUC displayed by pyrazole **17b**, which possessed similar structure and pKa to **170b**, the moderate bioavailability was somewhat unexpected. However, a full *in vivo* PK study of **17b** was never conducted, which may have displayed a similar profile in such a study. Although these data would improve the understanding of the relationship between the short oral absorption model and an i.v./p.o PK study, it was not considered ethically appropriate to use animal lives to this end.

Christopher J Tame

To further understand the oral absorption of **170b** and the potential for the administration of large doses, an oral PK study was undertaken in the mouse with a 30 mg/Kg dose.[126] This afforded an average bioavailability of 20%, a slight drop when compared to 35% obtained after 3 mg/Kg dose. This could indicate that the oral absorption of **170b** is partially driven by active transport, which is saturated at higher doses and results in a non-linear dose-PK relationship. These results are not considered to negatively impact the potential progression of **170b**, but rather help future dose predictions for *in vivo* studies.

In an attempt to understand the pharmacokinetic profile of **170b** across a number of species, and therefore provide a more reliable prediction of the human PK profile, an i.v./p.o. PK study was undertaken in the rat (**Table 37**).[126]
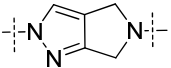
170b in female Wistar Han rats	p.o.	i.v. infusion
Dose (mg/kg)	1.0	1.0
AUC$_{(0-\infty)}$ (ng/h/mL)	693	1017
Bioavailability (F%)	-	67
Clearance (Cl$_b$) (mL/min/Kg)	-	17
Half life (T ½) (h)	-	1.6
Volume of distribution (V$_d$) (L/Kg)	-	0.9

Table 38: The rat PK profile for pyrazolopyrrolidine **170b**.[126]

The bioavailability of **170b** in the rat was measured at 68%, a vast improvement from the value of 35% obtained in the mouse. This could either reflect an increase in passive intestinal absorption or a higher occurrence of the relevant proteins required for active transport. The rat liver blood flow is similar to that of the mouse (85 and 90 mL/min/Kg, respectively),[244] which suggests that the clearance observed in the rat can still be considered low to moderate. The half life is also similar across both species, which may need further optimisation.

Christopher J Tame

To summarise, pyrazolopyrrolidine **170b** displayed moderate to excellent oral bioavailability and low to moderate clearance in rodent PK studies, whilst maintaining relatively low plasma protein binding. In an attempt to more accurately represent the free fraction of pyrazolopyrrolidine **170b**, and therefore the potential for *in vivo* efficacy, the whole blood binding data was obtained (**Table 39**). Whilst the mouse blood binding of pyrazolopyrrolidine **170b** is 5% lower than thiophene **84a**, the human blood binding is still considered very high at >99%. If it is considered that free fraction determines efficacy, then a blood binding value of less than 90% would help minimise the administered dose. This, along with solubility and permeability, has been shown to correlate to the *in vivo* performance of oral drugs in the developability classification system (DCS).[245]
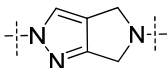
Species	170b whole blood binding (%)	85b whole blood binding (%)
Mouse	95.2	99.5
Rat	97.6	>99.9
Human	99.4	>99.9
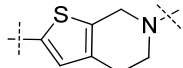
Table 39: Whole blood binding for pyrazolopyrrolidine **170b** and thiophene **85b**.[126]

The next stage of investigation would involve testing pyrazolopyrrolidine **170b** in an *in vivo* pharmacodynamic model, which would help elucidate the potential effect of free fraction on efficacy. This was expected to determine the potential for compounds with high blood binding, such **170b**, to be progressed as a therapy for IPF.

In order to facilitate an *in vivo* PD study, further investigation into the αvβ6 potency and the off-target activity of **170b** was required. Accordingly, pyrazolopyrrolidine **170b** was studied in the normal human bronchial epithelial (NHBE) cell assay, which provided a more accurate representation of αvβ6 potency. This resulted in a pIC50 of 6.3, which pleasingly confirms the ability for **170b** to reduce the release of PAI 1, a cytokine related to αvβ6 activity and the onset of fibrosis.[103]

Christopher J Tame

In addition to the NHBE assay, pyrazolopyrrolidine **170b** was tested against a wide range of other biological targets. These were selected for their potential to cause toxicity or other undesired off-target effects. Activity against these would be considered detrimental to the progression of **170b** as a drug candidate. Fortunately, pyrazolopyrrolidine **170b** did not significantly inhibit any of these targets (**Appendix 1**).

The availability of reliable *in vivo* pharmacodynamic models for fibrotic diseases was very low at the time this research was conducted. The very high blood binding of pyrazolopyrrolidine **170b** was also considered to be potentially detrimental to the chances of exhibiting efficacy in an *in vivo* PD model. As a result, further investigation of pyrazolopyrrolidine **170b** was postponed, in favour of further optimisation efforts to identify a selective αvβ6 antagonist with oral bioavailability and blood binding < 90%. Despite this, pyrazolopyrrolidine **170b** still represents a promising lead with excellent potency and acceptable αvβ6 selectivity. Compound **170b** could then represent an attractive back-up compound to other lead series.

3   Analysis of calculated and measured lipophilicity and basicity values

The research detailed in this thesis has relied on calculated lipophilicity and basicity values to help design new molecules with improved pharmacokinetic profiles. Indeed, this process has been used to triage a selection of compounds down to a small number of examples which are expected to represent specific areas of physicochemical property space predicted to be of interest. The search for unique molecules which balance the desired pharmacokinetic-pharmacodynamic relationship for a given biological target inevitably leads medicinal chemists into undefined physicochemical space within a given lead series. Accordingly, the use of calculated properties becomes less reliable, as they typically rely on measured values from fragments of existing and well studied compounds. The incorporation of novel or rare ring systems and behaviours such as intramolecular interactions are, therefore, less well predicted by these models. This may result in misleading calculated values. Therefore, it is pertinent to review the relationship between the calculated and

measured values to assist the development of more accurate models for future research. Accordingly, the calculated and measured lipophilicity and pKa values for a selection of RGD-integrin antagonists were compared. The results for lipophilicity are presented in **Table 40** and **Figures 36** and **37**, whilst the results for pKa are displayed in **Table 41** and **Figures 38** and **39**.

The lipophilicities were compared for both cLogP and cLogD values to investigate the ability of these models to predict the lipophilicity at physiological pH (7.4). Pleasingly, both models demonstrated moderate and similar levels of positive correlation, with calculated LogD values providing a marginally more accurate prediction (**Figures 36** and **37**).

The calculated logP values seem to more accurately predict the trend in lipophilicity in a particular structural series, which is demonstrated by the poor prediction of pyridine **12** and piperidine **13** (**Figure 36**). In addition, the cLogP model predicts greater differences in lipophilicity than the observed values. This supports the rule applied to the design of the compounds presented in this work which aimed to increase the lipophilicity. A minimum increase of 0.5 log units when compared to pyrazolopiperidine **17b** was required for the selection of replacement cores, which would have removed this error in the calculated values.

The relationship between the calculated and measured pKa values of the basic centre in the core of a range of integrin antagonists is displayed in **Figure 38**, which show a modest positive correlation. However, the accuracy of the model to predict the pKa values of the weakly basic triazole **168** was poor when compared to pyrazoles **170b** and **17b**. This inadequacy is also apparent between calculated and measured pKa of the tetrahydronaphthyridine (THN) in **Figure 39**, which fails to show any correlation. These findings highlight the limitation of the model when attempting to identify changes in the pKa of weakly basic integrin antagonists, which could be an area for further investigation.

Christopher J Tame

n	12	13	17b	84b	85b	86	89	168	170b
cLogP	5.5	5.9	3.5	5.3	5.3	4.8	4.3	3.1	3.2
cLogD pH 7.4	3.1	3.8	2.9	4.6	4.3	3.9	3.7	3.7	3.2
Chrom LogD pH 7.4	2.7	3.7	3.1	4.5	4.6	4.2	3.7	3.4	3.0

Table 40: The comparison of calculated and measured lipophilicity for a range of αvβ6 integrin antagonists
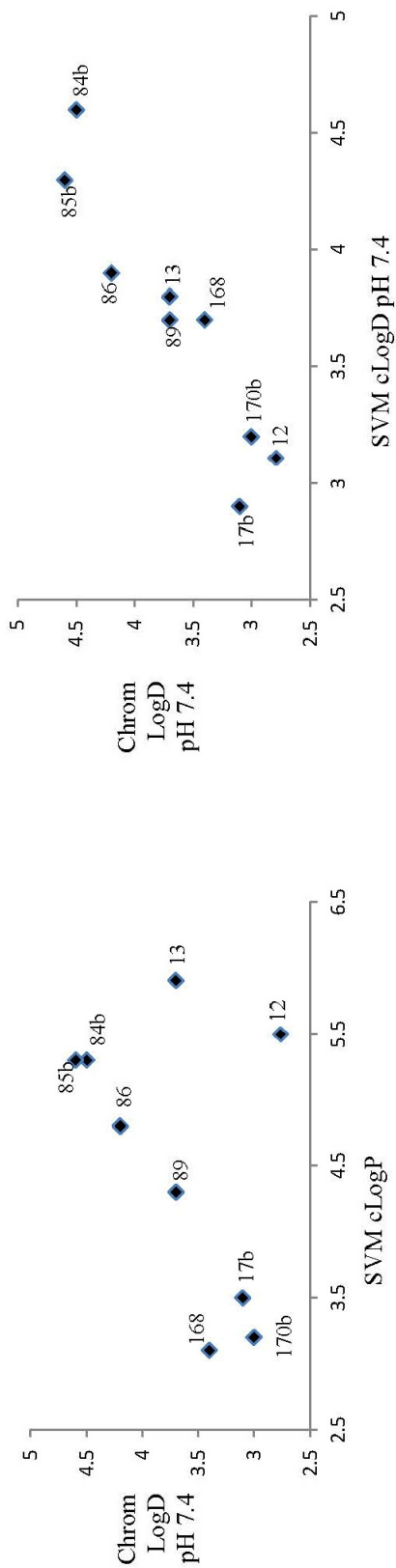
Figure 36: The comparison of cLogP and measured Chrom LogD.

Figure 37: The comparison of calculated and measured Chrom LogD.

n	12	13	17b	84b	85b	86	89	168	170b
PKa (core/THN)	NT	NT	7.8/5.5	8.2/6.8	NT	8.4/7.2	NT	6.6/5.7	7.4/5.7
calc. pKa (core/THN)	7.2/5.9	9.9/7.5	8.1/6.6	9.4/6.4	9.7/6.4	9.0/6.2	8.9/6.0	7.6/6.2	7.2/6.3

Table 41: The comparison of calculated and measured pKa values for a range of αvβ6 integrin antagonists
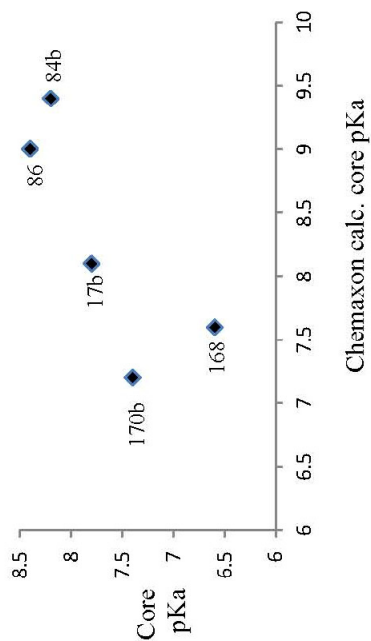
Figure 38: The comparison of calculated and measured pKa values.
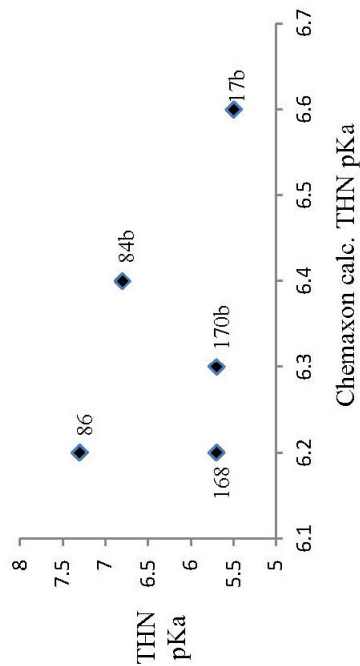
Figure 39: The comparison of calculated and measured pKa values.

Christopher J Tame

4   Future Work

The attractive potency, selectivity, and PK profile of pyrazolopyrrolidine **170b** makes it suitable for further optimisation strategies. This would have the aim of reducing the blood protein binding below 90%, whilst maintaining oral bioavailability in the mouse of around 30%.

The moderate bioavailability observed in the mouse and good bioavailability observed in the rat suggests that a reduction in the lipophilicity of pyrazolopyrrolidine **170b** could still maintain bioavailability at ~30%. If this reduction in lipophilicity did not affect the pKa, then it could result in a reduction of blood binding affinity.

Analysis of the potential structural modifications which could alter the lipophilicity of pyrazolopyrrolidine **170b** was subsequently undertaken (**Figure 40**). This revealed that manipulations to the phenyl ring would have the best chance of adjusting the lipophilicity without affecting the pKa. Such changes to a phenyl unit within an analogous series have been extensively investigated (**Table 9**), suggesting that these changes would be tolerated by αvβ6 and selectivity could be maintained.

Christopher J Tame
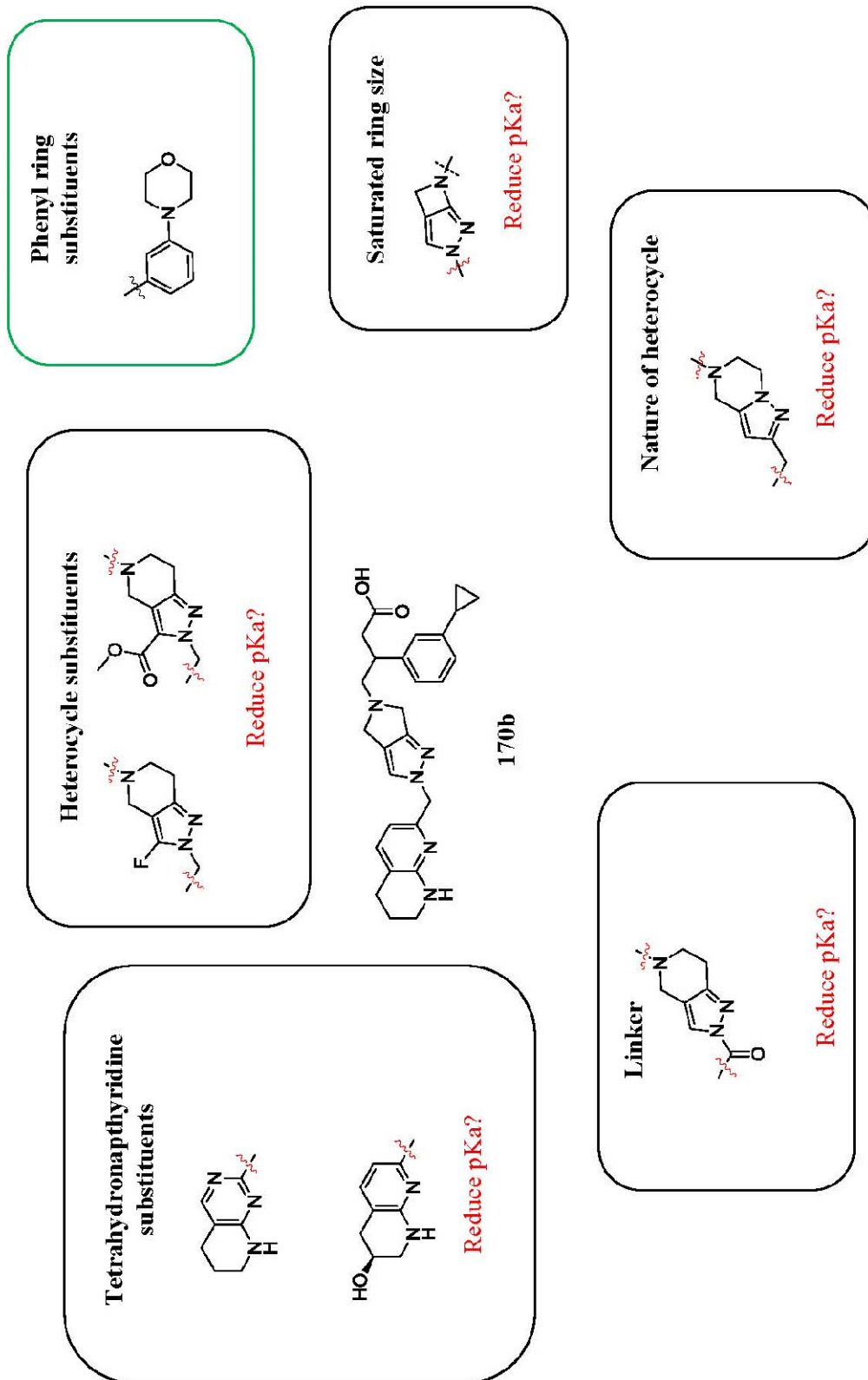
Figure 40: Potential modifications to compound **170b** for reduced lipophilicity.

Christopher J Tame

The synthetic chemistry used to access these compounds could follow the pre-validated route to access late stage intermediate **240** and exploit the commercial availability of numerous arylboronic acids (**265**), which highlights the feasibility of this approach (**Scheme 95**).
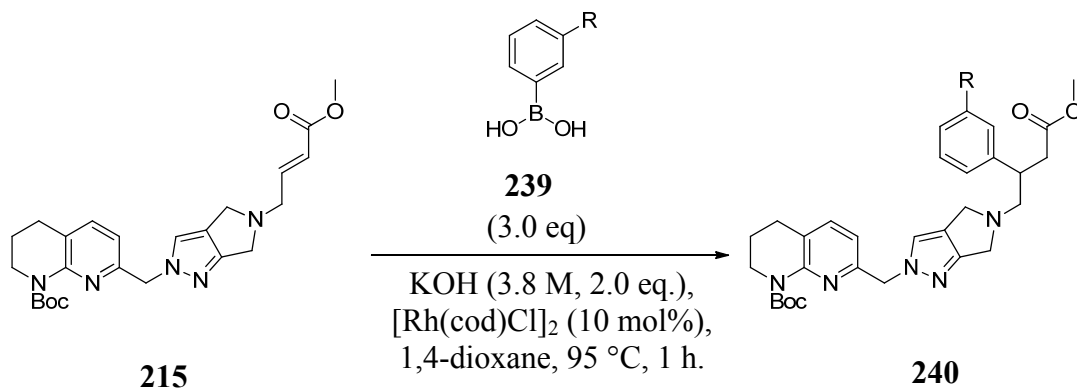
Scheme 95: The proposed synthetic route to access analogues of pyrazolopyrrolidine **170b** with modified phenyl ring substituents.

Initial efforts could utilise the commercial availability of the arylboronic acids to investigate a wide range of physicochemical properties. The results from this array approach could then be used to identify the desired physicochemical properties to balance oral absorption and blood binding, which may require bespoke synthesis of an appropriate arylboronic acid.

Christopher J Tame

5   Summary

The only small molecule therapy approved for IPF is Pirfenidone, which acts through multiple biological mechanisms and consequently possesses numerous severe side effects. In addition, Perfinidone has questionable efficacy from multiple clinical trials. Considering this, its world-wide approval for sale demonstrates the significant unmet need for safe and efficacious treatments of IPF.

In relation to this pressing objective, the selective modification of the integrin αvβ6 presents an opportunity for modification of IPF disease progression without undesirable side-effects. The lack of RGD-integrin selectivity or suitable oral PK profile of the αvβ6 antagonists published in the literature highlighted the benefit that further research towards the identification of a selective and orally-bioavailable small molecule αvβ6 antagonist would have for IPF patients

The biological data for all key compounds synthesised in this work have been collated and are presented in **Table 42**. This illustrates the improvements made to the oral PK profile of a selective αvβ6 antagonist through the optimisation of pyrazolopiperidine **17b** lipophilicity and pKa, and is summarised below.

The optimisation of the oral pharmacokinetic profile of lead **13** was attempted by reducing the basic pKa of a tertiary amine in the core of the molecule. Initial work focused on the resynthesis of a promising lead (**16**), which included structural modifications to improve RGD-integrin selectivity. This identified pyrazolopiperidine **17b**, which displayed low oral absorption and, more promisingly, low hepatic clearance in a mouse short oral absorption model.

Optimisation of the lipophilicity of pyrazolopiperidine **17b** identified thiophene **84b** as a potent and selective replacement, which displayed excellent oral bioavailability in mouse PK studies. Thiophene **84b** represented the first compound to display αvβ6-selectivity and good oral bioavailability when profiled in our assays. However, thiophene **86b** was also very highly bound to mouse, rat and human blood, limiting

Christopher J Tame

further investigation of this molecule in disease-relevant *in vivo* studies. Attempts to reduce the lipophilicity of thiophene **84b** with furan **86** and thiazole **89** were not successful in significantly reducing plasma protein binding.

Research then focused on improving the oral absorption of pyrazolopiperidine **17b** without increasing the lipophilicity. Subsequent modification of the basic pKa of the core template identified pyrazolopyrrolidine **170b**, which displayed good PK profiles in mice and rats after oral and i.v. administration. In addition, pyrazolopyrrolidine **170b** represented the most potent and RGD integrin selective αvβ6 antagonist to possess a suitable PK profile for oral administration, as well as promising activity in relevant pharmacological assays. The human blood binding of pyrazolopyrrolidine **170b** was reduced to 99.4%, although this was still considered very high and may limit efficacy in an *in vivo* pharmacodynamic study. However, pyrazolopyrrolidine **170b** also showed no toxicity issues after wider selectivity screening, which highlighted the promising safety profile of this template. Taken together, the data generated identified pyrazolopyrrolidine **170b** as a promising lead which can be used to probe the *in vivo* pharmacology of αvβ6 dependent idiopathic pulmonary fibrosis when a suitable assay becomes available.

Pharmacodynamic profiling of pyrazolopyrrolidine **170b** in an *in vivo* setting will help determine the relationship between free fraction and efficacy, and whether this needs to be optimised further.   In addition, testing pyrazolopyrrolidine **170b** alongside the αvβ6-selective antibody 3G9 and the pan-RGD integrin inhibitor **12** will help understand the pharmacological relevance of the *in vitro* selectivity assays, and whether further optimisation is required here also.

In conclusion, the research undertaken in this chapter has identified the first series of αvβ6-selective small molecules which possess a pharmacokinetic profile suitable for an orally administered treatment of IPF. This presents the potential for offering IPF patients a treatment with reduced side-effects and a more convenient mode of delivery when compared to existing therapies presented in the literature. This series has been optimised to improve the pharmacokinetic profile and reduce the level of

Christopher J Tame

blood binding, which identified pyrazolopyrrolidine **170b** as the optimal compound. Pharmacodynamic profiling in an *in vivo* setting is expected to provide further guidance on the potency, selectivity profile and free-fraction required for *in vivo* efficacy.

Christopher J Tame

n	12	13	17b	84b	85b	86	89	168	170b
MW	459	462	472	488	488	472	489	473	457
Chrom LogD pH 7.4	3.2	3.7	3.1	4.5	4.6	4.2	3.7	3.4	3.0
pKa	7.6/5.5/3.8†	9.7/8.1/3.9†	7.8/5.5/4.0	8.2/6.8/4.1	-	8.4/7.3/4.5	NT	6.6/5.7/4.0	7.4/5.7/4.1
Rotatable bonds	9	9	7	7	7	7	7	7	7
$\alpha v \beta 6$ (pIC50)	6.9	7.6	7.3	7.1	7.4	7.3	7.1	5.6	7.9
$\alpha v \beta 3/5/8$ (pIC50)	8.0/8.2/7.1	6.8/6.9/6.5	6.5/6.4/6.4	6.6/6.3/6.9	6.2/6.4/6.9	6.4/6.7/6.6	6.5/6.7/6.7	6.1/5.9/5.7	6.5/6.7/7.5
Species	Rat	Mouse*	Mouse*	Mouse	-	-	-	-	Mouse, Rat
Dose (i.v./p.o., mg/kg)	1.0/1.0	-/3.0*	-3.0*	1.2/3.2	-	-	-	-	1.1/3.1, 1.0/1.0
AUC(0-∞) (i.v./p.o., ng/h/mL)	2192/2133	-/382*	-/417*	441/1075	-	-	-	-	1015/1010 693/1017
Bioavailability (F%)	98	-	-	93	-	-	-	-	34, 67
Clearance (Cl, mL/min/Kg)	7.6	51*	23*	45	-	-	-	-	18, 17
Half life (T1/2, h)	1.75	-	-	2.0	-	-	-	-	1.9, 1.6
Volume of distribution (Vd, L/kg)	0.52	-	-	4.0	-	-	-	-	1.4, 0.9
PPB (HSA/AGP, %)	97/89	88/90	94/82	97/93	97/93	97/93	97/87	97/85	92/83
Blood binding (m/r/h, %)	-	-	-	-	100/100/100	-	-	-	95/98/99
Solubility (CLND, µg/mL)	153	218	173	162	228	147	182	136	216
Perm. (MDCK, nm/sec)	68	43	23	320	349	196	217	81*	32

Table 42: The RGD-binding integrin potencies and PK profiles for the compounds synthesised in this work, compared with benchmark compounds **12** and **13**. † denotes pKa measurements taken from representative compounds. Text highlighted in red denotes rat PK data. * Result from short oral absorption (SOA) study (3 mg/kg p.o. dose only). AUC values are taken from systemic blood (0-last) and clearance is only hepatic.

176

Christopher J Tame

CHAPTER 2

The Inhibition of Phosphoinositide-3-Kinase δ and γ for the Treatment of Asthma

1.   Introduction

1.1   Asthma

Asthma is a physiological condition typified by symptoms such as wheezing, shortness of breath and tightening of the chest. These are a result of the contraction of smooth muscle around the airways which is caused by an excessive reaction to an environmental trigger (**Figure 41**). Typical triggers include: house-dust mites, pollen, smoke, and animals.[246] A 2007 publication by the World Health Organisation claimed asthma to be responsible for 255,000 worldwide deaths in 2004, and estimated 300,000,000 people to be suffering from asthma in the same year.[247]
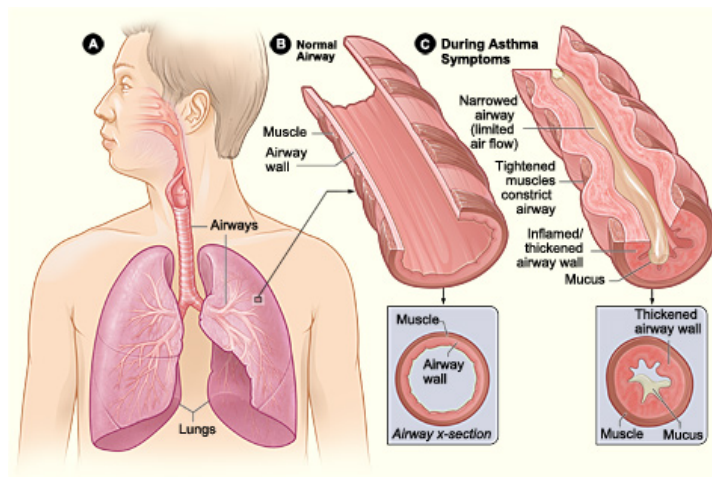
Figure 41: The comparison between a normal airway (B) and an airway during an asthmatic exacerbation (C) in a human lung (A).[248]

Christopher J Tame

Current treatments for asthmatic exacerbations generally involve the inhalation of bronchodilators (**Figure 42**). These medicines relax smooth muscle in the airways by stimulating the action of the beta-2-adrenergic receptor. Long-acting beta-agonists (LABAs), taken without corticosteroids, have been shown to increase the likelihood of death from asthma, as well as promoting bronchial inflammation.[249] Inhaled corticosteroids (IHCs) have also shown to have a number of undesired side-effects, including cataracts, glaucoma and stunted growth.[250] As a result of this, a long-acting asthma treatment with an improved safety profile is desired.

241

Salmeterol

242

Fluticosone Propionate

Traditional Inhaler
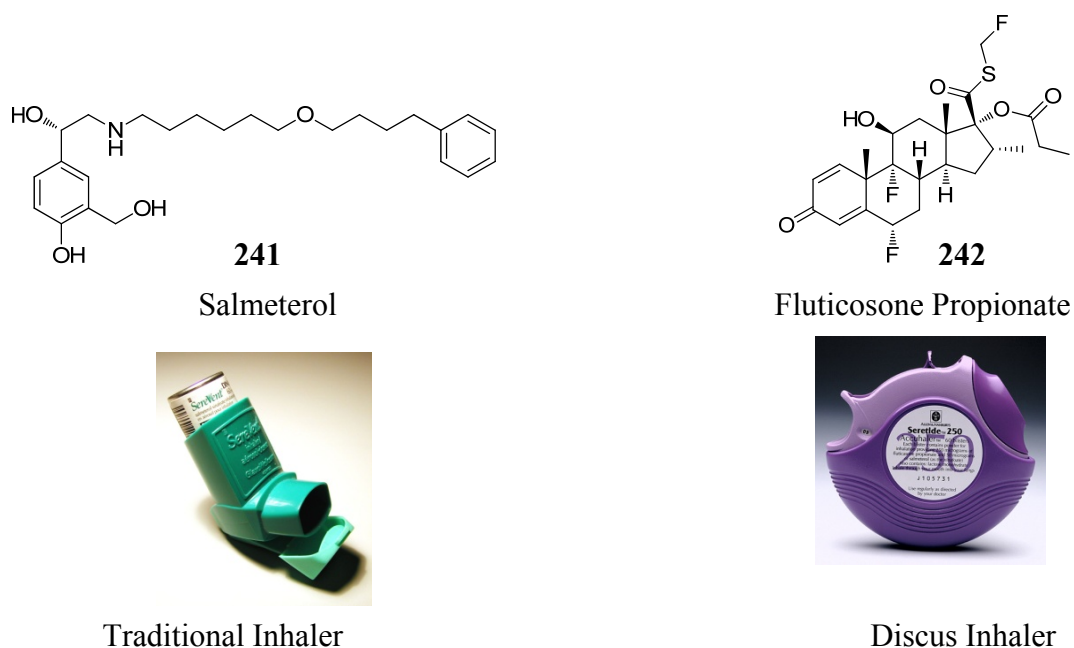
Discus Inhaler

Figure 42: The long-acting beta-agonist Salmeterol (**241**) in a traditional inhaler (left), and in combination with the steroid Flucticosone Propionate (**242**) in the Discus inhaler (right).

Kinases are a class of biological targets that play a role in cell signalling and have been shown to regulate a range of diseases including asthma.[251] Kinase activity has been modified using small molecules[252] and knowledge of their three dimensional structure facilitates X-ray crystal structure-driven drug discovery, an attractive technique which provides a window on target-ligand interactions for the medicinal chemist. Therefore, global research efforts are attempting to create new asthmatic treatments through the modulation of a range of kinases.[253]

Christopher J Tame

1.2   Kinases

Kinases are intracellular signalling proteins that transfer messages between each other in the form of phosphate groups.[254]   These messages regulate a range of processes such as gene expression and controlling the release of intercellular messengers such as cytokines. Cytokines are proteins, peptides or glycoproteins that bind to cell-surface receptors which initiate intra cellular messaging cascades, culminating in an immunomodulatory response. Examples of cytokines include the interleukins and interferons.[255]

Figure 43 illustrates a kinase-mediated intracellular message transfer.[256] A signal molecule (such as a cytokine) is recognised by a receptor at the cell surface. This process activates protein kinase 1, which in turn activates protein kinase 2 by transferring a phosphate group to it from adenosine triphosphate (ATP). Adensodine diphosphate (ADP) is produced and is regenerated to ATP elsewhere in the cell. Active protein kinase 2 then activates protein kinase 3 in a similar manner, which will activate other kinases in a domino effect (known as the phosphorylation cascade) until a final protein is activated, which invokes a different cellular response.

Christopher J Tame
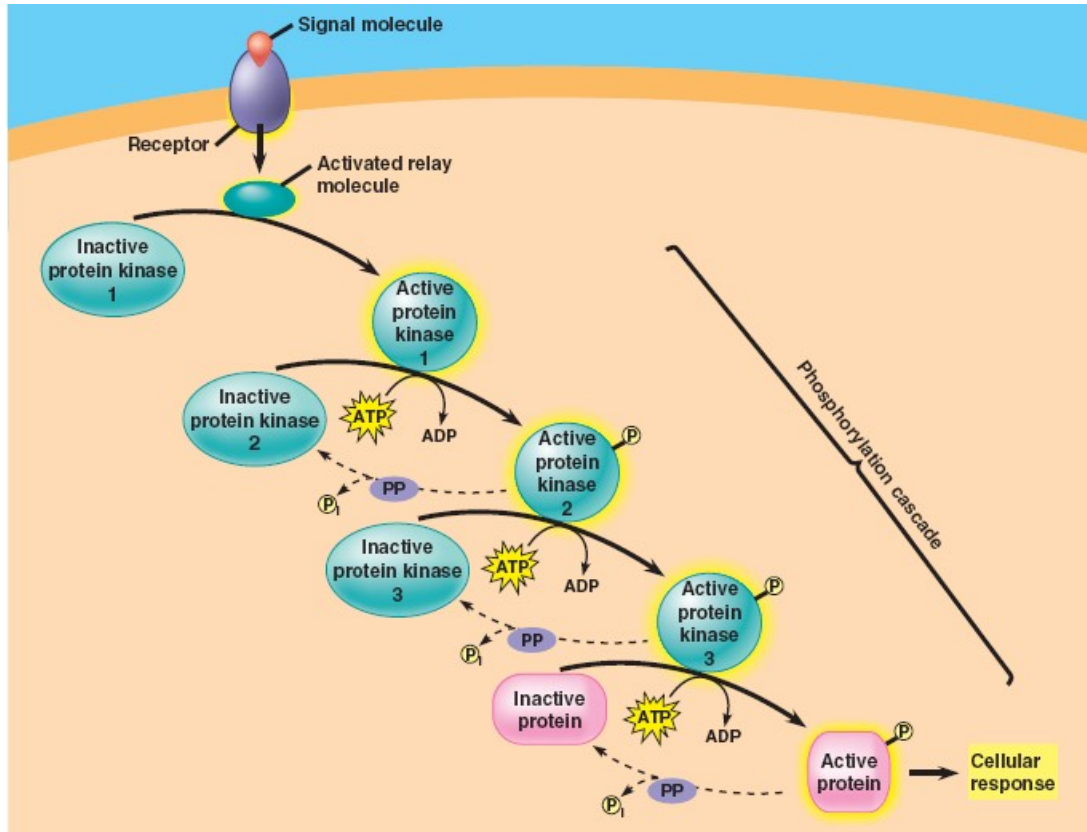
Figure 43: A kinase mediated phosphorylation cascade.[256]

There are over 500 structurally-related protein kinases which make up the human kinome (**Figure 44)**. Each kinase controls different cellular signalling pathways and they are grouped into seven families based on the amino-acid residues they phosphorylate:[257]

1. Tyrosine kinases (TK),
2. Tyrosine kinase-like kinases (TKL),
3. Homologs of yeast sterile 7, sterile 11 and sterile 20 kinases (STE),
4. Casein kinase 1 (CK1),
5. Protein kinase A, protein kinase G and protein kinase C (AGC),
6. Calcium/calmodulin-dependent protein kinase (CAMK), and
7. CDK, MAPK, GSK3, CLK families (CMGC).

Christopher J Tame
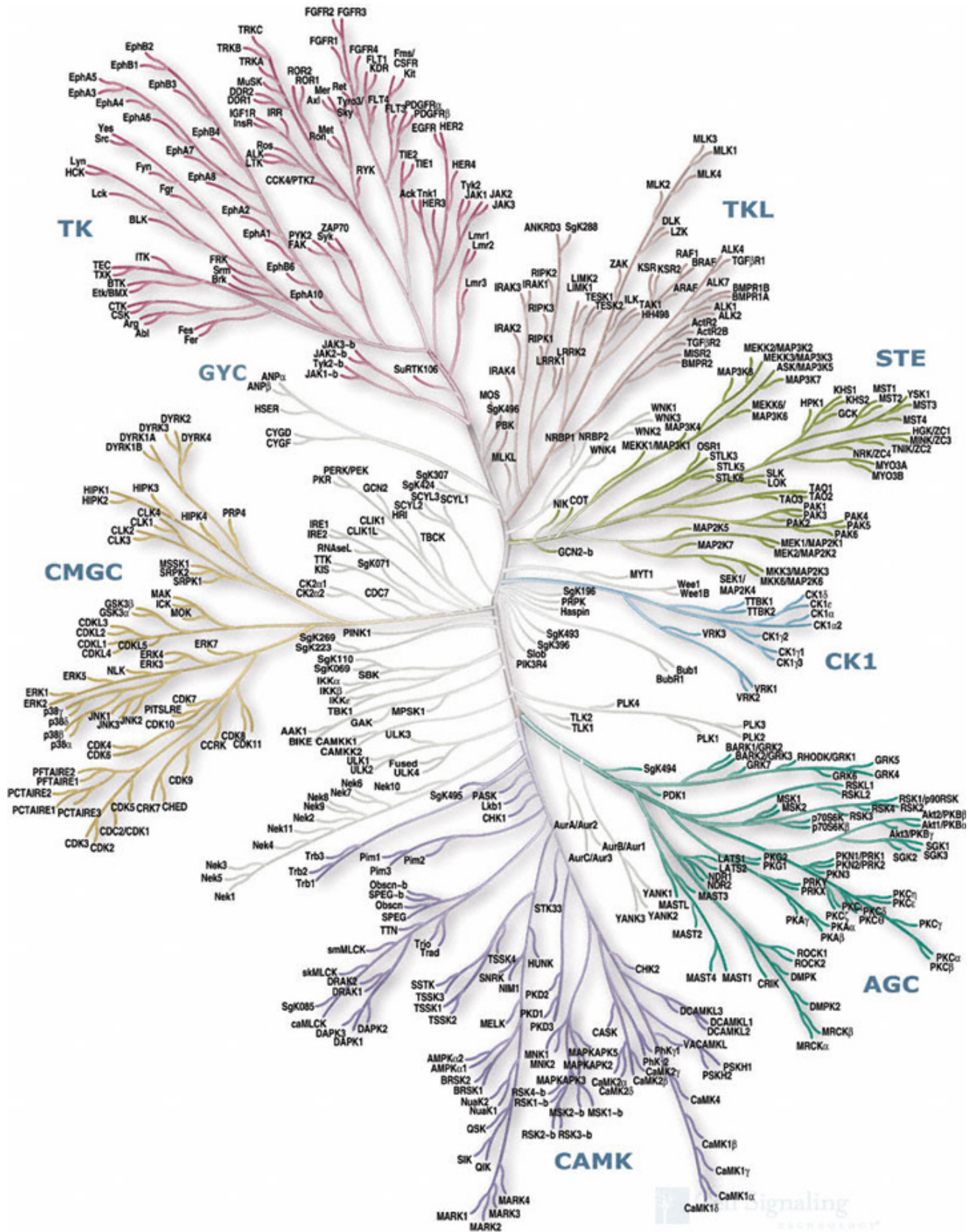
Figure 44: The human protein kinome.[258]

Christopher J Tame

The general three-dimensional structure of protein kinases are described as having two lobes, an *N*-terminus and a *C*-terminus. These are connected by a small strand of protein referred to as the hinge region or, more generally, the active site (or activation segment, **Figure 45**).[259] Changes to this region can alter the conformation of the entire kinase, therefore controlling its behaviour. It is at the active site where a phosphate group is obtained by abstraction from an adenosine triphosphate (ATP) molecule which activates the kinase towards other phosphorylation cascades. This area is typically targeted for small-molecule therapies by blocking the binding of ATP to the kinase.
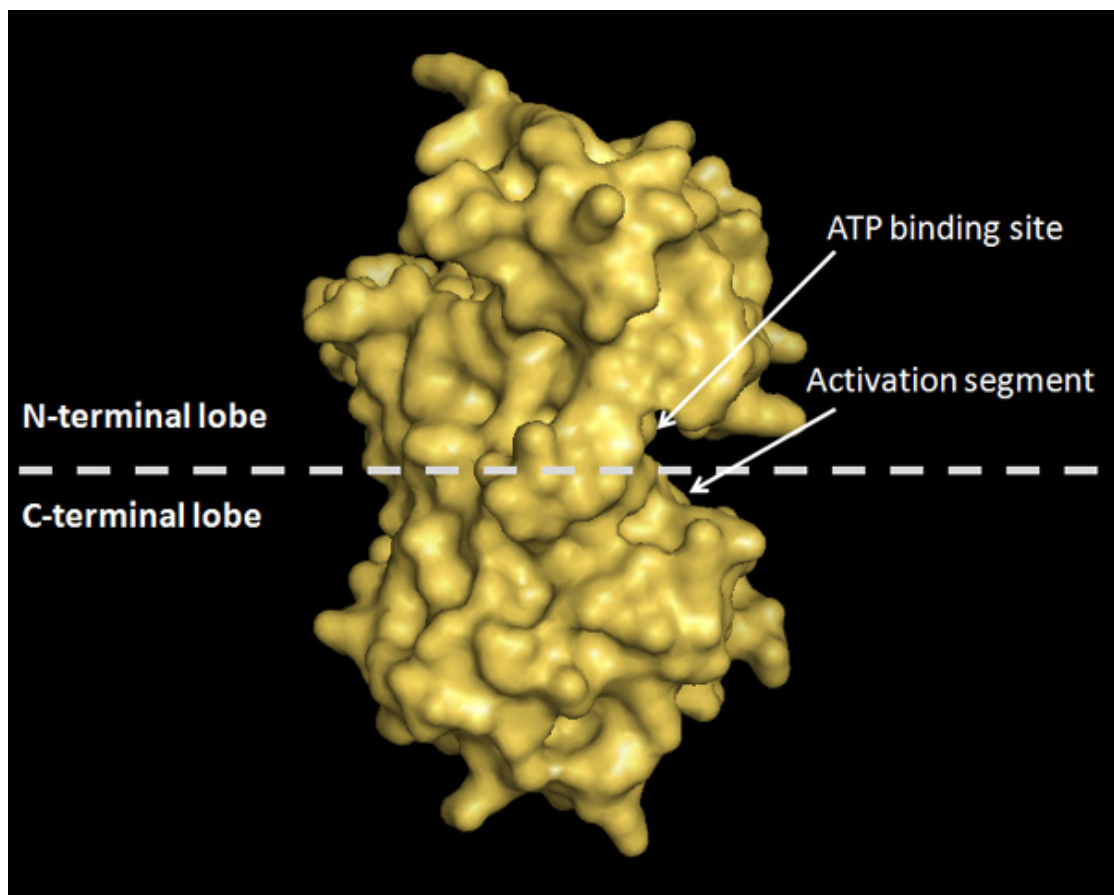
Figure 45: A solved x-ray crystal structure of a kinase.[259]

As a direct consequence of evolution, all kinases bind ATP, which means all active sites are structurally similar. An example of the typical interactions ATP makes with a kinase active site is illustrated for the case of PI3Kγ in **Figure 46**. A key hydrogen

Christopher J Tame

bonding interaction is made between the pyrimidine nitrogen of ATP and the hinge residue Val 882 in PI3Kγ. The phosphate residues are positioned in a polar region of the kinase and interact with a number of water molecules and other polar residues, such as the primary amine of Lys 833 and the alcoholic Ser 806.
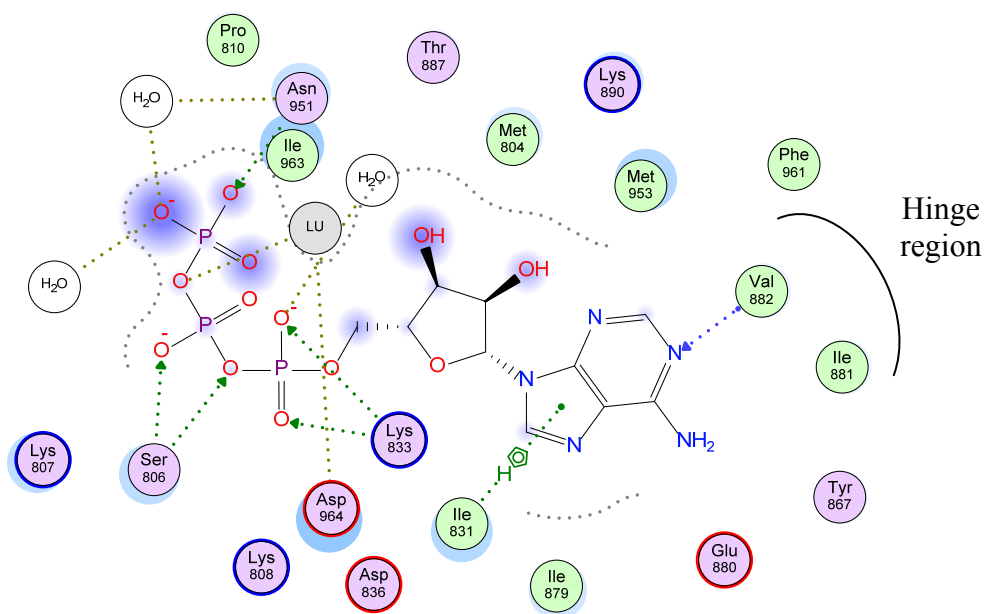
Figure 46: An interaction map of the solved crystal structure of ATP bound into the active site of PI3Kγ.[260]

There are three classes of kinase inhibitors, of which the majority are ATP-competitive and are termed type I. Typical type I small molecule kinase inhibitors require a strong hinge binding interaction that mimics the interaction between ATP and, for example, Val 882 in PI3Kγ (Val 826 in PI3Kδ). Carefully designing other polar and non-polar residues into complementary areas of the protein can help improve the potency and selectivity profile.

Kinases can exist in either active or inactive forms, which are dictated by the position of a specific protein chain called the activation loop. At one end the loop contains the residues aspartic acid (D), phenylalanine (F) and glycine (G), which are essential for phosphorylation and can exist in an 'in' or 'out' conformation.[261] Phosphorylation can only occur when the DFG motif exists in its 'in', or 'active'

Christopher J Tame

conformation. Type I kinase inhibitors compete with ATP to bind to the active form of the kinase. Type II inhibitors stabilise the inactive form of the kinase by binding to protein residues inside and outside of the ATP binding site. This inactive form prevents ATP from binding, and is therefore not directly competitive with ATP.

Kinase inhibition can also be achieved with small molecules that interact with amino acid residues that are distinct from that of the ATP binding site. These are type III inhibitors and their mode of action is termed allosteric modulation. This can have a number of effects but typically causes a change in the active site shape or prevents other interactions at the kinase surface. Changes in the active site shape can result in an incompatibility with ATP, which presents an orthogonal approach to ATP-competitive inhibition.

1.3   Kinases and disease

Changes in kinase expression have been observed in a range of diseases including asthma,[251] liver fibrosis,[262] and multiple cancers.[263] This suggests that restoring kinase function to normal levels could treat the related disease and, accordingly, a common approach to disease modification is to reduce the activity of a specific kinase. This can be achieved by using a small molecule to inhibit the binding of ATP in the active site of the kinase. Such an approach has been successful, with kinase inhibitors such as the Anti-Estrogen Receptor b1, b2 (ERB1/2) inhibitor Lapatinib (**3**)[264] for breast cancer and the BCR-ABL[265] inhibitor Imatinib (**4**)[266] for chronic myelogenous leukaemia, approved for sale by the food and drug administration (FDA) in 2007 and 2001, respectively (**Figure 47**). A solved crystal structure of Imatinib in c-Abl, the kinase for which it was designed to inhibit, is shown in **Figure 48**,[267] highlighting the utility of a structure based drug design approach in identifying kinase inhibitors.

Christopher J Tame

243 **244**
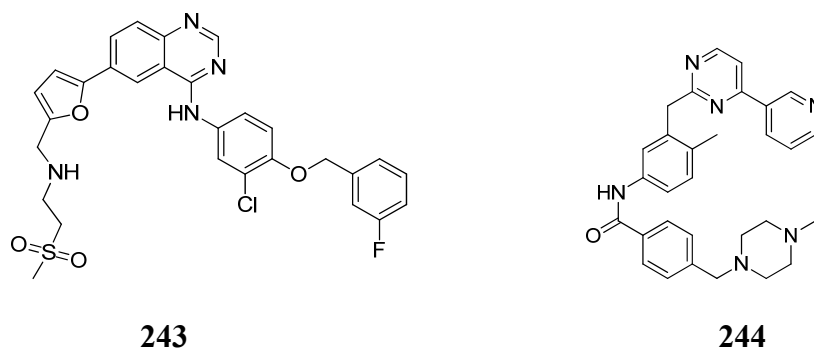
Figure 47: Kinase active site inhibitors Lapatinib (**3**) and Imatinib (**4**).
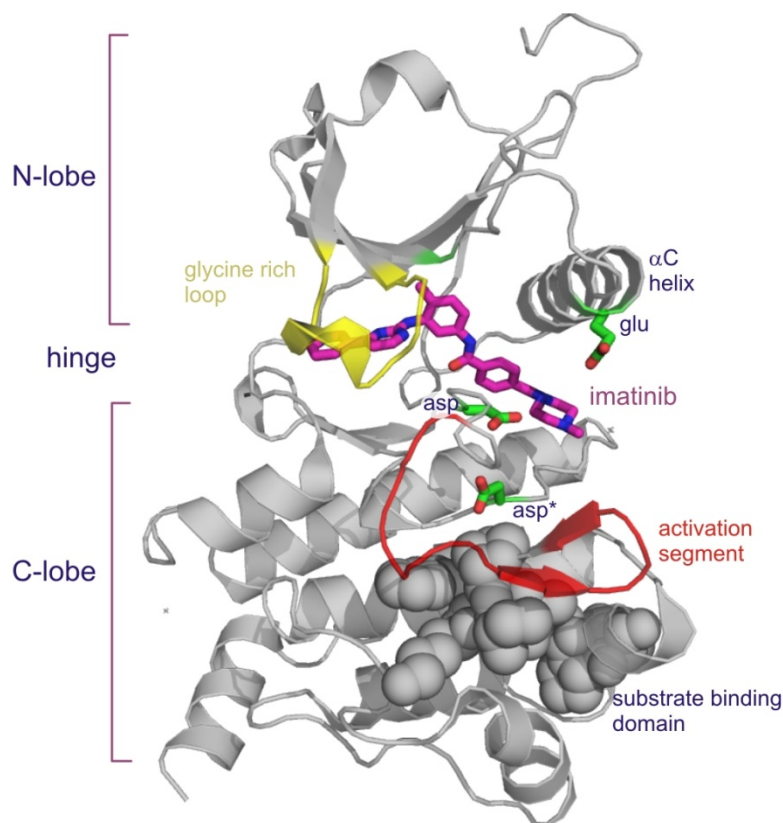
Figure 48: A solved X-ray crystal structure of Imatinib (**4**) in c-Abl.[267]

Despite being targeted at a small number of kinases, these drugs rely on a degree of promiscuity across the human kinome for their wide range of therapeutic indications. Imatinib, for example, has been granted approval by the FDA for treatments of 10 different cancers, some of which are controlled by different kinases. This lack of selectivity is also the likely cause of a range of undesired side-effects, ranging from nausea and vomiting to joint swelling and yellowing of the skin.[268]

Christopher J Tame

Cancer treatments like Imatinib can afford to exhibit such a profile due to the overall improvement in the quality of life to the patient. Side effects like these, however, outweigh the clinical benefits offered by asthma treatments, and are therefore unacceptable liabilities. For this reason asthma treatments that are selective across the human kinome are urgently required.

All kinases bind ATP in their active site, and are therefore structurally very similar in this region. There are however subtle differences which could be exploited to achieve selectivity. As a result, the main aim of drug discovery programmes that target protein kinases for asthma is to exploit these differences to achieve selectivity. To date, there have been no small molecule inhibitors of kinases that have been approved to treat asthma, which illustrates the difficulty of the task.

1.4   Phosphoinositide-3-kinases (PI3Ks)

The phosphoinositide-3-kinases (PI3Ks) are a family of lipid kinases that are implicated in the development of a range of diseases, including respiratory inflammation.[269,270] They comprise three classes based on structure, mode of regulation and phospholipid substrate. The class I targets have been extensively investigated due to their role in various cancers and inflammatory diseases, and will be the subject of this research.[269,271] By contrast, comparatively little is known about the structure or function of class II and III targets.

Class I PI3Ks phosphorylate phosphatidylinositol (4,5)-diphosphate (PtdIns(4,5)P2), to produce phosphatidylinositol (3,4,5)-triphosphate (PtdIns(3,4,5)P3).[272] By distinction, the class II and III PI3Ks phosphorylate phosphatidylinositol (PtdIns), to produce phosphatidylinositol (3)-monophosphate (PtdIns(3)P).[273,274] The physiological role of each kinase can vary, depending on their expression levels in specific tissues.

Two of the three PI3K class II targets (PI3K-C2α, PI3K-C2β) are expressed in the clathrin-coated or endocytic compartment, and influence vascular biology.[275] A

Christopher J Tame

recent study has identified an independent role of PI3K-C2α in angiogenesis and vascular barrier integrity.[276] This can be explained by subtle differences in the expression of these targets in endothelial cells. The third PI3K class II target (PI3K-C2γ) is primarily expressed in the liver, and is involved in the Bcr-Abl mediated pathway in leukaemia.[277]

The sole PI3K class III target, vacuolar protein-sorting mutagen 34 (Vps34), is also expressed in the endocytic compartment.[278] Its physiological role has been more extensively studied than the PI3K class II targets, and is involved in endocytosis and vesicular trafficking.[279] A recent study has also identified the involvement of Vps34 in mTOR-mediated nutrient sensing and macroautophagy, which are related processes.[280,281] Macroautophagy is the process of cytosolic degradation, and is implicated in innate immunity.[282]

The four PI3K class I targets (PI3Kα, PI3Kβ, PI3Kγ and PI3Kδ) are heterodimers, consisting of a regulatory and a catalytic subunit (**Table 43**).[283] The regulatory subunit localises the heterodimer to the cell membrane, where the phosphatidylinositol lipids are located.[284,285] The catalytic subunit binds adenosine triphosphate (ATP), where it transfers a phosphate group to PtdIns(4,5)P2, producing PtdIns(3,4,5)P3.[286] Each PI3K class I isoform has a unique catalytic subunit, from which their name derives.[287]

	Catalytic subunits	Regulatory subunits
Class Ia		
PI3Kα	p110α	
PI3Kβ	p110β	p85α (p55α, p50α), p85β, p55γ
PI3K δ	p110δ	
Class Ib		
PI3Kγ	p110γ	p101, p84/p87

Table 43: The PI3K class I catalytic and regulatory subunits.[269]

Christopher J Tame

The process of up-regulation to the cell membrane is controlled by binding of the regulatory subunit to an activated receptor. The receptor may be produced from either receptor tyrosine kinases (RTKs)[284] or G-protein coupled receptors (GPCRs).[285] Consequently, two distinct sub-classes of PI3K class I targets are identified. These PI3K classes are Ia and Ib, which are activated by RTKs and GPCRs, respectively.

The formation of PtdIns(3,4,5)P3 from PtdIns(4,5)P2 is negatively regulated by phosphatase and tensin homologue (PTEN) (**Figure 49**).[288,289] Another phosphatase, SH-2 domain-containing inositol phosphatase (SHIP) converts PtdIns(3,4,5)P to PtdIns(3,4)P.[290] The role PTEN and SHIP have in regulating PtdIns(3,4,5)P3 levels make them interesting therapeutic targets for diseases which class I PI3K targets have been shown to influence.

Figure 49: The catalytic cycle of phosphate transfer between PtdIns(4,5)P2 and PtdIns(3,4,5)P3.[291]

A range of biological targets involved in cell signalling are activated by binding PtdIns(3,4,5)P3 to their pleckstrin homology (PH) or phoxy lipid (PX) domains.[292,293] The protein kinase Akt plays a key role in cell survival, and is translocated to the cell membrane upon interaction with PtdIns(3,4,5)P3.[294] The role of PtdIns(3,4,5)P3 in respiratory inflammation is complex, but a number of studies have highlighted the correlation between PI3K-mediated PIP3 production and mast cell recruitment,[295]

Christopher J Tame

neutrophil chemotaxis,[296] and the production of reactive oxygen species.[297] These cell behaviours have been implicated in the development of respiratory inflammation and a range of cancers.[298]

PI3Kα and β are ubiquitously expressed and control cell growth and proliferation.[299] These isoforms are up-regulated or mutated in some carcinomas, making PI3Kα and β inhibitors potential anti-cancer treatments.[299] PI3Kδ and γ predominantly modify the behaviour of T-lymphocytes, the cells of the immune system.[300,301] During an inflammatory response, T-lymphocytes are up-regulated to the site of infection by a gradient-controlled process known as chemotaxis. The associated increased expression of PI3Kδ and γ make them attractive targets for anti-inflammatory treatments.

The inhibition of PI3Kδ and γ has shown to reduce a number of processes related to respiratory inflammation. These include: T-lymphocyte trafficking into the airways, T-cell survival, mast cell function and eosinophil function, such as the release of cytotoxic molecules (degranulation) and inflammatory mediators (cytokines).[295,302,303] Studies on genetically engineered mice have identified potential differences in the expression of PI3Kδ and γ in the cells involved in an inflammatory response.[304,305] These differences show that the inhibition of PI3Kδ and γ would result in a complementary profile and, therefore, highlight the advantage of developing selective PI3Kδ and γ inhibitors.[306]

In summary, PI3Kδ and γ are implicated in the inflammation of the airways, which can cause a range of respiratory diseases such as asthma. It has also been shown that PI3Kδ and γ have different roles in lymphocytes, which may be exploited by selective inhibition to deliver differentiated asthma treatments. The aim of this research is to contribute towards the development of two orthogonal PI3K-modulated asthma treatments. This will be attempted by optimising two series of small molecule inhibitors for the selective inhibition of PI3Kδ and PI3Kγ, respectively.

Christopher J Tame

1.5 Contrasting oral and inhaled delivery methods for small-molecule asthma therapies.

Traditional asthma therapies have been developed for inhaled delivery, whilst current research focuses on both oral and inhaled routes. It is therefore useful to evaluate both of these methods of administration to help rationalise the aims of the research programmes presented in this document.

Inhaled medicines are designed to possess an orthogonal pharmacokinetic (PK) profile to orally administered treatments. An inhaled PK profile would include low oral bioavailability and high systemic clearance, which results in the action of the drug being limited to the administered tissue (in this case, the lung). Concentrating the action of the drug to the lung helps deliver efficacy whilst minimising off-target activity from systemic exposure. Toxicity arising from off-target activity is a major cause of drug candidate attrition for orally-administered molecules, reducing this risk is therefore particularly pertinent.[307]

There are, however, a number of challenges associated with the inhaled approach. These include achieving sufficient duration of action, without causing irritation in the lung, and patient compliance.[308] The requirements of duration differ for each biological target, whilst there are little published findings on predicting irritation and other adverse reactions in the lung.

Historically, medicinal chemistry approaches within our laboratories aimed to achieve duration of action by designing compounds with low solubility or permeability.[308] This was expected to increase the residence time, and therefore the efficacy, of the drug in the lung whilst minimising oral bioavailability and systemic exposure.

Low permeability was typically achieved by designing a hydrophobic compound with a hydrophilic side chain and a cationic charge. The hydrophilic, cationic moiety imparts sufficient solubility for nebulised dosing, whilst reducing passive cellular

Christopher J Tame

penetration, due to its ionised nature. Therefore, these cationic, ambiphilic drugs (CADs) reduce the rate of diffusion from the airways to the blood stream, *via* the tissue. CAD-like compounds, however, increase the risk of adverse events in the lung, such as phospholipidosis.[309] This is the name given to the accumulation of phospholipid-drug complexes in cells, which can lead to degradation of cell function and toxicity.

Similarly, compounds with low solubility have been used to increase duration, through slow dissolution of the compound in the lung. Recent studies in our laboratories have shown such compounds to cause foamy macrophages, a condition where the macrophage ingests a drug particle which it cannot digest, and subsequently becomes inactive.[308] The accumulation of these foamy macrophages has been linked with increased respiratory inflammation, and is therefore undesired.[310]

A study in 2003 showed that patient compliance is a major cause of untreated disease in the United States.[311] Another study showed that patients are less likely to adhere to the prescribed dosing regimen with metered-dose inhalers (MDIs) due to the complexity of administration.[312] Without the cost of design and manufacture of inhalers, orally-administered drugs are also cheaper to make available to patients, and could result in greater patient compliance. However, based on all of the above, both topically and orally administered delivery mechanisms are of value.

Work in our laboratories is currently focused on delivering a first-in-class, selective PI3Kγ inhibitor for inhaled administration, and optimising an existing PI3Kδ inhaled series for oral administration. Both of these programmes have been designed initially for asthmatic indications.

Christopher J Tame

2   PI3K δ inhibitors

2.1   Background

2.1.1   Literature PI3Kδ inhibitors

The PI3Kδ-selective inhibitor Zydelig (**245**, **Figure 50**) was recently granted approval by the USA's Food and Drug Administration (FDA) and the European Medicines Agency (EMA) for treatment of non-Hodgkin lymphomas and chronic lymphocytic leukaemia (**Figure 50**).[313,314] The enhanced expression of PI3Kδ in leukocytes complements these cancers of the immune system. However, Zydelig carries a 'Boxed Warning', alerting patients and medical professionals to fatal and serious toxicities which can occur as a consequence of treatment with Zydelig. These side-effects render the drug unsuitable for the treatment of asthmatic patients when compared to the existing standard of care.

245
Zydelig (Idelalisib)
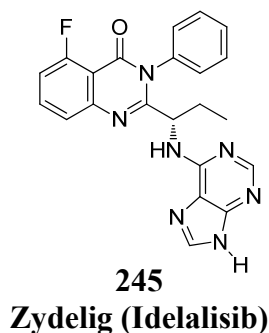
Figure 50: The selective PI3Kδ inhibitor Zydelig (Idelalisib).

Whilst there are no publications regarding the structure-activity relationships (SAR) of Zydelig, ideas can be generated from its extensively-studied predecessor IC-87114 (**246**, **Figure 51**). A co-crystal structure of IC-87114 (**246**) in PI3Kδ has been solved recently using X-ray crystallography and provides some insight into the origins of the potency and selectivity of these compounds (**Figure 52**).[315] Two hinge interactions are shown to be made between the adenenine moiety and the residues Valine 828 and Glutamic acid 826. The more interesting interaction involves the perpendicular arrangement of the pyrimidinone moiety with respect to the hinge.

Christopher J Tame

This moiety is positioned in between a tryptophan (Trp 760, shown on the left) and a methionine (Met 752, shown on the right). **Figure 52** also includes the electrostatic surface of these residues, which help illustrate how the ligand tightly fits between the cleft formed.

246
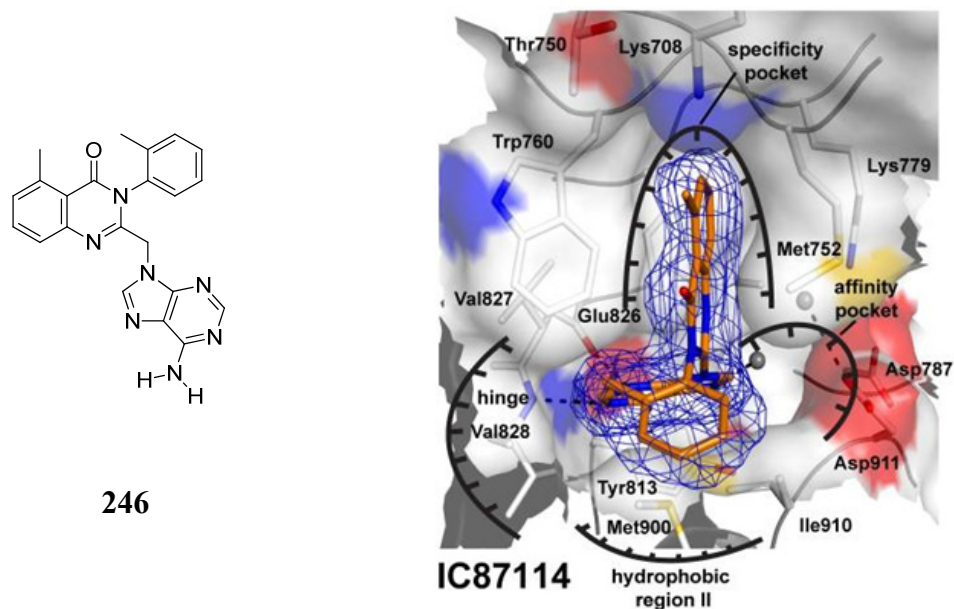
Figure 51: The interactions made between IC-87114 and PI3Kδ.[315]
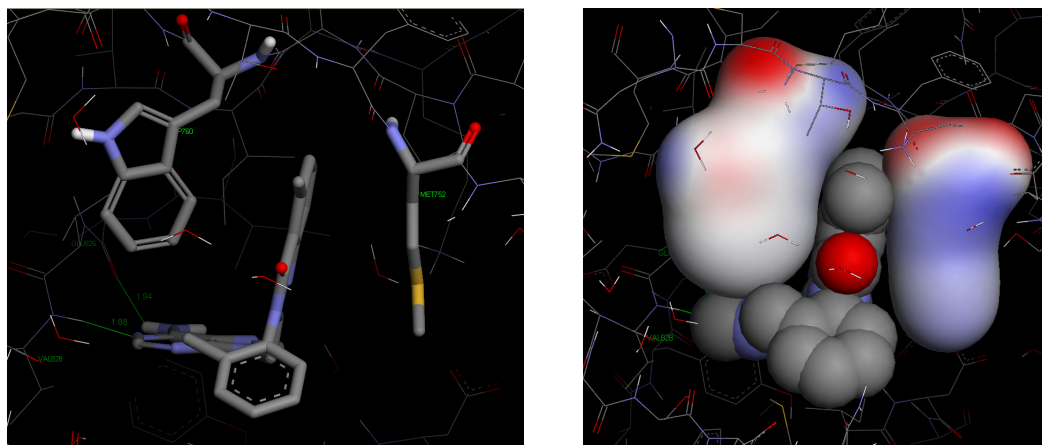
Figure 52: X-ray crystal structure of IC-87114 (**246**) in PI3Kδ. The interactions with the hinge residues Val 828 and Glu 826 are highlighted in green.

The origin of selectivity is predicted to involve the ability of the Met 752 residue in PI3Kδ to move and accommodate the ligand, whereas the other PI3K class I isoforms

Christopher J Tame

cannot. This could be explained by the subtle differences in the residues present on the strand of protein that contains Met 752, known as the P-loop.[315]

A pharmacokinetic study of Zydelig was carried out in our laboratories with a 1 mg/kg oral (p.o.) dose in mice.[316] The results showed poor oral absorption, with a low area under curve (AUC) value of 127.0 ng/h/mL and a half life of just 0.25 hours. Accordingly, improvements in the oral pharmacokinetic profile of a PI3Kδ-selective inhibitor is likely to reduce the required dose, which has the potential to eliminate undesired side-effects and improve the safety profile.

The most advanced clinical trial for asthma with a PI3K inhibitor is a Phase II study with the PI3Kγ/δ dual compound IPI-145 by Infinity Pharmaceuticals (formally known as INK1197 by Intellikine).[317] This compound is also being studied for a range of indications including haematological cancer, arthritis, multiple sclerosis, COPD and allergies. To date, no structure has been disclosed for this compound. IPI-145 demonstrates good oral absorption into the systemic circulation (denoted as bioavailability) in three of the four species studied (**Table 44**).[318] This promising pharmacokinetic profile was reinforced with a successful pharmacodynamic study. Prophylactic and therapeutic dosing of IPI-145 in an ovalbumin-challenged rat pharmacodynamic model demonstrated significant knockdown of eosinophil count from the bronchial alveolar lavage (BAL) (**Figure 53**).[318]

Species	Dose (mg/Kg)	Bioavailability, F(%)
Mouse	10	7
Rat	10	57
Dog	5	97
Monkey	5	40

Table 44: The oral bioavailability of IPI-145 in a range of species.[318]

Christopher J Tame
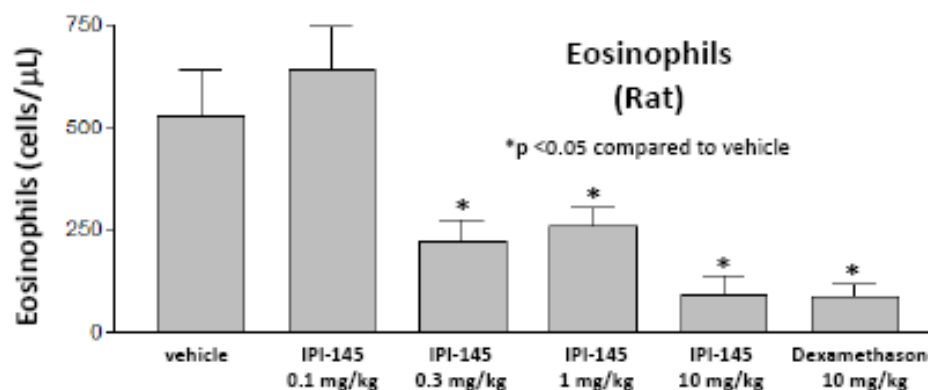
Figure 53: A pharmacodynamic study of IPI-145 in ovalbumin-challenged rats.[318]

To date, there have been no PI3Kδ-selective compounds disclosed in the literature which demonstrate good oral absorption in pharmacokinetic studies conducted in our laboratories. This highlights the potential benefits to the scientific community from further research into the development of an improved orally-administered PI3Kδ selective inhibitor. Access to such a tool compound could prove to be a valuable asset in further delineating the role of these kinases in inflammatory disease, and could provide a path forward towards new treatments for asthma.

2.1.2   PI3Kδ inhibitors previously identified in our laboratories

The aim of this research programme was to access a novel series of PI3Kδ inhibitors for oral administration, which would complement the existing portfolio of inhaled respiratory medicines. One method of achieving this was to optimise the PK profile of an existing inhaled series which had been previously identified within our laboratories.[319] An example from this series (**247**) is displayed in **Figure 54**, which uses an interaction map from a solved crystal structure to highlight the key interactions it makes with the PI3Kδ protein.[320] Isolated enzyme assay results indicate a high level of potency at PI3Kδ, whilst demonstrating at least 100 fold selectivity over the other PI3K class I isoforms.

Christopher J Tame
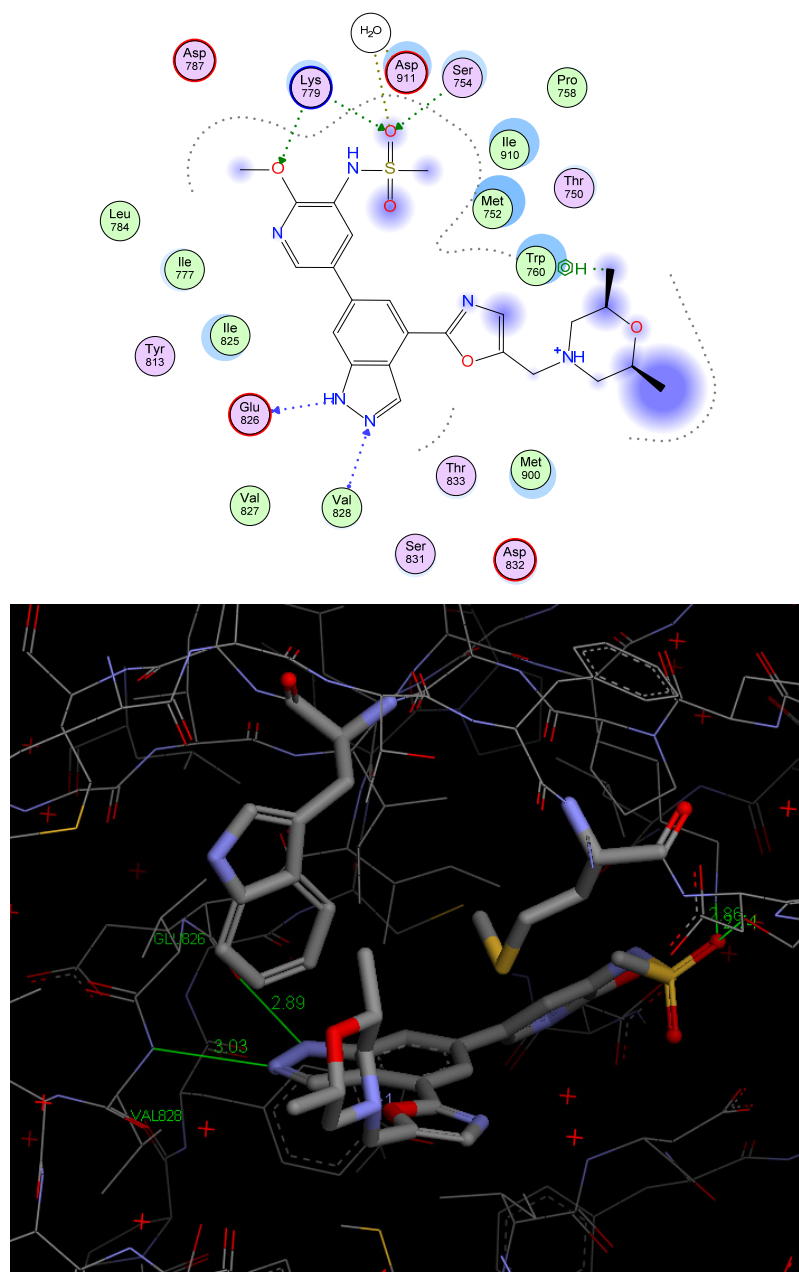
Isolated enzyme assay	pIC$_{50}$
PI3Kδ	9.1
PI3Kα, β, and γ	6.3, 6.2, 6.3

Figure 54: An existing inhaled series of PI3Kδ inhibitors, exemplified by compound **247**.

The indazole ring of **247** participates in a donor-acceptor hydrogen bonding interaction with hinge residues Glu 826 and Val 828, which is also shown with Idelalisib (**245**, **Figure 51**) and with ATP when bound to the analogous residues in PI3Kγ (**Figure 46**). As discussed previously, the drug-protein interactions at the hinge typically impart the highest binding affinity in protein kinases. Lipid kinases, however, have shown that the hydrophilic region in the back-pocket, defined in this case by residues Lys 779, Asp 911 and Ser 754, are responsible for the majority of potency. The oxazole ring does not make any noticeable interactions and is likely to act as a flat spacer between the indazole and the morpholine moieties.

Structure-activity relationship (SAR) studies carried out elsewhere in our laboratories have shown that the morpholine induces the selectivity observed (**Table 45**),[319] however this cannot be reliably explained by molecular modelling using the available crystal structures or homology models of the P13K isoforms. For example, the morpholine moiety does not reach far enough to induce the conformational change between Trp 760 and Met 752 seen with IC-87114 (**Figures 43** and **44**). However, one hypothesis is that the selectivity is due to subtle differences in interaction between the methyl groups of the morpholine moiety and the Trp 760 residue in each PI3K isoform.

Christopher J Tame
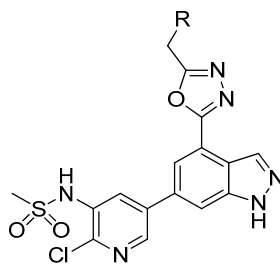
n	R	PI3Kδ pIC$_{50}$	PI3Kα, β, γ pIC$_{50}$ (ratio vs PI3Kδ)
248	Me	8.2	6.5 (50.1), 6.4 (63.1), 6.8 (25.1)
249		8.4	6.4 (100), 6.3 (125.9), 6.8 (39.8)
250		9.2	6.6 (501), 6.2 (1000), 6.7 (316)
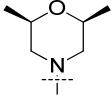
Table 45: The PI3K class I selectivity profile of compounds with different substitutents on an oxadiazole ring. The template possesses a 2-chloropyridine and an oxadiazole ring, which is in contrast to the 2-methoxypyridine and oxazole ring in compound **247,** respectively.[319,359]

The rat pharmacokinetic (PK) data indicates high clearance and low bioavailability **(Table 46)**.[316] The area-under-curve (AUC) value for oral administration (p.o.) is very low, suggesting poor oral absorption or rapid first pass hepatic clearance. This PK profile is suitable for inhaled delivery, as it allows the compound to deliver efficacy when dosed to the lung, with limited systemic exposure. For oral administration the PK profile must be reversed, demonstrating good bioavailability and absorption, as well as low clearance and an improved half-life in order to maintain an acceptable dosing regimen.

Christopher J Tame
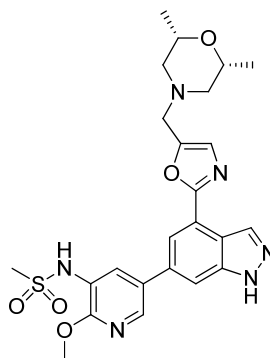
247

Pharmacokinetic Profile	i.v. (1.0 mg/Kg)	p.o. (3.0 mg/Kg)
AUC (ng/h/mL)	333	24.0
Half Life, $T_{1/2}$ (i.v.) (h)	2.6	-
Cl_p, (i.v.) (mL/min/Kg)	50.0	-
Bioavailability, F (%)	-	< 2.0

Table 46: Pharmacokinetic (PK) profile of an inhaled PI3Kδ inhibitor, **247**.

As discussed in Chapter 1, the *in vitro* permeability, solubility and physicochemical properties of marketed drugs have been shown to influence oral absorption.[131,133,135,138] **Table 47** summarises the ideal physicochemical property space required for sufficient oral exposure, and is presented alongside the physicochemical properties of compound **247**. This analysis shows that the reduction of molecular weight, number of aromatic rings, and topological polar surface area (TPSA) could potentially improve the chances of identifying an orally-active PI3Kδ inhibitor relative to lead molecule **247**.

Physicochemical property	Guideline values for an oral candidate	247
MW	<500	513
cLogP	<4	2.8
Chrom LogD pH 7.4	<3	3.3
TPSA	>75, <140	135
No. of Ar rings	≤3	4
No. of Rotatable bonds	≤7	6

Table 47: The physicochemical properties required for an orally-active drug are compared against the properties displayed by compound **247**.

Christopher J Tame

2.1.3   Identification of the dihydroisobenzofuran series

Previous work carried out elsewhere in our laboratories focused on the reduction of TPSA and aromatic rings by replacing the indazole motif in the molecule.[321]   This work was undertaken on a truncated version of the original series, due to synthetic tractability enabling rapid access to exemplar compounds.

Based on this earlier work, the pyridylsulfonamide functionality was responsible for a significant increase in potency and was therefore maintained.   This provided sufficient potency to facilitate the identification of structure-activity relationships (SAR) among the different indazole replacements (**Scheme 96**).

The functionality at the 6-position of the indazole ring was mainly responsible for selectivity and was therefore temporarily removed to facilitate efficient synthesis. Functionality at this vector was planned to be re-introduced once a suitable replacement core had been identified, with the aim of regaining the selectivity profile observed in the inhaled series.
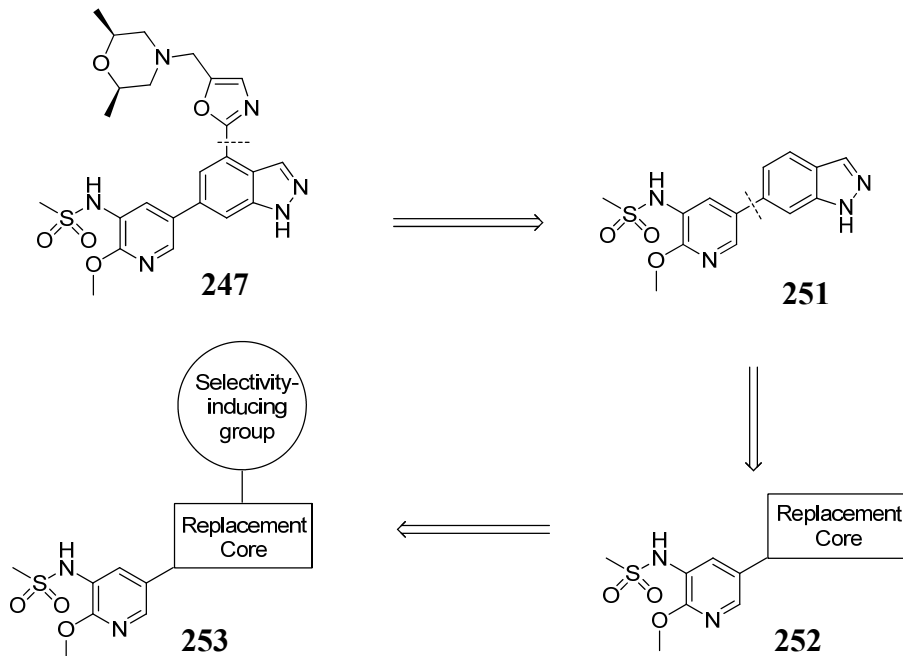
Scheme 96: A reduced-complexity approach was adopted with the aim of replacing the indazole core of an existing series of PI3Kδ inhibitors.

Christopher J Tame

The results from this work identified a dihydroisobenzofuran motif as a suitable replacement for the indazole core (**Table 48**).[321] The screening results from an isolated enzyme assay showed potency to be maintained, whilst *in silico* calculations predicted the TPSA to be reduced and the physicochemical assays indicated that solubility was improved. This correlated well with findings from Ritchie and Macdonald, who proposed the dependency of solubility on the molecular weight and the number of aromatic rings of a compound.[138]
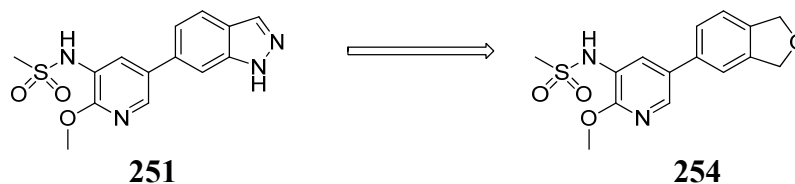
	251	**254**
PI3Kδ Enzyme pIC$_{50}$	6.0	6.1
MW	318	320
cLog P	2.3	2.3
Chrom LogD pH 7.4	2.6	3.5
TPSA	97	78
No. of Ar rings	3	2
Solubility (μg/mL)	31	92

Table 48: Results of isostere screening identified the dihydroisobenzofuran core.[321] The new motif showed improved TPSA and number of aromatic rings, whilst the reduction in molecular weight and Chrom LogD remained unoptimised.

Christopher J Tame

2.2   PI3Kδ research aims

The aim of this research was to optimise the PI3K class I selectivity profile and oral bioavailability of a series of dihydroisobenzofuran-containing PI3Kδ inhibitors. This was attempted by applying the structure-activity relationships identified from an indazole-containing series of PI3Kδ inhibitors   The compounds were designed within the physicochemical property guidelines set for good oral absorption, with the aim of achieving suitable bioavailability for oral administration.

2.3   Methodology

2.3.1   Medicinal chemistry

Having identified the replacement core, the next step was to design and synthesise a selection of fully functionalised molecules. The compounds were designed to enable a more complete comparison with analogues from the indazole series, which would help understand how well the structure-activity-relationships (SAR) are related between the two. These compounds were designed and prioritised in order to adhere to the physicochemical guidelines described earlier for orally-active compounds.

In order to select appropriate functional groups for incorporation at the 6-position of the dihydroisobenzofuran, the database of PI3Kδ compounds synthesised within our laboratories was analysed and molecules that contained the key pyridylsulfonamide moiety were selected. These molecules were then filtered based on ideal physicochemical values anticipated to be compatible with oral delivery when incorporated into the dihydroisobenzofuran core. This afforded a small subset of compounds, from which six distinct motifs were identified. These motifs had different PI3K class I selectivity profiles and spanned four distinct pharmacophores. **Table 49** displays these motifs on the dihydroisobenzofuran core, and therefore the targets required for synthesis.

Christopher J Tame

255

256

257

258

259

260
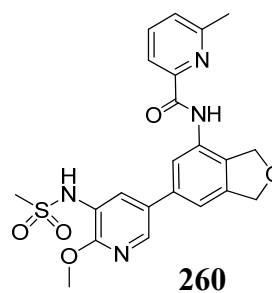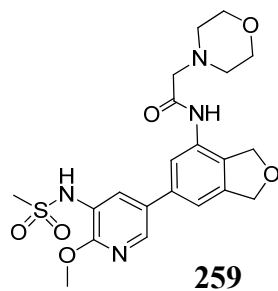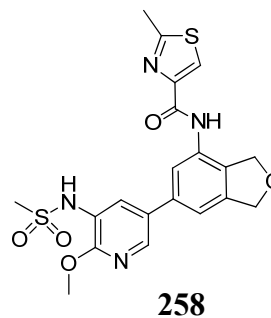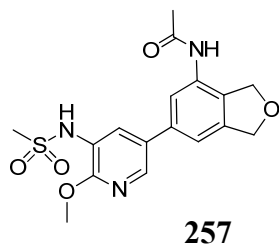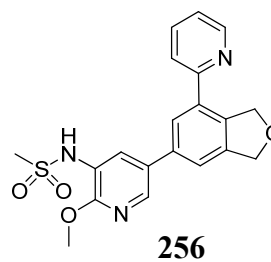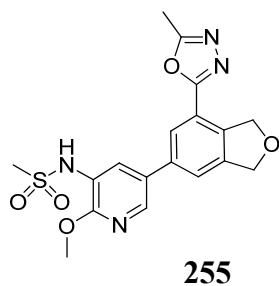
Phys. Chem. Property	255	256	257	258	259	260
MW	402	397	377	461	463	455
cLog P	1.1	2.9	1.5	2.8	2.9	1.6
TPSA	116	90	107	120	120	120
No. Ar rings	3	3	2	3	2	3
Rotatable bonds	4	4	4	5	6	5

Table 49: The six targets designed as PI3Kδ inhibitors for oral administration.

Christopher J Tame

2.3.2   Synthetic approaches to target compounds

Retrosynthetic analysis of the target compounds revealed common intermediate **263** (**Scheme 97**), which contained an iodine as a handle for functional group modifications. The synthetic transformations to access biaryl **255** and **256** required palladium-catalysed cross-coupling techniques. To achieve this, the oxadiazole and pyridyl coupling partners would require activating metal groups such as boron, zinc or tin at the relevant position (**Figure 55**).
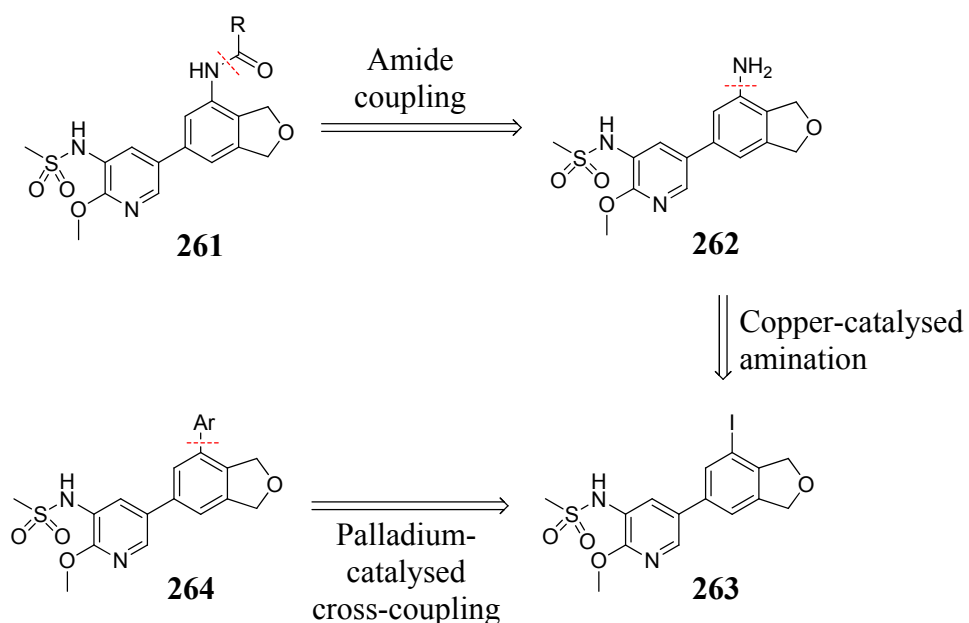
Scheme 97: Retrosynthetic analysis of the target compounds.
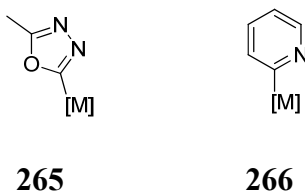
Figure 55: The synthesis of pyridyl and oxadiazole-functionalised inhibitors of PI3Kδ are to be accessed from the appropriately metallated starting materials shown.

Christopher J Tame

Turning our attention to the necessary metallated coupling partners, 2-methyl 5-*H* oxadiazole is the only commercially available source of this moiety. One-pot zinc chloride functionalisation, followed by palladium-catalysed cross-coupling with an aromatic iodide, is expected to afford the desired target (**Scheme 98**).[322]
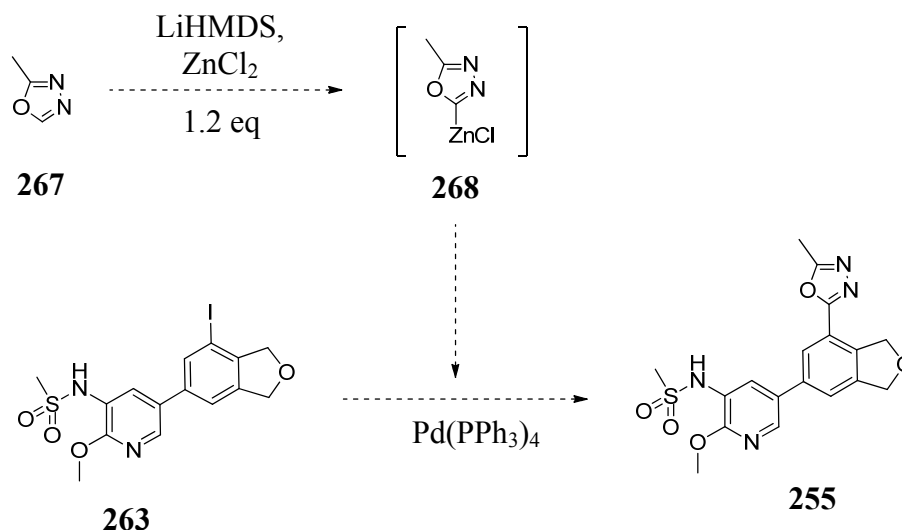
Scheme 98: The proposed one-pot zinc-chloride functionalisation and palladium-catalysed cross coupling to access the oxadiazole-containing target (**255**).

Pyridin-2-ylboronic acid is commercially available; however, these 2-heterocyclic boronic acids readily undergo proto-deboronation during metal-catalysed cross-coupling reactions.[323] Based on this, a recent study has shown that the addition of copper(I) chloride can facilitate cross-coupling reactions involving 2-heterocyclic boronic acids.[323] The proposed mechanism involves initial transmetallation of the boronic acid to copper. This softer nucleophile is proposed to be more stable under the reaction conditions and will transmetallate to palladium at a slower rate than the borylated analogue (**Figure 48**). Based on this precedent, these conditions will be attempted in the case of pyridin-2-ylboronic acid to form the desired target.

Christopher J Tame
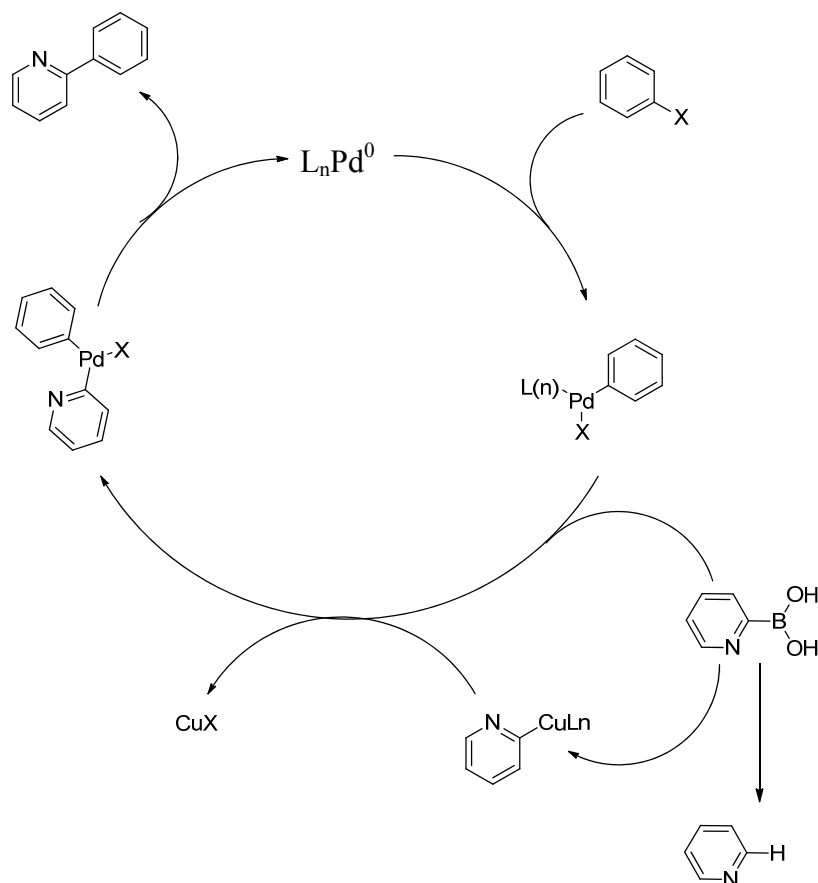
Figure 56: Palladium-catalysed cross coupling of halogenated arenes with 2-borylated heterocycles using a copper(I) chloride additive. **X** typically refers to iodide or bromide.

Returning to retrosynthetic analysis, the iodine-functionalised core can be converted to the required aniline (**262**) by copper(I) iodide catalysed amination. Recent studies have demonstrated direct amination of aryl iodides using aqueous ammonia solution at room temperature (**Scheme 99**).[324] These conditions improve upon traditional methods involving stoichiometric copper, harsh reaction conditions and protected amines; which would only furnish the desired aniline after a further deprotection step.[325] Once formed, the aniline can facilitate the formation of compounds **257-260** *via* HATU-mediated amide coupling conditions.[326]

Christopher J Tame
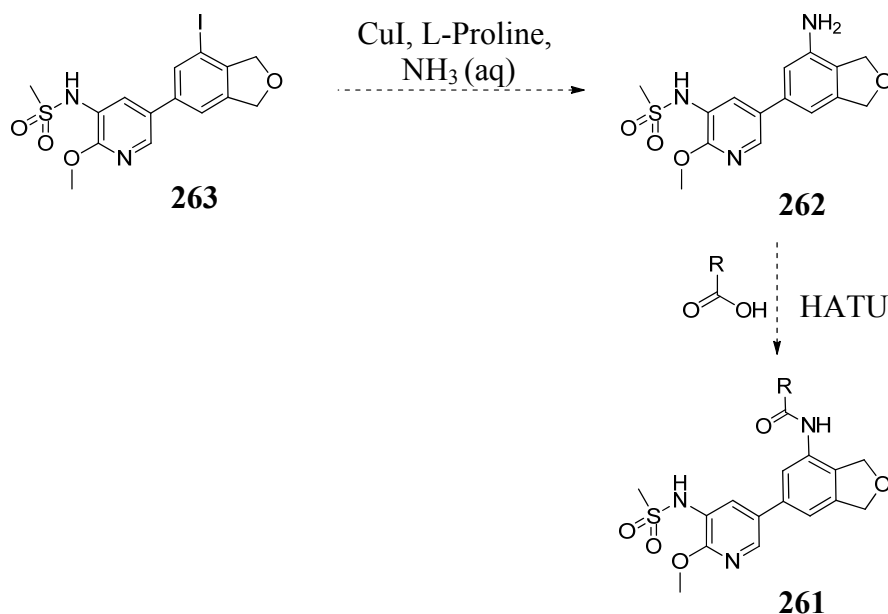
Scheme 99: Copper-catalysed room temperature amination of aryl iodides with aqueous ammonia followed by HATU-mediated amide coupling.

The requisite 4,6-substituted dihydroisobenzofurans were not commercially available and lacked relevant literature precedence for their synthesis. Based on this, a novel synthetic strategy was therefore required. A synthetic route that utilised well-established synthetic transformations would require an appropriately substituted phenyl ring as a starting point, in this case, a 1,2,3,5-substituted benzene. This substitution pattern is unusual and therefore precedence for the required synthetic transformations is scarce. An example of a potential route towards the target core is presented in **Scheme 100**.[327]

The seven step synthesis towards the target products is linear up to the last step, which is likely to result in a low overall yield and would require significant optimisation due to the lack of literature precedence.. Furthermore, the pyridylsulfonamide functional group is fixed early on in the route, which would require redesigning if it were to be modified during a subsequent medicinal chemistry iteration. This perhaps outlines the difficulty in utilising the dihydroisobenzofuran motif in small molecule drug discovery.

Christopher J Tame
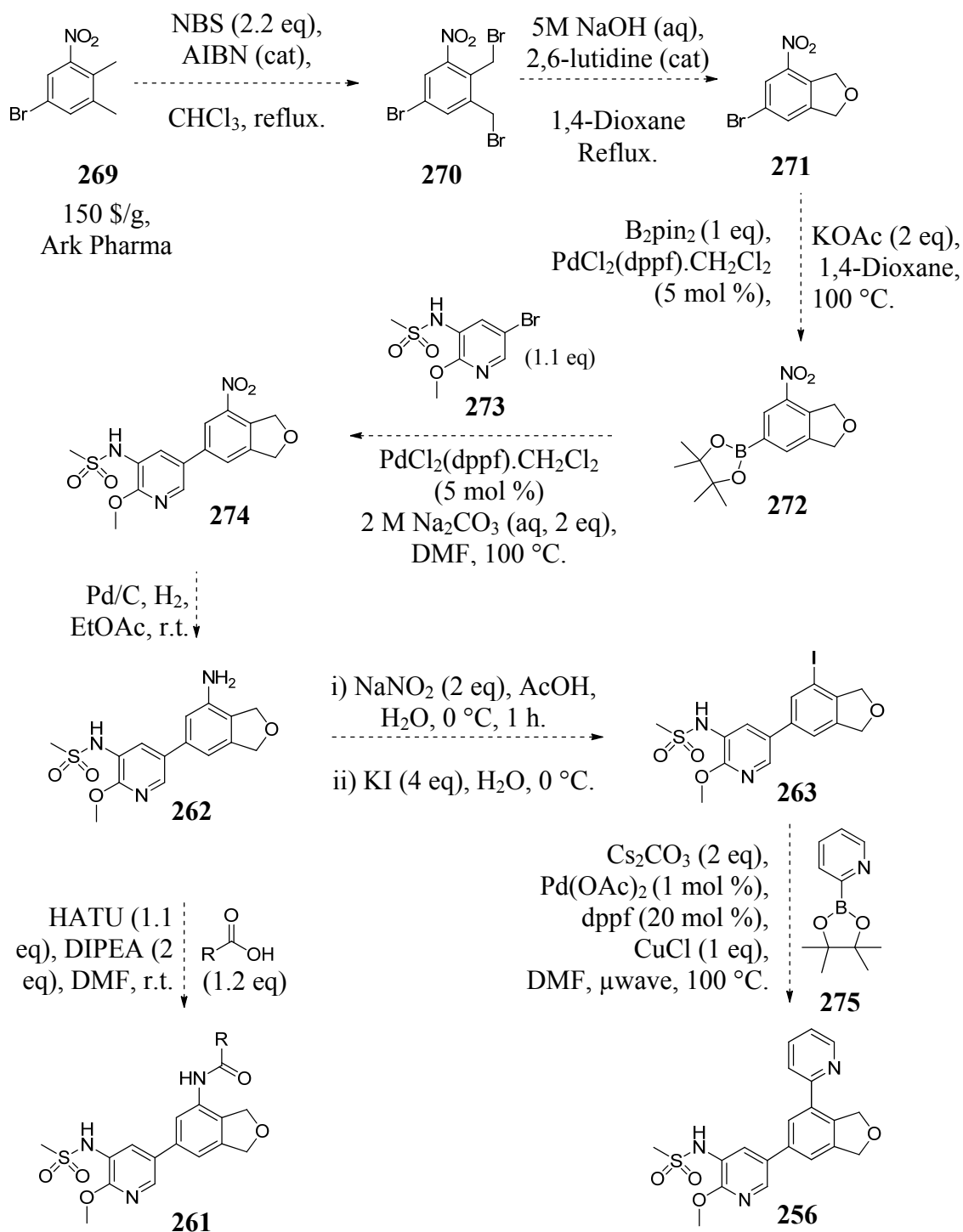
Scheme 100: A potential synthetic route to access a 4,6-substituted dihydroisobenzofuran from a 1,2,3,5-substituted benzene.

Another strategy could involve functionalisation of a less-substituted ring system, for example, electrophilic aromatic substitution or metal-catalysed C-H insertion of a 1,2,3-substituted phenyl ring. **Scheme 101** applies this concept to the synthesis of

Christopher J Tame

272, a key intermediate in **Scheme 100** above. Whilst this route requires much cheaper starting materials and one less synthetic step, the route still relies on little or no literature precedence.[328] This lack of precedence encouraged the search for other methods of forming 4,6-substituted dihydroisobenzofurans.
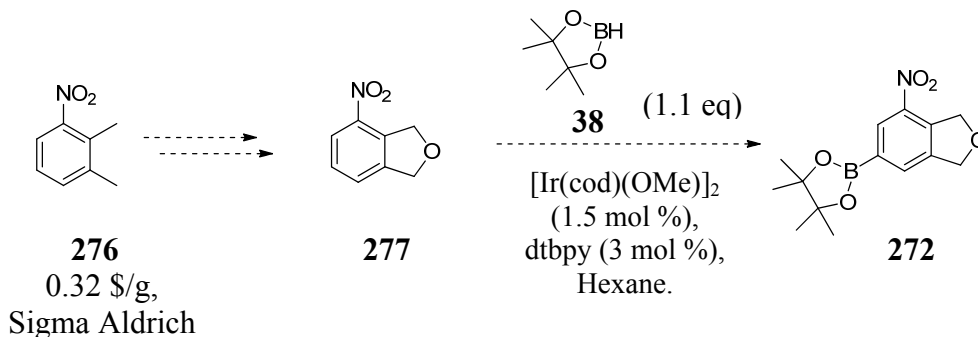
Scheme 101: The modification of **Scheme 100** with iridium catalysed C-H insertion of pinacol borane.

Subsequent discussions identified alkyne cyclotrimerisation reactions as a potential approach to access the desired dihydroisobenzofurans.[329] Examination of the literature revealed that the cyclotrimerisation reactions of bispropargyl ether with a functionalised alkyne are prevalent amongst the published methods for the formation of 4,6-disubstituted dihydroisobenzofurans (**Scheme 102**).[330] These reactions require low loadings of a transition metal catalyst together with degassed, anhydrous conditions, and can access the desired product at room temperature and in short reaction times. The high *meta*-regioselectivity (rationalised later) makes this method applicable for the synthesis of PI3Kδ inhibitors. It is therefore pertinent to review the literature pertaining to this synthetic approach.
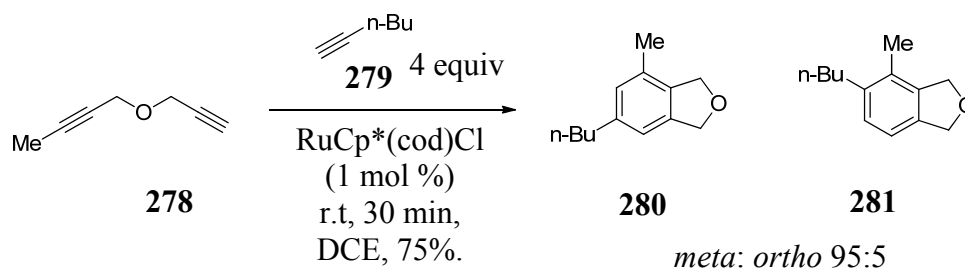
Scheme 102: Formation of 4,6-disubstituted dihydroisobenzofurans using [2+2+2] cyclotrimerisation of functionalised alkynes with ether-tethered diynes.[330]

Christopher J Tame

Metal-mediated cyclotrimerisation reactions were first developed by Reppe in 1948, and involved the reaction of nickel and a range of alkynes to form benzene and its substituted derivatives (**Scheme 103**).[331] The addition of triphenylphosphine was required to occupy one of the nickel coordination sites to prevent the formation of cyclooctatetraene.
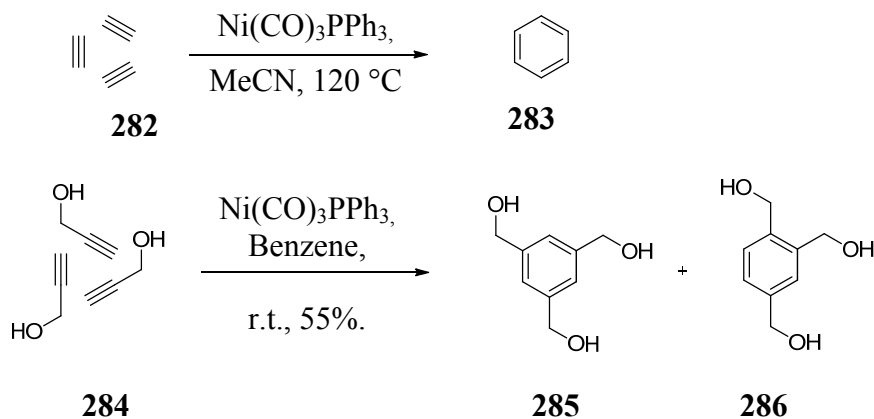
Scheme 103: The first metal mediated cyclotrimerisation reactions.

The synthesis of functionalised phenyl rings was further developed using cyclotrimerisation conditions by Muller in 1971, which required stoichiometric amounts of expensive rhodium (**Scheme 104**).[332] Catalytic conditions were subsequently developed by Vollhardt and Bergmann, which displayed efficient formation of substituted phenyl rings with only 2 mol% loading of cobalt. (**Scheme 105**).[333]
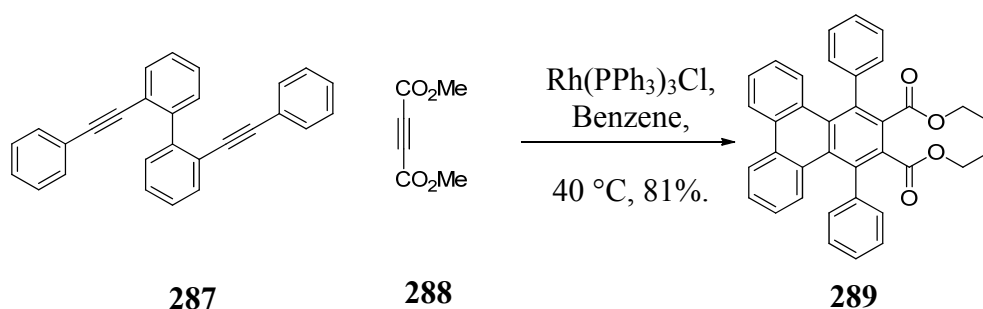
Scheme 104: The formation of poly-substituted phenyl rings using rhodium-mediated cyclotrimerisation conditions by Muller in 1971.

Christopher J Tame
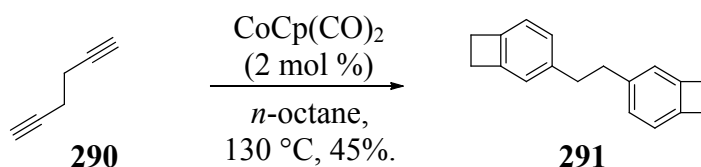
Scheme 105: The first catalytic cyclotrimerisation conditions were disclosed by Vollhardt and Bergmann in 1974.

Throughout the following 20 years, Vollhardt contributed a number of advancements in this area, including mechanistic studies of the cyclotrimerisation catalytic cycle[334] and the cobalt catalysed synthesis of pyridines from nitriles and tethered diynes (**Scheme 106**).[335]
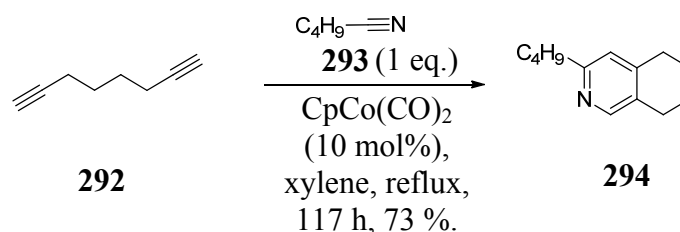
Scheme 106: Pyridine ring formation via catalytic cyclotrimerisation conditions.

This research was supplemented by the studies of Grigg and Mori, who investigated different catalysts and tethered diynes (**Schemes 107** and **108**).[336,337] These results demonstrate the high tolerability of the catalytic cyclotrimerisation reaction towards a range of functional groups, some of which may require protection in other metal-catalysed cross-coupling protocols. The reactions outlined below do, however, rely on suitable functionality on the diyne tether to facilitate the reaction, as well as a large excess of the mono alkyne.
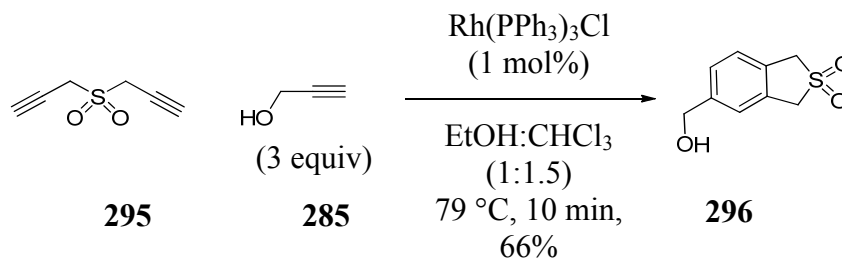
Scheme 107: The cyclotrimerisation of unprotected propyn-1-ol with a sulfone-tethered diyne reported by Grigg.

Christopher J Tame
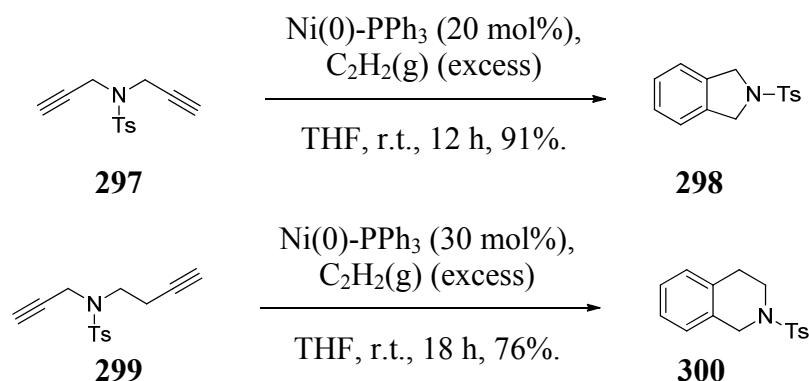
Scheme 108: The cyclotrimerisation of tosyl-protected amines with acetylene by Mori.

To date, 15 different metals have been utilised in the cyclotrimerisation of a range of substrates to form complex aromatic, heteroaromatic, and semi-saturated systems.[338,339] The examples in **Schemes 109** and **110** help demonstrate the utility of cyclotrimerisations in complex ring synthesis. **Scheme 109** presents a key ring-forming step in Reisman's total synthesis of Salvileucalin B, which shows no epimerisation upon ring formation.[340] This example not only demonstrates the complex synthesis of a substituted dihydroisobenzofuran, but also illustrates the presence of this ring system in a biologically-active natural product. This fact further supports the application of the cyclotrimerisation process in our drug discovery efforts.
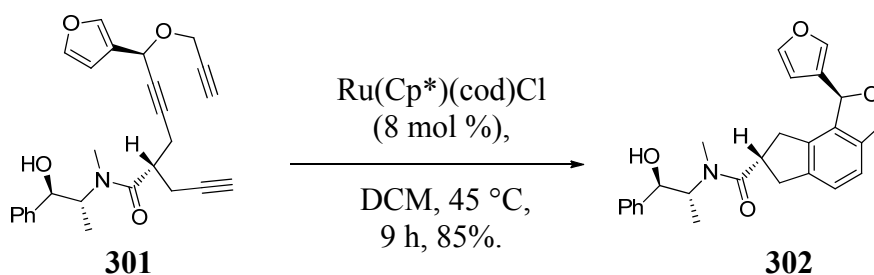
Scheme 109: The key step in the total synthesis of Salvileucalin B utilises an intramolecular alkyne cyclotrimerisation reaction.[340]

Pyridone rings are often used by medicinal chemists and are difficult to access when multi-substituted. **Scheme 110** presents the formation of a fully-substituted pyridone

Christopher J Tame

ring, although the use of a symmetrical diyne prevents any insight into potential regioisomeric control from being gained.[341]
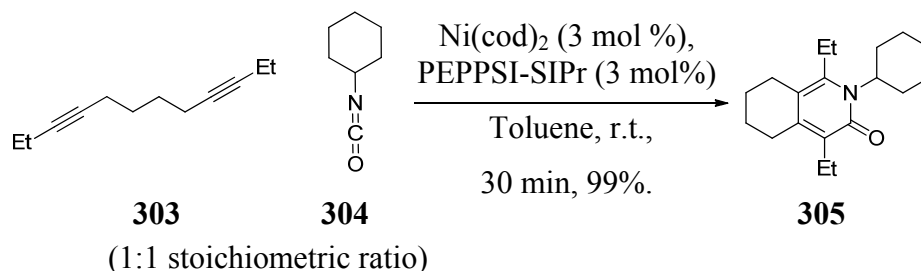
Scheme 110: The formation of a pyridone ring system by cyclotrimerisation of an isocyanate with a diyne. [341]

A number of investigations have been conducted to help identify the mechanism of cyclotrimerisation reactions. The majority of these studies utilised density functional theory (DFT) calculations to identify the most energetically favourable pathway,[330,334,342] whilst others have synthesised and isolated intermediates in the catalytic cycle.[343] The results have shown that the exact mechanism can vary based on the transition metal, ligand and solvent used.

An extensive study into the mechanism of cobalt-catalysed acetylene cyclotrimerisation reactions was undertaken by Vollhardt and co-workers using DFT calculations. They showed that two catalytic cycles are possible, depending on the nature of ligand or solvent used (**Figure 57**).[334] Whilst variances exist, this remains the accepted mechanism for the broad range of cyclotrimerisation reactions.[338]

Christopher J Tame
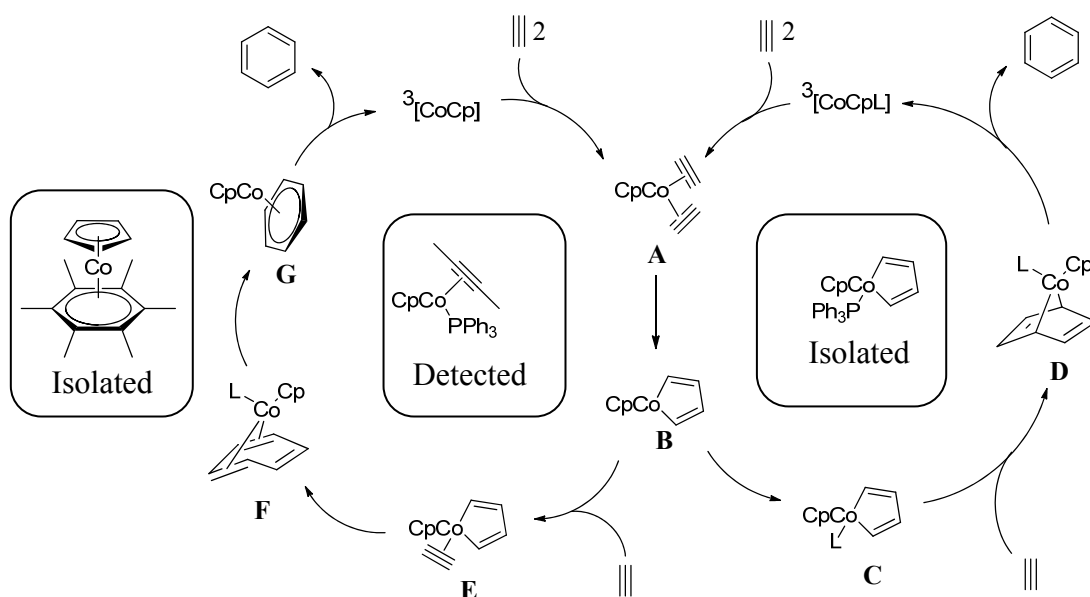
Figure 57: The widely accepted mechanism for cobalt and ruthenium-catalysed cyclotrimerisation of acetylene. L = alkene, CO or PR_3.

The mechanism shows the coordination of two alkynes to the metal centre **(A)**, which then forms a 5-membered metallocycle **(B)**. There are then two possible routes that may be taken, depending on the nature of solvent and ligand. If strong σ-donor ligands or solvents are present, then co-ordination of these will precede the addition of the final alkyne (**C**). It is therefore plausible to suggest that the presence of a ligand bound-metal may invoke steric or electronic effects with the alkyne substituents, potentially influencing regioselectivity.

The co-ordination of the final alkyne is followed by insertion to form an aromatic ring. In the right-hand catalytic cycle, intermediate (**D**) shows the metal bridging the ring, which is then eliminated to afford benzene. The left-hand catalytic cycle shows the metal initially co-ordinating in an η^4 fashion (**F**), which then moves to an η^6 complex (**G**). Elimination of the metal affords benzene and regenerates the catalyst.

The mechanism of ruthenium-catalysed cyclotrimerisations has been investigated with two DFT studies on acetylene,[330,344] both of which indicate an alkyne insertion

Christopher J Tame

mechanism comparable with the right hand catalytic cycle in **Figure 57**. One study is used to rationalise the regioselective synthesis of 4,6-disubstituted dihydroisobenzofurans (**280**, **Scheme 102**), and is, therefore, of particular relevance. This DFT study was conducted with [CpRuCl] fragments and acetylene (**Figure 58**).

The key difference between ruthenium and cobalt catalysed cyclotrimerisations is the inclusion of the third alkyne component into the catalytic cycle. The [CpRuCl] fragment is considered to undergo a formal [2+2] cycloaddition between the ruthenacycle (**IV**) and acetylene to eventually afford a 7-membered ruthenacycle (**VI**), which reductively eliminates benzene. In contrast, the [CpCo] fragment undergoes a formal [4+2] cycloaddition to directly form a 6-membered ring (**Figure 22**). The reason for the formation of 7-membered ruthenacycle (**VI**) is due to the low energy barrier of just 0.1 kcal/mol to access transition state (**TS$_{IV-V}$**). This is in comparison to an energy barrier of 14.5 kcal/mol, which is required to form a transition state suitable for a Diels-Alder type [4+2] cycloaddition.

Intermediate (**VI**) includes a cyclopentadienyl ligand bound in η^1-fashion to ruthenium. This ring slippage could possibly erode regioselectivity, due to the removal of steric constraint around the ruthenium centre. However, this is unlikely to occur with the more electron-releasing pentamethylcyclopentadienyl (Cp*) ligand, which is the optimal π-ligand for regioselective 4,6-disubstituted dihydroisobenzofuran formation.[330]

Christopher J Tame
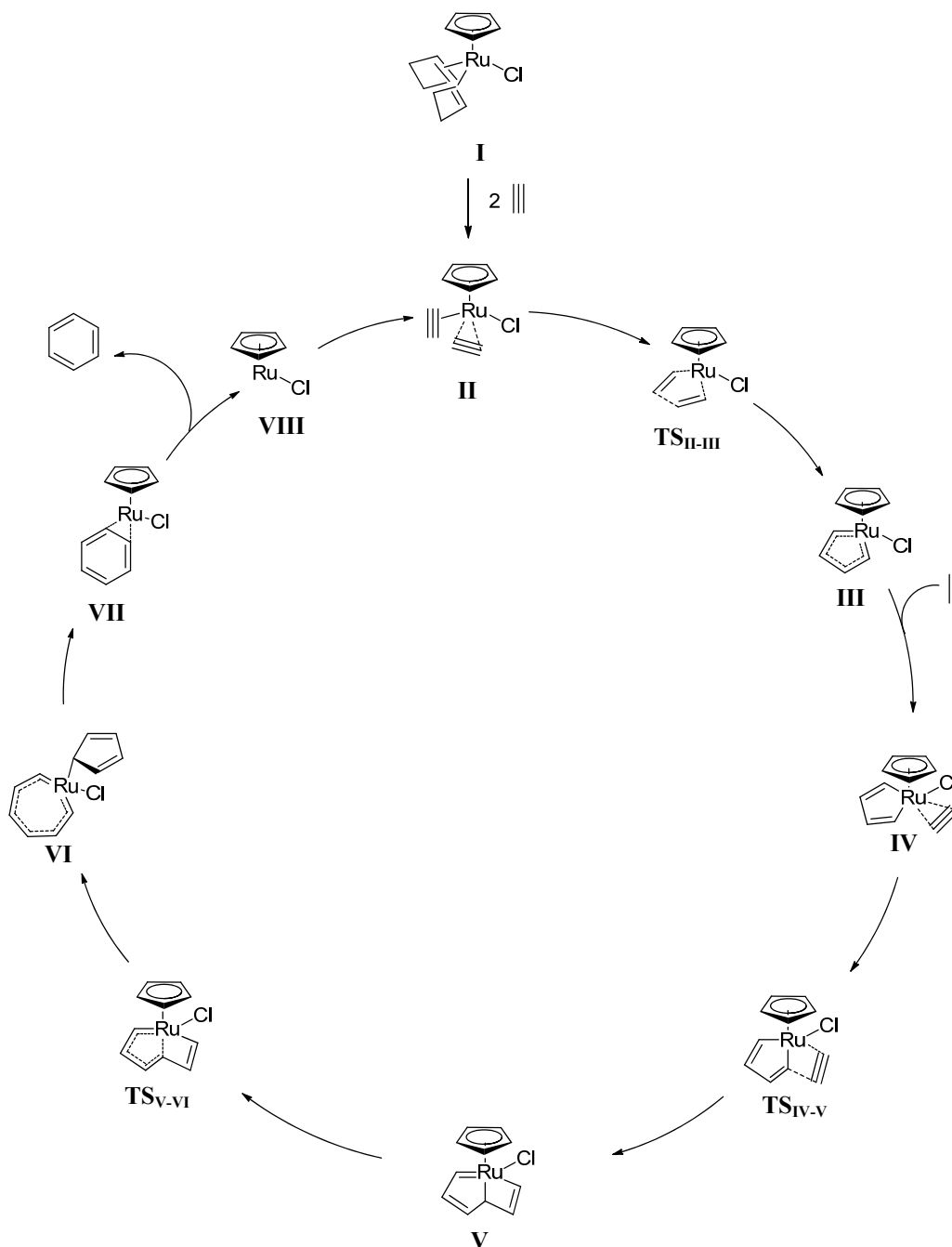
Figure 58: A proposed mechanism for the [CpRuCl] catalysed cyclotrimerisation of acetylene, identified from DFT calculations.

One potential drawback of cyclotrimerisation reactions is regioselective control. Tethering the alkynes helps to overcome this issue, as there are fewer potential products that can form (**Scheme 111**). As the degree of tethering increases, so does

Christopher J Tame

the regioselectivity, unfortunately at the expense of synthetic flexibility. For the synthesis of dihydroisobenzofurans, two alkynes required to be tethered with an ether-containing linker (**Scheme 112**). The nature of the metal,[330] solvent,[345] and alkyne substituent[346] have all been shown to control the formation of these regioisomers, which will help identify the ideal reaction conditions for 4,6-regioisomer formation.

Alkyne component

Possible products

(excluding homocoupling)
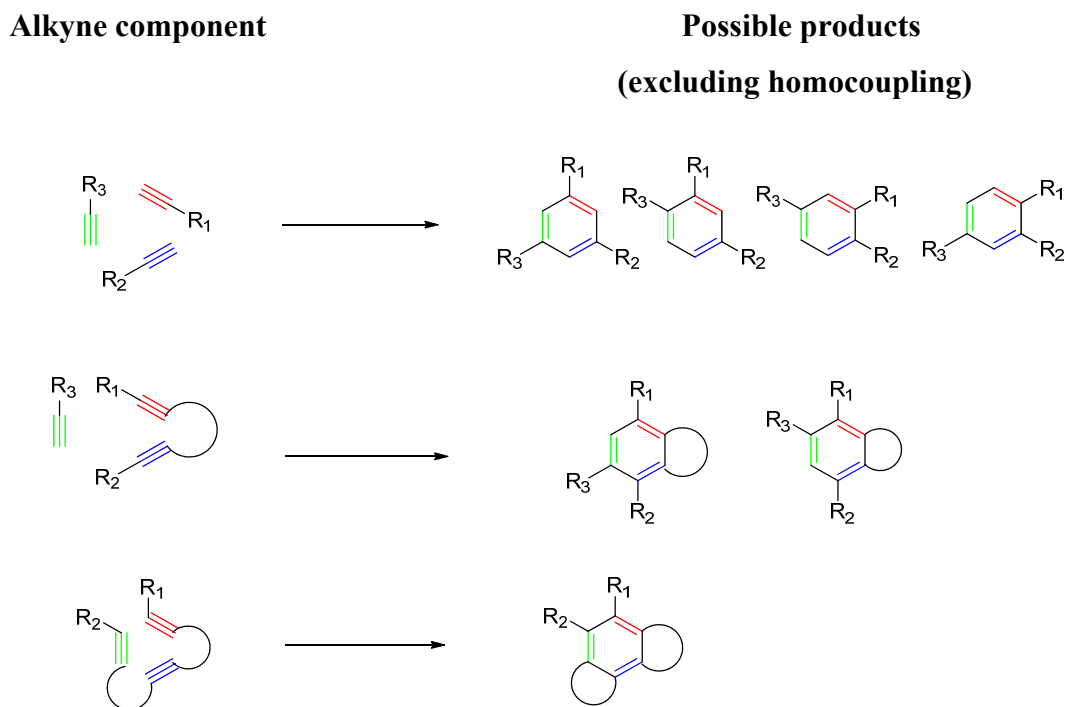
Scheme 111: The possible cyclotrimerisation products when using varying alkyne tethers.

Focusing on the preparation of the templates needed in the current study, Yamamoto's synthesis of 4,6-disubstituted dihydroisobenzofurans required low catalyst loadings and mild conditions to afford the desired regioisomers in high yield, thus providing the optimum protocol (**Scheme 102**).[330] In addition, Yamamoto also conducted a study into the control of regioselectivity depending on alkyne substituent (**Table 50**).[330] This was undertaken using a diethyl malonate-tethered diyne, which had been previously shown to display similar results to bispropargyl ether, required for dihydroisobenzofuran synthesis. This study identified the trimethylsilyl group to

Christopher J Tame

impart optimal regioselectivity for the 4,6-regioisomer. All substituents examined gave the desired regioselectivity, which may help facilitate the synthesis of a range of functional groups for PI3Kδ inhibitors.
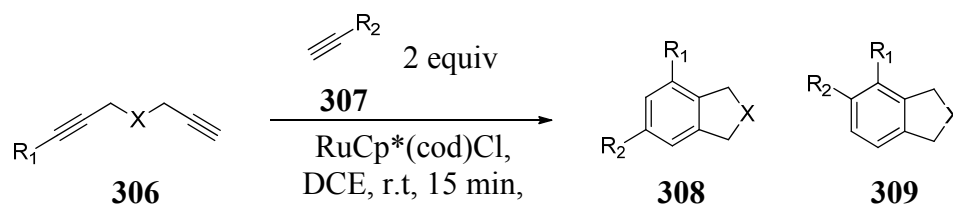
R^1	R^2	Catalyst loading	Time	Isolated yield	308:309 ratio
Me	^{n}Bu	1 mol %	1 h	85%	93:7
Me	CH_2OMe	1 mol %	3 h	86%	94:6
Me	Ph	3 mol %	24 h	82%	88:12
CH_2OMe	^{n}Bu	3 mol %	12 h	78%	92:8
Ph	^{n}Bu	10 mol %	24 h	80%	95:5
$SiMe_3$	^{n}Bu	5 mol %	7 h	94%	98:2

Table 50: Study conducted to investigate effects of R-groups on cyclotrimerisation regioselectivity.[330] $X = C(CO_2Et)_2$.

The regioselectivity observed was rationalised based on steric interactions between the diyne substituent and the bulky π-ligand (**Scheme 112**). *Ortho*-coordination of the mono alkyne is shown in **Route 2**. Here the diyne substituent (R) is forced upwards to avoid clashing with the R' group (**75**). This however causes steric repulsion with the methyl groups of the (pentamethyl)cyclopentadienyl ligand, resulting in an unfavourable pathway. *Meta*-arrangement of the R groups minimise steric interactions between the diyne substituent R and the Cp* ligand, and is therefore more favourable.

Christopher J Tame
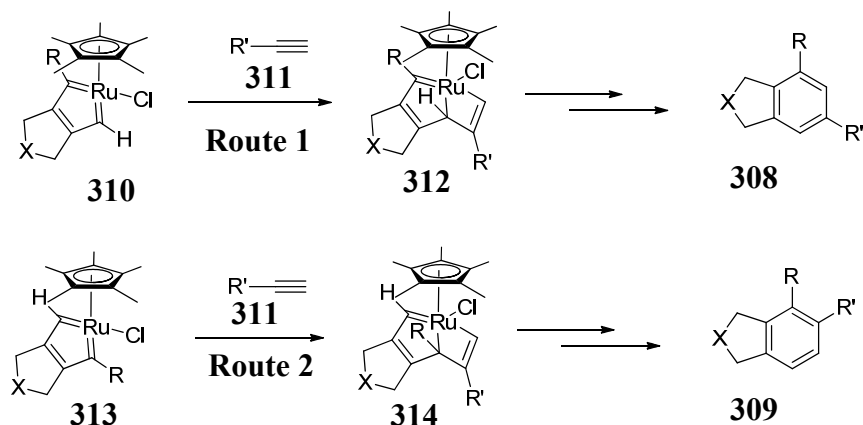
Scheme 112: Rationalisation of meta regioselectivity.[330]

Some of Yamamoto's own findings, however, contradict this trend, with bulky boronic ester and carboxylate-functionalised bispropargyl ethers exhibiting no significant regioselectivity (**Scheme 113**).[346]   The reasons behind the loss of regioselectivity are unclear but may be rationalised as the result of the formation of an electronically-modified ruthenacycle intermediate, which may change the coordination geometry required from the monoalkyne. This could result in the monoalkyne substituent being positioned in a different plane to the diyne, removing the potential for steric interactions.[334]

R^1	R^2	Isolated yield	308:309 ratio
(carboxylic ester)	nBu	46%	49:51
	CH$_2$OMe	74%	45:55
(boronic ester)	nBu	70%	45:55
	CH$_2$OMe	58%	30:70
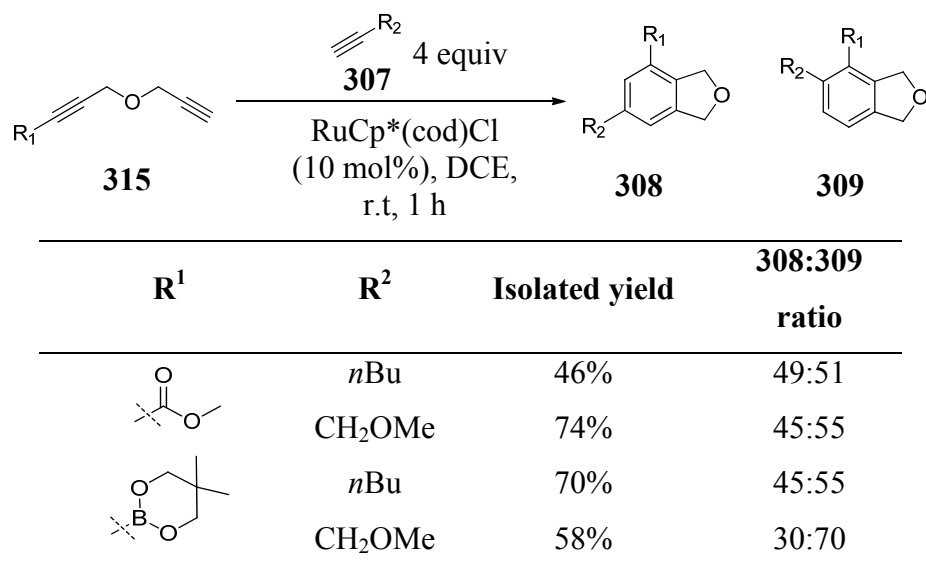
Scheme 113: Boronic and carboxylic esters show no regioselectivity in cyclotrimerisation reactions with n-hexyne and methoxypropyne.

Christopher J Tame

From consideration of the data presented in **Table 50**, the synthesis of a dihydroisobenzofuran functionalised with a trimethylsilyl group at the 6-position will provide the best opportunity for regioselectivity. Additionally, it was suggested by another member of our laboratory[348] that *ipso*-substitution of the trimethylsilyl group with iodine monochloride would be expected to form the desired common intermediate **263** (**Scheme 114**),[347] ready for downstream manipulation.
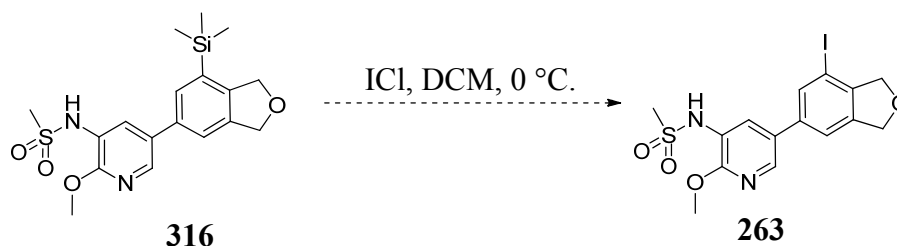
Scheme 114: ICl mediated *ipso*-substitution of trimethylsilyl **83** to afford aryl iodide **263**.

The full retrosynthetic plan in **Scheme 116** illustrates the potential for an efficient and convergent method of accessing densely functionalised dihydroisobenzofurans. This requires the incorporation of pyridyl sulfonamide, which was prepared elsewhere in our laboratories and is displayed in **Scheme 115**.[348]

Christopher J Tame
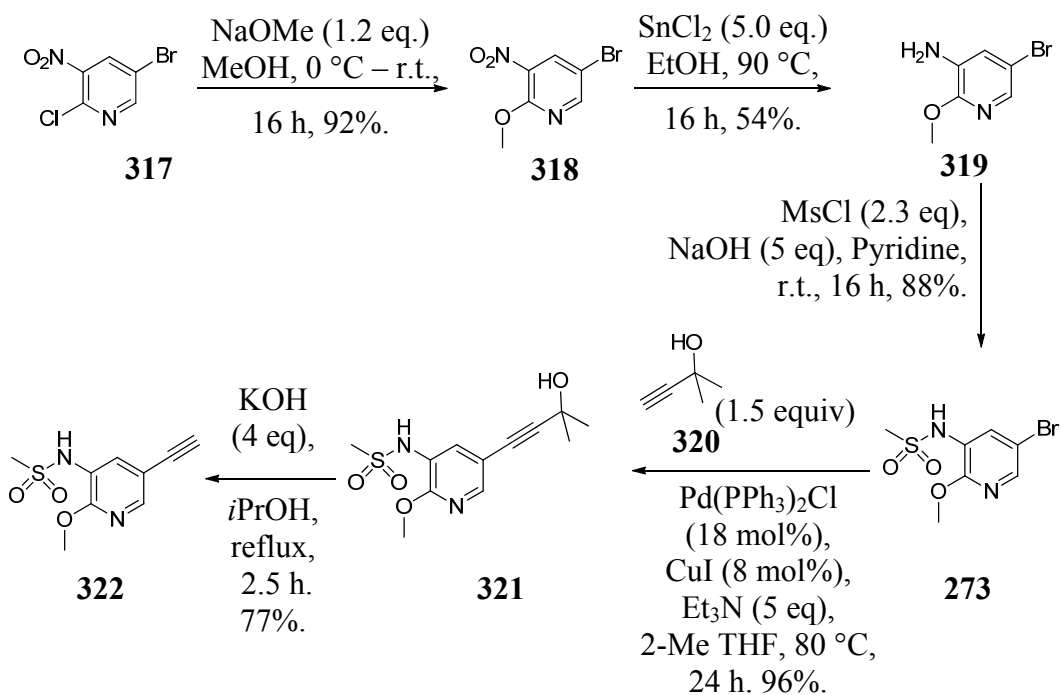
Scheme 115: The synthetic route used to access pyridyl sulfonamide (**322**).[348]

Despite the apparent synthetic efficiency, a drawback of this route is the lack of literature precedence in the cyclotrimerisation of functionalised, highly polar alkynes, which was expected to require initial optimisation to achieve appropriate conversion and regioselectivity levels.

The convergent nature of cyclotrimerisation chemistry, however, will enable future investigations to access a range of substituents at any position of the dihydroisobenzofuran without the need to design a new synthetic route. Therefore, the initial investment in route optimisation was expected to facilitate rapid medicinal chemistry iterations in the future.
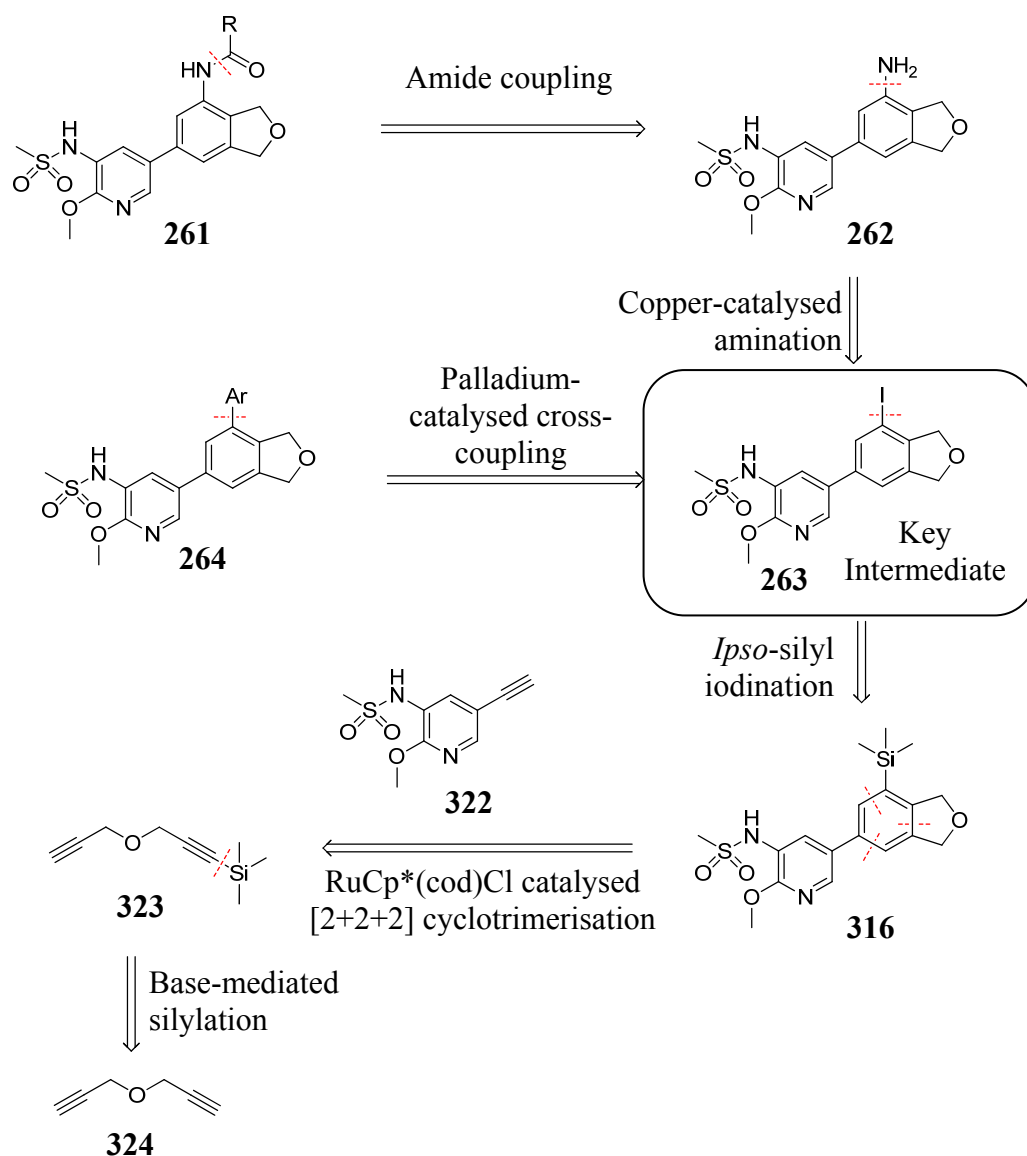
Scheme 116: Retrosynthetic analysis of the target compounds.

2.4   Results and discussion

2.4.1   Synthetic chemistry

The synthesis of trimethylsilyl bispropargyl ether (**323**) followed literature precedence, using lithium hexamethyldisilylazide (LHMDS, 1 eq) in tetrahydrofuran (THF), **Scheme 117**.[349] Optimisation efforts found that leaving the reaction to warm

Christopher J Tame

slightly from -78 °C to -30 °C overnight afforded optimal conversion to the desired product.
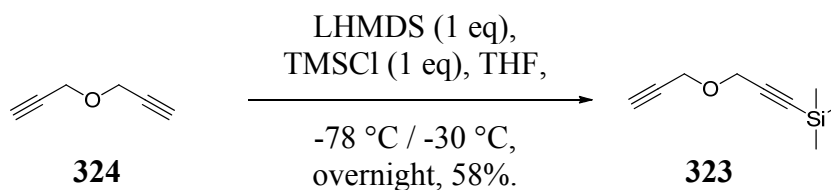
Scheme 117: Base-mediated formation of trimethylsilyl bispropargyl ether (323).

Initial purification attempts utilised silica column chromatography and afforded low yields. This was rationalised as instability of the trimethylsilyl group on the weakly acidic silica. In addition, the similar polarity of mono- and disubstituted products hampered purification by this method. Vacuum-assisted fractional distillation facilitated the isolation of the desired product with the highest purity and acceptable yields.

With the appropriately functionalised diyne (323) in hand, the standard literature conditions for cyclotrimerisation were tested using a model system. Phenylacetylene 325 resembled the most analogues alkyne to pyridylsulfonamide 322 investigated in the literature and was, therefore, chosen as the mono alkyne component (Scheme 118).

The catalyst loading of 5 mol% was selected for the trimethylsilyl-functionalised diyne, which again was in accord with literature conditions. The reactions were monitored at 30 min and 120 min time intervals by liquid chromatography-mass spectrometry (LCMS) analysis.

An excess of mono-alkyne is used in the literature to prevent homo-coupling of the diyne. Yamamoto suggests the use of two equivalents to be sufficient to prevent this, although up to four equivalents has been employed to give optimal yields.[330] In the interests of reaction efficiency, the initial cyclotrimerisation reactions used only two equivalents of mono-alkyne.

Christopher J Tame
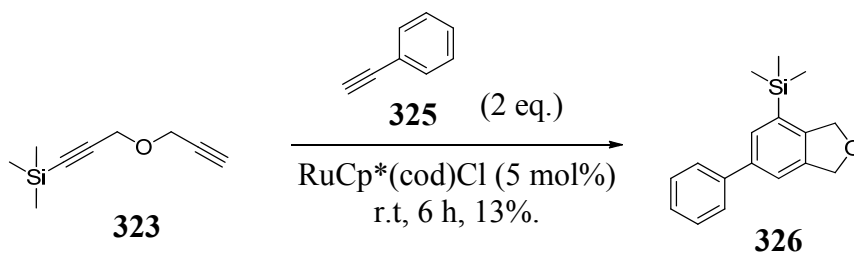
Scheme 118: Yamamoto's findings were successfully reproduced with diyne **323** and phenylacetylene (**325**).

The reaction mixture was submitted to aqueous work-up conditions and formic acid modified mass-directed auto preparative chromatography to afford the desired product in 13% yield. ^{1}H NMR analysis confirmed the presence of the desired *meta*-product due to the absence of doublets on the dihydroisobenzofuran aromatic ring, which would have resulted from *ortho*- substitution. Optimisation of this protocol was not attempted due to the expected change in reaction profile and retention time when transitioning to the more polar 5-pyridyl sulfonamide monoyne component.

These conditions were applied to the desired reaction of pyridyl sulfonamide alkyne **322** and TMS-diyne **323** (**Scheme 119**). Dichloroethane has been shown to increase the risk of carcinogenic side effects upon exposure,[350] and as a result requires approval before use in our laboratories. For these reasons it was replaced with dichloromethane, which provides similar anhydrous properties with a slightly reduced risk of carcinogenicity.
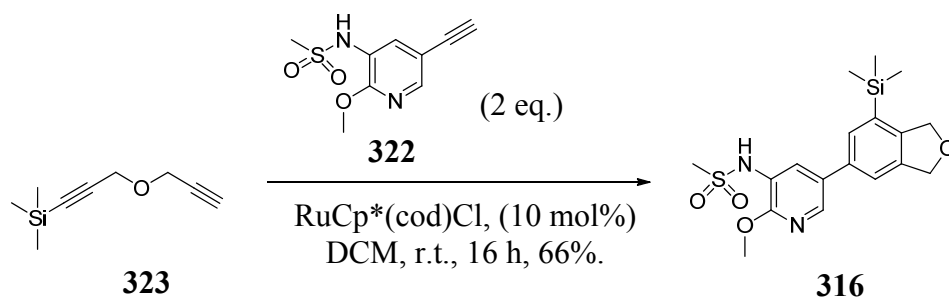
Scheme 119: The regioselective cyclotrimerisation of TMS-diyne (**323**) with pyridyl sulfonamide (**322**).

Christopher J Tame

A further 5 mol% RuCp*(cod)Cl was used due to an expected reduction in catalytic turnover efficiency resulting from potential coordination of the sulfonamide group to the ruthenium metal centre, which was confirmed by subsequent investigations undertaken by another team member.[351]

The reaction mixture was submitted to aqueous work-up conditions and normal phase silica-gel column chromatography in an attempt to optimise the recovery observed with the model reaction. This afforded the desired pyridyl sulfonamide-containing dihydroisobenzofuran **316** in 66% yield. Column chromatography also facilitated the recovery of unreacted monoyne in 31% yield, with respect to the two equivalents of monoyne used. The ability to successfully recover the synthetically valuable monoyne provides a significant improvement in reaction efficiency, effectively requiring just 1.4 equivalents of the monoyne component. Whilst ^{1}H NMR analysis of the crude reaction mixture was not undertaken, the ortho-substituted dihydroisobenzofuran product was never observed, which is in contrast to the previously published results by Yamamoto.

The reactions undertaken in medicinal chemistry laboratories typically involve reagents that possess increased polarity and functional group diversity than those disclosed in academic publications. Furthermore, experimental techniques in academic laboratories often provide more controlled environments (for example, through the use of glove boxes and solvent stills) which are not routinely available to medicinal chemists within an industrial setting. As a result, literature conditions are often more difficult to reproduce by medicinal chemists operating outside of an academic environment.

Based on this, a study into the optimisation of solvent and reaction conditions (**Table 51**) was undertaken on the model system with phenylacetylene. Solvents were selected based on increased polarity (relative to DCE) and their environmental sustainability,[352] whilst anhydrous and degassed conditions were avoided. The reaction in DCE was repeated to allow for accurate comparisons to be made. The

Christopher J Tame

reactions were monitored by LCMS at set time intervals to determine reaction progression.
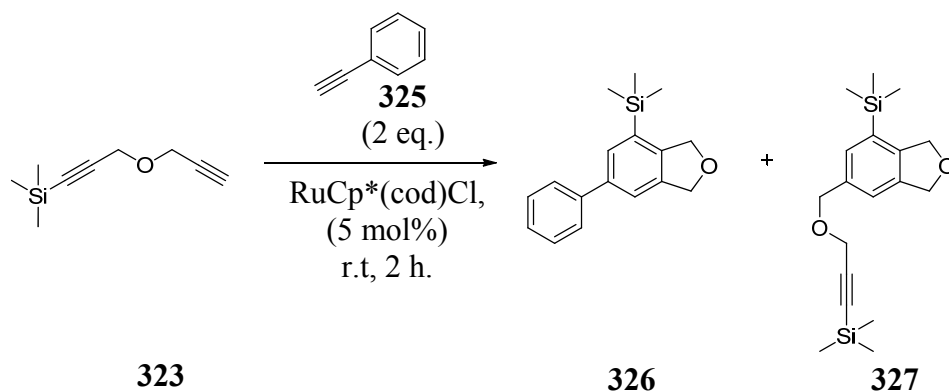
Solvent	326 (%)*	
	t = 30 min	t = 120 min
DCE	10	14
CPME	36	59
2-MeTHF	5	5
2-BuOH	40	52
EtOH	34	37
Water	35	43
EtOH:H$_2$O (1:1)	14	17

*[% absorption by LCMS diode array detection (DAD)]

Table 51: A range of solvents were screened under 'bench-top' conditions to identify an optimal reaction protocol for a medicinal chemistry laboratory setting.

The percentage conversion is calculated relative to the amount of phenylacetylene (**325**) present in the reaction mixture, which is in an excess of 2 equivalents and has a different chromophore to the product. Accordingly, these results are not suitable for the identification of reaction end points and absolute conversion rates. The results can however be used as an indication to the relative conversions between the different solvents. The results suggest that water, CPME and 2-butanol display encouraging reaction profiles under these conditions.

Christopher J Tame

Based on the above data, the reactions in DCE, CPME and water were submitted to work-up and purification procedures, in an attempt to identify an isolated yield. Unfortunately column chromatography failed to isolate the desired 4,6-regioisomer (**326**) from the co-eluting homo-coupled diyne impurity **327**. The ratio of **326**:**327** was identified using ^{1}H NMR analysis, which was used to calculate the yield of desired product **326** (**Table 52**). The presence of the homo-coupled impurity (**327**) was not observed in the cyclotrimerisation of TMS-diyne (**323**) and pyridyl sulfonamide (**322**) (**Scheme 120**), therefore, further chromatographic investigations were not attempted.

LCMS analysis of the crude reaction mixture and ^{1}H NMR analysis of the chromatographed material could not identify the presence of the *ortho*-regioisomeric product, which had been observed in an analogous reaction with diyne **323** and 1-hexyne as reported in the literature (**Table 50**).[330] Whilst it is plausible that the purification steps may have removed this product, another explanation is that the increased steric bulk of the phenyl ring (compared to 1-hexyne) has prevented any of the *ortho*-regioisomer from forming.
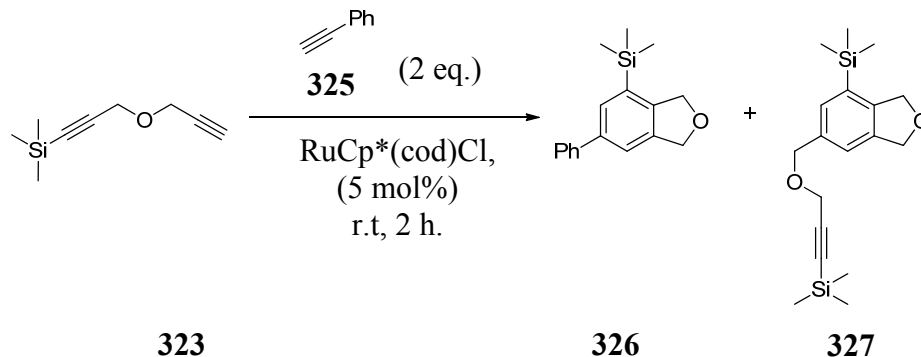
Solvent	Crude Yield (326 + 327)	Ratio by ^{1}H NMR (326:327)	Corrected Yield (326)
DCE	23	6.0 : 1	19
Water	67	2.3 : 1	47
CPME	97	4.1 : 1	78

Table 52: The use of water and CPME as solvent showed improved reaction efficiency when compared to DCE.

Christopher J Tame

Interestingly, all three solvents gave different yields and desired product (**326**) to homo-coupled product (**327**) ratios. This could be rationalised as a solvent effect on the rate of reaction, which may be due to differences in solubility of the catalyst or particular alkyne components. An alternative explanation could involve differences in interaction between the solvent and the rhodium catalyst.

The influence of solvent on cobalt-catalysed cyclotrimerisations has been demonstrated previously, both through theoretical and practical studies. Vollhardt and co-workers used density functional theory (DFT) calculations to identify possible reaction pathways, which depended on the σ-bonding capability of the ligand or solvent (**Figure 57**).[334] In addition to this, Hilt and co-workers identified the dependency of solvent on the regioselectivity observed in cobalt-catalysed cyclotrimerisations with phenylacetylene.[345] However, further investigation is required with the catalytic system presented in **Table 52** before more reliable conclusions can be drawn about the effect of solvent on ruthenium-catalysed cyclotrimerisations. These studies could include a wider set of solvents and ^{1}H NMR analysis of crude reaction mixtures.

The superior reaction efficiency and green credentials of CPME[352] prompted its replacement for DCM in the key reaction between pyridyl sulfonamide **322** and TMS-diyne **323** (**Scheme 120**). This was undertaken under non-anhydrous conditions, and encouragingly gave a comparable yield to anhydrous DCM. As a result, CPME was selected as the desired solvent for further optimisation efforts.
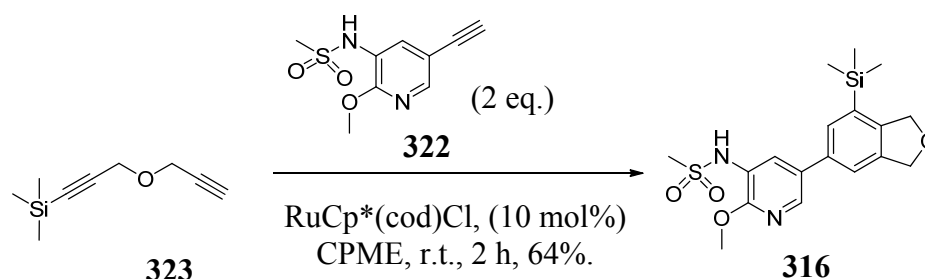
Scheme 120: The regioselective cyclotrimerisation of TMS-diyne (**323**) with pyridyl sulfonamide (**322**).

Christopher J Tame

The heavily substituted monoyne (**322**) is perhaps the most valuable component of this cyclotrimerisation reaction, requiring a 5 step synthesis from **317** in an overall yield of 32% (**Scheme 115**). This monoyne has so far been used in excess to prevent homo-coupling of the diyne component. These conditions are utilised in the literature due to the comparably-increased value of the diyne. However, in this case the diyne is readily made in one step from bispropargyl ether, and as a result is less valuable than the monoyne. It is, therefore, important to consider optimising the stoichiometric equivalents of these two components to reflect their value.

The reaction between pyridyl sulfonamide (**322**) and TMS-diyne (**323**) was then repeated with a slight excess of the diyne component (**Scheme 121**). The results show that efficient formation of the desired product is maintained when the reaction is optimised to reflect the value of each alkyne component.
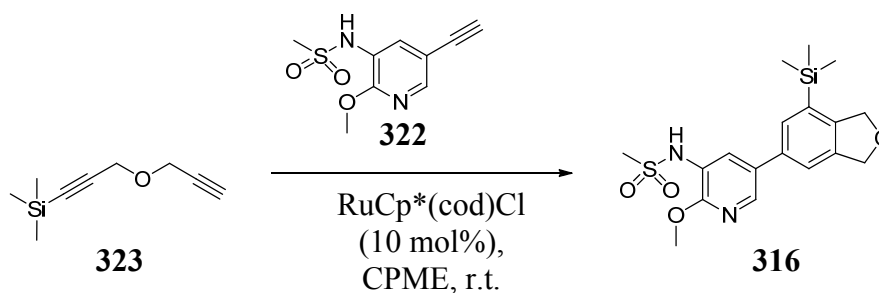
323:322 (ratio)	Isolated Yield 316 (%)*
1 : 2	64
1.2 : 1	64

* Yield based on lowest component in reaction.

Scheme 121: The cyclotrimerisation of TMS-diyne (**323**) with pyridyl sulfonamide (**322**).

These efforts have shown that the cyclotrimerisation reaction conditions originally developed by Yamamoto *et al.* can tolerate a bench-top environment, and are therefore amenable for use in a medicinal chemistry laboratory setting. In addition to this, it has also been shown that an excess of the monoyne component is not required

Christopher J Tame

for the reaction between TMS-diyne (**323**) and pyridyl sulfonamide (**322**), thus greatly enhancing the efficiency of these reactions.

Following on from the successful cyclotrimerisation, *ipso*-substitution of the trimethylsilyl group with iodine monochloride proceeded smoothly to afford the desired iodo intermediate (**263**) in 80% yield (**Scheme 122**). This was then converted to aniline (**262**) using aqueous ammonia and catalytic CuI (**Scheme 123**). The transformation required the use of stoichiometric amounts of L-proline, which may act as a solubilising ligand for the copper as well as creating an active Cu(III) complex. Initial screening on small scale showed this reaction to follow literature precedent and furnish the product at room temperature. Solubility played an important role in this reaction and transformations at the desired scale (1 g) required heating to 110 °C and increased reagent levels in order to afford the desired product in 77% isolated yield.
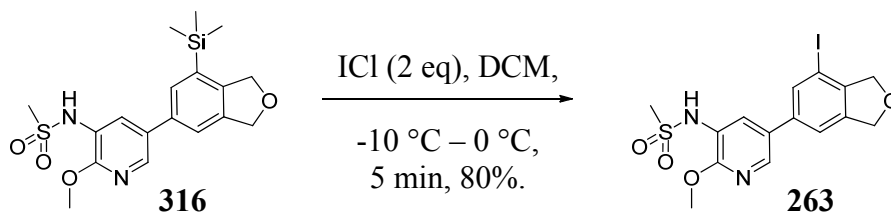
Scheme 122: *Ipso*-substitution of trimethylsilyl intermediate **316**.
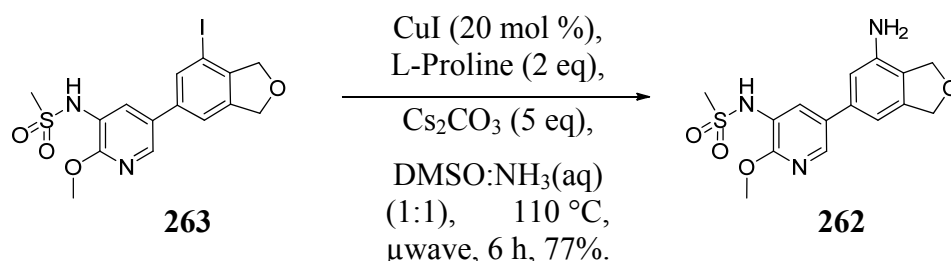
Scheme 123: Copper-catalysed amination of aryl iodide (**263**) with aqueous ammonia solution.

The aniline (**262**) was then submitted to amide coupling conditions with HATU, DIPEA and commercially available carboxylic acids to afford the desired amides (**257-260**) (**Table 53**). Whilst efficient conversion was observed for all of these

Christopher J Tame

reactions by *in situ* LCMS analysis, the isolated yields were low. This may be attributed to the purification method; all compounds were submitted to mass directed auto-preparative (MDAP) chromatography in order to isolate material with purity in excess of 95% for biological screening. Clearly this purification method is at the detriment of isolated yield and is not an accurate reflection on the efficiency of these acylation reactions. Having stated this, sufficient material was isolated from each reaction to enable subsequent biological profiling.
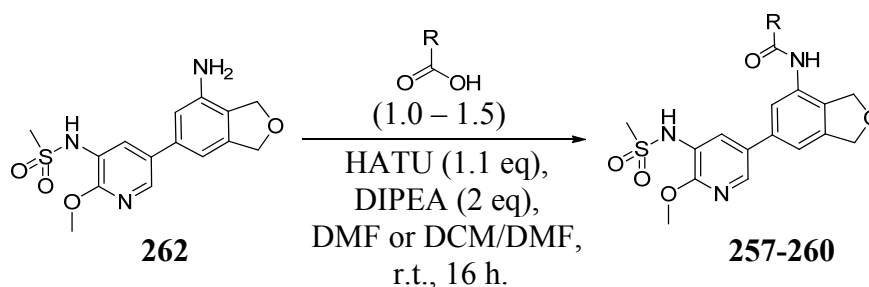
Product	R	Yield
257	CH₃	21 %
258		21 %
259		22 %
260		28 %

Table 53: HATU-mediated amide formation was utilised to access desired targets **257-260**.

The 1,3,4-oxadiazole-containing target (**255**) and the pyridyl-containing target (**256**) were successfully accessed from the iodo-intermediate (**263**) using the synthetic strategy described earlier (**Schemes 124** and **125**). The formation of the zinc-functionalised oxadiazole was undertaken in a microwave vial, which facilitated the initial formation of the zincate at low temperature and the palladium-catalysed biaryl coupling at high temperature in an anhydrous and degassed environment.

Christopher J Tame
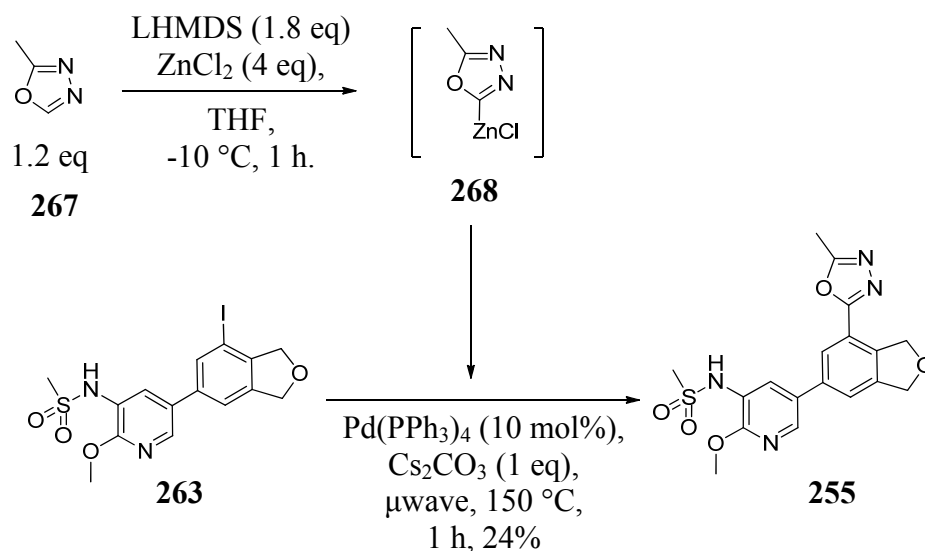
Scheme 124: One-pot zinc-chloride functionalisation and palladium-catalysed cross coupling to access the oxadiazole-containing target (**15**).
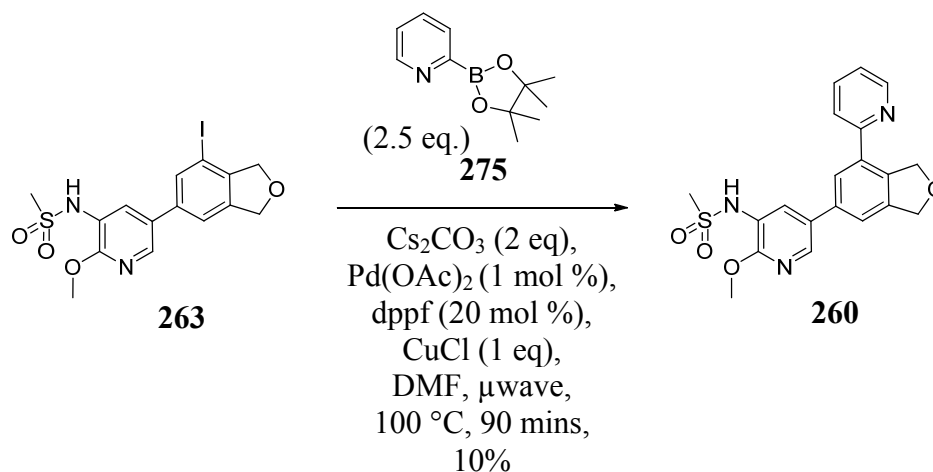
Scheme 125: Palladium-catalysed cross coupling of an unstable 2-pyridyl pinacolboronate (**275**).

The formation of the 2-pyridyl target (**260**) proceeded in very low yield (10%). This is still considered a relatively successful outcome due to the inherent instability of pinacolboronate (**275**). Other methods have shown that forming the pyridyl-*N*-oxide can facilitate C-H metallation at the 2-position, which would circumvent any decomposition issues (**Scheme 126**).[353] However the lack of literature precedence

Christopher J Tame

and the extra synthetic steps required to add and remove the *N*-oxide make this approach less attractive.
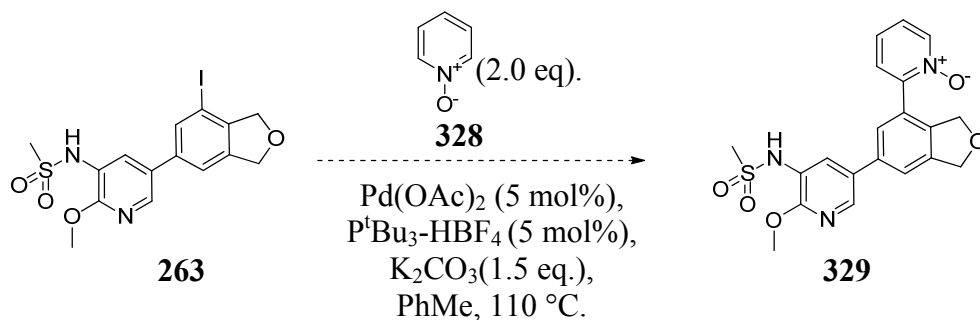
Scheme 126: Proposed palladium-catalysed C-H activation route towards target **329**.[353]

Despite the low reported yields for these two reactions, sufficient material for biological screening was afforded and therefore re-synthesis and reaction optimisation was not attempted at this stage. The reaction could potentially be optimised by removing the sulfonamide group, as it could co-ordinate to the palladium metal, which would reduce the catalytic turnover and, therefore, the catalytic activity. **Scheme 127** demonstrates a potential route to achieve this, which incorporates a bis-benzyl protecting group on the aniline, which is removed after functionalisation at the 6 position of the dihydroisobenzofuran.[354] Mesylation with methanesulfonyl chloride would then afford the desired target.[355] This route, however, requires two extra synthetic steps, and may not sufficiently improve the overall yield to make this worthwhile.

Christopher J Tame
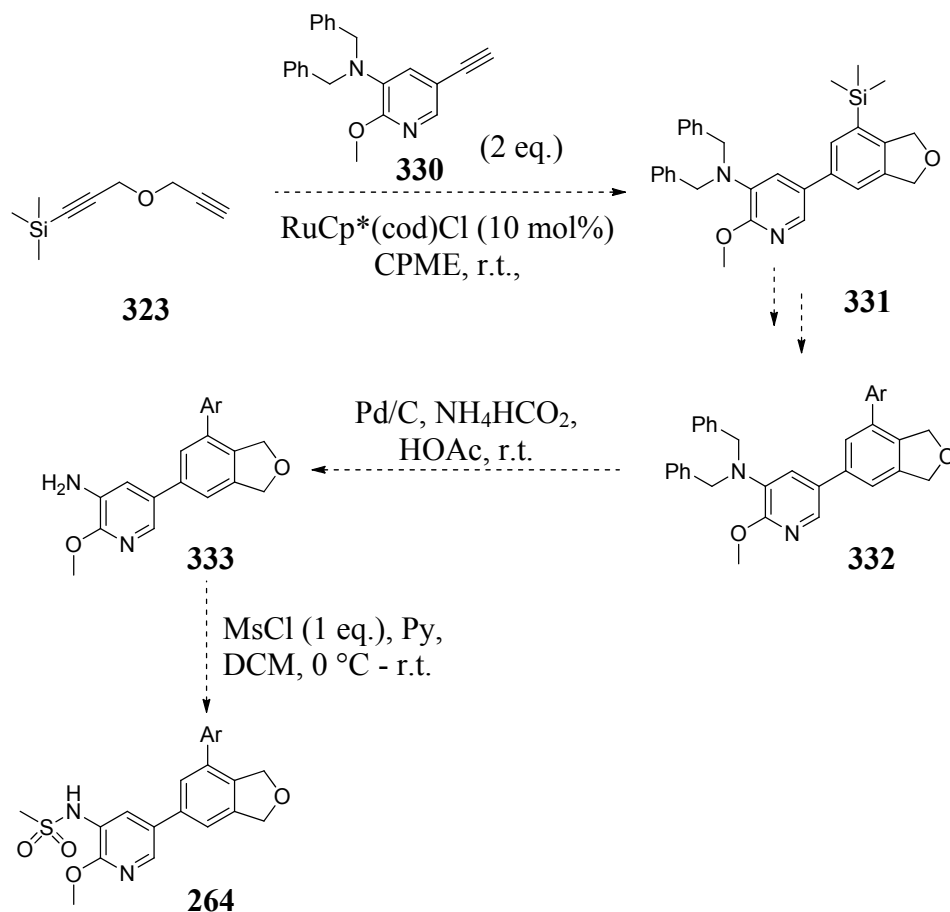
Scheme 127 – Masking the sulfonamide moiety may improve the yields for palladium-catalysed cross-coupling steps.

An alternative strategy could involve the direct functionalisation of bispropargyl ether with the requisite aromatic rings already in place. This would avoid any functional group interconversions in the presence of the pyridylsulfonamide moiety. Such functionalised diyne intermediates could be accessed using palladium-catalysed cross-coupling of bispropargyl ether with the appropriate halogenated heterocycle (**Scheme 128**).[356]   The formation of 2-bromo-5-methyl-1,3,4-oxadiazole can be envisaged by treatment of 1,3,4-oxadiazole with bromine,[357] whilst 2-bromopyridine is commercially available.

One potential drawback of this approach could be the removal of regioselectivity observed with the trimethylsilyl group. Yamamoto's original research showed that a

Christopher J Tame

methyl group can exhibit the same regioselectivity profile as a trimethylsilyl group. Based on this finding, the regioselectivity is unlikely to be affected by the difference in size between the trimethylsilyl and aromatic moieties.
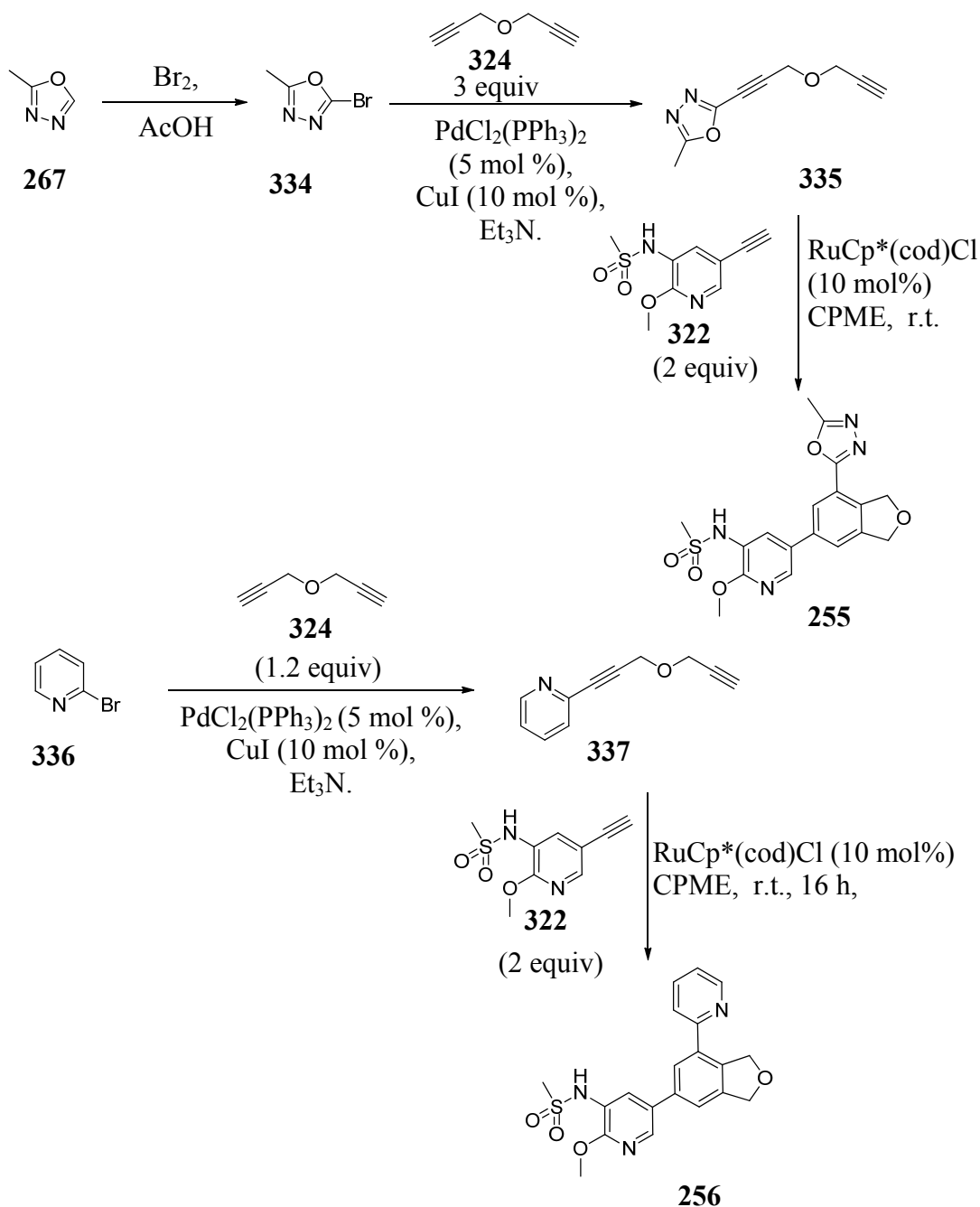
Scheme 128 – The direct formation of functionalised diynes removes the necessity for low-yielding palladium-catalysed cross-couplings of potentially unstable heterocycles.

Christopher J Tame

2.4.2   Medicinal chemistry

The aim of this research was to access a series of PI3Kδ inhibitors that possess a suitable pharmacokinetic (PK) profile for oral administration.   This has been attempted by reducing the topological polar surface area (TPSA) and the number of aromatic rings of an existing inhaled series.   Initial work focused on replacing the indazole core with a dihydroisobenzofuran, which demonstrated retention of potency on related fragments.   The current study involved elaborating the structures at the 6-position of the dihydroisobenzofuran in order to improve potency and selectivity.   As described in the previous section, six analogues were made and represent the different pharmacophoric elements explored in the original inhaled series (**Table 11**).
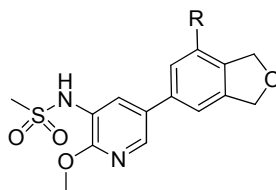
Compound Number	R	Mwt	cLog P	TPSA	Ar. Ring count
255		402	1.1	116	3
256		397	2.9	90	3
257		377	1.5	107	2
258		461	2.8	120	3
259		463	1.6	119	2
260		455	2.9	120	3

Table 54:   The calculated physicochemical properties are displayed for the six compounds designed as orally-active PI3Kδ inhibitors.

Christopher J Tame

The selectivity requirements for this series concern the closely related PI3K class I isoforms and the wider lipid and protein kinases. Isolated enzyme assays provide useful information of a compound's affinity for a particular target and for this reason are run routinely for all compounds made.

Whilst enzyme data displays the affinity of a ligand to a target, cellular assays provide a more accurate representation of an *in vivo* system. The potency values from whole blood cellular assays are influenced by factors such as cell permeability, metabolic stability and plasma protein binding (ppb). Promising compounds from the isolated enzyme assays will be run in a whole blood assay to assess whether good levels of potency can be achieved in this more biologically relevant system. The results from this assay, along with data from pharmacokinetic (PK) studies, will support the progression of successful compounds to pharmacodynamic (PD) studies. This will then be used to establish levels of efficacy in a disease relevant model.

PK studies provide understanding of the absorption, distribution and metabolism of the molecule and therefore its suitability for oral administration. Compounds which show appropriate stability will be progressed to *in vivo* PD studies, which are initially conducted in rodents and are the first examples of the compound's activity in a living organism. Detailed studies in a range of organisms are required by law before an appropriate molecule is selected for human trials. The screening cascade utilised in this research programme is illustrated in **Figure 24**, which has been constructed based on the consideration above.

Christopher J Tame

Isolated enzyme assays.
- PI3Kδ pIC50 > 7.0.
- 100 fold selectivity over PI3K class I isoforms (α, β, γ), and wider lipid and protein kinases.

Whole blood cellular assay.

- PI3K δ pIC50 > 6.0.

in vitro and *in vivo* PK studies.
- In vitro clearance (IVC): (microsomes and hepatocytes) p450 enzymes, MDCK permeability.
- Bioavailability (F%), half life ($T_{1/2}$), volume of distribution (V_{dss}), clearance (Cl_p).

in vivo PD studies.

- OVA-stimulated Brown Norway rat model.

Pre-candidate selection
- Safety studies (Ames test, hERG, eXp).
- Toxicity studies
- Large scale synthesis

Figure 59: The screening cascade for the identification of an efficacious, orally administered PI3Kδ inhibitor.

Christopher J Tame

The *in vitro* potencies of these compounds were measured against the isolated PI3K class I isoforms using biotinylated PIP$_3$ and a homogenous time-resolved fluorescence (HTRF) assay, supplied by Millipore.[358] The results from these assays (**Table 55**) show good potency against the PI3Kδ isoform, with pIC$_{50}$ values ranging from 6.4 to 8.3.[359] The more structurally elaborated compounds thiazole **258** and pyridine **260** display the best potency and selectivity profiles, supporting the hypothesis that functionalisation at the 6-position of the dihydroisobenzofuran core would provide an enhancement of activity and selectivity.
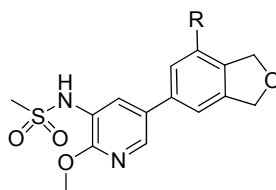
Compound Number	R	PI3K Class I isoforms			
		pIC$_{50}$ δ	Selectivity vs PI3K δ (Ratio)		
			α	β	γ
247	Inhaled PI3Kδ lead	9.1	631	794	631
255		7.7	5	13	5
256		7.2	10	20	6
257		6.4	4	13	13
258		8.1	50	63	25
259		6.8	25	63	50
260		8.3	50	126	25

Table 55: The isolated enzyme assay results for the PI3K class I isoforms.

239

Christopher J Tame

Whilst the potency data is encouraging, optimisation of selectivity is still required. Further elaboration at the 6-position would be aimed at reaching the pocket created by the Trp 760 and Met 752 residues in PI3Kδ, which has been used to tune selectivity. This has been previously rationalised to account for the selectivity profile observed in both literature and compounds from our earlier efforts on this target such as Idelalisib (**245, Figure 48**) and inhaled compound **247 (Figure 54)**, respectively. If this is exploited in the same manner as in previous internal PI3K δ series it will likely afford the desired selectivity profile of 100 fold over the Class I isoforms.

The isolated enzyme assay results for the PI3K class I isoforms are also represented as a bar chart to help compare the selectivity profiles of the compounds (**Figure 60**). Four of the six compounds display sufficient potency at PI3Kδ ($pIC_{50} > 7.0$), with thiazole **258** and pyridine **260** offering the best selectivity profile with this targeted set of compounds.
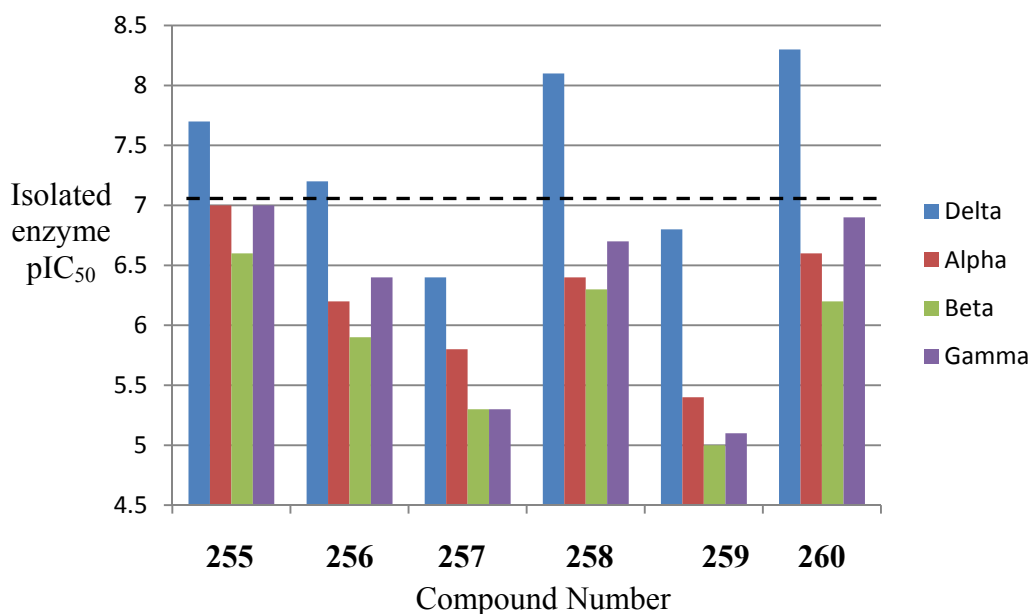
Figure 60: The isolated enzyme assay results for the PI3K class I isoforms.

The wider selectivity was also investigated and included screening against both lipid and protein kinases.[359] Screening against a panel of 17 protein kinases available in our laboratories revealed no measurable potency, which represents an average selectivity of 1000 fold when compared to PI3Kδ. Again, whilst these results are

Christopher J Tame

encouraging, screening against a wider set of protein kinases would help generate a more accurate view of the compounds' activity across the kinome.

Results from screening against lipid kinases available in our laboratories are shown in **Table 56** and are represented graphically in **Figure 61**. The compounds display excellent selectivity relative to FRAP 1, the catalytic subunit for the mTOR kinase, which has been shown to be associated with the PI3K/pAkt pathway.[360] Excellent selectivity was also observed against another related kinase, PIK3C2B (not shown in **Table 56**). The Class III PI3K Vps34 is shown to be strongly inhibited, as is DNA-PK. DNA-PK influences the cell cycle and, therefore, activity at this target is undesirable.[361] Vps34 is involved in mTOR-mediated nutrient sensing and macroautophagy, which are related processes.[280,281] Macroautophagy is the process of cytosolic degradation, and is implicated in innate immunity.[282] Vps34 inhibition, therefore, could cause undesired immunosuppressive side-effects.

Christopher J Tame
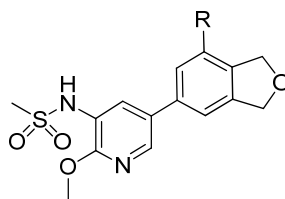
Compound Number	Structure of 'R'	Lipid Kinase (pIC$_{50}$)			
		PI3K δ	DNA PK	Vps34	FRAP 1
255		7.7	8.5	9.3	6.6
256		7.2	6.8	-	5.5
257		6.4	6.1	-	5.0
258		8.1	7.3	8.6	5.0
259		6.8	5.6	8.2	4.5
260		8.3	7.7	-	5.3

Table 56: The isolated enzyme assay results for PI3Kδ compared with selected lipid kinase targets.

Christopher J Tame
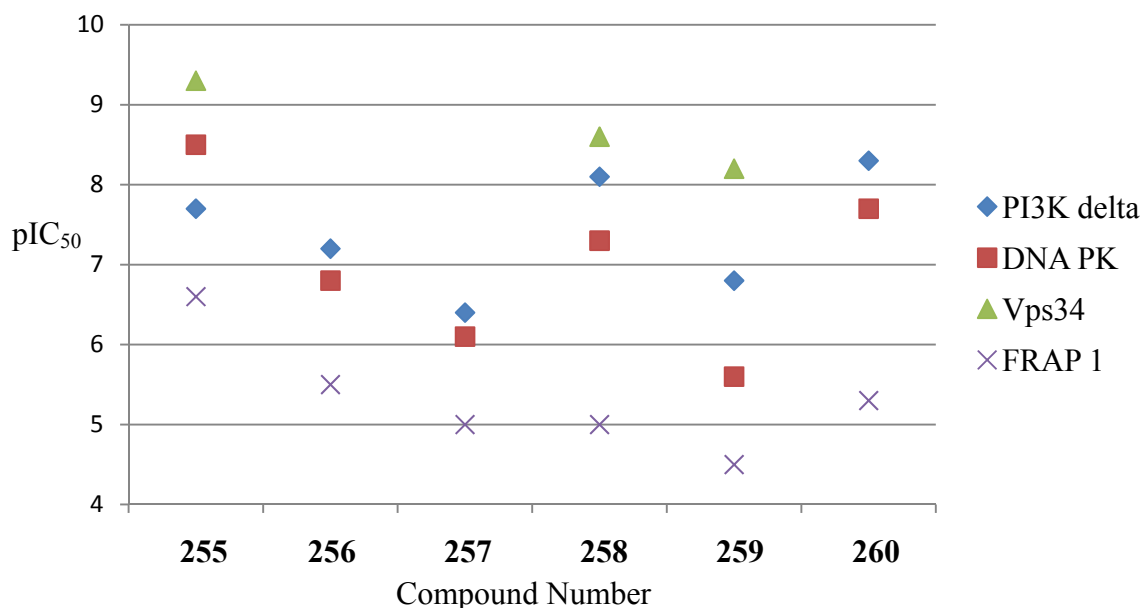
Figure 61: The wider lipid kinase selectivity for the PI3K δ inhibitors.

Selectivity relative to Vps34 and DNA-PK has been demonstrated previously by our research group (**Table 14**).[319] Comparing the structures with our current assets, these selective molecules have larger substituents at the 4-position of the indazole, which may extend towards Trp 760. Interactions with this residue are considered to be responsible for the high selectivity seen in this series (*cf.* inhaled compound **247**, **Figure 46**). Applying this SAR to the same position in the dihydroisobenzofuran series is expected to afford the desired selectivity profile and, therefore, could provide a means of enhancing selectivity within this new series.

Christopher J Tame

Table 57: The comparison of DNA-PK and Vps34 activity.
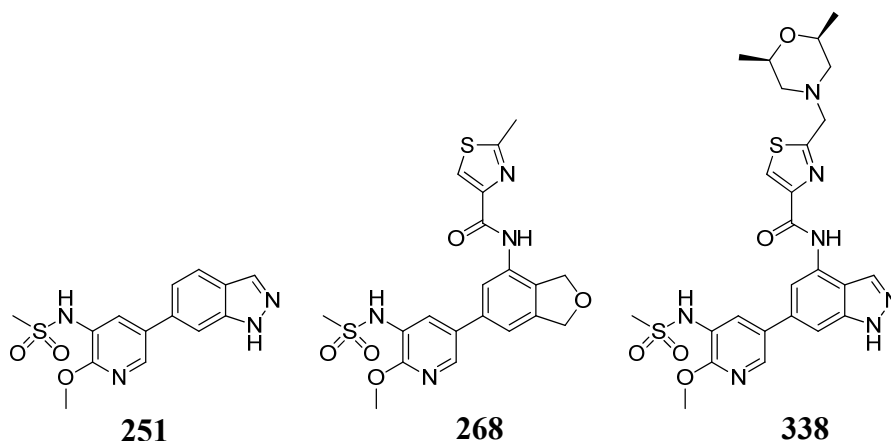
Isolated enzyme assay	251	268	338
PI3Kδ (pIC50)	6.0	8.1	9.2
PI3Kα, β, γ (pIC50)	5.1, 5.1, 5.5	6.4, 6.3, 6.7	6.4, 5.6, 6.5
DNA-PK (pIC50)	6.1	7.3	7.7
Vps34 (pIC50)	-	8.6	7.0

In order to more completely benchmark the series, three compounds were selected for further study based on their variation in potency, lipophilicity, and substitution at the 6-position of the dihydroisobenzofuran core. Oxadiazole **255** has a biaryl motif, morpholine **259** possesses an amide and methylene linker to a saturated ring whilst pyridine **260** has an amide-linked aromatic ring. The results from the whole blood assays[362] and PK studies[316] are shown in **Table 58**.

Christopher J Tame

	Inhaled PI3Kδ lead	R		
Compound number	**247**	**255**	**259**	**260**
PI3Kδ isolated enzyme (pIC$_{50}$)	9.1	7.7	6.8	8.3
PI3Kδ whole blood (pIC$_{50}$)	8.4	6.7	6.6	6.7
IVC (rat, mouse, human microsomes) (mL/min/g)	1.9, 5.9, 3.2	<0.5, 1.0, <0.5	<0.5, <0.5, <0.5	1.2, 1.4, <0.5
AUC (p.o) (after 1 mg/kg dose) (ng/hr/mL)	< 24	1130	576	42
Half Life, T $_{1/2}$ (i.v.) (hr)	2.6	0.9	1.3	3.4
Cl (i.v.) (mL/min/Kg)	50.0	6.9	14	6.0
Bioavailability, F (%)	**< 2.0**	**56**	**54**	**1.5**
V$_{dss}$ (L/Kg)	3.5	0.5	1.1	1.6
HSA binding (%)	90	90	64	93
Solubility (µg/mL)	182	195	185	50
MDCK perm. (nm/min)	213	803	122	758

Table 58: The results of *in vitro* and rat *in vivo* pharmacokinetic (PK) testing for compounds oxadiazole **255**, morpholine **259** and pyridine **260**, compared with that of the inhaled lead **247**.

The drop-off in potency between isolated enzyme and whole blood assays is represented graphically in **Figure 62**. The low drop-off exhibited by morpholine **259** compared to the other two analogues may be due to the low human serum albumin (HSA) binding, given that all other properties are similar. Accordingly, this would allow a higher free-fraction of compound available to interact with the kinase in an *in vivo* setting.

Christopher J Tame
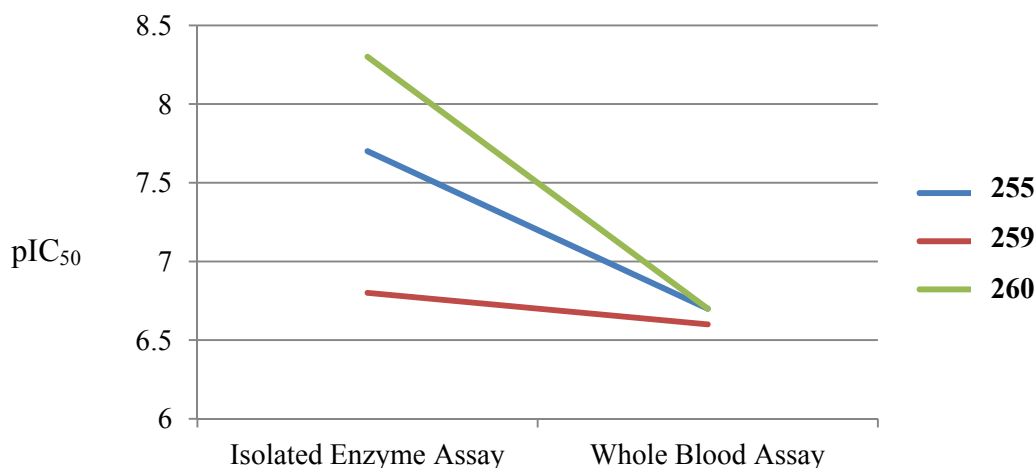
Figure 62: The drop-off in potency from the PI3Kδ isolated enzyme assay and the whole blood assay.

The HSA binding assay measures the affinity of a compound towards proteins present in the blood. When bound to HSA, the compound is shielded from interactions with the systemic environment, which includes the target of choice and metabolic enzymes. High HSA binding is therefore expected to result in longer compound duration but possibly at a lower potency level. **Figure 63** displays a reasonable correlation between HSA and enzyme-to-cell drop-off, suggesting that morpholine **259** is more exposed to the PI3Kδ target in the whole blood system as a result of lower HSA binding.
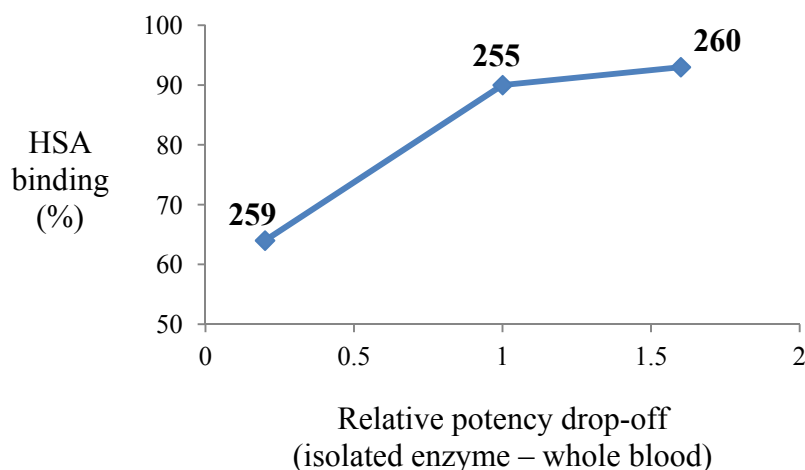
Figure 63: The positive correlation between HSA binding and potency drop off between enzyme and whole blood cellular assays.

Christopher J Tame

All three compounds display much improved clearance levels when compared to the inhaled compound **247** in *in vitro* and *in vivo* studies. *In vitro* clearance (IVC) levels in mouse (m), rat (r) and human (h) microsomes are low to moderate, whilst rat *in vivo* clearance of less than 14 mL/min/Kg equates to less than 20% liver blood flow (**Table 58**).[316] The slightly elevated clearance of morpholine **259** with respect to oxadiazole **255** and pyridine **260** could be attributed to the lower level of protein binding (HSA), which increases exposure towards metabolic enzymes, as discussed previously.

Bioavailability (F%) is defined as the ratio of the area under the curve for intravenous (IV) and oral administration in *in vivo* studies. This value represents the level of compound present in the systemic compartment and therefore the percentage of the dose available to interact with the target of choice. Low bioavailability is observed for pyridine **260**, which may be attributed to poor absorption into the systemic circulation, indicated by the low level of compound detected throughout the study (area under curve (AUC) value). This is likely to be due to the low solubility of pyridine **260** (50 µg/mL) when compared to the other two analogues examined. Interestingly, the low oral absorption does not correlate to MDCK permeability, which is high for all three compounds. This demonstrates the limitation of using *in vitro* assays as representative models for *in vivo* pharmacokinetic profiles. This information will be useful for the design of the next iteration of compounds.

Oxadiazole **255** and morpholine **259** show significantly improved bioavailability when compared to inhaled compound **247** and, to our knowledge, represents the first time good oral bioavailability has been achieved in any PI3Kδ selective inhibitor. Furthermore, morpholine **259** is the first bioavailable PI3Kδ inhibitor that possesses greater than 20 fold PI3K class I selectivity in our isolated enzyme assays. This then represents a significant advance in the design of selective PI3Kδ compounds which are suitable for oral administration.

The volume of distribution (V_{dss}) is a mathematical term derived from measured *in vivo* PK data, and is used to describe the amount of compound present in the blood

and tissue at any one time. A low V_{dss} defines the compound to be present mainly in the blood, whilst a high number would refer to the compound being present mainly in the tissues. This number can help explain the half life of a compound, as it is considered that a compound cannot be metabolised (or interact with the target) in the tissue. Accordingly, 'protection' from metabolism can prolong the half life. The half lives and volume of distribution correlate well in compounds **247**, **255**, **259**, **260**, supporting this hypothesis.

The half lives of oxadiazole **255**, morpholine **259** and pyridine **260** will likely have to be improved in order to satisfy a reasonable once-daily dosing regimen. This could be achieved by increasing the lipophilicity of the compounds, which should increase their volume of distribution. Increasing the lipophilicity, however, may negatively impact other parameters such as solubility, which is a key descriptor for oral absorption.[133,138] These factors will need to be closely monitored if this approach was adopted, and it is likely that a balance will need to be made between all of these factors.

Despite the caveats mentioned above, the promising bioavailability and PI3K class I selectivity results led to morpholine **259** being progressed to an *in vivo* pharmacodynamic (PD) study[363] to determine its efficacy in a disease relevant animal model (**Figure 64**).

Christopher J Tame
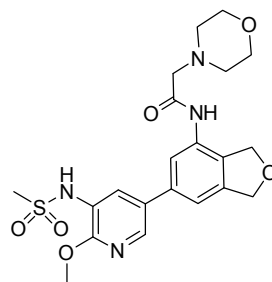
259
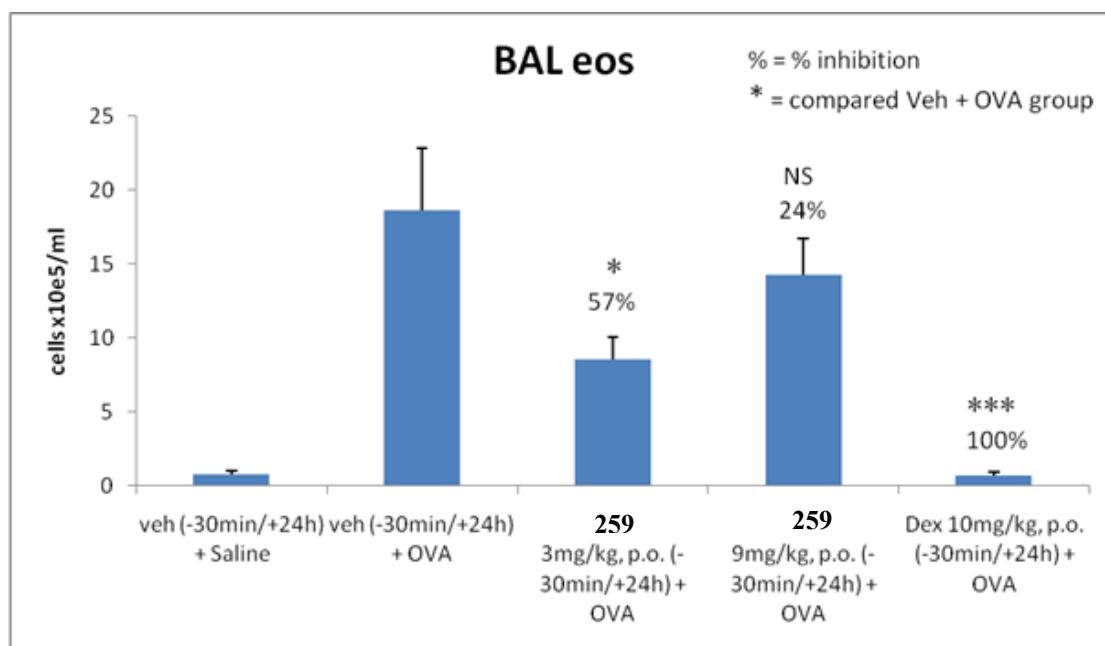
Figure 64: Results from a pharmacodynamic study of orally administered **19** in Brown Norway rats. (* = p < 0.05).

The study was undertaken on ovalbumin (OVA)–stimulated Brown Norway rats and the compound was dosed orally at two levels, 3 mg/kg and 9 mg/kg at 30 min and 24 hour intervals after the OVA challenge. Ovalbumin invokes an inflammatory response, causing the up-regulation of a range of inflammatory cell types. This replicates the disease state of an asthmatic patient and therefore provides a more realistic model with which to investigate the effect of morpholine **259**.

The dose was formulated in a 0.5% HPMC/0.2% Tween-80 solution in water and the study was run with a control and a standard (Dexamethasone). After 48 hours the

Christopher J Tame

lungs were washed out with brine, known as a Bronchial Alveolar Lavage (BAL). The eosinophil cells were isolated from the collected brine washings and their number was determined. Eosinophils have been shown to be upregulated at the site of inflammation, and therefore provide a reasonable marker for measuring the possible anti-inflammatory effect of the compound.[303]

The 3 mg/kg dose shows significant knock-down of eosinophil cells when compared to the control, however the 9 mg/kg dose shows no statistically significant inhibition. This phenomena has been found in other PI3Kδ compounds investigated by our group and the cause is not well understood, but seems to correlate with increased dose levels.[319] This is considered to be a limitation of the assay rather than of the efficacy of the compounds tested, but would need to be investigated further before the compound could be progressed towards clinical studies, for example.

The next investigation could involve a dose-response study of morpholine **259** in another PD model, perhaps in a different species such as mouse, or with a different stimulator, such as bleomycin. These results would be compared with that of the OVA-stimulated Brown Norway rat model presented in **Figure 64**, which would help determine a more realistic representation of the *in vivo* efficacy of the compound.

From consideration of all the above data, morpholine **259** represents the first PI3Kδ-selective inhibitor with good oral bioavailability and *in vivo* efficacy tested in our laboratories. This is compared to the benchmark set by the orally bioavailable dual PI3Kγ/δ dual inhibitor IPI-145, which demonstrates similar levels of *in vivo* efficacy in a similar PD study and is currently undergoing a Phase 2a trial for asthma.[318]

This study has shown that the pharmacokinetic profile of the existing PI3Kδ series has been significantly improved, based on the initial inhaled lead, and represents a major breakthrough in the research of an orally active PI3Kδ-selective inhibitor. **Table 59** compares the oral profiles of the lead inhaled compound **247** with that of morpholine **259**, highlighting the significant progress made. The reduction of key

Christopher J Tame

physicochemical parameters has correlated well with the improved oral PK profile of **259**, which further supports the literature evidence for this relationship.

The next steps with this series will be to optimise the selectivity profile amongst the PI3K class I and wider lipid kinases, as well as the duration of the compound in the body, represented as the half life ($T_{1/2}$).
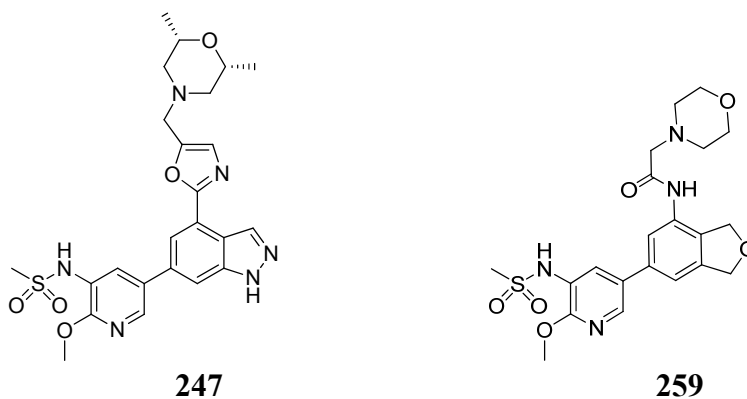
247   **259**

Compound number	247	259
Molecular weight (Da)	513	463
Chrom LogD pH 7.4	3.3	2.6
TPSA	135	120
Aromatic ring count	4	3
Rotatable bond count	6	5
PI3Kδ Isolated enzyme (pIC_{50})	9.1	6.8
PI3K α, β, γ Isolated enzyme (ratio)	631, 794, 631	25, 63, 50
PI3Kδ Whole Blood (pIC_{50})	8.5	6.6
IVC (rat, mouse, human microsomes) (mL/min/g)	1.9, 5.9, 3.2	<0.5, <0.5, <0.5
Half Life, $T_{1/2}$ (i.v.) (hr)	2.6	1.3
Clb, (i.v.) (mL/min/Kg)	50.0	14
Bioavailability, F (%)	< 2.0	54
Vdss (L/Kg)	3.5	1.1
HSA binding (%)	90	64
Solubility (µg/mL)	182	185
MDCK perm. (nm/min)	213	122

Table 59: Comparison of physicochemical properties and oral PK profile of inhaled compound **247** and morpholine **259**. Data in green highlights the improvements made.

Christopher J Tame

2.5   Summary and next steps

A specific set of dihydroisobenzofuran-containing small molecules has been designed and synthesised with the aim of achieving sufficient potency and selectivity and delivering a suitable PK profile for oral administration. These compounds were accessed efficiently from the relevant precursor alkynes using ruthenium-catalysed [2+2+2] cyclotrimerisation reactions. These reactions were optimised from literature conditions by eradicating the excess of the valuable monoyne component required, demonstrating the tolerability of a novel heteroaromatic alkyne substituent, removing the requirement of anhydrous and degassed conditions, and incorporating a range of environmentally sustainable solvents.

The dihydroisobenzofuran series has shown good levels of potency and encouraging degrees of selectivity, which may be enhanced through further optimisation based on existing knowledge of a progenitor series of compounds. The current off-target activity at lipid kinases DNA-PK and Vps34 will need to be addressed and may again be solved by application of in-house knowledge from previous PI3Kδ programmes prosecuted within our laboratories.

Oxadiazole **255**, morpholine **259** and pyridine **260** were selected for further study and show good activity in a whole blood cellular assay. The minimal drop off in potency between enzyme and cellular assays of morpholine **259** appears to be a result of low human serum albumin binding (HSA), which could be attributed to the reduced number of aromatic rings when compared to oxazole **255** and pyridine **260**.

All three compounds display low clearance in mouse, rat and human IVC studies, which was reflected *in vivo*. The low bioavailability of pyridine **260** may be a result of relatively low solubility, an aspect that should be considered in future design processes. Oxadiazole **255** and morpholine **259** displayed encouraging half-lives, however, these may require optimisation to achieve consistency with once daily dosing. It is expected that increasing the lipophilicity may result in a longer half life through a higher volume of distribution.

Christopher J Tame

Morpholine **259** demonstrates significant knockdown of eosinophil cell recruitment in an OVA-challenged PD model at 3 mg/kg dose, underlining the viability of this series as orally-active PI3Kδ inhibitors. This is the first example of an orally efficacious PI3Kδ inhibitor with good levels of selectivity over the other PI3K class I isoforms when tested in our laboratories. The parabolic dose-response curve is not well understood but reflects what has been previously shown to be dose-dependent with other classes of PI3Kδ inhibitors.[319] Further investigation is necessary to fully validate the *in vivo* efficacy of these compounds in complementary pharmacodynamic models. However, morpholine **259** represents a valuable asset to probe the oral activity of PI3Kδ inhibitors against a raft of inflammatory diseases.

Future work should focus on the optimisation of lipid kinase selectivity and PI3Kδ potency. Literature compounds have identified a 'selectivity pocket' between Trp 760 and Met 752, which is considered to be responsible for generating significant PI3Kδ specificity. This could be reached with further elaboration at the 6-position of the dihydroisobenzofuran, as demonstrated in the indazole series previously identified in our group (**Figure 65**).[321]
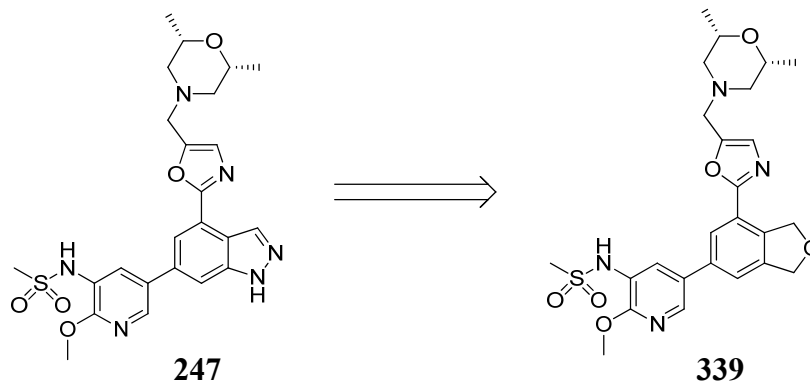
Figure 65: The lipid kinase selectivity of the dihydroisobenzofuran series could be improved by accessing the Trp 760 and Met 752 residues, as done with the indazole series.

The physicochemical properties of the indazole series have been previously optimised by replacing the pyridylsulfonamide moiety with an indole, which marginally increases the lipophilicity and reduces the molecular weight by almost

100 daltons.[319] These changes are made whilst maintaining an excellent PI3K class I selectivity profile (**Figure 66**).   Combining the indole moiety with the dihydroisobenzofuran may therefore facilitate further improvement in physicochemical profile, which could potentially contribute to an improved half-life and bioavailability in the series.

Christopher J Tame
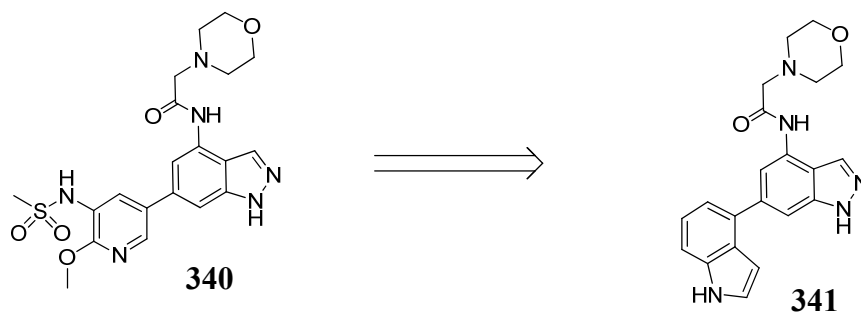
Compound number	104	341
PI3Kδ (pIC$_{50}$)	7.3	6.5
PI3K α, β, γ (ratio)	631, 794, 631	6309, 398, 794
Mwt	460	375
cLog P	2.1	3.2
TPSA	139	86
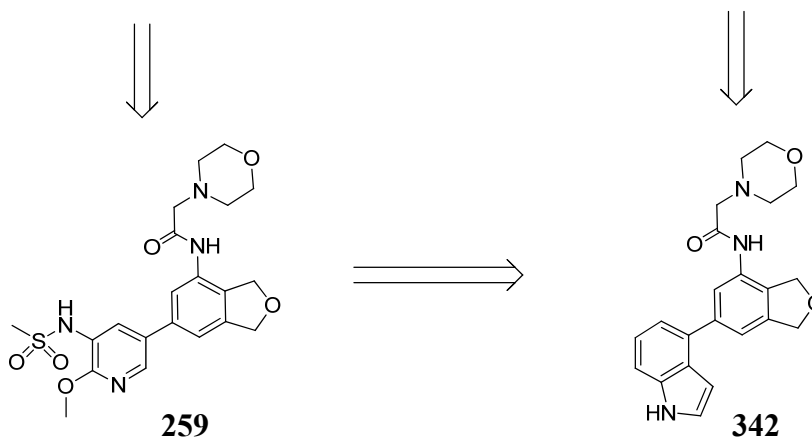
Compound number	259	342
PI3Kδ (pIC$_{50}$)	6.8	-
PI3K α, β, γ (ratio)	25, 63, 50	-
Mwt	463	377
cLog P	1.6	2.7
TPSA	120	67

Figure 66: Rationale for improved lipophilicity and molecular weight by replacing the pyridylsulfonamide with an indole moiety.

Examining the physicochemical properties of this series suggests that the predicted polar surface area of the new indole-functionalised dihydroisobenzofuran (**342**) is

255

below the low-level guideline for orally efficacious, non toxic compounds.[137] This could be increased by incorporating polar groups to re-establish the hydrogen-bonding interactions made by the sulfonamide analogue. This may have the effect of also improving the potency and selectivity profile. A potentially simpler approach to increase the polar surface area could be achieved through the introduction of an aza-dihydroisobenzofuran (**Figure 67**). In principle, this could be accessed using cyclotrimerisation methodology with a monoyne and a nitrile-tethered alkyne (**Figure 68**).

343

Mwt	378
cLog P	2.2
TPSA	79
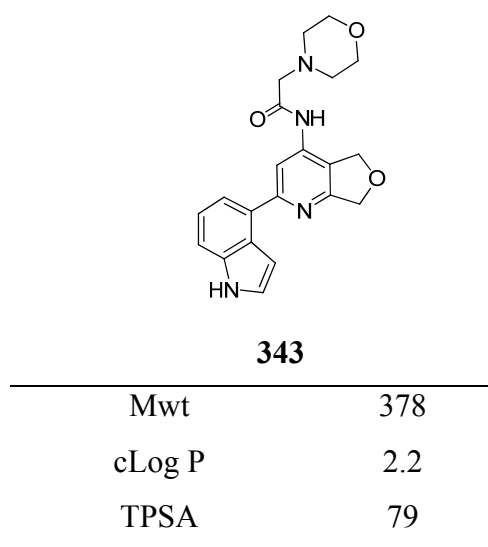
Figure 67: The introduction of an aza-dihydroisobenzofuran for improved TPSA.
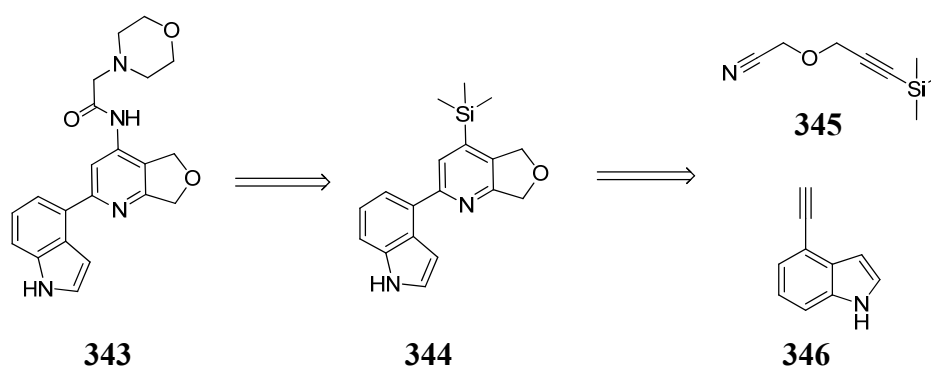
Figure 68: Retrosynthetic analysis of **343** utilising a cyclotrimerisation strategy. Modifying the sp^2 centre at the 6-position with an sp^3 centre has also been identified as another manipulation of groups at this vector. An sp^3 centre situated here will

Christopher J Tame

reduce the planarity of the molecule, which has shown to influence solubility,[364,365] a property that had a demonstrable effect upon the bioavailability of the series.[138]

All of these modifications can be efficiently investigated through exploitation of alkyne cyclotrimerisation chemistry. This approach allows the relevant vectors to be accessed from simple alkynes in fewer steps than compared to the functionalisation of activated phenyl rings.

3   PI3Kγ Inhibitors

3.1   Background

3.1.1   Literature PI3Kγ Inhibitors

The development of a small molecule inhibitor of PI3Kγ has attracted interest from a large number of pharmaceutical companies, illustrated by the significant number of publications and patents in this area.[366] The most advanced compound is the PI3Kγ/δ dual inhibitor IPI-145, which is currently undergoing a Phase II study for asthma.[367] There are, however, very few publications disclosing the discovery of selective PI3Kγ inhibitors.

The most advanced compound in terms of potency and selectivity that has been profiled in our laboratories is compound **347** from Shionogi,[368] which demonstrates at least 100 fold selectivity against all the kinases tested so far. This includes all PI3K Class I and III isoforms and over 20 protein kinases. This compound has also shown good rat oral PK after 1 mg/kg i.v. and 2 mg/kg p.o. dosing (**Table 60**).

Christopher J Tame

347
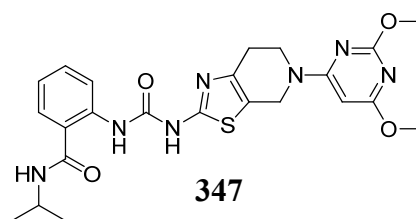
PI3Kγ (pIC$_{50}$)	8.6	Artificial Membrane Permeability (nm/sec)	800	
PI3K α, β, δ (ratio)	7943, 501, 501	MDCK Permeability (nm/sec)	565	
Mwt	498	CLND Solubility (μg/mL)	13	
Chrom LogD pH 7.4	5.5	HSA (%)	95	
cLog P	4.3	Bioavailability (F%)	51	
TPSA	131	Half-life (T$_{1/2}$)	5.0	
Aromatic ring count	3	Cl$_b$ (mL/min/kg)	7.5	
Rotatable bond count	7	V$_{dss}$ (L/kg)	2.3	

Table 60: A selective inhibitor of PI3Kγ discovered by Shionogi.

A solved crystal structure of compound **347** in PI3Kγ is displayed in **Figure 69**.[369] The results confirm a key hinge binding interaction between the donor-acceptor motif of the aminothiazole moiety and Val 882. Potency is likely to also be derived from hydrogen-bonding interactions between the pyrimidine moiety and Lys 833. This residue is commonly targeted by PI3Kγ inhibitors, such as the natural product wortmannin, which binds irreversibly to Lys 833 (**Figure 70**).[370] The origin of selectivity is unclear but could be due to the urea-linked isopropylbenzamide group, which the crystal structure suggests is involved in lipophilic interactions distant from the hinge.[320]

Christopher J Tame
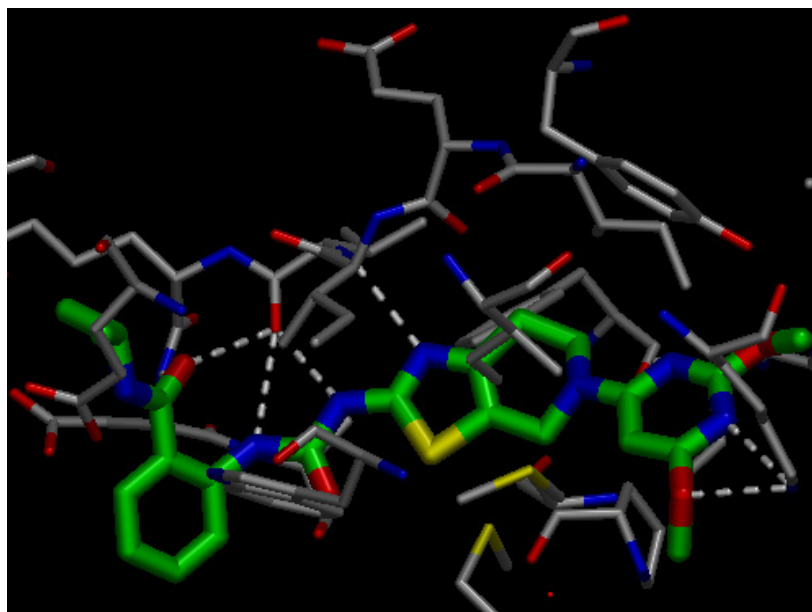
Figure 69: A solved crystal structure of PI3Kγ and **347** to 2.9Å.[369]
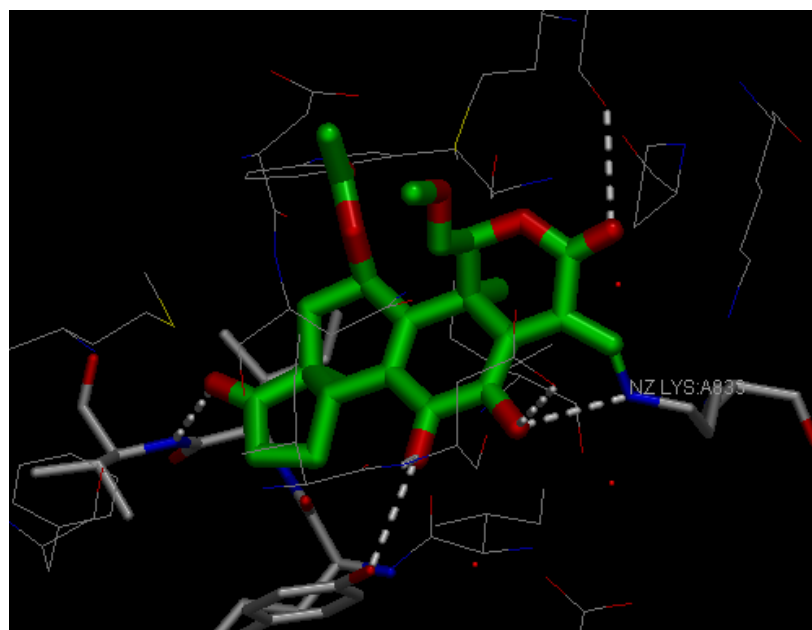
Figure 70: Crystal structure of wortmannin irreversibly bound to PI3Kγ.[370]

The main potential issues associated with this compound include the high molecular weight, high lipophilicity and low solubility, which attrition studies have predicted to increase the risk of undesirable developability issues as an orally administered

Christopher J Tame

compound.[136,138] This compound also contains aminothiazole and aniline moieties, which are known toxicophores, features which are not attractive in a development compound.[371]

The low solubility may also be undesirable for inhaled delivery, as this can exacerbate the build up of foamy macrophages – inactive immune cells formed from the excessive consumption of particulates as described in the introduction. These foamy macrophages can initiate inflammation of the lung, causing other inflammatory mediators and cell types to be up-regulated to the site of infection. This would cause the opposite pharmacological effect to that which is desired.

The origin of the difficulties in achieving both selectivity and developability is that only three residues are exclusive to the PI3Kγ active site amongst the class I isoforms.[372] In order to achieve selectivity, an inhibitor must interact more favourably with residues in the desired active site than in others.   Therefore, interaction with the three unique residues in PI3Kγ is likely to be important for optimal selectivity. These residues are Thr 886, Lys 802 and Lys 890 which are located on the periphery of the active site, distanced from the hinge region where interactions are typically required for an ATP competitive inhibitor (**Figure 71**).[320]
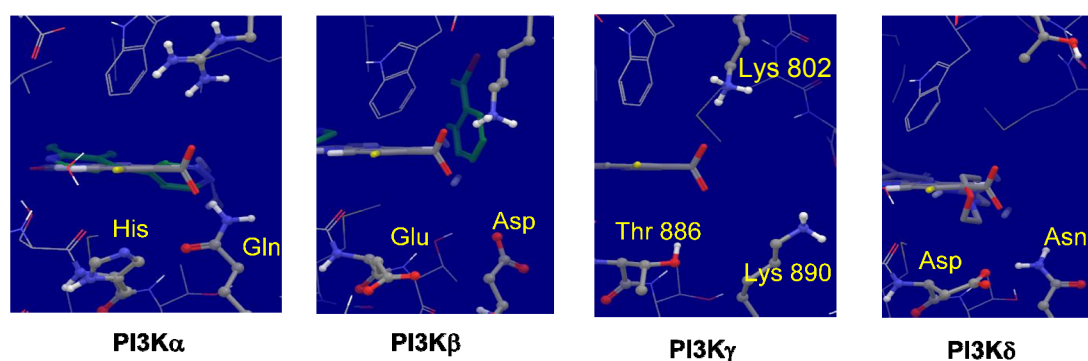
Figure 71: The varying residues present amongst the PI3K Class I isoforms.[320]

Reaching this region from the hinge therefore requires large molecules, and consequently many of the reported compound classes possess undesirable properties for either oral or inhaled administration routes.[366] The current difficulty in accessing

a selective and developable PI3Kγ inhibitor allows competitive research in this area to remain viable.

3.1.2 PI3Kγ inhibitors identified in our laboratories

Previous investigations in our laboratories identified a class of compounds which exploit a key interaction between a pyridone carbonyl and the Valine 882 residue at the hinge.[373] An example of this series and its associated PI3K class I selectivity profile is displayed in **Table 61**. A crystal structure of an exemplar compound is also shown in **Figure 72**.[374]

348
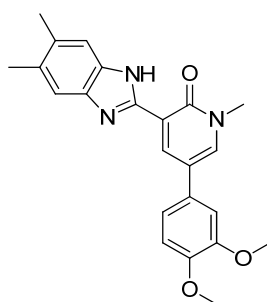
348	
PI3K γ (pIC$_{50}$)	7.0
PI3K α, β, δ (pIC$_{50}$)	5.4, <4.6, 6.1
10 protein kinases (pIC$_{50}$)	< 5.0
MW	389
cLogP	4.3
Chrom LogD pH 7.4	5.1
TPSA	69
Ar Ring Count	4
CLND Solubility (µg/mL)	11
Artificial Membrane Permeability (nm/sec)	160

Table 61: The PI3K class I isoform enzyme affinity and physicochemical properties for a previously optimised internal series of PI3Kγ inhibitors.[375]

Christopher J Tame
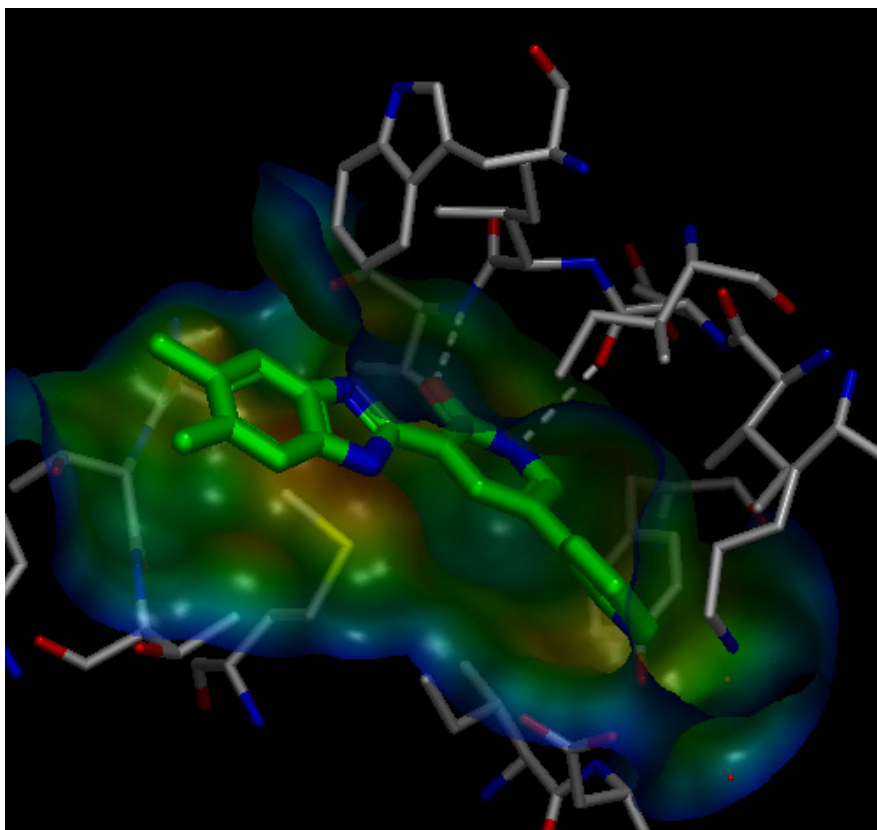
Figure 72: A crystal structure of PI3Kγ and inhibitor **348**, solved to 2.3Å.[374]

Benzimidazole **348** exhibits reasonable potency against PI3Kγ whilst showing no measurable affinity towards PI3Kβ or a range of unrelated protein kinases. However, optimisation is required at PI3Kα and δ to achieve the required selectivity window of 100 fold necessary for further development of this chemical series.

Earlier optimisation efforts by our research team identified a carboxylic acid-containing molecule that exhibited improved selectivity against PI3Kδ and improved solubility (**Table 62**), but with significantly reduced permeability.[373]

Christopher J Tame

349
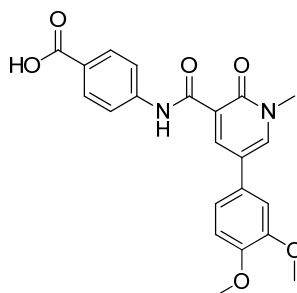
	349
PI3Kγ (pIC$_{50}$)	7.4
PI3Kα, β, δ (pIC$_{50}$)	5.0, <4.5, 5.7
CLND Solubility (μg/mL)	132
Artificial Membrane Permeability (nm/sec)	3.0

Table 62: The potency and selectivity profile is improved when replacing the dimethylbenzimidazole moiety with a 4-aminobenzoic acid moiety.

The data generated to date indicate that the structure activity relationships (SAR) correlate well between the benzimidazole and aniline templates, which is exemplified by benzimidazole **348** and carboxylate **349**, respectively. The aniline is accessed from robust synthetic chemistry methodology, which can facilitate rapid synthesis and testing cycles during the optimisation campaign. Subsequent medicinal chemistry efforts will therefore utilise the aniline, which can be replaced with the benzimidazole once the molecule is optimised, so as to avoid any potential toxic metabolism of anilines in the body.[376]

Attempts to obtain X-ray crystallography data of carboxylate **349** were unsuccessful. However, molecular modelling predicted the acidic residue to interact with the lysine and threonine residues unique to PI3Kγ (**Figure 71**).[320] The improved selectivity over PI3Kδ can be rationalised when the residues in this region of the kinase are compared. PI3Kδ possesses an aspartate (Asp) residue, which would not interact

Christopher J Tame

favourably with the carboxylate moiety **349**, whereas threonine (Thr) 886 in PI3Kγ could potentially form a favourable hydrogen-bonding interaction.
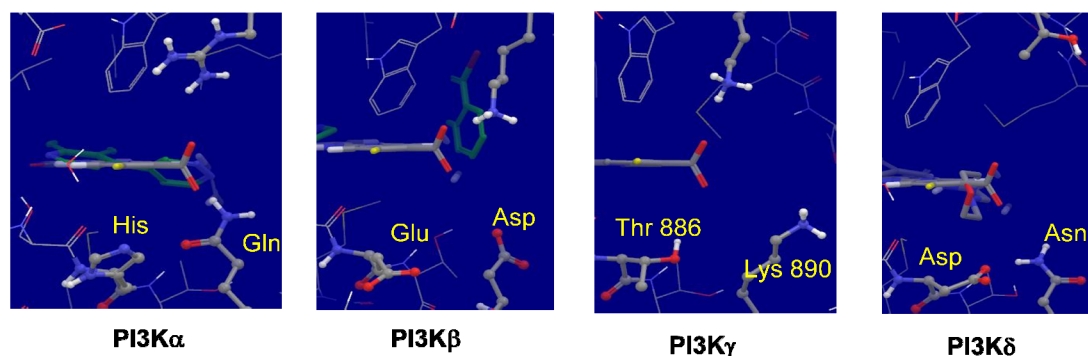
Figure 71: A solved crystal structure for PI3Kγ was used to develop models of the other PI3K class I isoforms.[320]

This carboxylic acid-containing pyridone represented the most advanced molecule in this programme within our laboratories, due to the improved selectivity profile it exhibited; however the potency at PI3Kγ still required extensive optimisation.

The objective of this research was to develop a safe and efficacious small molecule inhibitor of PI3Kγ for the treatment of asthma. Topical administration presented the best opportunity to expediently investigate this aim, as the action of the drug is targeted at the diseased tissue and systemic toxicity is limited (explained previously in **Chapter 1**). The PK and PD profiles of existing compound series within our laboratory were therefore optimised to complement the inhaled route of administration.

The target profile for an inhaled inhibitor of PI3Kγ is shown in **Table 63**. The high potency requirements at PI3Kγ would allow the desired therapeutic effect to be achieved with a minimal dose, which is expected to minimise irritation in the lung.

Christopher J Tame

Target values for an inhaled PI3Kγ inhibitor	
PI3Kγ (pIC$_{50}$)	>9
PI3Kα, β, δ	100 fold selective
General kinase selectivity	100 fold selective
Solubility (μg/mL)	>100
Permeability (nm/sec)	>100

Table 63: The key requirements for an inhaled PI3Kγ candidate molecule.

The potency and selectivity levels required for a PI3Kγ clinical candidate molecule are much higher than those exhibited by the pyridone series. The aim of accessing these levels is expected to be achieved through *irreversibly* binding to a residue in the PI3Kγ active site. Based on consideration of molecular modelling studies, the carboxylic acid moiety of compound **349** was predicted to interact with Lys 890, so conversion of this acid to a cell-hydrolysable ester would be anticipated to afford a selective covalent inhibitor.

Covalent inhibition of lysine residues with electrophilic esters had been recently demonstrated in other biological targets, and provided an opportunity to overcome the potency and selectivity requirements of the series (**Scheme 129**).[377] Initial work would focus on optimising the location of the carboxylic acid moiety before conversion to a suitable acylating agent.
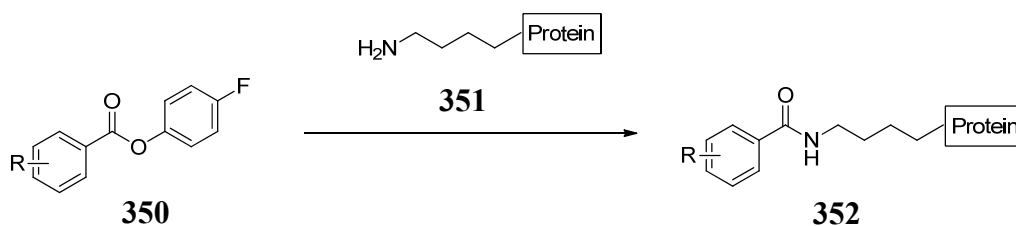
Scheme 129: The design of an irreversibly bound inhibitor through covalent interaction with a lysine residue in PI3Kγ has the aim of achieving the high potency levels required.

Christopher J Tame

Irreversible inhibition has seen a resurgence of interest within medicinal chemistry research as a method of identifying leads for challenging biological targets.[378] The main advantage of irreversible inhibition is the complete deactivation of a biological target. A potential disadvantage to this approach is off-target activity, for which covalent modification could enhance any unwanted side-effects.

In designing a covalent inhibitor, it is important to balance the level of electrophilicity of the ligand so that it can only undergo irreversible inhibition once selectively bound in the active site of the target of choice. If this is achieved the resulting selectivity profile will also be excellent.

Scheme 130 presents the kinetic profile of an irreversible inhibitor. The reversible inhibition of ligand (L) and protein (P) to form the bound complex (LP) is governed by the rate constants k_1 and k_{-1}, whilst irreversible inhibition to form inactivated protein (LP*) is governed by k_2. If k_2 is fast, the irreversible inhibition will readily occur and is likely to cause off-target activity. If k_2 is slow then the ligand can exhibit selectivity towards the desired active site before undergoing covalent inhibition, which would dramatically improve the activity profile against other biological targets.

Irreversible Inhibition

$$L+P \underset{k_{-1}}{\overset{k_1}{\rightleftharpoons}} LP \overset{k_2}{\dashrightarrow} LP*$$

Reversible Inhibition
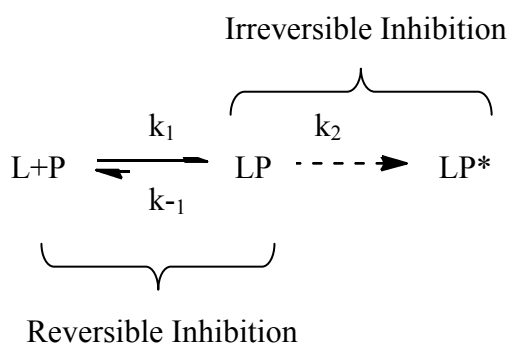
Scheme 130: The kinetic profile of an irreversible inhibitor.

Christopher J Tame

3.2   PI3Kγ research aims

The aim of this research was to optimise the potency and PI3K class I selectivity profile of a series of carboxylic acid-containing reversible PI3Kγ inhibitors. Specifically, this was to optimise the location of the carboxylic acid moiety with respect to nearby lysine residues unique to PI3Kγ. Key compounds which exploited this interaction were then planned to be used as leads to be further optimised as irreversible inhibitors of PI3Kγ. These compounds were expected to covalently bind to the appropriate lysine residue of PI3Kγ by replacing the carboxylic acid moiety with an electrophilic ester.

The use of irreversible inhibition had the aim of achieving sufficient potency for *in vivo* efficacy, whilst targeting a nucleophilic residue specific to PI3Kγ was designed to achieve PI3Kγ selectivity. To help reduce the potential toxicity associated with off-target effects of irreversible inhibitors and to increase the chances of achieving suitable efficacy *in vivo*, the PK profile was designed for inhaled administration.

3.3   Methodology

3.3.1   Medicinal chemistry

Optimisation of the carboxylic acid was attempted by varying the location it occupies in the active site and its electronic nature. A range of carbon linkers at the *para*- and *meta*-positions of the phenyl ring were examined to investigate the optimum location of the acid (**Figure 73**). This probed the protein for improved interactions with the desired threonine and lysine residues unique to PI3Kγ. Both saturated and unsaturated chains were included to assess the effect of rigidity and entropic strain in this region of the protein.

Christopher J Tame

353   **354**
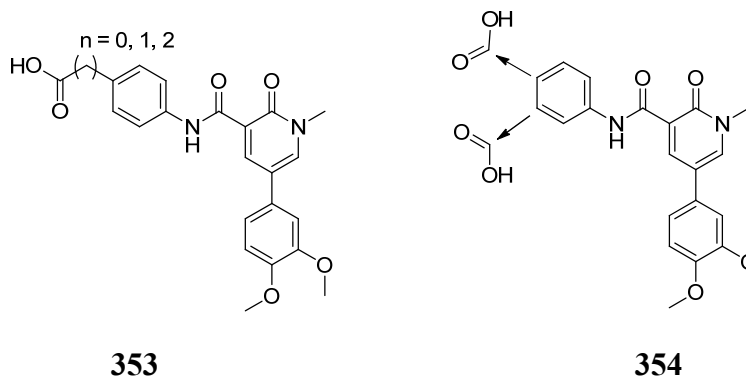
Figure 73: The optimisation of the carboxylate motif through variation in chain length and aniline substitution pattern.

Substituents were also introduced *ortho* to the benzoic acid moiety in order to adjust the electronic nature of the acid and, therefore, the potential interaction with the protein. Substituents of differing electronic and steric nature were selected to investigate how variation of pKa and dihedral angle may influence ligand-protein interactions. An example of this is shown in **Figure 74**.

Benzoic acid   2-Fluorobenzoic acid   2-Chlorobenzoic acid

Flat, no electronic effect   Flat, EWG   Perpendicular, EWG
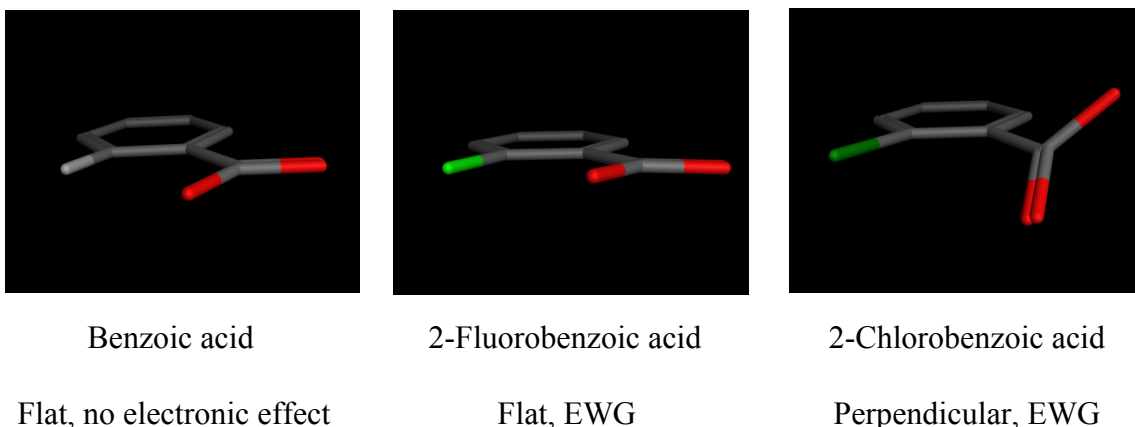
Figure 74: The orientation and electronics of the carboxylic acid moiety can be modified by varying the *ortho*-substituents.

The dihedral angle for a range of *ortho* substituents, as well as the pKa of the acid were calculated (**Table 64**). The dihedral angles were calculated from energy minimisations using the molecular modelling program, MOE[379] and the corresponding pKas were calculated using the ACD predictor.[380]

Christopher J Tame
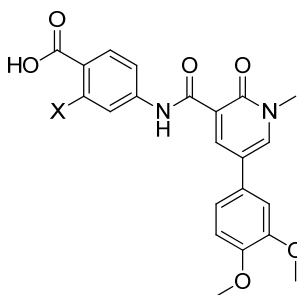
Compound Number	X	Dihedral angle (°)	ACD v11 pKa
349	H	0.1	4.3
355	F	15.7	3.4
356	Cl	48.3	3.0
357	Me	33.3	3.9
358	OMe	45.9	4.2
359	Br	52.2	2.7
360	NH$_2$	0.0	4.4
361	NHMe	0.0	1.9

Table 64: The calculated dihedral angles and pKa values for the carboxylate moiety of a variety of *ortho*-substituted compounds.

These substituents provide a range of dihedral angles and acidities, which was anticipated to provide useful SAR for carboxylate modification. The *ortho*-methylamine containing derivative (**361**) interestingly provides a low pKa value which could be a result of its zwitterionic nature (**Figure 75**).
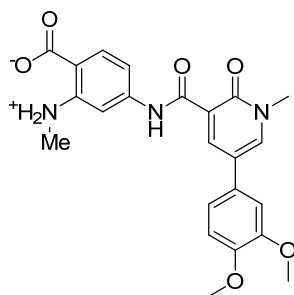
361

Figure 75: The zwitterionic nature of **361** is expected to cause the low calculated pKa value

Christopher J Tame

3.3.2   Synthetic chemistry

The synthetic route towards the amide-linked benzoic acids required two to three steps and exploited the extensive commercial availability of aminobenzoic acid analogues. This facilitated rapid construction of a range of analogues for structure-activity relationship (SAR) exploration (**Scheme 126**). The chemistry to access **364** was enabled previously within our laboratories and is well-validated.[373] A range of conditions were utilised to access the appropriate amides and some required subsequent hydrolysis, depending on the nature of the starting materials.
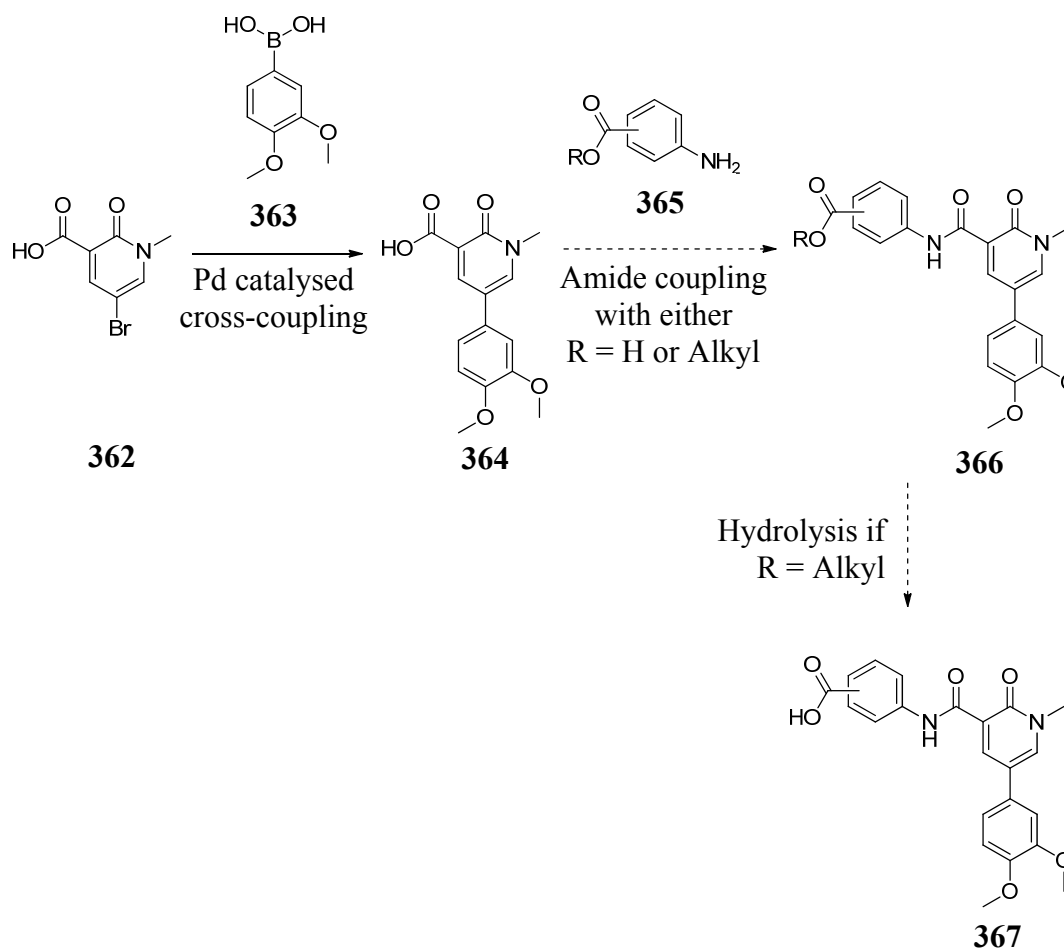
Scheme 131: The synthetic route used to access the *ortho*-substituted carboxylic acid targets.

Christopher J Tame

3.4   Results and discussion

3.4.1   Synthetic chemistry

The common intermediate **364** was accessed in one step from the commercially available pyridone **362** in 85% yield *via* palladium-catalysed cross-coupling with boronic acid **363** (**Scheme 132**).[381]
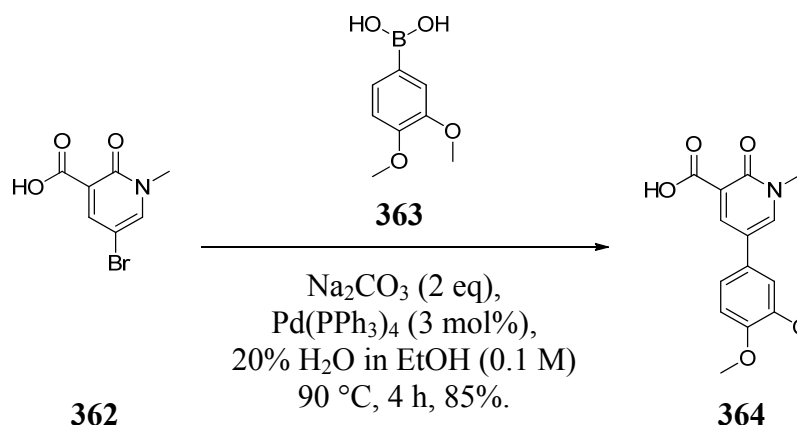
Scheme 132: Palladium-catalysed cross coupling of bromopyridone **362** with aryl boronic acid **363**.

The synthesis of compounds **349** and **370-373** was undertaken by another member of our laboratory, who utilised parallel reaction and purification techniques to facilitate their expedient synthesis.[382] This afforded the desired products with yields ranging 15-40% (**Scheme 133**). The requisite *meta*-benzoic acid (**369**) was accessed from oxalyl chloride-mediated acyl chloride formation, followed by reaction with 3-aminobenzoic acid (**368**, **Scheme 134**).

Christopher J Tame
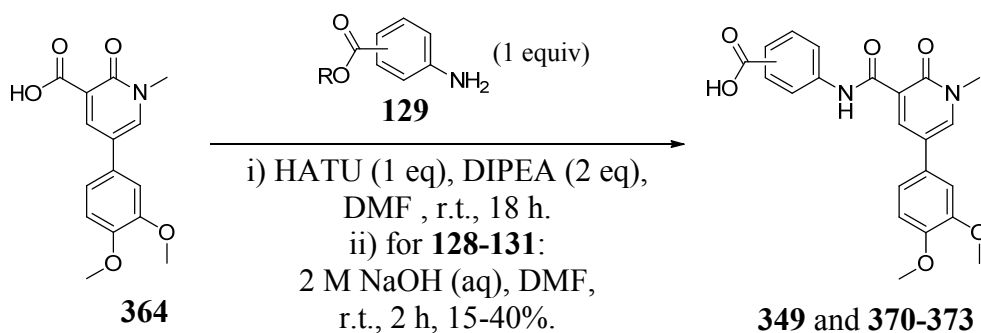
Scheme 133: HATU-mediated amide coupling of carboxylic acid **364** with a range of commercially available anilines.[382] R = H or alkyl.
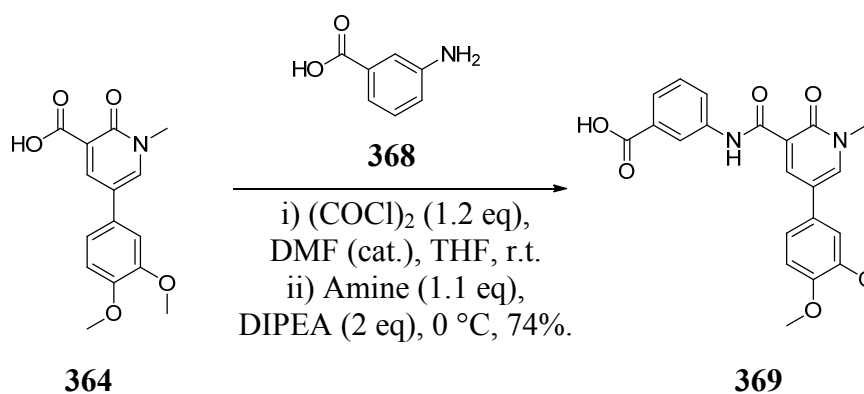
Scheme 134: *Meta*-functionalised benzoic acid **369** was accessed from the acid chloride intermediate by treatment of **364** with oxalyl chloride and DMF.

The yields and isolated enzyme affinities are shown for the PI3K class I isoforms in **Table 65**. The results show that all compounds are tolerated in the active site, which is encouraging when considering the incorporation of bulky esters in this region for covalent inhibition. All examples show a degree of erosion of selectivity against PI3Kα and β when compared to the original lead **349**, however many of these values remain above the acceptable 200-fold level. There is no evidence of significant change in the selectivity profile against PI3Kδ, which suggests that the selectivity of **349** may not be attributable to specific hydrogen-bonding interactions with the protein. This provides optimism that the selectivity profile can be improved by enhancing the interactions between the ligand and the protein in this region.

Christopher J Tame
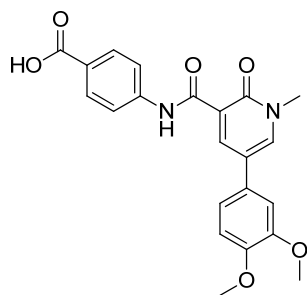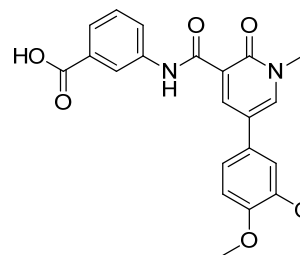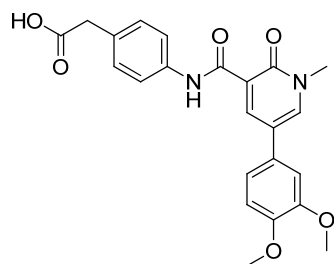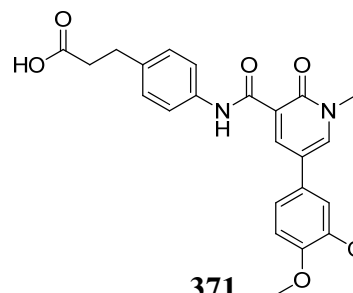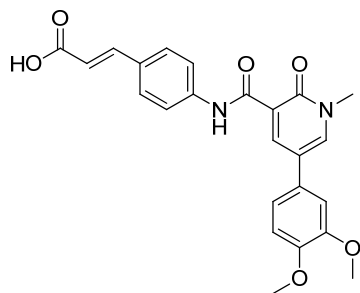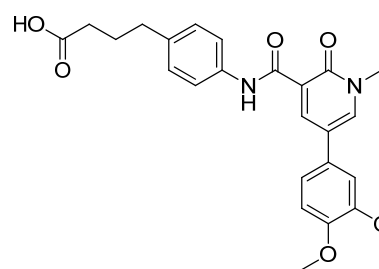
Compound number	Isolated yield	PI3K isoform isolated enzyme			
		γ (pIC$_{50}$)	α (ratio)	β (ratio)	δ (ratio)
349	22%	7.4	251	>794	50
369	74%	6.8	50	200	63
370	16%	7.0	200	>316	50
371	40%	7.1	63	>398	40
372	15%	7.2	79	>501	40
373	29%	7.0	126	-	10

Table 65: The yields and PI3K class I isolated enzyme data for a series of carboxylic acid-containing PI3Kγ inhibitors.

Christopher J Tame

A number of different approaches were utilised to access the different *ortho*-substituted benzoic acids depending on the commercial availability of the aniline monomers. The fluoro- and chloro-containing anilines were available as benzoic acids and their reasonable solubility in THF facilitated formation of the products *via* in-situ acid chloride generation of the pyridone core with oxalyl chloride and catalytic DMF (**Scheme 135**).[383] Subsequent purification *via* mass directed chromatography (MDAP) afforded the desired products in low yields.
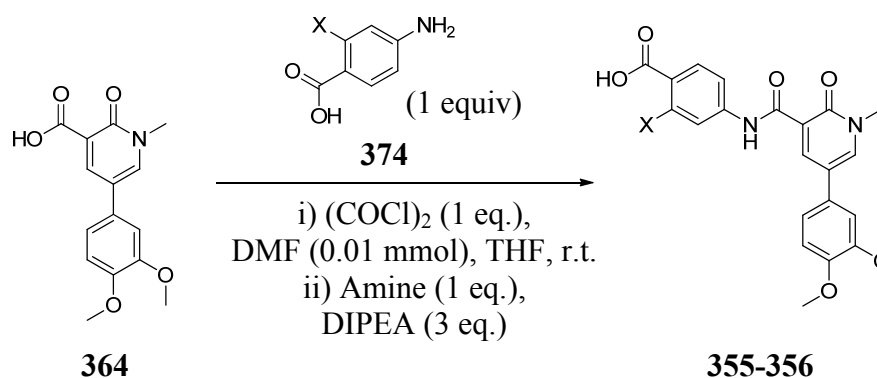
Compound number	X	Yield
355	F	5%
356	Cl	18%

Scheme 135: Oxalyl chloride-mediated formation of anilines **355** and **356** in low yields.

Through analysis of the reaction mixture by LCMS, it was observed that the acid chloride decomposed to the starting material during addition of the aniline monomers, which is likely to be responsible for the low yields. This could potentially be attributed to anhydride formation between the acid chloride (**375**) and the benzoic acid starting material (**374**) (**Scheme 136**). Upon LCMS analysis or work-up procedures, the anhydride would hydrolyse to afford two molecules of starting material.

Christopher J Tame

Protecting the carboxylic acid as the methyl ester would circumvent any anhydride formation, thereby potentially optimising the reaction conversion. This is the most straightforward method of optimising the reaction as it relies on robust esterification and ester hydrolysis transformations. The disclosed route was used due to the reduced number of synthetic steps, which offers greatest synthetic expediency. These reactions were also undertaken on a sufficient scale to afford appropriate amounts of the target compounds for biological screening.
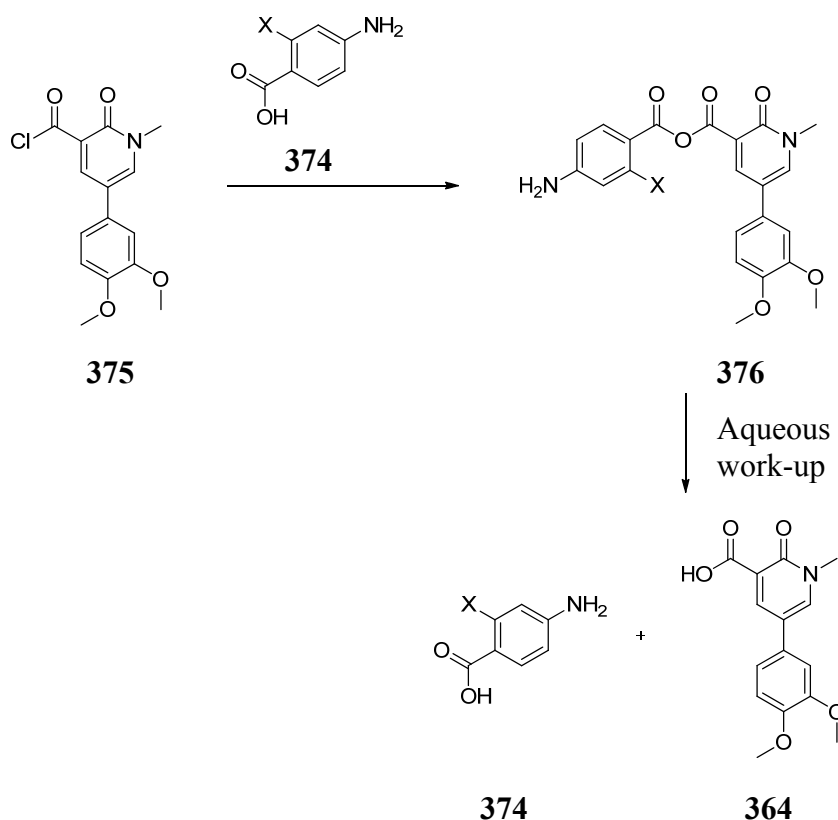
Scheme 136: Anhydride formation could be responsible for the low reported yields when executing amide couplings with aminobenzoic acids.

In addition to potential side reactions, the low aqueous solubility of the products may also be responsible for the low recovery observed. Precipitation during reverse-phase chromatography is likely with poorly-soluble compounds, which would hamper efficient recovery of material. This could be overcome by utilising normal-phase purification techniques, which are more likely to maintain compound dissolution.

Christopher J Tame

Future work in this area should involve investigation in to protection of the acid and the development of chromatography for improved reaction yields.

The methyl and methoxy *ortho*-substituted targets (**357** and **358**) were accessed by another member of our laboratory, who applied HATU-activated amide coupling conditions followed by aqueous sodium hydroxide-mediated hydrolysis to access the desired targets (**Scheme 137**).[382]
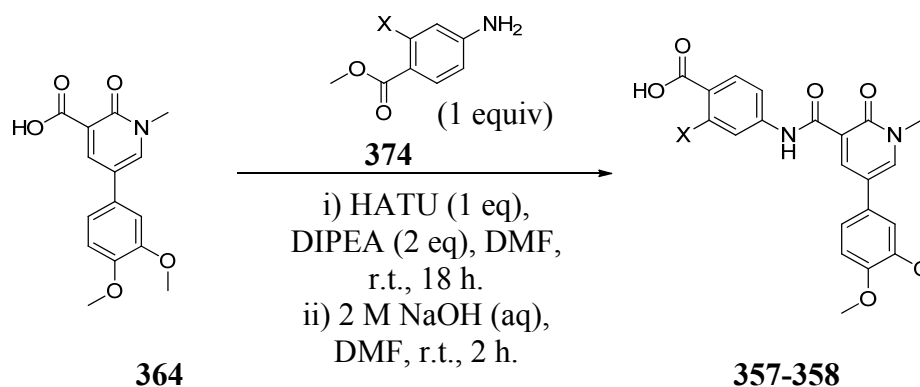
Compound number	X	Overall Yield
357	Me	3%
358	OMe	8%

Scheme 137: HATU-mediated amide formation of **357** and **358**.[382]

The isolation procedure of targets **357** and **358** involve hydrochloric acid-mediated neutralisation followed by evaporation of the volatiles. The resulting crude gum is then taken up in a minimal amount of DMSO and purified by reverse phase mass-directed chromatography. This procedure does not remove the large excesses of salt produced during neutralisation, which may hamper solubility during automated injection onto the column. This could contribute towards the exceptionally low yields observed. As with previous examples **355** and **356**, the low overall yields seen with **357** and **358** could also be due to the low solubility of the intermediates and products, for which optimisation of reaction solvent and chromatography eluents may help improve.

Christopher J Tame

Correspondingly, the formation of bromo-functionalised product **359** utilised aqueous work-ups after both amide coupling and ester hydrolysis steps (**Scheme 138**). The overall yield of 17% is at least double that of targets **357** and **358**, supporting the removal of salts before undertaking chromatographic techniques. Other contributing factors to the improvement of yield could include the marginal excess of aniline **377** and HATU starting materials used, as well as the elevated temperature of hydrolysis. The yield is expected to improve further if the reaction solvent and chromatographic eluents are optimised.
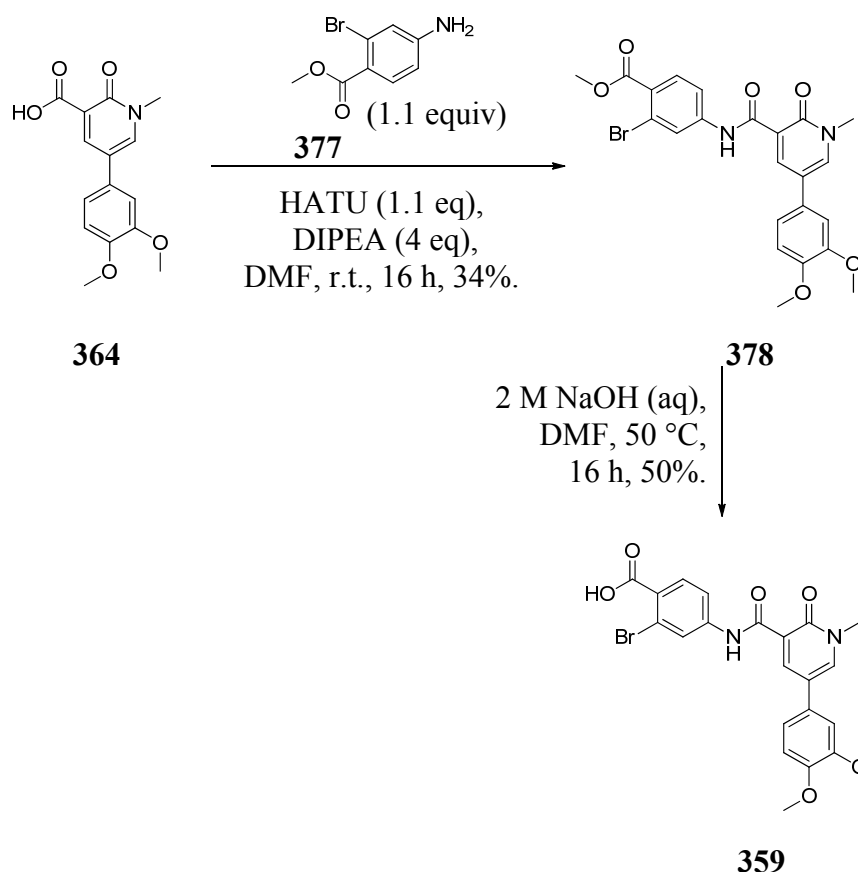
Scheme 138: The formation of bromo-functionalised target **359**.

The formation of the primary amine-containing product **360** proved particularly challenging. The commercially available methyl ester failed to react with the acid chloride of the pyridone core or undergo HATU-mediated amide coupling. The product was eventually accessed from the isotoic anhydride (**379**) (**Scheme 139**). Although very insoluble, the isotoic anhydride intermediate (**380**) could be prepared *via* HATU-assisted amide coupling in DMF. *In situ* hydrolysis of the intermediate

Christopher J Tame

anhydride furnished the product in 1% overall yield. Whilst this is an extremely low yield it provided enough material to be submitted for biological screening. The poor solubility of the product may not only rationalise the low yield but also be indicative of properties not compatible in the context of a biological system.
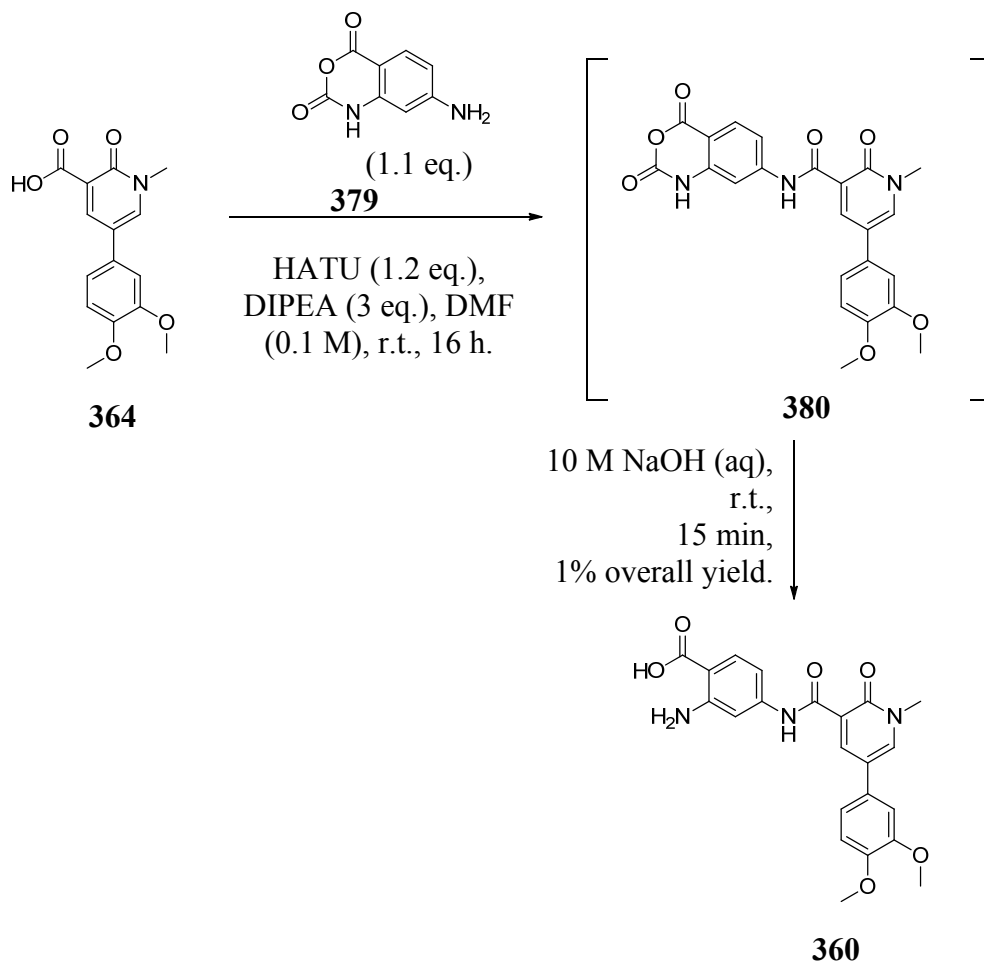
Scheme 139: Masking the α-amino benzoic acid as an isotoic anhydride was required to access **360**.

The methylamine-functionalised aniline was not commercially available, either as the benzoic acid or its methyl ester. It has been shown that $S_N Ar$ of activated aromatic fluorine derivatives with a range of aliphatic amines can be achieved at elevated temperatures.[384] The poor yield obtained from accessing fluoro **355** (5%) prompted an alternative route to be devised. The methyl ester analogue **382** was accessed via HATU-mediated amide coupling in a similar manner to that previously described, although disappointingly at an even lower yield than with the benzoic acid

Christopher J Tame

analogue (3%) (**Scheme 140**). Screening a range of alternative amide coupling reagents is expected to identify an optimal protocol to improve the yield of this reaction. This, however, was not required, as sufficient intermediate was isolated to access the desired target **361**. Subsequent optimisation could be attempted if warranted based on the biological data of the compound.

Nucleophilic displacement of fluoro **382** with methylamine afforded **383** in 49% yield. Subsequent hydrolysis to access the desired benzoic acid **361** gave a yield of 81% in the last step. 1,4-Dioxane replaced DMF as solvent for the hydrolysis due to the improved solubility of reactants observed in the previous step.
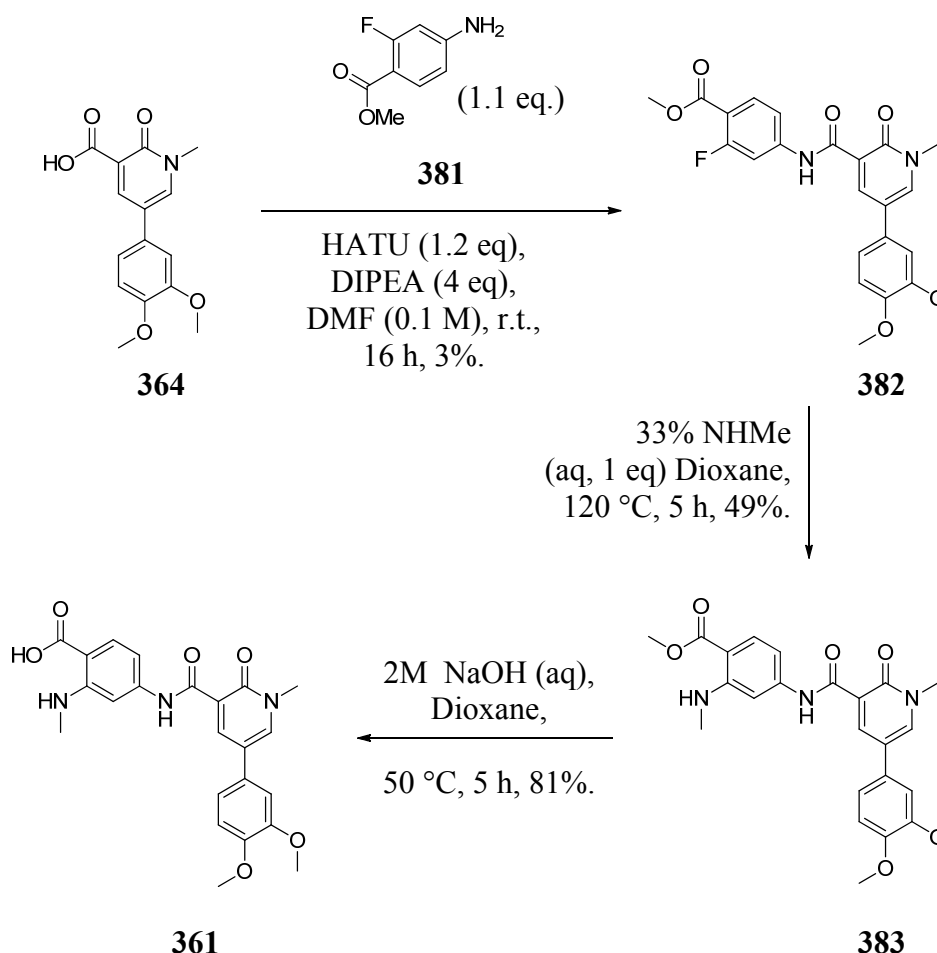
Scheme 140: S_NAr of fluoro **382** successfully accessed methylamine **383**, which afforded the desired target **361** after base-mediated ester hydrolysis.

Christopher J Tame

3.4.2 Medicinal chemistry

The isolated enzyme data for the PI3K class I isoforms are presented in **Table 66**. The data generated indicated that improvements were observed for both potency and selectivity profiles of PI3Kγ. Pleasingly, all compounds exhibit in excess of 100-fold selectivity for PI3Kγ over PI3Kδ, apart from **119** and **125**. This represents the first time 100-fold selectivity has been achieved over PI3Kδ with this series of compounds, a significant finding given the level of homology between the active sites of the kinase.

Compound number	Ortho Substituent	PI3K isoform isolated enzyme			
		γ (pIC$_{50}$)	α (ratio)	β (ratio)	δ (ratio)
349	H	7.4	251	>794	50
355	F	7.5	63	>794	25
356	Cl	7.9	251	>1258	200
357	Me	7.5	501	>1000	200
358	OMe	7.8	794	>1995	631
359	Br	7.4	398	>1584	794
360	NH$_2$	7.6	200	>1258	200
361	NHMe	6.8	159	>200	20

Table 66: *Ortho*-substituted benzoic acids represent the first time 100-fold selectivity over the other PI3K class I isoforms has been achieved.

The excellent selectivity over PI3Kδ is illustrated in **Figure 76** and indicates chloro **356**, methoxy **358** and bromo **359** to exhibit the best selectivity profiles for the PI3K class I isoforms.

Christopher J Tame
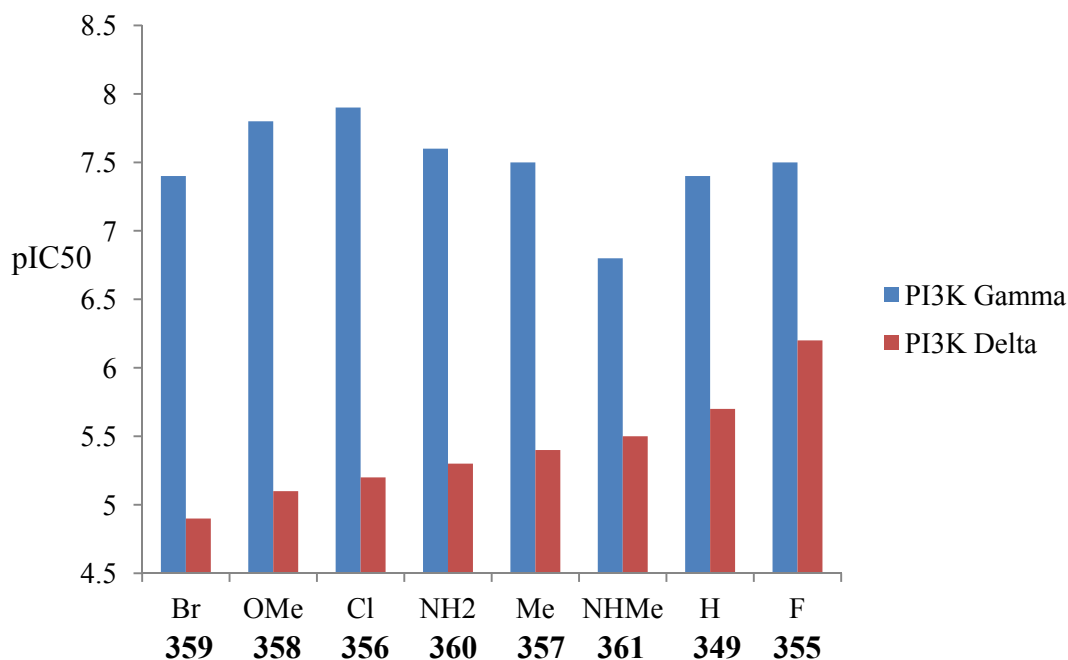
Figure 76: Isolated enzyme affinity at PI3Kγ and PI3Kδ are compared for a range of ortho-substituted benzoic acids.

The methoxy-substituted compound **358** represents the most selective PI3Kγ inhibitor identified in our laboratories at the time of synthesis and in **Table 67** is compared with the a literature compound **347** from Shionogi.[368] Methoxy **358** is more selective over PI3Kβ and PI3Kδ than the competitor compound **347** and therefore exhibits the largest selectivity window of any PI3Kγ inhibitor over PI3Kδ in our hands. This is a significant development when considering that **347** is the only compound in the literature to demonstrate a 100 fold selectivity window when profiled in our assays.

Christopher J Tame
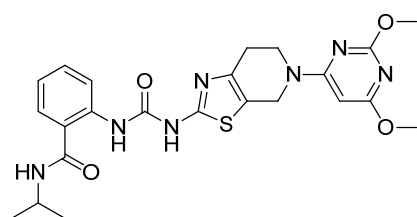
347
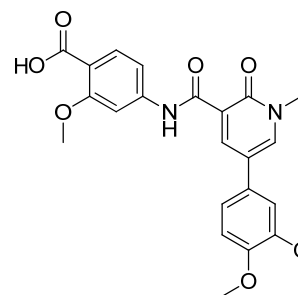
358

Compound number	**347**	**358**
PI3Kγ (pIC$_{50}$)	8.6	7.8
PI3K α, β, δ (ratio)	7943, 501, 501	1794, 1995, 630
TPSA	131	116
No. of aromatic rings	3	3
Solubility (μg/mL)	13	216
Artificial membrane Permeability (nm/sec)	800	10

Table 67: The comparison of **358** with competitor compound **347**.

Methoxy **358** also possesses improved solubility, which is likely to be due to the polarity and hydrogen-bonding capability of the carboxylic acid functionality. However, this motif is also likely to be responsible for the poor permeability observed. The development of methoxy **358** into an irreversible inhibitor will involve the conversion of the carboxylic acid to an electrophilic ester, which will affect the solubility and permeability values. It will therefore be more valuable to address the optimisation of these properties as carboxylic esters.

The potencies of the compounds were compared with their pKa values and dihedral angles in an attempt to rationalise the structure-activity relationships observed. In order to facilitate this analysis the pKa values for each compound were measured,[385] which display excellent correlation with the calculated values (**Figure 77**). This provides confidence in the use of pKa calculations for iterative design of acids in this series.

Christopher J Tame
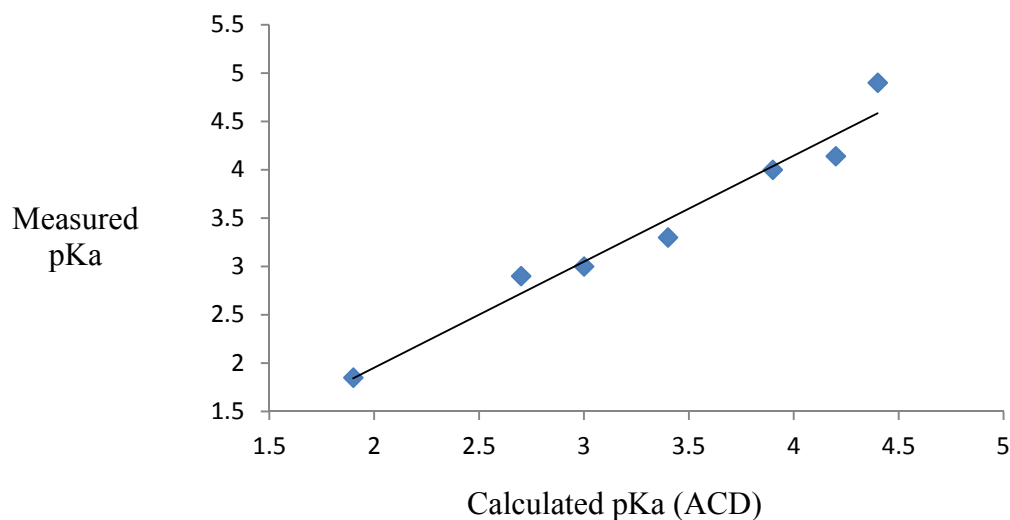
Figure 77: A strong correlation is observed between calculated and measured pKa values for the acid series.

Potency data for PI3Kγ and δ has been compared with the measured pKa values and dihedral angles of the compounds and are presented in **Figures 78** and **79**, respectively. Neither of these parameters shows any correlation with potency at either isoform, suggesting another explanation is needed for the exhibited potencies and selectivities observed within this sub-series.
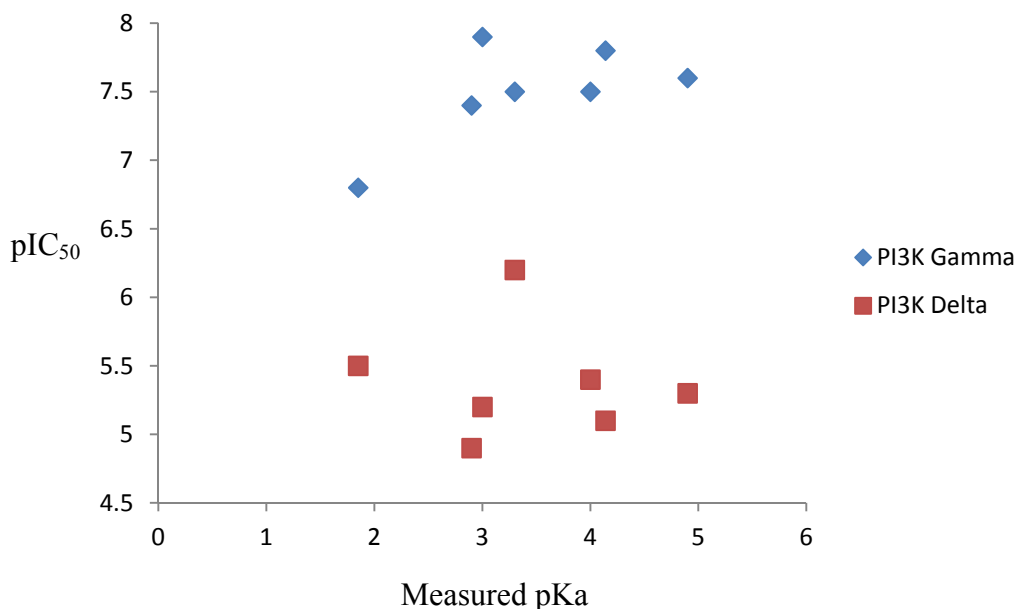
Figure 78: No correlation is observed between PI3Kγ or δ isolated enzyme potency and measured pKa values.

Christopher J Tame
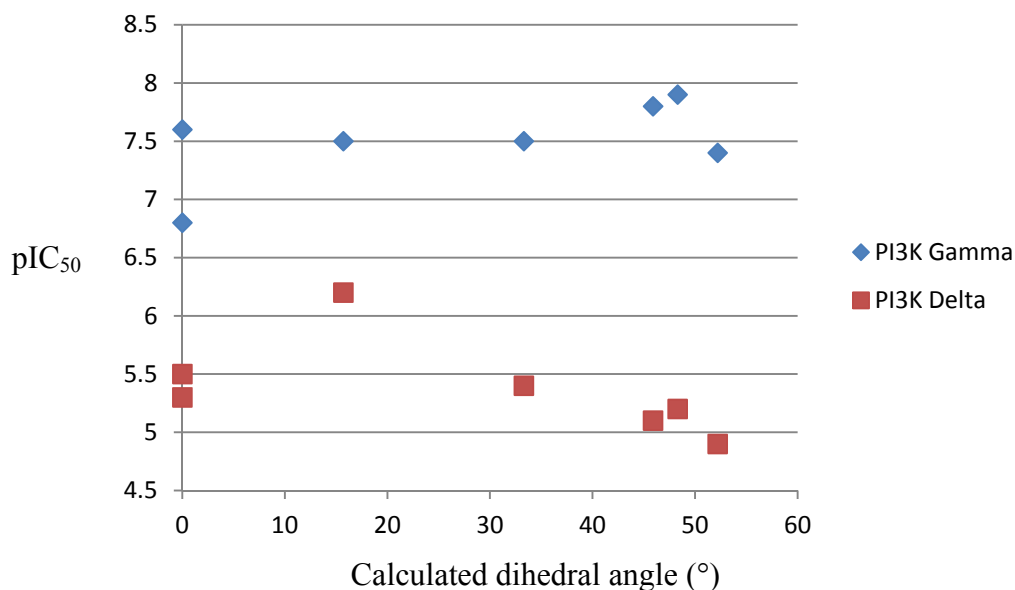
Figure 79: No correlation is observed between PI3Kγ or δ isolated enzyme potency and the calculated dihedral angle of the carboxylate moiety.

An X-ray crystal structure of methoxy **358** in PI3Kγ has been solved to 3.2 Å resolution and is displayed in **Figure 80**. Whilst electron density is observed for the acid, there are no obvious interactions with the protein, which is consistent with the observed SAR. **Figure 80** measures the length between the carboxylate and Threonine 886 to 3.2 Å; a suitable distance for hydrogen bonding to occur. However, efforts to optimise the distance of the acid from the core showed no significant change in potency or selectivity profile, suggesting that this interaction is not important for this template.

Christopher J Tame
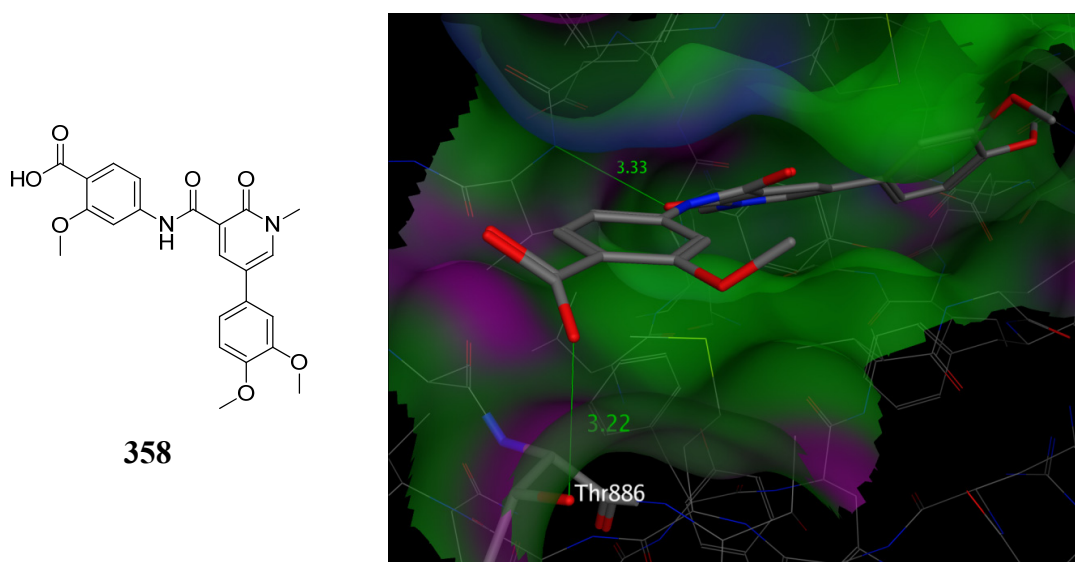
Figure 80: A solved X-ray crystal structure of methoxy **358** in PI3Kγ does not show any specific interactions between the carboxylic acid moiety and the protein.

3.5   Summary and next steps

The potential differences in role of PI3Kδ and γ in a range of lymphocytes provides an opportunity for differentiated modification of airway inflammation through selective inhibition of each biological target. Previous studies in our laboratories have struggled to develop suitable potent and selective PI3Kγ inhibitors, which prompted investigation into selective covalent modification of PI3Kγ.

Lead compound carboxylate **349** was predicted to form key acidic interactions with a polar region unique to PI3Kγ[372] and was investigated for optimisation of potency and selectivity. A selection of optimised molecules were then planned to be developed into electrophilic esters with the aim of covalently interacting with Lysine 890, a residue unique to PI3Kγ.

An effort to gain new interactions with protein residues *distant* from the hinge region was attempted by increasing the length of the linker between the aniline and carboxylate moieties. This gave no improvement in overall potency or selectivity

profiles, indicating that no specific interactions are being made between the carboxylic acid and this region of the protein.

Altering the substituent *ortho* to the carboxylate gave minor improvements in potency and for the first time displayed 100-fold selectivity against PI3Kδ within our laboratories. In addition, methoxy **358** represents the most selective PI3Kγ inhibitor to date, and is therefore a valuable asset which will be of potential utility in exploring the biology of PI3Kγ-selective ligands.

Attempts to correlate the SAR with the electronic nature or orientation of the acid were unsuccessful. A subsequently solved X-ray crystal structure of methoxy **358** also showed no significant interactions with the protein and the carboxylate moiety at this level of resolution. These observations suggest that there may be another reason for the observed potency and selectivity profiles of these compounds, which as yet remains unclear.

The tolerance of larger substituents and apparent flexibility in this region of the protein supports the feasibility of incorporating bulky esters for covalent inhibition. The results from the optimisation of the acid moiety show no sustained interactions with Lys 890. This is not a concern for covalent inhibition because the irreversible nature of interaction with the protein will drive the equilibrium of interaction towards the covalently-bound complex over time. A range of precursors with varying activity and selectivity profiles (and therefore varying interactions with the protein) was considered to offer the most effective staring point to explore the covalent approach.

Accordingly, the four examples of carboxylic acid-containing motifs displayed in **Figure 81** could be targeted for investigation as covalent inhibitors. Compounds **349**, **358**, and **369** provide a variety of vectors which the carboxylate projects, whilst compound **384** provides an example with an alternative benzimidazole core.

Christopher J Tame
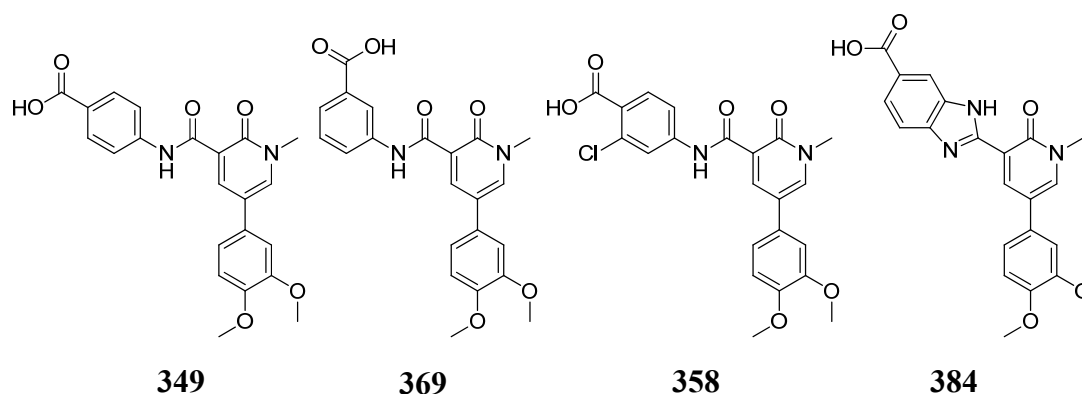
Figure 81: The four cores selected for further investigation as irreversible inhibitors of PI3Kγ.

The electrophilic component of the molecules could be composed of the three electrophilic esters (**385-387**) highlighted in a recent publication detailing their successful covalent modification of lysine residues (**Figure 82**).[377]   The more structurally simple ethyl ester **388** will also be investigated to provide a simple alternative to the other examples.
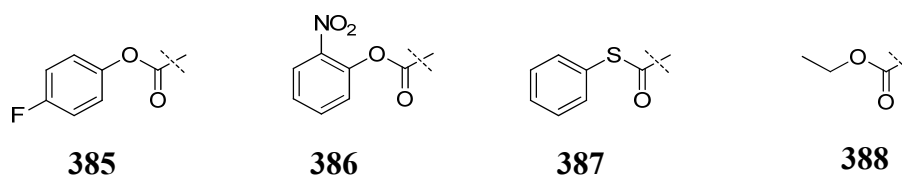
Figure 82: The four esters to be incorporated onto the cores displayed in **Figure 81**.

To summarise, this research has identified the first orally efficacious PI3Kδ-selective inhibitor in our laboratories and a sufficiently-selective PI3Kγ inhibitor to facilitate subsequent studies in the identification of a covalent PI3Kγ inhibitor.   These advancements can be used to improve the understanding of the role of PI3Kδ and γ in a range of inflammatory diseases by both oral and inhaled routes of administration.   These developments provide encouragement that therapies of respiratory inflammation with improved safety and efficacy is possible through selective modification of PI3Kδ and γ.

Christopher J Tame

Experimental

1   General experimental procedures

Unless otherwise stated, all solvents and reagents were purchased from Sigma-Aldrich and used as received. Reactions were monitored by LCMS using an Agilent A1100 series utilising UPLC BEH C18 1.7 μm column (50 mm x 2.1 mm) at 40 °C and analysed with electron spray ionisation (ESI). ^{1}H NMR spectra were recorded on a Bruker Spectrospin spectrometer at 400 or 600 MHz and ^{13}C NMR spectra were recorded on a Bruker Spectrospin spectrometer at 101 MHz. The NMR data are reported relative to internal DMSO (^{1}H, δ = 2.50 ppm and ^{13}C, δ = 39.5 ppm) or chloroform (^{1}H, δ = 7.26 ppm and ^{13}C, δ = 77.0 ppm) Data for ^{1}H NMR spectra are reported as follows: chemical shift (δ ppm) (multiplicity, coupling constant (Hz), integration). Multiplicity and qualifier abbreviations are as follows: s = singlet, d = doublet, t = triplet, q = quartet, m = multiplet, br = broad, app = apparent. Infra-red spectroscopy was obtained from solid or pure liquid samples using a Perkin-Elmer Spectrum One Fourier-Transform infra-red spectrometer with an attenuated total reflectance (ATR) accessory. IR values are reported in frequency of absorption (cm^{–1}). Only the major absorbances are listed. High resolution mass spectra (HRMS) were recorded on a Micromass Autospec 500 OAT spectrometer. HRMS were recorded by Bill Leavens, Analytical Chemistry Mass Spectrometry Department, GSK, Stevenage. Only the major peaks are listed. Melting point (m.p.) analysis were recorded on a Bibby Scientific STUART SMP40 automatic melting point apparatus. Microwave reactions were carried out using a Biotage Initiator microwave with a Biotage 60 autosampler. All animal studies were ethically reviewed and carried out in accordance with Animals (Scientific Procedures) Act 1986 and the GSK Policy on the Care, Welfare and Treatment of Animals

Liquid Chromatography Mass Spectrometry (LCMS) Methods

Method A:

The UPLC analysis was conducted on an Acquity UPLC BEH C18 column (50 mm x 2.1 mm i.d. 1.7 μm packing diameter) at 40 °C. The solvents employed were:

Christopher J Tame

A = 0.1% v/v solution of Formic Acid in Water.
B = 0.1% v/v solution of Formic Acid in Acetonitrile.

The gradient employed was:

Time (min)	Flow Rate (ml/min)	% A	% B
0	1	97	3
1.5	1	0	100
1.9	1	0	100
2.0	1	97	3

The UV detection was a summed signal from wavelength of 210nm to 350nm.

MS Conditions
MS : Waters ZQ
Ionisation mode : Alternate-scan Positive and Negative Electrospray
Scan Range : 100 to 1000 AMU
Scan Time : 0.27 seconds
Inter scan Delay : 0.10 seconds

Method B:

The UPLC analysis was conducted on an Acquity UPLC BEH C18 column (50 mm x 2.1 mm i.d. 1.7 μm packing diameter) at 40 °C. The solvents employed were:
A = 0.1% v/v solution of Ammonium Bicarbonate in Water.
B = 0.1% v/v solution of Ammonium Bicarbonate in Acetonitrile.

The gradient employed was:

Time (min)	Flow Rate (ml/min)	% A	% B
0	1	97	3
1.5	1	0	100
1.9	1	0	100
2.0	1	97	3

The UV detection was a summed signal from wavelength of 210 nm to 350 nm.

MS Conditions
MS : Waters ZQ
Ionisation mode : Alternate-scan Positive and Negative Electrospray
Scan Range : 100 to 1000 AMU
Scan Time : 0.27 seconds
Inter scan Delay : 0.10 seconds

Christopher J Tame

2　　　Experimental procedures for RGD integrin antagonists

7-((4,5,6,7-Tetrahydro-2*H*-pyrazolo[4,3-*c*]pyridin-2-yl)methyl)-1,2,3,4-tetrahydro-1,8-naphthyridine (22) and **7-((4,5,6,7-tetrahydro-1*H*-pyrazolo[4,3-*c*]pyridin-1-yl)methyl)-1,2,3,4-tetrahydro-1,8-naphthyridine (23)**

To a stirred solution of *tert*-butyl 6,7-dihydro-1*H*-pyrazolo[4,3-*c*]pyridine-5(4*H*)-carboxylate (1.71 g, 7.64 mmol) in DMF (70 mL) was added sodium hydride (60% w/w dispersed in mineral oil, 0.458 g, 11.5 mmol) portionwise at 0 ºC over nitrogen. The mixture was then stirred for 20 min at 0 ºC. To the mixture was added a solution of *tert*-butyl 7-(bromomethyl)-3,4-dihydro-1,8-naphthyridine-1(2*H*)-carboxylate (2.50 g, 7.64 mmol) in DMF (7 mL) dropwise at 0 ºC under nitrogen. The flask was then removed from the cooling bath and stirred at room temperature for 16 h. To the mixture was added aqueous lithium chloride solution (1% w/v, 200 mL) and EtOAc (200 mL) was added the separated aqueous phase was extracted twice with EtOAc (2 x 200 mL). The combined organics were washed with aqueous lithium chloride solution (1% w/v, 200 mL) then passed through a hydrophobic frit and the filtrate was concentrated under reduced pressure to afford a crude solid. To a stirred solution of the crude solid in MeOH (75 mL) was added a solution of HCl in 1,4-dioxane (4 M, 10.7 mL, 42.6 mmol) dropwise at room temperature under nitrogen. The mixture was stirred at room temperature for 16 h. The mixture was then neutralised with saturated aqueous sodium bicarbonate solution. To the mixture was added EtOAc (200 mL) and water (200 mL) and the separated organic fraction was extracted twice with water (2 x 200 mL). The combined aqueous phase was concentrated under reduced pressure to afford a white solid. The solid was dissolved in minimal MeOH and loaded onto an SCX pre-packed column (70 g) and eluted with water (100 mL), MeOH (100 mL) and a solution of NH$_3$ in MeOH (2 M, 100 mL), respectively. The relevant fractions were combined and concentrated under

Christopher J Tame

reduced pressure to afford a mixture of 7-((4,5,6,7-tetrahydro-2*H*-pyrazolo[4,3-*c*]pyridin-2-yl)methyl)-1,2,3,4-tetrahydro-1,8-naphthyridine and 7-((4,5,6,7-tetrahydro-1*H*-pyrazolo[4,3-*c*]pyridin-1-yl)methyl)-1,2,3,4-tetrahydro-1,8-naphthyridine. (1.31 g, 4.86 mmol, 64% yield). LCMS (Method B): 0.68 min, [M+H]$^+$ 270 m/z. ^{1}H NMR (400 MHz, DMSO-d$_6$) δ 7.34 (s, 0.57H), 7.16 (s, 0.43H), 7.06 (d, *J* = 7.3 Hz, 0.57H), 7.04 (d, *J* = 7.3 Hz, 0.43H), 6.39 (br. s., 0.57H), 6.38 (br. s., 0.43H), 6.08 (d, *J* = 7.3 Hz, 0.57H), 5.87 (d, *J* = 7.3 Hz, 0.43H), 4.96 (s, 2H), 3.66 (d, *J* = 5.8 Hz, 1.14H), 3.63 (d, *J* = 5.5 Hz, 0.86H), 3.20 - 3.26 (m, 2H), 2.83 - 2.91 (m, 2H), 2.57 - 2.64 (m, 2H), 2.45 - 2.52 (m, 2H), 2.09 - 2.19 (m, 1H), 1.74 (m, 2H) ppm.

Methyl 3-(3-cyclopropylphenyl)-4-(2-((5,6,7,8-tetrahydro-1,8-naphthyridin-2-yl)methyl)-6,7-dihydro-2*H*-pyrazolo[4,3-*c*]pyridin-5(4*H*)-yl)butanoate (55) and methyl 3-(3-cyclopropylphenyl)-4-(1-((5,6,7,8-tetrahydro-1,8-naphthyridin-2-yl)methyl)-6,7-dihydro-1*H*-pyrazolo[4,3-*c*]pyridin-5(4*H*)-yl)butanoate (56)
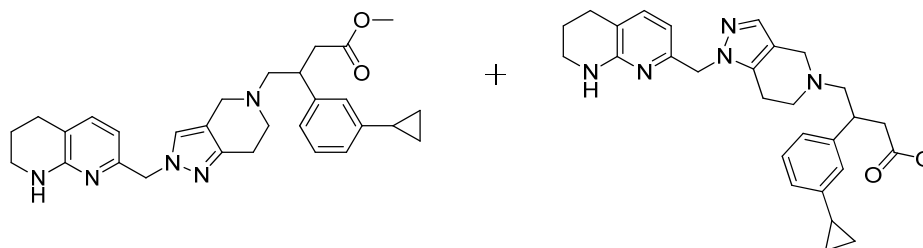
To a stirred solution of a mixture of 7-((4,5,6,7-tetrahydro-2*H*-pyrazolo[4,3-*c*]pyridin-2-yl)methyl)-1,2,3,4-tetrahydro-1,8-naphthyridine and 7-((4,5,6,7-tetrahydro-1*H*-pyrazolo[4,3-*c*]pyridin-1-yl)methyl)-1,2,3,4-tetrahydro-1,8-naphthyridine (1.31 g, 4.86 mmol), and triethylamine (1.36 mL, 9.73 mmol) in CH$_2$Cl$_2$ (60 mL) at 0 ºC was added (*E*)-methyl 4-bromobut-2-enoate (0.580 mL, 4.86 mmol) dropwise. The flask was removed from the cooling-bath and the mixture was stirred at room temperature for 1 h. EtOAc (50 mL) and aqueous lithium chloride solution (10%, 50 mL) was added and the separated organic phase was washed twice with aqueous lithium chloride solution (10% w/v, 2 x 50 mL). The combined aqueous phase was extracted twice with EtOAc (2 x 50 mL) and the combined

Christopher J Tame

organic phase was passed through a hydrophobic frit and concentrated under reduced pressure to afford a crude orange gum. To a solution of the orange gum (1.0 g) and (3-cyclopropylphenyl)boronic acid (1.32 g, 8.16 mmol) in 1,4-dioxane (26 mL) was added degassed aqueous potassium hydroxide solution (3.8 M, 1.4 mL, 5.4 mmol) and chloro(1,5-cyclooctadiene)rhodium(II) dimer (0.40 g, 0.82 mmol) sequentially. The solution was further degassed with three alternative applications of vacuum and nitrogen and was then heated to 95 ºC for 45 min. The mixture was concentrated under reduced pressure then dissolved in EtOAc (200 mL) and water (200 mL). The separated organic phase was washed twice with water (2 x 200 mL) and the combined organic phase was passed through a hydrophobic frit. The filtrate was concentrated under reduced pressure, then loaded in minimal CH_2Cl_2 onto a silica pre-packed column (100 g) and eluted with 0-15% MeOH (+ 1% triethylamine) in CH_2Cl_2 over 60 min. The relevant fractions were combined and concentrated under reduced pressure to afford a crude gum (1.5 g). The gum was dissolved in DMSO (16.5 mL) and purified by HPLC (33 x 0.5 mL injections, XSelect CSH C18 column, 150 mm x 30 mm, 40 mL/min, 50-100% aqueous ammonium bicarbonate solution in MeCN). The relevant fractions were combined and concentrated under a stream of nitrogen to afford methyl 3-(3-cyclopropylphenyl)-4-(2-((5,6,7,8-tetrahydro-1,8-naphthyridin-2-yl)methyl)-6,7-dihydro-2*H*-pyrazolo[4,3-*c*]pyridin-5(4*H*)-yl)butanoate (**55**) (190 mg, 390 µmol, 8% yield) as a yellow gum and methyl 3-(3-cyclopropylphenyl)-4-(1-((5,6,7,8-tetrahydro-1,8-naphthyridin-2-yl)methyl)-6,7-dihydro-1*H*-pyrazolo[4,3-*c*]pyridin-5(4*H*)-yl)butanoate (**56**) (43 mg, 90 µmol, 2% yield) as a yellow gum.

Methyl 3-(3-cyclopropylphenyl)-4-(2-((5,6,7,8-tetrahydro-1,8-naphthyridin-2-yl)methyl)-6,7-dihydro-2*H*-pyrazolo[4,3-*c*]pyridin-5(4*H*)-yl)butanoate (**55**): LCMS (Method B): 1.26 min, $[M+H]^+$ 486 m/z. ^{1}H NMR (400 MHz, DMSO-d_6) δ = 7.39 (s, 1H), 7.14 (t, *J* = 7.6 Hz, 1H), 7.06 (d, *J* = 7.3 Hz, 1H), 7.01 (d, *J* = 7.8 Hz, 1H), 6.98 (s, 1H), 6.86 (d, *J* = 7.6 Hz, 1H), 6.40 (s, 1H), 6.07 (d, *J* = 7.3 Hz, 1H), 4.96 (s, 2H), 3.48 (d, *J* = 13.6 Hz, 1H), 3.40 (s, 3H), 3.36 (d, *J* = 13.6 Hz, 1H), 3.26 - 3.19 (m, 2H), 2.85 - 2.70 (m, 2H), 2.68 - 2.58 (m, 5H), 2.57 - 2.52 (m, 4H), 1.92 - 1.82

Christopher J Tame

(m, 1H), 1.78 - 1.67 (m, 2H), 0.97 - 0.86 (m, 2H), 0.64 (ddd, J = 2.0, 4.0, 5.0 Hz, 2H) ppm.

Methyl 3-(3-cyclopropylphenyl)-4-(1-((5,6,7,8-tetrahydro-1,8-naphthyridin-2-yl)methyl)-6,7-dihydro-1H-pyrazolo[4,3-c]pyridin-5(4H)-yl)butanoate (**56**): LCMS (Method B): 1.27 min, [M+H]$^+$ 486 m/z. ^{1}H NMR (400 MHz, DMSO-d$_6$) δ = 7.19 (s, 1H), 7.15 (t, J = 7.6 Hz, 1H), 7.06 - 6.99 (m, 2H), 6.98 (s, 1H), 6.87 (d, J = 7.8 Hz, 1H), 6.39 (br. s, 1H), 5.87 (d, J = 7.1 Hz, 1H), 4.96 (s, 2H), 3.45 (d, J = 13.4 Hz, 1H), 3.37 (s, 3H), 3.35 - 3.31 (m, 1H), 3.27 - 3.20 (m, 2H), 2.83 - 2.72 (m, 2H), 2.70 - 2.56 (m, 5H), 2.55 - 2.43 (m, 4H), 1.93 - 1.82 (m, 1H), 1.79 - 1.69 (m, 2H), 0.97 - 0.89 (m, 2H), 0.65 (ddd, J = 1.8, 4.3, 5.1 Hz, 2H) ppm.

Christopher J Tame

Methyl 3-(3-cyclopropylphenyl)-4-(2-((5,6,7,8-tetrahydro-1,8-naphthyridin-2-yl)methyl)-6,7-dihydro-2*H*-pyrazolo[4,3-*c*]pyridin-5(4*H*)-yl)butanoate (55) ^{1}H NMR NOESY analysis. Irradiation at 4.96 ppm.
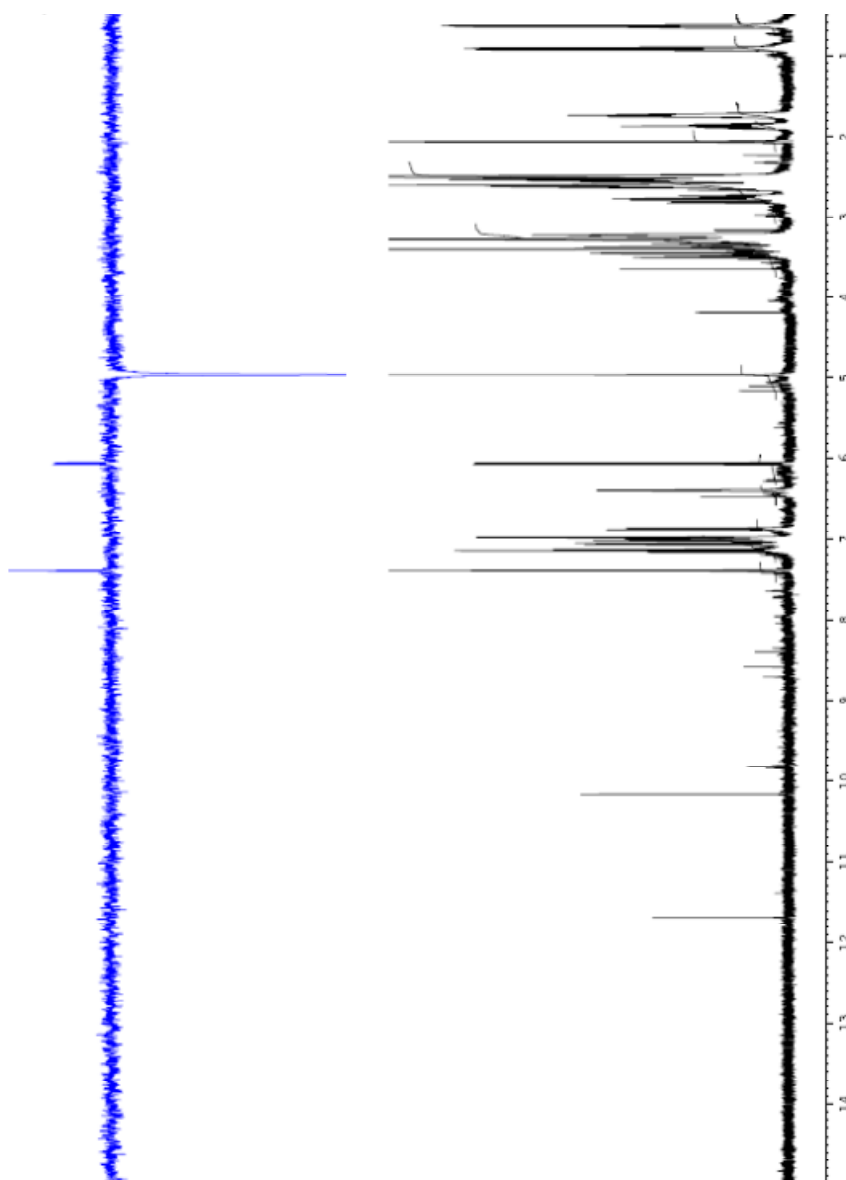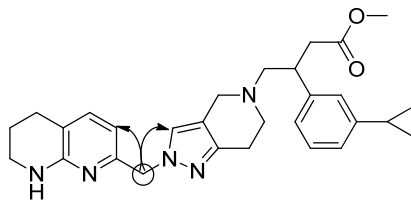
Christopher J Tame

Methyl 3-(3-cyclopropylphenyl)-4-(1-((5,6,7,8-tetrahydro-1,8-naphthyridin-2-yl)methyl)-6,7-dihydro-1*H*-pyrazolo[4,3-*c*]pyridin-5(4*H*)-yl)butanoate (56) ^{1}H NMR NOESY analysis. Irradiation at 4.96 ppm.
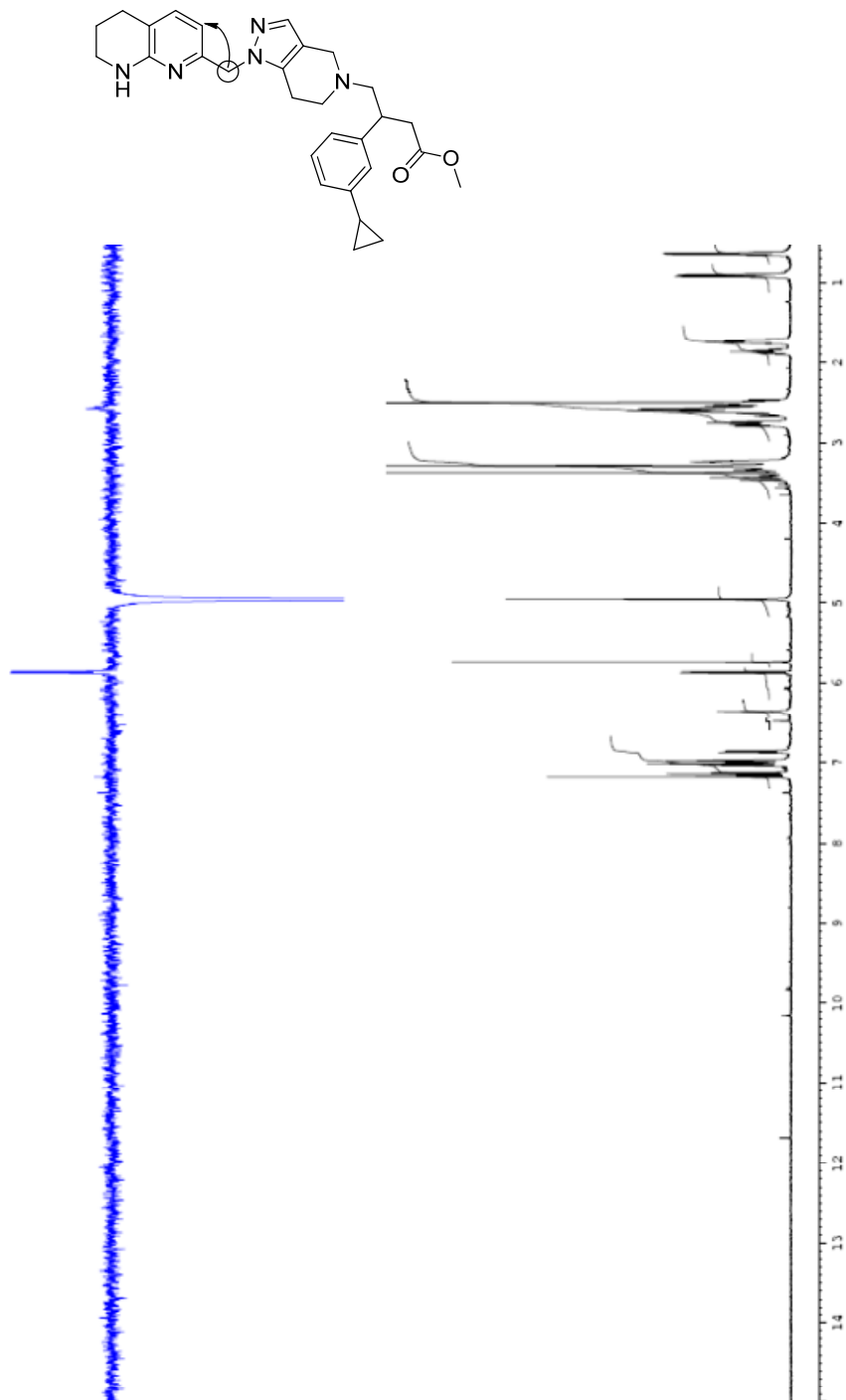
Christopher J Tame

3-(3-Cyclopropylphenyl)-4-(1-((5,6,7,8-tetrahydro-1,8-naphthyridin-2-yl)methyl)-6,7-dihydro-1*H*-pyrazolo[4,3-*c*]pyridin-5(4*H*)-yl)butanoic acid, formic acid salt (58)
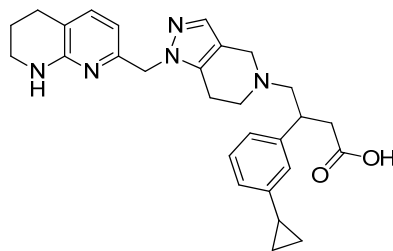
To a stirred solution of methyl 3-(3-cyclopropylphenyl)-4-(1-((5,6,7,8-tetrahydro-1,8-naphthyridin-2-yl)methyl)-6,7-dihydro-1*H*-pyrazolo[4,3-*c*]pyridin-5(4*H*)-yl)butanoate (40 mg, 82 μmol) in MeCN (0.4 mL) was added aqueous NaOH solution (2 M, 0.21 mL, 0.41 mmol) dropwise at room temperature under nitrogen and the mixture was stirred at 50 ºC for 2 h. The mixture was purified directly *via* mass-directed auto-preparative (MDAP) chromatography using a Sunfire C18 column and ammonium bicarbonate -modified MeCN/water gradient. The relevant fractions were combined and concentrated under a stream of nitrogen to afford a crude solid. The solid was loaded in DMSO (1 mL) and purified *via* mass-directed auto-preparative (MDAP) chromatography using a Sunfire C18 column and a formic acid-modified MeCN/water gradient. The relevant fractions were combined and concentrated under a stream of nitrogen to afford the desired product (25 mg, 50 μmol, 60% yield) as a yellow gum. LCMS (Method B): 0.78 min, [M+H]$^+$ 472 m/z. ^{1}H NMR (400 MHz, CDCl$_3$) δ = 8.38 (br. s, 1H), 7.34 (s, 1H), 7.21 (t, *J* = 7.7 Hz, 1H), 7.17 (d, *J* = 7.3 Hz, 1H), 6.96 - 6.88 (m, 3H), 6.09 (d, *J* = 7.3 Hz, 1H), 5.16 (s, 2H), 3.87 (d, *J* = 13.8 Hz, 1H), 3.81 (d, *J* = 13.8 Hz, 1H), 3.46 - 3.40 (m, 2H), 3.40 - 3.25 (m, 2H), 3.00 - 2.84 (m, 6H), 2.70 (t, *J* = 6.3 Hz, 2H), 1.95 - 1.82 (m, 3H), 1.01 - 0.93 (m, 2H), 0.72 - 0.64 (m, 2H) ppm.

Note: 2H missing from ^{1}H NMR (exchangeable).

Christopher J Tame

Methyl 3-(3-cyclopropylphenyl)-4-(2-((5,6,7,8-tetrahydro-1,8-naphthyridin-2-yl)methyl)-6,7-dihydro-2*H*-pyrazolo[4,3-*c*]pyridin-5(4*H*)-yl)butanoate (57a and **57b)**
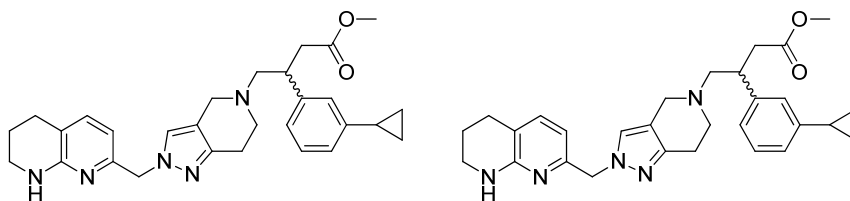
Methyl 3-(3-cyclopropylphenyl)-4-(2-((5,6,7,8-tetrahydro-1,8-naphthyridin-2-yl)methyl)-6,7-dihydro-2*H*-pyrazolo[4,3-*c*]pyridin-5(4*H*)-yl)butanoate (190 mg, 390 μmol) was dissolved in EtOH (4 mL) and purified by chiral HPLC chromatography (2 x 2 mL injections, 100% EtOH, Chiralpak IA column (30 mm x 25 cm), flow rate: 15 mL/min). The relevant fractions were combined and concentrated under reduced pressure to afford methyl 3-(3-cyclopropylphenyl)-4-(2-((5,6,7,8-tetrahydro-1,8-naphthyridin-2-yl)methyl)-6,7-dihydro-2*H*-pyrazolo[4,3-*c*]pyridin-5(4*H*)-yl)butanoate (**57a**, **enantiomer 1** (23-29 min): 70 mg, 0.14 mmol, 36% yield, >99% e.e.) and methyl 3-(3-cyclopropylphenyl)-4-(2-((5,6,7,8-tetrahydro-1,8-naphthyridin-2-yl)methyl)-6,7-dihydro-2*H*-pyrazolo[4,3-*c*]pyridin-5(4*H*)-yl)butanoate (**57b**, **enantiomer 2** (36-80 min): 76 mg, 0.16 mmol, 40% yield, >99.5% e.e.) as yellow gums. Enantiomeric excess was determined using chiral HPLC analysis (100% EtOH, Chiralpak IA column (4.6 mm x 25 cm), flow rate: 1 mL/min).

Christopher J Tame

3-(3-Cyclopropylphenyl)-4-(2-((5,6,7,8-tetrahydro-1,8-naphthyridin-2-yl)methyl)-6,7-dihydro-2*H*-pyrazolo[4,3-*c*]pyridin-5(4*H*)-yl)butanoic acid (17a enantiomer 1)
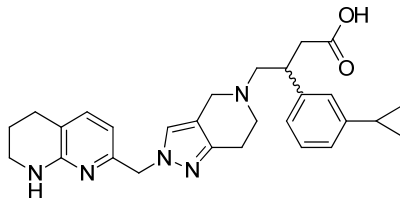
To a stirred solution of methyl 3-(3-cyclopropylphenyl)-4-(2-((5,6,7,8-tetrahydro-1,8-naphthyridin-2-yl)methyl)-6,7-dihydro-2*H*-pyrazolo[4,3-*c*]pyridin-5(4*H*)-yl)butanoate (**enantiomer 1**, 70 mg, 0.14 mmol) in MeCN (0.5 mL) was added aqueous NaOH solution (2 M, 0.72 mL, 1.44 mmol) dropwise at room temperature under nitrogen and the mixture was stirred at 50 ºC for 2 h. The mixture was purified directly *via* mass-directed auto-preparative (MDAP) chromatography using a Sunfire C18 column and ammonium bicarbonate -modified MeCN/water gradient. The relevant fractions were combined and concentrated under a stream of nitrogen to afford the desired product (41 mg, 90 µmol, 61% yield) as a yellow gum. LCMS (Method B): 0.80 min, $[M+H]^+$ 472 m/z. ^{1}H NMR (400 MHz, DMSO-d$_6$) δ = 7.40 (s, 1H), 7.14 (t, *J* = 7.8 Hz, 1H), 7.06 (d, *J* = 7.3 Hz, 1H), 7.01 (d, *J* = 7.8 Hz, 1H), 6.98 (s, 1H), 6.86 (d, *J* = 7.8 Hz, 1H), 6.41 (br. s, 1H), 6.11 (d, *J* = 7.3 Hz, 1H), 4.96 (s, 2H), 3.51 (d, *J* = 13.6 Hz, 1H), 3.42 (d, *J* = 13.6 Hz, 1H), 3.36 - 3.26 (m, 1H), 3.26 - 3.18 (m, 2H), 2.84 - 2.74 (m, 2H), 2.73 - 2.63 (m, 2H), 2.64 - 2.54 (m, 5H), 2.42 (dd, *J* = 7.9, 15.7 Hz, 1H), 1.92 - 1.80 (m, 1H), 1.80 - 1.64 (m, 2H), 0.95 - 0.88 (m, 2H), 0.68 - 0.60 (m, 2H) ppm.

Note: 1H missing from ^{1}H NMR (exchangeable).

Christopher J Tame

3-(3-Cyclopropylphenyl)-4-(2-((5,6,7,8-tetrahydro-1,8-naphthyridin-2-yl)methyl)-6,7-dihydro-2*H*-pyrazolo[4,3-*c*]pyridin-5(4*H*)-yl)butanoic acid (17b enantiomer 2)
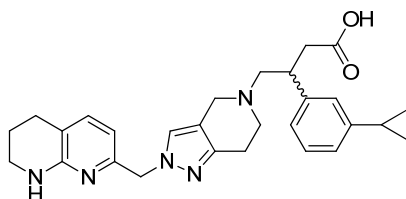
To a stirred solution of methyl 3-(3-cyclopropylphenyl)-4-(2-((5,6,7,8-tetrahydro-1,8-naphthyridin-2-yl)methyl)-6,7-dihydro-2*H*-pyrazolo[4,3-*c*]pyridin-5(4*H*)-yl)butanoate (**enantiomer 2**, 76 mg, 0.16 mmol) in MeCN (0.5 mL) was added aqueous NaOH solution (2 M, 780 μL, 1.56 mmol) dropwise at room temperature under nitrogen and the mixture was stirred at 50 ºC for 2 h. The mixture was purified directly *via* mass-directed auto-preparative (MDAP) chromatography using a Sunfire C18 column and ammonium bicarbonate-modified MeCN/water gradient. The relevant fractions were combined and concentrated under a stream of nitrogen to afford the desired product (59 mg, 0.13 mmol, 80% yield) as a yellow gum. LCMS (Method B): 0.80 min, $[M+H]^+$ 472 m/z. IR (solid) 3287 (N-H stretch), 2930 (sp^3 C-H stretch), 2810 (N-H$^+$ stretch) 1600, 1460 (O-C-O$^-$ stretch) cm^{-1}. ^{1}H NMR (400 MHz, DMSO-d$_6$) δ = 7.39 (s, 1H), 7.14 (t, J = 7.6 Hz, 1H), 7.06 (d, J = 7.3 Hz, 1H), 7.01 (d, J = 7.8 Hz, 1H), 6.98 (s, 1H), 6.85 (d, J = 7.8 Hz, 1H), 6.41 (br. s., 1H), 6.11 (d, J = 7.1 Hz, 1H), 4.96 (s, 2H), 3.51 (d, J = 13.6 Hz, 1H), 3.46 - 3.38 (m, 1H), 3.34 - 3.25 (m, 1H), 3.26 - 3.19 (m, 2H), 2.83 - 2.72 (m, 2H), 2.72 - 2.63 (m, 2H), 2.63 - 2.52 (m, 5H), 2.41 (dd, J = 7.9, 15.7 Hz, 1H), 1.92 - 1.81 (m, 1H), 1.79 - 1.68 (m, 2H), 0.95 - 0.88 (m, 2H), 0.67 - 0.60 (m, 2H) ppm. ^{13}C NMR (101 MHz, CDCl$_3$) δ = 174.7, 155.4, 150.8, 145.0, 144.8, 142.5, 137.1, 128.8, 126.3, 124.3, 123.7, 122.1, 118.4, 116.3, 111.6, 110.7, 64.1, 56.8, 51.0, 44.4, 41.5, 38.9, 26.3, 21.7, 20.9, 15.5, 9.2 ppm. HRMS (ESI) calc'd for C$_{28}$H$_{34}$N$_5$O$_2$ $[M+H]^+$ 472.2707, found 472.2684.

Note: 1H missing from ^{1}H NMR (exchangeable). Optical rotation could not be obtained due to the coloured nature of the isolated product.

Christopher J Tame

Benzyl 6,7-dihydrothieno[3,2-*c*]pyridine-5(4*H*)-carboxylate (106)
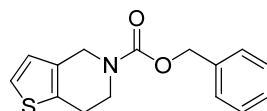
To an ice-cooled stirred solution of 4,5,6,7-tetrahydrothieno[3,2-*c*]pyridine, hydrochloride (3.20 g, 18.2 mmol) (Activate Scientific) and DIPEA (9.54 mL, 54.6 mmol) in *tert*-butylmethyl ether (170 mL) was added benzyl chloroformate (2.86 mL, 20.0 mmol) dropwise at 0 ºC under nitrogen. The mixture was allowed to reach room temperature then stirred for 30 min at room temperature under nitrogen. Water (100 mL) was added and the separated organic phase was washed twice with water (2 x 100 mL). The combined organic phase was passed through a hydrophobic frit and the filtrate was concentrated under reduced pressure to afford the desired product as a colourless oil, which crystallised upon standing (5.30 g, 18.4 mmol, 100% yield). LCMS (Method A): 1.20 min, [M+H]$^+$ 274 m/z. ^{1}H NMR (400 MHz, DMSO-d$_6$) δ = 7.41 - 7.34 (m, 5H), 7.33 (d, *J* = 5.3 Hz, 1H), 6.89 (d, *J* = 5.3 Hz, 1H), 5.12 (s, 2H), 4.50 (br. s., 2H), 3.71 (t, *J* = 5.4 Hz, 2H), 2.81 (t, *J* = 5.7 Hz, 2H) ppm.

Attempted synthesis of **Benzyl 2-(4,4,5,5-tetramethyl-1,3,2-dioxaborolan-2-yl)-6,7-dihydrothieno[3,2-*c*]pyridine-5(4*H*)-carboxylate (108)**
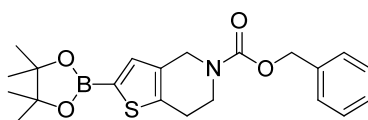
(1,5-Cyclooctadiene)(methoxy)iridium(I) dimer (34.6 mg, 52.0 µmol) and 4,4'-di-*tert*-butyl-2,2'-bipyridine (28 mg, 0.10 mmol) were charged to a 50 mL round bottomed flask and degassed with three alternative applications of vacuum and nitrogen. A solution of benzyl 6,7-dihydrothieno[3,2-*c*]pyridine-5(4*H*)-carboxylate (950 mg, 3.48 mmol) in cyclohexane (20 mL) was added, followed by 4,4,5,5-tetramethyl-1,3,2-dioxaborolane (560 µL, 3.82 mmol) dropwise. The mixture was stirred at 25 ºC for 3 h. LCMS (Method A): 1.38 min, [M+H]$^+$ 400 m/z, which

indicated borylation of the starting material. To the mixture was added water (50 mL) and EtOAc (50 mL) and the separated aqueous phase was extracted twice with EtOAc (2 x 100 mL). The combined organic phase was washed twice with brine (2 x 100 mL) then filtered through a hydrophobic frit. The filtrate was concentrated under reduced pressure to afford the desired product (1.15 g, 2.88 mmol, 83% yield) as red oil. LCMS (Method A): 1.38 min, [M+H]$^+$ 400 m/z. ^{1}H NMR (400 MHz, DMSO-d$_6$) δ = 7.89 (s, 1H), 7.42 - 7.28 (m, 5H), 5.12 (s, 2H), 4.58 - 4.47 (m, 2H), 3.74 - 3.65 (m, 2H), 2.90 - 2.81 (m, 2H), 1.27 (s, 12H) ppm, which indicated borylation of the thiophene ring. The oil was left to stand at room temperature for 48 h. LCMS (method A): 1.20 min, [M+H]$^+$ 274 m/z, indicated deborylation of the intermediate back to starting material.

Benzyl 2-((8-(*tert*-butoxycarbonyl)-5,6,7,8-tetrahydro-1,8-naphthyridin-2-yl)methyl)-6,7-dihydrothieno[3,2-*c*]pyridine-5(4*H*)-carboxylate (109)
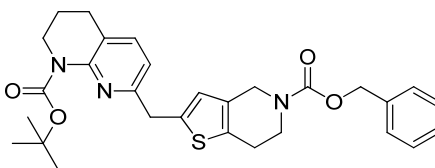
(1,5-Cyclooctadiene)(methoxy)iridium(I) dimer (35 mg, 50 μmol) and 4,4'-di-*tert*-butyl-2,2'-bipyridine (28 mg, 0.10 mmol) were charged to a 150 mL round bottomed flask and degassed with three alternative applications of vacuum and nitrogen. Degassed cyclohexane (18 mL), degassed 4,4,5,5-tetramethyl-1,3,2-dioxaborolane (0.550 mL, 3.82 mmol) and a degassed mixture of benzyl 6,7-dihydrothieno[3,2-*c*]pyridine-5(4*H*)-carboxylate (1.00 g, 3.48 mmol) in cyclohexane (2 mL) were added dropwise, sequentially at room temperature under nitrogen. The mixture was stirred at room temperature for 2 h. A degassed mixture of chloro(2-dicyclohexylphosphino-2′,4′,6′-triisopropyl-1,1′-biphenyl)[2-(2′-amino-1,1′-biphenyl)]palladium(II) (270 mg, 350 μmol) and *tert*-butyl 7-(bromomethyl)-3,4-dihydro-1,8-naphthyridine-1(2*H*)-carboxylate (750 mg, 2.29 mmol) in THF (5 mL)

was added dropwise at room temperature, followed by the addition of degassed aqueous potassium phosphate solution (500 mM, 9.24 mL, 4.62 mmol) dropwise at room temperature. The resulting solution was stirred at room temperature under nitrogen for 16 h. Brine (50 mL) and EtOAc (50 mL) were added and the separated organic phase was washed twice with brine (2 x 100 mL). The combined aqueous phase was extracted with EtOAc (100 mL) and the combined organic phase was filtered through a hydrophobic frit. The filtrate was concentrated under reduced pressure to afford a red oil. The gum was loaded in minimal CH_2Cl_2 onto two silica pre-packed columns (2 x 100 g) and eluted with 0-25% EtOAc in cyclohexane over 60 min. The relevant fractions were combined and concentrated under reduced pressure to afford the desired product (1.15 g, 2.10 mmol, 92% yield) as a brown gum. LCMS (Method A): 1.10 min, $[M+H]^+$ 520 m/z. IR (solid) 2931 (sp^3 C-H stretch), 1691 (C=O stretch), 1461, 1416 (C-N stretch) 1227, 1150, 1147, 1096 (C-O stretch). ^{1}H NMR (400 MHz, DMSO-d_6) δ = 7.44 (d, J = 7.8 Hz, 1H), 7.40 - 7.34 (m, 5H), 6.93 (d, J = 7.6 Hz, 1H), 6.66 (br. s., 1H), 5.11 (s, 2H), 4.40 (br. s., 2H), 4.05 (s, 2H), 3.71 - 3.64 (m, 2H), 3.61 (t, J = 6.0 Hz, 2H), 2.75-2.65 (m, 4H), 1.81 (quin, J = 6.5 Hz, 2H), 1.38 (s, 9H) ppm. ^{13}C NMR (150 MHz, DMSO-d_6) δ = 155.3, 154.6, 153.5, 150.6, 139.7, 137.5, 136.8, 131.3, 128.3, 127.8, 127.5, 123.5, 122.1, 117.9, 79.7, 66.3, 44.2, 43.7, 41.3, 37.7, 27.8, 25.4, 24.3, 22.7 ppm. HRMS (ESI) calc'd for $C_{29}H_{34}N_3O_4S$ $[M+H]^+$ 520.2270, found 520.2272.

1 C missing from ^{13}C NMR spectrum.

Key correlations observed from NMR experiments:
COSY (^{1}H to ^{1}H): δ = 7.44 to 6.93 ppm; 3.71-3.64 to 2.75-2.65 ppm; 3.61 to 2.75-2.65 to 1.81 ppm. **HSQC** (^{1}H to ^{13}C): δ = 7.44 to 137.5 ppm; 7.40 - 7.34 to 128.5, 127.8 and 127.5 ppm; 6.93 to 117.9 ppm; 6.66 to 123.5 ppm; 5.11 to 66.3 ppm; 4.40 to 43.7 ppm; 4.05 to 37.7 ppm; 3.71 - 3.64 to 41.3 ppm; 3.61 to 44.2 ppm; 2.75-2.65 to 25.4 and 24.3 ppm; 1.81 to 22.7 ppm; 1.38 to 27.8 ppm. **HMBC** (^{1}H to ^{13}C): δ = 7.44 to 155.3 ppm; 7.44 to 25.4 ppm; 7.44 to 37.7 ppm; 7.40 – 7.34 to 66.3 ppm; 6.93 to 37.7 ppm; 6.66 to 139.7 ppm; 6.66 to 37.7 ppm; 4.05 to 139.7 ppm; 4.05 to

Christopher J Tame

155.3 ppm. **NOE** Irradiated at 4.05 ppm. (^{1}H to ^{1}H): δ = 4.05 to 6.93 and 6.66 ppm. No correlation observed to 4.40 ppm.

Benzyl 2-((8-(*tert*-butoxycarbonyl)-5,6,7,8-tetrahydro-1,8-naphthyridin-2-yl)methyl)-6,7-dihydrothieno[3,2-*c*]pyridine-5(4*H*)-carboxylate (109) ^{1}H **NMR Correlation Spectroscopy (**COSY).
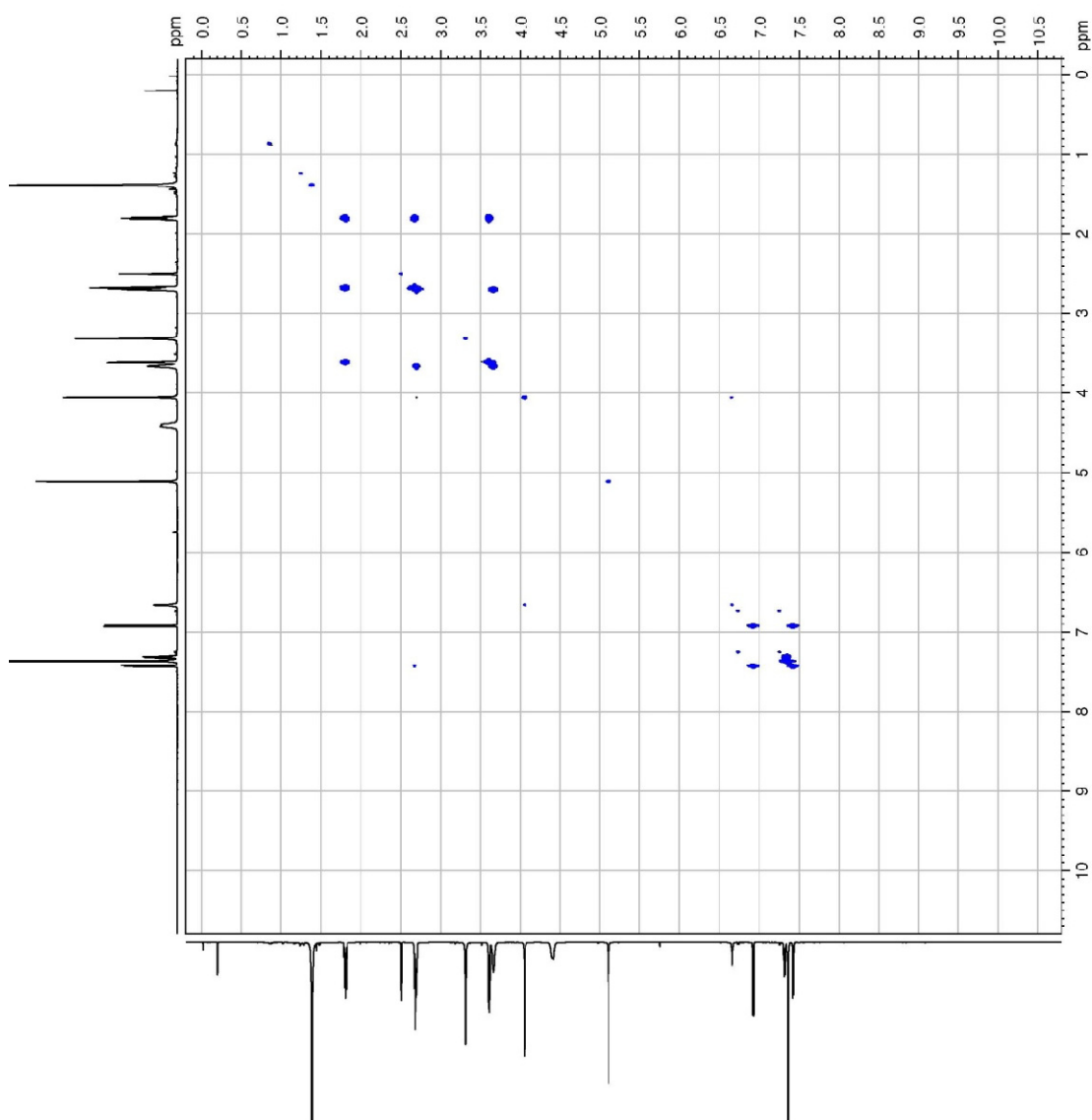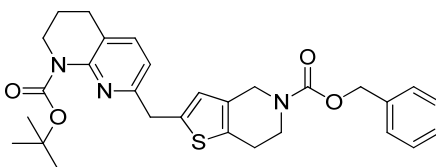
Christopher J Tame

dihydrothieno[3,2-*c*]pyridine-5(4*H*)-carboxylate (109) Heteronuclear Single Quantum Coherence (HSQC) ^{1}H and ^{13}C NMR spectroscopy.
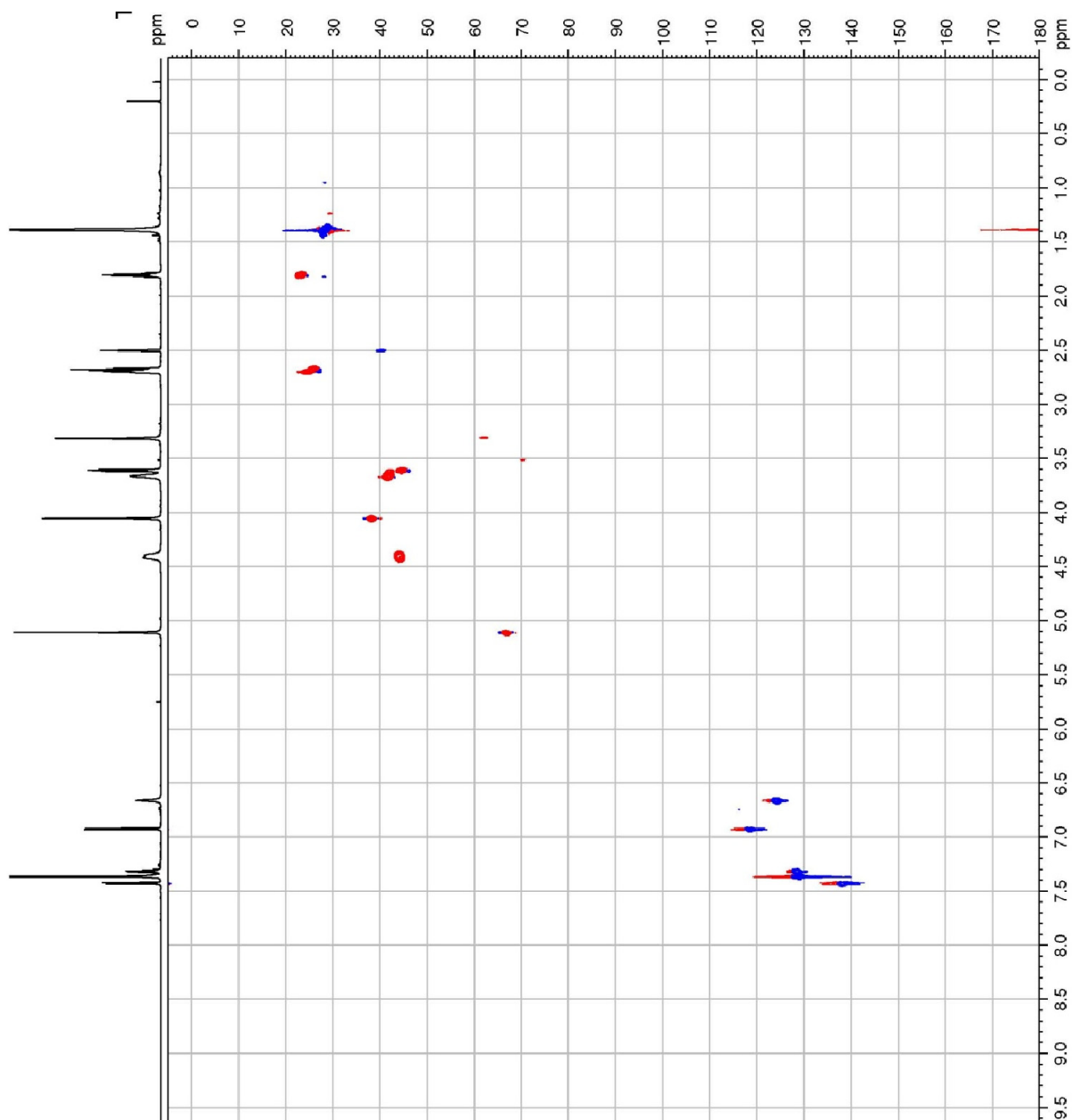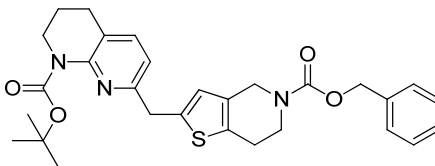
Christopher J Tame

Benzyl 2-((8-(*tert*-butoxycarbonyl)-5,6,7,8-tetrahydro-1,8-naphthyridin-2-yl)methyl)-6,7-dihydrothieno[3,2-*c*]pyridine-5(4*H*)-carboxylate (109) **Heteronuclear Multiple Bond Correlation (HMBC) ^{1}H and ^{13}C NMR spectroscopy.**

305

Christopher J Tame
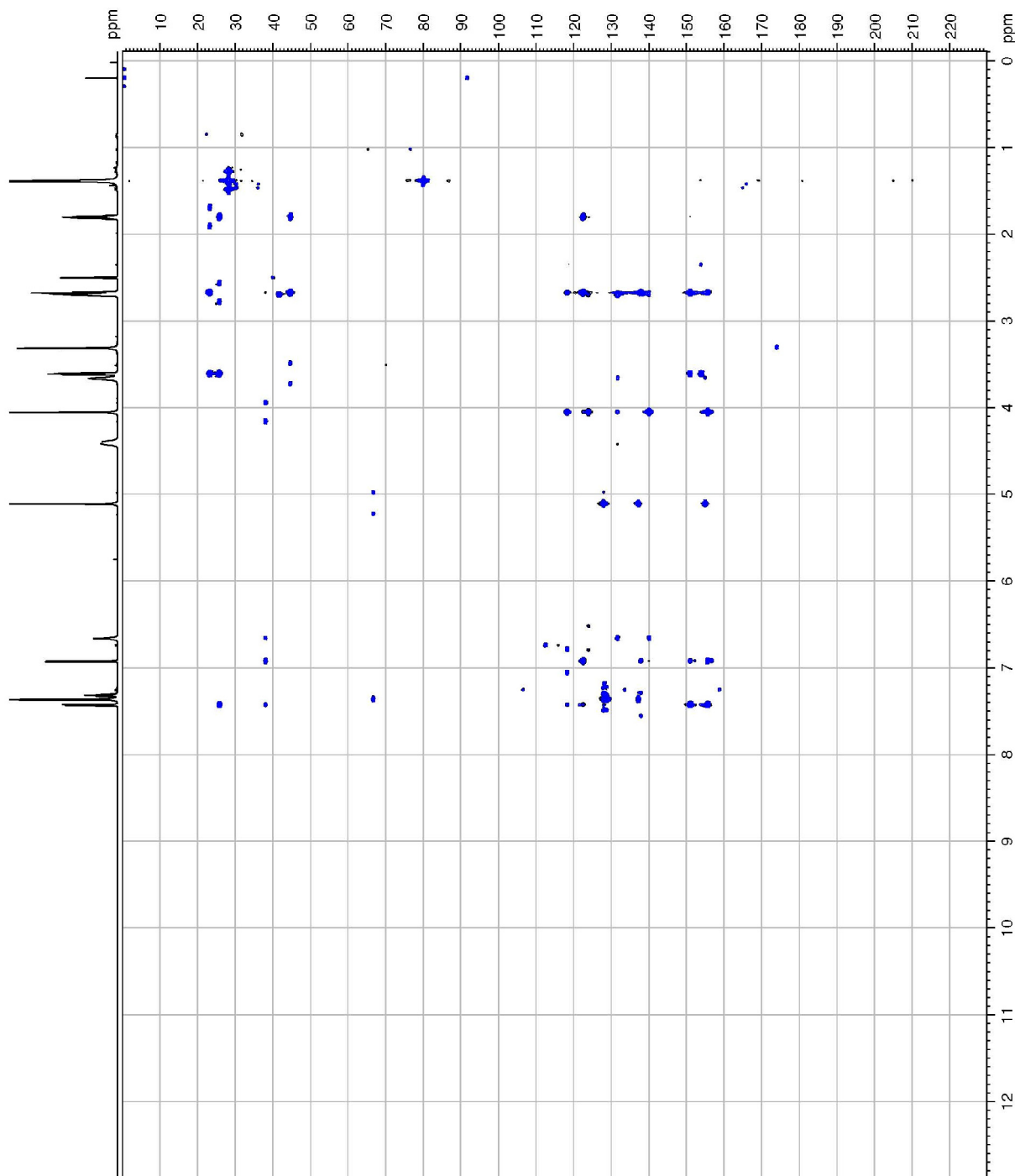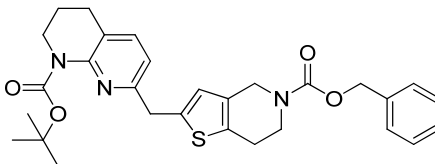
Benzyl 2-((8-(*tert*-butoxycarbonyl)-5,6,7,8-tetrahydro-1,8-naphthyridin-2-yl)methyl)-6,7-dihydrothieno[3,2-*c*]pyridine-5(4*H*)-carboxylate (109) Nuclear Overhauser Effect (NOE) ^{1}H NMR spectroscopy.

Christopher J Tame
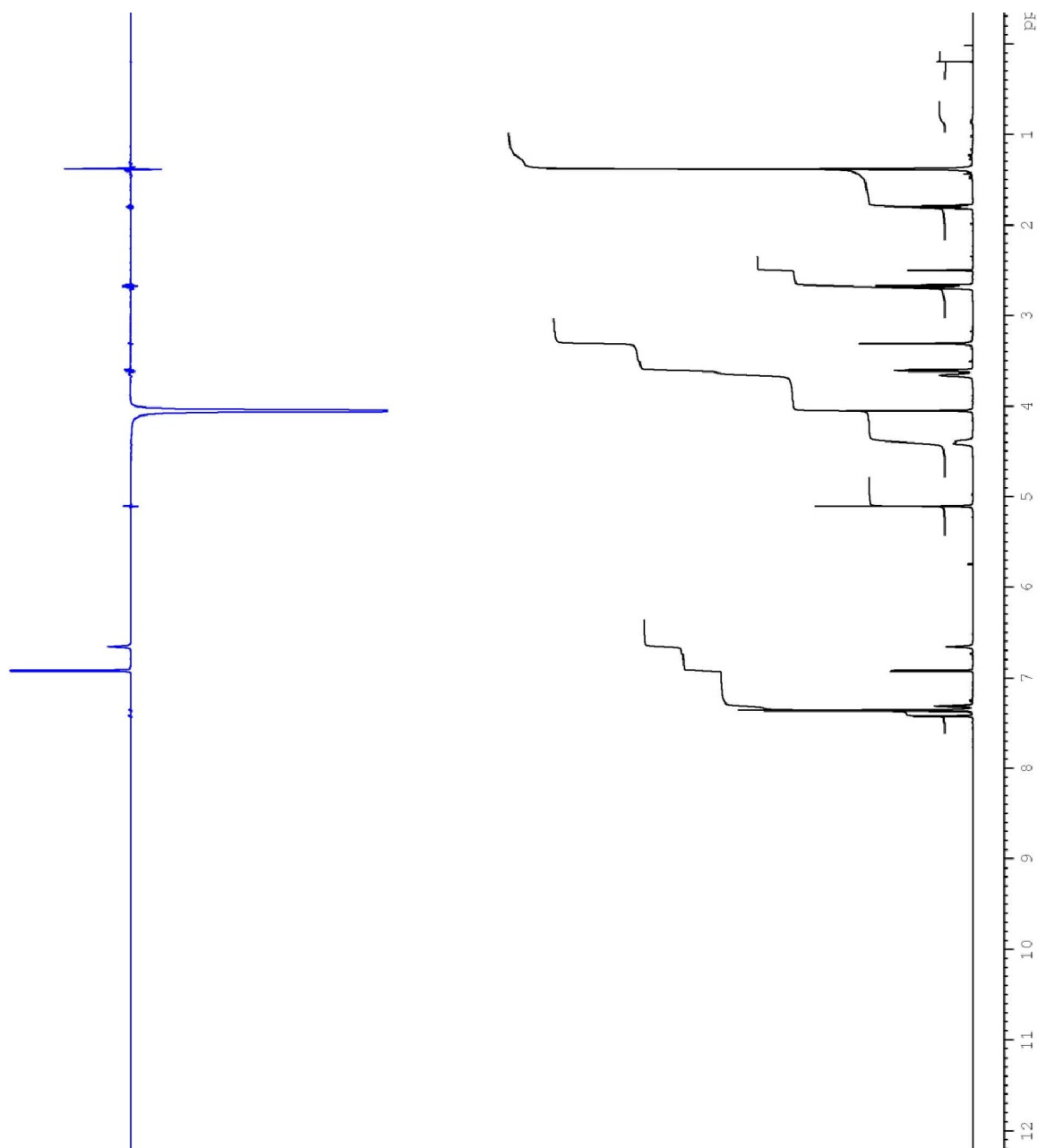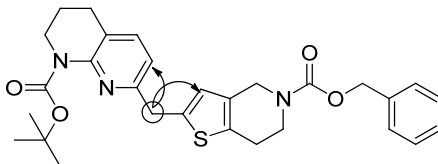
2-((5,6,7,8-Tetrahydro-1,8-naphthyridin-2-yl)methyl)-4,5,6,7-tetrahydrothieno[3,2-*c*]pyridine (91).
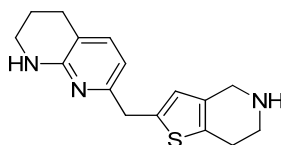
To a stirred solution of benzyl 2-((8-(tert-butoxycarbonyl)-5,6,7,8-tetrahydro-1,8-naphthyridin-2-yl)methyl)-6,7-dihydrothieno[3,2-*c*]pyridine-5(4*H*)-carboxylate (1.00 g, 1.93 mmol in acetonitrile (15 mL) at 0 ºC under nitrogen was added iodotrimethylsilane (1.37 mL, 9.62 mmol) dropwise. The flask was removed from the ice bath and the mixture was stirred at room temperature for 1 h. The mixture was concentrated under reduced pressure to afford a brown gum. The gum was taken up in EtOAc (100 mL) and aqueous hydrochloric acid solution (2 M, 100 mL) and the mixture separated. The organic phase was extracted twice with aqueous hydrochloric acid solution (2 M, 100 mL) and the combined aqueous phase was neutralised with aqueous sodium hydroxide solution (10 M). The aqueous mixture was extracted twice with EtOAc (2 x 100 mL) and the combined aqueous phase was purified directly by ion-exchange silica column chromatography (Isolute SCX column, 50 g). The column was sequentially eluted with water (100 mL), MeOH (100 mL) and ammonia in MeOH solution (2M, 100 mL). The relevant fractions were combined and concentrated under reduced pressure to afford the desired product (474 mg, 1.66 mmol, 86 % yield as an orange gum. LCMS (Method A): 0.96 min, [M+H]$^+$ 286 m/z. ^{1}H NMR (400 MHz, DMSO-d$_6$) δ = 7.03 (d, *J* = 7.3 Hz, 1H), 6.46 (s, 1H), 6.31 (s, 1H), 6.27 (d, *J* = 7.3 Hz, 1H), 4.07 (br. s., 1H), 3.83 (s, 2H), 3.64 - 3.58 (m, 2H), 3.25 - 3.19 (m, 2H), 2.92 - 2.86 (m, 2H), 2.59 (t, *J* = 6.3 Hz, 2H), 2.57 - 2.52 (m, 2H), 1.77 - 1.69 (m, 2H) ppm.

Christopher J Tame

(**E**)-Methyl 4-(2-((5,6,7,8-tetrahydro-1,8-naphthyridin-2-yl)methyl)-6,7-dihydrothieno[3,2-*c*]pyridin-5(4*H*)-yl)but-2-enoate (90)
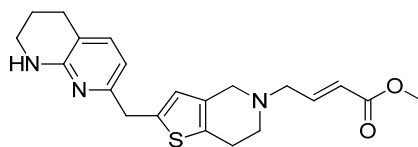
To a stirred solution of 2-((5,6,7,8-tetrahydro-1,8-naphthyridin-2-yl)methyl)-4,5,6,7-tetrahydrothieno[3,2-*c*]pyridine (474 mg, 1.58 mmol) and triethylamine (495 µL, 3.55 mmol) in CH_2Cl_2 (16 mL) at room temperature under nitrogen was added (*E*)-methyl 4-bromobut-2-enoate (207 µL, 1.74 mmol) dropwise. The mixture was stirred at room temperature for 1 h. Water (50 mL) and CH_2Cl_2 (50 mL) was added and the mixture separated. The organic phase was washed twice with water (2 x 50 mL) and the combined organic phase was passed through a hydrophobic frit. The filtrate was concentrated under reduced pressure to afford the desired product (400 mg, 1.04 mmol, 66% yield) as an orange solid. LCMS (Method B): 1.13 min, $[M+H]^+$ 384 m/z. ^{1}H NMR (400 MHz, DMSO-d$_6$) δ = 7.04 (d, *J* = 7.3 Hz, 1H), 6.88 (dt, *J* = 5.8, 15.6 Hz, 1H), 6.50 (s, 1H), 6.32 (br. s., 1H), 6.28 (d, *J* = 7.3 Hz, 1 H), 6.06 (d, *J* = 15.9 Hz, 1H), 3.83 (s, 2H), 3.65 (s, 2H), 3.39 (s, 2H), 3.30 (s, 3H), 3.22 (s, 2H), 2.68 (s, 4H), 2.64 - 2.53 (m, 2H), 1.79 - 1.65 (m, 2H) ppm.

Christopher J Tame

Methyl 3-(3-cyclopropylphenyl)-4-(2-((5,6,7,8-tetrahydro-1,8-naphthyridin-2-yl)methyl)-6,7-dihydrothieno[3,2-*c*]pyridin-5(4*H*)-yl)butanoate (110)
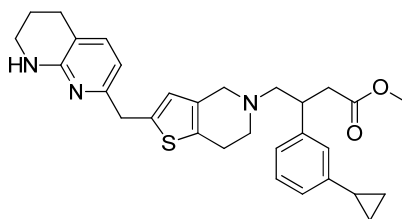
(3-Cyclopropylphenyl)boronic acid (436 mg, 2.69 mmol) and (*E*)-methyl 4-(2-((5,6,7,8-tetrahydro-1,8-naphthyridin-2-yl)methyl)-6,7-dihydrothieno[3,2-*c*]pyridin-5(4*H*)-yl)but-2-enoate (400 mg, 900 µmol) were charged to a 150 mL round bottom flask. The flask was sealed and degassed with 3 alternative applications of vacuum and nitrogen. Anhydrous and degassed 1,4-dioxane (8 mL) was added and the resulting solution was degassed under a stream of nitrogen for 20 min. To this solution was added aqueous potassium hydroxide solution (3.8 M, 0.47 mL, 1.8 mmol) and chloro(1,5-cyclooctadiene)rhodium(II) dimer (133 mg, 270 µmol) sequentially and the solution was further degassed with 3 alternative applications of vacuum and nitrogen. The solution was then heated and stirred under reflux at 95 ºC for 45 min. The reaction mixture was concentrated under reduced pressure to afford a brown gum. The gum was dissolved in CH_2Cl_2 (100 mL) and was washed three times with water (3 x 100 mL). The combined organic fractions were passed through a hydrophobic frit under atmospheric pressure. The filtrate was concentrated under reduced pressure to afford a brown gum. The gum was loaded in minimal CH_2Cl_2 onto a silica pre-packed column (100 g) and eluted with 0-15% MeOH in CH_2Cl_2 over 60 min. The appropriate fractions were combined and concentrated under reduced pressure to afford the desired product (400 mg, 800 µmol, 89% yield) as a brown gum. LCMS (Method B): 1.48 min, [M+H]$^+$ 502 m/z. ^{1}H NMR (400 MHz, DMSO-d$_6$) δ = 7.14 (t, *J* = 7.6 Hz, 1H), 7.04 (d, *J* = 7.3 Hz, 1H), 7.00 (d, *J* = 7.8 Hz, 1H), 6.97 (s, 1H), 6.85 (d, *J* = 7.6 Hz, 1H), 6.49 (s, 1H), 6.32 (br. s., 1H), 6.27 (d, *J* = 7.3 Hz, 1H), 3.83 (s, 2H), 3.48 - 3.42 (m, 1H), 3.41 (s, 3H), 3.37 - 3.30 (m, 2H), 3.26 - 3.19 (m, 2H), 2.83 - 2.72 (m, 2H), 2.66 - 2.56 (m, 6H), 2.55 - 2.51 (m, 1H), 2.45 -

Christopher J Tame

2.39 (m, 1H), 1.90 - 1.81 (m, 1H), 1.77 - 1.68 (m, 2H), 0.95 - 0.88 (m, 2H), 0.67 - 0.60 (m, 2H) ppm.

Methyl 3-(3-cyclopropylphenyl)-4-(2-((5,6,7,8-tetrahydro-1,8-naphthyridin-2-yl)methyl)-6,7-dihydrothieno[3,2-*c*]pyridin-5(4*H*)-yl)butanoate, (110a, enantiomer 1) and **methyl 3-(3-cyclopropylphenyl)-4-(2-((5,6,7,8-tetrahydro-1,8-naphthyridin-2-yl)methyl)-6,7-dihydrothieno[3,2-*c*]pyridin-5(4*H*)-yl)butanoate, (110b, enantiomer 2)**
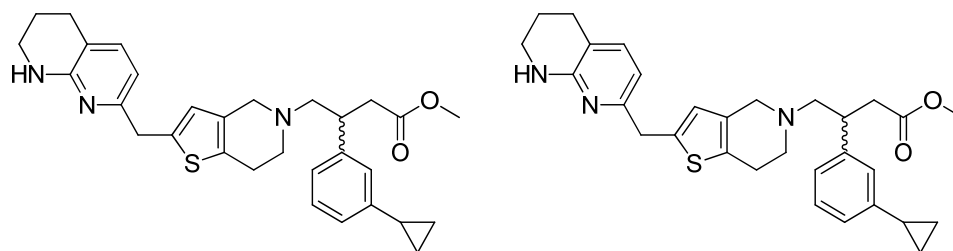
Methyl 3-(3-cyclopropylphenyl)-4-(2-((5,6,7,8-tetrahydro-1,8-naphthyridin-2-yl)methyl)-6,7-dihydrothieno[3,2-*c*]pyridin-5(4*H*)-yl)butanoate (400 mg, 800 µmol) was dissolved in an EtOH-heptane mixture (1:1, 2 mL) and filtered through a silica frit. The filtrate was purified by chiral HPLC chromatography (5 x 0.4 mL injections, 10% EtOH in heptane, Chiralcel OD-H column (30 mm x 25 cm), flow rate: 30 mL/min). The relevant fractions were combined and concentrated under reduced pressure to afford methyl 3-(3-cyclopropylphenyl)-4-(2-((5,6,7,8-tetrahydro-1,8-naphthyridin-2-yl)methyl)-6,7-dihydrothieno[3,2-*c*]pyridin-5(4*H*)-yl)butanoate (**110a**, **enantiomer 1** (20.5 - 24.5 min): 131 mg, 260 µmol, 33% yield, >99% e.e.) and methyl 3-(3-cyclopropylphenyl)-4-(2-((5,6,7,8-tetrahydro-1,8-naphthyridin-2-yl)methyl)-6,7-dihydrothieno[3,2-*c*]pyridin-5(4*H*)-yl)butanoate (**110b**, **enantiomer 2** (27.5 - 36.5 min): 125 mg, 250 µmol, 31% yield, >99% e.e.) as yellow gums. Enantiomeric excess was determined using chiral HPLC analysis (15% EtOH in heptane, Chiralcel OD-H column (4.6 mm x 25 cm), flow rate: 1 mL/min).

Christopher J Tame

3-(3-Cyclopropylphenyl)-4-(2-((5,6,7,8-tetrahydro-1,8-naphthyridin-2-yl)methyl)-6,7-dihydrothieno[3,2-*c*]pyridin-5(4*H*)-yl)butanoic acid (84a, enantiomer 1)
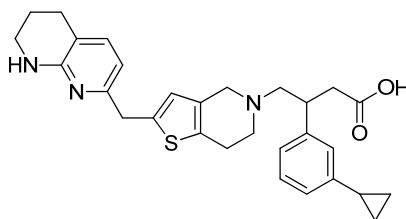
To a stirred solution of methyl 3-(3-cyclopropylphenyl)-4-(2-((5,6,7,8-tetrahydro-1,8-naphthyridin-2-yl)methyl)-6,7-dihydrothieno[3,2-c]pyridin-5(4*H*)-yl)butanoate (**110a**, **enantiomer 1**, 131 mg, 260 µmol) in MeOH (5 mL) at room temperature was added aqueous sodium hydroxide solution (200 mM, 653 µL, 1.31 mmol) dropwise. The mixture was stirred at 50 ºC for 2 h. The mixture was concentrated under reduced pressure to afford a brown gum. The gum was dissolved in DMSO (0.5 mL) and MeOH (0.5 mL) and purified by ammonium bicarbonate modified mass-directed auto-preparative (MDAP) chromatography. The relevant fractions were combined and concentrated under reduced pressure to afford the desired product (**84a**, **enantiomer 1**: 105 mg, 220 µmol, 82% yield) as a brown gum. LCMS (Method B): 0.95 min, $[M+H]^+$ 488 m/z. IR (solid) 3300 (N-H stretch), 2820 (N-H$^+$ stretch), 2923 (sp^3 C-H stretch), 1601, 1460 (O-C-O$^-$ stretch) cm^{-1}. ^{1}H NMR (400 MHz, CDCl$_3$) δ = 7.17 (t, *J* = 7.6 Hz, 1H), 7.07 (d, *J* = 7.3 Hz, 1H), 6.98 (d, *J* = 7.6 Hz, 1H), 6.93 (s, 1H), 6.88 (d, *J* = 7.6 Hz, 1H), 6.49 (s, 1H), 6.29 (d, *J* = 7.3 Hz, 1H), 3.94 (s, 2H), 3.71 (d, *J* = 14.9 Hz, 1H), 3.60 (d, *J* = 14.9 Hz, 1H), 3.44 - 3.29 (m, 3H), 3.07 - 2.95 (m, 1H), 2.89 (d, *J* = 9.1 Hz, 1H), 2.87 - 2.83 (m, *J* = 9.3 Hz, 1H), 2.81 (br. s., 4H), 2.73 (br. s., 1H), 2.66 (t, *J* = 6.1 Hz, 2H), 1.91 - 1.79 (m, 3H), 0.96 - 0.88 (m, 2H), 0.70 - 0.62 (m, 2H) ppm. ^{13}C NMR (101 MHz, CDCl$_3$) δ 175.8, 155.1, 144.5, 143.0, 139.7, 137.7, 131.7, 131.2, 128.7, 124.8, 124.0, 123.9, 115.3, 110.5, 64.2, 52.6, 50.6, 43.6, 41.2, 39.1, 36.4, 26.2, 24.0, 20.7, 15.3, 9.2 ppm. HRMS (ESI) calc'd for C$_{29}$H$_{34}$N$_3$O$_2$S $[M+H]^+$ 488.2366, found 488.2348.

2H missing from ^{1}H NMR spectrum (exchangeable). 2C not observed in ^{13}C NMR spectrum. Optical rotation could not be obtained due to the coloured nature of the isolated product.

Christopher J Tame

3-(3-Cyclopropylphenyl)-4-(2-((5,6,7,8-tetrahydro-1,8-naphthyridin-2-yl)methyl)-6,7-dihydrothieno[3,2-*c*]pyridin-5(4*H*)-yl)butanoic acid (84b, enantiomer 2)
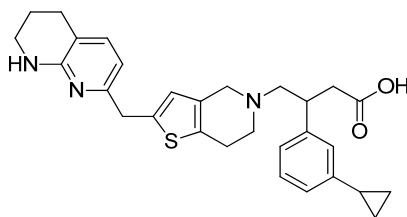
To a stirred solution of methyl 3-(3-cyclopropylphenyl)-4-(2-((5,6,7,8-tetrahydro-1,8-naphthyridin-2-yl)methyl)-6,7-dihydrothieno[3,2-*c*]pyridin-5(4*H*)-yl)butanoate (**110b**, **enantiomer 2**: 125 mg, 250 μmol) in MeOH (5 mL) at room temperature was added aqueous sodium hydroxide solution (2.0 M, 0.62 mL, 1.3 mmol) dropwise. The mixture was stirred at 50 ºC for 2 h. The mixture was concentrated under reduced pressure to afford a brown gum. The gum was dissolved in DMSO (0.5 mL) and MeOH (0.5 mL) and purified by ammonium bicarbonate modified mass-directed auto-preparative (MDAP) chromatography. The relevant fractions were combined and concentrated under reduced pressure to afford the desired product (**84b**, **enantiomer 2**: 101 mg, 210 μmol, 83% yield) as a brown solid. m.p. 206.4 °C. $[\alpha]_D$ = -20.0 (c = 1.00 in MeOH). LCMS (Method B): 0.95 min, $[M+H]^+$ 488 m/z. IR (solid) 3300 (N-H stretch); 2930 (sp^3 C-H stretch); 2820 ($[N-H]^+$ stretch); 1650, 1320 (O-C-O$^-$ stretch) cm^{-1}. ^{1}H NMR (400 MHz, CDCl3) δ = 7.17 (t, *J* = 7.6 Hz, 1H), 7.09 (d, *J* = 7.3 Hz, 1H), 6.96 (d, *J* = 7.6 Hz, 1H), 6.91 (s, 1H), 6.89 (d, *J* = 7.8 Hz, 1H), 6.56 (br. s., 1H), 6.50 (s, 1H), 6.31 (d, *J* = 7.3 Hz, 1H), 3.95 (s, 2H), 3.74 (d, *J* = 14.7 Hz, 1H), 3.65 (d, *J* = 14.4 Hz, 1H), 3.40 - 3.34 (m, 3H), 3.11 - 3.02 (m, 1H), 2.92 - 2.88 (m, 1H), 2.92 - 2.79 (m, 5H), 2.75 (dd, *J* = 3.5, 15.9 Hz, 1H), 2.68 (t, *J* = 6.1 Hz, 2H), 1.91 - 1.81 (m, 3H), 0.94 (dd, *J* = 1.9, 8.5 Hz, 2H), 0.66 (dd, *J* = 1.6, 4.9 Hz, 2H) ppm. ^{13}C NMR (101 MHz, DMSO-d$_6$) δ = 172.2, 151.2, 145.4, 144.1, 141.0, 140.8, 137.7, 131.1, 128.5, 127.6, 125.0, 124.9, 124.7, 124.2, 119.6, 110.3, 66.4, 59.2, 40.6, 36.9, 31.8, 24.8, 21.3, 18.8, 15.1, 9.6, 9.5 ppm. HRMS (ESI) calc'd for $C_{29}H_{34}N_3O_2S$ $[M+H]^+$ 488.2366, found 488.2367

1H missing from ^{1}H NMR spectrum (exchangeable). 1C missing from ^{13}C NMR.

Christopher J Tame

4-(3-Cyclopropylphenyl)dihydrofuran-2(3*H*)-one (120)
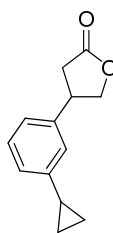
Method 1

To a mixture of (3-cyclopropylphenyl)boronic acid (66 mg, 0.40 mmol) and chloro(1,5-cyclooctadiene)rhodium(II) dimer (5 mg, 0.01 µmol) under nitrogen was added a solution of furan-2(5*H*)-one (14 µL, 0.20 mmol) in 1,4-dioxane and water (5.5 mL, 10:1) followed by triethylamine (28 µL, 0.20 mmol). The mixture was stirred at room temperature for 18 h then filtered over a celite pad covered with MgSO$_4$. The celite pad was rinsed with Et$_2$O and the filtrate was concentrated under reduced pressure to afford a crude orange gum. The gum was loaded in minimal CH$_2$Cl$_2$ onto a silica pre-packed column (5 g) and eluted with 0-50% EtOAc in cyclohexane. The relevant fractions were combined and concentrated to afford the desired product (8.3 mg, 40 µmol, 20% yield) as a colourless oil.

Method 2

To a nitrogen-degassed mixture of (3-cyclopropylphenyl)boronic acid (5.0 g, 31 mmol) and furan-2(5*H*)-one (4.3 mL, 61 mmol) in 1,4-dioxane (67 mL) and water (6.7 mL) was added chloro(1,5-cyclooctadiene)rhodium(II) dimer (1.5 g, 3.1 mmol) and aqueous potassium hydroxide solution (3.8 M, 24 mL, 93 mmol) sequentially at room temperature and the reaction mixture was stirred at room temperature for 10 min. To the mixture was added water (250 mL) and EtOAc (250 mL) and the separated aqueous phase was extracted twice with EtOAc (2 x 250 mL). The combined organic phase was passed through a hydrophobic frit and the filtrate was concentrated under reduced pressure to afford a yellow gum. The gum was loaded in minimal CH$_2$Cl$_2$ onto a silica pre-packed column (340 g) and eluted with 0-50% EtOAc in cyclohexane over 60 min. The relevant fractions were combined and

Christopher J Tame

concentrated under reduced pressure to afford the desired product (2.25 g, 11.1 mmol, 36% yield) as a clear oil.

Method 3

To a nitrogen-degassed mixture of (3-cyclopropylphenyl)boronic acid (100 mg, 620 µmol) and furan-2(5*H*)-one (0.22 mL, 3.1 mmol) in 1,4-dioxane (2 mL) and water (0.2 mL) was added chloro(1,5-cyclooctadiene)rhodium(II) dimer (30 mg, 60 µmol) and aqueous potassium hydroxide solution (3.8 M, 0.49 mL, 1.9 mmol) sequentially at room temperature and the reaction mixture was stirred at room temperature for 10 min. Water (10 mL) and EtOAc (10 mL) were added and the separated aqueous phase was extracted twice with EtOAc (2 x 10 mL). The combined organic phase was passed through a hydrophobic frit and the filtrate was concentrated under reduced pressure to afford a yellow gum. The gum was loaded in minimal CH_2Cl_2 onto a silica pre-packed column (20 g) and eluted with 0-50% EtOAc in cyclohexane over 40 min. The relevant fractions were combined and concentrated under reduced pressure to afford the desired product (71 mg, 0.35 mmol, 57% yield) as a clear oil. LCMS (Method A): 1.00 min, $[M+H]^+$ 203 m/z. IR (oil) 3003 (sp^3 C-H stretch), 1771, (C=O stretch), 1164, 1015 (C-O stretch) cm^{-1}. ^{1}H NMR (400 MHz, acetonitrile-d_3) δ = 7.14 (t, *J* = 8.1 Hz, 1H), 7.06 - 6.99 (m, 2 H), 6.90 (d, *J* = 7.8 Hz, 1H), 4.55 (t, *J* = 8.3 Hz, 1H), 4.12 (t, *J* = 8.4 Hz, 1H), 3.74 (quin, *J* = 8.6 Hz, 1H), 2.77 (dd, *J* = 17.1, 8.6 Hz, 1H), 2.62 (dd, *J* = 17.1, 9.6 Hz, 1H), 1.86 - 1.78 (m, 1H), 0.86 (ddd, *J* = 8.3, 4.5, 2.0 Hz, 2H), 0.64 - 0.56 (m, 2H) ppm. ^{13}C NMR (101MHz, DMSO-d_6) δ = 177.1, 144.7, 140.2, 129.0, 124.8, 124.5, 124.4, 73.9, 41.0, 35.6, 15.5, 9.9 ppm. HRMS (ESI) calc'd for $C_{13}H_{15}O_2$ [M+H]+ 203.1072, found 203.1065.

Christopher J Tame

4-(3-Cyclopropylphenyl)dihydrofuran-2(3*H*)-one (120a)
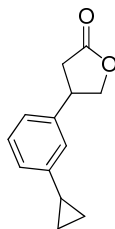
Method 1

(3-Cyclopropylphenyl)boronic acid (270 mg, 1.67 mmol), bisethylenerhodium acetylacetonate (9 mg, 36 μmol) and 2,2'-bis(diphenylphosphino)-1,1'-binaphthalene (22 mg, 36 μmol) were charged to a microwave vial equipped with a microwave stirrer bar. The vial was sealed and degassed with three alternative applications of vacuum and nitrogen. 1,4-dioxane (0.6 mL) was added and the mixture degassed with nitrogen for 10 min. Water (60 μL) and furan-2(5*H*)-one (100 mg, 1.19 mmol) were added sequentially and the vial was then heated and stirred at 100 ºC for 5 h. LCMS analysis (Method A) indicated only partial conversion to the desired product.

Method 2

To a nitrogen-degassed mixture of (3-cyclopropylphenyl)boronic acid (100 mg, 620 μmol) and furan-2(5*H*)-one (0.22 mL, 3.1 mmol) in 1,4-dioxane (2 mL) and water (0.2 mL) was added a degassed solution of chloro(1,5-cyclooctadiene)rhodium(II) dimer (30 mg, 60 μmol) and 2,2'-bis(diphenylphosphino)-1,1'-binaphthalene ((*R*)-BINAP) (77 mg, 0.12 mmol) in 1,4-dioxane (0.5 mL). To the mixture was added aqueous potassium hydroxide solution (3.8 M, 0.5 mL, 1.9 mmol) and the mixture was stirred at room temperature for 10 min. Water (10 mL) and EtOAc (10 mL) were added and the separated aqueous phase was extracted twice with EtOAc (2 x 10 mL). The combined organic phase was passed through a hydrophobic frit and the filtrate was concentrated under reduced pressure to afford a yellow gum. The gum was dissolved in DMSO (2 mL) and a 1 mL aliquot was purified by formic acid modified mass-directed auto preparative (MDAP) chromatography. The relevant fractions were combined and concentrated under reduced pressure to afford the desired product (32 mg, 0.16 mmol, 26% yield) as a colourless oil. Chiral HPLC

Christopher J Tame

analysis (5% EtOH in heptane, Chiralpak AD-H column (4.6 mm x 25 cm), flow rate: 1 mL/min): 0% e.e.

Method 3

To a nitrogen-degassed solution of (3-cyclopropylphenyl)boronic acid (101 mg, 620 μmol) and 1,4-dioxane (0.7 mL) was added bis(norbornadiene)rhodium(I) tetrafluoroborate (11 mg, 0.03 mmol) and 2,2'-bis(diphenylphosphino)-1,1'-binaphthalene ((*R*)-BINAP) (21 mg, 36 μmol) under a nitrogen atmosphere and the mixture was stirred for 2 h at room temperature. To the mixture was added water (109 μL), furan-2(5*H*)-one (42 μL, 0.60 mmol) and triethylamine (83 μL, 0.60 mmol) sequentially and the mixture was stirred at 50 ºC for 15 h. The mixture was diluted with EtOAc (20 mL) and water (20 mL) and the separated aqueous phase was extracted twice with EtOAc (2 x 20mL). The combined organic phase was passed through a hydrophobic frit and the filtrate was concentrated under reduced pressure to afford a gum. The gum was loaded in DMSO (2 x 1 mL) and purified by formic acid modified mass-directed auto-preparative (MDAP) chromatography. The relevant fractions were combined and concentrated under reduced pressure to afford the desired product (20 mg, 0.10 mmol, 17% yield) as a clear oil. LCMS (Method A): 1.00 min, [M+H]$^+$ 203 m/z. Chiral HPLC analysis (5% EtOH in heptane, Chiralpak AD-H column (4.6 mm x 25 cm), flow rate: 1 mL/min): 96% e.e. ^{1}H NMR (400 MHz, CDCl$_3$) δ = 7.27 (t, *J* = 3.5 Hz, 1H), 7.04 - 6.90 (m, 3H), 4.65 (t, *J* = 7.8 Hz, 1H), 4.26 (d, *J* = 8.8 Hz, 1H), 3.74 (quin, *J* = 8.5 Hz, 1H), 2.91 (dd, *J* = 17.4, 8.8 Hz, 1H), 2.67 (dd, *J* = 17.7, 9.1 Hz, 1H), 1.89 (tt, *J* = 8.5, 5.1 Hz, 1H), 0.98 (ddd, *J* = 8.3, 4.8, 3.5 Hz, 2H), 0.73 - 0.65 (m, 2H) ppm.

Christopher J Tame

Ethyl 4-bromo-3-(3-cyclopropylphenyl)butanoate (121) and **ethyl 4-bromo-3-(3-(1-bromopropyl)phenyl)butanoate (122)**
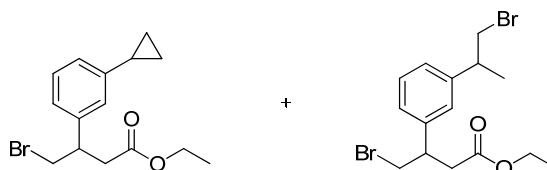
Method 1

To EtOH (0.1 mL) was added acetyl bromide (84 µL, 1.1 mmol) and a solution of 4-(3-cyclopropylphenyl)dihydrofuran-2(3*H*)-one (77 mg, 0.38 mmol) in EtOH (0.1 mL) dropwise, sequentially at 0 °C. The mixture was allowed to reach room temperature then stirred at room temperature for 2 h. LCMS analysis indicated incomplete conversion to a new peak that ionised at $[M+H]^+$ 311 and 313 m/z. No further investigation was undertaken.

Method 2

To EtOH (0.3 mL) at 0 ºC was added acetyl bromide, (480 µL, 6.52 mmol) dropwise at 0 ºC and the mixture was stirred at 0 ºC for 10 min. To the mixture was added a solution of 4-(3-cyclopropylphenyl)dihydrofuran-2(3H)-one (150 mg, 740 µmol) in EtOH (0.3 mL) dropwise at 0 ºC. The mixture was allowed to reach room temperature, then stirred for 2 h at room temperature, then concentrated under reduced pressure to afford a crude gum. The gum was loaded in DMSO (2 mL) and purified by formic acid modified mass directed auto-preparative (MDAP) chromatography (2 x 1 mL injections). The relevant fractions were combined and concentrated to afford ethyl 4-bromo-3-(3-cyclopropylphenyl)butanoate (**121**) (117 mg, 380 µmol, 51% yield) as a colourless oil and ethyl 4-bromo-3-(3-(1-bromopropyl)phenyl)butanoate (**122**) (100 mg, 260 µmol, 34% yield) as a yellow gum.

Ethyl 4-bromo-3-(3-cyclopropylphenyl)butanoate (**121**): LCMS (Method A): 1.31 min, $[^{79}Br\ M+H]^+$ 310, $[^{81}Br\ M+H]^+$ 312 m/z. IR (oil) 2981 (sp^3 C-H stretch), 1730

Christopher J Tame

(C=O stretch), 1179, 1032 (C-O stretch) cm^{-1}. ^{1}H NMR (400 MHz, DMSO-d$_6$) δ = 7.18 (t, *J* = 7.6, Hz, 1H), 7.04 (d, *J* = 7.8 Hz, 1H), 7.00 (s, 1H), 6.92 (d, *J* = 7.8 Hz, 1H), 3.96 (q, *J* = 7.3 Hz, 2H), 3.76 (dd, *J* = 10.1, 7.1 Hz, 1H), 3.70 (dd, *J* = 10.1, 6.8 Hz, 1H), 3.42 - 3.31 (m, 1H), 2.88 (dd, *J* = 15.9, 5.8 Hz, 1H), 2.68 (dd, *J* = 15.9, 9.1 Hz, 1H), 1.92 - 1.82 (m, 1H), 1.06 (t, *J* = 7.1 Hz, 3H), 0.96 - 0.90 (m, 2H), 0.69 - 0.62 (m, 2H) ppm. ^{13}C NMR (101 MHz, DMSO-d6) δ = 171.5, 144.2, 141.3, 128.6, 125.3, 124.9, 124.4, 60.3, 44.3, 39.2, 39.0, 15.4, 14.4, 9.9 ppm. HRMS (ESI) calc'd for C$_{15}$H$_{20}$O$_2$Br [M+H]$^+$ 311.0647, found 311.0639.

Ethyl 4-bromo-3-(3-(1-bromopropyl)phenyl)butanoate (**122**): LCMS (Method A): 1.35 min, [^{79}Br M+H]$^+$, [^{79}Br M+H]$^+$ 390; [^{79}Br M+H]$^+$, [^{81}Br M+H]$^+$ 392 m/z; [^{81}Br M+H]$^+$, [^{81}Br M+H]$^+$ 394. ^{1}H NMR (600 MHz, DMSO-d$_6$) δ = 7.37 (s, 1H), 7.33 (t, *J* = 6.6 Hz, 1H), 7.30 (d, *J* = 7.3 Hz, 1H), 7.24 (d, *J* = 7.3 Hz, 1H), 5.15 (t, *J* = 7.2 Hz, 1H), 3.99 - 3.90 (m, 2H), 3.81 - 3.76 (m, 1H), 3.76 - 3.70 (m, 1H), 3.46 - 3.38 (m, 1H), 2.91 (dd, *J* = 15.8, 5.9 Hz, 1H), 2.74 - 2.67 (m, 1H), 2.29 - 2.18 (m, 1H), 2.15 - 2.07 (m, 1H), 1.08 - 1.01 (m, 3H), 0.91 (t, *J* = 7.2 Hz, 3H). ^{13}C NMR (101 MHz, DMSO-d6) δ = 171.3, 142.2, 141.8, 129.0, 128.0, 127.2, 126.7, 60.1, 58.4, 43.9, 38.8, 38.6, 32.8, 14.3, 13.0 ppm.

Method 3

To EtOH (4.5 mL) was added acetyl bromide (4.93 mL, 66.7 mmol) and a solution of 4-(3-cyclopropylphenyl)dihydrofuran-2(3*H*)-one (2.25 g, 11.1 mmol) in EtOH (4.5 mL) dropwise, sequentially at 0 °C. The mixture was allowed to reach room temperature then stirred at room temperature for 1 h. The reaction mixture was then concentrated under reduced pressure to afford a gum. The gum was dissolved in EtOAc (100 mL) and water (100 mL) and the separated aqueous phase was extracted twice with EtOAc (2 x 100 mL). The combined organic phase was passed through a hydrophobic frit and the filtrate was concentrated under reduced pressure to afford a crude gum. The gum was loaded in minimal CH$_2$Cl$_2$ onto a silica pre-packed column (100 g) and eluted with 0-50% EtOAc in cyclohexane over 60 min. The

Christopher J Tame

relevant fractions were combined and concentrated under reduced pressure to afford the desired product **121** (1.66 g, 4.537 mmol, 41% yield) as a clear oil.

3-(3-Cyclopropylphenyl)-4-(2-((5,6,7,8-tetrahydro-1,8-naphthyridin-2-yl)methyl)-6,7-dihydrothieno[3,2-*c*]pyridin-5(4*H*)-yl)butanoic acid (84)
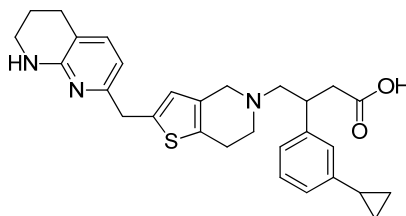
To a stirred suspension of 2-((5,6,7,8-tetrahydro-1,8-naphthyridin-2-yl)methyl)-4,5,6,7-tetrahydrothieno[3,2-*c*]pyridine (50 mg, 0.18 mmol) and ethyl 4-bromo-3-(3-cyclopropylphenyl)butanoate (71 mg, 0.23 mmol) in isopropanol (1 mL) was added DIPEA (90 μL, 0.53 mmol) dropwise at room temperature. The mixture was sealed in a microwave vial and heated at 150 ºC for 1 h in a Biotage initiator microwave. The mixture was concentrated under reduced pressure to afford a brown gum. To the brown gum was added EtOAc (50 mL) and water (50 mL) and the mixture separated. The aqueous phase was extracted twice with EtOAc (2 x 50mL) and the combined organic phase was passed through a hydrophobic frit and concentrated under reduced pressure to afford a crude orange solid. To a solution of the crude solid in MeCN (1 mL) was added an aqueous solution of NaOH (2 M, 2.2 mL, 0.90 mmol) at room temperature and the resulting mixture was stirred vigorously at 50 °C for 2 h. The mixture was cooled to room temperature and neutralised with an aqueous solution of HCl (2 M). The mixture was concentrated under reduced pressure to afford a crude orange gum. The crude solid was loaded in DMSO (1 mL) and purified by ammonium-bicarbonate modified mass directed auto preparative (MDAP) chromatography. The relevant fractions were combined and concentrated under reduced pressure to afford a crude gum. The gum was dissolved in DMSO (1 mL) and purified by formic acid modified mass directed auto preparative (MDAP) chromatography. The relevant fractions were combined and concentrated under a stream of nitrogen to afford a colourless gum. The gum was triturated from minimal

Christopher J Tame

diethyl ether and the mixture concentrated under a stream of nitrogen to afford the desired product (12 mg, 30 μmol, 14% yield) as a white solid. LCMS (Method C): 0.69 min, [M+H]$^+$ 488 m/z. ^{1}H NMR (400 MHz, DMSO-d$_6$) δ = 7.14 (t, J = 7.6 Hz, 1H), 7.05 (d, J = 7.3 Hz, 1H), 7.02 - 6.96 (m, 2H), 6.85 (d, J = 7.6 Hz, 1H), 6.50 (s, 1H), 6.32 (br. s., 1H), 6.28 (d, J = 7.3 Hz, 1H), 3.83 (s, 2H), 3.48 (d, J = 14.6 Hz, 1H), 3.38 (d, J = 14.9 Hz, 1H), 3.25 - 3.20 (m, 3H), 2.81 - 2.72 (m, 2H), 2.70 - 2.62 (m, 4H), 2.59 (t, J = 6.3 Hz, 2H), 2.57 - 2.52 (m, 1H), 2.41 (d, J = 8.1 Hz, 1H), 1.91 - 1.82 (m, 1H), 1.78 - 1.69 (m, 2H), 0.95 - 0.89 (m, 2H), 0.67 - 0.61 (m, 2H) ppm.

1H missing from ^{1}H NMR spectrum (exchangeable).

(*E*)-Methyl 4-(4,5-dihydrothieno[2,3-*c*]pyridin-6(7*H*)-yl)but-2-enoate (128)
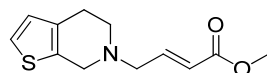
To a stirred solution of 4,5,6,7-tetrahydrothieno[2,3-*c*]pyridine, hydrochloride (1.0 g, 5.4 mmol) and triethylamine (2.26 mL, 16.2 mmol) in CH$_2$Cl$_2$ (50 mL) was added (*E*)-methyl 4-bromobut-2-enoate (970 μL, 8.11 mmol) dropwise at room temperature under nitrogen and the mixture was stirred at room temperature for 1 h. To the mixture was added water (50 mL) and CH$_2$Cl$_2$ (50 mL) and the separated organic phase was washed twice with water (2 x 50 mL). The combined organic phase was then passed through a hydrophobic frit and the filtrate was concentrated under reduced pressure to afford the title compound (1.39 g, 5.27 mmol, 97 % yield) as a crude orange gum. LCMS (Method B): 0.99 min, [M+H]$^+$ 238 m/z. ^{1}H NMR (400 MHz, DMSO-d$_6$) δ = 7.28 (d, J = 5.0 Hz, 1H), 6.89 (dt, J = 15.6, 6.0 Hz, 1H), 6.82 (d, J = 5.0 Hz, 1H), 6.07 (dt, J = 15.6, 1.5 Hz, 1H), 3.67 (s, 3H), 3.63 (s, 2H), 3.33 (dd, J = 6.0, 1.8 Hz, 2H), 2.74 - 2.67 (m, 2H), 2.65 (m, 2H) ppm.

Christopher J Tame

Methyl 3-(3-cyclopropylphenyl)-4-(4,5-dihydrothieno[2,3-*c*]pyridin-6(7*H*)-yl)butanoate (127)
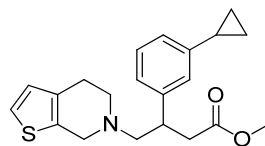
To a nitrogen- degassed solution of (3-cyclopropylphenyl)boronic acid (2.56 g, 15.8 mmol) and (*E*)-methyl 4-(4,5-dihydrothieno[2,3-*c*]pyridin-6(7*H*)-yl)but-2-enoate (1.39 g, 5.27 mmol) in 1,4-dioxane (8 mL) was added an aqueous solution of potassium hydroxide (3.8 M, 2.8 mL, 11 mmol) and chloro(1,5-cyclooctadiene)rhodium(II) dimer (780 mg, 1.58 mmol) sequentially. The solution was then further degassed with 3 alternative applications vacuum and nitrogen and then heated and stirred under reflux at 95 ºC for 45 min. The reaction mixture was cooled to room temperature then concentrated under reduced pressure to afford a brown gum. The gum was then dissolved in CH_2Cl_2 (100 mL) and washed three times with water (3 x 100 mL). The combined organic phase was passed through a hydrophobic frit and the filtrate was concentrated under reduced pressure to afford a brown gum. The gum was loaded in minimal CH_2Cl_2 onto a silica pre-packed column (100 g) and eluted with 0-25% TBME in cyclohexane over 60 min. The appropriate fractions were combined and concentrated under reduced pressure to afford the desired product (1.68 g, 4.73 mmol, 90 % yield) as a brown gum. LCMS (Method B): 1.41 min, $[M+H]^+$ 356 m/z. ^{1}H NMR (400 MHz, DMSO-d_6) δ = 7.27 (d, *J* = 5.0 Hz, 1H), 7.15 (t, *J* = 7.6 Hz, 1H), 7.03 (d, 7.8 Hz, 1H), 7.00 (s, 1H), 6.88 (d, *J* = 7.6 Hz, 1H), 6.80 (d, *J* = 5.0 Hz, 1H), 3.68 (d, *J* = 14.9 Hz, 1H), 3.58 (d, *J* = 15.1 Hz, 1H), 3.41 (s, 3H), 3.37 - 3.31 (m, 1H), 2.86 - 2.75 (m, 2H), 2.73 - 2.63 (m, 2H), 2.63 - 2.56 (m, 2H), 2.52 - 2.47 (m, 2H), 1.92 - 1.84 (m, 1H), 0.96 - 0.90 (m, 2H), 0.68 - 0.62 (m, 2H) ppm.

Christopher J Tame

***tert*-Butyl 7-((6-(2-(3-cyclopropylphenyl)-4-methoxy-4-oxobutyl)-4,5,6,7-tetrahydrothieno[2,3-*c*]pyridin-2-yl)methyl)-3,4-dihydro-1,8-naphthyridine-1(2*H*)-carboxylate (129)**
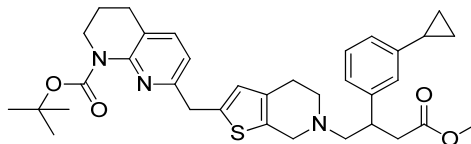
(1,5-Cyclooctadiene)(methoxy)iridium(I) dimer (13 mg, 20 µmol) and 4,4'-di-tert-butyl-2,2'-bipyridine (11 mg, 40 µmol) were charged to a 150 mL round bottomed flask and degassed with three alternative applications of vacuum and nitrogen. Degassed cyclohexane (4 mL), degassed 4,4,5,5-tetramethyl-1,3,2-dioxaborolane (210 µL, 1.44 mmol) and a degassed mixture of methyl 3-(3-cyclopropylphenyl)-4-(4,5-dihydrothieno[2,3-*c*]pyridin-6(7*H*)-yl)butanoate (500 mg, 1.31 mmol) in cyclohexane (3 mL) were added dropwise, sequentially, at room temperature under nitrogen. The mixture was then stirred at 20 ºC for 3 h. To the mixture was added a degassed mixture of chloro(2-dicyclohexylphosphino-2′,4′,6′-triisopropyl-1,1′-biphenyl)[2-(2′-amino-1,1′-biphenyl)]palladium(II) (103 mg, 130 µmol) and *tert*-butyl 7-(bromomethyl)-3,4-dihydro-1,8-naphthyridine-1(2H)-carboxylate (300 mg, 920 µmol) in THF (3 mL) dropwise at room temperature, followed by the addition of a degassed aqueous solution of potassium phosphate (500 mM, 3.48 mL, 1.74 mmol) dropwise at room temperature.   The resulting solution was stirred at room temperature under nitrogen for 16 h. To the mixture was added brine (50 mL) and EtOAc (50 mL) and the separated organic phase was washed twice with brine (2 x 100 mL). The combined aqueous phase was extracted with EtOAc (100 mL) and the combined organic phase was then filtered through a hydrophobic frit and the filtrate was concentrated under reduced pressure to afford a red oil. The oil was loaded in minimal CH_2Cl_2 onto a silica pre-packed column (100 g) and eluted with 0-25% EtOAc in cyclohexane over 60 min. The appropriate fractions were combined and concentrated under reduced pressure to afford the desired product (183 mg, 283 µmol, 22 % yield) as an orange gum. LCMS (Method A): 0.86 min, [M+H]$^+$ 302 m/z. ^{1}H NMR (600 MHz, CDCl3) δ = 7.32 (d, *J* = 7.7 Hz, 1H), 7.20 (t, *J* = 7.7 Hz,

1H), 7.01 (d, J = 7.7 Hz, 1H), 6.96 (s, 1H), 6.92 (d, J = 7.7 Hz, 1H), 6.86 (d, J = 7.7 Hz, 1H), 6.56 (s, 1H), 4.18 (s, 2H), 3.78 (t, J = 6.2 Hz, 2H), 3.71 (d, J = 15.0 Hz, 1H), 3.59 (d, J = 15.0 Hz, 1H), 3.51 (s, 3H), 3.46 - 3.40 (m, 1H), 2.90 (dd, J = 7.0, 15.4 Hz, 2H), 2.75 (t, J = 6.8 Hz, 2H), 2.72 - 2.66 (m, 2H), 2.64 (s, 2H), 2.58 (dd, J = 7.7, 15.8 Hz, 1H), 1.98 - 1.92 (m, 2H), 1.89 (s, 1H), 1.52 (s, 9H), 0.99 - 0.95 (m, 2H), 0.72 - 0.68 (m, 2H) ppm. ^{13}C NMR (101 MHz , CDCl$_3$) δ = 173.2, 156.3, 154.1, 151.0, 144.1, 142.7, 138.9, 137.4, 133.3, 131.9, 128.4, 125.7, 125.1, 124.3, 123.8, 122.2, 118.0, 80.8, 63.3, 52.1, 51.2, 50.7, 44.7, 40.3, 39.3, 38.5, 28.3, 26.3, 25.4, 23.2, 15.4, 9.2 ppm.

2D NMR key correlations:

HSQC (^{1}H NMR to ^{13}C NMR): δ = 6.56 to 125.7 ppm; 4.18 ppm to 38.5 ppm.
HMBC (^{1}H NMR to ^{13}C NMR): δ = 6.56 ppm to 25.4, 38.5, 131.9, 133.3, 138.9 ppm; 4.18 to 118.0, 125.7, 138.9, 156.3 ppm.

Christopher J Tame

***tert*-Butyl 7-((6-(2-(3-cyclopropylphenyl)-4-methoxy-4-oxobutyl)-4,5,6,7-tetrahydrothieno[2,3-*c*]pyridin-2-yl)methyl)-3,4-dihydro-1,8-naphthyridine-1(2*H*)-carboxylate (129) ^{1}H NMR Correlation Spectroscopy (COSY)**

Christopher J Tame

tert-Butyl 7-((6-(2-(3-cyclopropylphenyl)-4-methoxy-4-oxobutyl)-4,5,6,7-tetrahydrothieno[2,3-*c*]pyridin-2-yl)methyl)-3,4-dihydro-1,8-naphthyridine-1(2*H*)-carboxylate (129) Heteronuclear Single Quantum Coherence (HSQC) ^{1}H and ^{13}C NMR spectroscopy.
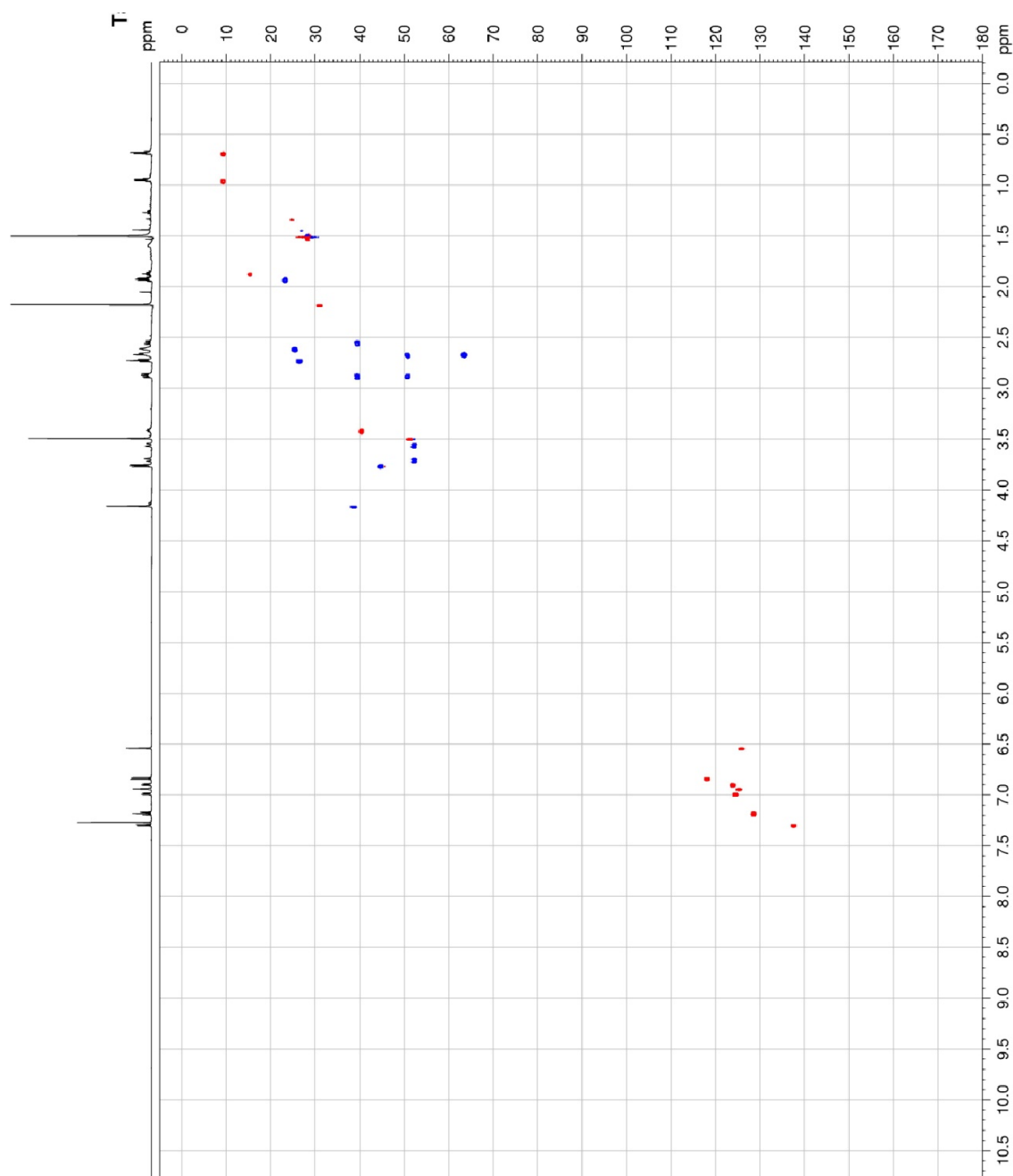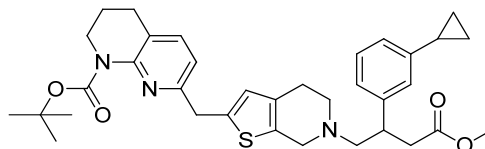
Christopher J Tame

tert-Butyl 7-((6-(2-(3-cyclopropylphenyl)-4-methoxy-4-oxobutyl)-4,5,6,7-tetrahydrothieno[2,3-*c*]pyridin-2-yl)methyl)-3,4-dihydro-1,8-naphthyridine-1(2*H*)-carboxylate (129) Heteronuclear Multiple Bond Correlation (HMBC) ^{1}H and ^{13}C NMR spectroscopy.

Christopher J Tame
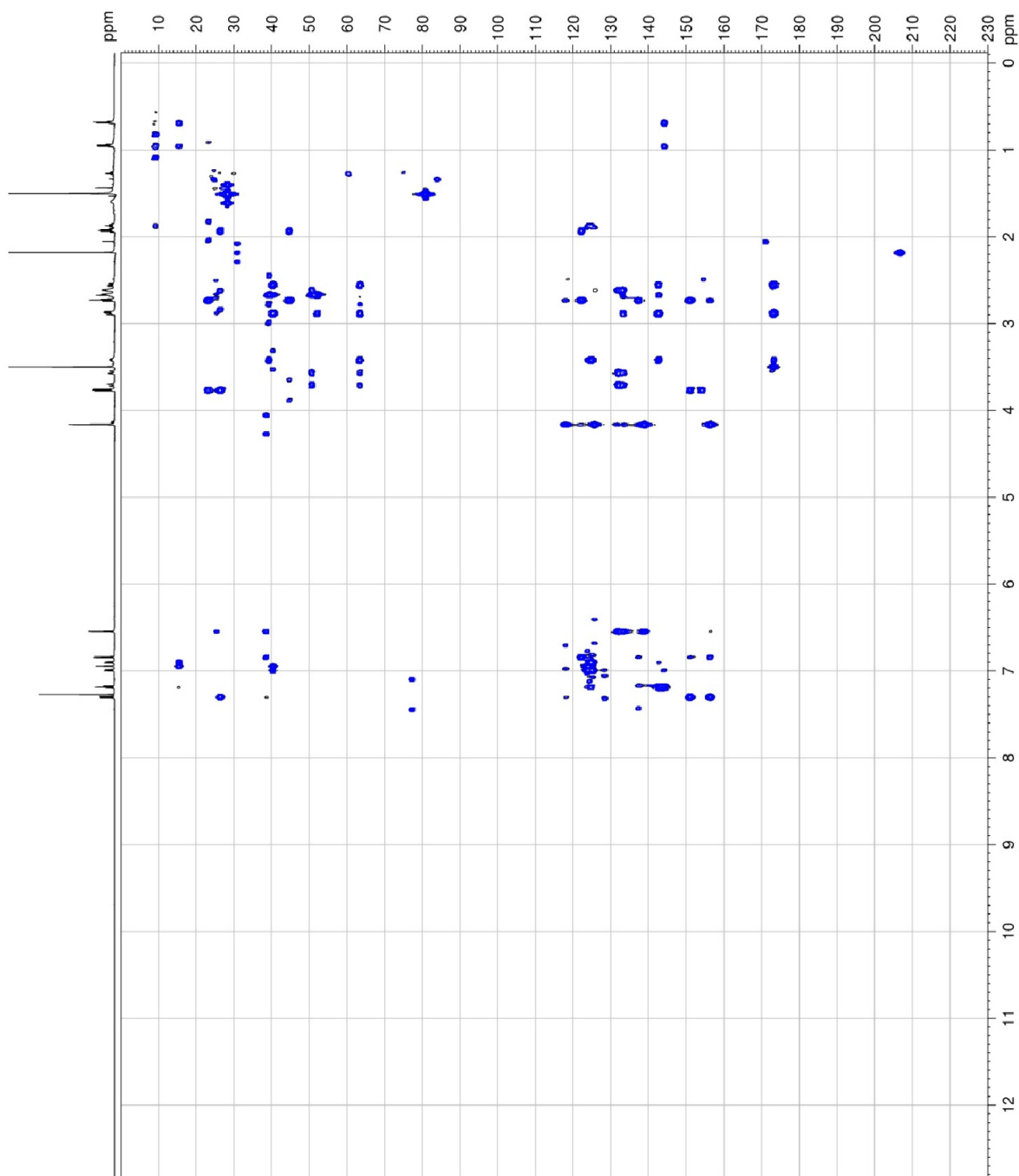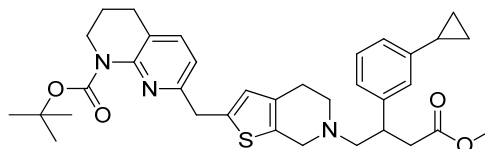
3-(3-Cyclopropylphenyl)-4-(2-((5,6,7,8-tetrahydro-1,8-naphthyridin-2-yl)methyl)-4,5-dihydrothieno[2,3-c]pyridin-6(7H)-yl)butanoic acid, formic acid salt (85)

To a stirred solution of tert-butyl 7-(((6-(2-(3-cyclopropylphenyl)-4-methoxy-4-oxobutyl)-4,5,6,7-tetrahydrothieno[2,3-c]pyridin-2-yl)methyl)-3,4-dihydro-1,8-naphthyridine-1(2H)-carboxylate (100 mg, 0.17 mmol) in MeOH (1.5 mL) was added a solution of HCl in 1,4-dioxane (4.0 M, 0.415 mL, 1.66 mmol) dropwise at room temperature and the mixture was stirred at 50 ºC for 2 h. The mixture was then loaded onto an aminopropyl-functionalised silica cartridge (20 g) and eluted with MeOH. The filtrate was then concentrated under reduced pressure to afford a crude gum. To a solution of the crude gum in MeCN (1.5 mL) was added an aqueous solution of NaOH (2.0 M, 0.83 mL, 1.66 mmol) dropwise and the resulting mixture was stirred at 50 ºC for 2 h. The mixture was then cooled to room temperature and concentrated to 1 mL under a stream of nitrogen, then purified by ammonium-bicarbonate modified, mass-directed auto-preparative (MDAP) chromatography. The relevant fractions were combined and concentrated under reduced pressure to afford a crude gum. The gum was dissolved in DMSO (1 mL) and purified by formic acid modified, mass-directed auto-preparative (MDAP) chromatography. The relevant fractions were combined and concentrated under reduced pressure the title compound as a formic acid salt (20 mg, 37 μmol, 23% yield). LCMS (Method B): 0.91 min, [M+H]$^+$ 488 m/z. ^{1}H NMR (400 MHz, DMSO-d$_6$) δ = 8.17 (s, 1H), 7.20 - 7.10 (m, 1H), 7.07 - 6.99 (m, J=15.2, 7.4 Hz, 2H), 6.99 (s, 1H), 6.86 (d, J = 7.8 Hz, 1H), 6.52 (s, 1H), 6.34 (br. s., 1H), 6.30 (d, J = 7.3 Hz, 1H), 3.84 (s, 2H), 3.60 (d, J = 14.9 Hz, 1H), 3.52 (d, J = 14.9 Hz, 1H), 3.34 - 3.26 (m, 1H), 3.24 (d, J = 4.3 Hz, 2H), 2.82 - 2.71 (m, 2H), 2.70 - 2.55 (m, 5H), 2.52 (br. s., 2H), 2.42 (dd, J = 15.7, 8.2 Hz, 1H), 1.92 - 1.81 (m, 1H), 1.80 - 1.66 (m, 2H), 0.97 - 0.81 (m, 2H), 0.68 - 0.56 (m, 2H) ppm.

Christopher J Tame

2H missing from ^{1}H NMR spectrum (exchangeable). Full characterisation undertaken on page 334.

(*E*)-Methyl 4-(4,5-dihydrothieno[2,3-*c*]pyridin-6(7*H*)-yl)but-2-enoate (128)
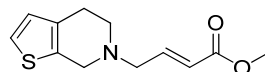
To a stirred solution of 4,5,6,7-tetrahydrothieno[2,3-*c*]pyridine, hydrochloride (10.0 g, 54 mmol) and triethylamine (22.6 mL, 162 mmol) in *tert*-butylmethyl ether (200 ml) and CH_2Cl_2 (50 mL) at room temperature under nitrogen was added (*E*)-methyl 4-bromobut-2-enoate (9.69 mL, 81.0 mmol) dropwise. The mixture was stirred at room temperature for 1 h. Water (50 mL) and CH_2Cl_2 (50 mL) was added and the seperated organic phase was washed twice with water (2 x 50 mL). The combined organic phase was passed through a hydrophobic frit and the filtrate was concentrated under reduced pressure to afford a brown oil. The oil was loaded in minimal CH_2Cl_2 onto a silica pre-packed column (750 g) and eluted with 0-100% EtOAc in cyclohexane over 60 min. The relevant fractions were combined and concentrated under reduced pressure to afford the title compound (9.28 g, 39.1 mmol, 72% yield) as a colourless oil. LCMS (Method B): 0.99 min, [M+H]$^+$ 238 m/z. ^{1}H NMR (400 MHz, DMSO-d$_6$) δ = 7.28 (d, *J* = 5.0 Hz, 1H), 6.89 (dt, *J* = 15.6, 6.0 Hz, 1H), 6.82 (d, *J* = 5.0 Hz, 1H), 6.07 (dt, *J* = 15.6, 1.5 Hz, 1H), 3.67 (s, 3H), 3.63 (s, 2H), 3.33 (dd, *J* = 6.0, 1.8 Hz, 2H), 2.74 - 2.67 (m, 2H), 2.65-2.64 (m, 2H) ppm.

Methyl 3-(3-cyclopropylphenyl)-4-(4,5-dihydrothieno[2,3-*c*]pyridin-6(7*H*)-yl)butanoate (127)
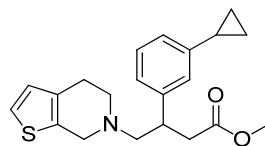
Method 1

To a nitrogen-degassed solution of (3-cyclopropylphenyl)boronic acid (139 mg, 858 µmol) in 1,4-dioxane (2 mL) was added an aqueous solution of potassium hydroxide (3.8 M, 0.24 mL, 0.89 mmol), (*R*)-2,2'-bis(diphenylphosphino)-1,1'-binaphthalene (28 mg, 50 µmol) and chloro(1,5-cyclooctadiene)rhodium(II) dimer (11 mg, 20 µmol) sequentially and the solution was further degassed under a stream of nitrogen for 30 min. To the solution was added a solution of (*E*)-methyl 4-(4,5-dihydrothieno[2,3-*c*]pyridin-6(7*H*)-yl)but-2-enoate (106 mg, 450 µmol) in 1,4-dioxane (2 mL) dropwise at room temperature. The solution was then heated and stirred under reflux at 95 ºC for 1 h. The reaction mixture was cooled to room temperature then concentrated under reduced pressure to afford a brown gum. The gum was dissolved in CH$_2$Cl$_2$ (100 mL) and then washed three times with water (3 x 100 mL). The combined organic phase was passed through a hydrophobic frit and the filtrate was concentrated under reduced pressure to afford a brown gum. The gum was loaded in DMSO (1 mL) and purified by formic acid modified mass directed auto-preparative (MDAP) chromatography. The appropriate fractions were combined and concentrated to afford the title compound (46.4 mg, 0.130 mmol, 29% yield) as a brown gum. LCMS (Method B): 1.41 min, [M+H]$^+$ 356 m/z. Chiral HPLC analysis (10% EtOH in heptane, Chiralcel OD-H column (4.6 mm x 25 cm), flow rate: 1 mL/min): 67% e.e

Method 2

To a nitrogen-degassed solution of (3-cyclopropylphenyl)boronic acid (72 mg, 0.44 mmol) in 1,4-dioxane (0.5 mL) was added bis(norbornadiene)rhodium(I) tetrafluoroborate (2.5 mg, 6.7 µmol) and 2,2'-bis(diphenylphosphino)-1,1'-binaphthalene ((*R*)-BINAP) (4.5 mg, 7.2 µmol) under a nitrogen atmosphere and the mixture was stirred for 2 h at room temperature. To the mixture was added water

Christopher J Tame

(50 µL), a solution of (*E*)-methyl 4-(4,5-dihydrothieno[2,3-*c*]pyridin-6(7*H*)-yl)but-2-enoate (100 mg, 421 µmol) in 1,4-dioxane (100 µL) and triethylamine (60 µL, 0.42 mmol), sequentially, and the mixture was stirred at 23 ºC for 15 h. LCMS analysis of the crude reaction mixture indicated no desired reaction to have occurred. To the reaction mixture was added bis(norbornadiene)rhodium(I) tetrafluoroborate (2.5 mg, 6.7 µmol) and (*R*)-2,2'-bis(diphenylphosphino)-1,1'-binaphthalene (4.5 mg, 7.2 µmol) and the mixture was stirred at 50 ºC for 2 h. LCMS analysis of the crude reaction mixture indicated partial conversion to the desired product. The mixture was then stirred at 70 ºC for 2 h. The mixture cooled to room temperature then concentrated under reduced pressure to afford a brown gum. The gum was dissolved in CH_2Cl_2 (50 mL) and was washed three times with water (3 x 50 mL). The combined organic fractions were passed through a hydrophobic frit and the filtrate was concentrated under reduced pressure to afford a brown gum. The gum was loaded in DMSO (1 mL) and purified by formic acid modified mass directed auto-preparative (MDAP) chromatography. The appropriate fractions were combined and concentrated to afford the title compound (8.4 mg, 20 µmol, 6% yield) as a brown gum. LCMS (Method B): 1.41 min, $[M+H]^+$ 356 m/z. Chiral HPLC analysis (10% EtOH in heptane, Chiralcel OD-H column (4.6 mm x 25 cm), flow rate: 1 mL/min): 37% e.e

Method 3

To a degassed solution of (3-cyclopropylphenyl)boronic acid (12.1 g, 74.8 mmol) in 1,4-dioxane (300 mL) was added aqueous potassium hydroxide solution (3.8 M, 20 mL, 75 mmol), (*R*)-2,2'-bis(diphenylphosphino)-1,1'-binaphthalene (2.33 g, 3.74 mmol) and chloro(1,5-cyclooctadiene)rhodium(II) dimer (921 mg, 1.87 mmol) sequentially and the solution was further degassed under a stream of nitrogen for 30 min. To the mixture was added a solution of (*E*)-methyl 4-(4,5-dihydrothieno[2,3-*c*]pyridin-6(7*H*)-yl)but-2-enoate (8.87 g, 37.4 mmol) in 1,4-dioxane (50 mL) dropwise at room temperature. The solution was then heated and stirred under reflux at 95 ºC for 1 h. The reaction mixture was concentrated under reduced pressure to afford a brown gum. The gum was dissolved in EtOAc (300 mL) and was washed three times with water (3 x 300 mL). The combined organic fractions were passed

through a hydrophobic frit and the filtrate was concentrated under reduced pressure to afford a brown gum. The oil was loaded in minimal CH_2Cl_2 onto a silica pre-packed column (330 g) and eluted with 0-25% *tert*-butylmethyl ether in cyclohexane over 60 min. The appropriate fractions were combined and concentrated to afford a crude oil. The oil was diluted in EtOAc (50 mL) and loaded onto a silica SCX pre-packed column and eluted with EtOAc (200 mL), then EtOAc/ 2 M NH_3 in MeOH (1:1, 200 mL). The relevant fractions were combined and concentrated under reduced pressure to afford the title compound (9.90 g, 27.8 mmol, 75% yield) as a pale yellow oil. LCMS (Method B): 1.41 min, $[M+H]^+$ 356 m/z. Chiral HPLC analysis (10% EtOH in heptane, Chiralcel OD-H column (4.6 mm x 25 cm), flow rate: 1 mL/min): 72% e.e. ^{1}H NMR (400 MHz, DMSO-d$_6$) δ = 7.27 (d, *J* = 5.0 Hz, 1H), 7.15 (t, *J* = 7.6 Hz, 1H), 7.03 (d, *J* = 7.8 Hz, 1H), 7.00 (s, 1H), 6.88 (d, *J* = 7.8 Hz, 1H), 6.80 (d, *J* = 5.0 Hz, 1H), 3.68 (d, *J* = 14.9 Hz, 1H), 3.58 (d, *J* = 14.9 Hz, 1H), 3.41-3.39 (m, 3H), 3.34 (s, 1H), 2.85 - 2.75 (m, 2H), 2.72 - 2.52 (m, 6H), 1.93 - 1.81 (m, 1H), 0.96 - 0.89 (m, 2H), 0.68 - 0.62 (m, 2H) ppm.

Methyl 3-(3-cyclopropylphenyl)-4-(4,5-dihydrothieno[2,3-*c*]pyridin-6(7*H*)-yl)butanoate (127a, enantiomer 1) and **methyl 3-(3-cyclopropylphenyl)-4-(4,5-dihydrothieno[2,3-*c*]pyridin-6(7*H*)-yl)butanoate (127b, enantiomer 2)**
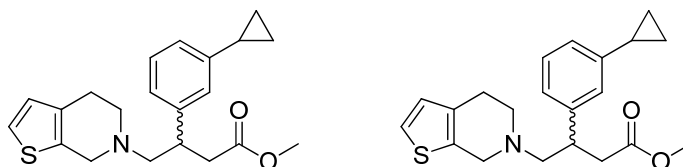
Methyl 3-(3-cyclopropylphenyl)-4-(2-((5,6,7,8-tetrahydro-1,8-naphthyridin-2-yl)methyl)-6,7-dihydrothieno[2,3-*c*]pyridin-5(4*H*)-yl)butanoate (**151**) (9.90 g, 27.8 mmol) was dissolved in EtOH (50 mL) and heptane (50 mL) and purified by chiral HPLC chromatography (100 x 1 mL injections, 10% EtOH in heptane, Chiralcel OD-H column (30 mm x 25 cm), flow rate: 25 mL/min). The relevant fractions were combined and concentrated under reduced pressure to afford methyl 3-(3-

Christopher J Tame

cyclopropylphenyl)-4-(2-((5,6,7,8-tetrahydro-1,8-naphthyridin-2-yl)methyl)-6,7-dihydrothieno[2,3-*c*]pyridin-5(4*H*)-yl)butanoate (**127a**, **enantiomer 1** (8.0 – 9.0 min): 1.00 g, 2.81 mmol, 10% yield, >99% e.e.) and methyl 3-(3-cyclopropylphenyl)-4-(2-((5,6,7,8-tetrahydro-1,8-naphthyridin-2-yl)methyl)-6,7-dihydrothieno[2,3-*c*]pyridin-5(4*H*)-yl)butanoate (**127b**, **enantiomer 2** (9.0 – 12.0 min): 7.75 g, 21.8 mmol, 78% yield, >99% e.e.) as yellow oils. Enantiomeric excess was determined using chiral HPLC analysis (10% EtOH in heptane, Chiralcel OD-H column (4.6 mm x 25 cm), flow rate: 1 mL/min). No further analysis was undertaken.

tert-Butyl 7-((6-(2-(3-cyclopropylphenyl)-4-methoxy-4-oxobutyl)-4,5,6,7-tetrahydrothieno[2,3-*c*]pyridin-2-yl)methyl)-3,4-dihydro-1,8-naphthyridine-1(2*H*)-carboxylate (129b)
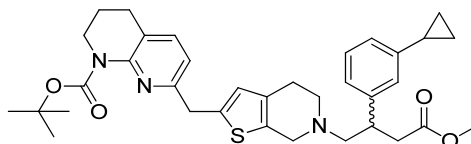
(1,5-Cyclooctadiene)(methoxy)iridium(I) dimer (220 mg, 330 µmol) and 4,4'-di-*tert*-butyl-2,2'-bipyridine (180 mg, 650 µmol) were charged to a 1.0 L round bottomed flask and degassed with three alternative applications of vacuum and nitrogen. Degassed cyclohexane (50 mL), degassed 4,4,5,5-tetramethyl-1,3,2-dioxaborolane (4.74 mL, 32.7 mmol) and a degassed solution of methyl 3-(3-cyclopropylphenyl)-4-(4,5-dihydrothieno[2,3-*c*]pyridin-6(7*H*)-yl)butanoate (7.75 g, 21.8 mmol) in cyclohexane (20 mL) was added dropwise sequentially at room temperature under nitrogen. The mixture was stirred at 20 ºC for 3 h. To the mixture was added a degassed mixture of chloro(2-dicyclohexylphosphino-2′,4′,6′-triisopropyl-1,1′-biphenyl)[2-(2′-amino-1,1′-biphenyl)]palladium(II) (1.72 g, 2.18 mmol) and *tert*-butyl 7-(bromomethyl)-3,4-dihydro-1,8-naphthyridine-1(2*H*)-carboxylate (7.13 g, 21.8 mmol) in THF (45 mL), and degassed aqueous potassium phosphate solution (500 mM, 58.0 mL, 29.0 mmol) sequentially in a dropwise fashion at room temperature. The resulting solution was stirred at room temperature under nitrogen

Christopher J Tame

for 16 h. Brine (200 mL) and EtOAc (200 mL) was added and the separated organic phase was washed twice with brine (2 x 200 mL). The combined aqueous phase was extracted with EtOAc (200 mL) and the combined organic phase was dried over MgSO$_4$, filtered and concentrated under reduced pressure to afford a red oil. The oil was loaded in minimal CH$_2$Cl$_2$ onto a silica pre-packed column (330 g) and eluted with 0-25% EtOAc in cyclohexane over 40 min. The relevant fractions were combined and concentrated under reduced pressure to afford the desired product (5.21 g, 6.93 mmol, 40% yield) as an orange gum. LCMS (Method A): 0.86 min, [M+H]$^+$ 302 m/z. ^{1}H NMR (400 MHz, CDCl$_3$) δ = 7.31 (d, J = 7.8 Hz, 1H), 7.20 (t, J = 7.6 Hz, 1H), 7.01 (d, J = 7.3 Hz, 1H), 6.96 (s, 1H), 6.92 (d, J = 7.6 Hz, 1H), 6.86 (d, J = 7.6 Hz, 1H), 6.56 (s, 1H), 4.18 (s, 2H), 3.78 (t, J = 5.9 Hz, 2H), 3.73 (d, J = 15.1 Hz, 1H), 3.58 (d, J = 14.6 Hz, 1H), 3.51 (s, 3H), 3.44 (t, J = 7.3 Hz, 1H), 2.90 (dd, J = 15.9, 6.8 Hz, 2H), 2.74 (t, J = 6.8 Hz, 2H), 2.68 (d, J = 7.8 Hz, 2H), 2.63 (br. s., 3H), 2.57 (dd, J = 15.2, 7.4 Hz, 1H), 1.98 - 1.91 (m, 2H), 1.91 - 1.85 (m, 1H), 1.52 (s, 9H), 1.00 - 0.93 (m, 2H), 0.74 - 0.66 (m, 2H) ppm. ^{13}C NMR (101 MHz, CDCl$_3$) δ = 173.2, 156.3, 154.1, 151.0, 144.1, 142.7, 138.9, 137.4, 133.3, 131.9, 128.4, 125.7, 125.1, 124.3, 123.8, 122.2, 118.0, 80.8, 63.3, 52.1, 51.2, 50.7, 44.7, 40.3, 39.3, 38.5, 26.3, 25.4, 23.2, 15.4, 9.2 ppm.

1C missing from ^{13}C NMR.

Christopher J Tame

3-(3-Cyclopropylphenyl)-4-(2-((5,6,7,8-tetrahydro-1,8-naphthyridin-2-yl)methyl)-4,5-dihydrothieno[2,3-*c*]pyridin-6(7*H*)-yl)butanoic acid (85b)
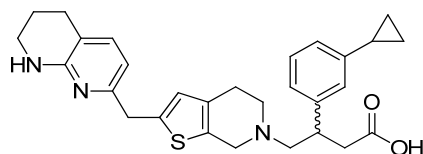
To a stirred solution of *tert*-butyl 7-(((6-(2-(3-cyclopropylphenyl)-4-methoxy-4-oxobutyl)-4,5,6,7-tetrahydrothieno[2,3-*c*]pyridin-2-yl)methyl)-3,4-dihydro-1,8-naphthyridine-1(2*H*)-carboxylate (5.21 g, 8.66 mmol) in MeOH (25 mL) at room temperature was added a solution of HCl in 1,4-dioxane (4.0 M, 11 mL, 43 mmol) dropwise and the mixture was stirred at 50 ºC for 2 h. The mixture was then loaded directly onto an 70 g aminopropyl silica pre-packed cartridge and eluted with MeOH (100 mL). The filtrate was concentrated under reduced pressure to afford a crude gum. To a solution of the gum in MeCN (15 mL) was added aqueous NaOH solution (2.0 M, 22 mL, 43 mmol) dropwise at room temperature and the mixture was stirred at 50 ºC for 2 h.   The mixture was cooled to room temperature, then neutralised with aqueous HCl solution (2 M). The solution was then loaded directly onto a 70 g SCX silica pre-packed cartridge and eluted with aqueous MeCN solution (50% v/v, 200 mL) and a solution of ammonium hydroxide solution (28-30% NH₃ basis) in MeCN (10% v/v, 200 mL). The relevant fractions were combined and concentrated under reduced pressure to afford a crude gum. The gum was dissolved in water (200 mL) and CH_2Cl_2 (200 mL) and the separated aqueous phase was extracted twice with EtOAc (2 x 200 mL).   The combined organic phase was filtered through a hydrophobic frit and the filtrate was concentrated under reduced pressure to afford a crude gum. The gum was loaded in minimal CH_2Cl_2 onto a 100 g silica pre-packed column and eluted with EtOAc (200 mL), CH_2Cl_2 (200 mL) and an aqueous MeCN solution (10% v/v, 200 mL). The relevant fractions were combined and concentrated under reduced pressure to afford the desired product (750 mg, 1.54 mmol, 18% yield) as an orange solid. m.p. = 200.1 °C. IR (solid) 3250 (N-H stretch); 2900 (C-H sp³ stretch); 2800 ([N-H]⁺ stretch); 1600, 1450 (O-C-O⁻ stretch) cm⁻¹.   LCMS

Christopher J Tame

(Method B): 0.91 min, [M+H]$^+$ 488 m/z. ^{1}H NMR (400 MHz, CDCl$_3$) δ = 7.19 (t, J = 7.6 Hz, 1H), 7.11 (d, J = 7.3 Hz, 1H), 6.99 (d, J = 7.6 Hz, 1H), 6.95 (s, 1H), 6.91 (d, J = 7.6 Hz, 1H), 6.57 (s, 1H), 6.33 (d, J = 7.3 Hz, 1H), 3.98 (s, 2H), 3.84 (d, J = 14.9 Hz, 1H), 3.77 (d, J = 14.9 Hz, 1H), 3.43 - 3.35 (m, 3H), 3.07 - 3.00 (m, 1H), 2.95 - 2.89 (m, 1H), 2.86 (d, J = 7.3 Hz, 2H), 2.81 (dd, J = 12.5, 6.2 Hz, 1H), 2.77 (d, J = 4.5 Hz, 1H), 2.73 (d, J=4.3 Hz, 1H), 2.71 - 2.64 (m, 3H), 1.93 - 1.82 (m, 3H), 0.95 (ddd, J = 6.8, 4.5, 2.0 Hz, 2H), 0.69 (ddd, J = 6.3, 4.5, 2.0 Hz, 2H) ppm. ^{13}C NMR (101 MHz, CDCl$_3$) δ = 176.4, 155.1, 153.3, 144.4, 143.2, 139.3, 137.7, 132.9, 130.1, 128.6, 125.6, 125.0, 124.1, 123.8, 115.3, 110.5, 63.6, 51.8, 50.3, 43.2, 41.2, 39.6, 36.3, 26.3, 24.4, 20.8, 15.4, 9.2 ppm. HRMS (ESI) calc'd for C$_{29}$H$_{34}$N$_3$O$_2$S [M+H]$^+$ 488.2372, found 488.2374.

2H missing from ^{1}H NMR spectrum (exchangeable). Optical rotation could not be obtained due to the coloured nature of the isolated product.

(*E*)-Methyl 4-(6,7-dihydrofuro[3,2-*c*]pyridin-5(4*H*)-yl)but-2-enoate (131)
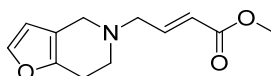
To a stirred solution of 4,5,6,7-tetrahydrofuro[3,2-*c*]pyridine, hydrochloride (250 mg, 1.49 mmol) and triethylamine (620 µL, 4.46 mmol) in CH$_2$Cl$_2$ (15 mL) was added (*E*)-methyl 4-bromobut-2-enoate (210 µL, 1.79 mmol) dropwise at room temperature under nitrogen. The mixture was stirred at room temperature for 1 h, then water (50 mL) and CH$_2$Cl$_2$ (50 mL) was added and the separated organic phase was washed twice with water (2 x 50 mL). The combined organic phase was filtered through a hydrophobic frit and the filtrate was concentrated under reduced pressure to afford the desired product (323 mg, 1.24 mmol, 83% yield) as an orange oil. LCMS (Method B): 0.87 min, [M+H]$^+$ 222 m/z. ^{1}H NMR (400 MHz, DMSO-d$_6$) δ = 7.44 (s, 1H), 6.88 (dt, J = 15.9, 5.8 Hz, 1H), 6.28 (s, 1H), 6.06 (dt, J = 15.9, 1.5 Hz, 1H), 3.67 (s, 3H), 3.38 - 3.27 (m, 4H), 2.74 (t, J = 5.8 Hz, 2H), 2.63 (t, J = 5.5 Hz, 2H) ppm.

Christopher J Tame

Methyl 3-(3-cyclopropylphenyl)-4-(6,7-dihydrofuro[3,2-*c*]pyridin-5(4*H*)-yl)butanoate (132)
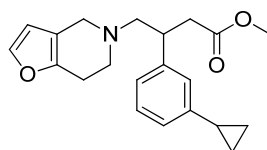
To a stirred solution of (3-cyclopropylphenyl)boronic acid (597 mg, 3.69 mmol) and (*E*)-methyl 4-(6,7-dihydrofuro[3,2-*c*]pyridin-5(4*H*)-yl)but-2-enoate (320 mg, 1.23 mmol) in 1,4-dioxane (12 mL) was added aqueous potassium hydroxide solution (3.8 M, 0.65 mL, 2.5 mmol) and chloro(1,5-cyclooctadiene)rhodium(II) dimer (182 mg, 0.370 mmol) sequentially and the solution was degassed with 3 alternative applications vacuum and nitrogen. The solution was then heated and stirred under reflux at 95 ºC for 1 h. The reaction mixture was cooled to room temperature, loaded directly onto an SCX pre-packed silica cartridge (20 g) and eluted with MeOH (40 mL) and a solution of NH_3 in MeOH (40 mL). The relevant fractions were concentrated under reduced pressure to afford an orange gum. The gum was loaded in minimal CH_2Cl_2 onto a silica pre-packed column (20 g) and eluted with 0-100% EtOAc in cyclohexane over 60 min. The relevant fractions were combined and concentrated under reduced pressure to afford the desired product (219 mg, 650 µmol, 53% yield) as a pale yellow oil. LCMS (Method B): 1.36 min, $[M+H]^+$ 340 m/z. ^{1}H NMR (600 MHz, DMSO-d₆) δ = 7.42 (d, *J* = 1.5 Hz, 1H), 7.15 (t, *J* = 7.7 Hz, 1H), 7.01 (d, *J* = 7.7 Hz, 1H), 6.98 (s, 1H), 6.87 (d, *J* = 7.7 Hz, 1H), 6.28 (d, *J* = 1.5 Hz, 1H), 3.41 (s, 3H), 3.38 (d, *J* = 13.9 Hz, 1H), 3.35 - 3.29 (m, 1H), 2.86 - 2.75 (m, 2H), 2.71 - 2.62 (m, 2H), 2.60 - 2.55 (m, 3H), 2.55 - 2.47 (m, 2H), 1.87 (s, 1H), 0.92 (ddd, *J* = 8.4, 4.4, 2.4 Hz, 2H), 0.68 - 0.61 (m, 2H) ppm.

Christopher J Tame

***tert*-Butyl 7-((5-(2-(3-cyclopropylphenyl)-4-methoxy-4-oxobutyl)-4,5,6,7-tetrahydrofuro[3,2-*c*]pyridin-2-yl)methyl)-3,4-dihydro-1,8-naphthyridine-1(2*H*)-carboxylate (133)**
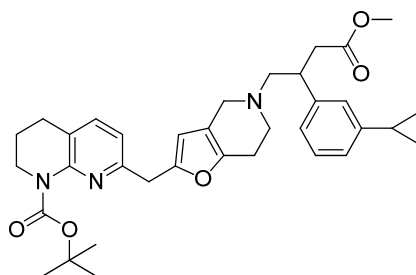
To a nitrogen-degassed mixture of (1,5-cyclooctadiene)(methoxy)iridium(I) dimer (3 mg, 0.005 mmol) and 4,4'-di-*tert*-butyl-2,2'-bipyridine (8 mg, 0.03 mmol) in cyclohexane (0.5 mL) was added a nitrogen-degassed solution of 4,4,5,5-tetramethyl-1,3,2-dioxaborolane (50 μL, 0.35 mmol) and methyl 3-(3-cyclopropylphenyl)-4-(6,7-dihydrofuro[3,2-*c*]pyridin-5(4*H*)-yl)butanoate (100 mg, 270 μmol) in cyclohexane (1 mL) dropwise at room temperature under nitrogen. The mixture was stirred at 20 ºC for 16 h. To the mixture was added a nitrogen-degassed mixture of chloro(2-dicyclohexylphosphino-2′,4′,6′-triisopropyl-1,1′-biphenyl)[2-(2′-amino-1,1′-biphenyl)]palladium(II) (22 mg, 30 μmol) and *tert*-butyl 7-(bromomethyl)-3,4-dihydro-1,8-naphthyridine-1(2*H*)-carboxylate (63 mg, 0.19 mmol) in THF (1.5 mL) dropwise, followed by aqueous potassium phosphate solution (500 mM, 730 μL, 360 μmol) dropwise, sequentially at room temperature under nitrogen. The resulting solution was stirred at room temperature under nitrogen for 2 h. The mixture was loaded directly onto an SCX pre-packed silica cartridge (20 g) and eluted with MeOH (40 mL) and a solution of NH₃ in MeOH (2.0 M, 40 mL) sequentially. The relevant fractions were combined and concentrated under reduced pressure to afford a crude gum. The gum was loaded in minimal CH₂Cl₂ onto a silica pre-packed column (20 g) and eluted with 0-25% EtOAc in cyclohexane over 60 min. The relevant fractions were combined and concentrated under reduced pressure to afford the desired product (51.3 mg, 90.0 μmol, 32% yield) as a pale yellow gum. LCMS (Method B): 1.53 min, [M+H]⁺ 586 m/z. ¹H NMR (600 MHz, DMSO-d₆) δ = 7.43 (d, *J* = 7.7 Hz, 1H), 7.13 (t, *J* = 7.7 Hz, 1H), 7.00 (d, *J* = 7.7 Hz, 1H), 6.96 (s, 1H), 6.90 - 6.84 (m, 2H), 5.97 (s, 1H), 3.93 - 3.90

(m, 2H), 3.63 - 3.59 (m, 2H), 3.42 (s, 3H), 3.35 - 3.31 (m, 1H), 3.28 - 3.26 (m, 1H), 3.25 - 3.21 (m, 1H), 2.82 - 2.75 (m, 2H), 2.70 - 2.67 (m, 2H), 2.66 - 2.60 (m, 2H), 2.56 - 2.51 (m, 2H), 2.50 - 2.46 (m, 2H), 1.89 - 1.84 (m, 1H), 1.84 - 1.78 (m, 2H), 1.39 (s, 9H), 0.93 - 0.89 (m, 2H), 0.67 - 0.61 (m, 2H) ppm.

Christopher J Tame

tert-Butyl 7-((5-(2-(3-cyclopropylphenyl)-4-methoxy-4-oxobutyl)-4,5,6,7-tetrahydrofuro[3,2-*c*]pyridin-2-yl)methyl)-3,4-dihydro-1,8-naphthyridine-1(2*H*)-carboxylate (133) Rotating Frame Nuclear Overhauser Effect (ROESY) ¹H NMR spectroscopy. Irradiated at 5.98 ppm.

Christopher J Tame
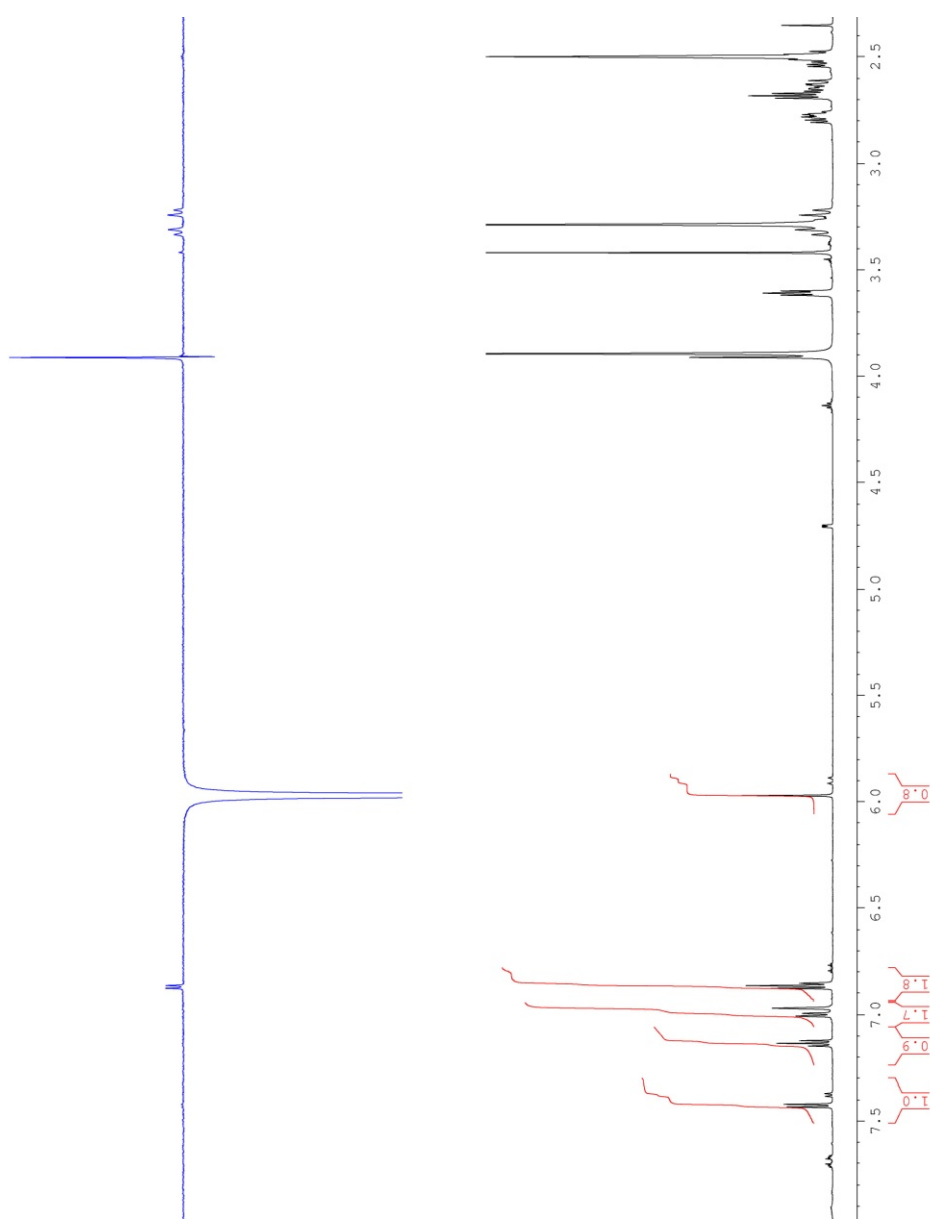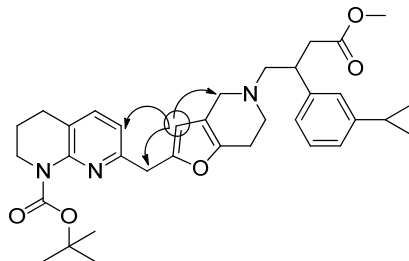
3-(3-Cyclopropylphenyl)-4-(2-((5,6,7,8-tetrahydro-1,8-naphthyridin-2-yl)methyl)-6,7-dihydrofuro[3,2-*c*]pyridin-5(4*H*)-yl)butanoic acid (86)
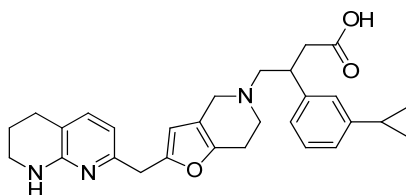
To a stirred solution of *tert*-butyl 7-((5-(2-(3-cyclopropylphenyl)-4-methoxy-4-oxobutyl)-4,5,6,7-tetrahydrofuro[3,2-*c*]pyridin-2-yl)methyl)-3,4-dihydro-1,8-naphthyridine-1(2*H*)-carboxylate (50 mg, 90 μmol) in MeOH (0.5 mL) was added a solution of HCl, 1,4-dioxane (4.0 M, 0.11 mL, 0.43 mmol) dropwise at room temperature and the mixture was stirred at 50 ºC for 2 h. The mixture was then loaded directly onto an aminopropyl pre-packed silica cartridge (20 g) and eluted with MeOH (40 mL). The filtrate was concentrated under reduced pressure to afford a crude orange solid. To a solution of the crude solid in MeCN (0.5 mL) was added aqueous NaOH solution (2.0 M, 0.21 mL, 0.43 mmol) dropwise at room temperature and the mixture was stirred at 50 ºC for 2 h. The mixture was purified directly *via* mass-directed auto-preparative (MDAP) chromatography using a Sunfire C18 column and an ammonium bicarbonate-modified MeCN/water gradient.   The relevant fractions were combined and concentrated under a stream of nitrogen to afford a crude gum. The gum was loaded in DMSO (1 mL) and purified *via* mass-directed auto-preparative (MDAP) chromatography using a Sunfire C18 column and a formic acid-modified MeCN/water gradient. The relevant fractions were combined and concentrated under a stream of nitrogen to afford the desired product (28.3 mg, 50.0 μmol, 53% yield) as a white solid. m.p. 139-140 °C. LCMS (Method B): 0.93 min, $[M+H]^+$ 472 m/z. IR (solid) 3300 (N-H stretch), 2923 (sp^3 C-H stretch), 2852 (N-H$^+$ stretch), 1601, 1460 (O-C-O$^-$ stretch) cm^{-1}. ^{1}H NMR (600 MHz, CDCl$_3$) δ = 7.25 (d, *J* = 7.3 Hz, 1H), 7.22 - 7.12 (m, 2H), 6.94 (d, *J* = 7.7 Hz, 1H), 6.93 - 6.89 (m, 2H), 6.35 (d, *J* = 7.3 Hz, 1H), 6.00 (s, 1H), 3.88 (s, 2H), 3.73 - 3.68 (m, 1H), 3.62 (d, *J* = 13.9 Hz, 1H), 3.41 (t, *J* = 5.5 Hz, 2H), 2.94 - 2.87 (m, 4H), 2.83 (dd, *J* = 16.1, 2.9 Hz, 2H), 2.70 (t, *J* = 6.1 Hz, 2H), 1.94 - 1.84 (m, 3H), 1.73 - 1.70 (m, 1H),

Christopher J Tame

1.70 - 1.65 (m, 2H), 0.99 - 0.93 (m, 2H), 0.71 - 0.65 (m, 2H) ppm. ^{13}C NMR (151 MHz, CDCl$_3$) δ 175.1, 144.7, 142.7, 137.9, 137.9, 129.0, 128.8, 128.2, 125.3, 124.7, 124.1, 123.8, 114.4, 110.9, 106.1, 69.1, 64.0, 63.8, 44.1, 41.3, 39.2, 26.2, 25.3, 22.3, 21.4, 20.7, 15.4, 9.2 ppm. HRMS (ESI) calc'd for C$_{29}$H$_{34}$N$_3$O$_3$ [M+H]$^+$ 472.2595, found 472.2578.

Note: 1H missing from ^{1}H NMR (exchangeable).

(*E*)-methyl 4-(6,7-dihydrothiazolo[5,4-*c*]pyridin-5(4*H*)-yl)but-2-enoate (135)
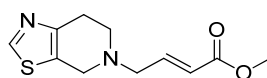
To a stirred solution of 4,5,6,7-tetrahydrothiazolo[5,4-*c*]pyridine, hydrochloride (880 mg, 4.73 mmol) and DIPEA (2.5 mL, 14 mmol) in CH$_2$Cl$_2$ (45 mL) at room temperature under nitrogen was added (*E*)-methyl 4-bromobut-2-enoate (850 µL, 7.10 mmol) dropwise and the mixture was stirred at room temperature for 1 h. Water (50 mL) and CH$_2$Cl$_2$ (50 mL) was added and the separated organic phase was washed twice with water (2 x 50 mL). The combined organic phase was passed through a hydrophobic frit and the filtrate was concentrated under reduced pressure to afford a crude gum. The gum was loaded in minimal CH$_2$Cl$_2$ onto a silica pre-packed column (100 g) and eluted with 0-100% EtOAc in cyclohexane over 60 min. The appropriate fractions were combined and concentrated to afford the desired (380 mg, 1.60 mmol, 34% yield) as an orange gum. LCMS (Method B): 0.71 min, [M+H]$^+$ 239 m/z. ^{1}H NMR (400 MHz, DMSO-d$_6$) δ = 8.90 (s, 1H), 6.89 (dt, *J* = 15.9, 5.8 Hz, 1H), 6.08 (dt, *J* = 15.9, 1.5 Hz, 1H), 3.72 (s, 2H), 3.67 (s, 2H), 3.37 (dd, *J* = 5.9, 1.6 Hz, 2H), 3.17 (d, *J* = 5.0 Hz, 2H), 2.81 (s, 3H) ppm.

Christopher J Tame

Methyl 3-(3-cyclopropylphenyl)-4-(6,7-dihydrothiazolo[5,4-*c*]pyridin-5(4*H*)-yl)butanoate (136)
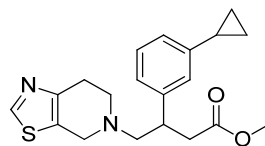
To a degassed solution of (3-cyclopropylphenyl)boronic acid (700 mg, 4.31 mmol) and (*E*)-methyl 4-(6,7-dihydrothiazolo[5,4-*c*]pyridin-5(4*H*)-yl)but-2-enoate (380 mg, 1.44 mmol) in 1,4-dioxane (14 mL) was added aqueous potassium hydroxide solution (3.8 M, 0.76 mL, 2.9 mmol) and chloro(1,5-cyclooctadiene)rhodium(II) dimer (210 mg, 430 μmol) sequentially and the solution was further degassed with 3 alternative applications vacuum and nitrogen. The solution was then heated and stirred under reflux at 95 ºC for 45 min. The reaction mixture was concentrated under reduced pressure to afford a brown gum. The gum was dissolved in CH$_2$Cl$_2$ (100 mL) and was washed three times with water (3 x 100 mL). The combined organic fractions were passed through a hydrophobic frit and the filtrate was concentrated under reduced pressure to afford a brown gum. The gum was loaded in minimal CH$_2$Cl$_2$ onto a silica pre-packed column (100 g) and eluted with 0-15% MeOH in CH$_2$Cl$_2$ over 60 min. The appropriate fractions were combined and concentrated to afford the desired product (450 mg, 1.26 mmol, 88 % yield) as a brown gum. LCMS (Method B): 1.21 min, [M+H]$^+$ 357 m/z. ^{1}H NMR (400 MHz, DMSO-d$_6$) δ = 8.88 (s, 1H), 7.18 - 7.11 (t, *J* = 7.6 Hz, 1H), 7.02 (d, *J* = 7.8 Hz, 1H), 6.99 (s, 1H), 6.87 (d, *J* = 7.8 Hz, 1H), 3.75 (d, *J* = 15.1 Hz, 1H), 3.68 (d, *J* = 15.1 Hz, 1H), 3.39 (s, 3H), 3.37 - 3.30 (m, 1H), 2.92 - 2.84 (m, 1H), 2.84 - 2.80 (m, 1H), 2.80 - 2.72 (m, 3H), 2.74 - 2.65 (m, 1H), 2.63 - 2.59 (m, 1H), 2.55 - 2.52 (m, 1H), 1.93 - 1.80 (m, 1H), 0.99 - 0.86 (m, 2H), 0.65 (m, 2H) ppm.

Christopher J Tame

Attempted synthesis of **_tert_-butyl 7-((5-(2-(3-cyclopropylphenyl)-4-methoxy-4-oxobutyl)-4,5,6,7-tetrahydrothiazolo[5,4-_c_]pyridin-2-yl)methyl)-3,4-dihydro-1,8-naphthyridine-1(2_H_)-carboxylate (154)**

(1,5-Cyclooctadiene)(methoxy)iridium(I) dimer (1.3 mg, 2.0 µmol) and 4,4'-di-_tert_-butyl-2,2'-bipyridine (1.1 mg, 4.0 µmol) were charged to a 25 mL round bottomed flask and degassed with three alternative applications of vacuum and nitrogen. Degassed cyclohexane (1 mL), degassed 4,4,5,5-tetramethyl-1,3,2-dioxaborolane (20 µL, 0.15 mmol) and a degassed mixture of methyl 3-(3-cyclopropylphenyl)-4-(6,7-dihydrothiazolo[5,4-_c_]pyridin-5(4_H_)-yl)butanoate (50 mg, 0.13 mmol) and CH$_2$Cl$_2$ (0.1 mL) was added dropwise, sequentially at room temperature under nitrogen. The mixture was stirred at 20 ºC for 3 h. LCMS analysis could not identify the desired boronate intermediate. A degassed mixture of chloro(2-dicyclohexylphosphino-2′,4′,6′-triisopropyl-1,1′-biphenyl)[2-(2′-amino-1,1′-biphenyl)]palladium(II) (10.5 mg, 13 µmol) and _tert_-butyl 7-(bromomethyl)-3,4-dihydro-1,8-naphthyridine-1(2_H_)-carboxylate (31 mg, 90 mmol) in THF (0.5 mL) was added dropwise at room temperature, followed by the addition of degassed aqueous potassium phosphate solution (500 mM 350 µL, 180 µmol) dropwise at room temperature. The resulting solution was stirred at room temperature under nitrogen for 16 h. LCMS analysis could not identify the desired product.

Christopher J Tame

tert-Butyl 7-(hydroxymethyl)-3,4-dihydro-1,8-naphthyridine-1(2_H_)-carboxylate (142)

To a stirred mixture of 1,1-dimethylethyl 7-formyl-3,4-dihydro-1,8-naphthyridine-1(2*H*)-carboxylate (21.5 g, 82.0 mmol) in THF (100 mL) was added sodium borohydride (3.41 g, 90.0 mmol) portionwise at 0 ºC under nitrogen and the mixture was stirred at 0 ºC for 1 h. To the mixture was added water (100 mL), brine (30 mL) and EtOAc (100 mL) and the separated aqueous phase was extracted twice with EtOAc (2 x 100 mL). The combined organic phase was passed through a hydrophobic frit and the filtrate was concentrated under reduced pressure to afford a crude solid. The solid was loaded in minimal CH_2Cl_2 onto a silica pre-packed column (750 g) and eluted with 0-100% EtOAc in cyclohexane over 60 min. The relevant fractions were combined and concentrated under reduced pressure to afford the desired product (21.4 g, 73.0 mmol, 89% yield) as a white powder. LCMS (Method B): 0.85 min, $[M+H]^+$ 265 m/z. ^{1}H NMR (400 MHz, DMSO-d$_6$) δ = 7.49 (d, *J* = 7.6 Hz, 1H), 7.09 (d, *J* = 7.6 Hz, 1H), 5.25 (t, *J* = 5.8 Hz, 1H), 4.45 (d, *J* = 5.8 Hz, 2H), 3.62 (t, *J* = 6.0 Hz, 2H), 2.70 (t, *J* = 6.5 Hz, 2H), 1.82 (quin, *J* = 6.5 Hz, 2H), 1.43 (s, 9H) ppm.

tert-Butyl 7-(((methoxycarbonyl)oxy)methyl)-3,4-dihydro-1,8-naphthyridine-1(2H)-carboxylate (144)
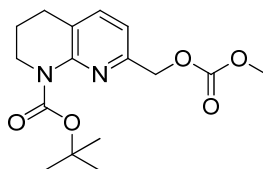
Tetrabutylammonium bisulfate (5 mg, 0.02 mmol) was charged to a 20 mL round bottomed flask and degassed using alternative applications of vacuum and nitrogen.

Christopher J Tame

A solution of *tert*-butyl 7-(hydroxymethyl)-3,4-dihydro-1,8-naphthyridine-1(2*H*)-carboxylate (200 mg, 760 µmol) and methyl chloroformate (97 µL, 1.3 mmol) in CH$_2$Cl$_2$ (600 µL) was added dropwise at room temperature. The flask was cooled to 0 ºC and aqueous NaOH solution (7.5 M, 0.33 mL, 2.4 mmol) was added dropwise. The mixture was stirred at 0 ºC for 30 min, then poured into water (50 mL) and extracted three times with CH$_2$Cl$_2$ (3 x 50 mL). The combined organic phase was filtered through a hydrophobic frit and the filtrate was concentrated under reduced pressure to afford a crude gum. The gum was loaded in minimal CH$_2$Cl$_2$ onto a 20 g silica pre-packed column, eluting with 0-100% EtOAc in cyclohexane over 60 min. The relevant fractions were combined and concentrated under a stream of nitrogen to afford the desired product (126 mg, 390 µmol, 52% yield) as a white solid. LCMS (Method B): 1.07 min, [M+H]$^+$ 323 m/z. ^{1}H NMR (400 MHz, CDCl$_3$) δ = 7.41 (d, *J* = 7.6 Hz, 1H), 7.05 (d, *J* = 7.6 Hz, 1H), 5.22 (s, 2H), 3.84 (s, 3H), 3.82 - 3.74 (t, *J* = 5.9 Hz, 2H), 2.77 (t, *J* = 6.6 Hz, 2H), 1.94 (quin, *J* = 6.4 Hz, 2H), 1.54 (s, 9H) ppm.

Attempted synthesis of ***tert*-butyl 7-((5-(2-(3-cyclopropylphenyl)-4-methoxy-4-oxobutyl)-4,5,6,7-tetrahydrothiazolo[5,4-*c*]pyridin-2-yl)methyl)-3,4-dihydro-1,8-naphthyridine-1(2*H*)-carboxylate (138)**
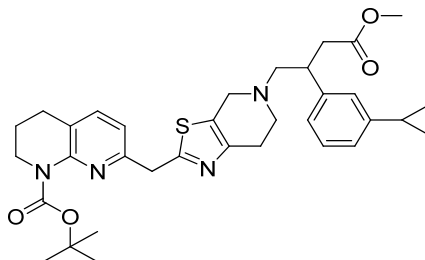
Methyl 3-(3-cyclopropylphenyl)-4-(6,7-dihydrothiazolo[5,4-*c*]pyridin-5(4*H*)-yl)butanoate (50 mg, 0.14 mmol), *tert*-butyl 7-(((methoxycarbonyl)oxy)methyl)-3,4-dihydro-1,8-naphthyridine-1(2*H*)-carboxylate (125 mg, 390 µmol), 1,3-Bis(diphenylphosphino)propane (dppp) (3 mg, 0.07 mmol), tris(dibenylideneacetone)dipalladium(0) (4 mg, 4 µmol) and potassium fluoride (17 mg, 0.29 mmol) in anhydrous DMSO (1.5 mL) were degassed with a stream of

Christopher J Tame

nitrogen for 30 min. The mixture was then heated at 120 ºC for 3 h. LCMS analysis could not identify the desired product.

tert-Butyl 7-(2-amino-2-oxoethyl)-3,4-dihydro-1,8-naphthyridine-1(2*H*)-carboxylate (149)
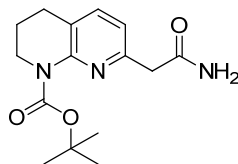
A sealed solution of *tert*-butyl 7-(2-methoxy-2-oxoethyl)-3,4-dihydro-1,8-naphthyridine-1(2*H*)-carboxylate (20.0 g, 65.3 mmol) in a solution of ammonia in MeOH (7.0 M, 0.30 L, 2.1 mol) was stirred at room temperature for 16 h, then concentrated under reduced pressure to afford the desired product (19.0 g, 65.2 mmol, 100% yield) as a yellow oil, which crystallised over time to give a pale yellow solid. LCMS (Method B): 0.85 min, $[M+H]^+$ 292 m/z. ^{1}H NMR (400 MHz, DMSO-d_6) δ = 7.69 (br. s, 1H), 7.45 (d, J = 7.6 Hz, 1H), 6.96 (d, J = 7.6 Hz, 1H), 6.93 (br. s, 1H), 4.16 (br. s, 2H), 3.65 (d, J = 6.0 Hz, 2H), 2.70 (t, J = 6.3 Hz, 2H), 1.83 (quin, J = 6.5 Hz, 2H), 1.45 (s, 9H) ppm.

tert-Butyl 7-(2-amino-2-thioxoethyl)-3,4-dihydro-1,8-naphthyridine-1(2*H*)-carboxylate (150)
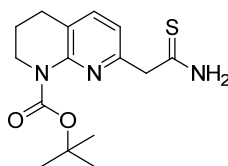
Method 1

To a stirred solution of *tert*-butyl 7-(2-amino-2-oxoethyl)-3,4-dihydro-1,8-naphthyridine-1(2*H*)-carboxylate (180 mg, 620 µmol) in THF (1 mL) at room temperature under nitrogen was added Lawesson's reagent (150 mg, 370 µmol) and the mixture was stirred at reflux for 2 h. LCMS (Method B) of the crude reaction mixture identified the Boc-deprotected analogue of the product 0.71 min, $[M+H]^+$

208 m/z, along with a range of unidentifiable impurities. No further investigation was undertaken.

Method 2

To a stirred solution of *tert*-butyl 7-(2-amino-2-oxoethyl)-3,4-dihydro-1,8-naphthyridine-1(2*H*)-carboxylate (515 mg, 1.77 mmol) in 1,4-dioxane (3.5 mL) was added Lawesson's reagent (357 mg, 880 μmol) and the mixture was stirred at room temperature under nitrogen for 16 h. The mixture was concentrated under reduced pressure to afford a crude orange solid. The solid was dissolved in EtOAc (50 mL) and brine (50 mL) and the separated aqueous phase was extracted twice with EtOAc (2 x 50 mL). The combined organic phase was passed through a hydrophobic frit and the filtrate was concentrated under reduced pressure to afford an orange solid. The solid was loaded in minimal CH_2Cl_2 onto a silica pre-packed column (100 g) and eluted with 0-100% EtOAc in cyclohexane over 60 min. The relevant fractions were combined and concentrated under reduced pressure to afford the desired product (200 mg, 650 μmol, 37% yield) as a yellow solid. LCMS (Method B): 1.06 min, [M+H]$^+$ 308 m/z. ^{1}H NMR (400 MHz, DMSO-d$_6$) δ = 9.75 - 9.54 (m, 2H), 7.48 (d, *J* = 7.6 Hz, 1H), 7.01 (d, *J* = 7.6 Hz, 1H), 3.94 (s, 2H), 3.73 - 3.62 (m, 2H), 2.76 - 2.63 (m, 2H), 1.89 - 1.74 (m, 2H), 1.46 (s, 9H) ppm.

Christopher J Tame

***tert*-Butyl 2-((5,6,7,8-tetrahydro-1,8-naphthyridin-2-yl)methyl)-6,7-dihydrothiazolo[5,4-*c*]pyridine-5(4*H*)-carboxylate (157)**
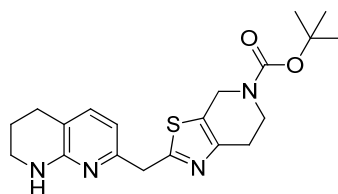
To a stirred mixture of *tert*-butyl 7-(2-amino-2-thioxoethyl)-3,4-dihydro-1,8-naphthyridine-1(2*H*)-carboxylate (200 mg, 650 µmol) in 1,4-dioxane (2 mL) was added *tert*-butyl 3-bromo-4-oxopiperidine-1-carboxylate (271 mg, 980 µmol) and calcium carbonate (130 mg, 1.30 mmol) under nitrogen at room temperature and the mixture was stirred at 70 ºC for 16 h. The reaction mixture was cooled to room temperature, then EtOAc (50 mL) and water (50 mL) were added and the separated aqueous phase was extracted twice with EtOAc (2 x 50 mL). The combined organic phase was filtered through a hydrophobic frit and the filtrate was concentrated under reduced pressure to afford a crude red oil. The oil was loaded in minimal CH$_2$Cl$_2$ onto a silica pre-packed column (50 g) and eluted with 0-100% EtOAc in cyclohexane over 60 min. The relevant fractions were combined and concentrated under reduced pressure to afford the desired product (186 mg, 480 µmol, 74% yield) as an orange solid. LCMS (Method B): 1.15 min, [M+H]$^+$ 387 m/z. ^{1}H NMR (400 MHz, CDCl$_3$) δ = 7.08 (d, *J* = 7.3 Hz, 1H), 6.46 (d, *J* = 7.3 Hz, 1H), 4.85 (br. s., 1H), 4.55 (br. s., 2H), 4.19 (s, 2H), 3.77 - 3.67 (m, 2H), 3.45 - 3.36 (m, 2H), 2.89 - 2.79 (m, 2H), 2.70 (t, *J* = 6.3 Hz, 2H), 1.96 - 1.82 (m, 2H), 1.47 (s, 9H) ppm.

Christopher J Tame

CONFIDENTIAL – DO NOT COPY

2-((5,6,7,8-Tetrahydro-1,8-naphthyridin-2-yl)methyl)-4,5,6,7-tetrahydrothiazolo[5,4-*c*]pyridine (153)
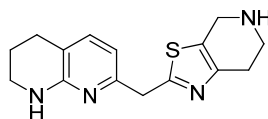
To a stirred solution of *tert*-Butyl 2-((5,6,7,8-tetrahydro-1,8-naphthyridin-2-yl)methyl)-6,7-dihydrothiazolo[5,4-*c*]pyridine-5(4*H*)-carboxylate (186 mg, 480 µmol) in MeOH (1.0 mL) was added a solution of HCl in 1,4-dioxane (4 M, 0.6 mL, 2.4 mmol) dropwise at room temperature and the mixture was stirred at room temperature overnight. The mixture was then loaded directly onto an aminopropyl silica pre-packed cartridge (20 g) and eluted with MeOH (40 mL). The filtrate was concentrated under reduced pressure to afford the desired product (114 mg, 400 µmol, 83% yield) as an orange solid. LCMS (Method B): 0.77 min, [M+H]$^+$ 287 m/z. ^{1}H NMR (400 MHz, CDCl$_3$) δ = 7.08 (d, *J* = 6.8 Hz, 1H), 6.46 (d, *J* = 7.3 Hz, 1H), 4.82 (br. s, 1H), 4.19 (s, 2H), 3.97 (s, 2H), 3.45 - 3.35 (m, 2H), 3.15 (t, *J* = 5.8 Hz, 2H), 2.85 - 2.75 (m, 2H), 2.69 (t, *J* = 6.3 Hz, 2H), 1.96 - 1.84 (m, 2H), 1.58 (br. s, 1H) ppm.

(*E*)-Methyl 4-(2-((5,6,7,8-tetrahydro-1,8-naphthyridin-2-yl)methyl)-6,7-dihydrothiazolo[5,4-*c*]pyridin-5(4*H*)-yl)but-2-enoate (154)
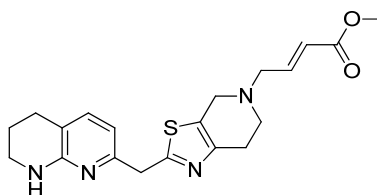
To a stirred solution of 2-((5,6,7,8-tetrahydro-1,8-naphthyridin-2-yl)methyl)-4,5,6,7-tetrahydrothiazolo[4,5-*c*]pyridine (114 mg, 380 µmol) and triethylamine (110 µL, 760 µmol) in CH$_2$Cl$_2$ (3.5 mL) was added a solution of (*E*)-methyl 4-bromobut-2-

enoate (50 μL, 0.38 mmol) in CH$_2$Cl$_2$ (0.5 mL) dropwise at 0 ºC under nitrogen. The mixture was stirred at room temperature for 1 h. To the reaction mixture was then added triethylamine (0.053 mL, 0.378 mmol) and a solution of (E)-methyl 4-bromobut-2-enoate (0.023 mL, 0.189 mmol) in DCM (0.5 mL) dropwise, sequentially at 0 ºC and the mixture was stirred at room temperature for 1 h. To the reaction mixture was then added triethylamine (0.053 mL, 0.378 mmol) and a solution of (E)-methyl 4-bromobut-2-enoate (0.023 mL, 0.189 mmol) in DCM (0.5 mL) dropwise, sequentially at 0 ºC and the mixture was stirred at room temperature for 1 h. Water (50 mL) and CH$_2$Cl$_2$ (50 mL) was added and the separated organic phase was washed twice with water (2 x 50 mL). The combined organic phase was filtered through a hydrophobic frit and the filtrate was concentrated under reduced pressure to afford the desired product (147 mg, 380 μmol, 96% yield) as a yellow solid. LCMS (Method B): 0.97 min, [M+H]$^+$ 385 m/z. ^{1}H NMR (400 MHz, CDCl$_3$) = 7.09 (d, J = 7.3 Hz, 1H), 7.00 (dt, J = 15.6, 6.0 Hz, 1H), 6.45 (d, J = 7.3 Hz, 1H), 6.04 (dt, J = 15.6, 1.5 Hz, 1H), 4.88 (br. s., 1 H), 4.20 (s, 2H), 3.75 (s, 3H), 3.67 (s, 2H), 3.44 - 3.38 (m, 2H), 3.35 (dd, J = 6.0, 1.8 Hz, 2H), 2.91 - 2.84 (m, 4H), 2.70 (t, J = 6.3 Hz, 2H), 1.96 - 1.87 (m, 2H) ppm.

3-(3-Cyclopropylphenyl)-4-(2-((5,6,7,8-tetrahydro-1,8-naphthyridin-2-yl)methyl)-6,7-dihydrothiazolo[5,4-c]pyridin-5(4H)-yl)butanoic acid, formic acid salt (89)
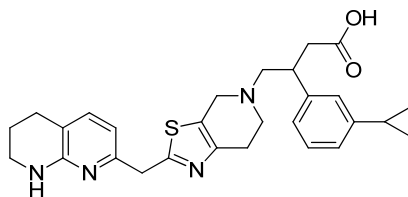
To a solution of (3-cyclopropylphenyl)boronic acid (178 mg, 1.10 mmol) and (E)-methyl 4-(2-((5,6,7,8-tetrahydro-1,8-naphthyridin-2-yl)methyl)-6,7-dihydrothiazolo[5,4-c]pyridin-5(4H)-yl)but-2-enoate (141 mg, 370 μmol) in degassed 1,4-dioxane (2.50 mL) was added degassed aqueous KOH solution (3.8 M, 190 μL, 730 μmol) and chloro(1,5-cyclooctadiene)rhodium(II) dimer (54 mg, 0.11 mmol) sequentially at room temperature under nitrogen. The reaction mixture was

Christopher J Tame

then heated to 95 ºC for 5 min. The reaction mixture was concentrated under reduced pressure to afford a brown gum. The gum was dissolved in CH_2Cl_2 (5 mL), MeOH (5 mL) and water (5 mL) and loaded onto an SCX pre-packed silica cartridge (5 g). The column was eluted with MeOH (50 mL), CH_2Cl_2 (50 mL), water (50 mL) and a solution of NH_3 in MeOH (2 M, 50 mL), respectively. The relevant fractions were concentrated under reduced pressure to afford a crude brown gum. To a solution of the brown gum in MeOH (1 mL) at room temperature was added aqueous NaOH solution (2.0 M, 0.92 mL, 1.8 mmol) and the solution was stirred at 50 ºC for 1 h. The solution was concentrated under reduced pressure to afford a brown gum. The gum was dissolved in MeCN (1.00 mL) and water (1.00 mL) and purified *via* mass-directed auto-preparative (MDAP) chromatography using a Sunfire C18 column (2 x 1.00 mL injections) and an ammonium bicarbonate-modified MeCN/water gradient. The relevant fractions were combined and concentrated under a stream of nitrogen to afford the desired product (113 mg, 210 µmol, 63% yield) as a brown solid. m.p. 127.1 – 127.4 °C. LCMS (Method B): 0.96 min, $[M+H]^+$ 489 m/z. IR (solid) 3300 (N-H stretch), 2926 (sp^3 C-H stretch), 1600, 1275 ($O-C-O^-$ stretch) cm^{-1}. ^1H NMR (400 MHz, $CDCl_3$) δ = 8.39 (s, 1H), 7.24 (d, J = 7.3 Hz, 1H), 7.20 (t, J = 7.6 Hz, 1H), 6.96 - 6.85 (m, 4H), 6.42 (d, J = 7.3 Hz, 1H), 4.31 (s, 2H), 3.96 (d, J = 14.9 Hz, 1H), 3.88 (d, J = 14.9 Hz, 1H), 3.46 (t, J = 5.6 Hz, 2H), 3.38 - 3.29 (m, 1H), 3.29 - 3.18 (m, 1H), 2.97 (s, 2H), 2.91 (d, J = 7.3 Hz, 2H), 2.89 - 2.79 (m, 2H), 2.84 - 2.78 (m, 1H), 2.72 (t, J = 6.2 Hz, 2H), 1.96 - 1.80 (m, 3H), 1.00 - 0.92 (m, 2H), 0.72 - 0.64 (m, 2H) ppm. ^{13}C NMR (101 MHz, DMSO-d_6) δ = 173.2, 173.2, 165.4, 155.9, 153.3, 147.2, 143.5, 143.1, 136.1, 127.9, 126.0, 124.8, 122.8 , 113.4, 110.2, 61.9, 49.6, 49.5, 40.8, 40.1, 39.1, 38.6, 26.1, 25.6, 20.5, 14.4, 9.1 ppm. HRMS (ESI) calc'd for $C_{28}H_{33}N_4O_2S$ $[M+H]^+$ 489.2324, found 489.2325.

Key 2D correlations:

HMBC (^1H NMR to ^{13}C NMR): δ = 4.01 to 110.2, 153.3, 165.4 ppm; 3.96 and 3.88 to 49.6, 126.0, 147.2 ppm; 2.88 to 49.5, 147.2 ppm; 2.82 to 26.1, 61.9, 147.2 ppm.

Christopher J Tame

3-(3-Cyclopropylphenyl)-4-(2-((5,6,7,8-tetrahydro-1,8-naphthyridin-2-yl)methyl)-6,7-dihydrothiazolo[5,4-*c*]pyridin-5(4*H*)-yl)butanoic acid, formic acid salt (89) ^{1}H NMR Correlation Spectroscopy (COSY).
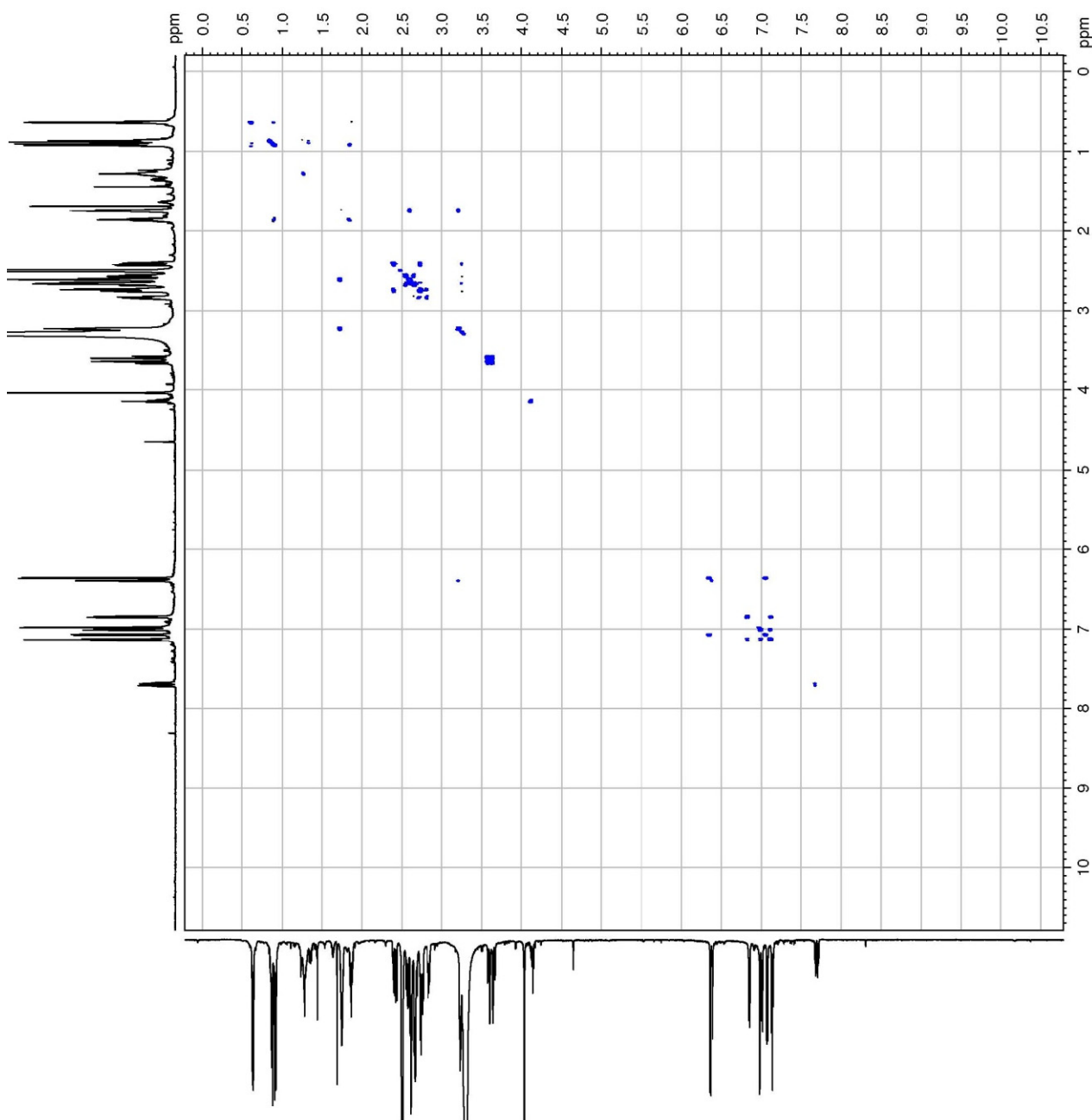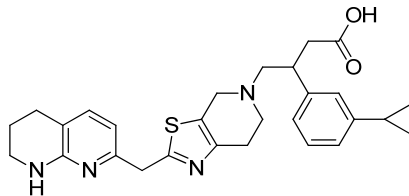
352

Christopher J Tame

3-(3-Cyclopropylphenyl)-4-(2-((5,6,7,8-tetrahydro-1,8-naphthyridin-2-yl)methyl)-6,7-dihydrothiazolo[5,4-c]pyridin-5(4H)-yl)butanoic acid, formic acid salt (89) Heteronuclear Single Quantum Coherence (HSQC) ^{1}H and ^{13}C NMR spectroscopy
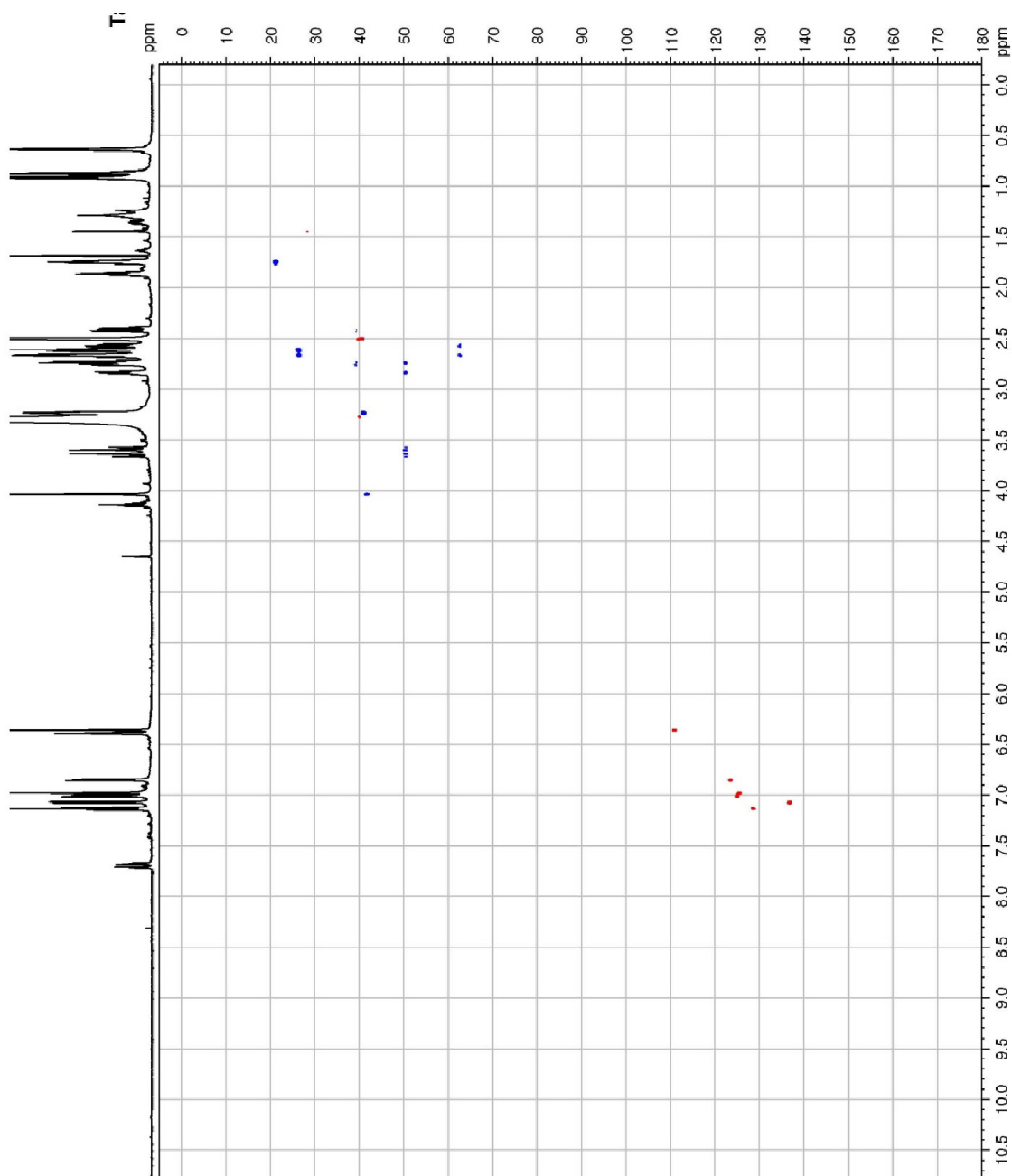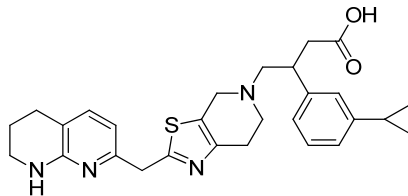
Christopher J Tame

3-(3-Cyclopropylphenyl)-4-(2-((5,6,7,8-tetrahydro-1,8-naphthyridin-2-yl)methyl)-6,7-dihydrothiazolo[5,4-*c*]pyridin-5(4*H*)-yl)butanoic acid, formic acid salt (89) Heteronuclear Multiple Bond Correlation (HMBC) ^{1}H and ^{13}C NMR spectroscopy.

Christopher J Tame
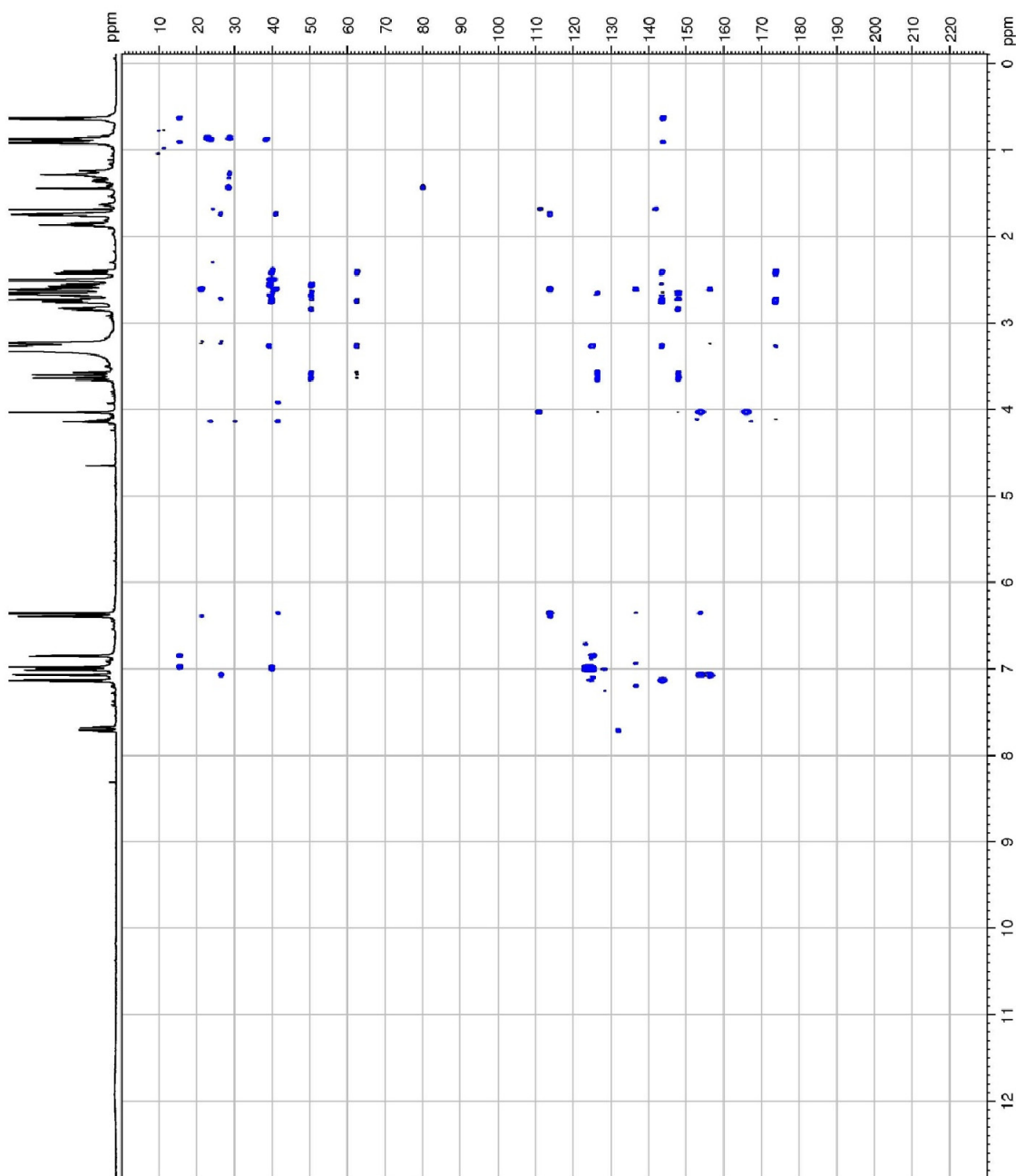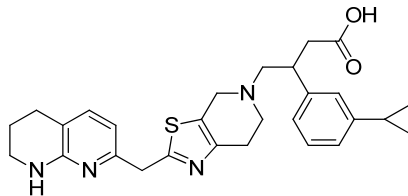
5,6,7,8-Tetrahydro-[1,2,4]triazolo[1,5-*a*]pyrazine (173)
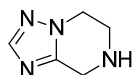
A mixture of [1,2,4]triazolo[1,5-*a*]pyrazine (1.00 g, 8.33 mmol) and palladium on carbon (10%, dry basis, 90 mg, 0.83 mmol) in EtOH (30 mL) was stirred under a hydrogen atmosphere at room temperature for 20 h. The mixture was filtered through a celite plug under reduced pressure and the filtrate was concentrated under reduced pressure to afford the desired product (1.03 g, 8.33 mmol, 100% yield) as a white solid. ^{1}H NMR (400 MHz, CDCl$_3$) δ = 7.87 (s, 1H), 4.13 - 4.19 (m, 6H), 3.33 (br. s, 1H) ppm.

Benzyl 5,6-dihydro-[1,2,4]triazolo[1,5-*a*]pyrazine-7(8*H*)-carboxylate (174)
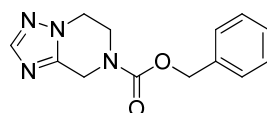
To a stirred mixture of 5,6,7,8-tetrahydro-[1,2,4]triazolo[1,5-*a*]pyrazine (1.00 g, 6.23 mmol) and triethylamine (1.74 mL, 12.5 mmol) in CH$_2$Cl$_2$ (60 mL) was added benzyl (2,5-dioxopyrrolidin-1-yl) carbonate (1.71 g, 6.85 mmol) portionwise at room temperature and the mixture was stirred at room temperature for 2 h. To the mixture was added water (100 mL) and the separated aqueous layer was extracted twice with CH$_2$Cl$_2$ (2 x 100 mL). The combined organic phase was washed with water (100 mL) and filtered through a hydrophobic frit. The filtrate was concentrated under vacuum to afford a crude orange gum. The gum was loaded in minimal CH$_2$Cl$_2$ onto a 50 g silica pre-packed column and eluted with 0-100% EtOAc in cyclohexane, then 0-20% MeOH (1% Et$_3$N) over 60 min. The relevant fractions were combined and concentrated under reduced pressure to afford the desired product (640 mg, 2.48 mmol, 40%). LCMS (Method B): 0.76 min, [M+H]$^+$ 259 m/z. ^{1}H NMR (400 MHz,

Christopher J Tame

DMSO-d$_6$) δ = 7.96 (s, 1H), 7.44 - 7.30 (m, 5H), 5.15 (s, 2H), 4.73 (br. s, 2H), 4.18 (t, J = 5.4 Hz, 2H), 3.94 (m, 2H) ppm.

Attempted synthesis of *tert*-Butyl 7-((7-((benzyloxy)carbonyl)-5,6,7,8-tetrahydro-[1,2,4]triazolo[1,5-*a*]pyrazin-2-yl)methyl)-3,4-dihydro-1,8-naphthyridine-1(2*H*)-carboxylate (176)
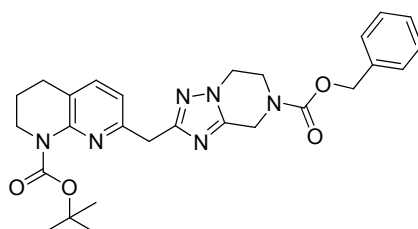
Method 1

To a degassed mixture of (1,5-cyclooctadiene)(methoxy)iridium(I) dimer (13 mg, 20 µmol) and 4,4'-di-tert-butyl-2,2'-bipyridine (10 mg, 40 µmol) was added degassed cyclohexane (1.5 mL), degassed pinacolborane (80 µL, 580 µmol) and a degassed solution of benzyl 5,6-dihydro-[1,2,4]triazolo[1,5-*a*]pyrazine-7(8*H*)-carboxylate (100 mg, 390 µmol) in CHCl$_3$ (0.5 mL) dropwise at room temperature under nitrogen. Addition of pinacolboroane was accompanied with a colour change from orange to deep red. The mixture was stirred at 70 ºC under reflux for 1 h. LCMS analysis (MeCN, Method B) indicated incomplete consumption of the starting material and new peaks at 1.02 min, [M+H]$^+$ 385 m/z, and 0.53 min, [M+H]$^+$ 303 m/z, which suggested the presence of pinacol boronate and boronic acid intermediates, respectively. To the reaction mixture was added a degassed solution of chloro(2-dicyclohexylphosphino-2′,4′,6′-triisopropyl-1,1′-biphenyl)[2-(2′-amino-1,1′-biphenyl)]palladium(II) (31 mg, 40 µmol) and *tert*-butyl 7-(bromomethyl)-3,4-dihydro-1,8-naphthyridine-1(2*H*)-carboxylate (89 mg, 0.27 mmol) in THF (1.5 mL) and aqueous K$_3$PO$_4$ solution (0.5 M, 1.0 mL, 0.52 mmol) dropwise, sequentially, at 70 ºC under nitrogen. Gas evolution was observed during both additions. LCMS analysis (MeCN, Method B) indicated complete conversion back to the starting material 0.76 min, [M+H]$^+$ 259 m/z.

Christopher J Tame

Method 2

To a degassed mixture of (1,5-cyclooctadiene)(methoxy)iridium(I) dimer (13 mg, 20 μmol) and 4,4'-di-*tert*-butyl-2,2'-bipyridine (dtbpy) (10 mg, 40 μmol) was added degassed cyclohexane (1.5 mL), degassed pinacolborane (0.14 mL, 0.97 mmol) and a degassed solution of benzyl 5,6-dihydro-[1,2,4]triazolo[1,5-*a*]pyrazine-7(8*H*)-carboxylate (100 mg, 390 μmol) in chloroform (0.5 mL) dropwise at room temperature under nitrogen. The addition of pinacolborane was accompanied with a colour change from orange to deep red. The mixture was stirred at 70 ºC under reflux for 1 hour then cooled to 0 ºC or 50 °C. LCMS analysis indicated a major peak which corresponded to the boronic acid intermediate and mono-substituted dtbpy: (method B) 0.53 min, [M+H]$^+$ 303 m/z; 1.02 min, [M+H]$^+$ 385 m/z. Note: LCMS samples were dissolved in MeCN and were run on ammonium-bicarbonate modified LCMS, 2 minute system. Samples taken in MeOH only show starting material, suggesting rapid protodeboronation. To the reaction mixture was added a degassed solution of chloro(2-dicyclohexylphosphino-2′,4′,6′-triisopropyl-1,1′-biphenyl)[2-(2′-amino-1,1′-biphenyl)]palladium(II) (31 mg, 39 μmol) and *tert*-butyl 7-(bromomethyl)-3,4-dihydro-1,8-naphthyridine-1(2*H*)-carboxylate (89 mg, 0.27 mmol) in THF (1.5 mL) and an aqueous solution of potassium phosphate (500 mM 1.00 mL, 520 μmol) dropwise respectively at 0 ºC or 50 °C. Gas evolution was observed during both additions. The reaction mixture was then stirred either at room temperature or 50 °C overnight, under nitrogen. LCMS analysis (method B) could only identify degradation of the pinacolboronate intermediate to starting material.

2-Bromo-7-trityl-5,6,7,8-tetrahydro-[1,2,4]triazolo[1,5-*a*]pyrazine (189)
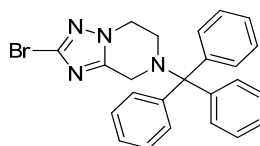
To a stirred mixture of trityl chloride (755 mg, 2.71 mmol) and 2-bromo-5,6,7,8-tetrahydro-[1,2,4]triazolo[1,5-*a*]pyrazine (500 mg, 2.46 mmol) in CH$_2$Cl$_2$ (2.5 mL) was added DIPEA (1.29 mL, 7.39 mmol) dropwise at room temperature, which was

Christopher J Tame

accompanied by the evolution of a white gas. The resulting solution was stirred at room temperature for 1 h. CH_2Cl_2 (5 mL) was added to re-dissolve a yellow precipitate which formed during the reaction. Water (10 mL) and CH_2Cl_2 (10 mL) was added and the isolated aqueous phase was extracted twice with CH_2Cl_2 (2 x 10 mL) and the combined organic phase was concentrated to ~5 mL under reduced pressure, then loaded onto a silica-gel pre-packed column (100 g) and eluted with 0-50% EtOAc in cyclohexane over 40 min. The relevant fractions were combined and concentrated to afford the desired product (852 mg, 1.91 mmol, 78% yield) as a white solid. LCMS (Method B): 1.39 min, 445 [^{79}Br M+H]$^+$, 447 [^{81}Br M+H]$^+$ m/z. ^{1}H NMR (400 MHz, DMSO-d_6) δ = 7.46 (d, J = 7.6 Hz, 6H), 7.35 (t, J = 7.8 Hz, 6H), 7.27 - 7.19 (m, 3H), 4.29 (t, J = 5.3 Hz, 2H), 3.43 (br. s, 2H), 2.72 - 2.62 (m, 2H) ppm.

2-(8-(*tert*-Butoxycarbonyl)-5,6,7,8-tetrahydro-1,8-naphthyridin-2-yl)acetic acid (190)
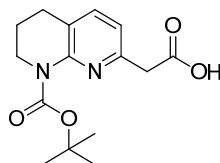
To a stirred solution of *tert*-butyl 7-(2-methoxy-2-oxoethyl)-3,4-dihydro-1,8-naphthyridine-1(2*H*)-carboxylate (6.00 g, 19.6 mmol) in MeCN (25 mL) was added aqueous NaOH solution (2.0 M, 20 mL, 39 mmol) dropwise over 20 min and the mixture was stirred at room temperature for 10 min. The mixture was neutralised with aqueous HCl solution (2 M), concentrated under reduced pressure to half the original volume then acidified to pH 5 with aqueous hydrochloric acid solution (2 M). Water (50 mL) and EtOAc (50 mL) was added and the separated aqueous phase was extracted twice with EtOAc (2 x 100 mL). The combined organic fractions were filtered through a hydrophobic frit and the filtrate was concentrated under reduced pressure to afford the desired product (4.72 g, 15.3 mmol, 78% yield) as a yellow oil. LCMS (Method B): 0.60 min, [M+H]$^+$ 293 m/z. ^{1}H NMR (400 MHz, DMSO-d_6) δ =

Christopher J Tame

12.54 (br. s, 1H), 7.48 (d, J = 7.8 Hz, 1H), 6.98 (d, J = 7.6 Hz, 1H), 3.67 - 3.61 (m, 4H), 2.71 (t, J = 6.5 Hz, 2H), 1.83 (quin, J = 6.5 Hz, 2H), 1.44 (s, 9H) ppm.

7-Methyl-1-(5,6,7,8-tetrahydro-[1,2,4]triazolo[1,5-*a*]pyrazin-2-yl)-1,2,3,4-tetrahydro-1,8-naphthyridine (191)
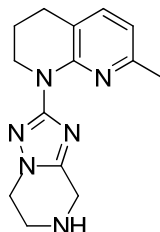
To a stirred solution of 2-(8-(*tert*-butoxycarbonyl)-5,6,7,8-tetrahydro-1,8-naphthyridin-2-yl)acetic acid (350 mg, 1.08 mmol) in MeCN (6 mL) was added an aqueous solution of potassium hydroxide (1.0 M, 1.1 mL, 1.1 mmol) dropwise at room temperature . The mixture was stirred at room temperature for 5 min, then concentrated under reduced pressure to afford an orange solid (356 mg, 1.08 mmol). The orange solid (326 mg, 990 μmol), 2-bromo-7-trityl-5,6,7,8-tetrahydro-[1,2,4]triazolo[1,5-*a*]pyrazine (400 mg, 900 μmol), tris(dibenzylideneacetone)dipalladium (82 mg, 90 μmol) and 4,5-bis(diphenylphosphino)-9,9-dimethyl xanthene (156 mg, 270 μmol) were charged to an oven-dried round bottomed flask then sealed and degassed with three alternative applications of nitrogen and vacuum. To the solids was added degassed 1,3,5-trimethylbenzene (1.8 mL) and the resulting mixture was transferred to a pre-heated oil bath set at 150 ºC and stirred under nitrogen for 16 h. The reaction mixture was concentrated under reduced pressure then loaded in minimal CH_2Cl_2 and purified by silica gel chromatography, eluting with 0-100% EtOAc in cyclohexane, followed by 0-20% MeOH in CH_2Cl_2. The relevant fractions were combined and concentrated under reduced pressure to afford an orange solid. The solid was dissolved in minimal CH_2Cl_2 and purified by SCX ion exchange column chromatography, eluting with MeOH, followed by a solution of ammonia in MeOH (2 M). LCMS analysis of the ammonia-containing fractions suggested a mixture of the trityl-deprotected analogue of the product, and 2-methyl tetranaphthyridine in a 1:2 ratio. LCMS

Christopher J Tame

(method B) 0.59 min, $[M+H]^+$ 271 m/z; 0.79 min, $[M+H]^+$ 149 m/z. The mixture was concentrated under reduced pressure to afford a gum. The gum was loaded in MeOH (1 mL) and purified by formic acid-modified mass-directed auto preparative (MDAP) chromatography. The relevant fractions were combined and passed through an ammonium bicarbonate-functionalised silica column under atmospheric pressure, eluting with MeOH. The filtrate was combined and concentrated under reduced pressure to afford a crude white solid. LCMS (Method B): 0.59 min, [M+H]+ 271 m/z. ^{1}H NMR (400 MHz, CDCl3) δ = 7.23 (d, *J* = 7.3 Hz, 1H), 6.61 (d, *J* = 7.6 Hz, 1H), 4.10 - 4.16 (m, 4H), 3.90 - 3.95 (m, 2H), 3.35 (t, *J* = 5.4 Hz, 2H), 2.79 (t, *J* = 6.4 Hz, 2H), 2.42 (s, 3H), 2.04 (quin, *J* = 6.0 Hz, 2H) ppm.

7-((5,6-Dihydropyrrolo[3,4-*c*]pyrazol-2(4*H*)-yl)methyl)-1,2,3,4-tetrahydro-1,8-naphthyridine (203) and **7-((5,6-dihydropyrrolo[3,4-*c*]pyrazol-1(4*H*)-yl)methyl)-1,2,3,4-tetrahydro-1,8-naphthyridine (204)**

To a stirred solution of *tert*-butyl 4,6-dihydropyrrolo[3,4-*c*]pyrazole-5(1*H*)-carboxylate (1.02 g, 4.89 mmol) in DMF (44.5 mL) was added sodium hydride (60% dispersion in mineral oil, 290 mg, 7.33 mmol) portionwise at 0 ºC under nitrogen, and the mixture was then stirred for 20 min at 0 ºC. To the mixture was added a solution of *tert*-butyl 7-(bromomethyl)-3,4-dihydro-1,8-naphthyridine-1(2*H*)-carboxylate (1.60 g, 4.89 mmol) in DMF (4.5 mL) dropwise at 0 ºC. The mixture was then allowed to reach room temperature and stirred at room temperature for 16 h. Aqueous lithium chloride solution (1% (w/v), 200 mL) and EtOAc (200 mL) were added and the separated aqueous phase was extracted twice with EtOAc (2 x 200 mL), and the combined organics were washed with aqueous lithium chloride solution (1% (w/v), 200 mL). The combined organic phase was filtered through a hydrophobic frit and the filtrate was concentrated under reduced pressure to afford a crude solid (1.7 g). To a stirred solution of the crude solid in MeOH (30 mL) was

Christopher J Tame

added a solution of HCl, in 1,4-dioxane (4.0 M, 4.4 mL, 18 mmol) dropwise at room temperature under nitrogen and the mixture was stirred at room temperature for 16 h. The reaction mixture was neutralised with saturated aqueous sodium bicarbonate solution. To the mixture was added EtOAc (200 mL) and water (200 mL) and the separated organic phase was washed twice with water (2 x 200 mL). The combined aqueous phase was concentrated under reduced pressure to afford a white solid. The solid was loaded in minimal water onto an SCX pre-packed column (50 g) and eluted with water (100 mL), MeOH (100 mL) and a solution of NH$_3$ in MeOH (2 M, 100 mL), respectively. The relevant fractions were combined and concentrated under reduced pressure to afford a mixture of 7-((5,6-dihydropyrrolo[3,4-*c*]pyrazol-2(4*H*)-yl)methyl)-1,2,3,4-tetrahydro-1,8-naphthyridine (**203**) and 7-((5,6-dihydropyrrolo[3,4-*c*]pyrazol-1(4*H*)-yl)methyl)-1,2,3,4-tetrahydro-1,8-naphthyridine (**204**) (530 mg, 2.08 mmol, 43% yield) as a yellow gum. LCMS (Method B): 0.59 min, [M+H]$^+$ 256 m/z. ^{1}H NMR (400 MHz, DMSO-d$_6$) δ = 7.38 (s, 1H), 7.11 - 7.04 (m, 1H), 6.43 (br. s, 0.33H), 6.40 (br. s, 0.67H), 6.13 (d, *J* = 7.3 Hz, 0.33H), 6.07 (d, *J* = 7.3 Hz, 0.67H), 5.02 (s, 1.34H), 4.94 (s, 0.66H), 3.82 - 3.77 (m, 2H), 3.77 - 3.70 (m, 2H), 3.18 (s, 1H), 3.28 - 3.20 (m, 2H), 2.67 - 2.55 (m, 2H), 1.74 (quin, *J* = 5.9 Hz, 2H) ppm. Integration of peaks at 6.13 and 6.07 ppm indicate a 2:1 ratio of components in the mixture.

Methyl 3-(3-cyclopropylphenyl)-4-(2-((5,6,7,8-tetrahydro-1,8-naphthyridin-2-yl)methyl)pyrrolo[3,4-*c*]pyrazol-5(2*H*,4*H*,6*H*)-yl)butanoate, formic acid salt (209) and **methyl 3-(3-cyclopropylphenyl)-4-(1-((5,6,7,8-tetrahydro-1,8-naphthyridin-2-yl)methyl)pyrrolo[3,4-*c*]pyrazol-5(1*H*,4*H*,6*H*)-yl)butanoate, formic acid salt (210)**
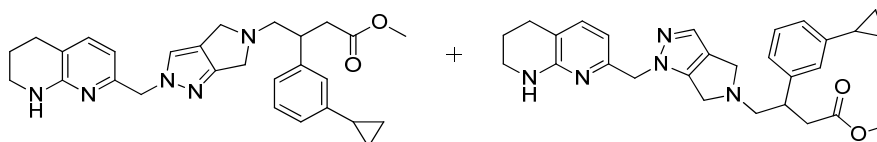
To a stirred solution of 7-((5,6-dihydropyrrolo[3,4-*c*]pyrazol-2(4*H*)-yl)methyl)-1,2,3,4-tetrahydro-1,8-naphthyridine (585 mg, 2.29 mmol) and triethylamine (640

Christopher J Tame

μL, 4.58 mmol) in CH_2Cl_2 (22 mL) was added (*E*)-methyl 4-bromobut-2-enoate (342 μL, 2.86 mmol) dropwise at 0 ºC under nitrogen. The mixture was allowed to reach room temperature and stirred at room temperature for 1 h. EtOAc (50 mL) and aqueous lithium chloride solution (10% (w/v), 50 mL) was added and the separated organic phase was washed twice with aqueous lithium chloride solution (10 % (w/v), 2 x 50 mL). The combined aqueous phase was extracted twice with EtOAc (2 x 50 mL) and the combined organic phase was passed through a hydrophobic frit and the filtrate was concentrated under reduced pressure to afford a crude orange gum (450 mg). To a stirred nitrogen-degassed mixture of the crude orange gum and (3-cyclopropylphenyl)boronic acid (619 mg, 3.82 mmol) in 1,4-dioxane (12 mL) was added degassed aqueous potassium hydroxide solution (3.8 M, 0.67 mL, 2.6 mmol) and chloro(1,5-cyclooctadiene)rhodium(II) dimer (188 mg, 380 μmol) sequentially. The solution was further degassed with alternative applications of vacuum and nitrogen and then heated to 95 ºC for 15 min. The mixture was concentrated under reduced pressure then dissolved in EtOAc (100 mL) and water (100 mL). The separated organic phase was washed twice with water (2 x 200 mL) and the combined organic phase was passed through a hydrophobic frit and the filtrate was concentrated under reduced pressure to afford a crude solid. The solid was loaded in minimal CH_2Cl_2 onto a silica pre-packed column (100 g) and eluted with 0-15% MeOH (+ 1% Et_3N) in CH_2Cl_2 over 60 min. The relevant fractions were combined and concentrated under reduced pressure to afford a crude gum. The gum was dissolved in DMSO (4.3 mL) and purified by HPLC (43 x 100 μL injections, Waters Atlantis C18 column, 100 mm x 19.0 mm, 20 mL/min, 20-100% MeOH (0.1% (v/v) formic acid) in water (0.1% (v/v) formic acid) over 18 min). The relevant fractions were combined and concentrated under a stream of nitrogen to afford methyl 3-(3-cyclopropylphenyl)-4-(2-((5,6,7,8-tetrahydro-1,8-naphthyridin-2-yl)methyl)pyrrolo[3,4-*c*]pyrazol-5(2*H*,4*H*,6*H*)-yl)butanoate, formic acid salt (**209**) (90 mg, 0.17 mmol, 8% yield) and methyl 3-(3-cyclopropylphenyl)-4-(1-((5,6,7,8-tetrahydro-1,8-naphthyridin-2-yl)methyl)pyrrolo[3,4-*c*]pyrazol-5(1*H*,4*H*,6*H*)-yl)butanoate, formic acid salt (**210**) (125 mg, 240 μmol, 11% yield).

Christopher J Tame

Methyl 3-(3-cyclopropylphenyl)-4-(2-((5,6,7,8-tetrahydro-1,8-naphthyridin-2-yl)methyl)pyrrolo[3,4-*c*]pyrazol-5(2*H*,4*H*,6*H*)-yl)butanoate, formic acid salt (**209**): LCMS (Method B): 1.23 min, [M+H]$^+$ 472 m/z. ^{1}H NMR (600 MHz, DMSO-d$_6$) δ = 8.37 (br. s, 1H), 7.39 (s, 1H), 7.15 (t, *J* = 7.7 Hz, 1H), 7.05 (d, *J* = 7.3 Hz, 1H), 7.03 (d, *J* = 7.7 Hz, 1H), 7.00 (s, 1H), 6.87 (d, *J* = 7.7 Hz, 1H), 6.40 (br. s, 1H), 6.03 (d, *J* = 7.3 Hz, 1H), 5.01 (s, 2H), 3.68 - 3.57 (m, 4H), 3.44 (s, 3H), 3.25 - 3.19 (m, 3H), 2.93 - 2.78 (m, 3H), 2.60 (t, *J* = 6.1 Hz, 2H), 2.55 - 2.51 (m, 1H), 1.92 - 1.84 (m, 1H), 1.79 - 1.67 (m, 2H), 0.97 - 0.88 (m, 2H), 0.72 - 0.59 (m, 2H) ppm.

Methyl 3-(3-cyclopropylphenyl)-4-(1-((5,6,7,8-tetrahydro-1,8-naphthyridin-2-yl)methyl)pyrrolo[3,4-*c*]pyrazol-5(1*H*,4*H*,6*H*)-yl)butanoate, formic acid salt (**210**): LCMS (Method B): 1.23 min, [M+H]$^+$ 472 m/z. ^{1}H NMR (600 MHz, DMSO-d$_6$) δ = 8.40 (br. s, 1H), 7.14 (t, *J* = 7.7 Hz, 1H), 7.10 (s, 1H), 7.08 (d, *J* = 7.3 Hz, 1H), 7.00 (d, *J* = 7.7 Hz, 1H), 6.97 (s, 1H), 6.86 (d, *J* = 7.7 Hz, 1H), 6.43 (br. s, 1H), 6.12 (d, *J* = 7.3 Hz, 1H), 4.95 (s, 2H), 3.72 - 3.61 (m, 4H), 3.43 (s, 3H), 3.25 (t, *J* = 4.8 Hz, 2H), 3.16 - 3.11 (m, 1H), 2.88 - 2.82 (m, 2H), 2.79 (dd, *J* = 15.4, 6.2 Hz, 1H), 2.62 (t, *J* = 6.2 Hz, 2H), 2.55 - 2.51 (m, 1H), 1.90 - 1.83 (m, 1H), 1.75 (quin, *J* = 6.2 Hz, 2H), 0.94 - 0.89 (m, 2H), 0.66 - 0.62 (m, 2H) ppm.

Christopher J Tame

Methyl 3-(3-cyclopropylphenyl)-4-(2-((5,6,7,8-tetrahydro-1,8-naphthyridin-2-yl)methyl)pyrrolo[3,4-c]pyrazol-5(2H,4H,6H)-yl)butanoate, formic acid salt (209) ^{1}H NMR NOESY analysis. Irradiation at 5.01 ppm.
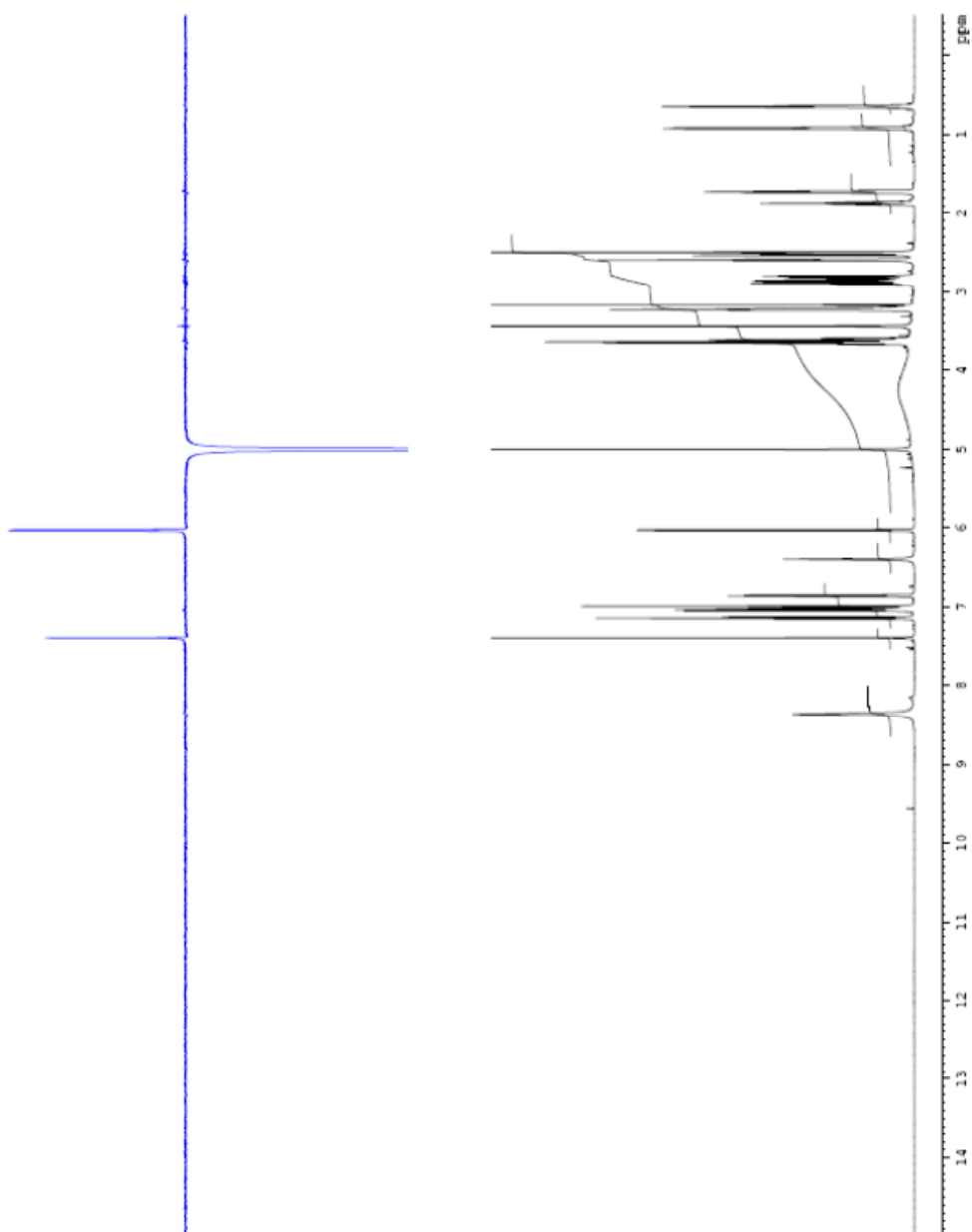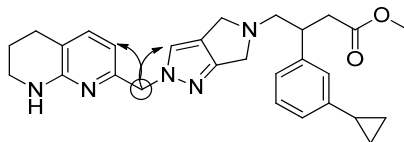
Christopher J Tame

Methyl 3-(3-cyclopropylphenyl)-4-(1-((5,6,7,8-tetrahydro-1,8-naphthyridin-2-yl)methyl)pyrrolo[3,4-c]pyrazol-5(1H,4H,6H)-yl)butanoate, formic acid salt (210) ^{1}H NMR NOESY analysis. Irradiation at 4.95 ppm.
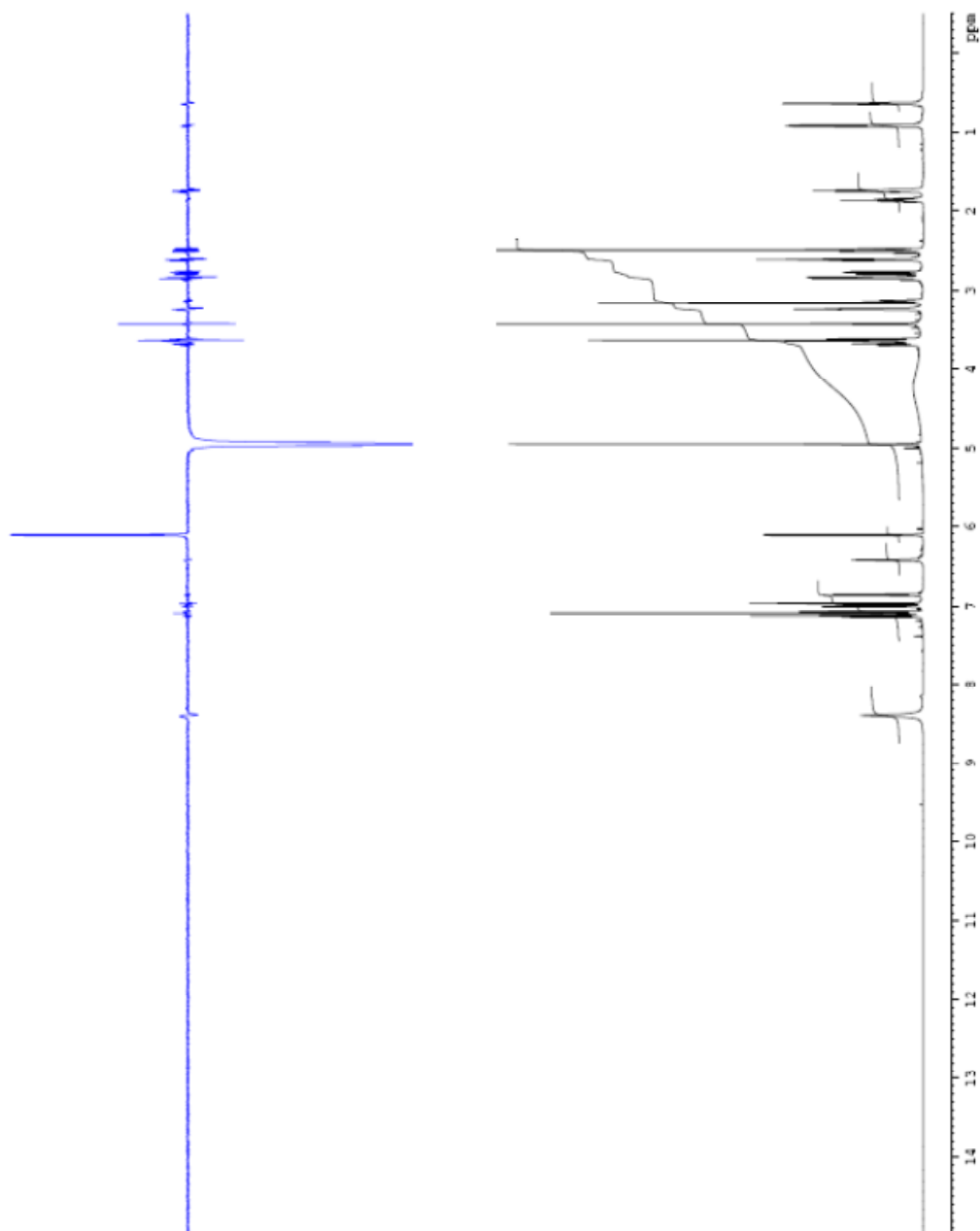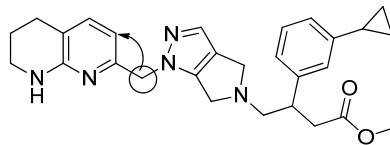
Christopher J Tame

Methyl 3-(3-cyclopropylphenyl)-4-(2-((5,6,7,8-tetrahydro-1,8-naphthyridin-2-yl)methyl)pyrrolo[3,4-*c*]pyrazol-5(2*H*,4*H*,6*H*)-yl)butanoate (209a and 209b).
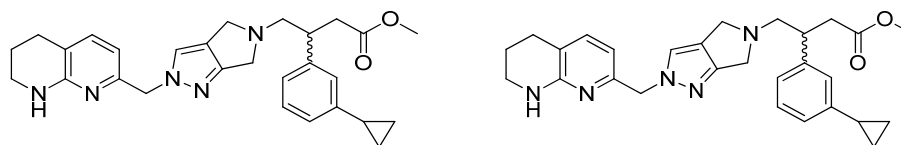
Methyl 3-(3-cyclopropylphenyl)-4-(2-((5,6,7,8-tetrahydro-1,8-naphthyridin-2-yl)methyl)pyrrolo[3,4-*c*]pyrazol-5(2*H*,4*H*,6*H*)-yl)butanoate (**235**) (90 mg, 0.17 mmol) was dissolved in EtOH (3 mL) and the supernatant was decanted, diluted with heptane (3 mL) and purified by chiral HPLC chromatography (6 x 1 mL injections, 20% EtOH in heptane, Chiralcel OD-H column (30 mm x 25 cm), flow rate: 30 mL/min). The relevant fractions were combined and concentrated under reduced pressure to afford methyl 3-(3-cyclopropylphenyl)-4-(2-((5,6,7,8-tetrahydro-1,8-naphthyridin-2-yl)methyl)pyrrolo[3,4-*c*]pyrazol-5(2*H*,4*H*,6*H*)-yl)butanoate (**209a**, **enantiomer 1** (18.5-21 min): 18 mg, 40 μmol, 20% yield, >96% e.e.) and methyl 3-(3-cyclopropylphenyl)-4-(2-((5,6,7,8-tetrahydro-1,8-naphthyridin-2-yl)methyl)pyrrolo[3,4-*c*]pyrazol-5(2*H*,4*H*,6*H*)-yl)butanoate (**209b**, **enantiomer 2** (23-27 min): 19 mg, 40 μmol, 21% yield, >99% e.e.) as yellow gums. Enantiomeric excess was determined using chiral HPLC analysis (30% EtOH in heptane, Chiralcel OD-H column (4.6 mm x 25 cm), flow rate: 1 mL/min).

3-(3-Cyclopropylphenyl)-4-(2-((5,6,7,8-tetrahydro-1,8-naphthyridin-2-yl)methyl)pyrrolo[3,4-*c*]pyrazol-5(2*H*,4*H*,6*H*)-yl)butanoic acid (170a, enantiomer 1)
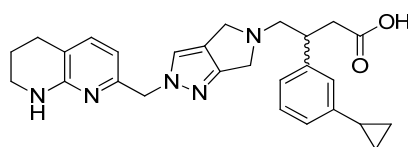
To a stirred solution of methyl 3-(3-cyclopropylphenyl)-4-(2-((5,6,7,8-tetrahydro-1,8-naphthyridin-2-yl)methyl)pyrrolo[3,4-*c*]pyrazol-5(2*H*,4*H*,6*H*)-yl)butanoate (enantiomer 1, 18 mg, 40 μmol) in MeCN (0.2 mL) was added aqueous NaOH solution (2.0 M, 0.19 mL, 0.38 mmol) dropwise at room temperature under nitrogen

Christopher J Tame

and the mixture was stirred at 50 ºC for 2 h. The mixture was purified directly *via* mass-directed auto-preparative (MDAP) chromatography using a Sunfire C18 column and ammonium bicarbonate-modified MeCN/water gradient. The relevant fractions were combined and concentrated under a stream of nitrogen to afford the desired product (11.5 mg, 30.0 μmol, 66% yield) as a yellow gum. LCMS (Method B): 0.77 min, [M+H]$^+$ 458 m/z. IR (solid) 3300 (N-H stretch); 2930 (sp^3 C-H stretch); 2800 (N-H$^+$ stretch) 1600, 1393 (O-C-O$^-$ stretch) cm^{-1}. $[\alpha]_D$ = +0.14 (c = 0.45 in MeOH). ^{1}H NMR (600 MHz, DMSO-d$_6$) δ = 7.39 (s, 1H), 7.15 (t, *J* = 7.7 Hz, 1H), 7.06 (d, *J* = 7.3 Hz, 1H), 7.03 (d, *J* = 7.7 Hz, 1H), 7.01 (s, 1H), 6.85 (d, *J* = 7.7 Hz, 1H), 6.38 (br. s, 1H), 6.08 (d, *J* = 7.0 Hz, 1H), 5.01 (s, 2H), 3.71 - 3.60 (m, 4H), 3.26 - 3.16 (m, 3H), 2.92 (dd, *J* = 8.8, 3.3 Hz, 1H), 2.87 (dd, *J* = 7.0, 5.1 Hz, 1H), 2.77 (dd, *J* = 15.4, 5.9 Hz, 1H), 2.60 (t, *J* = 6.2 Hz, 2H), 2.42 (dd, *J* = 15.6, 8.3 Hz, 1H), 1.90 - 1.84 (m, 1H), 1.77 - 1.70 (m, 2H), 0.94 - 0.88 (m, 2H), 0.67 - 0.61 (m, 2H) ppm. ^{13}C NMR (101 MHz, MeOD-d$_4$) δ = 177.7, 156.1, 153.4, 151.6, 144.7, 142.3, 136.8, 128.5, 124.6, 124.4, 123.9, 123.7, 118.4, 116.0, 109.7, 61.9, 56.7, 52.4, 51.9, 43.2, 40.9, 39.8, 26.1, 20.8, 14.8, 8.3, 8.2 ppm. HRMS (ESI) calc'd for C$_{27}$H$_{32}$N$_5$O$_2$ [M+H]$^+$ 458.2551, found 458.2529.

Note: 1H missing from ^{1}H NMR (exchangeable).

3-(3-Cyclopropylphenyl)-4-(2-((5,6,7,8-tetrahydro-1,8-naphthyridin-2-yl)methyl)pyrrolo[3,4-c]pyrazol-5(2H,4H,6H)-yl)butanoic acid (170b, enantiomer 2)
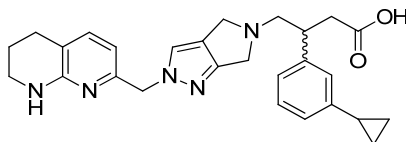
To a stirred solution of methyl 3-(3-cyclopropylphenyl)-4-(2-((5,6,7,8-tetrahydro-1,8-naphthyridin-2-yl)methyl)pyrrolo[3,4-c]pyrazol-5(2H,4H,6H)-yl)butanoate (enantiomer 2, 19 mg, 40 μmol) in MeCN (0.2 mL) was added aqueous NaOH solution (2.0 M, 0.20 mL, 0.40 mmol) dropwise at room temperature under nitrogen

and the mixture was stirred at 50 ºC for 2 h. The mixture was purified directly *via* mass-directed auto-preparative (MDAP) chromatography using a Sunfire C18 column and ammonium bicarbonate-modified MeCN/water gradient. The relevant fractions were combined and concentrated under a stream of nitrogen to afford the desired product (12 mg, 30 μmol, 65% yield) as a yellow gum. LCMS (Method B): 0.77 min, [M+H]$^+$ 458 m/z. IR (solid) 3300 (N-H stretch); 2930 (sp^3 C-H stretch); 2800 (N-H$^+$ stretch); 1600, 1393 (O-C-O$^-$ stretch) cm^{-1}. [α]$_D$ =   -0.16 (c = 0.50 in MeOH). ^{1}H NMR (600 MHz, DMSO-d$_6$) δ = 7.39 (s, 1H), 7.15 (t, *J* = 7.7 Hz, 1H), 7.06 (d, *J* = 7.3 Hz, 1H), 7.03 (d, *J* = 7.7 Hz, 1H), 7.01 (s, 1H), 6.85 (d, *J* = 7.7 Hz, 1H), 6.38 (br. s, 1H), 6.08 (d, *J* = 7.0 Hz, 1H), 5.01 (s, 2H), 3.71 - 3.60 (m, 4H), 3.26 - 3.16 (m, 3H), 2.92 (dd, *J* = 8.8, 3.3 Hz, 1H), 2.87 (dd, *J* = 7.0, 5.1 Hz, 1H), 2.77 (dd, *J* = 15.4, 5.9 Hz, 1H), 2.60 (t, *J* = 6.2 Hz, 2H), 2.42 (dd, *J* = 15.6, 8.3 Hz, 1H), 1.90 - 1.84 (m, 1H), 1.77 - 1.70 (m, 2H), 0.94 - 0.88 (m, 2H), 0.67 - 0.61 (m, 2H) ppm. ^{13}C NMR (101 MHz, DMSO-d$_6$) δ = 173.5, 155.3, 154.7, 152.0, 143.0, 142.2, 135.0, 126.9, 124.0, 123.4, 122.1, 121.5, 119.5, 113.0, 107.8, 60.7, 55.6, 50.3, 50.2, 40.2, 39.5, 39.4, 25.0, 19.7, 14.0, 8.3, 8.2 ppm. HRMS (ESI) calc'd for $C_{27}H_{32}N_5O_2$ [M+H]$^+$ 458.2556, found 458.2557.

Note: 1H missing from ^{1}H NMR (exchangeable

Christopher J Tame

Benzyl 4,6-dihydropyrrolo[3,4-*c*]pyrazole-5(2*H*)-carboxylate (212), dibenzyl pyrrolo[3,4-*c*]pyrazole-2,5(4*H*,6*H*)-dicarboxylate (216) and **dibenzyl pyrrolo[3,4-*c*]pyrazole-1,5(4*H*,6*H*)-dicarboxylate (217)**
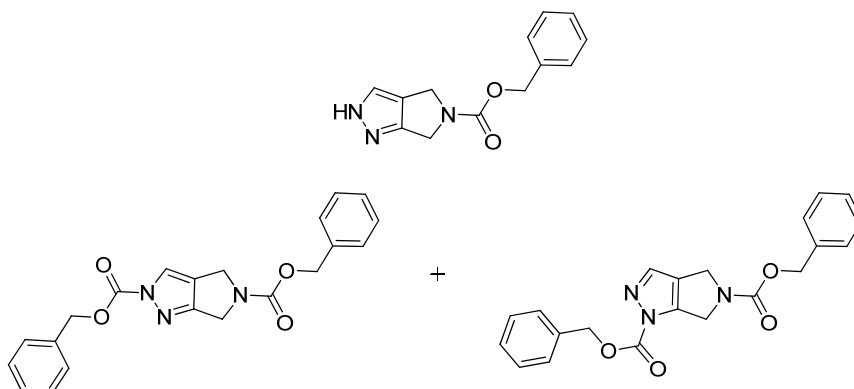
To a stirred mixture of 2,4,5,6-tetrahydropyrrolo[3,4-*c*]pyrazole, 4-methylbenzenesulphonic acid salt (3.30 g, 11.7 mmol) in 1,4-dioxane (40 mL) was added triethylamine (6.5 mL, 47 mmol) dropwise at room temperature. The flask was cooled to 0 ºC under nitrogen and benzyl (2,5-dioxopyrrolidin-1-yl) carbonate (2.92 g, 11.7 mmol) was added portionwise. The flask was removed from the cooling bath and the solution was stirred at room temperature for 1 h. Aqueous sodium bicarbonate solution (5 mL) was added and the reaction mixture was concentrated under reduced pressure to afford a crude gum. The gum was dissolved in EtOAc (100 mL) and washed three times with water (3 x 100 mL). The combined aqueous fractions were combined and extracted twice with EtOAc (2 x 100 mL). The combined organic fractions were passed through a hydrophobic frit and the filtrate was concentrated under reduced pressure to afford a brown gum. The gum was loaded in minimal CH$_2$Cl$_2$ onto two silica pre-packed columns (2 x 100 g) and eluted with 0-100% EtOAc in cyclohexane over 60 min. The relevant fractions were combined and concentrated under reduced pressure to afford benzyl 4,6-dihydropyrrolo[3,4-*c*]pyrazole-5(2*H*)-carboxylate (**212**) (1.00 g, 4.11 mmol, 35% yield) and a mixture of dibenzyl pyrrolo[3,4-*c*]pyrazole-2,5(4*H*,6*H*)-dicarboxylate (**216**) and dibenzyl pyrrolo[3,4-*c*]pyrazole-1,5(4*H*,6*H*)-dicarboxylate (**217**) (680 mg, 1.80 mmol, 15% yield) as white solids.

Christopher J Tame

Benzyl 4,6-dihydropyrrolo[3,4-*c*]pyrazole-5(2*H*)-carboxylate (**212**): LCMS (Method B): 0.82 min, [M+H]$^+$ 244 m/z. ^{1}H NMR (400 MHz, DMSO-d$_6$) δ = 12.69 (br. s., 1H), 7.53 (d, *J* = 10.8 Hz, 1H), 7.48 - 7.26 (m, 5H), 5.15 (s, 2H), 4.46 (s, 2H), 4.39 (s, 2H) ppm.

Dibenzyl pyrrolo[3,4-*c*]pyrazole-2,5(4*H*,6*H*)-dicarboxylate (**216**) and dibenzyl pyrrolo[3,4-*c*]pyrazole-1,5(4*H*,6*H*)-dicarboxylate (**217**): LCMS (Method B): 1.19 min, [M+H]$^+$ 378 m/z. ^{1}H NMR (400 MHz, DMSO-d$_6$) δ = 8.13 (d, *J* = 14.4 Hz, 0.5H), 7.72 (d, *J* = 12.7 Hz, 0.5H), 7.52 - 7.31 (m, 10H), 5.44 (s, 2H), 5.15 (s, 2H), 4.52 (s, 1H), 4.48 (s, 1H), 4.45 (s, 1H), 4.41 (s, 1H) ppm. Integration of peaks at 8.13 and 7.72 ppm indicate a 1:1 ratio of components in the mixture.

Benzyl 4,6-dihydropyrrolo[3,4-*c*]pyrazole-5(2*H*)-carboxylate (212)
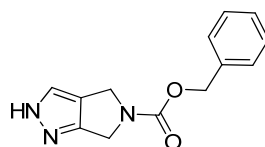
Method 1

To a stirred solution of dibenzyl pyrrolo[3,4-*c*]pyrazole-2,5(4*H*,6*H*)-dicarboxylate (100 mg, 265 μmol) in MeOH (2 mL) was added isopropylamine (68 μL, 0.80 mmol) dropwise at room temperature and the mixture was stirred for 2 h at room temperature. LCMS indicated complete conversion to the mono protected product. No further isolation or characterisation was undertaken.

Method 2

To a stirred mixture of 2,4,5,6-tetrahydropyrrolo[3,4-*c*]pyrazole, 4-methylbenzenesulphonic acid salt (4.93 g, 17.6 mmol) and DIPEA (12.3 mL, 70.2 mmol) in 2-MeTHF (80 mL) was added benzyl (2,5-dioxopyrrolidin-1-yl) carbonate (8.75 g, 35.1 mmol) portionwise at room temperature and the mixture was stirred at room temperature for 1 h. To the reaction mixture was added isopropylamine (3.0 mL, 35.1 mmol) dropwise and the solution was stirred at room temperature for 20

Christopher J Tame

min. Aqueous sodium bicarbonate solution (5 mL) was added dropwise and the reaction mixture was concentrated under reduced pressure to afford a crude gum. The gum was dissolved in EtOAc (100 mL) and washed three times with water (3 x 100 mL). The combined aqueous fractions were extracted twice with EtOAc (2 x 100 mL). The combined organic fractions were passed through a hydrophobic frit and the filtrate was concentrated under reduced pressure to afford a brown gum. The gum was loaded in minimal CH₂Cl₂ onto two silica pre-packed columns (2 x 100 g) and eluted with 0-100% EtOAc in cyclohexane over 60 min. The relevant fractions were combined and concentrated under reduced pressure to afford the desired product (2.80 g, 11.5 mmol, 66% yield) as a white solid. LCMS (Method B): 0.82 min, $[M+H]^+$ 244 m/z. ^{1}H NMR (400 MHz, DMSO-d_6) δ = 12.69 (br. s., 1H), 7.53 (d, J = 10.8 Hz, 1H), 7.48 - 7.26 (m, 5H), 5.15 (s, 2H), 4.46 (s, 2H), 4.39 (s, 2H) ppm.

tert-Butyl 7-((5-((benzyloxy)carbonyl)-5,6-dihydropyrrolo[3,4-_c_]pyrazol-2(4_H_)-yl)methyl)-3,4-dihydro-1,8-naphthyridine-1(2_H_)-carboxylate (213)
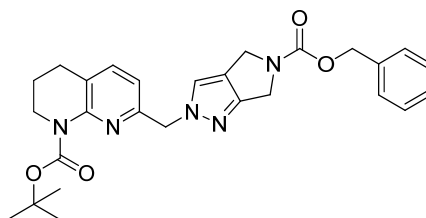
To a stirred solution of benzyl 4,6-dihydropyrrolo[3,4-_c_]pyrazole-5(1_H_)-carboxylate (29.3 g, 78.0 mmol) in DMF (350 mL) at 0 ºC was added sodium hydride (9.40 g, 235 mmol) portionwise under nitrogen and the mixture was stirred for 30 min at 0 ºC. A solution of _tert_-butyl 7-(bromomethyl)-3,4-dihydro-1,8-naphthyridine-1(2_H_)-carboxylate (25.6 g, 78.0 mmol) in DMF (35 mL) was added dropwise over 1 h at 0 ºC and the mixture was then stirred for a further 20 min at 0 ºC. Aqueous lithium chloride solution (1% (w/v), 500 mL) and EtOAc (500 mL) was added and the separated aqueous phase was extracted twice with EtOAc (2 x 500 mL). The combined organic phase was then washed with aqueous lithium chloride solution

Christopher J Tame

(1% w/v, 500 mL). The combined organic phase was then passed through a hydrophobic frit and the filtrate was concentrated under reduced pressure to afford a crude solid. The gum was loaded in minimal CH$_2$Cl$_2$ onto a silica pre-packed column (1.50 Kg) and eluted with 0-100% EtOAc in cyclohexane over 60 min. The relevant fractions were combined and concentrated under reduced pressure to afford the desired product (11.0 g, 22.5 mmol, 29% yield) as a clear oil. LCMS (Method A): 1.02 min, [M+H]$^+$ 490 m/z. ^{1}H NMR (600 MHz, DMSO-d$_6$) δ = 7.68 - 7.63 (m, 1H), 7.47 (d, J = 7.5 Hz, 1H), 7.42 - 7.35 (m, 4H), 7.34 - 7.29 (m, 1H), 6.74 (dd, J = 2.4, 7.7 Hz, 1H), 5.28 (s, 2H), 5.15 (s, 2H), 4.49 - 4.32 (m, 4H), 3.65 - 3.59 (m, 2H), 2.69 (t, J = 6.6 Hz, 2H), 1.81 (quin, J = 6.3 Hz, 2H), 1.40 (s, 9H) ppm.

Attempted synthesis of: ***tert*-butyl 7-((5,6-dihydropyrrolo[3,4-*c*]pyrazol-2(4*H*)-yl)methyl)-3,4-dihydro-1,8-naphthyridine-1(2*H*)-carboxylate (214)**
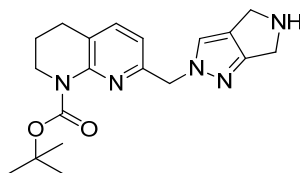
Method 1

A representative procedure is described below for the hydrogenation of **238** with three different solvents, EtOH, EtOAc and CHCl$_3$:

A solution of *tert*-butyl 7-((5-((benzyloxy)carbonyl)-5,6-dihydropyrrolo[3,4-*c*]pyrazol-2(4*H*)-yl)methyl)-3,4-dihydro-1,8-naphthyridine-1(2*H*)-carboxylate (50 mg, 0.10 mmol) in [EtOH, EtOAc or CHCl$_3$] (2 mL) was added to a nitrogen-degassed Biotage-carousel boiling tube charged with palladium (10%) on carbon (20 mg, 19 μmol) dropwise at room temperature. The atmosphere was replaced with hydrogen *via* alternative applications of vacuum and hydrogen and the solution was stirred at room temperature for 30 min. The mixture was degassed with nitrogen and submitted to LCMS analysis. LCMS analysis for each reaction suggested incomplete conversion to the desired product, along with a range of impurities LCMS (Method

Christopher J Tame

B): 0.53 min, [M+H]$^+$ 356 m/z. The most favourable reaction profile was observed with EtOAc and the least favourable reaction profile was observed with EtOH.

Method 2

To a nitrogen-degassed hydrogenation flask charged with 10% palladium on carbon (1.5 g, 3.1 mmol) was added a solution of *tert*-butyl 7-((5-((benzyloxy)carbonyl)-5,6-dihydropyrrolo[3,4-*c*]pyrazol-2(4*H*)-yl)methyl)-3,4-dihydro-1,8-naphthyridine-1(2H)-carboxylate (1.50 g, 3.06 mmol) and acetic acid (526 µL, 9.19 mmol) in EtOAc (30 mL) dropwise at room temperature. The atmosphere was replaced with hydrogen *via* alternative applications of vacuum and hydrogen and the solution was stirred at room temperature for 2 h. LCMS analysis indicated the presence of the desired product (LCMS (Method B): 0.53 min, [M+H]$^+$ 356 m/z). The reaction mixture was filtered through celite and the filtrate was washed three times with water (3 x 30 mL). The aqueous phase was then extracted with 2-BuOH (3 x 100 mL). LCMS analysis showed the presence of product in both organic and aqueous phases. The organic phase was concentrated under reduced pressure to afford an orange gum. The gum was loaded in DMSO (1 mL) and submitted to formic acid modified mass directed auto-preparative (MDAP) chromatography, which failed to isolate the desired product.

Method 3

To a nitrogen-degassed hydrogenation flask charged with 10% palladium on carbon (2.5 g, 2.4 mmol) was added a solution of *tert*-butyl 7-((5-((benzyloxy)carbonyl)-5,6-dihydropyrrolo[3,4-*c*]pyrazol-2(4*H*)-yl)methyl)-3,4-dihydro-1,8-naphthyridine-1(2*H*)-carboxylate (4.50 g, 9.19 mmol) and acetic acid (1.6 mL, 27.6 mmol) in EtOAc (90 mL) dropwise at room temperature. The atmosphere was replaced with hydrogen *via* alternative applications of vacuum and hydrogen and the solution was stirred at room temperature for 3 h. The reaction mixture was filtered through celite and the filtrate was concentrated under reduced pressure (water bath < 40 ºC) to 1/3 of its original volume. The filtrate was loaded on to an aminopropyl silica cartridge

Christopher J Tame

(50 g) and eluted with EtOAc (100 mL), followed by EtOH (100 mL). The EtOH-containing fractions were combined and concentrated under reduced pressure to afford the desired product (2.54 g, 6.72 mmol, 73% yield) as a yellow oil. LCMS (Method B): 0.53 min, $[M+H]^+$ 356 m/z. ^{1}H NMR (400 MHz, CDCl$_3$) δ = 7.26 (d, J = 7.3 Hz, 1H), 7.16 (s, 1H), 6.63 (d, J = 7.8 Hz, 1H), 4.00 - 3.90 (m, 4H), 3.77 - 3.62 (m, 2H), 3.34 (s, 2H), 2.67 (d, J = 6.5 Hz, 2H), 1.93 - 1.75 (m, 2H), 1.45 (s, 9H) ppm.

(*E*)-*tert*-butyl 7-((5-(4-methoxy-4-oxobut-2-en-1-yl)-5,6-dihydropyrrolo[3,4-*c*]pyrazol-2(4*H*)-yl)methyl)-3,4-dihydro-1,8-naphthyridine-1(2*H*)-carboxylate (215)
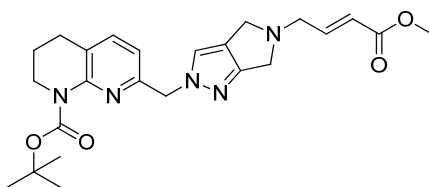
To a stirred solution of *tert*-butyl 7-((5,6-dihydropyrrolo[3,4-*c*]pyrazol-2(4*H*)-yl)methyl)-3,4-dihydro-1,8-naphthyridine-1(2*H*)-carboxylate (240 mg, 675 µmol) and DIPEA (236 µL, 1.35 mmol) in CH$_2$Cl$_2$ (6 mL) at room temperature under nitrogen was added (*E*)-methyl 4-bromobut-2-enoate (80 µL, 0.68 mmol) dropwise. The mixture was stirred at room temperature for 1 h. CH$_2$Cl$_2$ (50 mL) was added and the mixture was washed three times with water (3 x 50 mL). The combined organic phase was passed through a hydrophobic frit and concentrated under reduced pressure to afford an orange gum. The gum was loaded in minimal CH$_2$Cl$_2$ onto a silica pre-packed column (50 g) and eluted with 0-10% MeOH in CH$_2$Cl$_2$ over 60 min. The relevant fractions were combined and concentrated under reduced pressure to afford the desired product (150 mg, 330 µmol, 49% yield) as a yellow solid. LCMS (Method A): 0.66 min, $[M+H]^+$ 454 m/z. ^{1}H NMR (400 MHz, DMSO-d$_6$) δ = 7.50 (s, 1H), 7.46 (d, J = 7.6 Hz, 1H), 6.90 (dt, J = 5.8, 15.6 Hz, 1H), 6.68 (d, J = 7.6 Hz, 1H), 6.07 (dt, J = 1.8, 15.6 Hz, 1H), 3.70 (s, 2H), 3.67 (s, 3H), 3.63 (t, J = 6.0 Hz, 2H), 3.55 (dd, J = 1.6, 5.7 Hz, 2H), 3.17 (d, J = 5.3 Hz, 4H), 2.70 (s, 2H), 1.89 - 1.74 (m, 2H), 1.41 (s, 9H) ppm.

Christopher J Tame

Methyl 3-(3-cyclopropylphenyl)-4-(2-((5,6,7,8-tetrahydro-1,8-naphthyridin-2-yl)methyl)pyrrolo[3,4-*c*]pyrazol-5(2*H*,4*H*,6*H*)-yl)butanoate (209)
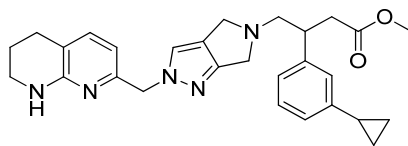
To a degassed solution of 3-cyclopropylphenyl boronic acid (273 mg, 1.69 mmol), (*E*)-*tert*-butyl 7-((5-(4-methoxy-4-oxobut-2-en-1-yl)-5,6-dihydropyrrolo[3,4-*c*]pyrazol-2(4*H*)-yl)methyl)-3,4-dihydro-1,8-naphthyridine-1(2*H*)-carboxylate (255 mg, 560 μmol) and (*R*)-2,2'-bis(diphenylphosphino)-1,1'-binaphthalene (70 mg, 0.11 mmol) in 1,4-dioxane (5.5 mL) was added aqueous potassium hydroxide solution (3.8 M, 300 μL, 1.13 mmol) and chloro(1,5-cyclooctadiene)rhodium(II) dimer (28 mg, 60 μmol) at room temperature. The mixture was degassed with alternative applications of vacuum and nitrogen and then heated to 95 ºC for 1 h. The reaction mixture was cooled to room temperature, loaded directly onto an SCX pre-packed column (10 g) and eluted with MeOH (20 mL) and a solution of NH₃ in MeOH (2 M, 20 mL), respectively. The relevant fractions were combined and concentrated under reduced pressure to afford a crude gum. To a solution of the gum in MeOH (5 mL) was added a solution of hydrochloric acid in 1,4-dioxane (4.0 M, 0.71 mL, 2.8 mol) and the solution was stirred at 50 °C for 2 h. The reaction mixture was loaded directly onto an aminopropyl pre-packed column (20 g) and eluted with MeOH (50 mL). The filtrate was concentrated under reduced pressure to afford a crude solid. The solid was dissolved in minimal DMSO and loaded onto a C18 pre packed silica cartridge (30 g) and eluted with 50-95% MeCN (0.1% NH3) in water (0.1% ammonium bicarbonate) over 30 min. The relevant fractions were combined and concentrated to afford the desired product (95 mg, 0.201 mmol, 36%) as a yellow gum. LCMS (Method B): 1.22 min, [M+H]⁺ 472 m/z. Chiral HPLC analysis (30% EtOH in heptane, Chiralcel OD-H column (4.6 mm x 25 cm), flow rate: 1 mL/min): 75% e.e. ¹H NMR (400 MHz, CDCl₃) δ = 7.19 (t, *J* = 7.6 Hz, 1H), 7.13 (s, 1H), 7.07 (d, *J* = 7.3 Hz, 1H), 7.02 (d, *J* = 7.8 Hz, 1H), 6.97 (s, 1H), 6.91 (d, *J* = 7.8 Hz, 1H), 6.24 (d, *J* = 7.3 Hz, 1H), 5.11 (s, 2H), 4.83 (br. s., 1H), 3.88 - 3.79 (m, 2H), 3.79 - 3.73 (m, *J* = 12.3 Hz, 1H), 3.70 (d, *J* = 11.3 Hz, 1H), 3.53 (s, 3H), 3.43 - 3.38

Christopher J Tame

(m, 2H), 3.38 - 3.30 (m, 1H), 2.95 (d, J = 7.6 Hz, 2H), 2.89 (dd, J = 15.1, 7.1 Hz, 1H), 2.69 (t, J = 6.3 Hz, 2 H), 2.56 (dd, J = 15.2, 7.7 Hz, 1H), 1.96 - 1.81 (m, 3H), 0.99 - 0.90 (m, 2H), 0.72 - 0.64 (m, 2H) ppm.

4　Experimental procedures for PI3Kδ inhibitors

Trimethyl[3-(2-propyn-1-yloxy)-1-propyn-1-yl]silane (323) [349]
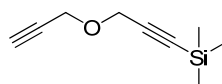
Lithium bis(trimethylsilyl)amide in THF (1 M, 103 mL, 103 mmol) was added dropwise to a stirred solution of 3-(prop-2-yn-1-yloxy)prop-1-yne (10.6 mL, 103 mmol) in THF (400 mL) at -78 ºC under nitrogen. Following stirring at -78 °C for 1 h, chlorotrimethylsilane (13.1 mL, 103 mmol) was added dropwise at -78 ºC under nitrogen.   The reaction mixture was allowed to warm to -30 ºC over 16 h, then saturated ammonium chloride solution (200 mL) was added dropwise. The flask was then removed from the bath and allowed to warm to room temperature. The mixture was then extracted three times with diethyl ether (3 x 500 mL) and the combined organic phases were passed through a hydrophobic frit and evaporated under reduced pressure (>100 mbar, <35 °C) to afford an orange oil. Trimethyl[3-(2-propyn-1-yloxy)-1-propyn-1-yl]silane was isolated by fractional distillation as a colourless oil, b.p. 120-130°C at 135 mbar (9.98 g, 60.0 mmol, 58%). ^{1}H NMR (DMSO-d$_6$, 400 MHz): δ = 4.20 (s, 2H), 4.17 (d, J = 2.3 Hz, 2H), 3.47 (t, J = 2.4 Hz, 1H), 0.16 (s, 9H) ppm.

Christopher J Tame

Trimethyl(6-phenyl-1,3-dihydroisobenzofuran-4-yl)silane (326)
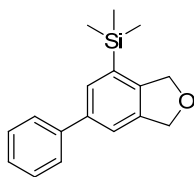
To chloro(pentamethylcyclopentadienyl)(cyclooctadiene)ruthenium(II) (13 mg, 30 μmol) and ethynylbenzene (130 μL, 1.18 mmol) was added anhydrous dichloroethane (DCE) (2.5 mL) and the mixture was degassed with three alternative applications of nitrogen and vacuum. To the mixture was added a solution of trimethyl[3-(2-propyn-1-yloxy)-1-propyn-1-yl]silane (98 mg, 0.59 mmol) in dichloroethane (2.5 mL) dropwise at room temperature and the mixture was stirred under nitrogen for 6 h. The mixture was diluted with dichloroethane (150 mL) and then filtered under atmospheric pressure. The filter cake was dissolved in MeOH (1 mL) and purified by formic acid modified mass directed auto preparative chromatography. The relevant fractions were combined and concentrated under reduced pressure to afford trimethyl(6-phenyl-1,3-dihydroisobenzofuran-4-yl)silane (21 mg, 80 μmol, 13%). LCMS (Method A): 1.47 min, [M+H]$^+$ 269 m/z. ^{1}H NMR (600 MHz, DMSO-d$_6$) δ = 7.48 (s, 1H), 7.47 (s, 1H), 7.42 (s, 2H), 7.31 (t, J = 7.3 Hz, 2H), 7.21 (t, J = 7.3 Hz, 1H), 4.93 (s, 2H), 4.89 (s, 2H), 0.14 (s, 9H) ppm.

Christopher J Tame

N-{2-(Methyloxy)-5-[7-(trimethylsilyl)-1,3-dihydro-2-benzofuran-5-yl]-3-pyridinyl}methanesulfonamide (316)
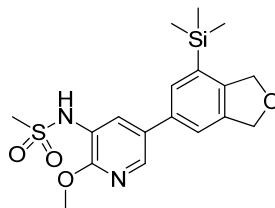
To chloro(pentamethylcyclopentadienyl)(cyclooctadiene)ruthenium(II) (45.8 mg, 120 μmol) and N-[5-ethynyl-2-(methyloxy)-3-pyridinyl]methanesulfonamide (544 mg, 2.41 mmol) was added anhydrous CH_2Cl_2 (10 mL) and the mixture was degassed with alternative applications of nitrogen and vacuum. To the mixture was added a solution of trimethyl[3-(2-propyn-1-yloxy)-1-propyn-1-yl]silane (200 mg, 1.20 mmol) in CH_2Cl_2 (10 mL) dropwise at room temperature under nitrogen. The reaction mixture was stirred at room temperature overnight. Water (100 mL) and CH_2Cl_2 (100 mL) was added to the flask and the mixture separated. The aqueous phase was extracted three times with CH_2Cl_2 (3 x 100 mL) and the combined organic fractions were washed twice more with brine (2 x 100 mL). The organic fractions were combined, passed through a hydrophobic frit and concentrated under reduced pressure to afford a crude gum. The crude gum was dissolved in a minimum volume of CH_2Cl_2 and purified by silica gel column chromatography (100g Si, 0-100% EtOAc in Cyclohexane, 40 min.). The relevant fractions were combined and concentrated under reduced pressure to afford a yellow gum. The crude gum was dissolved in a minimum volume of CH_2Cl_2 and purified by silica gel column chromatography (100g Si, 0-10% EtOAc in CH_2Cl_2, 40 min.). The relevant fractions were combined and concentrated under reduced pressure to N-{2-(methyloxy)-5-[7-(trimethylsilyl)-1,3-dihydro-2-benzofuran-5-yl]-3-pyridinyl}methanesulfonamide (310 mg, 0.79 mmol, 66% yield) as a white solid and N-[5-ethynyl-2-(methyloxy)-3-pyridinyl]methanesulfonamide (167 mg, 0.74 mmol, 31%) as a white solid.

N-{2-(methyloxy)-5-[7-(trimethylsilyl)-1,3-dihydro-2-benzofuran-5-yl]-3-pyridinyl}methanesulfonamide (**316**): m.p. 166 - 167 °C. LCMS (Method A): 1.19 min, [M+H]$^+$ 393 m/z. IR (solid) 3171 (N-H stretch); 1327, 1137 (O=S=O) cm^{-1}. ^{1}H

Christopher J Tame

NMR (DMSO-d$_6$, 400 MHz) δ = 9.33 (s, 1H), 8.28 (d, J = 2.3 Hz, 1H), 7.85 (d, J = 2.3 Hz, 1H), 7.57 (s, 1H), 7.54 (s, 1H), 5.09 (s, 2H), 5.05 (s, 2H), 3.97 (s, 3H), 3.08 (s, 3H), 0.30 (s, 9H) ppm. ^{13}C NMR (DMSO-d$_6$, 101 MHz): δ = 157.2, 144.5, 141.5, 140.3, 136.4, 134.2, 132.2, 132.1, 131.2, 122.4, 121.3, 73.9, 73.3, 54.8, 41.8, 0.0 ppm. HRMS (ESI) calc'd for C$_{18}$H$_{25}$N$_2$O$_4$SSi [M+H]$^+$ 393.1299, found 393.1298.

N-[5-ethynyl-2-(methyloxy)-3-pyridinyl]methanesulfonamide (**322**): LCMS (Method A): 0.73 min, [M+H]$^+$ 226 m/z. ^{1}H NMR (DMSO-d$_6$, 400 MHz) δ = 9.38 (s, 1H), 8.13 (d, J = 2.0 Hz, 1H), 7.66 (d, J = 2.3 Hz, 1H), 4.28 (s, 1H), 3.94 (s, 3H), 3.08 (s, 3H) ppm.

Trimethyl(6-phenyl-1,3-dihydroisobenzofuran-4-yl)silane (326) and Trimethyl(3-((7-(trimethylsilyl)-1,3-dihydroisobenzofuran-5-yl)methoxy)prop-1-yn-1-yl)silane (327)
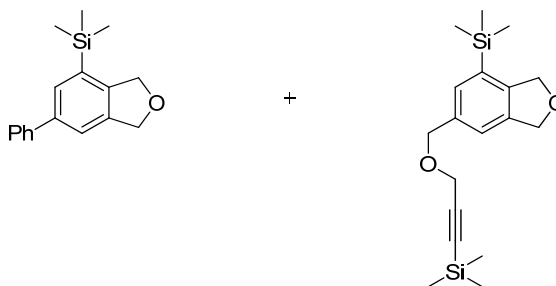
Procedure used for investigating the effect of solvent on cyclotrimerisation.

The solvents under investigation were submitted to the same reaction conditions, detailed below: The 7 solvents investigated were: 1,2-dichloroethane (DCE), 2-methyl THF, cyclopentylmethyl ether (CPME), 2-butanol, ethanol, water and water: ethanol (50:50)

Chloro(pentamethylcyclopentadienyl)(cyclooctadiene)ruthenium(II) (4.66 mg, 12.0 μmol) was charged to 7 Radley's carousel tubes, each equipped with a stirrer bar. To each of the 7 tubes was added a solution of ethynylbenzene (53.8 μL, 489 μmol) in

[Solvent, (1.30 mL)], followed by a solution of trimethyl[3-(2-propyn-1-yloxy)-1-propyn-1-yl]silane (40.7 mg, 245 μmol) in [Solvent, (1.30 mL)] at room temperature. The 7 vials were stirred simultaneously in a Radley's carousel for 2 h and analysed by LCMS after 30 min and 2 h.

The reactions using the solvents DCE, water and CPME were selected for work-up and purification, details for this are shown below.

Dichloroethane (DCE):

To the reaction mixture was added water (10 mL) and the mixture separated. The aqueous phase was extracted four times with 2-MeTHF (4 x 10 mL) and the combined organic phase was concentrated under reduced pressure to afford a crude solid. The crude solid was dissolved in minimal DCM and purified by silica gel column chromatography (10g Si, 0-25% EtOAc in cyclohexane, 60 min). The relevant fractions were combined and concentrated under reduced pressure to afford a mixture of trimethyl(6-phenyl-1,3-dihydroisobenzofuran-4-yl)silane (**326**) and trimethyl(3-((7-(trimethylsilyl)-1,3-dihydroisobenzofuran-5-yl)methoxy)prop-1-yn-1-yl)silane (**327**), respectively (15 mg). ^{1}H NMR (400 MHz, DMSO-d$_6$) δ = 7.48 (m), 7.42 (s), 7.31 (t, J = 7.3Hz), 7.24-7.20 (m), 7.15 (s), 7.12-7.10 (m), 4.93 (s), 4.89 (br. s.), 4.82 (s), 4.36 (s), 4.02 (s), 0.14 (s), 0.09 (s), 0.00 (s) ppm. The ratio of the products was determined by the integration of peaks at δ = 4.93 and 4.82 ppm. This gave a ratio for **326**:**327** of 6.0:1. Accordingly, the adjusted yield for trimethyl(6-phenyl-1,3-dihydroisobenzofuran-4-yl)silane (**326**) is 19%.

Water:

To the reaction mixture was added 2-MeTHF (10 mL) and the mixture separated. The aqueous phase was extracted four times with 2-MeTHF (4 x 10 mL) and the combined organic phase was concentrated under reduced pressure to afford a crude solid. The crude solid was dissolved in minimal DCM and purified by silica gel column chromatography (10g Si, 0-25% EtOAc in cyclohexane, 60 min). The relevant fractions were combined and concentrated under reduced pressure to afford

Christopher J Tame

a mixture of trimethyl(6-phenyl-1,3-dihydroisobenzofuran-4-yl)silane (**326**) and trimethyl(3-((7-(trimethylsilyl)-1,3-dihydroisobenzofuran-5-yl)methoxy)prop-1-yn-1-yl)silane (**327**), respectively (44 mg). ^{1}H NMR (400 MHz, DMSO-d_6) δ = 7.47 (m), 7.42 (s), 7.31 (t, J = 7.3 Hz), 7.24-7.18 (m), 7.15 (s), 7.10 (s), 4.93 (s), 4.88 (br. s.), 4.82 (s), 4.35 (s), 4.02 (s), 0.14 (s), 0.09 (s), 0.00 (s) ppm. The ratio of the products was determined by the integration of peaks at δ = 4.93 and 4.82 ppm. This gave a ratio for **326**:**327** of 2.3:1. Accordingly, the adjusted yield for trimethyl(6-phenyl-1,3-dihydroisobenzofuran-4-yl)silane (**326**) is 47%.

CPME:

To the reaction mixture was added water (10 mL) and the mixture was extracted four times with 2-MeTHF (4 x 10 mL). The combined organic phase was concentrated under reduced pressure to afford a crude solid. The crude solid was dissolved in minimal DCM and purified by silica gel column chromatography (10g Si, 0-25% EtOAc in cyclohexane, 60 min). The relevant fractions were combined and concentrated under reduced pressure to afford a mixture of trimethyl(6-phenyl-1,3-dihydroisobenzofuran-4-yl)silane (**326)** and trimethyl(3-((7-(trimethylsilyl)-1,3-dihydroisobenzofuran-5-yl)methoxy)prop-1-yn-1-yl)silane (**92**) respectively (64 mg). ^{1}H NMR (400 MHz, DMSO-d_6) δ = 7.48 (m), 7.42 (s), 7.31 (t, J = 7.6 Hz), 7.24-7.18 (m), 7.15 (s), 7.11 (s), 4.94-4.92 (m), 4.88 (br. s.) 4.82 (s), 4.35 (s), 4.02 (s), 0.14 (s), 0.10-0.08 (m), 0.00 (m) ppm. The ratio of the products was determined by the integration of peaks at δ = 4.93 and 4.82 ppm. This gave a ratio for **326**:**327** of 4.1:1. Accordingly, the adjusted yield for trimethyl(6-phenyl-1,3-dihydroisobenzofuran-4-yl)silane (**327**) is 78%.

Christopher J Tame

***N*-{2-(Methyloxy)-5-[7-(trimethylsilyl)-1,3-dihydro-2-benzofuran-5-yl]-3-pyridinyl}methanesulfonamide (316)**
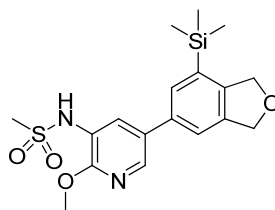
To chloro(pentamethylcyclopentadienyl)(cyclooctadiene)ruthenium(II) (344 mg, 902 μmol) was added a solution of *N*-[5-ethynyl-2-(methyloxy)-3-pyridinyl]methanesulfonamide (4.1 g, 18 mmol) in CPME (65 mL) and the mixture was degassed with three alternative applications of vacuum and nitrogen. To the mixture was added a solution of trimethyl[3-(2-propyn-1-yloxy)-1-propyn-1-yl]silane (1.5 g, 9.0 mmol) in CPME (40 mL) sequentially, dropwise at room temperature. The reaction mixture was then stirred at room temperature for 2 h. The reaction mixture was diluted with ethyl acetate (100 mL) and washed with brine (3x 50 mL). The aqueous extracts were back extracted with ethyl acetate (50 mL). The combined organic extracts were dried under reduced pressure to afford a crude gum. The gum was loaded in minimal CH$_2$Cl$_2$ onto a silica pre-packed column (340 g) and eluted with 0-10% EtOAc in CH$_2$Cl$_2$ over 12 column volumes. The combined relevant fractions were concentrated under reduced pressure to give *N*-{2-(methyloxy)-5-[7-(trimethylsilyl)-1,3-dihydro-2-benzofuran-5-yl]-3-pyridinyl}methanesulfonamide (2.26 g, 5.76 mmol, 64 % yield) as a yellow solid. LCMS (Method A): 1.19 min, ^{1}H NMR (DMSO-d$_6$, 400 MHz): δ = 9.25 - 9.40 (m, 1H), 8.21 - 8.33 (m, 1H), 7.75 - 7.95 (m, 1H), 7.56 (s, 1H), 7.54 (s, 1H), 5.08 (s, 2H), 5.05 (s, 2H), 3.97 (s, 3H), 3.07 (s, 3H), 0.29 (s, 9H) ppm.

Christopher J Tame

N-{2-(Methyloxy)-5-[7-(trimethylsilyl)-1,3-dihydro-2-benzofuran-5-yl]-3-pyridinyl}methanesulfonamide (316)
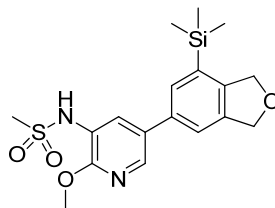
To a nitrogen degassed solution of chloro(pentamethylcyclopentadienyl)(cyclooctadiene)ruthenium(II) (38 mg, 0.10 mmol) and *N*-[5-ethynyl-2-(methyloxy)-3-pyridinyl]methanesulfonamide (226 mg, 0.1 mmol) in CPME (7.5 mL) was added a solution of trimethyl[3-(2-propyn-1-yloxy)-1-propyn-1-yl]silane (200 mg, 1.20 mmol) in CPME (7.5 mL) sequentially, dropwise at room temperature. The mixture was then stirred at room temperature for 24 h. The mixture was concentrated under reduced pressure to afford a crude gum. The gum was loaded in minimal CH_2Cl_2 onto a silica pre-packed column (10 g) and eluted with 0-100% EtOAc in cyclohexane over 60 min. The combined relevant fractions were concentrated under reduced pressure to give *N*-{2-(methyloxy)-5-[7-(trimethylsilyl)-1,3-dihydro-2-benzofuran-5-yl]-3-pyridinyl}methanesulfonamide (250 mg, 640 µmol, 64%) as a white solid. LCMS (Method A): 1.19 min. ^{1}H NMR (DMSO-d$_6$, 400 MHz): δ = 9.25 - 9.40 (m, 1H), 8.21 - 8.33 (m, 1H), 7.75 - 7.95 (m, 1H), 7.56 (s, 1H), 7.54 (s, 1H), 5.08 (s, 2H), 5.05 (s, 2H), 3.97 (s, 3H), 3.07 (s, 3H), 0.29 (s, 9H) ppm.

Christopher J Tame

N-[5-(7-Iodo-1,3-dihydro-2-benzofuran-5-yl)-2-(methyloxy)-3-pyridinyl]methanesulfonamide (263)
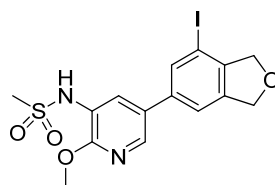
Iodine monochloride in CH_2Cl_2 (1 M, 4.33 mL, 4.33 mmol) was added dropwise to a solution of N-{2-(methyloxy)-5-[7-(trimethylsilyl)-1,3-dihydro-2-benzofuran-5-yl]-3-pyridinyl}methanesulfonamide (850 mg, 2.17 mmol) in CH_2Cl_2 (20 mL) under nitrogen at -10 ºC. The reaction mixture was allowed to warm to 0 ºC and stirred for 5 minutes, during which a white solid precipitated from solution. Saturated sodium thiosulfate solution (50 mL) was added and the resulting mixture stirred at room temperature for 20 min. The reaction mixture was filtered under reduced pressure and washed with CH_2Cl_2 (5 mL). The filtrate was poured onto CH_2Cl_2 (50 mL) and water (30 mL) and the separated aqueous phase was extracted with CH_2Cl_2 (2 x 50 mL). The combined organic fractions were passed through a hydrophobic frit then concentrated under vacuum to afford a yellow solid. The yellow solid and white solid were combined and triturated in methanol (5 mL). The mixture was filtered under reduced pressure and the solid was dried in a vacuum oven for 2 h to afford N-[5-(7-iodo-1,3-dihydro-2-benzofuran-5-yl)-2-(methyloxy)-3-pyridinyl]methanesulfonamide (774 mg, 1.73 mmol, 80%) as a white solid. LCMS (Method A): 1.06 min, [M+H]$^+$ 447 m/z. ^{1}H NMR (DMSO-d$_6$, 400 MHz): δ = 9.26 - 9.39 (m, 1H), 8.28 (d, J = 2.3 Hz, 1H), 7.89 (s, 1H), 7.85 (d, J = 2.3 Hz, 1H), 7.59 (s, 1H), 5.21 (s, 2H), 4.92 (s, 2H), 3.96 (s, 3H), 3.09 (s, 3H) ppm. ^{13}C NMR (101 MHz, DMSO-d$_6$): δ = 156.8, 143.2, 141.5, 141.1, 138.8, 134.3, 131.0, 128.8, 121.9, 119.8, 89.0, 76.9, 74.7, 54.3, 41.2 ppm.

Christopher J Tame

N-(5-(7-Amino-1,3-dihydroisobenzofuran-5-yl)-2-methoxypyridin-3-yl)methanesulfonamide (262)
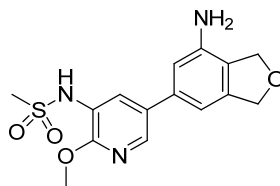
L-proline (413 mg, 3.59 mmol), copper(I) iodide (68 mg, 0.36 mmol), cesium carbonate (1.75 g, 5.38 mmol) and *N*-(5-(7-iodo-1,3-dihydroisobenzofuran-5-yl)-2-methoxypyridin-3-yl)methanesulfonamide (800 mg, 1.79 mmol) were evenly changerd over 2 microwave vials (2 x 20 mL). The vials was sealed and degassed before aqueous ammonia solution 0.88 (35%, 8.0 mL, 0.13 mol) and DMSO (8 mL) were added *via* syringe and the vials were heated and stirred in a Biotage microwave reactor at 50 ºC for 2 h. After this time aqueous ammonia solution 0.88 (35%, 2 x 4 mL, 0.2 mol) and cesium carbonate (2 x 500 mg, 1.53 mmol) was added *via* syringe to both vials and the vials were heated and stirred at 110 ºC for 6 h. The reaction mixtures were combined and filtered under reduced pressure, then washed with methanol. The blue filtrate was loaded directly onto a SCX cartridge (70 g) and flushed with methanol (200 mL) under reduced pressure. The column was then eluted with ammonia in methanol solution (7 M, 300 mL) under reduced pressure. The filtrate was concentrated under reduced pressure to afford a crude gum. The gum was dissolved in CH_2Cl_2 (30 mL) and washed three times with water. The combined organic fractions were filtered through a hydrophobic frit and concentrated under reduced pressure to afford *N*-(5-(7-amino-1,3-dihydroisobenzofuran-5-yl)-2-methoxypyridin-3-yl)methanesulfonamide (460 mg, 1.37 mmol, 77%) as a white solid. m.p. 295 - 301 °C. LCMS (Method A): 0.65 min, [M+H]$^+$ 336 m/z. IR (solid) 3467, 3377 (H-N-H stretch); 3049 (N-H stretch); 1303, 1138 (O=S=O) cm^{-1}. ^{1}H NMR (DMSO-d_6, 400 MHz): δ = 9.28 (br. s., 1H), 8.17 (d, *J* = 2.3 Hz, 1H), 7.77 (d, *J* = 2.3 Hz, 1H), 6.64 - 6.78 (m, 2H), 5.25 (s, 2H), 4.97 (s, 2H), 4.88 (s, 2H), 3.96 (s, 3H), 3.07 (s, 3H) ppm. ^{13}C NMR (DMSO-d_6, 101 MHz): δ = 155.8, 142.9, 140.8, 140.0, 137.1, 130.6, 130.5, 122.3, 121.1, 110.7, 106.6, 73.2, 71.5, 53.7, 40.6 ppm. HRMS (ESI) calc'd for $C_{15}H_{18}N_3O_4S$ [M+H]$^+$ 336.1013, found 336.1017.

Christopher J Tame

N-(6-(6-Methoxy-5-(methylsulfonamido)pyridin-3-yl)-1,3-dihydroisobenzofuran-4-yl)acetamide (257)
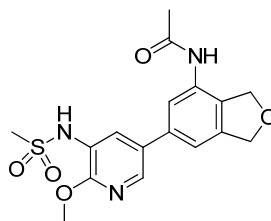
Acetic acid (10 μL, 0.15 mmol) was added dropwise to a stirred suspension of HATU (62 mg, 0.16 mmol) and DIPEA (50 μL, 0.30 mmol) in CH_2Cl_2 (1 mL) at room temperature. The mixture was stirred for 10 min at room temperature, during which time the milky suspension turned into a yellow solution. A suspension of *N*-(5-(7-amino-1,3-dihydroisobenzofuran-5-yl)-2-methoxypyridin-3-yl)methanesulfonamide (50 mg, 0.15 mmol) in CH_2Cl_2 (1 mL) was then added dropwise to the mixture at room temperature. DMF (10 μL) was added and the solution was stirred for 16 h at room temperature. The solution was poured onto EtOAc (2 mL) and brine (3 mL) and the separated organic phase was washed with brine (2 x 3 mL). The combined organic phase was concentrated under a stream of nitrogen to give an orange gum. The gum was dissolved in DMSO/MeOH (1 mL, 1:1 v/v) and purified *via* mass directed auto-preparative (MDAP) chromatography using a Sunfire C18 column and an ammonium bicarbonate-modified MeCN/water gradient. The relevant combined fractions were concentrated under reduced pressure to give a white solid. Water (10 mL) and diethyl ether (10 mL) was added and the mixture filtered and the filter cake was dried under reduced pressure to give *N*-(6-(6-methoxy-5-(methylsulfonamido)pyridin-3-yl)-1,3-dihydroisobenzofuran-4-yl)acetamide (12 mg, 30 μmol, 21%) as a white solid. m.p. 225 - 228 °C. LCMS (Method A): 0.67 min, $[M+H]^+$ 378 m/z. IR (solid) 3240 (N-H stretch); 3080 (N-H stretch); 1629 (C=O); 1321, 1144 (O=S=O) cm^{-1}. ^{1}H NMR (DMSO-d$_6$, 400 MHz): δ = 9.77 (s, 1H), 9.37 (s, 1H), 8.23 (s, 1H), 7.81 (s, 1H), 7.65 (s, 1H), 7.34 (s, 1H), 5.05 (s, 2H), 4.96 (s, 2H), 3.96 (s, 3H), 3.07 (s, 3H), 2.07 (s, 3H) ppm. ^{13}C NMR (101 MHz, DMSO-d$_6$) δ = 168.3, 156.1, 141.6, 140.3, 136.6, 132.9, 130.7, 130.4, 129.6,

Christopher J Tame

121.3, 118.9, 115.0, 72.8, 72.1, 53.8, 40.7, 23.4 ppm.   HRMS (ESI) calc'd for C$_{17}$H$_{20}$N$_3$O$_5$S [M+H]$^+$ 378.1118, found 378.1120.

_N_-(6-(6-Methoxy-5-(methylsulfonamido)pyridin-3-yl)-1,3-dihydroisobenzofuran-4-yl)-2-methylthiazole-4-carboxamide (258)
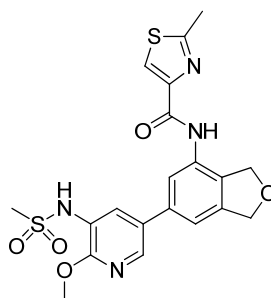
DIPEA (50 μL, 0.30 mmol) and HATU (62 mg, 0.16 mmol) were added sequentially to a stirred solution of 2-methyl-1,3-thiazole-4-carboxylic acid (34 mg, 24 μmol) in DMF (0.5 mL) at room temperature and the solution stirred for 10 min.   A solution of _N_-(5-(7-amino-1,3-dihydroisobenzofuran-5-yl)-2-methoxypyridin-3-yl)methanesulfonamide (50 mg, 0.15 mmol) in DMF (0.5 mL) was then added dropwise at room temperature and the solution stirred at room temperature for 16 h, during which time a white solid precipitated. The mixture was filtered under reduced pressure and washed with water (10 mL) then diethyl ether (10 mL). The white solid was dried in a vacuum oven for 16 h to afford _N_-(6-(6-methoxy-5-(methylsulfonamido)pyridin-3-yl)-1,3-dihydroisobenzofuran-4-yl)-2-methylthiazole-4-carboxamide (23.5 mg, 50.0 μmol, 21%) as a white solid. m.p. 274 - 277 °C. LCMS (Method A): 0.89 min, [M+H]$^+$ 461 m/z. IR (solid) 3379 (N-H stretch); 3141 (N-H stretch); 1671 (C=O); 1324, 1136 (O=S=O) cm^{-1}. ^{1}H NMR (DMSO-d$_6$, 400 MHz): δ = 10.30 (s, 1H), 9.39 (s, 1H), 8.25 - 8.44 (m, 2H), 7.93 (d, _J_ = 2.3 Hz, 1H), 7.71 (s, 1H), 7.49 (s, 1H), 5.15 (s, 2H), 5.07 (s, 2H), 4.03 (s, 3H), 3.14 (s, 3H), 2.83 (s, 3H) ppm. ^{13}C NMR (DMSO-d$_6$, 101 MHz): δ = 166.2, 158.8, 156.0, 148.7, 142.1, 140.1, 136.9, 132.6, 132.1, 130.6, 129.3, 125.4, 121.5, 120.8, 115.8, 72.7, 72.2, 53.7, 40.7, 18.8 ppm. HRMS (ESI) calc'd for C$_{20}$H$_{21}$N$_4$O$_5$S$_2$ [M+H]$^+$ 461.0948, found 461.0951.

Christopher J Tame

N-(6-(6-Methoxy-5-(methylsulfonamido)pyridin-3-yl)-1,3-dihydroisobenzofuran-4-yl)-2-morpholinoacetamide (259)
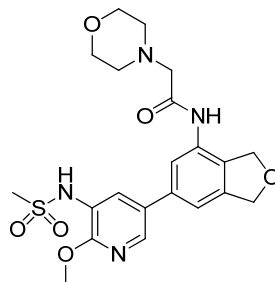
DIPEA (80 μL, 0.48 mmol) and HATU (100 mg, 260 μmol) were added sequentially to a stirred solution of morpholin-4-yl-acetic acid (35 mg, 0.24 mmol) in DMF (0.5 mL) at room temperature. The reaction was stirred for 10 min at room temperature. A solution of N-(5-(7-amino-1,3-dihydroisobenzofuran-5-yl)-2-methoxypyridin-3-yl)methanesulfonamide (80 mg, 0.24 mmol) in DMF (0.5 mL) was then added dropwise to the reaction mixture at room temperature and the mixture was stirred at room temperature for 16 h. The mixture was poured onto EtOAc (2 mL) and brine (3 mL) and the separated organic phase was washed with brine (2 x 3 mL). The combined organic phase was concentrated under a stream of nitrogen to give an orange gum. The gum was dissolved in DMSO/MeOH (1 mL, 1:1 v/v) and purified *via* mass directed auto-preparative (MDAP) chromatography using a Sunfire C18 column and an ammonium bicarbonate-modified MeCN/water gradient. The relevant fractions were combined and the volume reduced by 70% under a stream of nitrogen. A white solid precipitated from solution. The mixture was filtered under reduced pressure and washed with water (10 mL) then diethyl ether (10 mL) and then dried in a vacuum oven for 1 hour to afford N-(6-(6-methoxy-5-(methylsulfonamido)pyridin-3-yl)-1,3-dihydroisobenzofuran-4-yl)-2-morpholinoacetamide (25 mg, 50 μmol, 22%) as a white solid. m.p. 218 - 220 °C. LCMS (Method A): 0.54 min, [M+H]$^+$ 463 m/z. IR (solid) 3224 (N-H stretch); 2925 (N-H stretch); 2852 (C-H stretch); 1658 (C=O); 1318, 1142 (O=S=O) cm^{-1}. ^{1}H NMR (DMSO-d$_6$, 400 MHz): δ = 9.63 (s, 1H), 9.24 - 9.46 (m, 1H), 8.24 (d, J = 2.3 Hz, 1H), 7.83 (d, J = 2.3 Hz, 1H), 7.67 (s, 1H), 7.37 (s, 1H), 5.07 (s, 2H), 4.98 (s, 2H), 3.96 (s, 3H), 3.65 (t, J = 4.5 Hz, 4H), 3.15 (s, 2H), 3.07 (s, 3H), 2.53 (t, J = 4.5 Hz, 4H) ppm. ^{13}C NMR (DMSO-d$_6$, 101 MHz): δ = 168.0, 156.1, 141.6, 140.3, 136.6,

Christopher J Tame

133.1, 130.7, 130.4, 129.6, 121.3, 118.8, 115.0, 72.8, 72.1, 53.8, 40.7, 40.2, 38.9, 23.4 ppm. HRMS (ESI) calc'd for $C_{21}H_{27}N_4O_6S$ $[M+H]^+$ 463.1651, found 463.1656.

***N*-(6-(6-Methoxy-5-(methylsulfonamido)pyridin-3-yl)-1,3-dihydroisobenzofuran-4-yl)-6-methylpicolinamide (260)**
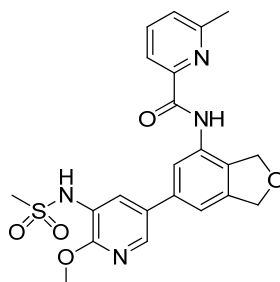
DIPEA (50 μL, 0.30 mmol) and HATU (62 mg, 0.16 mmol) were added sequentially to a stirred solution of 6-methylpicolinic acid (33 mg, 0.24 mmol) in DMF (0.5 mL) at room temperature and the solution stirred for 10 min. A solution of *N*-(5-(7-amino-1,3-dihydroisobenzofuran-5-yl)-2-methoxypyridin-3-yl)methanesulfonamide (50 mg, 0.15 mmol) in DMF (0.5 mL) was then added dropwise at room temperature and the mixture stirred at room temperature overnight. The reaction mixture was poured onto EtOAc (2 mL) and brine (3 mL) and the separated organic phase was washed with brine (2 x 3 mL). The combined organic phase was concentrated under a stream of nitrogen to give an orange gum. The gum was loaded in a solution of DMSO/MeOH (1 mL, 1:1 v/v) and purified *via* mass directed auto-preparative (MDAP) chromatography using a Sunfire C18 column and an ammonium bicarbonate-modified MeCN/water gradient. The relevant fractions were combined and concentrated under a stream of nitrogen to give *N*-(6-(6-methoxy-5-(methylsulfonamido)pyridin-3-yl)-1,3-dihydroisobenzofuran-4-yl)-6-methylpicolinamide (30 mg, 60 μmol, 28%) as a white solid. LCMS (Method A): 0.99 min, $[M+H]^+$ 455 m/z. ^1H NMR (DMSO-d$_6$, 400 MHz): δ = 10.49 (s, 1H), 9.26 - 9.57 (br. s, 1H), 8.31 (d, *J* = 2.3 Hz, 1H), 7.94 - 7.99 (m, 2H), 7.89 (d, *J* =2.3 Hz, 1H), 7.81 (s, 1H), 7.56 (dd, *J* = 6.2, 2.4 Hz, 1H), 7.46 (s, 1H), 5.11 (s, 2H), 5.07 (s, 2H), 3.98 (s, 3H), 3.09 (s, 3H), 2.64 (s, 3H) ppm.

Christopher J Tame

***N*-(2-Methoxy-5-(7-(5-methyl-1,3,4-oxadiazol-2-yl)-1,3-dihydroisobenzofuran-5-yl)pyridin-3-yl)methanesulfonamide (255)**
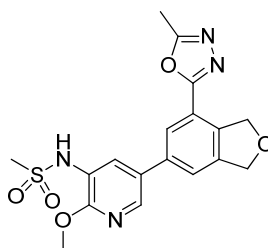
A microwave vial was charged with 2-methyl-1,3,4-oxadiazole (45 mg, 0.54 mmol) and THF (1.5 mL). Zinc chloride (244 mg, 1.79 mmol) was added and the mixture was degassed and cooled to -10 ºC under nitrogen. A solution of lithiumhexamethyldisilazide in THF (1 M, 810 μL, 810 μmol) was then added dropwise over 15 min at -10 °C. The resulting mixture was stirred at -10 °C (+/-5 °C) for 1 h. *N*-(5-(7-Iodo-1,3-dihydroisobenzofuran-5-yl)-2-methoxypyridin-3-yl)methanesulfonamide (200 mg, 450 μmol), tetrakis(triphenylphosphine)palladium(0) (52 mg, 45 μmol) and cesium carbonate (146 mg, 448 μmol) were then added at -10 °C. The mixture was then degassed with three alternative applications of vacuum and nitrogen, then heated in a Biotage microwave at 150 ºC for 1 h. The mixture was poured onto CH_2Cl_2 (20 mL) and the mixture was filtered under reduced pressure. The filtrate was extracted with CH_2Cl_2 (3 x 50 mL) and the combined organic phase was treated with water (50 mL). The resulting mixture was filtered under reduced pressure and washed with CH_2Cl_2 (3 x 50 mL). The filtrate was passed through a hydrophobic frit and then concentrated under reduced pressure to afford a yellow solid. The solid was loaded in DMSO (1 mL) and purified *via* mass directed auto-preparative (MDAP) chromatography using a Sunfire C18 column and an ammonium bicarbonate-modified MeCN/water gradient. The relevant combined fractions were concentrated under reduced pressure to give *N*-(2-methoxy-5-(7-(5-methyl-1,3,4-oxadiazol-2-yl)-1,3-dihydroisobenzofuran-5-yl)pyridin-3-yl)methanesulfonamide (45 mg, 0.11 mmol, 24%) as a white solid. LCMS (Method A): 0.78 min, $[M+H]^+$ 403. IR (solid) 2929 (N-H stretch); 1331, 1149 (O=S=O) cm^{-1}. ^{1}H NMR (DMSO-d$_6$, 400 MHz): δ = 9.37 (s, 1H), 8.37 (d, *J* = 2.3 Hz, 1 H), 8.02 (d, *J* = 1.3 Hz, 1H), 7.94 (d, *J* = 2.3 Hz,

Christopher J Tame

1H), 7.84 (s, 1H), 5.34 (s, 2H), 5.17 (s, 2H), 3.99 (s, 3H), 3.10 (s, 3H), 2.62 (s, 3H) ppm. ^{13}C NMR (101 MHz, DMSO-d_6) δ = 164.4, 163.3, 156.9, 142.7, 140.6, 137.8, 137.7, 130.6, 129.1, 123.7, 122.8, 122.6, 118.5, 73.9, 73.0, 54.3, 41.2, 11.1 ppm. HRMS (ESI) calc'd for $C_{18}H_{19}N_4O_5S$ [M+H]$^+$ 403.1071, found 403.1070.

N-(2-Methoxy-5-(7-(pyridin-2-yl)-1,3-dihydroisobenzofuran-5-yl)pyridin-3-yl)methanesulfonamide (256)
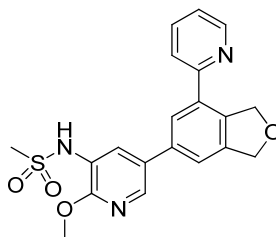
A microwave vial was charged with *N*-(5-(7-iodo-1,3-dihydroisobenzofuran-5-yl)-2-methoxypyridin-3-yl)methanesulfonamide (70 mg, 0.16 mmol), 2-(4,4,5,5-tetramethyl-1,3,2-dioxaborolan-2-yl)pyridine (80 mg, 0.39 mmol), cesium carbonate (102 mg, 0.310 mmol), copper(I) chloride (16 mg, 0.16 mmol), palladium(II) acetate (0.5 mg, 2 µmol), 1,1'-bis(diphenylphosphino)ferrocene (dppf) (18 mg, 30 µmol) and DMF (1.5 mL). The vial was sealed and degassed then heated and stirred in a Biotage microwave reactor at 100 ºC for 90 min. The mixture was poured onto water (20 mL) and EtOAc (20 mL) and the mixture was then filtered under reduced pressure. The separated aqueous phase was extracted with EtOAc (3 x 20 mL) and the combined organic phase was filtered. The filtrate was concentrated under reduced pressure to afford a brown solid. The solid was loaded in DMSO/MeOH solution (1:1 (v/v) 1 mL) and purified *via* mass directed auto-preparative (MDAP) chromatography using a Sunfire C18 column and an ammonium bicarbonate-modified MeCN/water gradient. The relevant combined fractions were concentrated under reduced pressure to give *N*-(2-methoxy-5-(7-(pyridin-2-yl)-1,3-dihydroisobenzofuran-5-yl)pyridin-3-yl)methanesulfonamide (6 mg, 0.02 mmol, 10%) as a white solid. LCMS (Method A): 0.89 min, [M+H]$^+$ 398 m/z. ^{1}H NMR (DMSO-d_6, 400 MHz,) δ = 9.07-9.43 (m, 1H), 8.70 (d, *J* = 4.03 Hz, 1H), 8.41 (d, *J* = 2.01 Hz, 1H), 8.06 (s, 2H), 7.90-8.00 (m, 2H), 7.65 (s, 1H), 7.39 (dd, *J* = 5.16, 6.92 Hz, 1H), 5.38 (s, 2H), 5.11 (s, 2H), 3.99 (s, 3H), 3.09 (s, 3H) ppm.

Christopher J Tame

4   Experimental procedures for PI3Kγ inhibitors

5-[3,4-*Bis*(Methyloxy)phenyl]-1-methyl-2-oxo-1,2-dihydro-3-pyridinecarboxylic acid (364)
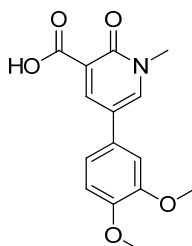
5-Bromo-1-methyl-2-oxo-1,2-dihydro-3-pyridinecarboxylic acid (Charnwood Molecular Limited, 31.9 g, 137 mmol), (3,4-dimethoxyphenyl)boronic acid (25.0 g, 137 mmol), sodium bicarbonate (29.1 g, 275 mmol) and tetrakis(triphenylphosphine)palladium(0) (4.76 g, 4.12 mmol) were suspended in ethanol (1.0 L) and water (0.25 L) and heated and stirred at 90 ºC for 4 h. The ethanol was removed under reduced pressure and the remaining solution was acidified with aqueous hydrochloric acid solution (2M) and a white solid precipitated from solution. The mixture was filtered under vacuum and washed with water. The solid was then dried under vacuum to afford 5-[3,4-bis(methyloxy)phenyl]-1-methyl-2-oxo-1,2-dihydro-3-pyridinecarboxylic acid (33.8 g, 117 mmol, 85%) as a white solid. LCMS (Method A): 0.75 min, m/z 290 $[M+H]^+$. ^{1}H NMR (DMSO-d_6, 400 MHz): δ = 13.6 (br. s, 1H), 8.15 - 8.37 (m, 2H), 7.15 (d, J = 2.0 Hz, 1H), 7.07 - 7.13 (m, 1H), 6.99 - 7.05 (m, 1H), 3.84 (s, 3H), 3.78 (s, 3H), 3.61 (s, 3H) ppm.

Christopher J Tame

3-(5-(3,4-Dimethoxyphenyl)-1-methyl-2-oxo-1,2-dihydropyridine-3-carboxamido)benzoic acid (369)
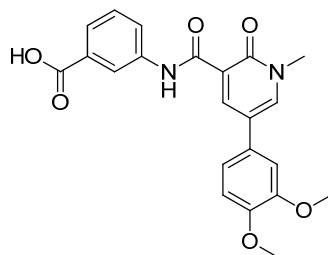
Oxalyl chloride (109 µL, 1.24 mmol) was added dropwise to a stirred mixture of 5-(3,4-dimethoxyphenyl)-1-methyl-2-oxo-1,2-dihydropyridine-3-carboxylic acid (300 mg, 1.04 mmol) and DMF (one drop) in THF (10 mL) at room temperature, which was accompanied by the evolution of gas. Once the evolution of gas ceased, the reaction mixture was evaporated under reduced pressure, redissolved in THF (10 mL) and added dropwise to an ice-cooled stirred solution of 3-aminobenzoic acid (156 mg, 1.14 mmol) and DIPEA (361 µL, 2.08 mmol) in THF (10 mL) at 0 ºC. The reaction mixture was stirred and allowed to reach room temperature over 10 minutes. Water (50 mL) and CH_2Cl_2 (50 mL) was added and a white solid precipitated from solution. The mixture was filtered under vacuum, washed with water (50 mL) and dried under reduced pressure to afford 3-(5-(3,4-dimethoxyphenyl)-1-methyl-2-oxo-1,2-dihydropyridine-3-carboxamido)benzoic acid (312 mg, 760 µmol, 74%) as a white solid. LCMS (Method A): 0.86 min, m/z 409 [M+H]+. ^{1}H NMR (DMSO-d$_6$, 400 MHz): δ = 12.37 (s, 1H), 8.71 (d, *J* = 2.8 Hz, 1H), 8.50 (d, *J* = 2.8 Hz, 1H), 8.39 (s, 1H), 7.77 - 7.93 (m, 1H), 7.69 (d, *J* = 7.8 Hz, 1H), 7.49 (t, *J* = 7.8 Hz, 1H), 7.21 (d, *J* = 1.8 Hz, 1H), 7.13 - 7.18 (m, 1H), 7.05 (d, *J* = 8.3 Hz, 1H), 3.86 (s, 3H), 3.80 (s, 3H), 3.73 (s, 3H) ppm.

Note: 1H missing from ^{1}H NMR (exchangeable).

Christopher J Tame

4-(5-(3,4-Dimethoxyphenyl)-1-methyl-2-oxo-1,2-dihydropyridine-3-carboxamido)-2-fluorobenzoic acid (355)
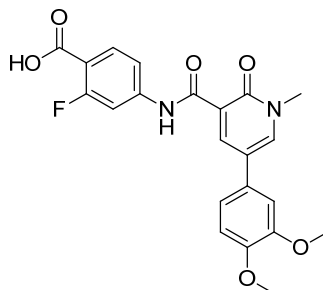
A solution of oxalyl chloride (16 μL, 0.18 mmol) in THF (1 mL) was added dropwise to a stirred mixture of 5-(3,4-dimethoxyphenyl)-1-methyl-2-oxo-1,2-dihydropyridine-3-carboxylic acid (52 mg, 0.18 mmol) and DMF (10 μL) at room temperature, which was accompanied by the evolution of gas. Once the evolution of gas ceased, the reaction mixture was concentrated under reduced pressure to give a pale yellow solid. The solid was azeotroped with toluene (2 x 10 mL) and then dissolved in CH_2Cl_2 (5 mL) and added dropwise over 1 min to an ice-cooled, stirred suspension of 4-amino-2-fluorobenzoic acid (28 mg, 0.18 mmol) and DIPEA (94 μL, 0.54 mmol) in THF at 0 ºC under nitrogen. Following stirring at 0 ºC for 10 min, the flask was removed from the ice bath and the reaction was stirred at room temperature for 20 min. LCMS indicated reaction completion. The solution was poured onto water (10 mL) and CH_2Cl_2 (10 mL) and the separated aqueous phase was extracted with CH_2Cl_2 (2 x 10 mL). The combined aqueous phase was acidified with aqueous hydrochloric acid solution (2 M) and a yellow solid precipitated from solution. The mixture was filtered under vacuum to afford a yellow solid. The solid was loaded in DMSO (1 mL) and purified *via* mass-directed auto-preparative (MDAP) chromatography using a Sunfire C18 column and a formic acid-modified MeCN/water gradient. The relevant fractions were combined and concentrated under a stream of nitrogen to give 4-(5-(3,4-dimethoxyphenyl)-1-methyl-2-oxo-1,2-dihydropyridine-3-carboxamido)-2-fluorobenzoic acid (4 mg, 8 μmol, 5%) as a yellow solid. LCMS (Method A): 0.90 min, m/z 427 $[M+H]^+$. ^{1}H NMR (DMSO-d$_6$, 400 MHz): δ = 12.46 (s, 1H), 8.65 - 8.77 (d, *J* = 2.8 Hz 1H), 8.46 - 8.62 (d, *J* = 2.8

Christopher J Tame

Hz, 1H), 7.73 - 7.82 (m, 2H), 7.30 - 7.39 (m, 1H), 7.21 - 7.25 (d, J = 2.3 Hz, 1H), 7.14 - 7.20 (dd, J = 8.0, 2.3 Hz 1H), 7.02 - 7.10 (d, J = 8.5 Hz, 1H), 3.86 (s, 3H), 3.80 (s, 3H), 3.73 (s, 3H) ppm.

Note: 1H missing from ^{1}H NMR (exchangeable).

2-Chloro-4-(5-(3,4-dimethoxyphenyl)-1-methyl-2-oxo-1,2-dihydropyridine-3-carboxamido)benzoic acid (356)
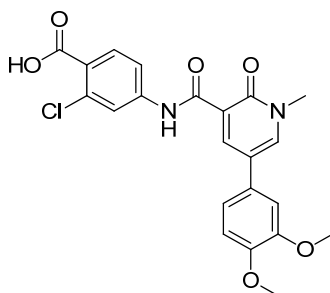
A solution of oxalyl chloride (45 µL, 0.52 mmol) in THF (5 mL) was added dropwise to a stirred mixture of 5-(3,4-dimethoxyphenyl)-1-methyl-2-oxo-1,2-dihydropyridine-3-carboxylic acid (125 mg, 430 µmol) and DMF (10 µL) at room temperature, which was accompanied by the evolution of gas. Once the evolution of gas ceased, the reaction mixture was concentrated under vacuum to afford a yellow gum. The gum was loaded in THF (2 mL) and added dropwise to an ice-cooled stirred solution of 4-amino-2-chloro benzoic acid (74 mg, 0.43 mmol) and DIPEA (225 µL, 1.29 mmol) in THF (3 mL) at 0 ºC and the mixture stirred at room temperature for 1 h. The mixture was poured onto water (10 mL) and CH_2Cl_2 (10 mL) and the separated aqueous phase was acidified with aqueous hydrochloric acid (2M) and a precipitate formed. The mixture was filtered under reduced pressure and the solid was loaded in DMSO (1 mL) and purified *via* mass-directed auto-preparative (MDAP) chromatography using a Sunfire C18 column and a formic acid-modified MeCN/water gradient. The relevant fractions were combined and concentrated under a stream of nitrogen to give 2-chloro-4-(5-(3,4-dimethoxyphenyl)-1-methyl-2-oxo-1,2-dihydropyridine-3-carboxamido)benzoic acid (35 mg, 80 µmol, 18%) as a yellow solid. m.p. 272 - 273 °C. LCMS (Method A): 0.91 min, m/z 443 [M+H]$^+$. IR (solid) 2945 (N-H stretch); 1694 (C=O); 1575 (C=O);

1515 (C=O); 1285 (C-O) cm^{-1}. ^{1}H NMR (DMSO-d_6, 400 MHz): δ = 13.00 - 13.31 (m, 1H), 12.50 (s, 1H), 8.70 (d, J = 2.8 Hz, 1H), 8.56 (d, J = 2.8 Hz, 1H), 8.10 (d, J = 2.0 Hz, 1H), 7.79 - 7.89 (m, 1H), 7.49 - 7.64 (m, 1H), 7.22 (d, J = 2.0 Hz, 1H), 7.15 - 7.19 (m, 1H), 7.07 (s, 1H), 3.86 (s, 3H), 3.80 (s, 3H), 3.73 (s, 3H) ppm. ^{13}C NMR (DMSO-d_6, 101 MHz): δ = 165.9, 161.9, 161.0, 149.2, 148.5, 141.8, 141.4, 133.0, 132.2, 127.6, 120.7, 119.3, 118.3, 117.9, 117.7, 112.2, 109.5, 55.7, 55.6, 38.1 ppm. HRMS (ESI) calc'd for $C_{22}H_{20}ClN_2O_6$ [M+H]$^+$ 443.1010, found 443.0994.

Note: 2C missing from ^{13}C NMR (overlapping peaks).

Methyl 2-Bromo-4-(5-(3,4-dimethoxyphenyl)-1-methyl-2-oxo-1,2-dihydropyridine-3-carboxamido)benzoate (378)
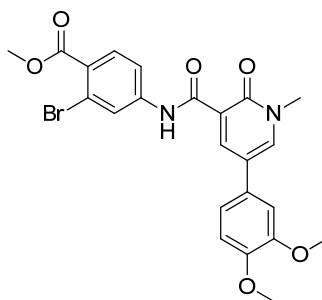
DIPEA (1.21 mL, 6.91 mmol) was added to a stirred solution of 5-(3,4-dimethoxyphenyl)-1-methyl-2-oxo-1,2-dihydropyridine-3-carboxylic acid (500 mg, 1.73 mmol) and HATU (723 mg, 1.90 mmol) in DMF (3.5 mL) at room temperature and the solution stirred for 10 min. A solution of methyl 4-amino-2-bromobenzoate (437 mg, 1.90 mmol) in DMF (3.5 mL) was then added dropwise at room temperature and the solution stirred for 16 h. The solution was poured onto ethyl acetate (2 mL) and brine (5 mL) and the separated organic phase was washed with brine (2 x 3 mL) then concentrated under reduced pressure to give a brown solid. The solid was triturated with CH$_2$Cl$_2$ and the mixture filtered under reduced pressure. The solid was dried under reduced pressure to give methyl 2-bromo-4-(5-(3,4-dimethoxyphenyl)-1-methyl-2-oxo-1,2-dihydropyridine-3-carboxamido)benzoate (290 mg, 580 μmol, 34%) as a yellow solid. LCMS (Method A): 1.17 min, m/z 501

[^{79}Br M+H]$^+$, 503 [^{81}Br M+H]$^+$. ^{1}H NMR (DMSO-d$_6$, 400 MHz): δ = 12.55 (s, 1H), 8.69 (d, J = 2.7 Hz, 1H), 8.58 (d, J = 2.7 Hz, 1H), 8.35 (d, J = 2.0 Hz, 1H), 7.87 (d, J = 8.6 Hz, 1H), 7.69 (dd, J = 8.6, 1.8 Hz, 1H), 7.22 (d, J = 1.8 Hz, 1H), 7.17 (dd, J = 8.3, 1.8 Hz, 1H), 7.06 (d, J = 8.3 Hz, 1H), 3.86 (s, 3H), 3.84, (s, 3H), 3.80 (s, 3 H), 3.73 (s, 3H) ppm.

2-Bromo-4-(5-(3,4-dimethoxyphenyl)-1-methyl-2-oxo-1,2-dihydropyridine-3-carboxamido)benzoic acid (359)
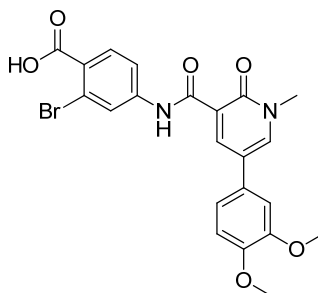
Aqueous sodium hydroxide solution (2 M, 0.2 mL, 0.4 mmol) was added dropwise to a stirred solution of methyl 2-bromo-4-(5-(3,4-dimethoxyphenyl)-1-methyl-2-oxo-1,2-dihydropyridine-3-carboxamido)benzoate (20 mg, 40 µmol) in DMF (10 mL) at room temperature and the solution was heated at 50 ºC for 16 h. The mixture was extracted three times with CH$_2$Cl$_2$ (3 x 10 mL) and the separated aqueous phase was adjusted to pH 4 with aqueous hydrochloric acid solution (2 M) and a yellow solid precipitated from solution. The solid was filtered and dried under reduced pressure. The solid was loaded in DMSO (1 mL) and purified *via* mass-directed auto-preparative (MDAP) chromatography using a Sunfire C18 column and a formic acid-modified MeCN/water gradient. The relevant fractions were combined and concentrated under a stream of nitrogen to give 2-bromo-4-(5-(3,4-dimethoxyphenyl)-1-methyl-2-oxo-1,2-dihydropyridine-3-carboxamido)benzoic acid (9.7 mg, 20 µmol, 50%) as a yellow solid. LCMS (Method A): 0.96 min, m/z 487 [^{79}Br M+H]$^+$, 489 [^{81}Br M+H]$^+$. ^{1}H NMR (DMSO-d$_6$, 400 MHz): δ = 12.26 (s, 1H), 8.69 (d, J = 2.8 Hz, 1H), 8.53 (d, J = 2.8 Hz, 1H), 8.40 (s, 1H), 8.08 (d, J = 2.0 Hz, 1H), 7.44 - 7.49 (d, J = 8.3 Hz, 1H), 7.40-7.47 (dd, J = 8.0, 2.3 Hz, 1H), 7.22 (d, J =

Christopher J Tame

2.0 Hz, 1H), 7.17 (dd, *J* = 8.3, 2.3 Hz, 1H), 7.06 (d, *J* = 8.5 Hz, 1H), 3.82 - 3.89 (m, 3H), 3.76 - 3.82 (m, 3H), 3.73 (s, 3H) ppm.

2-Amino-4-(5-(3,4-dimethoxyphenyl)-1-methyl-2-oxo-1,2-dihydropyridine-3-carboxamido)benzoic acid (360)
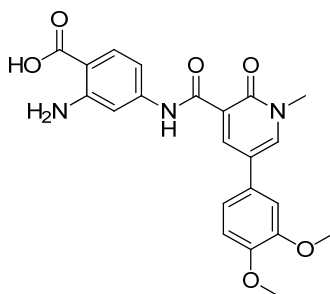
DIPEA (960 μL, 5.50 mmol) was added dropwise to a stirred solution of 5-(3,4-dimethoxyphenyl)-1-methyl-2-oxo-1,2-dihydropyridine-3-carboxylic acid (530 mg, 1.83 mmol) and HATU (766 mg, 2.02 mmol) in DMF (3.5 mL) at room temperature and the reaction stirred for 10 min. A solution of 7-amino-1*H*-benzo[*d*][1,3]oxazine-2,4-dione (359 mg, 2.02 mmol) in DMF (3.5 mL) was then added dropwise to the reaction mixture at room temperature and the mixture was stirred for 16 h. The solution was poured onto water (50 mL) and a brown solid precipitated from solution. The mixture was filtered under vacuum and washed with water (50 mL) to afford the isotoic anhydride intermediate as a brown solid. The solid was suspended in aqueous sodium hydroxide solution (10 M, 2 mL) and stirred for 15 min. Water (50 mL) was added and the pH adjusted to pH 4 using aqueous hydrochloric acid solution (2 M). A solid precipitated out of solution and the mixture was filtered under reduced pressure to give a brown solid. The solid was dissolved in DMSO (1 mL) and purified *via* mass-directed auto-preparative (MDAP) chromatography using a Sunfire C18 column and a formic acid-modified MeCN/water gradient. The relevant fractions were combined and concentrated under a stream of nitrogen to give 2-amino-4-(5-(3,4-dimethoxyphenyl)-1-methyl-2-oxo-1,2-dihydropyridine-3-carboxamido)benzoic acid (10 mg, 20 μmol, 1%) as a yellow solid. LCMS (Method A): 0.87 min, m/z 424 [M+H]$^+$. ^{1}H NMR (DMSO-d$_6$, 600 MHz,) δ = 12.24 (s, 1H), 8.68 (d, *J* = 2.9 Hz, 1H), 8.54 (d, *J* = 2.9 Hz, 1H), 7.68 (d,

Christopher J Tame

J = 8.8 Hz, 1H), 7.28 (s, 1H), 7.21 (d, *J* = 2.2 Hz, 1H), 7.16 (dd, *J* = 2.2, 8.1 Hz, 1H), 7.06 (d, *J* = 8.4 Hz, 1H), 6.75 (dd, *J* = 1.8, 7.0 Hz, 1H), 3.86 (s, 3H), 3.80 (s, 3H), 3.72 (s, 3H) ppm.

Note: 3H missing from ¹H NMR (exchangeable).

Methyl 4-(5-(3,4-dimethoxyphenyl)-1-methyl-2-oxo-1,2-dihydropyridine-3-carboxamido)-2-fluorobenzoate (382)
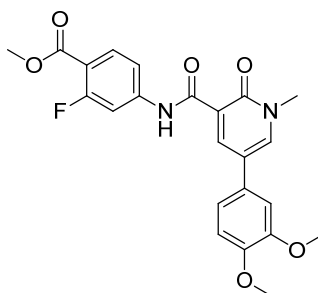
DIPEA (910 µL, 5.19 mmol) was added dropwise to a stirred solution of 5-(3,4-dimethoxyphenyl)-1-methyl-2-oxo-1,2-dihydropyridine-3-carboxylic acid (500 mg, 1.73 mmol) and HATU (723 mg, 1.90 mmol) in DMF (3.5 mL) at room temperature and the solution stirred for 10 min. A solution of methyl 4-amino-2-fluorobenzoate (322 mg, 1.90 mmol) in DMF (3.5 mL) was then added dropwise to the reaction mixture at room temperature and the solution stirred at room temperature for 16 h. The solution was then partitioned between EtOAc (2 mL) and brine (3 mL) and the separated organic phase was washed with brine (2 x 3 mL) and concentrated under reduced pressure to give a brown solid. The solid was triturated with CH₂Cl₂ and filtered under reduced pressure. The solid was dried under reduced pressure to afford methyl 4-(5-(3,4-dimethoxyphenyl)-1-methyl-2-oxo-1,2-dihydropyridine-3-carboxamido)-2-fluorobenzoate (20 mg, 50 µmol, 3%) as a yellow solid. LCMS (Method A): 1.11 min, m/z 441 [M+H]⁺. ¹H NMR (DMSO-d₆, 400 MHz): δ = 12.62 (s, 1H), 8.69 (d, *J* = 3.0 Hz, 1H), 8.57 (d, *J* = 3.0 Hz, 1H), 7.85 - 7.98 (m, 2H), 7.48 (dd, *J* = 8.7, 1.9 Hz, 1H), 7.22 (d, *J* = 2.0 Hz, 1H), 7.14 - 7.19 (m, 1H), 7.06 (d, *J* = 8.3 Hz, 1H), 3.86 (s, 3H), 3.84 (s, 3H), 3.80 (s, 3H), 3.73 (s, 3H) ppm.

Christopher J Tame

Methyl 4-(5-(3,4-dimethoxyphenyl)-1-methyl-2-oxo-1,2-dihydropyridine-3-carboxamido)-2-(methylamino)benzoate (383)
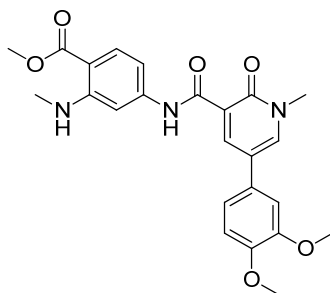
A solution of 33% methylamine in ethanol (1.0 mL, 50 μmol) was added to a microwave vial containing a stirred solution of methyl 4-(5-(3,4-dimethoxyphenyl)-1-methyl-2-oxo-1,2-dihydropyridine-3-carboxamido)-2-fluorobenzoate **142** (20 mg, 50 μmol) in 1,4-dioxane (0.2 mL). The vial was sealed and heated in a Biotage microwave reactor at 120 ºC for 5 h. The solution was poured onto water (50 mL) and CH$_2$Cl$_2$ (50 mL) and the separated aqueous phase was extracted with CH$_2$Cl$_2$ (50 mL). The combined organic phase was concentrated under reduced pressure to give an orange gum. The gum was loaded in DMSO (1 mL) and purified *via* mass-directed auto-preparative (MDAP) chromatography using a sunfire C18 column and an ammonium bicarbonate-modified MeCN/water gradient. The relevant fractions were combined and concentrated under a stream of nitrogen to give methyl 4-(5-(3,4-dimethoxyphenyl)-1-methyl-2-oxo-1,2-dihydropyridine-3-carboxamido)-2-(methylamino)benzoate (10 mg, 20 μmol, 49%) as a yellow solid. LCMS (Method A): 1.16 min, m/z 452 [M+H]$^+$. ^{1}H NMR (DMSO-d$_6$, 400 MHz) δ = 12.39 (s, 1H), 8.72 (d, J = 3.0 Hz, 1H), 8.56 (d, J = 3.0 Hz, 1H), 7.80 (d, J = 8.6 Hz, 1H), 7.65 (q, J = 4.6 Hz, 1H), 7.31 (d, J = 2.0 Hz, 1H), 7.23 (d, J = 2.3 Hz, 1H), 7.17 (dd, J = 8.3, 2.3 Hz, 1H), 7.07 (d, J = 8.3 Hz, 1H), 6.81 (dd, J = 2.0, 8.6 Hz, 1H), 3.87 (s, 3H), 3.81 (s, 3H), 3.78 (s, 3H), 3.74 (s, 3H), 2.88 (d, J = 5.1 Hz, 3H) ppm.

Christopher J Tame

4-(5-(3,4-Dimethoxyphenyl)-1-methyl-2-oxo-1,2-dihydropyridine-3-carboxamido)-2-(methylamino)benzoic acid (361)
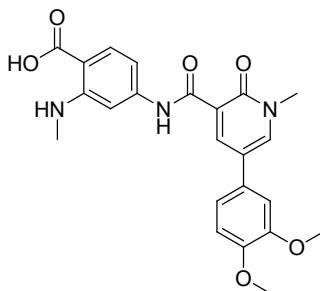
Aqueous sodium hydroxide solution (2 M, 220 µL, 440 µmol) was added to a stirred solution of methyl 4-(5-(3,4-dimethoxyphenyl)-1-methyl-2-oxo-1,2-dihydropyridine-3-carboxamido)-2-(methylamino)benzoate (20 mg, 40 µmol) in 1,4-dioxane (1 mL) in a microwave vial. The vial was sealed and heated in a Biotage microwave reactor at 50 ºC for 5 h. The mixture was acidified with aqueous hydrochloric acid solution (2.0 M, 0.44 mL, 0.89 mmol) and a green solid precipitated from solution. The mixture was filtered and washed with aqueous hydrochloric acid solution (2.0 M, 1.0 mL) and MeOH (1 mL). The solid was dried under a stream of nitrogen to give 4-(5-(3,4-dimethoxyphenyl)-1-methyl-2-oxo-1,2-dihydropyridine-3-carboxamido)-2-(methylamino)benzoic acid (16 mg, 40 µmol, 81%) as a yellow solid. LCMS (Method A): 0.94 min, m/z 438 [M+H]$^+$. ^{1}H NMR (DMSO-d$_6$, 400 MHz) δ = 12.35 (s, 1H), 8.72 (d, J = 2.8 Hz, 1H), 8.55 (d, J = 3.0 Hz, 1H), 7.78 (d, J = 8.6 Hz, 1H), 7.28 (d, J = 1.8 Hz, 1H), 7.23 (d, J = 2.0 Hz, 1H), 7.18 (dd, J = 8.3, 2.0 Hz, 1H), 7.08 (d, J = 8.3 Hz, 1H), 6.78 (dd, J = 8.6, 2.3 Hz, 1H), 3.87 (s, 3H), 3.81 (s, 3H), 3.74 (s, 3H), 2.87 (s, 3H) ppm. ^{13}C NMR (DMSO-d$_6$, 101 MHz) δ = 169.2, 167.3, 152.7, 149.3, 146.4, 143.7, 143.4, 141.8, 141.6, 136.5, 132.8, 119.2, 118.9, 117.9, 112.3, 109.6, 105.8, 55.7, 55.6, 38.1, 30.4 ppm. HRMS (ESI) calc'd for C$_{23}$H$_{24}$N$_3$O$_6$ [M+H]$^+$ 438.1660, found 438.1665.

Note: 2H missing from ^{1}H NMR (exchangeable). 2C missing from ^{13}C NMR (overlapping peaks).

Christopher J Tame

References

1. Irwin, R. S.; Richardson, N. D. *Chest* **2006**, *130*, 41S-53S.

2. http://www.nice.org.uk/nicemedia/live/14156/63713/63713.pdf **Accessed 19/05/2014**.

3. Barnett, S. B.; Nurmagambetov, T. A. *J. Allergy Clin. Immunol*. **2011**, *127*, 145-52.

4. Mosby's Medical Dictionary, 8th Edition, *Elsevier*, **2009**.

5. http://medical-dictionary.thefreedictionary.com/fibrosis. **Accessed 29/04/2013**.

6. Raghu, G.; Collard, H. R.; Egan, J. J.; Martinez, F. J.; Behr, J.; Brown, K. K.; Colby, T. V.; Cordier, J.-F.; Flaherty, K. R.; Lasky, J. A.; Lynch, D. A.; Ryu, J. H.; Swigris, J. J.; Wells, A. U.; Ancochea, J.; Bouros, D.; Carvalho, C.; Coastabel, U.; Ebina, M.; Hansell, D. M.; Johkoh, T.; Kim, D. S.; King, T. E. Jr.; Kondoh, Y.; Myers, J.; Müller, N. L.; Nicholson, A. G.; Richeldi, L.; Selman, M.; Dudden, R. F.; Griss, B. S.; Protzko, S. L.; Schünemann, H. J. *Am. J. Respir. Crit. Care Med*. **2011**, *183*, 788-824.

7. Rosenstein, B. J.; Cutting, G. R. *J. Pediatr*. **1998**, *132*, 589-595.

8. Connor, D. H.; Somers, K.; Hutt, M. S. R.; Manion, W. C.; D'Arbela, P. G. *Am. Heart J*. **1968**, *75*. 107-124.

9. Smedema, J. P.; Winckels, S. K. G.; Snoep, G.; Vainer, J.; Bekkers, S. C. A. M.; Crijins, H. J. G. M. *Int. J. Cardiovascular Imag*. **2004**, *20*, 517-522.

10. Krenning, G.; Zeisberg, E. M.; Kalluri, R. *J. Cell Physiol*. **2010**, *225*, 631-637.

11. Vaglio, A.; Salvarni, C.; Buzio, C. *Lancet* **2006**, *367*, 241-251.

12. Liu, Y. *Kidney Int*. **2006**, *69*, 213-217.

13. Fernandez, I. E.; Eickleberg, O. *Lancet* **2012**, *380*, 680-688.

14. Maher, T. M.; Wells, A. U.; Laurent, G. J. *Eur. Respir. J*. **2007**, *30*, 835-9.

15. Raghu. G.; Weycker, D.; Edelsberg, J.; Bradford, W. Z.; Oster, G. *Am. J. Respir. Crit. Care Med.* **2006**,*174*, 810–816.

16. Maher, T. M. *Expert Opin. Med. Diagn*. **2008**, *2*, 1317-1331.

17. Selman, M.; King, T. E.; Pardo, A. *Ann. Intern. Med*. **2001**, *134*, 136-151.

18. Leslie, K. O.; Wick, M. R. *Practical Pulmonary Pathology: A Diagnostic Approach*. 2nd Ed. Philadelphia: Churchill Livingstone, **2005**.

Christopher J Tame

19. Turner-Warwick, M.; Burrows, B.; Johnson, A. *Thorax* **1980**, *35*, 171-180.

20. American Thoracic Society board of directors and European Respiratory Society executive committee, *Am. J. Respir. Crit. Care Med*. **2002**, *165*, 277-304.

21. Ley, B.; Collard, H. R.; King, T. E. Jr. *Am. J. Respir. Crit. Care Med.* **2011**, *183*, 431-440.

22. King, T. E. Jr.; Tooze, J. A.; Schwarz, M. I.; Brown, K.; Chermiack, R. M. *Am. J. Respir. Crit. Care Med.* **2001**, *164*, 1171-1181.

23. Raghu G. *Chest* **1987**, *92*, 148–154.

24. Mejia, M.; Carrillo, G.; Rojas-Serrano, J.; Estrada, A.; Suarez, T.; Alonso, D.; Barrientos, E.; Gaxiola, M.; Navarro, C.; Selman, M. *Chest* **2009**, *136*, 10–15.

25. Selman, M.; Carrillo, G.; Estrada, A.; Meija, M.; Becerril, C.; Cisneros, J.; Gaxiola, M.; Perez-Padilla, R.; Navarro, C.; Richards, T.; Dauber, J.; King, T. E. Jr.; Pardo, A.; Kaminski, N. *PLos ONE* **2007**, *2*, e482.

26. Boon, K.; Bailey, N. W.; Yang, J.; Steel, M. P.; Groshong, S.; Kervitsky, D.; Brown, K. K.; Schwarz, M. I.; Schwarz, D. A. *PLoS ONE* **2009**, e5134.

27. http://www.intermune.com/pirfenidone **Accessed 02/05/2013.**

28. http://www.nice.org.uk/nicemedia/live/13039/63134/63134.pdf. **Accessed 02/05/2013.**

29. http://www.ema.europa.eu/docs/en_GB/document_library/EPAR_-_Product_Information/human/002154/WC500103049.pdf **Accessed 02/05/2013**.

30. Lin, X.; Yu, M.; Wu, K.; Yuan, H.; Zhong, H. *Invest. Opthalmol. Vis. Sci*. **2009**, *50*, 3763-3770.

31. Di Sario, A.; Emmanuele, B.; Baroni, G. S.; Ridolfi, F.; Casini, A.; Ceni, E.; Saccomanno, S.; Marzioni, M.; Trozzi, L.; Sterpetti, P.; Taffetani, S.; Benedetti, A. *J. Hepatol*. **2002**, *37*, 584-591.

32. Schaefer, C. J.; Ruhrmund, D. W.; Pan, L.; Seiwert, S. D.; Kossen, K. *Eur. Repir. Rev*. **2011**, *20*, 85-97.

33. Hilberg, O.; Simonsen, U.; du Bois, R.; Bendstrup, E. *Clin. Respir. J*. **2012**, *6*, 131–143.

Christopher J Tame

34. Taniguchi, H.; Ebina, M.; Kondoh, Y.; Ogura, T.; Azuma, A.; Suga, M.; Taguchi, Y.; Takahashi, H.; Nakata, K.; Sato, A.; Takeuchi, M.; Raghu, G.; Kudoh, S.; Nukiwa, T. *Eur. Respir. J*. **2010**, *35*, 821–829.

35. http://www.fda.gov/downloads/AdvisoryCommittees/ CommitteesMeetingMaterials/Drugs/Pulmonary-AllergyDrugsAdvisoryCommittee/ UCM203081.pdf. **Accessed 02/05/2013**.

36. http://www.prnewswire.com/news-releases/esbriet-pirfenidone-receives-positive- final-appraisal-determination-from-nice-for-idiopathic-pulmonary-fibrosis-ipf- 199269311.html. **Accessed 02/05/2013.**

37. Keating, D.; Levvey, B.; Kotsimbos, T.; Whitford, H.; Westall, G.; Williams, T.; Snell, G. *Transplant Proc*. **2009**, *41*, 289–291.

38. Thabut, G.; Mal, H.; Castier, Y.; Groussard, O.; Brugiere, O.; Marrash-Chahla, R.; Leseche, G.; Fournier, M. *J. Thorac. Cardiovasc. Surg*. **2003**, *126*, 469–475.

39. Raghu, G.; Freudenberger, T. D.; Yang, S.; Curtis, J. R.; Spada, C.; Hayes, J.; Sillery, J. K.; Pope, C. E. II; Pellegrini, C. A. *Eur. Respir. J*. **2006**, *27*, 136–142.

40. Davis, R. D. Jr.; Lau, C. L.; Eubanks, S.; Messier, R. H.; Hadjiliadis, D.; Steele, M. P.; Palmer, S. M. *J. Thorac. Cardiovasc. Surg*. **2003**, *125*, 533–542.

41. Clinical trial reference no. NCT01335464: http://clinicaltrials.gov/ct2/show/NCT01335464. **Accessed 02/05/2013**.

42. http://www.globaldata.com/PressReleaseDetails.aspx?PRID=811&Type=Industry & Title=Pharmaceuticals%20and%20Healthcare. **Accessed 03/05/2013**.

43. Hilberg, F.; Roth, G. J.; Krssak, M.; Kautschitsch, S.; Sommergruber, W.; Tontsch-Grunt, U.; Garin-Chesa, P.; Bader, G.; Zoephel, A.; Quant, J.; Heckel, A.; Rettig, W. J. *Cancer Res*. **2008**, *68*, 4774-4782.

44. Strieter, R. M.; Mehrad, B. *Chest* **2009**, *136*, 1364-1370

45. Mross, K.; Stefanic, M.; Gmehling, D.; Frost, A.; Baa, F.; Unger, C.; Strecker, R.; Henning, J.; Gaschler-Markefski, B.; Stopfer, P.; de Rossi, L.; Kaiser, R. *Clin. Cancer, Res*. **2010**, *16*, 311-319.

46. Waldmann, T. A. *Nat. Med*. **2003**, *9*, 269-277.

47. Werner, R. G. *J. Biotechnol*. **2004**, *113*, 171-182.

Christopher J Tame

48. Levëque, D.; Wisniewski, S.; Jehl, F. *Anticancer Res*. **2005**, *25*, 2327-2344.

49. Clinical trial reference no. NCT01766817: http://clinicaltrials.gov/ct2/show/NCT01766817. **Accessed 02/05/2013**.

50. http://gsk-pipeline.citeline.com/CpDrugInfo.aspx?DrugKey=31006&UserSearchID=0&Target=9. **Accessed 02/05/2013**.

51. Clinical trial reference no. NCT01725139: http://clinicaltrials.gov/ct2/show/NCT01725139?term=GSK+IPF&rank=1. **Accessed 02/05/2013**.

52. http://gsk-pipeline.citeline.com/CpResultDrugs.aspx?UserSearchID=266550. **Accessed 02/05/2013**.

53. Clinical trial reference no. NCT01371305: http://www.clinicaltrials.gov/ct2/show/NCT01371305. **Accessed 02/05/2013**.

54. Clinical trial reference no. NCT01769196: http://www.clinicaltrials.gov/ct2/show/NCT01769196. **Accessed 02/05/2013**.

55. Clinical trial reference no. NCT01262001: http://clinicaltrials.gov/ct2/show/study/NCT01262001. **Accessed 02/05/2013**.

56. Clinical trial reference no. NCT01629667: http://www.clinicaltrials.gov/ct2/show/NCT01629667. **Accessed 02/05/2013.**

57. Clinical trial reference no. NCT01529853: http://clinicaltrials.gov/show/NCT01529853. **Accessed 02/05/2013**.

58. Clinical trial reference no. NCT01254409: http://clinicaltrials.gov/ct2/show/NCT01254409. **Accessed 02/05/2013**.

59. Crystal, R. G.; Fulmer, J. D.; Roberts, W. C.; Moss, M. L.; Line, B. R.; Reynolds, H. Y. *Ann. Intern. Med*. **1976**, *85*, 769-788.

60. Selman, M.; Pardo, A. *Am. J. Respir. Crit. Care Med*. **2012**, *186*, 119-120.

61. http://www.histology.leeds.ac.uk/respiratory/respiratory.php **Accessed 01/05/2013**.

62. Weibel, E. R. *Physiol. Rev*. **1973**, *53*, 419-495.

63. Clark, R. A. *J. Dermatol. Surg. Oncol*. **1993**, *19*, 693-706.

64. Gabbiani, G.; Ryan, G. B.; Majno, G. *Experientia* **1971**, *27*, 549–550.

Christopher J Tame

65. Serini, G.; Gabbiani, G. *Exp. Cell Res*. **1999**, *250*, 273–283.

66. Caplan, A. I. *J. Orthop. Res*. **1991**, *9*, 641–650.

67. Kalluri, R.; Weiberg, R. A. *J. Clin. Invest*. **2009**, *119*, 1420-1428.

68. Nasreen, N.; Mohammed, K. A.; Mubarak, K. K. *Am. J. Physiol. Lung Cell Mol. Physiol*. **2009**, *297*, L115-L124

69. Kim, K. K.; Kugler, M. C.; Wolters, P. J. *Proc. Natl. Acad. Sci. USA* **2006**, *103*, 13180-13205.

70. Hong, K. M. Belperio, J. A.; Keane, M. P.; Burdick, M. D.; Strieter, R. M. *J. Biol. Chem*. **2007**, *282*, 22910-22920.

71. Sime, P. J.; Xing, Z.; Graham, F. L.; Csaky, K. G.; Gauldie, J. *J. Clin. Invest*. **1997**, *100*, 768-776.

72. Lee, C. G.; Cho, S. J.; Kang, M. J.; Chapoval, S. P.; Lee, P. J.; Noble, P. W.; Yehualaeshet, T.; Lu, B.; Flavell, R. A.; Milbrandt, J.; Homer, R. J.; Elias, J. A. *J. Exp. Med*. **2004**, *200*, 377-389.

73. Taylor, A. W. *J. Leukocyte Biol*. **2009**, *85*, 29-33.

74. Botfinger, E. P.; Letterio, J. J.; Roberts, A. B. *Kidney Int*. **1997**, *51*, 1355-1360.

75. Funke, M.; Zhao, Z.; Xu, Y.; Chun, J.; Tager, A. M. *Am. J. Respir. Cell Mol. Biol.* **2012**, *46*, 355-364.

76. Rodriguez, H. M.; Vaysberg, M.; Mikels, A.; McCaulay, S.; Velayo, A. C.; Garcia, C.; Smith, V. *J. Biol. Chem.* **2010**, *285*, 20964-20974.

77. Bolaños, A. L.; Milla, C. M.; Lira, J. C.; Ramírez, R.; Checa, M.; Barrera, L.; García-Alvarez, J.; Carbajal, V.; Becerril, C.; Gaxiola, M.; Pardo, A.; Selman, M. *Am. J. Physiol. Lung Cell Mol. Physiol*. **2012**, *303*, L978-L990.

78. Pandit, K. V.; Corcoran, D.; Yousef, H.; Yarlagadda, M.; Tzouvelekis, A.; Gibson, K. F.; Konishi, K.; Yousem, S. A.; Singh, M.; Handley, D.; Richards, T.; Selman, M.; Watkins, S. C.; Pardo, A.; Ben-Yehudah, A.; Bouros, D.; Eickelberg, O.; Ray, P.; Benos, P. V.; Kaminiski, N. *Am. J. Respir. Crit. Care Med*. **2010**, *182*, 220-229.

79. Yang, Z. H.; Wang, J. P.; Mi, S.; Cui, B.; Yan, H. M.; Yan, J.; Li, Z.; Liu, H.; Hua, F.; Lu, W.; Hu, Z. W. *Am. J. Pathol*. **2012**, *180*, 275-292.

Christopher J Tame

80. Olsen, K. C.; Sapinoro, R. E.; Kottmann, R. M.; Kulkarni, A. A.; Iismaa, S. E.; Johnson, G. V.; Thatcher, T. H.; Phipps, R. P.; Sime, P. J. *Am. J. Respir. Crit. Care Med*. **2011**, *184*, 699-707.

81. Königshoff, M.; Balsara, N.; Pfaff, E. M.; Kramer, M.; Chrobak, I.; Seeger, W.; Eickelberg, O. *PLoS One*, **2008**, *3*, e2142.

82. Liu, T.; Hu, B.; Choi, Y. Y.; Chung, M.; Ullenbruch, M.; Yu, H.; Lowe, J. B.; Phan, S. H. *Am. J. Pathol*. **2009**, *174*, 1745-1755.

83. Koli, K.; Myllärniemi, M.; Vuorinen, K.; Salmenkivi, K.; Ryynänn, M. J.; Kinnula, V. L.; Keski-Oja, J. *Am. J. Pathol*. **2006**, *169*, 61-71.

84. Shattil, S. J.; Kim, C.; Ginsberg, M. H. *Nat. Rev. Mol. Cell Biol*. **2010**, *11*, 288-300.

85. Hynes, R. O. *Cell* **2002**, *110*, 673-687.

86. Timpl, R.; Rohde, H.; Robey, P. G.; Rennard, S. I.; Foidart, J. M.; Martin, G. R. *J. Biol. Chem*. **1979**, *254*, 9933-9937.

87. Ferlatta, M.; Ekblom, P. *J. Cell Sci*. **1999**, *112*, 1-10.

88. Stipp, C. S. *Expert Rev. Mol. Med*. **2010**, *12*, e3.

89. Pouliot, N.; Nice, E. C.; Burgess, A. W. *Exp. Cell Res*. **2001**, *266*, 1-10.

90. Harris, E. S.; McIntyre, T. M.; Prescott, S. M.; Zimmerman, G. A. *J. Biol. Chem*. **2000**, *275*, 23409-23412.

91. Dustin, M. L.; Springer, T. A. *Nature*, **1989**, *341*, 619-624.

92. Kotovuori, A.; Morikawa-Pessa, T.; Kotovuori, P.; Nortamo, P.; Gahmberg, G. C. *J. Immunol*. **1999**, *162*, 6613-6620.

93. Kandula, S.; Abraham, C. *J. Immunol*. **2004**, *173*, 4443-4451.

94. Lodish, H.; Berk, A.; Zipursky, S. L.; Matsudaira, P.; Baltimore, D.; Darnell, J. *Molecular Cell Biology. 4th edition. Collagen: The Fibrous Proteins of the Matrix*. New York, **2000**. *22.3*, available from: http://www.ncbi.nlm.nih.gov/books/NBK21582. **Accessed 04/05/2013.**

95. De Fougerolles, A. R.; Sprague, A. G.; Nickerson-Nutter, C. L.; Chi-Rosso, G.; Rennert, P. D.; Gardner, H.; Gotwals, P. J.; Lobb, R. R.; Koteliansky, V. E. *J. Clin. Invest*. **2000**, *105*, 721-729.

96. Chandra, K. C. *Curr. Drug Targets* **2003**, *4*, 123-131.

Christopher J Tame

97. Brooks, P. C.; Clark, R. A.; Cheresh, D. A. *Science*, **1994**, *264*, 569-571.

98. Hahm, K.; Lukashev, M. E.; Luo, Y.; Yang, W. J.; Dolinski, B. M.; Weinred, P. H.; Simon, K. J.; Chun-Wang, L.; Leone, D. R.; Lobb, R. R.; McCrann, D. J.; Allaire, N. E.; Horan, G. S.; Fogo, A.; Kalluri, R.; Shield C. F. III; Sheppard, D.; Gardner, H. A.; Violette, S. M. *Am. J. Pathol*. **2007**, *170*, 110-125.

99. Sullivan, B. P.; Weinreb, P. H.; Violette, S. M.; Luvendyk, J. P. *Am. J. Pathol*. **2010**, *177*, 2837-2849.

100. Puthawala, K.; Hadjiangelis, N.; Jacoby, S.C.; Bayongan, E.; Zhao, Z.; Yang, Z.; Devitt, M. L.; Horan, G. S.; Weinreb, P. H.; Lukashev, M. E.; Violette, S. M.; Grant, K. S.; Colarossi, C.; Formenti, S. C.; Munger, J. S. *Am. J. Respir. Crit. Care Med*. **2008**, *177*, 82-90.

101. Munger, J. S.; Huang, X.; Kawakatsu, H.; Griffiths, M. J.; Dalton, S. L.; Wu, J.; Pittet, J. F.; Kaminski, N.; Matthay, M. A.; Rifkin, D. B.; Sheppard, D. *Cell* **1999**, *96*, 319-328.

102. Horan, G. S.; Wood, S.; Ona, V.; Li, D. J. Lukashev, M. E.; Weinreb, P. H.; Simon, K. J.; Hahm, K.; Allaire, N. E.; Rinaldi, N. J.; Goyal, J.; Feghali-Bostwick, C. A.; Matteson, E. L.; O'Hara, C.; Lafyatis, R.; Davis, G. S.; Huang, X.; Sheppard, D.; Violette, S. M. *Am. J. Respir. Crit. Care Med*. **2008**, *177*, 56-65.

103. Sheppard, D. *Eur. Respir. Rev*. **2008**, *109*, 157–162.

104. Khalil, N. *Microbes Infect*. **1999**, *1*, 1255-1263.

105. Ludbrook, S. B.; Barry, S. T.; Delves, C. J.; Horgan, C. M. *Biochem, J*. **2003**, *369*, 311-318.

106. Weinreb, P. H.; Simon, K. J.; Rayhorn, P.; Yang, W. J.; Leone, D. R.; Dolinski, B. M.; Pearse, B. R.; Yokota, Y.; Hisaaki, K.; Atakilit, A.; Sheppard, D.; Violette, S. M. *J. Biol. Chem*. **2004**, *279*, 17875-17887.

107. Schultz-Cherry, S.; Murphy-Ullich, J. E. *J. Cell Biol*. **1993**, *122*, 923-932.

108. Lyons, R. M.; Gentry, L. E.; Purchio, A. F.; Moses, H. L. *J. Cell Biol*. **1990**, *110*, 1361-1367.

109. Sato, Y.; Tsuobi, R.; Moses, H.; Rifkin, D. B. *J. Cell Biol*. **1990**, *111*, 757-763.

110. Barcellos-Hoff, M. H.; Dix, T. A. *Mol. Endocrinol*. **1996**, *10*, 1077-1083.

Christopher J Tame

111. Crawford, S. E.; Stellmach, V.; Murphy-Ullrich, J. E.; Ribeiro, S. M.; Lawler, J.; Hynes, R. O.; Boivin, G. P.; Bouck, N. *Cell* **1998**, *93*, 1159–1170.

112. Huang, X.; Wu, J.; Zhu, W.; Pytela, R.; Sheppard, D. *Am. J. Respir. Cell Mol. Biol*. **1998**, *19*, 636-642.

113. Christ, M.; McCartney-Francis, N.; Kulkarni, A.; Ward, J. M.; Mizel, D. E.; Mackall, C.; Gress, R. E.; Hines, K.; Tian, H.; Karlsson, S.; Wah, S. M. *J. Immunol*. **1994**, *153*, 1936-1946.

114. Cannistra, S. A.; Ottensmeier, C.; Niloff, J.; Orta, B.; DiCarlo, J. *Gynecol. Oncol*. **1995**, *58*, 216-225.

115. Beer, A. J.; Niemeyer, M.; Carlsen, J.; Sarbia, M.; Nährig, J.; Watzlowik, P.; Wester, H. J.; Harbeck, N.; Schwaiger, M. *J. Nucl. Med*. **2008**, *49*, 255-259.

116. Vonlaufen, A.; Wiedle, G.; Borisch, B.; Birrer, S.; Luder, P.; Imhof, B. A. *Mod. Pathol.* **2001**, *12*, 1126-1132.

117. Gladson, C. L. *J. Neuropathol. Exp. Neurol*. **1996**, *55*, 1143-1149.

118. Xiong, J.-P.; Stehle, T.; Zhang, R.; Joachimiak, A.; Frech, M.; Goodman, S. L.; Arnaout, M. A. *Science* **2002**, *296*, 151-155.

119. Xiong, J.-P.; Mahalingham, B.; Alonso, J. L.; Borrelli, L. A.; Rui, X.; Anand, S.; Hyman, B. T.; Rysiok, T.; Müller-Pompalla, D.; Goodman, S. L.; Arnaout, M. A. *J. Cell Biol*. **2009**, *126*, 589-600.

120. Dong, X.; Mi, L. Z.; Zhu, J.; Wang, W.; Hu, P.; Luo, B. H.; Springer, T. A. *Biochemistry* **2012**, *51*, 8814-8828.

121. Zartman, A. E.; Duong, L. T.; Fernandez-Metzler, C.; Hartman, G. D.; Leu, C.-T.; Prueksaritanont, T.; Rodan, G. A.; Rodan, S. B.; Duggan, M. E.; Meissner, R. S. *Bioorg. Med. Chem. Lett*. **2005**, *15*, 1647-1650.

122. Hartman, G. D.; Duggan, M. E. *Exp. Opin. Invest. Drugs* **2000**, *9*, 1281-1291.

123. Goodman, S. L.; Hölzemann, G.; Sulyok, G. A. G.; Kessler, H. *J. Med. Chem*. **2002**, *45*, 1045-1051.

124. Biological Assays and Development (BRAD), GlaxoSmithKline, unpublished work.

125. Pauletti, G. M.; Gangwar, S.; Siahaan, T. J.; Aubé, J.; Borchardt, R. *T. Adv. Drug Deliv. Rev*. **1997**, *27*, 235-256.

Christopher J Tame

126. Vitulli, G.; Graves, B.; Morrel, J.; Barrett, J. GlaxoSmithKline, unpublished work.

127. Macdonald, S. J. F.; Pritchard, J.; Anderson, N.; Wilson, C.; Redmond, J.; Campos, S.; Campbell-Crawford, M.; GlaxoSmithKline, unpublished work.

128. Roberts, F.; Freshwater-Turner, D. *Contin. Educ. Anaesth. Crit. Care. Pain*. **2007**, *7*, 25-29.

129. van de Waterbeemd, H.; Gifford, E. *Nat. Rev. Drug Discov*. **2003**, *2*, 192-204.

130. Amidon, G. L.; Lenneras, H.; Shah, V. P.; Crison, J. R. *Pham. Res*. **1995**, *12*, 413-420.

131. Butler, J. M.; Dressman, J. B. *J. Pharm. Sci*. **2010**, *99*, 4940-4954.

132. Irvine, J. D.; Takahashi, L.; Lockhart, K.; Cheong, J.; Tolan, J. W.; Selick, H. E.; Grove, J. R. *J. Pharm. Sci*. **1999**, *88*, 28-33.

133. Lipinski, C. A.; Lombardo, F.; Dominy, B. W.; Feeny, P. J. *Adv. Drug Deliv. Rev*. **1997**, *23*, 3-25.

134. Wenlock, M. C.; Austin, R. P.; Barton, P.; Davis, A. M.; Leeson, P. D. *J. Med. Chem*. **2003**, *46,* 1250-1256.

135. Veber, D. F.; Johnson, S. R.; Cheng, H.-Y.; Smith, B. R.; Ward, K. W.; Kopple, K. D. *J. Med. Chem*. **2002**, *45*, 2615-2623.

136. Gleeson, M. P. *J. Med. Chem.* **2008**, *51*, 817-834.

137. Hughes, J. D.; Blagg, J.; Price, D. A.; Bailey, S.; DeCrescenzo, G. A.; Devraj, R. V.; Ellsworth, E.; Fobian, Y. M.; Gibbs, M. E.; Gilles, R. W.; Greene, N.; Huang, E.; Krieger-Burke, T.; Loesel, J.; Wager, T.; Whitely, L.; Zhang, Y. *Bioorg. Med. Chem. Lett*. **2008**, *18*, 4872-4875.

138. a) Ritchie, T. J.; Macdonald, S. J. F. *Drug Discov. Today* **2009**, *14*, 1011-1020; and b) Ritchie, T. J.; Macdonald, S. J. F.; Young, R. J.; Pickett, S. D. *Drug Discov. Today* **2010**, *16*, 164-171.

139. Silverman, R. B. *The Organic Chemistry of Drug Design and Drug Action, Second Edition, Elsevier Academic Press*, *Waltham, MA, USA*. **2004**, *2.2*, 55-62.

140. Lombardo, F.; Shalaeva, M. Y.; Tupper, K. A.; Gao, F.; Abraham, M. H. *J. Med. Chem*. **2001**, 43, 2922.

Christopher J Tame

141. Moriguchi, I.; Hirono, S.; Liu, Q.; Nakagome, I.; Matisushita, Y. *Chem. Pharm. Bull*. **1992**, *40*, 127.

142. Scherrer, R. A.; Howard, S. M. *J. Med. Chem*. **1977**, *20*, 53-58.

143. Lombardo, F.; Shalaeva, M. Y.; Tupper, K. A.; Gao, F.; Abraham, M. H. *J. Med. Chem*. **2001**, 44, 2490.

144. Bhal, S. K.; Kassam, K.; Peirson, I. G.; Pearl, G. M. *Mol. Pharm*. **2007**, *4*, 556-560.

145. Lombardo, F.; Obach, R. S.; Shalaeva, M. Y.; Gao, F. *J. Med. Chem.* **2002**, *45,* 2867-2876.

146. Yamazaki, K.; Kanaoka, M. *J. Pharm. Sci*. **2004**, *93*, 1480-1494.

147. Shamovsky, I.; Connolly, S.; David, L.; Ivanova, S.; Norden, B.; Springthorpe, B.; Urbahns, K. *J. Med. Chem*. **2008**, *51*, 1162-1178.

148. Valko, K.; Bevan, C.; Reynolds, D. *Anal. Chem*. **1997**, *69*, 2022-2029.

149. Valko, K.; Du, C. M.; Bevan, C.; Reynolds, D. P.; Abraham, M. H. *Curr. Med. Chem*. **2001**, *8*, 1137-1146.

150. Valko, K. *J. Chromatogr. A*. **2004**, *1037*, 299-310.

151. Young, R. J.; Green, D. V. S.; Luscombe, C. N.; Hill, A. P. *Drug Discov. Today* **2011**, *16*, 822-830.

152. Hill, A.; Valko-Skegel, K. GlaxoSmithKline, unpublished work.

153. Lodish, H.; Berk, A.; Zipursky, S. L.; Matsudaira, P.; Baltimore, D.; Darnell, J. *Molecular Cell Biology. 4th edition. Diffusion of Small Molecules across Phospholipid Bilayers*. New York, **2000**. *22.3*, available from: http://www.ncbi.nlm.nih.gov/books/NBK21626. **Accessed 01/12/2013.**

154. http://en.wikipedia.org/wiki/Cell_membrane. **Accessed 27/10/2013**.

155. Macdonald, S. J. M.; Pritchard, J.; Hancock, A.; Campbell-Crawford, M. C. C. GlaxoSmithKline, unpublished work.

156. http://www.chem.wisc.edu/areas/reich/pkatable/index.htm. **Accessed 26/01/2014**. Crampton, M. R.; Robotham, I. A. *J. Chem. Res. (S)* **1997**, 22.

157. Rumley, S.; GlaxoSmithKline, unpublished work.

158. Ma, L. J.; Yang, H.; Gaspert, A.; Carlesso, G.; Barty, M. M.; Davidson, J. M.; Sheppard, D.; Fogo, A. B. *Am. J. Pathol*. **2003**, *163*, 1261-1273.

Christopher J Tame

159. Irvine, J. D.; Takahashi, L.; Lockhart, K.; Cheong, J.; Tolan, J. W.; Selick, H. E.; Grove, J. R. *J. Pharm. Sci*. **1999**, *88*, 28-33.

160. Redmond, J.; Pritchard, J.; Macdonald, S. J. F. GlaxoSmithKline, unpublished work.

161. Karasch, M. S.; Tawney, P. O. *J. Am. Chem. Soc*. **1941**, *63*, 2308-2316.

162. Feringa, B. L.; Badorrey, R.; Peña, D.; Harutyunyan, S. R. Minnaard, A. *J. Proc. Natl. Acad. Sci. U.S.A*. **2004**, *101*, 5834-5838.

163. Alexakis, A.; Bäckvall, J. E.; Krause, N.; Pàmies, O.; Dièguez, M. *Chem. Rev*. **2008,** *108,* 2796–2823.

164 . Miyaura, N.; Yanagi, T.; Suzuki, A. *Synth. Commun.* **1981**, *11*, 513-519.

165. Sakai, M.; Hayashi, H.; Miyaura, N. *Organometallics* **1997**, *16*, 4229-4231.

166. Takaya, Y.; Ogasawara, M.; Hayashi, T.; Sakai, M.; Miyaura, N. *J. Am. Chem. Soc.* **1998**, *120*, 5579-5580.

167. Yamamoto, T.; Iizuka, M.; Takenaka, H.; Ohta, T.; Ito, Y. *J. Organometallic Chem*. **2009**, *694*, 1325-1332.

168. Hayashi, T.; Tokunaga, N.; Okamoto, K.; Shintani, R. *Chem. Lett*. **2005**, *34*, 1480-1481.

169. Vautravers, N. R.; Breit, B. *Synlett* **2011**, 2517-2520.

170. Edwards, H. J.; Hargrave, J. D.; Penrose, S. D.; Frost, C. G. *Chem. Soc. Rev*. **2010**, *39*, 2093-2105.

171. Tian, P.; Dong, H.-Q.; Lin, G.-Q. *ACS Catal*. **2012**, *2*, 95-119.

172. Anderson, N. A.; Fallon, B. J.; Valverde, E.; MacDonald, S. J. F.; Pritchard, J. M.; Suckling, C. J.; Watson, A. J. B. *Synlett* **2012**, *23*, 2817-2821.

173. Hayashi, T.; Takahashi, M.; Takaya, Y.; Ogasawara, M. *J. Am. Chem. Soc.* **2002**, *124*, 5052–5058.

174. http://www.epa.gov/iris/subst/0070.htm and references therein. **Accessed 18/01/2014**.

175. Jackson, S.; Hortense, E.; Knaggs, A. GlaxoSmithKline, unpublished work.

176. Bravi, G. GlaxoSmithKline, unpublished work.

177. MCSI database, GlaxoSmithKline, unpublished work.

Christopher J Tame

178. Vitaku, E.; Ilardi, E. A.; Njardarson, J. T. http://cbc.arizona.edu/njardarson/group/sites/default/files/Top%20200%20Pharmace utical%20Products%20by%20US%20Retail%20Sales%20in%202011_small_0.pdf. **Accessed 17/10/2013**.

179. Saxena, A. K.; Jain, P. C.; Anand, N.; Dua, P. R. *J. Med. Chem*. **1973**, *16*, 560-564.

180. Lysek, R.; Schutz, C.; Favre, S.; O'Sullivan, A. C.; Pillonel, C.; Krulle, T.; Jung, P. M. J.; Clotet-Codina, I.; Este, J. A.; Vogel, P. *Bioorg. Med. Chem*. **2006**, *14*, 6255-6282.

181 . Likhosherstov, A. M.; Filippova, O. V.; Peresada, V. P.; Kryzhanovskii, S. A.; Vittnova, M. B.; Kaverina, N. V.; Reznikov, K. M. *Pharm. Chem. Jour*. **2003**, *37*, 6-9.

182. Casagrande, C.; Invernizzi, A.; Ferrini, R.; Ferrari, G. *J. Med. Chem*. **1968**, *11*, 765-770.

183. Fischer, P. M.; Wang, S. *Patent*: US 006531479 B2, WO 01/72745 A1.

184. Zhu, G.-D.; Gandhi, V. B.; Gong, J.; Luo, Y.; Liu, X.; Shi, Y.; Guan, R.; Magnone, S. R.; Klinghofer, V.; Johnson, E. F.; Bouska, J.; Shoemaker, A.; Oleksijew, A.; Jarvis, K.; Park, C.; De Jong, R.; Oltersdorf, T.; Li, Q.; Rosenberg, S. H.; Giranda, V. L. *Bioorg. Med. Chem. Lett*. **2006**, 16, 3424-3429.

185. Urban, S.; Beiring, B.; Ortega, N.; Paul, D.; Glorius, F. *J. Am. Chem. Soc*. **2012**, *134*, 15241-15244.

186. Nakamoto, K.; Tsukada, I.; Tanaka, K.; Matsukura, M.; Haneda, T.; Inoue, S.; Murai, N.; Abe, S.; Miyazaki, M.; Watanabe, N.; Asada, M.; Yoshimatsu, K.; Hata, K. *Bioorg. Med. Chem. Lett*. **2010**, *20*, 4624-4626.

187. O'Connor, M. J.; Haley, M. M. *Org. Lett*. **2008**, *10*, 3973-3976.

188. Tamao, K.; Kodama, S.; Nakajima, I.; Kumada, M. *Tetrahedron*, **1982**, *38*, 3347-3354.

189. Guo, Z.; Orth, P.; Zhu, Z.; Mazzola, R. D.; Chan, T. Y.; Vaccaro, H. A.; McKittrick, B.; Kozlowski, J. A.; Lavey, B. J.; Zhou, G.; Paliwal, S.; Wong, S.-C.; Shih, N.Y.; Ting, P. C.; Rosner, K. E.; Shipps, G. W. Jr.; Siddiqui, M. A.; Belanger,

Christopher J Tame

D. B.; Dai, C.; Li, D.; Girijavallabhan, V. M.; Popovici-Muller, J.; Yu, W.; Zhao, L. *Patent: WO2005/121130 A2*, **2005**

190. Burns, M. J.; Fairlamb, I. J. S.; Kapdil, A. R.; Sehnal, P.; Taylor, R. J. K. *Org. Lett*. **2007**, *9*, 5397-5400.

191. Kinzel, T.; Zhang, Y.; Buchwald, S. L. *J. Am. Chem. Soc*. **2010**, *132*, 14073-14075.

192. Keeling, S. GlaxoSmithKline, unpublished work.

193. Chen, Z.; Hamdouchi, C. H.; Hembre, E. J.; Jia, S.; Toth, J. L.; Hipskind, P. A. *Patent: WO2008/36541 A1*, **2008**.

194. Pars, M.; Hofmann, C. C.; Willinger, K.; Bauer, P.; Thelakkat, M.; Kohler, J. *Angew. Chem. Int. Ed*. **2011**, *50*, 11405-11408.

195. Zhao, Y.; Jiang, K.; Xu, W.; Zhu, D. *Tetrahedron* **2012**, *68*, 9113-9118.

196. Ishiyama, T.; Nobuta, Y.; Hartwig, J. F.; Miyaura, N. *Chem. Commun*. **2003**, 2924-2925.

197. Brown, G. R.; Hollinshead, D. M.; Stokes, E. S. E.; Waterson, D.; Clarke, D. S.; Foubister, A. J.; Glossop, S. C.; McTaggart, F.; Mirrless, D. J.; Smith, G. J.; Wood, R. *J. Med. Chem*. **2000**, *43*, 4964-4972.

198. Davis, F. A.; Xu, H.; Zhang, J. *J. Org. Chem*. **2007**, *72*, 2046-2052.

199. Bull, D. J.; Palmer, M. J.; Wythes, M. J. *Patent: US6610707 B1*, **2003**.

200. Anderson, N.; Hancock, A. GlaxoSmithKline, unpublished work.

201. Navarro, C.; Moreno, A.; Csǻkÿ, A. G. *J. Org. Chem*. **2009**, *74*, 466-469.

202. Hoefgen, B.; Decker, M.; Mohr, P.; Schramm, A. M.; Rostom, S. A. F.; El-Subbagh, H.; Schweikert, P. M.; Rudolf, D. R.; Kassack, M. U.; Lehmann, J. *J. Med. Chem*. **2006**, *49*, 760-769.

203. Aebi, J.; Binggeli, A.; Green, L.; Hartmann, G.; Maerki, H. P.; Mattei, P. *Patent: US2011/92698 A1*, **2011**.

204. Anderson, N. GlaxoSmithKline, Unpublished work.

205. Lukin, K.; Zhang, Q.; Leanna, M. R. *J. Org. Chem*. **2009**, *74*, 929-931.

206. Kelly, M. G.; Kincaid, J.; Gowlugari, S.; Kaub, C.; *Patent: WO2009/11904 A1,* **2009**

Christopher J Tame

207. Henderson, R. K.; Jimenez-Gonzalez, C.; Constable, D. J. C.; Alston, S. R.; Inglis, G. G. A.; Fisher, G.; Sherwood, J.; Binks, S. P.; Curzons, A. D. *Green Chem*. **2011**, *13*, 854-862.

208. Fasano, M.; Curry, S.; Terrano, E.; Galliano, M.; Fanali, G.; Narciso, P.; Notari, S.; Ascenzi, P. *IUBMB Life* **2005**, *57*, 787-796.

209. Smith, D. A.; Di, L.; Kerns, E. D. *Nat. Rev. Drug Discov*. **2010**, *9*, 929-939.

210. Zeitlinger, M. A.; Derendorf, H.; Mouton, J. W.; Cars, O.; Craig, W. A.; Andes, D.; Theuretzbacher, U. *Antimicrob. Agents Chemother*. **2011**, *55*, 3067-3074.

211. Virchow, J, Chr.; Bachert, C. *Resp. Med*. **2006,** *100*, 11, 1952-1959.

212. Cheng, H.; Leff, J. A.; Amin, R.; Gertz, B. J.; De Smet, M.; Noonan, N.; Rogers, J. D.; Malbecq, W.; Meisner, D.; Somers, G. *Pharm. Res.* **1996**, *13*, 3, 445-448.

213. Lanicek, M.; Laznickova, A. *J. Pharm. Biomed. Anal*. **1995**, *13*, 823-828.

214. Mukai, T.; Hirano, K.; Satoh, T.; Miura, M. *Org. Lett*., **2010**, *12*, 6, 1360-1363.

215. Boyd, R. E.; Press, J. B.; Rasmussen, C. R.; Raffa, R. B.; Codd, E. E.; Connelly, C. D.; Bennet, D. J.; Kirifides, A. L.; Gardocki, J. F.; Reynolds, B.; Hortenstein, J. T.; Reitz, A. B. *J. Med. Chem*. **1999**, *42*, 5064-5071.

216. Adams, A. D.; Szewczyk, J. W.; Green, A. I. *Patent: WO2007/64553 A2*, **2007**.

217. Rudolf, K.; Bischoff, D.; Dahnmann, G.; Grauert, M.; Kuelzer, R.; Wellenzohn, B. *Patent: WO2013/87739 A1*, **2013**.

218. Oberboersch, S.; Jostock, R.; Engels, M.; Schunk, S.; Hees, S.; Germann, T.; Klegraf, E.; Reich, M. *Patent: WO2009/124746 A1*, **2009**.

219. Wagner, J.; Matt, P. V.; Faller, B.; Cooke, N. G.; Albert, R.; Sedrani, R.; Wiegand, H.; Jean, C.; Beerli, C.; Weckbecker, G.; Evenou, J.-P.; Zenke, G.; Cottens, S. *J. Med. Chem*. **2011**, *54*, 6028-6039.

220. Bischoff, H.; Dittrich-Wengenroth, E.; Griebenow, N.; Kretschmer, A.; Krueger, J.; Woltering, E. *Patent: WO2005/97784 A1*, **2005**.

221. Hesse, C.; Luntz, S. P.; Siedler, H.; Unnebrink, K.; Mikus, G.; de Bruijn, M.; Zondang, E.; de Vries, M.; Seibert-Grafe, M.; Haefeli, W. E. *Br. J. Clin. Pharacol*. **2006**, *61*, 414-419.

Christopher J Tame

222. Al-Soud, Y. A.; Al-Dweri, M. N.; Al-Masoudi, N. A. *Farmaco*. **2004**, 59, 775-783.

223. Biftu, T.; Singh, S.; Weber, A. E.; Gao, Y.-D.; Feng, D. D. *Patent*: WO2006/9886 A1, **2006**.

224. Yamashita, M.; Hirano, K.; Satoh, T.; Miura, M. *Org. Lett*. **2010***, 12*, 592–595.

225. Zhao, D. B.; Gao, C.; Su, X. Y.; He, Y. Q.; You, J. S.; Xue, Y. *Chem. Commun*. **2010**, *46*, 9049–9051.

226. Goossen, L. J.; Lange, P. P.; Rodríguez, N.; Linder, C. *Chem. Eur. J*. **2010**, *16*, 3906–3909.

227. Goossen, L.; Rodriguez, N.; Melzer, B.; Linder, C.; Deng, G.; Levy, L. M. *J. Am. Chem. Soc.* **2007**, *129*, 4824-4833.

228. Shang, R.; Yang, Z.-W.; Wang, Y.; Zhang, S.-L.; Liu, L. *J. Am. Chem. Soc*. **2010**, *132*, 14391-14393.

229. Conditions adapted from: Bradley, T.; Campbell, M. GlaxoSmithKline, unpublished work.

230. Campeau, L. C.; Schipper, D. J.; Fagnou, K. *J. Am. Chem. Soc*. **2008**, *130*, 3266-3267.

231. Schipper, D. J.; Campeau, L.-C.; Fagnou, K. *Tetrahedro*n **2009**, *65*, 3155-3164.

232. Borthwick, A. D.; Davies, D. E.; Exall, A. E.; Hatley, R. J. D.; Hughes, J. A.; Irving, W. R.; Livermore, D. G.; Sollis, S. L.; Nerozzi, F.; Valko, K. L.; Allen, M. J.; Perren, M.; Shabbir, S. S.; Wollard, P. M.; Price, M. A. *J. Med. Chem*. **2006**, *49*, 4159-4170.

233. http://www.sigmaaldrich.com/MSDS/MSDS/DisplayMSDSPage.do?country=GB&language=en&productNumber=13631&brand=FLUKA&PageToGoToURL=http%3A%2F%2Fwww.sigmaaldrich.com%2Fcatalog%2Fproduct%2Ffluka%2F13631%3Flang%3Den **Accessed 21/01/2014**.

234. Leville, M. GlaxoSmithKline, unpublished work.

235. Gao, Y.; Lam, Y. *J. Comb. Chem*. **2010**, *12*, 69-74.

Christopher J Tame

236. Plouvier, B.; Beatch, G. N.; Jung, G. L.; Zolotoy, A.; Sheng, T.; Clohs, L.; Barrett, T. D.; Fedida, D.; Wang, W. Q.; Zhu, J. J.; Liu, Y.; Abraham, S.; Lynn, L.; Dong, Y.; Wall, R. A.; Walker, M. J. A. *J. Med. Chem*. **2007**, *50*, 2818-2841.

237. Peace, S. GlaxoSmithKline, unpublished work.

238. Craven, A. GlaxoSmithKline, unpublished work.

239. Takahashi, H.; Shinoyama, M.; Komine, T.; Nagao, M.; Suzuki, M.; Tsuchida, H.; Katsuyama, K. *Bioorg. Med. Chem. Lett*. **2011**, *21*, 1758-1762.

240. Malachowski, W. P.; Tie, C.; Wang, K.; Broadrup, R. L. *J. Org. Chem*. **2002**, *67*, 8962-8969.

241. Eatherton, A. J.; Giblin, G. M. P.; Hall, A.; Hurst, D. N.; Gibson, M. *Patent: WO2008/98978 A2*, 2008.

242. Biftu, T.; Caldwell, C. G.; Weber, A. E.; Chen, P.; Qian, X.; Feng, D.; Cox, J. M. *Patent*: WO2007/97931 A2, **2007**.

243. Hobbs, H. GlaxoSmithKline, unpublished work.

244. Ward, K. W.; Smith, B. R. *Drug Metab. Dispos*. **2004**, *32*, 603-611.

245. Butler, J. M.; Dressman, J. B. *J. Pharm Sci*. **2010**, *12*, 4940-4954.

246. Samet, J. S. *Tox. Lett*. **1995***, 81-83*, 33-38.

247. 'Global surveillance, prevention and control of chronic respiratory diseases – a comprehensive approach', *W.H.O*. **2007**, ISBN: 978 92 4 156346 8.

248. http://www.nhlbi.nih.gov/health/health-topics/topics/asthma. **Accessed 01/2011**.

249. Nelson, H. S.; Weiss, S. T.; Bleecker, E. R.; Yancey, S. W.; Dorinsky, P. M. *Chest* **2006**, *129*, 15-26.

250. Irwin, R. S.; Richardson, N. D. *CHEST* **2006**, *130*, 41S-53S.

251. Forssell, J.; Sideras, P.; Eriksson, C.; Malm-Erjefält, M.; Rydell-Törmänen, K.; Ericsson, P.-O.; Erjefält, J. S. *Am. J. Respir. Cell Mol. Biol*. **2005**, *32*, 6, 511-520.

252. Lee, S. J.; Wang, J. Y. J. *J. Biol*. **2009**, *8*, 30.

253. http://www.citeline.com/products/pharmaprojects/ **Accessed 21/01/2013**.

254. Hardie, D. G.; Hanks, S. K. *Protein Kinase Factsbook: Protein Serine Kinases*, Academic Press: London **1995** *1*, 7-47.

255. Dinarello, C. A. *Eur. J. Immunol*. **2007**, *37*, S34-S45.

Christopher J Tame

256.

http://bio1151b.nicerweb.com/Locked/media/ch11/phosphorylation_cascade.html, **Accessed 01/2011**.

257. Hanks, S. K.; Hunter, T. *FASEB J.* **1995**, *9*, 576-596.

258. Manning, G.; Whyte, D. B.; Martinez, R.; Hunter, T.; Sudarsanam, S. *Science* **2002**, *298*, 1912-1934.

259. Fu, J.; Jiang, Q.; Zhang, C. *Nature Education 3* **2010**, *9*, 82.

260. Walker, E. H.; Pacold, M. E.; Perisic, O.; Stephens, L.; Hawkins, P. T.; Whymann, M. P.; Williams, R. L. *Mol. Cell* **2000**, *6*, 909-919.

261. Kornev, A. P.; Haste, N. M.; Taylor, S. S.; Ten Eyck, L. F. *Proc. Natl. Acad. Sci. U.S.A.* **2006**, *103*, 17783-17788.

262. Bourbonnais, É.; Raymond, V. A.; Éthier, C.; Nguyen, B. N.; El-Leil, M. S.; Meloche, S.; Bilodeau, M. *Gastroenterology* **2012**, *142*, 130-139.

263. Tahara, E.; Kadara, H.; Lacroix, L.; Lotan, D.; Lotan, R. *Cancer Biol. Ther.* **2009**, *8*, 801-807.

264. Rusnak, D. W.; Lackey, K.; Affleck, K.; Wood, E. R.; Alligood, K. J.; Rhodes, N.; Keith, B. R.; Murray, D. M.; Knight, W. B.; Mullin, R. J.; Gilmer, T. M. *Mol. Cancer Ther.* **2001**, *1*, 85-94.

265. Bartram, C. R.; Kleinhauer, E.; de Klein, A.; Grosveldl, G.; Teyssier, J. R.; Heisterkamp, N.; Groffen, J. *EMBO J.* **1985**, *4*, 683-686.

266. Savage, D. G.; Antman, K. H. *N. Engl. J. Med.* **2002**, *346*, 683-693.

267. Foreman, J. C.; Johansen, T.; Gibb, A. J. *Textbook of Receptor Pharmacology, Third Edition*, CRC Press, **2010**, 303.

268. http://www.ncbi.nlm.nih.gov/pubmedhealth/PMH0000345/. **Accessed 01/2011**.

269. Ghigo, A.; Damilano, F.; Braccini, L.; Hirsch, E. *BioEssays* **2010**, 32, *3*, 185-196.

270. Chen, K.; Iribarren, P.; Gong, W.; Wang, J.-M. *Cell. & Mol. Immun.* **2005**, *2*, 241-252.

271. Paz-Ares, L.; Blanco-Aparicio, C.; Garcia-Carbonero, R.; Carnero, A. *Clin. Transl. Oncol.* **2009**, *11*, 9, 572-579.

272. Czech, M. P. *Cell* **2000**, *100*, 603–606.

Christopher J Tame

273. Falasca, M.; Hughes, W. E.; Dominguez, V.; Sala, G.; Fostira, F.; Fang, M. Q.; Cazzolli, R.; Shepherd P. R.; James, D. E.; Maffucci, T. *J. Biol. Chem.* **2007**, *282*, 28226-28236.

274. Takegawa, K.; DeWald, D. B.; Emr, S. D. *J. Cell Sci*. **1995**, *108*, 3745–3756.

275. Wheeler, M.; Domin, J. *J. Cell. Physiol*. **2006**, *206*, 586–593.

276. Yoshioka**,** K.; Yoshida, K.; Cui, H.; Wakayama, T.; Takuwa, N.; Okamoto, Y.; Du, W.; Qi, X.; Asanuma, K.; Sugihara, K.; Aki, S.; Miyazawa, H.; Biswas, K.; Nagakura, C.; Ueno, M.; Iseki, S.; Schwartz, R. J.; Okamoto, H.; Sasaki, T.; Matsui, O.; Asano, M.; Adams, R. H.; Takakura, N.; Takuwa, Y. *Nat. Med*. **2012**, *18*, 1560-1569.

277. Yu, W.; Sun, X.; Tang, H.; Tao, Y.; Dai, Z. *Leuk. Lymphoma*, **2010**, *51*, 6, 1098-1107.

278. Simonsen, A.; Tooze, S. A. *J. Cell Bio*. **2009**, *186*, 773-782.

279. Cantley, L. C. *Science* **2002**, *296*, 1655-1657.

280. Nobukuni, T.; Joaquin, M.; Roccio, M.; Dann, S. G.; Kim, S. Y.; Gulati, P.; Byfield, M. P.; Backer, J. M.; Natt, F.; Bos, J. L. Zwartkruis, F. J. T.; Thomas, G. *Proc. Natl. Acad. Sci. U.S.A*. **2005**, *102*, 14238–14243.

281. Kihara, A.; Noda, T.; Ishihara, N.; Ohsumi, Y. *J. Cell Biol*. **2001**, *152*, 519–530.

282. Deretic, V. *Curr. Opin. Immunol*. **2006**, *18*, 375–382.

283. Geering, B.; Cutillas, P. R.; Nock, G.; Gharbi, S. I.; Vanhaesebroeck, B. *Proc. Natl. Acad. Sci. U.S.A.* **2007**, *104*, 19, 7809-7814.

284. Rordorf-Nikolic, T.; Van Horn, D. J.; Chen, D.; White, M. F.; Backer, J. M. *J. Biol. Chem.* **1995**, *270*, 3662–3666.

285. Maier, U.; Babich, A.; Nurnberg, B. *J. Biol. Chem*. **1999**, *274*, 29311–29317.

286. Walker, E. H.; Perisic, O.; Reid, C.; Stephens, L.; Williams, R. L.; *Nature* **1999**, *402*, 6759, 313-320.

287. Vanhaesebroeck, B.; Waterfield, M. D. *Exp. Cell Res*. **1999**, *253*, 1, 239-54.

288. Kerr, W. G. *The Year in Immun.* **2010**, *1217*, 1-17.

289. Wishart, M. J.; Dixon, J. E. *Trends Cell Biol*. **2002**, *12*, 579-585.

290. Rohrschneider, L. R.; Fuller, J. F.; Wolf, I.; Liu, Y.; Lucas, D. M. *Genes Dev*. **2000**, *14*, 505-520.

Christopher J Tame

291. Gunn, R. M.; Hailes, H. C. *J. Chem. Biol*. **2008**, *1*, 49-62.

292. Saraste, M.; Hyviinen, M, *Curr. Opin. Struct. Biol*. **1995**, *5*, 403-408.

293. Wishart, M. J.; Taylor, G. S.; Dixon, J. E. *Cell* **2001**, *105*, 817-820.

294. Song, G.; Ouyang, G.; Bao, S. *J. Cell. Mol. Med*. **2005**, *9*, 1, 59-71.

295. Brown, J. M.; Wilson, T. M.; Metcalfe, D. D.; *Clin. Exp. Allergy*, **2007**, *38*, 4-18.

296. Sadhu, C.; Masinovsky, B.; Dick, K.; Sowell, C. G.; Staunton, D. E. *J. Immunol*. **2003**, *170*, 2647-2654.

297. Ellson, C. D.; Gobert-Gosse, S.; Anderson, K. E.; Davidson, K.; Erdjument-Bromage, H.; Tempst, P.; Thuring, J. W.; Cooper, M. A.; Lim, Z. Y.; Holmes, A. B.; Gaffney, P. R.; Coadwell, J.; Chilvers, E. R.; Hawkins, P. T.; Stephens, L. R. *Nat. Cell Biol*. **2001**, *3*, 7, 679-682.

298. Chen, K.; Iribarren, P.; Gong, W.; Wang, J.-M. *Cellular & Molecular Immunology*. **2005**, *2*, 241-252.

299. Hennessy, B. T.; Smith, D. L.; Ram, P. T.; Lu, Y.; Mills, G. B. *Nat. Rev. Drug. Discov*. **2005**, *12*, 988-1004.

300. Ali, K.; Bilancio, A.; Thomas, M.; Pearce, W.; Gilfillan, A. M.; Tkaczyk, C.; Kuehn, N.; Gray, A.; Giddings, J.; Peskett, E.; Fox, R.; Bruce, I.; Walker, C.; Sawyer, C.; Okkenhaug, K.; Finan, P.; Vanhaesebroeck, B. *Nature* **2004**, *431*, 1007–1011.

301. Sasaki, T.; Irie-Sasaki, J.; Jones, R. G.; Oliveira-dos-Santos, A. J.; Stanford, W. L.; Bolon, B.; Wakeham, A.; Itie, A.; Bouchard, D.; Kozieradzki, I.; Joza, N.; Mak, T. W.; Ohashi, P. S.; Suzuki, A.; Penninger, J. M. *Science* **2000**, *287*, 1040-1046.

302. Afshar, R.; Medoff, B. D.; Leuster, A. D. *Clin. Expe. Allergy* **2008**, *38*, 1847-1857.

303. Marwick, J. A.; Chung, K. F.; Adcock, I. M. *Ther. Adv. Resp. Dis*. **2009**, 1-16.

304. Okkenhaug, K. Bilancio, A.; Farjot, G.; Priddle, H.; Sancho, S.; Peskett, E.; Pearce, W.; Meek, S. E.; Salpekar, A.; Waterfield, M. D.; Smith, A. J. H.; Vanhaesebroeck, B. *Science* **2002**, *297*, 1031-1034.

305. Hirsch, E.; Katanaev, V. L.; Garlanda, C.; Azzolino, O.; Pirola, L.; Silengo, L.; Sozzani, S.; Mantovani, A.; Altruda, F.; Wymann, M. P. *Science* **2000**, *287*, 1049-1053.

306. Bohnacker, T.; Marone, R.; Collmann, E.; Calvez, R.; Hirsch, E.; Wymann, M. P. *Sci. Signal*. **2009**, *2*, 74, ra27, 1-12.

307. Kola, I.; Landis, J. *Nat. Rev. Drug Discov*. **2004**, *3*, 711-716.

308. Hassall, D.; Somers, G.; Bevan, N.; Allen, P. GlaxoSmithKline, *unpublished work*.

309. Halliwell, W. H. *Toxicol. Pathol.* **1997**, *25*, 53-60.

310. Lian, X.; Yan, C.; Yang, L.; Xu, Y.; Du, H. *Am. J. Physiol. Lung Cell Mol. Physiol.* **2004***, 286*, L801-L807.

311. Adherence to Long-Term Therapies: Evidence for Action. *W.H.O*. **2003**, ISBN 92 4 154599 2.

312. Wilson, S. R.; Scamages, P.; German, D. F.; Hughes, G. W.; Lulla, S.; Coss, S.; Thomas, R. G.; Starr-Scheidkraut, N.; Stancavage, F. B.; Arsham, G. M. *Am. J. Med*. **1993**, *94*, 564-576.

313. http://www.fda.gov/NewsEvents/Newsroom/PressAnnouncements/ucm406387.htm **Accesed 27/07/2014**.

314. http://www.ema.europa.eu/ema/index.jsp?curl=pages/news_and_events/news/2014/07/news_detail_002148.jsp. **Accessed 27/07/2014**.

315. Berndt, A.; Miller, S.; Williams, O.; Le, D. D.; Houseman, B. T.; Pacold, J. I.; Gorrec, F.; Hon, W.-C.; Liu, Y.; Rommel, C.; Gaillard, P.; Ruckle, T.; Schwarz, M. K.; Shokat, K. M.; Shaw, J. P.; Williams, R. L. *Nat. Chem. Biol*. **2010**, *6*, 117–124.

316. Vitulli, G.; *GlaxoSmithKline*, Unpublished work.

317. Sourced from clinicaltrials.gov. Study identifiers for the phase IIa trial for asthma: NCT01653756, IPI-145-03, 2012-001729-28. **Accessed 31/01/2013**.

318. Palombella, V. Poster: "Targeting PI3K-δ and PI3K-γ in inflammation" **2012**, http://infi.com/pdfs/palombella_nyas_2012.pdf, accessed **02/2013**.

Christopher J Tame

319. Hamblin, N. J.; Jones, P. S.; Keeling, S. E.; Le, J.; Mitchell, C. J.; Parr, N. J. Patent *US2013/0029985 A1*, **2012**.

320. Kranz, M. *GlaxoSmithKline*, Unpublished work.

321. Inglis, G. G. A.; Peace, S.; Barton, N.; Cooper, T. *GlaxoSmithKline*, unpublished work.

322. Erdik, E. *Tetrahedron* **1987**, *43*, 2203-2212.

323. Deng, J. Z.; Paone, D. V.; Ginnetti, A. T.; Kurihara, H.; Dreher, S. D.; Weissman, S. A.; Stauffer, S. R.; Burgey, C. S. *Org. Lett.* **2009**, *11,* 345-347.

324. Diao, X.; Wang, Y.; Jiang, Y.; Ma, D. *J. Org. Chem.* **2009**, *74*, 7974–7977.

325. Suzuki, H.; Miyoshi, K.; Shinoda, M. *Bull. Chem. Soc. Jpn*. **1980**, *53*, 1765-1766.

326. The area of amide bond formation is wide and varied. Below are two articles that review the current advances in amide coupling techniques. a) Joullie, M. M.; Lassen, K. M. *ARKIVOC* **2010**, 189-250; and b) Valeur, E.; Bradley, M. *Chem. Soc. Rev*. **2009**, *38*, 606-631.

327. Dihydrobenzofuran formation: Garcia, D.; Foubelo, F.; Yus, M. *Tetrahedron* **2008**, *64*, 4275-4286. Borylation and Pd catalysed cross coupling: Allan, M.; Chamoin, S.; Hu, Q.Y.; Imase, H.; Papillon, J. *Patent: WO2011/61168 A1* **2011**. Nitro reduction: Altenbach, R. J.; Khilevich, A.; Kolasa, T.; Rohde, J. J.; Bhatia, P. A.; Patel, M. V.; Searle, X. B.; Yang, F.; Bunnelle, W. H.; Tietje, K.; Bayburt, W. H.; Erol, K.; Carroll, W. A.; Meyer, M. D.; Henry, R.; Buckner, S. A.; Kuk, J.; Daza, A. V.; Millicic, I. V.; Cain, J. C.; Kang, C. H.; Ireland, L. M.; Carr, T. L.; Miller, T. R.; Hancock, A. A.; Nakane, M.; Esbenshade, T. A.; Brune, M. E.; O'Neill, A. B.; Gauvin, D. M.; Katwala, S. P.; Holladay, M. W.; Brioni, J. D.; Sullivan, J. P. *J. Med. Chem*. **2004**, *47*, 3220-3235. Diazotisation and aryl iodide formation: Funk, L. A.; Johnson, M. C.; Kung, P. P.; Meng, J. J.; Zhou, J. Z. *Patent: WO2006/117669 A1* **2006**.

328. Ishiyama, T.; Nobuta, Y.; Hartwig, J. F.; Miyaura, N. *Chem. Commun*. **2003**, 2924-2925.

329. Industrial supervisor Simon Peace suggested the use of alkyne cyclotrimerisations to access the appropriately functionalised dihydroisobenzofurans.

Christopher J Tame

330. Yamamoto, Y.; Arakawa, T.; Ogawa, R.; Itoh, K. *J. Am. Chem. Soc.* **2003**, *125*, 12143-12160.

331. Reppe, V. W.; Schweckendiek, W. J. Justus Liebigs Annalen der Chemie 1948, 560, 104-116.

332. Muller, E.; Thomas, R.; Sauberbier, M.; Langer, E.; Streichfuss, D. *Tetrahedron Lett.* **1971**, 521-524.

333. Vollhardt, K. P. C.; Bergman, R. G. *J. Am. Chem. Soc.* **1974**, *96*, 4996-4998.

334. Agnet, N.; Gandon, V.; Vollhardt, K. P. C.; Malacria, M.; Aubert, C. *J. Am. Chem. Soc*. **2007**, *129*, 8860-8871.

335. Naiman, A.; Vollhardt, K. P. C. *Angew. Chem. Int. Ed. Engl.* **1977**, *16*, 708-709.

336. Grigg, R.; Scott, R.; Stevenson, P. *Tetrahedron Lett*. **1982**, 23, 2691-2692.

337. Sato, Y.; Nishimata, T.; Mori, M. *J. Org. Chem.* **1994**, *59*, 6133-6135.

338. Inglesby, P. A.; Evans, P. A. *Chem. Soc. Rev*. **2010**, *39*, 2791-2805.

339. Dominguez, G.; Pérez-Castells, J. *Chem. Soc. Rev*. **2011**, *40*, 3430–3444.

340. Levin, S.; Nani, R. R.; Reisman, S. E. *J. Am. Chem. Soc*. **2010**, *133*, 774–776.

341. Duong, H. A.; Cross, M. J.; Louie, J. *J. Am. Chem. Soc.* **2004**, *126*, 11438-11439.

342. Verela, J. A.; Saa, C. *J. Org. Chem*. **2009**, *694*, 143-149.

343. Dutta, B.; Curchod, B. F. E.; Campomanes, P.; Solari, E.; Scopelliti, R.; Rothlisberger, U.; Severin, K. *Chem. Eur. J*. **2010**, *16*, 8400 – 8409.

344. Kirchner, K.; Calhorda, M. J.; Schmid, R.; Veiros, L. F. *J. Am. Chem. Soc*. **2003**, *125*, 11721-11729.

345. Hilt, G.; Hengst, C.; Hess, W. *Eur. J. Org. Chem*. **2008**, 2293-2297.

346. Yamamoto, Y.; Hattori, K.; Ishii, J.; Nishiyama, H. *Tetrahedron*, **2006**, *62*, 4294-4305.

347. Hillard, R. L.; III, Vollhardt, K. P. C. *J. Am. Chem. Soc.* **1977**, *99*, 4058-4069.

348. Peace, S. *GlaxoSmithKline*, unpublished work.

349. Trost, B.; Rudd, M. T.; Costa, M. G.; Lee, P. I.; Pomerantz, A. E. *Org. Lett*. **2004**, *6*, 4235-4238.

350. http://www.sigmaaldrich.com/MSDS/MSDS/DisplayMSDSPage.do?country=GB&la

Christopher J Tame

nguage=en&productNumber=437565&brand=SIAL&PageToGoToURL=http%3A%2F%2Fwww.sigmaaldrich.com%2Fcatalog%2Fproduct%2Fsial%2F437565%3Flang%3Den. **Accessed 21/01/2012**.

351. Bouisseau, A. *GlaxoSmithKline*, unpublished work.

352. Henderson, R. K.; Jimenez-Gonzalez, C.; Constable, D. J. C.; Alston, S. R.; Inglis, G. G. A.; Fisher, G.; Sherwood, J.; Binks, S. P.; Curzons, A. D. *Green Chem*. **2011**, *13*, 854-862

353. a) Schipper, D. J.; Campeau, L.-C.; Fagnou, K. *Tetrahedron* **2009,** *65,* 3155-3164; and b) Gosselin, F.; Savage, J.; Blaquiere, N.; Stabin, S. T. *Org. Lett.* **2012**, *14,* 862-865.

354. Nara, S. J.; Jha, M.; Brinkhorst, J.; Zemanek, T. J.; Pratt, D. A. *J. Org. Chem*. **2008**, *73*, 9326-9333.

355. Qian, D.; Han, A. Q.; Hamilton, M.; Wang, E. *Patent WO2009/155527 A2* **2009**.

356. Li, G.; Watson, K.; Buckheit, R. W.; Zhang, Y. *Org. Lett.* **2007**, *9*, 2043-2046

357. Vachal, P.; Toth, L. M.; Hale, J. J.; Yan, L.; Mills, S. G.; Chrebet, G. L.; Koehane, C. A.; Hajdu, R.; Milligan, J. A.; Rosenbach, M. J.; Mandala, S. *Bioorg. Med. Chem. Lett*. **2006**, *16*, 3684-3687.

358. www.millipore.com. **Accessed 21/01/2012**.

359. Smith, S. *GlaxoSmithKline*, unpublished work.

360. Collins, S. J.; DeWeese, T. L.; Jeggo, P. A.; Parker, A. R. *Oncogene* **2005**, *24*, 949–961.

361. Zoncu, R.; Efeyan, A.; Sabatini, D. M. *Nature Rev. Mol. Cell Biol*. **2011**, *12*, 21-35.

362. Lucas, F. *GlaxoSmithKline*, unpublished work.

363. Uddin, S. *GlaxoSmithKline*, unpublished work.

364. Ishikawa, M.; Hashimoto, Y. *J. Med. Chem.* **2011**, *54*, 1539-1554.

365. Lovering, F.; Bikker, J.; Humblet, C. *J. Med. Chem.* **2009**, *52*, 6752–6756.

366. Venable, J. D.; Ameriks, M. K.; Blevitt, J. M.; Thurmond, R. L.; Fung-Leung, W.-P. *Recent Patents on Inflamm. & Allergy Drug Discov*. **2010**, *4*, 1-15.

Christopher J Tame

367. Sourced from clinicaltrials.gov. Study identifiers for ongoing phase II trials for asthma: NCT01653756, 2012-001729-28. **Accessed 06/02/2013**.

368. Mitsuoka, Y.; Masuda, M.; Taniyama, D. *Patent US2011/0230472 A1*, **2011**.

369. Convery, M.; Neu, M. *GlaxoSmithKline*, unpublished work.

370. Walker, E. H.; Perisic, O.; Ried, C.;.Stephens, L.; Williams, R. L. *Nature* **1999**, *402*, 313-320.

371. Blagg, J. *Annu. Rep. Med. Chem*. **2006**, *41*, 353-368.

372. Ameriks, M. K.; Venable, J. D. *Current Topics in Med. Chem*. **2009**, *9*, 738-753.

373. Hamblin, N. J.; Down, K. D.; Hardy, C. J.; Hamadi, A.; Kranz, M.; Le, J. *GlaxoSmithKline*, unpublished work.

374. Elkins, T.; Smallwood, A. M.; Raha, K. *GlaxoSmithKline,* unpublished work.

375. Hill, A.; Valko, K.; Smith, S.; *GlaxoSmithKline*, unpublished work.

376. Kugler-Steigmeier, M. E.; Friederich, U.; Graf, U.; Lutz, W. K.; Schlatter, M. C. *Mutat. Res*. **1989**, *211*, 279-289.

377. Choi, S.; Connelly, S.; Reixach, N.; Wilson, I. A.; Kelly, J. W. *Nat. Chem. Biol*. **2010**, *6*, 133-139.

378. Singh, J.; Petter, R. C.; Baillie, T. A.; Whitty, A. *Nat. Rev. Drug Discov*. **2011**, *10*, 307-317.

379. http://www.chemcomp.com/software.htm. **Accessed 07/2011**.

380. http://www.acdlabs.com/company/media/pr/2008_03_pka.php. **Accessed 07/2011**.

381. Miyaura, N.; Yanagi, T.; Suzuki, A. *Synth. Commun*. **1981**, *11*, 513-519.

382. Wellaway, N. *GlaxoSmithKline*, unpublished work.

383. Wrobel, J.; Millen, J.; Sredy, J.; Dietrich, A.; Gorham, B. J.; Malamas, M.; Kelly, J. M.; Bauman, J. G.; Harrison, M. C.; Jones, L. R.; Guinosso, C.; Sestanj, K. *J. Med. Chem*. **1991**, *34*, 2504-2520.

384. Dong, Q.; Kanounl, T.; Wallace, M. B. *Patent US2009/118324 A1* **2009**.

385. Hill, A.; Reid, I. *GlaxoSmithKline*, unpublished work.

Christopher J Tame

Christopher J Tame